Conference Proceedings

Twentieth Annual Meeting of the American Society of Biomechanics

Georgia Tech
Atlanta, Georgia
October 17-19, 1996

founded 1977
AMERICAN SOCIETY OF BIOMECHANICS

GEORGIA INSTITUTE OF TECHNOLOGY
PROGRESS AND SERVICE
SEAL 1885

Conference Proceedings

AMERICAN SOCIETY OF BIOMECHANICS

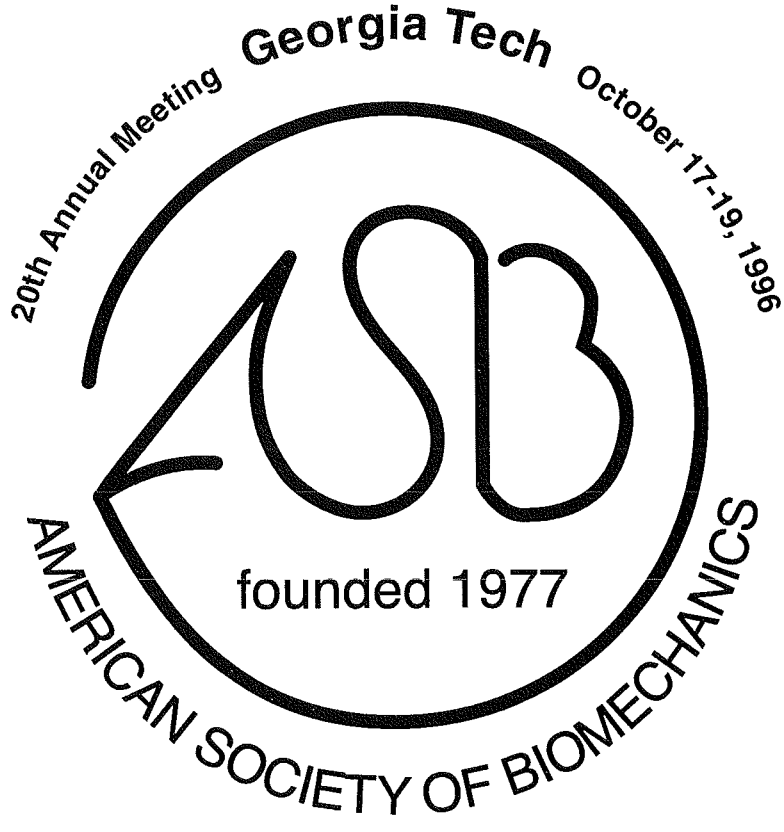

edited by
Dave Fyhrie Ph.D., Program Chair
Robert Gregor Ph.D., Meeting Chair

Local Organizing Committee

Robert J. Gregor, PhD
Department of Health and Performance Sciences
Georgia Institute of Technology

Robert Nerem, PhD
Director, Institute for Bioengineering and Bioscience
Georgia Institute of Technology

Ray Vito, PhD
Department of Mechanical Engineering
Georgia Institute of Technology

Richard Nichols, PhD
Department of Physiology
Emory University School of Medicine

Mike Sinclair
Director, Interactive Media and Technology Center
Georgia Institute of Technology

Jessica Hodgins, PhD
College of Computing
Georgia Institute of Technology

Ben Johnson, EdD
Department of Kinesiology and Health
Georgia State University

The organizers of the 20th Annual Meeting of the American Society of Biomechanics gratefully acknowledge the following organizations for their generous support of this Annual Meeting:

The Whitaker Foundation
for an educational grant to support student attendance and participation.

The Georgia Tech Foundation
to support student attendance and local Conference arrangements.

The Emory/Georgia Tech Biomedical Technology Research Center
in support of the Satellite Symposium at Emory University, October 20, 1996 and for student attendance at the Annual Meeting.

The Society for Neuroscience, Atlanta Chapter,
in support of the Satellite Symposium at Emory University, October 20, 1996.

❖ ❖ ❖ ❖ ❖ ❖ ❖ ❖ ❖ ❖ ❖

American Society of Biomechanics

The American Society of Biomechanics was formed in 1977. The purpose of the Society is to provide a forum for interaction among the diverse disciplines in biomechanics research and applications. The term biomechanics in this context refers to the study of structure and function of biological systems using the methods of mechanics. The active membership of the Society includes scientists who conduct research in the biological sciences, engineering and applied sciences, ergonomics and human factors, exercise and sports sciences, and the health sciences.

The principle activity of the Society is an annual scientific meeting. The meeting is held over a three-day period, and consists of keynote addresses, tutorial sessions, podium and poster presentations and student member functions. In keeping with the objectives of the Society, the papers address a wide range of topics and broad interests.

The Executive Board that has governed the Society during the past year is represented by the following individuals:

President:	Kai-Nan An, Mayo Clinic
Past President:	Philip E. Martin, Arizona State University
President-Elect:	Robert J. Gregor, Georgia Institute of Technology
Secretary-Treasurer:	Joan E. Bechtold, Orthopaedic Biomechanics Lab
Meeting Chairperson:	Robert J. Gregor, Georgia Institute of Technology
Program Chairperson:	David Fyhrie, Henry Ford Hospital
Program Chairperson-Elect:	Mary M. Rodgers, University of Maryland
Membership Committee Chairperson:	J.J. Trey Crisco, Brown University
EducationCommitteeChairperson:	Jill McNitt-Gray,University of Southern California

Sustaining Members of the Society

The Society would like to thank the following organizations for their continuing support as Sustaining Members:

Aircast
DePuy, Inc.
Howmedica, Inc.
Kistler Instrument Corporation
Motion Analysis Corporation
MTS Systems Corporation
Noraxon USA, Inc.
Orthofix, S.R.L.
Peak Performance Technologies, Inc.

Program Committee

David P. Fyhrie, Ph.D., Program Chair
Henry Ford Hospital

Mary M. Rodgers, Ph.D.
University of Maryland

Sharon Swartz, Ph.D.
Brown University

Scott Tashman, Ph.D.
Henry Ford Hospital

Exhibitors at the 1996 Meeting

AMTI
Bertec Corporation
BTS
Elsevier Science, Inc.
Georgia Tech College of Sciences
Instron Corporation
Kistler Instrument Corporation
Konigsberg Instruments, Inc.
Motion Analysis Corporation
MTS Systems Corporation
Noraxon USA, Inc.
Northern Digital, Inc.
Novel Electronics
Peak Performance Technologies
Qualisys, Inc.
Skill Technologies, Inc.

Conference Schedule

Wednesday, October 16, 1996

6:00 p.m. - 9:00 p.m.	Pre-registration at the Renaissance Hotel

Thursday, October 17, 1996

9:00 a.m. - 6:00 p.m.	Registration, Paul Weber Lobby
9:00 a.m. - 12:00 p.m.	Laboratory Tours - Georgia Tech and Emory
12:00 p.m. - 1:00 p.m.	Lunch (on your own)
1:00 p.m. - 2:30 p.m.	Tutorial Lecture #1, Paul Weber Rms. #4 & 5
2:30 p.m. - 5:30 p.m.	Exhibitors Display, Paul Weber Rm. #3
3:00 p.m. - 4:30 p.m.	Tutorial Lecture #2, Paul Weber Rms. #4 & 5
6:00 p.m. - 9:00 p.m.	Reception - Poster Session A, Student Success Center
7:00 p.m. - 10:00 p.m.	ASB Executive Board Meeting, Student Success Center

Friday, October 18, 1996

7:00 a.m. - 12:00 p.m.	Registration, Paul Weber Lobby
7:45 a.m. - 8:45 a.m.	Keynote Lecture, Paul Weber Rms. #4 & 5
9:00 a.m. - 1:00 p.m.	Poster Display A, Student Success Center
9:00 a.m. - 5:00 p.m.	Exhibitors Display, Paul Weber Rm. #3
9:00 a.m. - 10:15 a.m.	Free Communication, Sessions 1 & 2, Paul Weber Rms. #4 & 5
10:15 a.m. - 10:30 a.m.	Coffee Break
10:30 a.m. - 11:45 a.m.	Free Communication, Sessions 3 & 4, Paul Weber Rms. #4 & 5
12:00 p.m. - 1:15 p.m.	Student Member Meeting & Luncheon, Festival Area (Member lunch on your own)
1:30 p.m. - 2:45 p.m.	Keynote Symposium, Paul Weber Rms. #4 & 5
2:45 p.m. - 3:00 p.m.	Coffee Break
2:00 p.m. - 5:30 p.m.	Poster Display B, Student Success Center
3:00 p.m. - 4:30 p.m.	Free Communication, Sessions 5 & 6, Paul Weber Rms. #4 & 5
6:30 p.m. - 11:00 p.m.	Banquet/Buffet, The Carter Center

Saturday, October 19, 1996

7:45 a.m. - 8:45 a.m.	Keynote Lecture, Paul Weber Rms. #4 & 5
8:00 a.m. - 1:00 p.m.	Exhibitors Display, Paul Weber Rm. #3 Poster Display B, Student Success Center
9:00 a.m. - 10:15 a.m.	Free Communication, Sessions 7 & 8, Paul Weber Rms. #4 & 5
10:15 a.m. - 10:30 a.m.	Coffee Break
10:30 a.m. - 11:45 a.m.	Free Communication, Sessions 9 & 10, Paul Weber Rms. #4 & 5
12:00 p.m. - 1:30 p.m.	Awards Luncheon, Student Center Ballroom (3rd Floor)
1:45 p.m. - 2:45 p.m.	Borelli Award Lecture, Paul Weber Rms. #4 & 5
2:45 p.m. - 3:30 p.m.	ASB Business Meeting, Paul Weber Rms. #4 & 5
3:30 p.m. - 3:45 p.m.	Coffee Break
3:45 p.m. - 5:30 p.m.	Free Communication, Sessions 11 & 12, Paul Weber Rms. #4 & 5
6:30 p.m. - 11:00 p.m.	ASB Executive Board Meeting, Renaissance Hotel (Vintage Rm.)

Sunday, October 20, 1996

9:00 a.m. - 3:00 p.m.	Satellite Symposium "Biarticular Muscles: Biomechanics and Neural Control" at Emory University

Session Schedule

Friday, 18 October 1996

SST Room #4:

SST Room #5:

Saturday, 19 October 1996

SST Room #4:

SST Room #5:

Invited Sessions

Tutorial Lecture #1

Thursday, 1:00 p.m. - 2:30 p.m., SST Room #4 - 5

Biology, Physiology and Morphology of Bone
Clint Rubin — *State University of New York Stony Brook*

Tutorial Lecture #2

Thursday, 3:00 p.m. - 4:30 p.m., SST Room #4 - 5

Filtering of Kinesiological Data: A Biomechanist's Perspective
Scott Tashman — *Bone and Joint Center Henry Ford Hospital*

Keynote Lecture #1

Friday, 7:45 a.m. - 8:45 a.m., SST Room #4 - 5

Biomechanical Behavior of the Knee Ligaments In Vivo
Bruce Beynnon — *University of Vermont*

Keynote Symposium

Friday, 1:30 p.m. - 2:45 p.m., SST Room #4 - 5

The Regulation of Cell Structure and Function by Physical Forces
Bob Nerem — *Georgia Institute of Technology*

Localized Gene Therapy for Bone Repair
Steve Goldstein — *University of Michigan*

Keynote Lecture #2

Saturday, 7:45 a.m. - 8:45 a.m., SST Room #4 - 5

Biomechanical Behavior of Cortical Bone In Vivo
Dave Burr — *University of Indiana*

Satellite Symposium

Sunday, 9:00 a.m. - 3:00 a.m., Woodruff Health Sciences Center Administration Building, Emory University

Defining Muscular Function by Analyzing 3-D Musculoskeletal Mechanics
John Lawrence — *University of Kentucky*

Beyond Biarticular Muscles: The Distribution of Forces Between Multi-DOF Muscles
Arthur Kuo — *University of Michigan*

Functional Subdivision of Hindlimb Muscles for Postural Equilibrium: Evidence for Two Decoupled Controllers
Jane MacPhearson — *Dow-Neurological Institute*

Co-ordination of Two and One Joint Muscles in Static and Dynamic Tasks: Functional Consequences
Boris Prilutsky — *Georgia Institute of Technology*

Award Presentations

Borelli Award:

Post-Doctoral Young Scientist Award:

Pre-Doctoral Young Scientist Award:

Nominees for the Clinical Biomechanics Award:

ASB Travel Award:

Friday, October 18, TRACK 1
SESSION I - TISSUE AND CELL MECHANICS, Moderator: Don Anderson

Friday, October 18, TRACK 1
SESSION III - SPINE, Moderator: Vasanti M Gharpuray

Friday, October 18, TRACK 1
SESSION V - BONE, Moderator: Karl Jepsen

Friday, October 18, TRACK 2
SESSION II - HUMAN GAIT, Moderator: Scott Tashman

Friday, October 18, TRACK 2
SESSION IV - SPORT, Moderator: Rick Hinrichs

Friday, October 18, TRACK 2
SESSION VI - MOTOR CONTROL, Moderator: Art Kuo

Saturday, October 19, TRACK 1
SESSION VII - JOINT BIOMECHANICS I, Moderator: JJ (Trey) Crisco III

Saturday, October 19, TRACK 1
SESSION IX - JOINT BIOMECHANICS 2, Moderator: Michelle Grimm

Saturday, October 19, TRACK 1
SESSION XI - ORTHOPAEDICS, Moderator: Chris Jacobs

Saturday, October 19, TRACK 2
SESSION VIII - HUMAN MOVEMENT AND POSTURE I, Moderator: Eileen Fowler

Saturday, October 19, TRACK 2
SESSION X - MUSCLE, Moderator: Richard Nichols

Saturday, October 19, TRACK 2
SESSION XII - HUMAN MOVEMENT AND POSTURE 2/AGING, Steven Wolf

Thursday, October 17, 7:00pm-8:00pm
POSTER SESSION - A

NEUROMUSCULAR

SPORT

HAND

HARD AND SOFT TISSUE

Friday, October 18 4:30pm-5:30pm
POSTER SESSION - B

ORTHOPAEDICS

Invited Abstracts

BIOMECHANICAL BEHAVIOR OF THE ANTERIOR CRUCIATE LIGAMENT IN-VIVO

B. D. Beynnon

Dept. Orthopaedics and Rehabilitation
McClure Musculoskeletal Research Center, Stafford Hall
University of Vermont, Burlington, Vt. USA

Many factors have been associated with destruction of articular cartilage about the knee joint; however, only trauma such as that associated with disruption of the anterior cruciate ligament (ACL) is known to cause osteoarthritis. Another important concern associated with ACL disruption is that it is functionally disabling to an active individual and may lead to repetitive joint trauma. This is a concern because injuries to the ACL are occurring at epidemic proportions, especially those resulting from athletics. However, much diagnosis, treatment, and rehabilitation remain an enigma because of controversy regarding ACL function. The following is a summary of our recent work regarding the measurement of ACL strain in human subjects.

Participants were patient volunteers with normal ACLs undergoing diagnostic arthroscopic surgery performed under a local anesthesia. The subjects had normal knees, with no history of ligament trauma. After the surgical procedure was complete, the Hall Effect Strain Transducer (HEST), and in our more recent studies, the Differential Variable Reluctance Transducer (DVRT) was implanted in the ACL to measure its displacement pattern and calculate its strain behavior.

Recently, one of the primary efforts of our research has been to measure the strain behavior of the ACL during rehabilitation activities in-vivo (Beynnon 1996a, 1996c, and 1995). The rational for this research is founded on the fact that prior to studying the biomechanical effects of rehabilitation exercises on a knee with an ACL replacement, it is important to understand their effects on the normal ACL. We have determined that exercises which produce low or unstrained ACL values, and would not endanger a properly implanted ACL graft, are either dominated by the hamstrings muscles (isometric hamstring contraction), involve quadriceps muscle activity with the knee flexed at 60° or greater (isometric quadriceps, simultaneous quadriceps and hamstrings contraction), or involved active knee motion between 35° and 90° of flexion (Beynnon 1995). More recently, we determined the effect of weight-bearing exercises such as squatting (a closed-kinetic-chain exercise), and non-weight-bearing activities such as active flexion-extension of the leg in a open-kinetic-chain fashion on ACL strain (Beynnon 1996c). We revealed that the maximum ACL strain values obtained in the squatting condition did not differ from those obtained during active flexion-extension. Also, ACL strain values obtained during squatting were unaffected by the application of elastic resistance intended to increase muscle activity. These findings indicate that squatting (an activity that involves the compressive joint load produced by body weight and co-contraction of the hamstrings and quadriceps muscles groups) does not necessarily protect the ACL in comparison to active flexion-extension of the leg, which is characterized primarily by contraction of the dominant quadriceps muscles and which does not involve the compressive joint load produced by body weight. These

findings also demonstrate that increasing resistance with the Sport Cord during the squat exercise does not produce a significant increase in ACL strain values. This is in contrast to our earlier studies that demonstrated adding weight to increase resistance during open-kinetic-chain active flexion-extension of the leg produces a significant increase in ACL strain values. The similarity of ACL strain values obtained during these two common types of exercises leads us to question the practice of designating closed- and open-kinetic-chain exercise as safe and unsafe, respectively, during rehabilitation of an injured ACL or a healing ACL graft.

Functional knee braces have been used a means to treat instability of the knee due to injury of the ACL or to protect an ACL graft during healing. We have studied the effect of functional knee braces on ACL strain while "injury mechanism" loads were applied to the weight-bearing and non-weight-bearing knee for both braced and unbraced conditions (Beynnon 1996b and 1992). We determined that bracing can produce a protective effect on the ACL by significantly reducing ACL strain values for anterior-directed loadings of the tibia up to 140 N with the knee in both weight-bearing and non-weight-bearing conditions. Likewise, bracing produced a protective effect on the ACL by significantly reducing strain values in response to internal-external torque applied to the tibia up to 6 Nm with the knee non-weight-bearing. The protective strain shielding effect of the functional brace on the ACL was dependent on the magnitude of applied anterior load and internal torque: The protective effect of the brace on the ACL decreased as the magnitude of applied anterior load and internal-external torque increased.

Future studies are planned to expand these measurements to ACL grafts during healing, and further the development of analytic knee models to help interpret these data.

References:

1) Beynnon BD and Johnson RJ: Anterior Cruciate Ligament Injury Rehabilitation in Athlete. Sports Medicine 22(1):54-64, 1996a.

2) Beynnon BD et al: The effect of functional knee bracing on the anterior cruciate ligament in the weight-bearing and non-weight bearing knee. Accepted for publicaiton Amer J Sports Med 1996b.

3) Beynnon BD et al: The strain behavior of the anterior cruciate ligament during squatting and active flexion-extension : a comparison of an open and closed kineteic chain exercises. In review at the Amer J Sports Med 1996c.

4) Beynnon BD et al: Anterior Cruciate Ligament strain behavior during rehabilitation exercises In-vivo. Amer J Sports Med, 23(1):24-34, 1995.

5) Beynnon BD et al: The effect of functional knee braces on anterior cruciate ligament strain in-vivo. J Bone Joint Surg 74A:1298-1312, 1992

Acknowledgements:

Support for these studies was received from the National Institutes of Health grant RO1 AR39213

Regulation of Cell Structure and Function by Physical Forces

R.M. Nerem
Institute for Bioengineering and Bioscience
Georgia Institute of Technology
Atlanta, GA 30332-0363

Over the past decade much has been learned about the influence of physical forces on cell structure and function. Much of this knowledge has come from the study of vascular cells, with the endothelial cell being of particular interest.

As the interface between flowing blood and the underlying blood vessel wall, the endothelium resides in a very complex physical or mechanical environment. Not only is the endothelium exposed to flowing blood and the associated wall shear stress, but it also "sees" pressure and "rides" on a basement membrane which is being cyclically stretched. This complex physical environment alters many of the characteristics of endothelial cells, including cell morphology, cytoskeletal structure, the composition and organization of the extracellular matrix, cell proliferation, and the synthesis and secretion of various proteins. Furthermore, the effect of this physical environment extends to the gene expression level.

Studies on the influence of physical forces also have been conducted *in vitro* for the vascular smooth muscle cell (SMC) which *in vivo* resides in a cyclic stretch environment within the vessel wall. Again, results indicate profound effects on the structure and function of vascular SMC. Other cell types in addition have been studied. These include fibroblasts, cardiac myocytes, chondrocytes, osteoblasts, and neural-type cells. From such experiments, it is clear that virtually all cells are responsive to alterations in their physical environment.

Although much of biomechanics historically has focused at the tissue and organ level, studies of the type described above represent the emerging area of cellular biomechanics. From such studies much has been learned and much more will be learned. Particularly intriguing questions are "how does a cell recognize the physical environment in which it resides?" and having done so, "how does it transduce this recognition into the alterations in structure and function which have been observed?"

Beyond such basic questions, however, there will be a need to integrate the knowledge of cellular biomechanics into our understanding of biomechanics at the tissue and organ level. Only when we can do this, will we have achieved the integrated knowledge necessary to understand both normal biology and the pathology of injury and disease.

Localized Gene Therapy for Bone Repair

Steven A. Goldstein
University of Michigan, Ann Arbor, MI

Recent studies have documented the enormous potential benefit of stimulating fracture healing with the use of cytokines, growth factors or other biomolecules. Traditionally, these approaches have utilized implants containing recombinant proteins incorporated in carrier matrices. During the past three years, we have demonstrated novel, direct in vivo gene transfer into would repair fibroblasts. As a result, we have shown the potential of using DNA as a pharmaceutical to affect the process of would repair or tissue regeneration.

The verification of this concept was made using an animal model which involved the creation of a mid-diaphyseal critical size defect (5 mm) in the normal adult rat femur. Gene transfer was achieved by placing a biodegradable implant material impregnated with plasmid DNA at the osteotomy site. Fracture repair cells naturally migrated to the defect, transiently incorporated DNA and expressed it as functional protein.

Gene transfer was confirmed using three different marker genes as well as genes which encoded a functional bone stimulating protein. New bone formation in the osteotomy gap was seen in animals that received the functional genes as early as three weeks postoperatively. New bone formation was not identified in the gap of control animals that received the biodegradable implant alone or the marker genes. These studies have now been extended to large animals (dogs), and have been shown to be effective with a variety of carrier matrices. We have also shown that the process can be replicated in other tissues, including tendons, ligaments, and blood vessels.

The present studies demonstrate that (*i*) controlled release biomaterials can effectively deliver gene constructs to bone fracture repair cells in vivo; (*ii*) delivery of osteotropic transgenes can stimulate new bone formation *in vivo* and (*iii*) the gene transfer technology can be applied to wounds in many tissue types. It therefore appears wound healing cells can be genetically manipulated via gene transfer technology to act as bioreactors capable of producing a pharmaceutical at sites of tissue injury and repair.

BIOMECHANICAL BEHAVIOR OF CORTICAL BONE *IN VIVO*

David B. Burr
Depts. of Anatomy and Orthopedic Surgery, Biomechanics and Biomaterials Research Center, Indiana University School of Medicine, Indianapolis, IN 46202

Mechanical testing of devitalized bone shows that bone fails within 10^3 to 10^5 loading cycles at strain ranges of 5,000-10,000 microstrain (Carter et al., 1981a,b). Maximum principal and shear strains in the human tibia *in vivo* at a site known to be at risk for stress fracture never exceed 2,000 microstrain (Fig. 1) even for strenuous physical activities (Burr et al., 1996). Linearly extrapolating to the strain magnitudes found in the human tibia, fractures should not occur for at least 10^6 loading cycles (1,000 miles of running) if failure is caused solely by the repetitive application of load. However, the relationship between the number of loading cycles and failure in a bone at a given strain is not linear. Tensile fatigue tests of primary and Haversian bone at 1500 microstrain, more similar to the magnitude of strain measured in the human tibia, and strains rates similar to those developed during running (.03 strain/sec) show that healthy bone does not fail in tension by fatigue even after 37 million loading cycles (Schaffler et al., 1990). Factors besides repetitive loading alone must contribute to nontraumatic fractures in humans. Additional biomechanical factors may include locally high shear stresses caused by the geometry of bone and the inhomogeneity of bone tissue; muscular fatigue and loss of coordination; and high impact loads.

Stress fractures occur in regions where high bending loads are found. Large bending stresses can create high shear stresses, suggesting the possibility that shear leads to bone failure. Measurements of shear strain in the human tibia *in vivo* show that shear strains and strain rates can triple during vigorous activity, compared to walking (Fig. 1), implying an association between the elevation of strain magnitude/rate and fracture. Still, absolute magnitudes are too low to account for the occurrence of fracture with few loading cycles. However, bone is weak in shear; its transverse breaking strength in shear is similar to that in tension (ca. 69 MPa), about half of its compressive strength. But cortical bone shear strength in the longitudinal direction (17 MPa) is only 25% of its strength in tension or in transverse shear. Even small shear stresses may place some bone cortices dangerously close to failure.

Muscles can theoretically control bending strain that may elevate stresses. Muscles dissipate forces by eccentric contraction, and reduce strain rate by absorbing impact energy. Altered neuromuscular function associated with fatigue may prevent normal damping mechanisms and reduce the transfer of mechanical energy between the eccentric and concentric phases of muscle contraction. Muscular fatigue leads to a 50% increase in tibial acceleration (Verbitsky et al., submitted) and increases peak vertical ground reaction forces by about 25% (Nyland et al., 1994), probably due to an inability of the fatigued muscles to control knee extension and flexion. Muscular fatigue also increases bone strain by about 30% and changes the distribution of strain (Yoshikawa et al., 1994).

In vivo strain measurements of the human tibia of seven males between the ages of 23 and 50 indicate that tibial strain rates increase in younger subjects but decrease in older subjects, while strain

magnitude is unchanged in younger subjects, but increased in older subjects. Most stress fractures occur in younger people, and the age-dependence may result from the age-dependence of changes in strain and strain rate after fatiguing exercise. In particular, strain rate is implicated in the etiology of fractures caused by repetitive loading in subjects younger than 35 years.

Muscle fatigue can lead to a failure to control high strain rate loading and to absorb impact energy. High impact activities are associated with stress fractures (James et al., 1978). Higher loading rates increase the elastic modulus and material stress of bone, decreasing its fatigue resistance (Keller et al., 1985; Schaffler et al., 1989). Strain rates triple in the human tibia during strenuous physical activity, reaching 50,000 microstrain/sec.

Loading bone at magnitudes and rates consistent with normal human activity is insufficient alone to cause fracture within a reasonable physiologic period of time. It seems logical that fractures preferentially may occur in regions of high local stress concentration created by repetitive high impact loads uncontrolled by synergistic muscle action. Any change in training routine, which results in the loss of muscle coordination or prevents the normal attenuation of impact loads, can increase the risk for fracture.

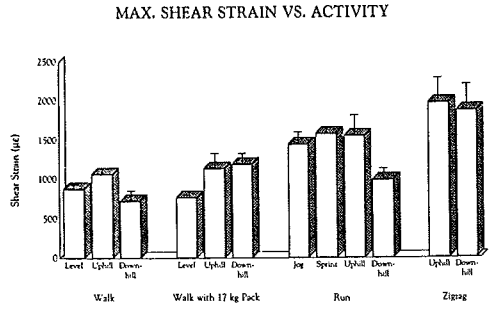

Fig. 1. Peak engineering shear strains on the human tibial midshaft. Mean ± SD.

REFERENCES

Burr, D.B. et al. Bone 18, 405-410, 1996.

Carter, D.R. et al. Acta Orthop. Scand. 52, 481-490, 1981a.

Carter, D.R. et al. J. Biomech. 14, 461-470, 1981b.

James, S.L. et al. Am. J. Sports Med. 6, 40-50, 1978.

Keller, T.S. et al. J. Biomech. 18, 297-304, 1985.

Schaffler, M.B. et al. Bone 10, 207-214, 1989.

Schaffler, M.B. et al. Bone 11, 321-326, 1990.

Verbitsky, O. et al. J. Biomech. (submitted).

Yoshikawa, T. et al. J. Exp. Biol. 188, 217-233, 1994.

ACKNOWLEDGEMENTS

Supported by NIH grants R01 AR39708 and R01 40655, and by the US-Israel Binational Science Foundation grant 93-00190. The author also acknowledges his collaborators: C. Milgrom, D. Fyhrie, M. Forwood (an NH and MRC NH Fairley Fellow), S. Hoshaw, M. Nyska, A. Finestone, A. Simkin, C. Turner, T. Yoshikawa and M. Schaffler.

Some Movements of Older Animals: What Leads to Age and Gender Differences in Balance Maintenance and Recovery?

Albert Schultz
University of Michigan

There will be two parts to this talk. The first will review some recent research about balance maintenance and recovery:

> Some old adults are unable to restore postural balance when it is disturbed, or to safely arrest falls that may occur when balance cannot be recovered. It is not clear to what extent these difficulties arise from declines in muscle function, and when they do, to what extent these declines are age or disease-related.
>
> The time available to recover balance or arrest a fall is often short. For example, only 200 to 300 ms are typically available for the initial responses needed to recover balance upon tripping. In contrast, the time required to develop maximum voluntary strengths may be 400 or more ms. Even old adults who are fit and healthy, compared to young adults, have diminished abilities to develop large torques rapidly. Recent findings suggest that the source of this decline at least sometimes lies in muscle physiology more than in central processing delays.
>
> Findings will be described regarding the biomechanics of age and gender differences found among healthy adults in stepping over suddenly-appearing, low-height obstacles; in suddenly turning away from or stopping in front of other obstacles while walking; and in regaining balance by stepping upon release from a forward lean. Analyses of whole-body, rapid response biomechanics through computer simulation that show the importance of strength development rates will also be described.

The second part of the talk will presents some highlights of the life of Giovanni Alfonso Borelli (1608-1679), and of his pioneering work, "On the Movement of Animals."

Abstracts

EFFECTS OF SKELETAL MATURITY AND STRAIN RATE ON THE MECHANICAL PROPERTIES OF PORCINE PATELLAR TENDON

G. W. Ringer, J. S. Wayne, W. A. Zuelzer
Orthopaedic Research Laboratory, Medical College of Virginia,
Virginia Commonwealth University, Richmond, VA 23298-0694

INTRODUCTION

Researchers have suggested the porcine knee is the animal model that best represents forces developed in the human anterior cruciate ligament (ACL) (Xerogeanes et al., 1995). Hence, the porcine model may be appropriate for in vivo studies of ACL reconstruction using a bone-patellar tendon (PT)-bone graft. To identify changes in the graft after implantation in this model, the mechanical properties of normal porcine PT must be known. Due to the characteristic nature of these tissues, the properties may be sensitive to certain variables in the experimental protocol, such as strain rate (Danto & Woo, 1993) and skeletal maturity of the donor (Woo et al., 1990). Therefore, the purpose of this study was to determine the mechanical properties of skeletally immature and mature porcine PT during uniaxial testing at two strain rates.

PROCEDURES

Twenty-five fresh porcine knees (17 immature & 8 mature, as verified by roentgenographic analysis) were isolated and dissected to leave only the patella-PT-tibia complex intact. The exposed tendon was kept moist throughout the testing procedure with a saline spray. The patella and tibia were clamped in a closed loop hydraulic testing machine (Instron, Model 1321) so that the PT was parallel to the direction of loading. The medial and lateral portions of the tendon were removed to isolate the central half. A preload of approximately 1 N was applied to the specimen. A rectangular cross section was assumed, and tissue dimensions were measured with digital calipers. A differential variable reluctance transducer (MicroStrain, Burlington, VT) with a gauge length of 10 mm was inserted to measure tissue strain. The specimen was conditioned for 20 cycles with a 1.5 mm amplitude triangular wave at an elongation rate of 20 mm/min. The 1 N preload was again applied to the specimen before loading to failure at either 20 (n=6 immature & 2 mature) or 200 mm/min (n = 11 immature & 6 mature). Tangent modulus, ultimate stress and strain, and failure mode were noted.

RESULTS

The cross-sectional areas determined for immature and mature specimens were 8.8 ± 0.4 and 10.8 ± 0.8 mm^2, respectively. Calculated strain rates corresponding to elongation rates of 20 and 200 mm/min were 0.23 ± 0.05%/s and 2.13 ± 0.65%/s, respectively. A representative stress versus time curve obtained during specimen conditioning is shown in Figure 1. This curve displays the typical relaxation behavior of a viscoelastic material when it is cycled over a fixed deformation. Representative stress-strain curves obtained during failure testing are shown in Figure 2. These curves display the nonlinear toe region, linear region, and nonlinear region prior to failure typically seen in the stress-strain relationship of these viscoelastic soft tissues. During avulsion, most deformation after the onset of failure occurred near the insertion site, which was outside of the region of strain determination. Hence, curves from specimens that failed in midsubstance exhibit an extended nonlinear region, while those from avulsed specimens end abruptly.

Both strain rate and skeletal maturity significantly affected failure mode of the tendons. At the slower rate, all immature specimens failed by avulsion from either the patella or tibia, while all mature specimens failed in midsubstance. At the faster rate, 7 of the 11 immature specimens failed in midsubstance, as did all mature specimens. The other immature specimens elongated at this rate failed by avulsion from the tibia. Ultimate properties can be reported only for specimens that failed in midsubstance. Therefore, ultimate properties were compared using two t-tests: one between immature and mature specimens elongated at the faster rate, and one between the different elongation rates for mature specimens (Table 1). Ultimate stress was significantly greater for mature specimens when compared with immature specimens ($p<.01$). Ultimate stress for mature specimens was also significantly greater at the faster elongation rate than at the slower rate ($p<.01$). Ultimate strain was not significantly affected by strain rate ($p=.17$) or maturity ($p=.29$). Because tangent modulus was determined for all specimens prior to failure, a two-way ANOVA was used to make statistical comparisons between all groups (Figure 3). Both strain rate and maturity significantly affected the tangent modulus ($p<.01$).

Table 1: Ultimate properties of porcine PT.

	Elongation Rate (mm/min)	
	20	200
Immature	failed by avulsion	$\sigma_U = 81.4 \pm 3.0$ $\varepsilon_U = 15.7 \pm 6.1$
Mature	$\sigma_U = 96.1 \pm 5.2$ $\varepsilon_U = 18.0 \pm 7.2$	$\sigma_U = 111.4 \pm 3.4$ $\varepsilon_U = 12.6 \pm 3.3$

Note: σ_U=ultimate stress, MPa; ε_U = ultimate strain, % (M ± se).

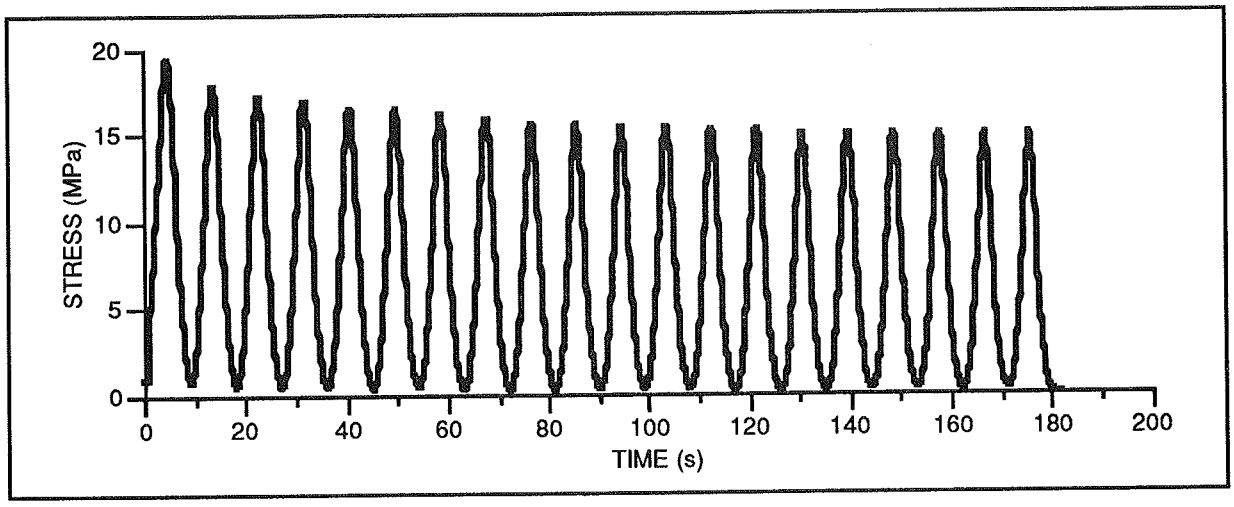

Figure 1: Stress relaxation of a mature specimen during conditioning.

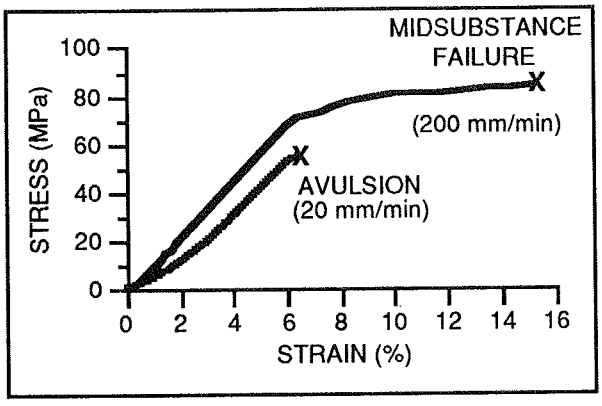

Figure 2: Stress-strain behavior for two immature specimens tested with different elongation rates.

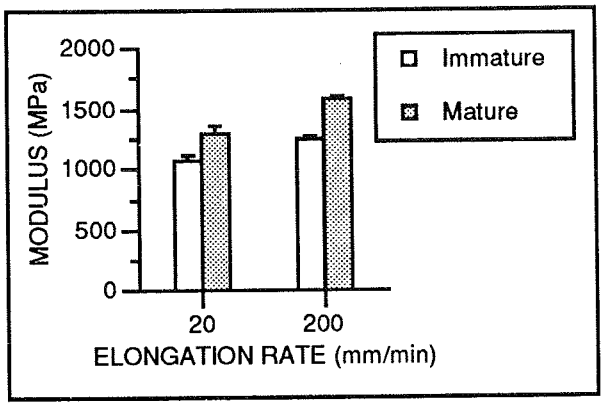

Figure 3: Modulus of specimens (M ± se).

DISCUSSION

Researchers have attributed an avulsion failure of a ligament during uniaxial testing either to a low strain rate or to skeletal immaturity (Woo et al., 1990). Skeletal maturity affected the failure mode of rabbit medial collateral ligament (MCL), but strain rate did not (Woo et al.). In the present study, however, both strain rate and skeletal maturity affected the failure mode of porcine PT. Increasing the strain rate increased the incidence of midsubstance failure in immature specimens. This finding suggests two possibilities. First, strain rate may be a more important factor in the failure mode of some soft tissues than in others due to structural differences in the insertion sites. Second, the effects of strain rate on the failure mode may be species-dependent. Anatomical differences near the insertion site, such as the pigs' greatly protruding tibial tubercle, may lead to a different fibrocartilage structure which is less apt to avulse.

A ten-fold increase in strain rate increased the tangent modulus of porcine PT by 15-20%. This finding is similar to those reported for rabbit PT (Danto & Woo, 1993) and MCL (Woo et al., 1990). However, the tangent modulus of human PT was not reported to be affected by strain rate (Blevins et al., 1994). Therefore, the issue of species-dependency is raised again. Because tangent modulus is characteristic of the tissue proper, differences in the insertion site cannot explain the varying reports.

REFERENCES

Blevins et al.: *Am J Sports Med*, 22: 328-333, 1994.
Danto & Woo: *J Orthop Res*, 11: 58-67, 1993.
Woo et al. in Daniel et al., eds. Knee ligaments: Structure, function, injury, and repair: Ch. 7: Fundamental studies in knee ligament mechanics: 115-134, 1990.
Xerogeanes et al.: *Trans ORS*, 20: 93, 1995.

STRESS WAVE VELOCITY IN LIGAMENTOUS TISSUE

J.J. Crisco[1,2], T.C. Dunn[2], R.D. McGovern[1]
[1]Department of Orthopaedics, Rhode Island Hospital, Providence, RI
[2]Division of Engineering, Brown University, Providence, RI

INTRODUCTION

Injuries to ligaments are common and vary from mild "sprains" to complete ruptures and bony avulsions. Although the specific etiologies associated with such ligament injuries are not fully understood, dynamic loading due to impact is typical. Dynamic loading, in contrast to quasi-static loading, implies that the effects of the impact are not transmitted instantaneously to all parts of the structure. Rather, these effects are transmitted through the structure as stress waves traveling at finite velocities. Stress wave propagation has been studied in a variety of biological tissues including lung, bone, and muscle, but has not been previously studied in ligamentous tissue.

REVIEW

Longitudinal stress waves propagate in elastic bodies at a velocity of

$$c = \sqrt{E/\rho}\,, \qquad [1]$$

where E is the elastic modulus and ρ is the density. The elastic modulus of ligaments increases with increasing strain and ligaments have been shown to be viscoelastic, as the elastic modulus increases at higher rates of loading. Stated more explicitly,

$$E = E(strain, strain\ rate).$$

Therefore, we would hypothesize that the velocity of the stress waves increases with increasing strain and that the velocity exceeds predictions based upon quasi-static loading.

The purpose of this study was to determine the velocity of stress waves in ligamentous tissue as a function of strain. These values were then compared to the velocities predicted using Eq. 1 and conventional load-deformation testing.

METHODS

Five bovine patella tendons were harvested and mounted in a low-melt alloy as bone-ligament-bone specimens.

Deformation tests were performed at a rate of 100 mm/s to a maximum of approximately 400 N. The load-deformation data was fit with a third order polynomial and then differentiated to obtain the stiffness (k) as a function of deformation. Ligament length (l) and cross-sectional area (A) were measured and the data were further reduced to estimates of the elastic modulus as a function of strain. Ligament mass (m) was measured after all testing had been completed.

Impact tests were performed by suspending various preloads from the ligament, impacting the lower end, and measuring the delay in force transmission. With piezoelectric load cells affixed to each end of the bone-ligament-bone specimen, preload masses of 0, 1, 5, 10, 15, and 17.5 kg were added to an impact apparatus (1.2 kg) suspended from the lower load cell. An impact was applied to the apparatus by dropping a 2 kg mass from a height of 5 cm. The delay in the propagation of the impulse was determined from the difference in the load cell signals, sampled at a rate of 500 kHz. This delay minus that attributed to the mechanical couplings and the bone segment was the delay due to the ligament (t).

The values for elastic modulus and wave velocity were derived and compared between the Deformation and Impact tests. The elastic modulus in the Deformation tests was given by $E_D = kl/A$. The elastic modulus in the Impact tests was defined as $E_I = ml/At^2$. The wave velocity in the Deformation tests was given by $c_D = l\sqrt{k/m}$. This equation is identical to Eq. 1, but is rewritten in terms of the specific variables measured. In the

Impact tests, the wave velocity was simply $c_I = l/t$.

The elastic modulus and wave velocity, first determined as functions of preload, were transformed using the load-deformation data to functions of strain for the purposes of a more general presentation of the results. Since the strains at a given preload varied between specimens, the elastic moduli and wave velocities were interpolated at strain values of 0.0075, 0.015, and 0.0225. Impact and Deformation tests were analyzed at each strain level using a paired, two-tailed, Student's t - test (n=5).

RESULTS

The elastic moduli predicted in the Impact tests were 160%, 120%, and 111% greater than the elastic moduli determined from the Deformation tests at the interpolated strain values of 0.0075, 0.015, and 0.0225, respectively. These increases were significant ($p \leq 0.02$) at each level of strain. Furthermore, the elastic modulus tended to increase with strain at a greater rate in the Impact tests than it did in the Deformation tests.

The wave velocities measured in the Impact tests were 260 ± 52 m/s, 360 ± 71 m/s, and 461 ± 94 m/s at strain values of 0.0075, 0.015, and 0.0225, respectively. These values were significantly faster ($p < 0.01$) by 52%, 46%, 41% than the values predicted from the Deformation tests.

DISCUSSION

In this study, the velocities of longitudinal stress waves in parallel fibered ligamentous tissue were determined and then demonstrated to increase with increasing preload and strain. This study was motivated in part by our interest in the mechanisms of musculoskeletal injuries, which typically occur in ligaments under impact loading. Whether or not stress wave propagation and reflection play a role in ligament injuries remains to be determined.

Excluding the possibility of measurement errors, the difference in stress wave velocity between the two tests was attributed to over a 110% increase in the effective elastic modulus with impact loading. This result suggests that impulsive loading may alter the mechanical properties of ligaments to a greater extent than previously documented with displacement controlled testing at varying rates.

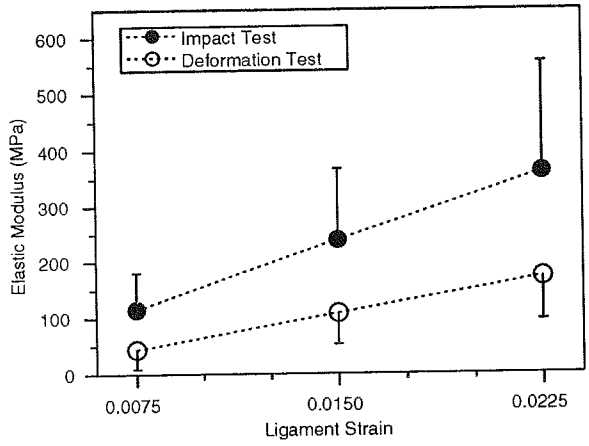

Figure 1. The elastic moduli calculated from the Impact tests were significantly greater then those determined from the Deformation tests.

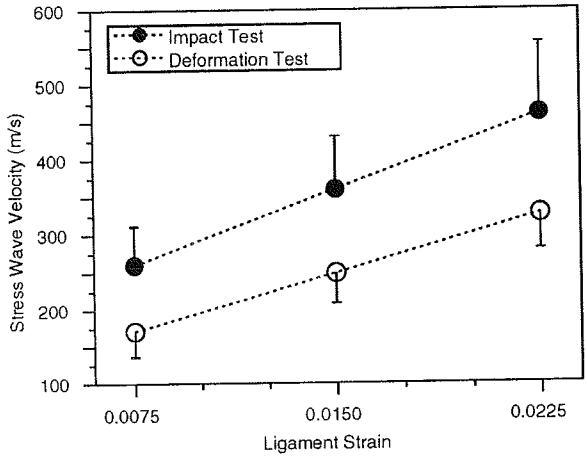

Figure 2. Stress wave velocity increased with increasing strain. The values measured in the Impact tests were significantly faster than those calculated from the Deformation tests.

AN APPLICATION OF POROELASTICITY TO THE MECHANICS OF TUMORS

M. Sarntinoranont[1,2], F. Rooney[2], & M. Ferrari[2]

[1]Department of Mechanical Engineering
University of California, Berkeley, CA 94720

[2]Biomedical Microdevices Center
Department of Materials Science and Mineral Engineering
Department of Civil and Environmental Engineering
University of California, Berkeley, CA 94720

INTRODUCTION

This study presents a simple spherically symmetric poroelastic model for a solid tumor. The model takes into account the stresses in the tumor and in the surrounding tissue as well as the interstitial pressures. Two different applications are elaborated for this poroelastic model. One application is the determination of the growth rate of the necrotic region in the core of the tumor. The second application is the determination of the distribution of therapeutic agents within a tumor as a function or time.

REVIEW AND THEORY

Poroelastic materials are assumed to consist of points of localized plastic flow and fluid injection in an otherwise elastic medium. Originally developed for applications in soil mechanics (Biot, 1955), poroelastic theory has been increasingly utilized to model the behavior of biological materials such as cartilage, heart muscle, and intervertebral discs (Armstrong et al., 1984, Yang et al., 1994, Simon et al., 1985). Recently, the application of poroelastic theory to neoplasms has been initiated by Jain and his coworkers (Netti et al., 1995) and our group (Rooney et al.) The structure of neoplasm is such that vessels and cancerous cells are supported in a collagen matrix, and, as such, this tissue lends itself towards poroelastic assumptions.

In recent years, there have been several attempts to mathematically model the growth and mechanical behavior of neoplasms. The emphasis has been on the matching of growth rates of mostly spherical models with the observed rates of growth of real tumors (Greenspan, 1972, Adam et al., 1990). However, there has not been significant work towards mathematically modeling the advancing front of the necrotic core of the tumor. This is defined as the region of the cancer where cells die because of lack of nutrients and the build up of metabolic wastes. In this context, most works assume a layer of constant thickness where viable cells exist only at the surface of the tumor. By using the interstitial pressure state given by the poroelastic model, regions of high pressure are determined. By postulating that nutrients are not transported to cells in regions of high pressure, the advancement of necrosis in the tumor core is modeled corresponding to an appropriate physiological basis.

Therapeutic agents entering into the tumor must overcome a number of obstacles in order to successfully reach the cancer cell. Jain and his coworkers have identified several such obstacles to delivery (Jain, 1994) among them being the high interstitial pressure (pore pressure) found within the tumor and non-uniform perfusion of blood to the tumor mass. These problems are mainly mechanical rather than biological in nature. Jain and Baxter have indeed modeled the spatial distribution of therapeutic agents within the tumor (Jain et al., 1988, Baxter et al., 1990). However, they solved for only the steady state case which is limited to large, mostly necrotic tumors. By utilizing the poroelastic pressure solution, a distribution model that is dependent on the age of the tumor is created in this paper. This new model is capable of modeling drug distribution in the tumor at all stages of tumor growth.

PROCEDURES

Solution of the spherically symmetric, poroelastic model for stress and interstitial pressure is determined in closed form (Fig. 1). A numerical method (method of lines) is used to find approximate solutions to the resulting one dimensional, parabolic partial differential equation that governs mass transport in the interstitial tissue. The resulting concentration profile for a therapeutic agent is illustrated in Fig. 2.

RESULTS AND DISCUSSION

The onset of the necrotic core and its subsequent growth is predicted by postulating that the onset of necrosis is caused by the inability of nutrients to reach cancer cells in regions of high pressure and stress. By analyzing the poroelastic interstitial pressure profile inside the tumor, nutrient deficient zones are identified at appropriately high pressure regions in the center of

the tumor. By incorporating an appropriate time lag, the outer radius of the necrotic region is defined at any given time. From this model, the growth rate of the necrotic core as a function of tumor size and age is determined.

Utilizing the poroelastic pressure solution in the equation governing mass transport, concentration profiles for the early stages of growth of the neoplasm are obtained. These concentration profiles first increase before decreasing with increasing age since the interstitial pressure is not yet high enough to act as a significant barrier to the delivery of the drug. Having the ability to model drug distribution at all stages of cancer growth, this model may eventually be used as a tool to the clinical oncologist. Given the age of the tumor, it could indicate when drugs can no longer penetrate the core of the tumor, and drug therapy will no longer be effective.

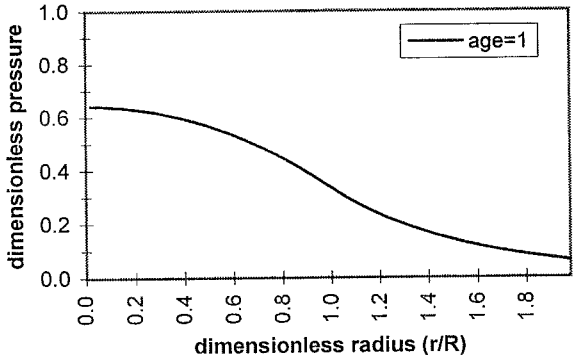

Figure 1: Solution of the spherically symmetric poroelastic model for dimensionless interstitial pore pressure ($p=2P\rho_o\kappa/qR^2$ where P=pressure, ρ_o=fluid density, κ=permeability, R=outer radius) for age=1(age=ct/R^2 where t=time, c=diffusivity). Homogeneous material properties inside and outside of the tumor were assumed.

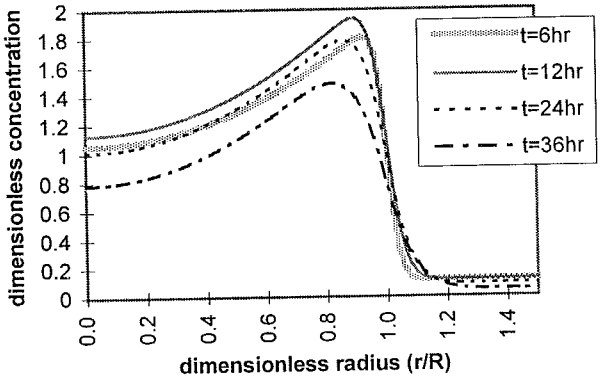

Figure 2: Dimensionless concentration (C_i/C_p) profile of a therapeutic agent (monoclonal antibody, Fab, Mr~50,000) in a spherical tumor of age = 1 for an exponentially decaying plasma concentration ($C_p=C_o\exp(-t/3hr)$, C_o is a constant). C_i is the concentration of agent in the interstitium, and C_p is the concentration in the plasma.

REFERENCE

Adam, J.A. et al. *Bull. of Math. Biol.* 52: 549-582, 1990.

Armstrong, C.G. et al. *Jo. of Biomech. Eng.* 106(2): 165-173, 1984.

Baxter, L.T. et al. *Microvasc. Res.* 40(2): 246-263, 1990.

Biot, M.A. *J. Appl. Phys.* 26: 182-185, 1955.

Greenspan, H.P. *Stud. Appl. Math.* 51: 317-340, 1972.

Jain, R.K. *Scientific American.* 271: 58-65, 1994.

Jain, R.K. et al. *Cancer Res.* 48: 7022-7032, 1988.

Netti, P.A. et al. *Biorheology.* 32(2-3):346, 1995.

Rooney, F. et al. *Math. Modelling and Sci. Comput.* (to appear).

Simon, B.R. et al. *Jo. of Biomech. Eng.* 107(4): 327-335, 1985.

Yang, M et al. *Jo. of Biomech. Eng.* 116(2): 213-223, 1994.

EFFECTS OF PRESSURE OVERLOAD VENTRICULAR HYPERTROPHY ON THE MECHANICAL PROPERTIES OF ISOLATED CARDIAC CELLS

M. R. Zile[1], J. M. Buckley[1], K. E. Richardson[1], G. Cooper IV[1], V. M. Gharpuray[2]
[1]Division of Cardiology, Department of Medicine, Medical University of South Carolina, Charleston, SC 29425
[2]Department of Bioengineering, Clemson University, Clemson, SC 29634

INTRODUCTION

Cardiac hypertrophy is a compensatory mechanism that develops in response to excessive hemodynamic loads. This hypertrophy results in the maintenance of systolic function, however it also causes abnormalities in ventricular diastolic function, which are in part responsible for the symptoms of congestive heart failure. Several investigators have shown that pressure overload hypertrophy results in an abnormal myocardium, and in increased passive myocardial stiffness (e.g., Tomita et al., 1990). Two possible mechanisms by which hypertrophy causes an increase in myocardial stiffness include a change in the cardiac muscle cells (cardiocytes) themselves or changes in the extracellular matrix surrounding the cardiocytes. In this study, the effect of hypertrophy on the mechanical properties of isolated cardiocytes was studied.

REVIEW AND THEORY

During diastole, the ventricle fills with blood, and expands. This causes the myocardium to lengthen passively, and cardiocytes within the tissue are also subjected to this passive elongation. Numerous innovative methods have been developed for measuring mechanical properties of cells - the micropipette technique, cell poking, cells in shear flow, magnetic beads, acoustic microscopy, etc. (Hochmuth, 1990). However, none of these techniques are able to accurately simulate the passive lengthening that cardiocytes are subjected to *in vivo*.

The passive lengthening properties of the myocardium and of isolated cardiocytes have been studied by many previous investigators (e.g., Granzier et al., 1995), using one of the above techniques. These previous studies have suggested that the lengthening properties of isolated cardiocytes may be expressed in terms of an exponential law given by $\sigma = C(e^{k\varepsilon} - 1)$, where σ=nominal stress, ε=natural strain, and C and k are constants that describe the mechanical behavior of the cardiocyte. To the best of our knowledge, however, the effect of hypertrophy on these constants has not yet been studied. We hypothesized that changes in mechanical properties of the cardiocyte itself play an important role in the increase in myocardial stiffness. Therefore, our primary objectives were (i) to develop a method to measure passive lengthening properties of isolated cardiocytes; and (ii) to determine whether hypertrophy causes changes in these properties.

PROCEDURES

Isolation of Cardiocytes

Ventricular hypertrophy (RVH) was created in the right ventricle of adult cats by banding the proximal pulmonary artery (see Tsutsui et al., 1993 for details). This method produced a doubling of the ventricular mass in 14 days. After 14 days, the heart muscle was excised, and cardiocytes from the right and left ventricular free walls were isolated using enzymatic techniques (Tsutsui et al., 1993).

Experimental Methods

To simulate cell elongation during diastole, the isolated cardiocytes were embedded in a 2% agarose gel (Seaprep agarose, FMC, ME). Mechanical testing determined that the gel is non-linear elastic and its constitutive relation is $\sigma = 51\varepsilon + 343\varepsilon^2$ kPa. The gel-cell mixture was molded into C-shaped specimens, and the specimens were placed in a custom designed stretch apparatus (Figure 1). A force transducer measured the force applied to the mandibles holding the specimen. During each loading cycle, only one cell within the gel aligned parallel to the long axis of the stretcher was examined using an inverted microscope (Zeiss Axiovert). Load was applied to the gel at a rate of 1gm/minute (up to a maximum load of 40 gm) and cell images were captured at 5 gm increments through a CCD camera (Hitachi Denshi). The gel was then unloaded at the same rate, and again cell images were captured at 5 gm increments. Cell adhesion to the gel was verified by ensuring that strains in the cell and the gel were of comparable magnitudes near the cell-gel interface. From these experiments, we could measure the stress in the gel, and the strain in the cardiocyte. However, we required a mechanical analysis to determine the properties of the cardiocyte, which we achieved using

the finite element method.

The Finite Element Model

Since cardiocytes are roughly rod-shaped, and the volume fraction of cells was very small (< 0.1%), an axisymmetric model that consisted of a single cell (12μm radius, 140μm length) within an infinite gel (150μm radius, 700μm length) was built using the commercial code ABAQUS (HKS, Inc.). Both the gel and the cell were modeled as incompressible hyperelastic materials, and an appropriate number of elements was determined from a convergence study. A uniaxial displacement in the longitudinal direction was applied in increments to the gel-cell model. An initial guess for the cell properties was made based on data available in the literature, and the model was executed. The cardiocyte strain predicted from the FE model was then compared to the experimentally observed values. Based on this comparison, cell properties were modified and these steps were repeated until a "good enough" estimate (determined from the t-test) for cell properties was obtained.

RESULTS

The experimental data indicated qualitatively that there were differences between normal and hypertrophied cells (Figure 2. Note that cell strain is plotted vs. gel stress). There were no differences between the loading curves of normal and RVH cells. However, the loading curve was significantly different from the unloading curve for both types of cells, and the normal cell unloading curve was significantly different from the RVH unloading curve. These curves show evidence of hysteresis, which suggests that the cardiocytes are viscoelastic. The curves also suggest that hypertrophy increases the energy absorbing capacity of the cardiocytes.

Table 1 shows the properties of the cells as predicted by the FE analysis. Granzier et al., reported a value of k=11.9 for murine cardiocytes; this compares well with our value of 15.39. However, their C (2.18) was much lower than ours (17.02). There are many reasons for this discrepancy, the most important of which is that C depends on the initial state of the cell and the loading rate. It is somewhat easier to compare the constants obtained for the different types of curves by noting that the slope of the stress-strain curve at $\sigma = 0$ is C*k. Thus the intial slope is approximately the same for both normal and RVH loading curves. However, the slope of the normal unloading curve at $\sigma=0$, is about twice that of the slope of the RVH unloading curve.

CONCLUSIONS

The results have shown that there are significant differences in the mechanical responses of normal and hypertrophied cardiocytes, especially during unloading. These results can now be used to define mechanisms by which ventricular hypertrophy alters ventricular passive stiffness, and further to develop mechanical and pharmacological techniques to treat these abnormalities.

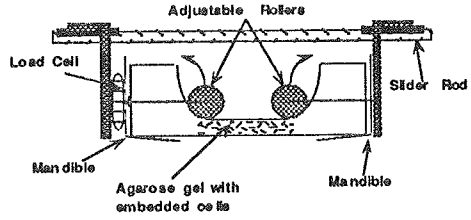

Figure 1. Gel Stretching Apparatus

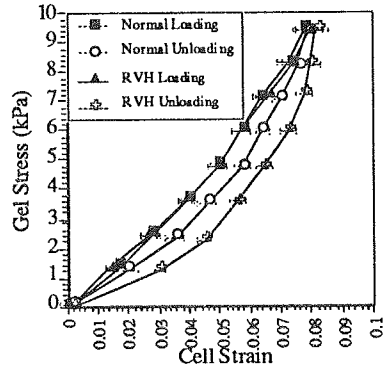

Figure 2. Gel stress vs. cell strain curves for normal and hypertrophied cardiocytes. Error bars show SE.

Table 1. FE predictions of cardiocyte properties described by $\sigma = C(e^{k\varepsilon} - 1)$

Cell Type	C (kPa)	k
Normal Loading	17.02	15.39
Normal Unloading	1.10	48.67
RVH Loading	28.34	10.29
RVH Unloading	0.56	45.19

REFERENCES

Granzier HL, et al., Biophy J, 68, 1027-1044, 1995

Hochmuth RM, J Biomech Eng, 112, 233-234, 1990.

Tsutsui H, et al., Science 260: 682-687, 1993.

Tomita M, et al., Circulation 83:635-644, 1991.

ACKNOWLEDGMENTS

Department of Veterans Affairs, Bioengineering Alliance of South Carolina, National Institutes of Health (P01-HL-48788) (financial support), M. Kelly Cowles (gel properties).

A FLUID-STRUCTURE-INTERACTION FORMULATION FOR COMPUTING NUTRIENT MEDIUM REACTIVE STRESSES IN MECHANICALLY STIMULATED CULTURES

T.D. Brown[1], D.R. Pedersen[1], M. Bottlang[1], and A.J. Banes[2]
[1]Department of Orthopaedic Surgery, University of Iowa, Iowa City IA 52242
[2]Department of Orthopaedic Surgery, University of North Carolina, Chapel Hill NC 27599

INTRODUCTION

Recent interest in the adaptive response of strain-sensitive musculoskeletal tissues has led to the development of various devices aimed at delivering well controlled mechanical stimuli to laboratory cell culture preparations (Brown, 1995). In several such devices, the targeted cells adhere to the surface of a compliant substrate membrane, which undergoes out-of-plane cyclic displacements induced by imposed pressure differentials. In these "cell stretching" systems, it is assumed that the induced substrate deformation is the dominant mechanical stimulus delivered to the target cells. Amost no attention has been directed to the potentially severe confounding effects of reactive shear and/or normal stress imparted to the adhered cells, by the coupled motion of the overlying fluid nutrient medium. These reactive stresses depend on the fluid motions relative to the moving culture substrate. However, the substrate motions are influenced by resistance of the overlying nutrient fluid, and the fluid motions in turn are influenced by the motion of the underlying substrate.

We report development of a new finite element computational formulation for addressing the full complexity of this fluid-structure interaction (FSI). Nonlinearities nested within the overall iterative treatment required by the transient FSI are: (1) a full Navier-Stokes treatment of inertial/viscous interactions in the nutrient fluid; (2) a time-dependent solution for the free surface interface between the nutrient medium and the incubator atmosphere, and (3) a finite-deformation (hyperelastic) continuum treatment of the substrate.

REVIEW AND THEORY

For the most widely used apparatus, the Flexercell® Strain Unit (Fig. 1), there have been several recent engineering studies of selected performance parameters, using both finite element models and direct experimental measurements. Gilbert et al. (1994) calculated axisymmetric static substrate strain distributions (in the absence of overlying nutrient) as a function of applied vacuum, demonstrating that the appreciable radial gradients of radial strain seen for plate-like 2.7-mm thick substrates largely disappear for membrane-like 0.5-mm thick substrates, but that appreciable radial gradients of circumferential strain persist. Using an experimentally validated dynamic nonlinear finite element formulation, Pedersen et al. (1992; 1995) demonstrated that substrate membrane strains were a function both of the vacuum duty cycle (frequency, waveform, peak amplitude) and of depth-dependent inertial restraint by overlying nutrient. Importantly, using a simplified constitutive characterization, they also showed that reactive inertial effects from the nutrient could be appreciable at instants of rapid substrate acceleration. Most recently, using a laser analog displacement sensor, Bottlang et al. (1996) documented the presence of previously unappreciated high-frequency oscillations of the culture substrate, a phenomenon dependent on both the vacuum pulse parameters and the nutrient depth. These studies demonstrate that the mechanical stimuli delivered to cells or tissues in the system are far more complex than what would be expected simply from static strains in the substrate. Since nearly two hundred of these systems are currently in operation around the world, with 600-1000 researchers actively using them, we have undertaken a rigorous mechanical characterization to address the interplay of normal stresses and shear stresses occurring atop the substrate.

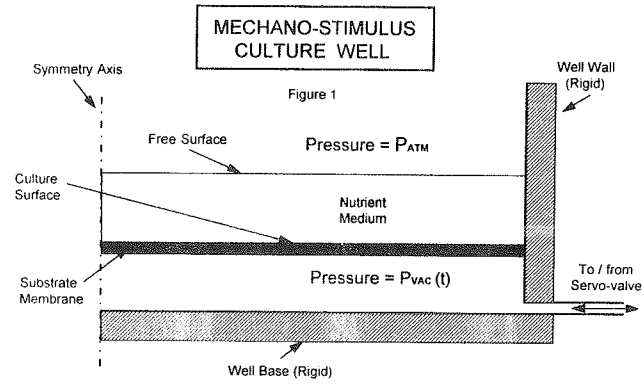

Figure 1

PROCEDURES

The finite element formulation involves two distinct axisymmetric problems, one for the nutrient medium and one for the culture substrate (Figure 2). These two problems are iteratively coupled so as to have mutually consistent solutions for displacement, velocity, pressure, and shear stress at their common interface, the substrate's growth surface.

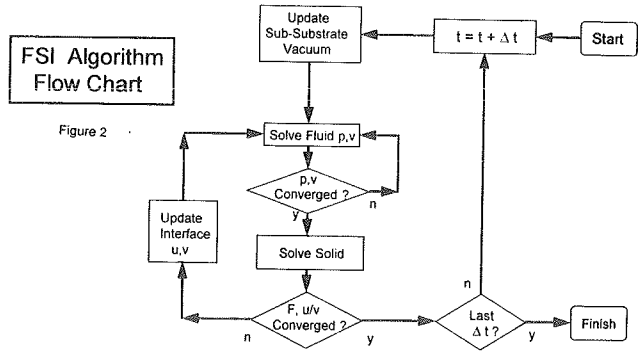

Figure 2

The nutrient medium is treated as a Newtonian fluid (kinematic viscosity = 1.0×10^{-3} kg/m-sec, density = 1.0×10^{3} kg/m^3), subjected to impenetrability boundary conditions at the symmetry axis and at the culture well wall. The fluid continuum is horizontally subdivided into two sub-regions, each having a different type of moving boundary: an upper free surface (atmospheric pressure) for the upper sub-region, and a lower moving substrate boundary for the lower sub-region. The fluid element nodes across the (initially horizontal) common boundary between sub-regions are constrained to move in proportion to the instantaneous local height differential between the free surface and the substrate. The substrate is treated as a hyperelastic continuum (density = 1.03 kg/m^3, Poisson's ratio = 0.5), using a five-term Mooney-Rivlin characterization whose material coefficients we measured experimentally using a standard biaxial inflation test: C_{10}, C_{01}, C_{20}, C_{11}, and C_{02} = 3.84×10^{7}, -3.64×10^{7}, 9.57×10^{8}, -1.47×10^{9}, and 5.79×10^{8}, respectively, all in units of kg/m-sec^2. Boundary conditions for the substrate were: rigid fixation at the culture well wall, zero radial displacement at the symmetry axis, normal and shear stress on the upper surface as computed from the nutrient finite element solution, and a time-variant vacuum on the lower surface (applied by Flexercell-controlled servovalve modulation of a reservoir vacuum.)

Finite element solutions were obtained using the ADINA (substrate) and ADINA-F (nutrient) programs, operating in concert using a fluid-structure interaction command procedure. At each time increment, the fluid pressure and velocity distributions were computed using the direct solution method, with Euler backward time integration and Newtonian iteration, convergence being assumed when the largest relative change in any field variable (nodal velocities, pressures, or moving boundary displacements) was less than 0.001. For the substrate, we performed direct time integration using the Newmark method (δ= 0.5, α=0.25), with direct solution of the equilibrium equation system. At any given time increment, the fluid-structure interaction was deemed convergent when the largest relative change in the (culture surface) interface nodal variables (force, displacement, velocity) was less than 0.01.

RESULTS

The FSI computations returned membrane centerline displacement histories that were fully consistent with our previous laser experimental measurements. Flow field results from a typical simulation illustrate the complexity of temporal and spatial distributions of nutrient medium pressures (Fig 3) and velocities (Fig 4.) During membrane downstroke in the first few tens of milliseconds after vacuum pulse initiation, computed oscillatory phenomena included not only membrane vibrations (Order(50 Hz), as had been observed experimentally), but also large fluctuations (O(80%)) of the nutrient pressures, and in some cases net reversals of instantaneous fluid velocities. A free surface wave of O(0.5 mm) initially propagated inward from the well wall, at celerity of O(3 m/sec), and was reflected with high attenuation (O(70%)) radially outward from the symmetry axis. For some cases with relatively deep (e.g., 10 mm) nutrient layers, weak annular vortices (velocity radially inward sub-surface, radially outward deep) developed in the late phase of the return membrane upstroke following vacuum release. In all cases considered, however, reactive fluid shear stresses at the culture surface were 2 to 3 orders of magnitude lower than the reactive normal stresses.

DISCUSSION

In a mechanical system with this degree of complexity, obtaining the physically credible numerical simulations here reported is obviously just a prelude to systematic exploration of the full parameter space. Implicitly, we assume that the presence of a thin layer of cells growing atop the membrane does not perceptibly alter the mechanical interactions otherwise present in the substrate-nutrient system. One factor potentially limiting the range of applicability of the present FSI formulation is that conditional numerical instabilities arise when the membrane's structural compliance is high, relative to imposed inertial accelerations of the nutrient medium. Another limiting factor is that because of the nested iterations, the computational procedure is fairly burdensome logistically, typically requiring 15-20 CPU hours on a DEC VaxStation 4000 to simulate a one-second Flexercell duty cycle at the mesh resolution in Figure 4. Downstroke inertial effects and high-frequency oscillations were typically only about 2/3 as pronounced during the second duty cycle as during the first (which necessarily started from rest), although the solutions became nearly periodic by the end of the second duty cycle.

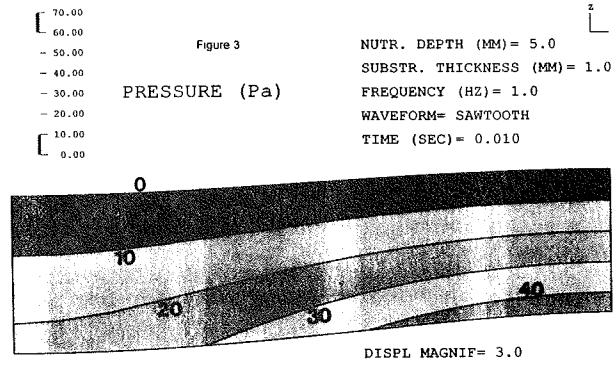

Figure 3

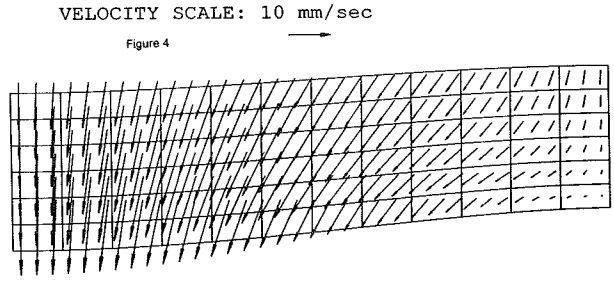

Figure 4

REFERENCES

Bottlang, M. et al. Trans. 42d ORS: 333, 1996.
Brown, T.D. Iowa Orthop. J. 15: 112-117, 1995.
Gilbert , J.A. et al. J. Biomech. 27: 1169-1177, 1994.
Pedersen, D.R. et al. Proc. NACOB II: 355-356, 1992.
Pedersen, D.R. et al. Trans. 41st ORS: 508, 1995.

ACKNOWLEDGEMENT

Financial support: NIH Grants AR/DE-42845 & AR-38121.

Biomechanics of Abdominal Belts

Effects of Abdominal Belts on Intra-abdominal Pressure and Intra-muscular Pressure in the Erector Spinae Muscles

Kei MIYAMOTO[1], Nobuki IINUMA[2], Masato MAEDA[1], Eiji WADA[3]

[1] Department of Orthopedic Surgery, Takayama Red Cross Hospital, Gifu, Japan

[2] Department of Orthopedic Surgery, Gifu Red Cross Hospital, Gifu, Japan

[3] Department of Orthopedic Surgery, Gifu University School of Medicine, Gifu, Japan

Introduction

Lifting task is one of the most common causes of low-back pain. Recently, abdominal belts are widely used by manual handling workers. The mechanism of the belts is commonly believed to be that, the belts raise the intra-abdominal pressure (IAP), which provides stability to the lumbar spine, and reduces pain or activities of trunk muscles. However, the effect of IAP is controversial (McGill et al, 1987). Many attempts had been made to evaluate the effectiveness of wearing belts, but some researchers concluded that justifying the effect of the belt in relieving load on the lumbar spine was difficult (McGill and Norman, 1990). We previously reported that the intra-muscular pressure of the erector spinae muscles (IMP) contributed to stabilization of the flexible spine against external forces (Iinuma et al, 1996). The purpose of this study was to evaluate the effect of abdominal belts on IAP, IMP and activity of trunk muscles during Valsalva maneuvers and maximum isometric lifting tasks.

Procedures

Seven healthy male volunteers (age:24-36) without low-back pain participated in this study. The study was done in 2 phases. Phase1: Performing Valsalva maneuvers on two conditions (Without-belt: WOB, With-belt: WB), Phase2: Performing maximum isometric lifting test for 7 seconds on two conditions (WOB, WB) in 2 lifting styles (leg and torso lift).
In both phases, IAP, IMP and myoelectric signals of trunk muscles were recorded simultaneously.
A weight-belt made of leather such as worn by weightlifters was used in this study. IAP was measured by a pressure sensitive transducer (Keller, Swiss) placed intra-rectally. IMP was measured using a saline filled catheter inserted sub-fascially 5 cm lateral to the L4 spinatous process and attached to the pressure transducer (Iinuma et al, 1996).

Myoelectric signals of trunk muscles (the erector spinae: ES, the external oblique: EO, the rectus abdominis: RA) were recorded using surface EMG electrodes. In phase 2, lifting force was measured using LIDO Lift System (Loredan Biomedical. Inc., California). All parameters were collected and interfaced to a computer via an A/D converter. Wilcoxon signed-ranks test was used for statistical analysis between two belt conditions.

Results and Discussion

Phase 1 : No statistical significant difference in IAP was recorded in Valsalva maneuvers, while IMP increased significantly by wearing the belt (Figure 1). Integrated EMG (IEMG) of RA increased significantly by wearing the belt ($p<0.01$). No significant change were observed in IEMG of ES and EO.
Phase 2 : Isometric lifting capacity (peak force), peak IAP and maximum increase in IAP were not significantly affected by wearing the belt in 2 types of lifting. IMP increased significantly by wearing the belt in all tasks (Table 1 and Figure 2). IEMG of RA increased significantly by wearing the belt ($p<0.05$).
When the belt is tightened around the abdomen and prevents the anterior protrusion of abdominal wall, increased activation of RA is hypothesized to pull the belt forward, thus, stiffen the trunk and raise the IMP of ES. To justify the effect of the belts, IAP had been measured by many researchers. However, some didn't find statistically significant increase in IAP by wearing the belts. One of the explanation for it may be that, abdominal cavity can extend to some extent. On the other hand, IMP of ES cannot leak because of firm fascia. Assuming that increased IMP stabilizes the lumbar spine, wearing weight-belts may contribute to the stabilization during Valsalva maneuvers and maximum lifting tasks.
The effectiveness can be objectively evaluated by measuring IMP of ES.

Conclusions

1) IMP (intra-muscular pressure) of the erector spinae muscles increased significantly by wearing the weight-belt in Valsalva maneuvers and maximum isometric lifting tasks, while maximum isometric lifting capacity and peak IAP were not affected by wearing the weight-belt.
2) IEMG of rectus abdominis increased significantly by wearing the weight-belt in Valsalva maneuvers and isometric leg lifting.
3) Wearing the weight-belts raised the IMP and were supposed to stiffen the trunk. Thus, the belts may contribute to the stabilization of the lumbar spine.

References

Iinuma, N., Miyamoto, K., Wada, E. et al. Acta Scholae Medicinalis Universitatis in Gifu 44: 70-79, 1996. (in Japanese)
McGill, SM., Norman, RW. Ergonomics 30: 1565-1588, 1987.
McGill, SM., Norman, RW., Sharratt, MT. Ergonomics 33: 147-160, 1990.

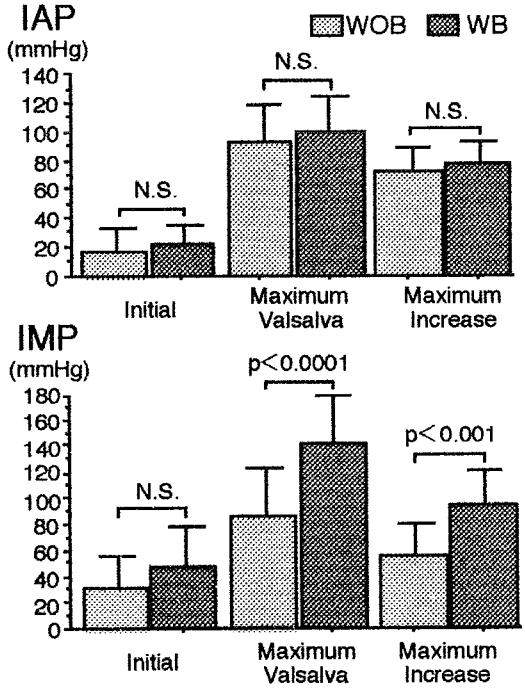

Figure 1. Means and S. D. of initial pressure, peak pressure and maximum increase in pressure (upper: IAP, lower: IMP) in Valsalva maneuvers. IMP increased significantly by wearing the belts. (Without-belt: WOB, With-belt: WB)

Table 1. Means and S. D. of peak force, maximum increase of IAP and maximum increase of IMP in 2 styles of maximum isometric lifting test.

	Without belt	With belt
Peak force (lbs)		
Leg lift	152.7 ± 44.7	143.5 ± 38.7
Torso lift	126.9 ± 26.8	120.5 ± 37.8
Maximum increase of IAP (mmHg)		
Leg lift	60.6 ± 18.4	59.8 ± 21.0
Torso lift	61.0 ± 24.8	56.2 ± 32.8
Maximum increase of IMP (mmHg)		
Leg lift	69.1 ± 61.4 *	109.1 ± 30.9 *
Torso lift	84.1 ± 67.3 **	180.2 ± 74.1 **
	*: $p < 0.05$	**: $p < 0.01$

No statistically significant difference was found in peak force and IAP. Maximum increase in IMP significantly increased by wearing the belts.

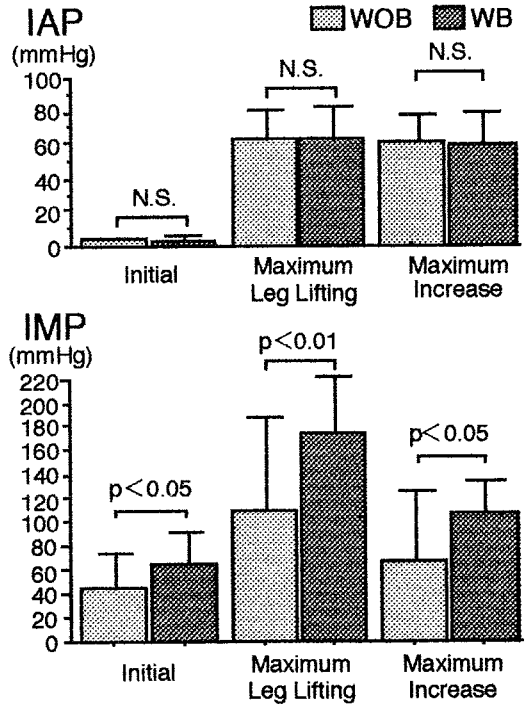

Figure 2. Means and S. D. of initial pressure, peak pressure and maximum increase in pressure (upper: IAP, lower: IMP) in isometric leg liftings. IMP increased significantly by wearing the belts. (Without-belt: WOB, With-belt: WB)

3D ANALYSIS OF SPINE LOADING DURING GAIT

J. P. Callaghan, , A.E. Patla, S. M. McGill
Department of Kinesiology, University of Waterloo, Waterloo, Ontario, Canada

INTRODUCTION

Thousands of low level loading cycles are endured by the spine every day. During normal gait the spinal musculature and accelerations of the trunk result in repeated spine loads. The magnitude of these loads in conjunction with spinal motion and muscular activity present a portrait of what is thought to be a non injurious activity. Clinically, walking has been found to help some individuals, yet hurt others. This motivated investigation into the loads during gait using an anatomically complex 3D model of the lumbar portion of the torso.

REVIEW AND THEORY

The literature to date consists of either 2D analyses or 3D analyses commencing at the cranial aspect of the body. The 2D studies have examined the low back moments from either a sagittal view[13] or from a frontal view[6] . Two dimensional planar analyses provide an excellent method of simplifying motion and facilitating calculations. However, rotations and translations from the plane of progression result in an inherent problem in interpretation of the moments and provide only one of three components acting at the joint examined. Cappozzo[1,2] calculated 3D moments at the low back from a top down model using inertial and kinematic variables as inputs. Calculating the low back moments from the top down does not incorporate any transient factors, such as the impact occurring at heel strike. In addition all these studies examined joint reaction loads, ignoring the muscular contribution to joint loads. A 3D analyses from the floor upwards was undertaken by Khoo et al.[5] , however, only the 2D (sagittal plane) forces and moments were analysed and joint loading was calculated with a single muscle equivalent model. Cappozzo[2] used a four muscle model, top down kinematic approach to determine compressive loads. In contrast, the data presented here used an anatomically complex, detailing 54 muscles, 3D EMG driven low back model[7,9] which incorporates normalized EMG and low back kinematics to calculate L4/L5 joint forces.

The overall goal of this portion of the study was to examine the 3D low back loads during gait. The specific purpose was to assess the effects of walking speed and arm placement on peak spinal loads, muscular activation, and lumbar spine motion.

PROCEDURES

Five male participants were recruited from a university student population (mean age 25 years, mass 78 kg, height 1.76 cm). The electromyogram (EMG) recording consisted of seven pairs of surface EMG electrodes applied to the right side of the body: rectus abdominis; external oblique; internal oblique; latissimus dorsi; thoracic erector spinae; lumbar erector spinae; and multifidus. Normalization was achieved by having the participants perform maximal isometric contractions for all monitored muscle groups[8]. The amplified signal was A/D converted at 1200 samples/s.

The segment kinematic profiles were determined through the collection of fifteen infrared emitting diodes (IREDS) in order to define a four segment rigid link model: right foot, right leg, right thigh, and pelvis. Three markers were attached to each segment and were used for segment tracking. An upright standing calibration posture and additional digitized points[4] provided the transformation matrix between the marker based axes and the segments principle axes. Segment lengths and perimeters were measured and moments of inertia were calculated based on regression equations[14]. Marker displacement data was recorded with a six camera optoelectronic system (OPTOTRAK) at a sample rate of 60 Hz. Lumbar spine kinematics were calculated using the six IREDS defining the pelvis and trunk. Rigid plates with three markers were attached to the posterior aspect of the sacrum and at the T12/L1 spine level. Lumbar curvature was normalized to normal upright standing (ie zero position). The rotational matrix (trunk with respect to pelvis) was decomposed (Euler XYZ) to yield three dimensional relative spine motion. The marker displacement data was digitally filtered with a 4th order zero lag butterworth low pass filter at 6 Hz[12].

Ground reaction forces were measured with a force plate and sampled at 1200 Hz. No filtering was performed on the forceplate data, however to synchronize the force data with the kinematic data (@ 60 Hz) every twentieth point was pulled to match the marker displacement data.

Collection protocol consisted of six different walking conditions (3 speeds: slow, normal, and fast; 2 arm postures: free swing, and arms crossed anterior to the trunk) with five repetitions of each . The point of initiation of gait was altered so that the right heel contact was recorded with a force plate following two complete strides. A calibration posture (trunk flexed to 60° from the vertical with a lordotic spine, holding a 10 kg mass in the hands) was recorded[11] to provide an EMG to moment relationship.

The left hip joint variables were generated based on an assumption of symmetric gait in the sagittal plane and corrected for anatomical sense (ie $-My_{Right\ Thigh}$ (external rotation) = $+My_{Left\ Thigh}$ (external rotation). The left hip joint forces and moments were shifted in time based on right foot event occurrence. The left side EMG was also generated with the same shifting method. This shifting of EMG patterns demonstrated good agreement with the bilateral patterns reported in the literature[2,3].

The resultant moments and forces, EMG activation, and spinal motion were three point ensemble averaged (one full stride from right heel contact) within condition and participants. The 3D low back joint loads and muscle forces were calculated using a 3D myoelectrically assisted model[7,9]. The reaction moment about the L4/L5 joint is partitioned into passive and active tissues based on spine curvature with forces allocated to musculature dependent on: activation; instantaneous length and velocity; and physiologic cross-sectional area. Forces in the restorative moment producing tissues are examined for their contribution to joint loading based on the EMG to moment relationship established in the calibration procedure. The dependent variables were compared using repeated measures ANOVA with a TUKEY post hoc analysis of significant findings.

RESULTS

The joint compressive loads peaked at weight acceptance with a magnitude of approximately 2.5 times body weight (figure 1,2). The two shear components (anterior-posterior and medial-lateral) were well below any in-vitro data used to estimate risk of injury (figure 3 and 4). There was no clear pattern to abdominal recruitment although it was consistently at a low level of activation (≈5 %MVC). The spinal musculature demonstrated a clear unimodal or bimodal activation pattern dependent on spinal level. The range of peak activation were 10 -15%MVC with clear rest periods between the peaks at toe off. The total lumbar spine range of motion with respect to the pelvis was: 6.2° flexion/extension, 6.6° lateral bend, and 7.2° in axial twist. These movements represent a small portion (≈10%) of the total range of

the lumbar spine[10]. The only two variables significantly affected by walking speed were the two shear force components. The arm swing versus no arm swing had no significant affect on any variable.

DISCUSSION

Tissue loading during walking appears to be below levels caused by many specific rehabilitation tasks, suggesting that walking is a wise choice for general back exercise and rehabilitation programs. Furthermore, the mild muscle activation levels combined with small spine motions reinforce this conclusion. Increasing walking speed and restricted arm movement increased the demands of the task, however not to statistically significant levels. The magnitudes of compressive joint loads are in agreement with previous studies[1,5] . No comparisons are available for the two joint shear components, however, joint reaction forces reported are within the same range[1]

REFERENCES

1. Cappozzo, A., J. Biomech. 16(4):265-277 1983.
2. Cappozzo, A., J. Orthop. Res. 1(3):292-301 1984.
3. Cromwell, R. et al. Ortop. Res. 7(3):371-377 1989.
4. Jian, Y. et al., Gait and Posture 1:9-22 1993.
5. Khoo, B.C.C. et al., Med. Eng. Phys. 17(1):27-35 1995.
6. MacKinnon, C.D., Winter, D.A., J. Biomech. 26(6):633-644 1993.
7. McGill S.M. et al., Spine 11:666-677 1986.
8. McGill SM., J. Orthop. Res. 9:91-103 1991.
9. McGill SM., J. Biomech. 25:395-414 1992.
10. McGregor, A.H. et al., Spine 20(22):2421-2428 1995.
11. Neumann, P. et al., 670-671, Xvth Congress of the International Society of Biomechanics, 670-671 1995.
12. Winter, D.A. Biomechanics and motor control of human movement 2nd ed., Wiley and Sons Inc. 1990.
13 .Winter, D.A. The biomechanics and motor control of human gait: Normal, elderly and pathological 2nd ed., University of Waterloo Press 1991.
14. Yeadon, M.R. et al., J. Biomech. 22:683-690 1989.

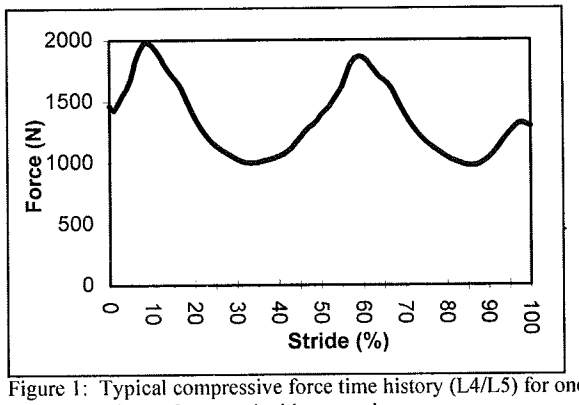

Figure 1: Typical compressive force time history (L4/L5) for one complete stride at fast speed with arm swing.

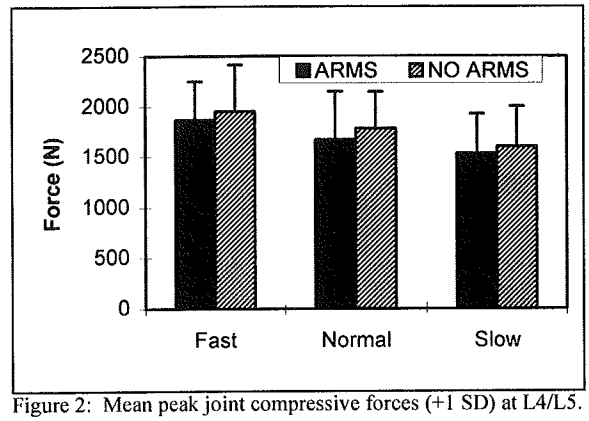

Figure 2: Mean peak joint compressive forces (+1 SD) at L4/L5.

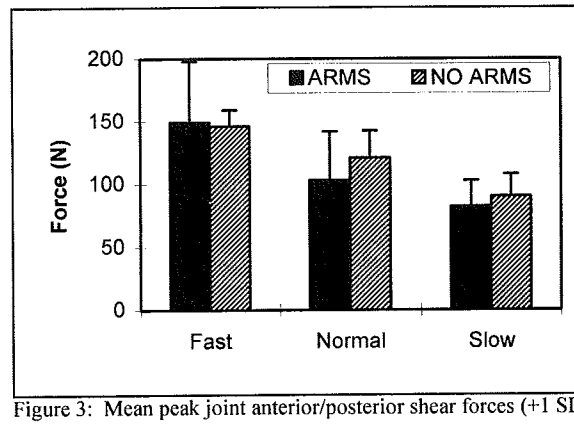

Figure 3: Mean peak joint anterior/posterior shear forces (+1 SD) at L4/L5.

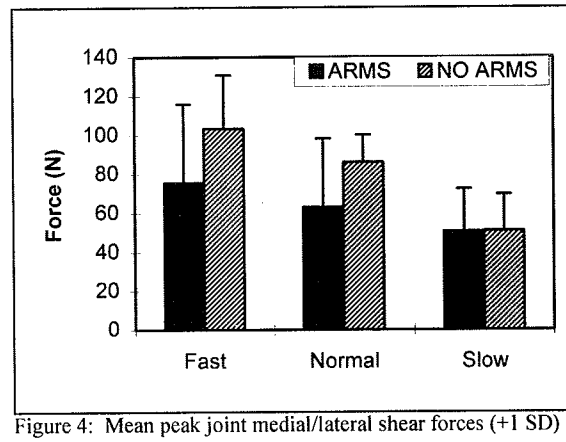

Figure 4: Mean peak joint medial/lateral shear forces (+1 SD) at L4/L5.

ACKNOWLEDGEMENTS

The authors would like to acknowledge the financial assistance of the Natural Science and Engineering Research Council, Canada (NSERC). The assistance and knowledge supplied by the following individuals were greatly appreciated: M. Ishac, C. Silcher, and S. Rietdyk.

INFLUENCE OF EXPERIENCE ON LIFTING KINEMATICS AND SPINAL LOADING

K.P. Granata, W.S. Marras and B. Kirking
Biodynamics Laboratory
The Ohio State University

INTRODUCTION

Low back disorders (LBD) are common in manual materials handling (MMH) occupations, yet some individuals survive many years of strenuous work without injury or complaint. Analyses of the lifting style and dynamic spinal loads were examined in experienced and inexperienced MMH employees. The objective of this effort was to identify some of the biomechanical parameters that help experienced employees survive without low-back injury. Experienced workers performed the prescribed lifting tasks smoother than their inexperienced counterparts. However, the spinal shear forces in the experienced group was greater than in the inexperienced group, contrary to our expectations.

REVIEW AND THEORY

Previous studies of lifting biomechanics have examined trunk motions, and modeled spinal load, however few have examined them in light of worker experience. It has been shown that lifting kinematics and dynamics are associated with LBD risk (Marras et al 1983). We hypothesize that experienced workers will demonstrate smoother motions. Spinal Loads have been correlated with low-back injury and is often used as a biomechanical measure of risk (Chaffin and Park, 1973; NIOSH 1981). We expected experienced workers to produce lower spinal compression and shear loads than inexperienced workers. This hypothesis was shown to be incorrect.

By virtue that the experienced workers have survived many years without injury may indicate their style of lifting is related to lower risk of LBD. Thus by comparing the motions and biomechanical loads of experienced versus inexperienced workers we may gain insight into the mechanisms of low-back injury.

PROCEDURES

Ten experienced warehouse order selectors (age 19 to 49 yr.; weight 80.1 ±8.4 kg.; height 180.3 ±7.1 cm.) were recruited from a local food distribution center. The subjects' experience as warehouse selectors ranged from 0.25 to 23 years. Five were categorized as experienced (greater than two years) and five as inexperienced (less than two years).

To simulate realistic warehouse working conditions, subjects were required to lift boxes ranging from 18.2 kg. to 27.3 kg. from one pallet to another until the entire pallet load, an average of 35 boxes, was transferred. Twelve pallets of boxes were moved at a frequency of 166 lifts per hour. Dynamic, three-dimensional trunk motion data were collected from the Lumbar Motion Monitor (LMM) (Marras et al 1993) and integrated myoelectric (EMG) activity of ten trunk muscles were collected from bi-polar surface electrodes (as per Mirka and Marras 1993) during the depalletizing tasks. Prior to beginning each pallet, a set of test exertions were performed on a force plate (Bertec 4060A) to supply calibration data for biomechanical analyses.

Each lifting task was assigned a probability of being at high risk for occupationally related LBD. The assessment was achieved from a multiple logistic regression risk model (Marras et al 1993). The epidemiologic risk model was developed from a database of trunk motion and workplace factors developed from on site measurements over 400 industrial workers, and incorporated factors including the lifting moment, lift rate, multi-dimensional trunk range of motion and velocities.

An EMG-assisted biomechanical model was employed to determine the dynamic spinal loads associated with the lifting exertions (Granata and Marras, 1995). The analysis incorporated normalized EMG data, muscle cross-sectional areas and vector directions as well as force-length and force-velocity relations to determine the force supplied by ten dynamically co-contracting muscles. Three-dimensional spinal loads were determined from the vector sum of the muscle forces, and trunk moments from the sum of vector products of muscle forces and moment arms. The model was calibrated by comparing the predicted trunk moments with values determined from the force plate data collected during the test exertions. Model output include peak spinal loads as well as the three-dimensional trunk range of motion (ROM), peak velocities and accelerations.

RESULTS AND DISCUSSION

Experienced selectors tended to perform the lifting tasks in a smoother, more fluid motion than their inexperienced counterparts. Although the range of

Table 1. Significance Summary of Kinematic, Kinetic an Spine Loading as a function of Experience.

	Sagtl	Latrl	Twist
ROM	p<.386	p<.001	p<.001
Vel	p<.005	p<.001	p<.001
Acc	p<.001	p<.001	p<.001
Moment		p<.05	
	Fx	**Fy**	**Fz**
Spinal Load	p<.030	p<.003	p<.407

Fx = Latrl Shear, Fy = AP Shear, Fz = Compression
Shaded regions indicates significance at p<.005

motion in the sagittal plane was not significantly different between the two groups, experienced subjects reduced lateral and twisting ROM. These results are important since epidemiological results indicate lateral and twisting motions increase the risk of LBD injury (Marras et al 1993, Punnet et al 1991).

Both groups were required to work at identical lift rates, but the experienced selectors were able to do so at lower peak trunk velocities (Figure 1). This indicates the motions were smoother for experienced workers. This is validated by significantly ($p<.001$) lower acceleration values for experienced workers relative to the less experienced selectors as measured in all three planes of motion.

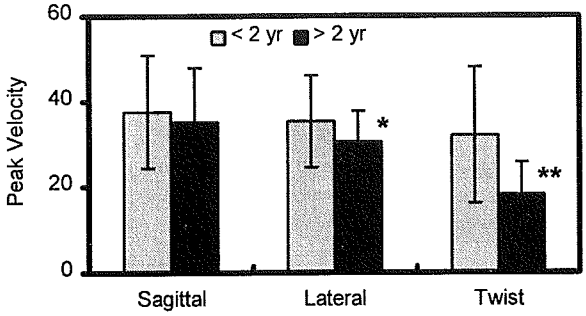

Figure 1. Experienced selectors performed the tasks using smoother motions than the inexperienced workers. * = $p<.05$, ** = $p<.005$

The probability of membership in the high risk category was significantly ($p<.01$) lower for experienced selectors (59%) than for less experienced workers (64%). The predicted LBD risk values were influenced primarily by the lateral and twisting velocity differences between the two groups. Thus, the smoother motions demonstrated by the experienced selectors may be related to reduced risk of low-back injury.

Compressive loads on the spine were not significantly different between the two levels of experience. Lateral and anterior-posterior shear loads were significantly greater in the experienced subjects, 3% and 7% respectively (Figure 2). However, the magnitude of these differences were physically small, 21 N in lateral shear and 45 N in AP shear.

The apparent paradox between reduced LBD risk and increased shear loading on the spine may be explained by several hypotheses. First, the sensitivity of the EMG-assisted model may be insufficient to identify the biomechanical parameters associated with the 5% difference in LBD risk between the two groups. Passive loads associated with increased range of motion demonstrated by the inexperienced workers may require more sophisticated biomechanical modeling. Second, the epidemiologic model may indicate a change in LBD

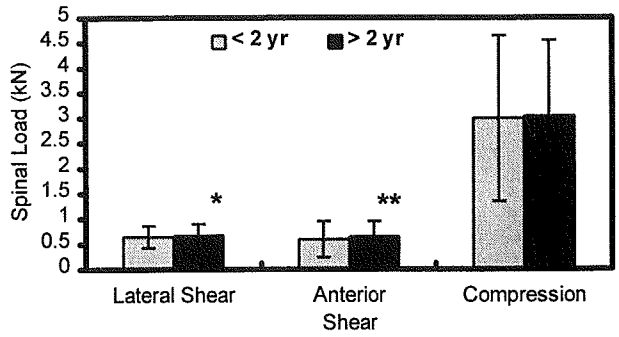

Figure 2. Biomechanical modeling indicates experienced selectors generate increased shear loads, possibly resulting from enhanced control and stability. * = $p<.05$, ** = $p<.005$

risk which is statistically significant but may not be interpretable given the current fidelity of the EMG-assisted model. However, by virtue that the experienced workers have survived many years without injury appears to indicate their style is related to lower risk of LBD. Finally, employing only maximum spinal loads (even those computed under dynamic conditions) to assess biomechanical risk may be insufficient to describe the mechanism of low-back injury.

Research has demonstrated that spinal compression alone is rarely sufficient to cause disk prolapse (Adams and Dolan 1985). During complex lifting tasks, the multi-dimensional loads on the spine increase the probability of disc injury (Shirazi-Adl et al. 1986). The results of this research indicate that reduced risk of LBD associated with experience and smoother motions does not necessarily correspond with reduced spinal loads. Hence, the injury mechanism may be related to the rate of spinal loading and the posture of the spine while being loaded. Musculoskeletal control issues may also influence the relation between spinal load and risk of LBD. Smoother motions may be related to muscle co-contraction patterns designed to increase the level of trunk stability, potentially at the expense of increased spinal load.

REFERENCES

Adams MA et al. *Spine* 10 (6), 524-531, 1985
Chaffin D.B. et al. *Am Ind Hyg Ass J* 34,: 513-525, 1973
Granata KP et al. *J. Biomechanics* 28 (11), 1309-1317, 1995
Marras WS et al. *Spine* 18 (5), 617-628, 1993
Mirka GA et al. *Spine* 18 (11), 1396-1409, 1993
NIOSH Report No.81-122, 1981
Punnet et al *Scand. J. Work Envir. Health.* 17 337-346, 1991
Shirazi-Adl et al. *Spine* 11 (9), 914-927, 1986

ACKNOWLEDGMENT

Funding was provided by the Food Marketing Institute. This work results from the efforts of Gary Allread.

PREDICTIONS OF MUSCLE AND L3-L4 AND L4-L5 DISC LOADS DURING FREESTYLE ASYMMETRIC LIFTING

D.M. Hooper, V.K. Goel, K.M. Bolte, M.H. Pope
Department of Biomedical Engineering
University of Iowa, Iowa City, IA 52242

INTRODUCTION

A three-dimensional optimization model of the muscles and discs of the L3-L5 levels was used to identify changes in loads resulting from increasing asymmetry during freestyle lifts. Loads in the discs were increased in all anatomic directions, particularly on the L4-L5 disc.

REVIEW AND THEORY

Epidemiological studies have long identified asymmetric lifting tasks as being more common and risky than symmetric tasks. However, investigations of freestyle asymmetric lifting are relatively few (Kromodihardjo 1987, Gagnon 1992, Hooper 1994). EMG based models have indicated increased amounts of antagonistic muscle contraction and predicted increased loads on the spine, Granata (1993). These models have typically been applied to constrained lifting and are not representative of true lifting techniques, but are improving (Granata 1995). Studies of external loads have shown that lateral bending and twisting moments are increased during asymmetric lifting (Hooper 1994).

PROCEDURES

Six subjects with no reported episodes of back pain were recruited for this study. Subjects were instrumented with infrared LEDs on the legs and lower back and asked to perform three types of lifts. While standing upon a force plate and keeping the feet stationary, the subjects lifted and 45 N load from knee level to chest level. The initial location of the load was in the midsagittal plane, followed by lifts from 45 and 90 degrees to the right of the sagittal plane. External loads on the L3-L4 and L4-L5 discs were determined from these experiments. The subjects completed the lifts again, but with a B-Tracker lumbar motion monitor (Isotechnologies) replacing the LEDs on the back. The B-Tracker measured the three-dimensional deformation in the spine between S1 and T12. These lifts were repeated three times so that the external load data could be best coupled with the spine motion measured by the B-Tracker. Matching of the data sets was done by comparing the times required to complete the task.

Muscle models of the trunk were constructed for each subject by scaling moment arms and area from archival data. The L3-L4 and L4-L5 levels were considered simultaneously using thirteen equivalent muscle groups; left and right multifidus, longissimus, iliocostalis, latissimus dorsi, psoas, quadratus lumborum, rectus abdominus, and anterior and medial sections of the external oblique, internal oblique and transverse abdominus. Forces in the iliocostalis, longissimus dorsi and rectus abdominus were equal at each level. Latissimus dorsi and quadratus lumborum were only present at L3-L4. Psoas and multifidus forces were independent at each level. Stresses in each of the oblique muscles were constant at each level. Muscle stresses were bounded by 125 N/cm^2. Passive loads borne by the L3-L4 and L4-L5 discs were included in the model by partitioning the spine deformation and considering the discs as elastic springs. The models were run at intervals of 0.10 seconds during each lift.

RESULTS

External lateral bending and twisting moments on each disc increased significantly with rotation, Figure 1. Lateral and A/P shear, and compression increased on both discs, most notably at L4-L5, Figure 2. Passive disc moments were predicted to reach about 22.0 Nm in flexion/extension and was similar in each

type of lift. Passive lateral bending moments reached 6.3 Nm during the 90° lift, and twisting moments were very small, <1 Nm.

The multifidus and psoas each produced greater forces at the L4-L5 level. For example, the multifidus produced a stress of 60 N/cm^2 at the L4-L5 level and 35 N/cm^2 at L3-L4. The contralateral psoas muscle was recruited heavily during asymmetric lifts, particularly at L4-L5. Stress in this muscle increased from 13 to 70 N/cm^2 during the 0 and 90° lifts. Increased forces were seen in most contralateral muscles during asymmetric lifts. The optimization model did predict activity of the abdominal muscles, typically 5-15 N/cm^2.

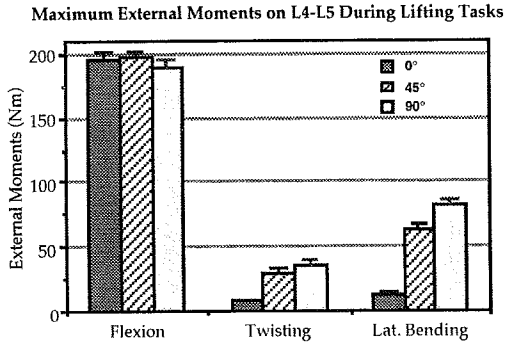

Figure 1: Maximum external moments on L3-L4, means and standard errors shown.

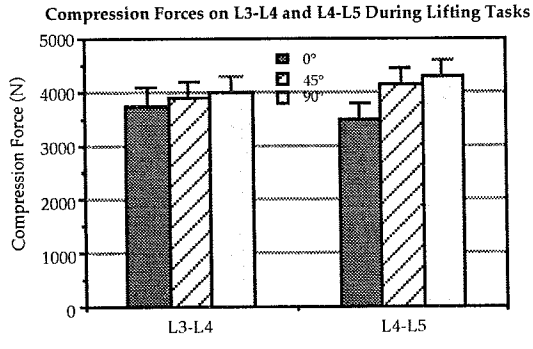

Figure 2: Maximum compression on L3-L4 and L4-L5 discs during asymmetric lifting. Means and standard errors shown.

DISCUSSION

This investigation sheds light on several aspects of freestyle asymmetric lifting. The external loads applied to the trunk have greater components of twisting and lateral bending moments. Also, the lumbar motion monitor indicated that there was very little twist in the spine despite placing the load 90° from the sagittal plane. The subjects accomplished their rotations using the legs and hips, and not the back.

The two level optimization model predicted that asymmetry increased the compression on the discs, particularly L4-L5. This may be due to increased activity of the contralateral psoas muscle. This muscle works through a short moment arm and resists lateral bending but also flexes the spine. This antagonistic flexion moment must be compensated by the erectors, thus increasing compression.

The multifidus was represented in this model as an intersegmental muscle, capable of independent forces at each level. A pilot study indicated that the model could not converge to a solution if all of the extensor muscles were assigned the same force at each level. This study indicates that when developing a multiple level model the muscle description must be refined. Furthermore, it seems that smaller muscles play an important role in maintaining equilibrium between levels.

The model did predict activity in all muscles during the lifts. Despite a maximum allowable muscle stress of 125 N/cm^2, the highest stress was only 80.3 N/cm^2. This stress was seen in the left iliocostalis during the 90° lift.

REFERENCES

Kromodihardjo, S. et al., J. Biomech. Eng., 109, 132-138, 1987.

Gagnon D, et al., J. Biomech., 25(8), 891-901, 1992

Granata K.P. et al, J. Biomech., 26, 12, 1429-1483, 1993.

Granata K.P. et al., J. Biomech., 28(11), 1309-1317, 1995.

Hooper D.M. et al., 1994 Adv. in Bioeng ASME 1994, 28, 333-334, 1994.

LUMBAR SPINE UNDER MECHANICAL LOAD: AN MRI STUDY *IN SITU*

Sherry L. Werner, Vladimir M. Zatsiorsky
Biomechanics Laboratory, Department of Kinesiology
The Pennsylvania State University, PA 16802

INTRODUCTION

The main idea of this study is to apply MRI to characterize the immediate effects of spine compression and decompression on the lumbar discs in living people.

METHODS

We constructed a spine compression unit (SCU) and registered sagittal MRI slices before, during and after compression. The SCU was construted from non-metallic materials. The compression load was about one body weight.

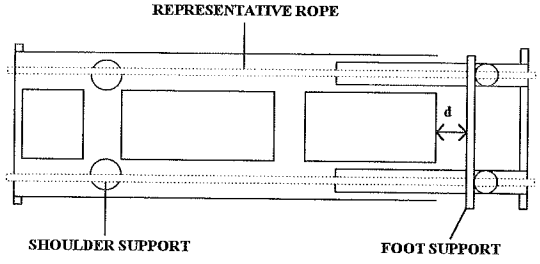

Figure. Overhead view of the spine compression unit (SCU) stretched a distance of 'd'. Pieces of PVC pipe of two different diameters form the telescopic frame with perpendicular extensions for shoulder and foot support. Rubber ropes (filled surgical tubing), extend the length of the unit inside of the telescopically arranged pipes. For the sake of clarity, only one rope on each side of the SCU is displayed.

A Picker International Vista MR system was used to collect images of the lumbar spine. Ten asymptomatic female volunteers between 20 and 25 years of age served as subjects. During experiment, the subject was assisted in positioning herself in a supine lying posture in the SCU on the scanning bed. As quickly as possible after situating the subject in the scanner, rf tuning, a 2 min scout and 12 min multi-echo scan were performed. Then the subject was exposed to an axial force. During the first 14 min after application of the load, a second set of scout and multi-echo scans were obtained. Forty-five minutes into the loading period a third 12 min scan was performed after a scout scan. After one hour of compression, the load was removed while the subject remained in the same position and the final scan was obtained.

The following disc parameters were identified for measurement and analysis:

(1) disc width (anterior-posterior); (2) anterior height, (3) posterior height, (4) mid-height, (5) sagittal area of the entire disc, (6) sagittal area of the hydrated portion of the disc, (7) disc volume, (8) hydrated disc volume, (9) average signal intensity of the pixels in the hydrated area of the disc. Signal intensity normalization for scanner variation and distance to the surface coil was achieved by dividing the disc signal intensity by the intensity of the cerebrospinal fluid (CSF) at the respective disc level. Because CSF is stable, its signal intensity was assumed to remain constant throughout the four scans.

RESULTS AND DISCUSSION

Conventional statistical analysis, a one-way, repeated measures ANOVA, did not reveal significant changes in the experimental parameters under the influence of the applied load. A more close inspection did reveal, however, that changes existed. In individual subjects, the changes (i.e. geometrical deformation) were not distributed evenly among all of the discs but were concentrated only in *some* discs and were camouflaged by opposite changes in other discs, see Table.

Table. Pre-compression values (h, mm) and changes (Δ, mm) between the first and third scans for disc anterior height. Height changes in excess of 20% and/or 2 mm are shown in bold type; discs with width changes in excess of 2 mm are underlined; and discs with area changes of ≥ 20% are in italics.

	L1-L2		L2-L3		L3-L4		L4-L5		L5-S1		Δ
#	h	Δ	h	Δ	h	Δ	h	Δ	h	Δ	total
1	5.00	-0.20	6.55	-0.55	7.05	1.10	10.20	0.00	11.80	0.00	0.35
2	4.25	0.60	***3.70***	***1.70***	7.65	-0.60	11.20	-1.15	**11.75**	**-3.55**	-3.00
3	**4.80**	**-1.10**	5.40	-0.10	7.10	0.55	6.30	-0.75	**5.80**	**-2.05**	-3.45
4	6.00	0.30	*7.20*	*0.10*	**12.90**	**-2.40**	12.20	0.00	13.60	-0.70	-2.70
5	***1.60***	***-0.60***	5.25	0.55	7.10	-0.65	**8.80**	**-4.05**	*5.20*	*0.00*	-4.75
6	3.70	0.00	*5.40*	*-0.60*	9.30	-0.60	9.60	0.40	11.20	-1.25	-2.05
7	4.80	0.60	6.00	0.15	8.80	-0.45	10.20	0.60	10.55	-0.05	0.85
8	6.55	0.00	7.60	-0.60	8.10	0.60	9.45	-0.20	12.60	-1.80	-2.00
9	**4.70**	**-3.10**	*6.00*	*1.10*	10.20	0.60	12.35	0.50	13.15	1.50	0.60
10	4.80	-0.55	**6.55**	**-1.75**	5.20	0.00	7.30	-0.65	**7.50**	**-2.00**	-4.95
Δ av	-0.41 ± 1.09		0.16 ± 0.76		-0.19±1.0		-0.53 ± 1.36		-0.99 ± 1.44		

The pattern of deformation was complex. The prevailing deformation was bending with the anterior (convex) side compressed. This is contrary to what was expected for the lordotic lumbar spine (concave side compression and convex side extension). The maximal magnitude of the local disc deformation reached 3-4 mm. The losses in hydrated disc area, volume and signal intensity agree commendably with the conventional explanation of disc behavior as an osmotic system that expels water when loaded. The gains in these parameters did not adhere well to this theory, however. An explanation was offered that under a moderate mechanical load, the osmotic pressure in some discs increases, thus counterbalancing the pressure enhancement due to mechanical loading. The changes in one motion segment did not correlate substantially with changes in other motion segments: Loss/gain of a certain parameter in a given segment was not associated in a perceptible manner with either loss or gain in other segments. The orientation of the lumbar spine during loading remained constant for all but one subject.

SUMMARY

The spine under (moderate) compression behaves as a dynamic living system, the behavior of which cannot be described by mechanical viscoelastic models. The cause→ effect relationship during loading of the spine is a three-link chain, *load→ physiological reaction→ deformation*, rather than a purely mechanical *load→ deformation* sequence. In summary: (a) mechanical loading of subjects in an MRI scanner is feasible, and (b) this method is sensitive enough to document changes in spine geometry and water content due to axial loading.

ACKNOWLEDGMENTS

The authors wish to thank J. Johnstonbaugh for constructing the compression unit and the staff at 611 Magnetic Imaging Associates, State College, PA for providing the MR images. The study was funded in part by grants from the College of Health and Human Development and the Alumni Society of the College, The Pennsylvania State University

A FLEXURAL FATIGUE MODEL FOR CORTICAL BONE

L.V. Griffin[1], J.C. Gibeling[1], R.B. Martin[2], V.A. Gibson[2], S.M. Stover[3]
[1]Division of Materials Science and Engineering, University of California, Davis, CA 95616
[2]Orthopaedic Research Laboratory, University of California, Sacramento, CA 95817
[3]Veterinary Orthopedic Research Laboratory, University of California, Davis, CA 95616

INTRODUCTION

An analytical flexural fatigue model was developed for bending of cortical bone beams. A mechanistic model of fatigue damage was used. The material model is based on an elastic damage formulation, which provides excellent agreement with axial fatigue data in both tensile and compressive fatigue of human cortical bone obtained by Pattin (1995). The model predictions provide good agreement with independently obtained flexural fatigue data for human femur tissue.

REVIEW AND THEORY

Fatigue damage accumulation mechanisms in cortical bone are of interest to researchers and clinicians who desire to determine causes and preventative measures for repetitive stress injuries. Long bones, such as the human femur, are subjected to complex multiaxial stress states which have been shown to produce damage in the form of microcracks, osteon debonds, and pulled out osteons, all of which tend to degrade the overall mechanical integrity of the bone structure. While there are volumes of literature dealing with the fatigue of composites and other engineering materials, the fatigue processes of bone remain virtually uncharacterized.

Previous investigations of cortical bone have demonstrated differences in tensile and compressive fatigue modulus degradation and fatigue life, as well as in the type of damage that forms in tensile and compressive fatigue. In agreement with Carter & Hayes (1977), we have observed that microcrack damage in tensile fatigue is largely limited to interstitial damage and osteonal debonding, while compressive fatigue produces cracks running between Haversian canals, crossing osteonal cement lines. While it seems reasonable to attribute fatigue behavior differences to the differences in damage, there has not been a theory which supports this hypothesis. Because one of the major loading modes of bone is bending, we are studying flexural fatigue damage accumulation. Therefore, we have developed a damage theory for flexural fatigue.

Assuming that the damage in four point bending experiments is predominately due to axial stresses, it was of interest to determine if modulus degradation and fatigue life could be modeled using uniaxial fatigue data in a damaged beam theory. If such a method can be validated, fatigue in flexure and other combined modes of loading may reasonably be modeled using data obtained from simpler, uniaxial tests.

Our model is based on laminated plate theory. As a first approximation, damage accumulation in flexure was assumed to be caused by axial stresses in tension and compression. A mechanistic fatigue damage model was developed using an approach which partitions damage into separate entities for osteons and interstitial bone matrix. The damage is mechanically manifest as a modulus reduction. The modulus for damaged Haversian bone was represented by an isostrain rule of mixtures,

$$E(N) = (1 - D_f)E_f V_f + (1 - D_m)E_m V_m \quad (1)$$

similar to that used by Ramakrishnan et al. (1992). In Eqn. (1), N is cycle number, E is modulus, V is volume fraction, D is damage, and the subscripts m and f stand for interstitial matrix and osteonal fibers, respectively. Damage is zero in an undamaged state, and one in a completely damaged (failed) state.

In *tensile* fatigue, damage evolution for the matrix was modeled as

$$dD_m/dN = K_m(D_t - D_m) \quad (2)$$

where matrix damage is assumed to have a stress-dependent upper limit, $D_t = K_t\sigma^m$. For the osteons, damage was assumed to evolve as

$$dD_f/dN = K_{fm} D_m + K_f D_f \quad (3)$$

In these equations, the K's are coefficients. In *compressive* fatigue, damage was postulated to evolve irrespective of osteonal boundaries, as a function of vascular canal stress concentrations and the existing damage,

$$dD_c/dN = K_{SF}\sigma^C + K_c D_c \quad (4)$$

where K_c and c are coefficients and $K_{SF}\ \sigma^C$ is a stress-sependent vascular channel "flaw factor." D_c was used for both D_f and D_m in Eqn. (1). Eqns. (1)-(4) were solved in closed form and the coefficients determined by a nonlinear regression analysis of human femur tissue uniaxial fatigue data by Pattin et al. (1995) using SAS (V 6.09, SAS Institute Inc., Cary, NC USA).

These relationships were then used in the laminated beam model, the plies of which do not represent the lamellae in the bone, but rather regions of approximately homogeneous stresses for computational purposes. The laminated beam assumes perfect bonding of the plies, which ensures that compatibility of strains is not violated. The governing equation for the laminated beam is

$$\frac{d^2y}{dx^2} = \frac{M}{C-(B^2/A)} \qquad (5)$$

where y is deflection, x is longitudinal position, and C, B, and A are functions of the geometry and elastic modulus of the plies. The beam was discretized into 40 segments along the length with each segment containing 20 plies. For each cycle of loading, the beam was numerically integrated, and the damage and modulus in each ply calculated from the above relationships. The discount method (i.e., setting the modulus value of the ply to zero at failure) was used to model individual ply failure. The beam was loaded one cycle at a time until beam failure was obtained, defined as 65% degradation of the effective beam modulus (calculated from its deflection).

PROCEDURES

Experimental data for flexural fatigue of human femur tissue were obtained using the four point bending protocol of Gibson, et al. (1995). Using inner and outer roller supports at 32 and 64mm, respectively, 4x10x100mm beams were fatigued in a 37°C saline bath at 2 hz under load control. Four specimens have been tested thus far.

RESULTS AND DISCUSSION

The damage model closely fits Pattin's uniaxial data (not shown here) with the advantage that its parameters have physical meaning (e.g., matrix microcracks). The model also provides excellent agreement with our preliminary but independently obtained experimental data (Fig. 1). The 6500 με prediction falls between data for two specimens tested at 6500με (initial strain). Model predictions also fall near data for beams tested at 6000 and 7500με. There seems to be a tendency for the model to underestimate fatigue life. This may be because of the limitations of the model (e.g., the ply discount method is too conservative) or different uniaxial and flexural test conditions (e.g., submersion in saline or not).

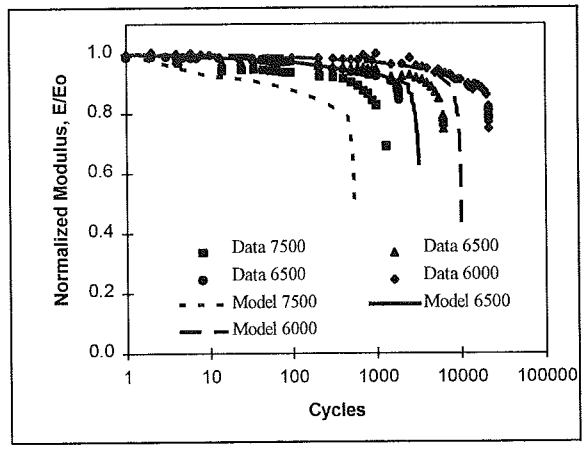

Figure 1: Model comparison with fatigue data. Legend values are initial microstrain.

These predictions suggest the model has good potential for further inquiry into the flexural fatigue processes of bone. The model can easily be adapted to other test configurations, such as three point or cantilever bending. The beam model may also be used to predict residual strength after fatigue loading.

REFERENCES

Carter D.R., Hayes W.C. CORR, 127, 265-274, 1977.
Gibson, V.A. et al. J Ortho Res, 13, 861-868, 1995.
Pattin, C.E. et al. J Biomech 29, 69-79, 1995.
Ramakrishnan V. et al. J Mat Sci, 28, 5592-5602, 1993.

ACKNOWLEDGEMENTS

This work was supported by NIH Grant AR41644; California Center for Equine Heath and Performance; UC Davis; Mr. and Mrs. Amory J. Cooke; and the Hearst Foundation.

RESIDUAL MECHANICAL PROPERTIES OF HUMAN CORTICAL BONE FOLLOWING FATIGUE LOADING

T.M. BOYCE, D.P. FYHRIE, F.R. BRODIE AND M.B. SCHAFFLER
Bone and Joint Center Breech Research Lab, Henry Ford Health Sciences Center, 2799 West Grand Boulevard, Detroit, MI 48202 USA

INTRODUCTION

Clinical fracture is often attributed to a single traumatic event, and the magnitude of trauma required to produce such a fracture decreases substantially with age (Hedlund & Lindgren, 1987) . In addition to age-related bone mass reductions, the lower magnitude of fracture-inducing loads may be accounted for by bone quality factors such as tissue-level material (Boyce & Bloebaum, 1993) and architectural changes (Heaney, 1993). Matrix damage effects from cyclic loading (Schaffler et al., 1994) , with their attendant reduction in cortical stiffness and strength (Carter & Hayes, 1977) suggest that bone fatigue may be a pre-disposing factor in fractures (Biewener 1993). The purpose of this study was to evaluate how matrix damage caused by cyclic loading influences the residual stiffness, strength and toughness of compact bone in a subsequent single-cycle failure.

PROCEDURES

Specimens were taken from paired femoral diaphyseal regions from one individual (49 y.o. male) to minimize inter-specimen variability. Diaphyseal pieces were lathe-turned to produce specimens with 3mm dia. gage region, and were moistened during all steps of fabrication. Half of the specimens, randomly chosen, were removed for use in a complementary microdamage histological study. The remaining specimens were randomly assigned to three groups: no fatigue (n=7), fatigue to 20% strain increase (n=6), fatigue to 40% strain increase (n=6), corresponding to 0%, 18.6±0.6% and 30.9±0.9% modulus loss, respectively. Two Hz cyclic loading, at a tensile load corresponding to 5000 με, was performed on a servohydraulic testing machine. Specimens were tested at 37°C under constant wetting with calcium supplemented saline solution (Gustafson et al., 1995). Tests were halted when the pre-determined strain increase was reached. Following cyclic loading, without disturbing the set-up, specimens were loaded at 20000 με/s in tension to failure. Initial and final elastic moduli were determined from the slope of linear trend lines through the first and last cycles of stress-strain data, except for the 0% group, where the initial elastic modulus was taken from the monotonic stress-strain curve. Residual properties (ultimate strength, ultimate strain, and energy absorption to failure) were determined. Data were analyzed by ANOVA with α=0.05 with post-hoc testing by Scheffe's Test.

RESULTS

Initial moduli of all three specimen groups were alike (Table 1, p=0.768). Stress-strain curves (fig. 1) from specimens loaded to 20% strain increase were qualitatively similar to non-fatigued specimens from comparable regions, albeit with somewhat reduced material properties. By contrast, 40% strain increase specimens had a radically different stress-strain relationship, characterized by an elastic region that deviates early from linearity, poorly-defined yield and a truncated post-yield region.

Between the no fatigue and 20% strain fatigue groups, residual properties were moderately reduced: ultimate strain (fig. 2) decreased by 13%, strength (fig. 3) fell by 9%, and failure energy (fig. 4) reduced by 16%. However, in the 40% deformation group, reductions were dramatically higher: 64%, 27% and 74% respectively. For all three material parameters, the 20% group was not significantly different from the control (0%) group ($0.125 < p < 0.215$). The 40% group differed very significantly from both the control group (p=0.0001 for each material parameter) and the 20% group ($0.0001 < p < 0.0037$).

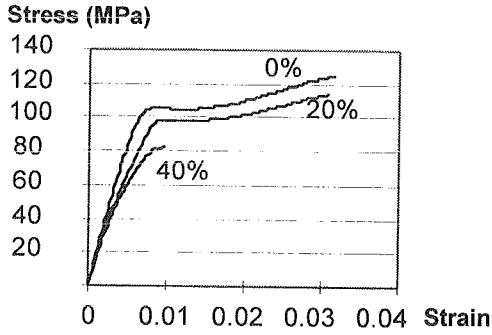

Figure 1 - Single-cycle stress-strain relationships for specimens fatigued to 0%, 20% and 40% displacement increase. Specimens taken from the anterior femoral diaphysis.

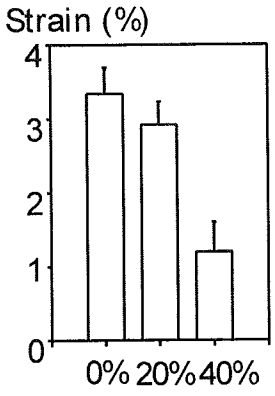

Figure 2 - Residual ultimate strain. Bars indicate SD.

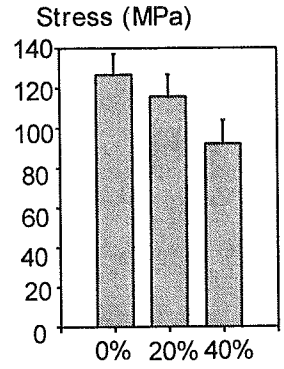

Figure 3 - Residual tensile strength.

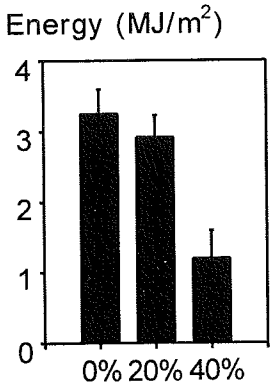

Figure 4 - Residual energy absorption to fracture.

Table 1: Fatigue and monotonic overload properties. (Mean ± SD)

Fatigue Group, %Displacement Increase	0% (n= 7)	20% (n= 7)	40% (n= 6)
Initial Modulus, GPa	16.6 ± 1.0	16.3 ± 1.0	16.2 ± 1.3
% Modulus Degradation	----------	18.6 ± 0.6	30.9 ± 0.9
Fatigue Cycles	----------	177 ± 147	1279 ± 1810
Residual Strain	3.34 ± 0.35%	2.92 ± 0.31%	1.20 ± 0.40%
Residual Tensile Stress, MPa	126.8 ± 10.3	115.9 ± 10.9	92.2 ± 11.7
Energy Absorption, MJ/m^3	3.25 ± 0.56	2.73 ± 0.36	0.83 ± 0.36

DISCUSSION

The present study shows that damage from low levels of fatigue, to about 20% modulus reduction (≈ 20% strain increase), are well-tolerated and do not significantly compromise the bone tissue properties. When fatigue damage reaches about 30% modulus reduction (≈ 40% strain increase) however, the material response changes dramatically. The elastic region of the stress-strain curve becomes nonlinear, and the plastic region is all but eliminated (fig. 1); these effects together account for reduced energy absorption to about one-quarter that of non-fatigued bone. With higher fatigue levels, stored energy is released in small amounts as local matrix damage (Carter & Hayes, 1977) and little additional energy may be absorbed during the subsequent single-cycle overload; by contrast, non-fatigued bone can store a large amount of energy during monotonic loading, which is released at once in catastrophic failure.

The current data indicate a nonlinear dependence of residual properties on matrix damage in bone, severely compromising its ability to withstand overload following higher levels of damage. These data also suggest that a buildup of unrepaired microdamage in bone, as in aging (Schaffler et al., 1994), will severely alter bone's residual properties and will contribute substantially to increased fragility in the aging skeleton.

REFERENCES

Hedlund, R., Lindgren U. *J Orthop Res* 5:242, 1987
Boyce, T.M., Bloebaum, R.D. *Bone* 14:769, 1993
Heaney, R.*Calcif Tissue Int* 53:S3, 1993
Schaffler, M.B. et al., *Trans ORS* 19:190, 1994
Carter, D.R., Hayes W.C. *J Biomech* 10:325, 1977
Biewener, A.A., *Calcif. Tissue Int* 53:S68, 1993
Gustafson, M.B., et al., *Trans ORS* 20:297, 1995

ACKNOWLEDGMENTS

Supported by NIH grants AR41210 (MBS) & NRSA AR0832 (TMB). Materials provided by the Musculoskeletal Transplant Foundation.

CORTICAL BONE ELASTICITY IN AGING RATS WITH AND WITHOUT GROWTH HORMONE TREATMENTS

S.S. KOHLES[1], G.D. CARTEE[2], R. VANDERBY JR[2]
[1] Department of Mechanical Engineering, University of Washington,
21703 20th Place West, Brier, WA 98036-8188
[2] University of Wisconsin, Madison, WI 53792-3228

INTRODUCTION

Aging deleteriously affects many issues associated with cortical bone including healing, fracture resistance, adaptability to physiological perturbations, and elastic properties. A potential means of slowing these age related changes as well as minimizing cortical bone loss is via growth hormone (GH) treatments (Bak *et al.*, 1991). In this study, the ultrasonic technique is used to test the hypothesis that treatments of GH may counter the age related elastic changes.

PROCEDURES

The ultrasonic elasticity test system included pulse and function generators, transmitting and receiving transducers, and a digital storage oscilloscope (Kohles *et al.*, 1996). Shear and longitudinal waves (5 and 20 MHz) were propagated. Density and wave propagation velocities were combined to describe the material stiffness matrix. Nine independent material properties were calculated including Young's moduli (E_{ii}), shear moduli (G_{ij}), and Poisson's ratios (ν_{ij}).

Sixty male Fischer 344 x Brown Norway F1 hybrid (F344/BNNia) rats of three ages (9, 20, or 31 months) were obtained. Each age group consisted of 20 rats, they were considered young adult (9 months), middle aged (20 months), and old (31 months). The rats were randomly assigned to vehicle control or GH treated groups. All rats received subcutaneous injections twice daily, at 0800 and 1500 hours, for 10 consecutive days. The GH group was injected with recombinant-derived human GH (0.7 mg/kg body weight) and the control group was injected with an equivalent volume of vehicle. All rats were euthanized, the femora harvested, and cubic specimens cut (2.0 x 2.0 x 0.8 mm) from the posterior cortex with surfaces oriented in the radial-1, circumferential-2, and longitudinal-3 directions for ultrasonic evaluation (i, j). Statistical evaluation of the cortical elasticity, density, thickness, and femoral length between the three age groups and the two treatment groups was undertaken using ANOVA with the Fisher's Protected Least Significant Differences analysis.

RESULTS

Cortical elastic moduli consistently increased with age with the strongest effects demonstrated in radial dependent properties such as E_{11} (+25.3% from 9 to 31 months, $p=0.0004$) and G_{12} (+12.6% from 20 to 31 months, $p=0.0419$). The ratio of transverse to axial displacement (Poisson's ratio) typically decreased with age (9 to 31 months) as seen in ν_{31} (-24.95%, $p=0.0134$) and ν_{32} (-20.7%, $p=0.0015$). Overall, a ten day treatment with GH produced no global statistical change in elastic properties ($p>0.05$). However, GH did minimize the age related differences that were measured for E_{22}, E_{33}, and ν_{32} between the 9 and 31 month old groups essentially returning old bone to its youthful elastic state.

Density exhibited a slight decrease (-1.11%) between 9 and 31 months ($p=0.0708$). This effect reached a maximum decrease (-1.79%) for the GH treated groups alone between 9 and 31 months ($p=0.0399$). Femoral length consistently increased over time ($p<0.05$) for all groups with a maximum increase from 9 to 20 months within the controls (+3.23%, $p=0.0001$). Mean cortical thickness increased for all groups from 9 to 20 months (+4.92%, $p=0.1262$) but decreased from 20 to 31 months (-4.28%, $p=0.1775$).

DISCUSSION

The results from this study indicate that the modulus of elasticity (E_{ii}) is a sensitive indicator of changes due to aging. This was especially demonstrated with the statistical increase of the radial modulus during tissue aging. Endosteal and periosteal surfaces provide the initial cellular and vascular responses to natural and synthetic perturbations thus establishing the first level of an adaptive response in the radial orientation. Although the overall elastic response to GH was minimal, the circumferential and longitudinal moduli indicated a sensitivity to the treatment, statistically mimimizing the age related increases.

REFERENCES

1. Bak *et al.*, *Clin. Orthop.*, 264, 295-301, 1991.
2. Kohles *et al.*, *Annals Biomed. Eng.*, 25, 1996.

ACKNOWLEDGEMENTS

Partial funding provided by the American Federation for Aging Research and the National Institute of Aging. Recombinant hGH was provided by Genentech Inc., San Francisco, CA.

DYNAMIC STRAIN AND INTRAMEDULLARY PRESSURE, FLUID FLOW MEDIATED BONE ADAPTATION

Y. Qin, K.J. McLeod, M.W. Otter, C.T. Rubin
Musculo-Skeletal Research Laboratory
State University of New York at Stony Brook, Stony Brook, NY 11794-8181

INTRODUCTION

We have previously shown that dynamic torsional loading of bone minimizes bone turnover, while axial loading elevates turnover[1]. Moreover, adaptation processes appear to be strongly frequency dependent[2]. Increasing the loading frequency from 1 to 60 Hz results in less periosteal new bone formation but substantially increased endosteal new bone formation. Finally, the sites of periosteal bone adaptive responses do not correlate well with the sites of strain magnitudes. These differential adaptive responses to different mechanical loads suggest that bone cells may be sensitive to multiple transduction processes.

Recently, we have shown that intramedullary (Im) pressure is dependent on the loading frequency[3] which may explain the frequency dependence of endosteal adaptation. Based on these information, we propose that fluid flow may play a role in bone adaptation, this fluid flow being driven by both strain-induced cortical deformation and Im pressure. The object of this study is to begin to characterize fluid flow dynamics in intact bone, evaluating transcortical fluid flow during axial and bending loads, and the influence of Im pressure on this flow. Measurements of *in vivo* transcortical streaming potentials (SPs), an electromechnical transduction[4] which occurs when fluid flow transports charge through the matrix, are utilized.

PROCEDURES

Under a general halothane anesthesia, the left ulnae of six adult male turkeys were functionally isolated via transverse epiphyseal osteotomies[1]. The metaphyses were then covered with stainless steel caps and sealed with PMMA. Pins inserted transcutaneously through the caps permitted mechanical loading of the bone. The bone was drilled and tapped for insertion of a saline filled 2 cm long tube. A 50 psi pressure transducer (Entran EPX-10IW) was connected with the medullary canal via this tube. Two Ag/AgCl electrodes were placed on the periosteal surface at the sites of near maximal and minimal strains corresponding to the distinct loading conditions (Fig. 1). Loading was accomplished using an Instron machine control to obtain peak longitudinal normal strain of approximately 600 με in both axial loading and bending. Sinusoidal loading was performed over the frequency range of 0.1 to 100 Hz. Pressure, load feedback and SPs were digitized at 409.6 Hz, with 16 bit resolution.

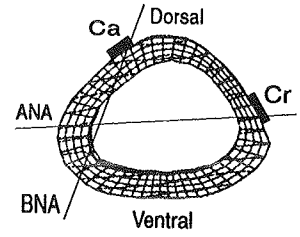

Figure 1: Cross section of the ulna showing the sites of electrode and the position of neutral axes under axial loading, dorsal and ventral bending. ANA--axial loading neutral axis; BNA--bending neutral axis. Cr--cranial electrode; Ca--caudal electrode.

The influence of Im pressure on transcortical fluid flow was investigated by pumping fluid in an oscillatory manner into the marrow cavity while measuring transcortical SPs, using the similar pressure magnitude generated by mechanical loading. A specially designed device, including a diaphragm, a syringe and an actuator, generated the dynamic pressure. Analysis consisted of normalizing peak-peak dynamic pressure, SP magnitudes to the load feedback signal at each frequency tested.

RESULTS

Dynamic axial loading and bending of the ulnae resulted in pressure and SPs reflecting complex

relaxation spectrums. Pressure was found to increase monotonically with increasing frequency for both loading cases. However, distinctly different frequency characteristics were found for the axial and bending loads (Fig 2). With axial loading, there is a relaxation time near 1 Hz. The normalized pressure at 30 Hz was 10x higher than that at 0.1 Hz. The Im pressures in axial loading are significant higher than these in bending, approximately 10x higher in the frequency band between 0.1 to 60 Hz.

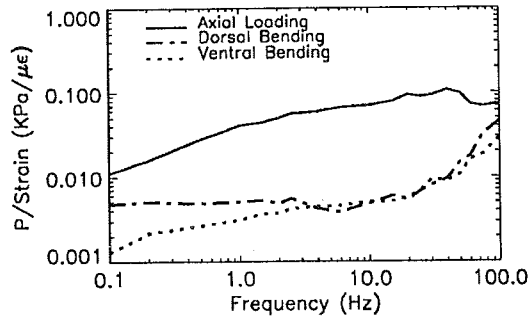

Figure 2: Normalized peak pressure vs. frequency during mechanical loading. Both axial and bending loads indicating a strong frequency dependence.

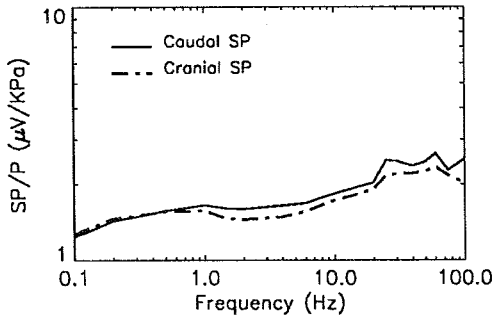

Figure 3: Streaming potentials per pressure unit at caudal and cranial sites by dynamic intramedullary pressure with the absence of matrix deformation.

SP magnitude and frequency dependence were similar at the two sites when marrow pressure was exogenously modified (Fig. 3). The SPs plateau around 20 to 50 Hz. There is a visible low value of SP/P near the frequency of 5 Hz. The peak appears around 30 Hz with the value of 2.46±0.41(s.d.) μV/KPa and 2.19±0.34(s.d.) μV/KPa at caudal and cranial sites, respectively.

DISCUSSION

It is well known that cortical deformation has the ability to produce SPs. Reported intracortical SP values[4], induced by bone matrix deformation, are on the order of 1~4μV/cm/με. Since the observed SPs induced by dynamic Im pressure, in the absence of mechanical loading, are similar in magnitude to SPs generated by axial loading at high frequency (~30 Hz), significant cortical fluid flow induced by mechanical loading appears to be partly generated by Im dynamic pressure. The Im pressure induced fluid flow would generate a uniform flow in the radial direction, while matrix deformation induced flow is likely to depend on local strain gradients. Thus, the patterns of fluid flow during mechanical loading, being a sum of these two fluid flow components, may not simply reflect the patterns of local matrix strains. Perhaps this finding can help to explain the lack of strong correlation between the sites of periosteal bone formation and the sites of maximum strains.

The combined frequency dependence of matrix deformation driven SPs and Im pressure driven SPs may partly explain the observation of a strong frequency dependent adaptation at the endosteal and periosteal surfaces. Further, the frequency dependence of both pressure and matrix deformation induced SPs are consistent with the observation that the strain magnitude for maintaining bone mass at higher frequency loads is much smaller than those required at lower frequency.

Interestingly, since the cortex at the caudal site is approximately 2 times thicker than that at the cranial site, the observed results of comparable SPs at two sites seems to indicates that the thickness of the cortex does not dramatically affect transcortical potential.

REFERENCE

1. Rubin et al., (1996) *JBJS* (accepted)
2. McLeod & Rubin, (1992) *ORS Tran* 38:533
3. Qin et al., (1995) *SPRBM Tran* 15:53
4. Otter et al., (1990) *JOR*, 8:119-126

ACKNOWLEDGMENTS

Supported by NIH AR40411 and Exogen, Inc.

BONE HYPEREMIA AS AN INITIATOR OF BONE RESORPTION

Ted S. Gross[1], Robert C. Bray[2], and Ronald F. Zernicke[2]
[1]Dept. of Orthopaedic Surgery, University of Cincinnati, Cincinnati, OH 45267
[2]McCaig Centre for Joint Injury and Arthritis, Univ. of Calgary, Calgary, Alta T2N 4N1

INTRODUCTION

The pathway by which disuse is translated into local osteoclastic resorption is poorly understood. In this study, we determined whether bone blood flow alterations associated with disuse precede the differentiation and recruitment of osteoclasts to bone surfaces. As blood flow was substantially altered prior to osteoclastic activity, we propose that blood flow may initiate cellular events that culminate in bone resorption.

REVIEW AND THEORY

Bone responds to physical stimuli by locally regulating cellular activity. When physical stimuli are severely diminished by immobilization or paralysis (i.e., disuse), bone mass is rapidly reduced via elevated osteoclastic resorption (1). One physiological process associated with cellular activity in a number of tissues is hyperemia (2). In bone, resorption caused by paraplegia, ovariectomy, and oophorectomy is accompanied by elevated blood flow (3,4,5). Typically, blood flow only returns to normal levels after tissue remodeling has been completed (4). As blood flow and bone cell activity increase and decrease in parallel, these processes may be coupled. It is not clear, however, whether blood flow actively initiates osteoclastic resorption, or is secondarily elevated by heightened cell activity. Evidence that blood flow is altered prior to osteoclastic activity, and therefore potentially initiates the process, is equivocal (6,7). In this study, we used an avian model of disuse osteopenia to determine whether bone blood flow alterations caused by disuse precede the differentiation and recruitment of osteoclasts. As 10 d are required for the onset of resorption in this model (8), we were able to identify the temporal relationship between blood flow alterations and the initiation of osteoclastic activity.

PROCEDURES

Adult male roosters (1 yr) were randomly assigned to zero-time control (n=6), 3 d disuse (n=3), 7 d sham surgery (n=6), 7 d disuse (n=6), and 14 d disuse groups (n=6). Zero-time controls animals did not undergo surgery. Within the disuse groups, the left ulna was isolated from mechanical loading via parallel metaphyseal osteotomies. In sham surgeries, partial osteotomies were performed through 1/3 of the cortex at both metaphyses. This procedure disrupted the marrow and bone blood supply at these sites, but maintained the structural integrity of the bone. The right ulnae served as an intact, contralateral control. At the appropriate time point, mid-diaphyseal bone blood flow was assessed in the left (exp) and right (control) ulnae. The rooster was anesthetized and the aortic root cannulated retrograde from the right carotid artery. Colored microspheres in mixed suspension with saline (6 million) were injected into the base of the aorta over a 30 s period. Starting 10 s prior to injection, a reference blood sample was drawn for 1 minute at 3 ml/min from a cannula placed in the left anterior tibial artery. After sacrifice, the ulnae were removed and 5 mm long cross-sections were extracted from the mid-diaphysis of each bone using a diamond saw. The sections were cleansed of marrow, decalcified, and digested. Microspheres trapped within the bone cross-sections were isolated by filtering the digested tissue through a 7 μm polyester filter. Once filtered, the microspheres were directly counted using a fluorescent microscope. The number of spheres within the reference blood sample was determined by filtering the sample, eluting the microspheres with DMF, taking spectrophotometer readings of the solution, and converting absorbance units using manufacturer calibration curves. Standardized blood flow (ml/min/100g) was determine by dividing the number of microspheres within the bone sample by the number contained within the reference blood

sample and normalizing this value by the dry mass of the tissue. Non-parametric Wilcoxon tests (p=0.05) were used to identify flow differences between the left and right ulnae within each group. Non-parametric Kruskal-Wallis one-way ANOVA was used to identify blood flow differences across treatment groups (non-parametric Tukey follow up; p=0.05).

RESULTS

Mean (± S.E.) blood flow was symmetric in the left and right ulnae of the zero-time (2.0 ± 0.6 vs 1.6 ± 0.8 ml/min/100g) and sham surgery groups (2.5 ± 0.6 vs 2.6 ± 1.3). Bone blood flow was elevated maximally at 7 days of disuse (10.3 ± 4.6; p=0.03; ***Fig 1***). Flow was also elevated at days 3 and 14, but to a lesser extent (***Fig 2***).

DISCUSSION

Three primary observations can be drawn from these data. First, symmetric blood flow in the zero-time ulnae indicated that the microspheres were evenly distributed throughout the animal (confirming a primary assumption of the microsphere technique). Second, contralateral bone blood flow was not altered in any of the treatment groups, and sham surgery did not induce mid-diaphyseal flow alterations. Thus, systemic and surgical effects were minimal, and any observed flow alterations may be attributed to physiologic processes associated with the bone's altered mechanical environment. Third, as 10 days are required for the activation of osteoclasts in this model (8), the extreme hyperemia observed at 7 days preceded osteoclastic resorption by 3 days. Importantly, this 3 day period is equivalent to the time that is required for osteoclasts to differentiate from marrow precursors (9). As endothelial cells are highly sensitive to local flow fluctuations and produce vasoactive substances that induce osteoclastic differentiation, they appear ideally situated to modulate this process. To our knowledge, this is the first *in vivo* study to suggest that blood flow may actively precipitate cellular events which result in bone resorption.

REFERENCES

1. Westlin, Clin Orthop, 102:194-199, 1994.
2. Salzman, New Horiz, 3:33-45, 1995.
3. Schoutens et al, CTI, 42:136-143, 1988.
4. Egrise et al, CTI, 50:536-541,1992.
5. Kapitola et al, Bone, 16:69-72, 1995.
6. Triffitt et al, JOR, 11:49-57, 1993.
7. Wilson et al., A J Phys, 264:H171-175, 1993.
8. Bain et al, JBMR, 5(S2):S217, 1990.
9. Jaworski et al, J Anat, 133:397-405, 1981.

ACKNOWLEDGMENTS

The authors thank Mr. Ariff Damjii, Mr. Michael Doschak and Mr. Stefan Judex for their surgical assistance. This work was supported, in part, by The Arthritis Society, Medical Research Council, Alberta Heritage Foundation for Medical Research, and the Natural Sciences and Engineering Research Council.

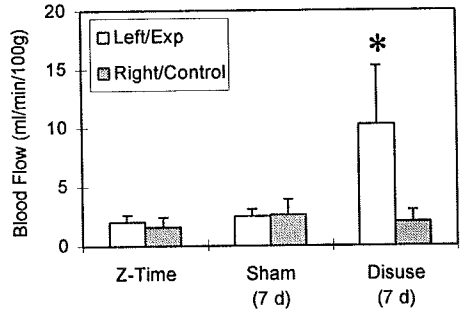

Fig. 1. *Mean mid-diaphyseal bone blood flow (+S.E.) in the left and right ulnae. Flow was symmetric in the zero-time group, was not altered by sham surgery, and was significantly elevated at 7 d of disuse vs zero-time and contralateral controls (*; p=0.03).*

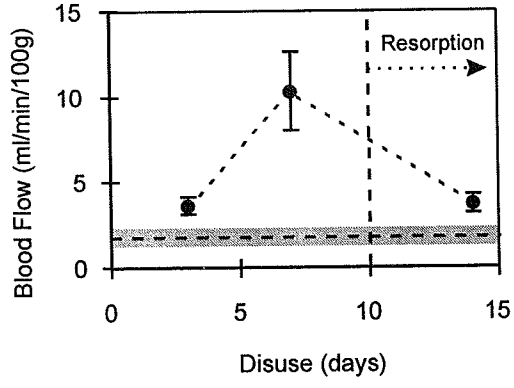

Fig. 2. *Mean (± S.E.) blood flow at 3, 7, and 14 d of disuse. Mean (± S.E.) zero-time control flow (horizontal dash and shaded area) is extended across the graph. Resorption is initiated 3 d after massive hyperemia at 7 d.*

EFFECTS OF LIMB-OBSTACLE PROXIMITY ON THE JOINT MOMENTS OF THE TRAILING LIMB

Li-Shan Chou and Louis F. Draganich

Section of Orthopaedic Surgery and Rehabilitation Medicine, Department of Surgery
The University of Chicago, Chicago, Illinois 60637

INTRODUCTION

The motivation for this study is the seriousness of falls in the elderly. In order to better understand the biomechanics of crossing obstacles in the elderly, base-line data in young healthy adults is needed. Arguably, tripping over an obstacle with the leading limb may be more dangerous than tripping over an obstacle with the trailing limb. The trailing limb supports the body when stepping over an obstacle with the leading limb. Thus, we studied the effects of obstacle location on the 3-D joint moments of the trailing limb in seven healthy young adults stepping over obstacles of 51, 102, and 204 mm heights positioned at distances from the trailing foot of 10, 20, 30, and 40% of the step length measured during unobstructed level walking.

REVIEW AND THEORY

Strong relationships of lower extremity strength to balance and to gait have been found in both nursing home and community-dwelling elder subjects (Wolfson et al., 1995). Furthermore, reductions in knee extensor and ankle plantar flexor strengths have been found in nursing home fallers (Whipple et al., 1987). The results of our previous study on healthy young adults showed that, except for the internal-external rotation moments at the ankle, significant increases were generated in the magnitudes of the 3-D moments about the joints of the trailing limb when the leading limb was crossing an obstacle (Chou and Draganich, 1996[a]).

When stepping over an obstacle the proximity between the limb and the obstacle would be expected to affect the motion of the lower limbs and, therefore, might also be expected to affect the magnitude of the 3-D moments about the joints. We are not aware of any studies reporting on the effects of limb-obstacle proximity on the 3-D moments of the joints of the trailing limb (stance limb) when the leading limb crosses an obstacle. Therefore, the purpose of this study was to investigate the effects of limb-obstacle proximity on the 3-D joint moments of the trailing limb during stance.

PROCEDURES

Gait analysis was performed on seven healthy young adults (5 males, 2 females) having a mean age of 24 years (range, 20 to 32 years). Their average height was 174 cm (range, 167 cm to 184 cm), and their average weight was 705 N (range, 637 N to 881 N). Subjects wore their own low-heel shoes. Three sets of experiments were performed. For each experiment subjects walked along a 9.5 m walkway at their comfortable, self-selected speeds. In the first experiment, each subject's average step length over several strides was measured. In the second experiment, the subject was instructed to walk along the walkway and step over an obstacle (white elastic band 1 mm thick and 6 mm wide) of 51, 102, or 204 mm height in his/her usual self-selected manner. To do this, the obstacle was placed beyond the force plate at a fixed location. The subject's beginning position was adjusted until with practice the subject had established a comfortable gait and the toe of the trailing foot landed within ±5 cm of a marker on the force plate before lifting the trailing foot to step over the obstacle. This beginning position was used in the third experiment. For the third experiment the average step length for the subject found in the first experiment was used to compute lengths of 10, 20, 30, and 40% of step length. The obstacle of each height was randomly placed at these distances from the marker on the force plate for a total of twelve tasks for this experiment (4 locations and 3 heights). The subject was instructed to maintain the stride attained in the second experiment until heel-strike of the trailing foot just prior to stepping over the obstacle. Thus, the distance from the trailing foot to the obstacle was controlled. Trials were accepted only if the toe of the trailing foot was within ±5 cm of the marker on the force plate.

Ground reaction forces were measured with a force platform in the center of walkway. Clusters of six or eight infrared light-emitting diodes were attached to the foot, shank, and thigh of the left lower limb and pelvis of the subject with elastic straps. Kinematic parameters were collected with the optoelectronic, 3-D digitizing

system. Kinematic and force parameters were sampled at a rate of 100 Hz. The overall accuracy of the system was better than 5 mm.

The 3-D moments about the hip, knee, and ankle joints of the stance limb were computed using inverse dynamics. The length, mass, location of mass center, and inertial properties of each body segment were calculated from data in the literature (Chaffin and Andersson, 1984). The moments were normalized to body weight times lower limb length. The effects of obstacle location on the maximum magnitudes of the 3-D joint moments were tested using two-way ANOVA with repeated measures. An α=0.01 level was used based on a Bonferroni adjustment for five comparisons of maximum moments during stance (i.e., flexion during early and late stance, extension during mid to late stance, adduction, and internal rotation). Only the 3-D external moments of the knee joint were reported here.

RESULTS

When crossing an obstacle positioned at 10, 20, 30, or 40% of step length the patterns of the 3-D moments at the knee were similar to those found when crossing the obstacle at the self-selected foot-obstacle distance (Fig. 1). Only the maximum flexion moment during late stance was significantly affected by limb-obstacle proximity (p=0.009). The magnitude decreased linearly (p=0.04) as limb-obstacle proximity decreased. The maximum extension moment during mid to late stance, maximum adduction moment during stance, and maximum internal rotation moment during stance were found to increase as limb-obstacle proximity decreased. However, significant differences were not found.

DISCUSSION

The maximum flexion moment during late stance (during double support phase) was significantly reduced as limb-obstacle proximity was decreased. An explanation for this is that the decrease in distance led to a decrease in the crossing stride length (Chou and Draganich, 1996[b]). This resulted in a decrease in distance between the leading and trailing feet during the double support phase (i.e., one limb on either side of the obstacle) which would in turn be expected to have led to a decrease in the sagittal plane moment arm between the knee and the body weight vector. This reduction in the external flexion moment and, hence, reduction in quadriceps force would prepare the trailing limb for the transition to hamstring force needed to flex the knee to cross the obstacle. Although we found only the maximum flexion moment during late stance to be significantly reduced, there were trends for the other peak moments which may become significant with a larger number of samples. We are currently investigating this possibility.

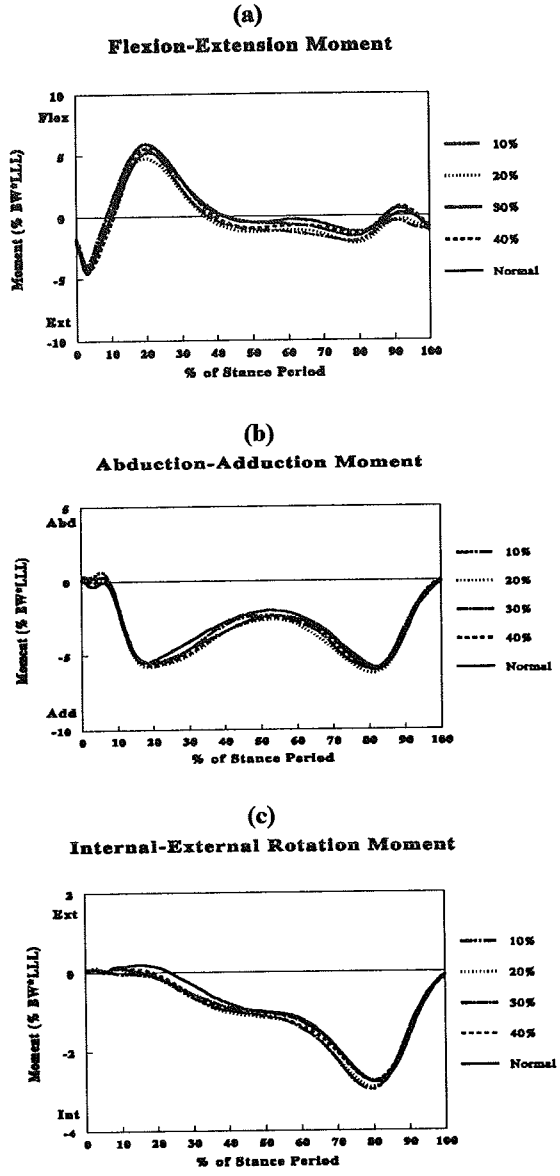

Figure 1. The ensemble-average external 3-D moments generated at the knee of the trailing limb during stance just prior to stepping over an obstacle of 204 mm height.

REFERENCES

1.Chaffin and Andersson,*Occupational Biomechanics*, John Wiley & Sons, Inc., NY, 1984.

2. Chou and Draganich, submitted to *J. Biomechanics.* 1996[a].

3. Chou and Draganich, submitted to *ASB* Meeting 1996[b].

4. Whipple et al. *J. Am. Geriatric Soc.*: 35, 13-20.

5. Wolfson et al. *J. Gerontology*: 50A: 64-67.

THE NONLINEAR DYNAMICS OF CHILDREN WITH TORSIONAL ANOMALIES OF THE LOWER LIMB JOINTS USING POINT MAPPING TECHNIQUES

Dan B. Marghitu[1], Prasad Nalluri[1], M.C. Hobatho[2], R. Darmana[2], J.P. Cahuzac[3]
[1]Department of Mechanical Engineering, Auburn University, Auburn, AL 36849
[2]INSERM U305, Hotel Dieu, Toulouse
[3]CHU Purpan, Service d'Orthopedie Pediatrique, Toulouse

INTRODUCTION

In this study we used the techniques of nonlinear dynamics to analyze the stability of normal and pathological gait in children. We based the analysis on the assumption that a human at steady state locomotion can be represented as a nonlinear periodic system. Kinematic data for the lower limb joints were used to construct phase plane portraits and first return maps for the hip, the knee and the ankle joints. Anomalies in the joint rotations of pathological individuals were graphically depicted by comparing the phase plane portraits and first return maps. Using the Floquet theory, an index of dynamic stability was used to compare normal and pathological gait.

REVIEW AND THEORY

Human locomotion studies have an extensive application in the diagnosis and treatment of gait abnormalities and their methodologies have diverse origins. Researchers studied the kinematics and dynamics of gait using inverted pendulum models of the lower limbs.[1] Some studies focused on studying and developing control algorithms for human locomotion.[2] Another widely used approach was to study experimentally acquired kinematic measures that are characteristic to gait. Abnormalities resulting from pathological gait were detected by comparing plots of joint rotations of the pathological subject with those of the normal subject.[3] In recent years, researchers have tried to analyze gait and human motion using the theories of nonlinear dynamics. Phase plane portraits were used to study the locomotion of neurologically impaired and normal individuals.[4] Phase plane portraits and reverse phase plane portraits were used to describe multijoint coordination in complex human actions.[5] First return maps along with phase plane portraits were used to distinguish gait abnormalities in humans.[6] A scalar measure based on characteristic multipliers was used to compare the dynamic stability of post-polio and normal gait.[7] In the present study, we analyze the gait stability of normal children and children with pathological disorders of the knee and ankle. The analysis is based on the periodic motions that arise a result of human locomotion. The walking human being can be represented as a periodically forced nonlinear dynamical system, given by a set of n first order ordinary differential equations $\dot{\mathbf{x}}(t) = \mathbf{F}(\mathbf{x}, t)$, where $\mathbf{x}$ is a vector in the phase space $\Re^n$. The vector field $\mathbf{F}(., t) = \mathbf{F}(., t + T)$ is periodic in time with the period T. A set of solutions representing the walking patterns of the human would then be given by $\mathbf{x}(t) = \mathbf{x}(t + T)$. The stability of the periodic solutions can be studied by constructing phase plane portraits of the significant joints. The closed orbits that are obtained on the phase plane are stable if the neighbouring trajectories approach them asymptotically. The discrete Poincaré maps eliminate the additional factor of time and are obtained by inserting fictitious planes transverse to the trajectories in phase space at specific instants of the gait cycle. The motion achieved between each heel strike event of the same foot was defined as a gait cycle. Using the Floquet theory, the local stability of the critical points of these discrete maps were analyzed. The state vector $\mathbf{x}$ was defined as $\mathbf{x} = \{q_i, \dot{q}_i\}$, where q_i represents the relative rotations of the hip, knee and ankle joints and $\dot{q}_i$ represents the corresponding angular velocities. A discrete nonlinear map that represents the dynamics of the system was then given by $\mathbf{x}_{k+1} = \mathbf{f}(\mathbf{x}_k)$ where, $\mathbf{x}_k$, and $\mathbf{x}_{k+1}$ represent the state vector sampled at the Poincaré section (maximum knee flexion) during the k-th and the $(k+1)$-th gait cycles and $\mathbf{f}$ is the discrete mapping function. Linearizing the map about the equilibrium points gives $\mathbf{x}_{k+1} = \mathbf{J}\ \mathbf{x}_k$, where $\mathbf{J}$ is called the Jacobian and is a constant coefficient matrix. The eigenvalues of this matrix are called the Floquet multipliers and are less than unity for a stable system. Also, the behaviour of a stable system is dominated by the largest multiplier and hence it

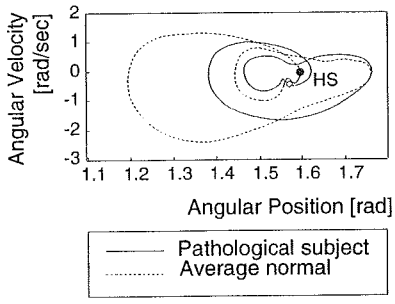

Figure 1: Phase Plane Portraits

can be used as a stability index to compare the gait of different subjects.

PROCEDURES

Kinematic data for the normal and pathological subjects were obtained by using a two dimensional motion analysis system. The joint angular rotations were numerically differentiated to obtain corresponding joint angular velocities. Phase plane portraits for each joint were obtained by plotting the joint rotations against the corresponding joint velocities. The Poincaré maps were defined at the instant of maximum knee flexion and were constructed by plotting the values of a joint rotation or velocity at one step with the same values obtained at the immediate next step. The Jacobian matrix was obtained by using curve fitting techniques and the Floquet multipliers were determined by computing the eigenvalues of this matrix.[6,7]

RESULTS

The phase plane portraits for all subjects were closed loops indicating a periodic motion. Comparison of the phase plane portraits for the normal and pathological subjects exhibited a significant difference in terms of both joint angular rotations and joint velocities for all pathological subjects (Fig. 1). The first return maps depicted similar discrepancies for the pathological subjects(Fig. 2). The Floquet multipliers for all subjects were found to be less than one in magnitude and the largest multiplier was defined as the stability index. It was observed that the stability indices of all the pathological subjects varied within a range of 0.55 to 0.78. These values were larger than the normal index of 0.48 indicating that the gait of the pathological subjects was less stable. The techniques used in this study provide a superior method of analyzing gait. The phase

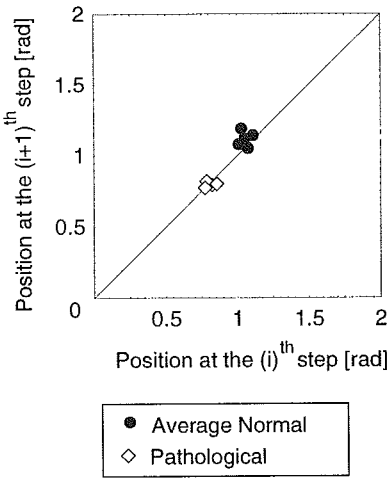

Figure 2: First Return Maps

portraits provide a direct correlation between the joint angular positions and their respective velocities. The first return maps provide a compact method of presenting the data at specific instants of the gait cycle. The stability index provides a quantitative measure of gait stability and can be used as an effective clinical analysis tool in conjunction with the above two methods.

REFERENCES

1. Apkarian J, Naumann S, Cairns B. *J Biomech* A three-dimensional kinematic and dynamic model of the lower limb, 22,143-155,1989.

2. Miyazaki F, Arimoto S. *Trans. Soc. Instrum. Control Eng* A control theoretic study on the dynamics of biped locomotion, 14,428,1978.

3. Cappozzo, *Human Movement Science* A. Gait analysis methodology, 3,27-50,1984.

4. Winstien CJ, Garfinkel A. *Journal of Motor Behaviour* Qualitative dynamics of disordered human locomotion: A preliminary investigation, 21,4,373-391,1989.

5. Scholz JP. *Human Movement Science* Organizational principles for the coordination of lifting, 12,537-536,1993.

6. Hurmuzlu Y et al. *J Biomech* Presenting joint kinematics of human locomotion using phase plane portraits and the Poincaré maps, 27,12,1495-1499,1994.

7. Hurmuzlu Y, Basdogan C. *J of Biomech Eng* On the measurement of stability in human locomotion, 116,30-36,1994.

VARIABILITY OF GAIT TIME-DISTANCE PARAMETERS

K.R. Kaufman, A. Lauer, H.G. Chambers, D.H. Sutherland
University of California, San Diego
Motion Analysis Laboratory, Children's Hospital, San Diego

INTRODUCTION

Human gait demonstrates cycle-to-cycle variability. A gait cycle is defined as foot contact to ipsilateral contact. This study quantifies the minimum number of cycles which are required to obtain a precise representation of a subject's gait during a testing session. 234 clinical studies from 165 subjects were evaluated. Two levels of error were considered. At least 6 to 9 gait cycles are needed to obtain temporal-distance data which is low in precision, whereas at least 20 to 29 gait cycles are needed to obtain more precise data, high in precision.

REVIEW

Gait analysis techniques can provide objective information to assess gait disorders. Humans demonstrate cycle-to-cycle variability in their gait patterns. Many laboratories graph two cycles of a subject's walking patterns on the same graph to assess the repeatability of the measurements. Other laboratories average several cycles to obtain the mean of several trials. It is important to know how many cycles need to be collected to represent the gait for a subject. The purpose of this study was to quantify the minimum number of gait cycles needed to obtain a precise representation of an individual's gait during a laboratory testing session.

PROCEDURES

The variability of gait time and distance variables in 234 gait studies was assessed. The sample population consisted of 165 clinical subjects with a mean age of 12.7 ± 10.2 years (range 2-64). Several of the subjects in the test group had repeat gait studies. Most (78%) of the test subjects had cerebral palsy. Kinematic data was acquired using a computer aided motion analysis system (VICON, Oxford Metrics, Ltd., Oxford, England). Each subject walked at a self-selected walking speed, along a six meter walkway. Trajectories of markers placed on the heel and fifth metatarsal head were used to track the motion of the feet during the gait cycle. The position of the markers, along with the camera speed, was used to calculate stride length, cadence, time, and velocity. Ten to twenty gait cycles were collected for each subject in a given gait testing session. A larger number of gait cycles was collected when the subject demonstrated more variability. The beginning and end of the gait cycles were identified using the foot contact patterns. The temporal distance parameters were calculated from the individual gait cycles. The mean and standard deviations of the spatial temporal parameters were computed for each gait study.

The minimum required number of gait cycles(n) to obtain accurate data for each gait study was calculated, based on the maximum allowable error (E), the estimated sample standard deviation (σ), and a desired confidence level of 95% $\left(t_{df,\frac{\alpha}{2}}\right)$. The formulation was as follows:

$$n = \left[t_{df,\frac{\alpha}{2}}\left(\frac{\sigma}{E}\right)\right]^2$$

Two scenarios of acceptable error (E) were utilized (Table 1). The high precision requirement represents a 5% error and the low precision represents a 10% error from the mean gait parameters for each time-distance parameter for a normal individual. The required number of gait cycles was calculated for each parameter and each subject. The number of gait cycles for each subject were tabulated and cumulative percentages were calculated.

Gait Parameter	Precision	
	High	Low
Stride Length (cm)	5	10
Cadence (steps/min)	7	14
Velocity (cm/sec)	6	12

Table 1. Maximum Allowable Error

RESULTS

The required number of cycles to obtain precise velocity data differed with the precision requirements (See figure). If high precision was required, 13% of the subjects studied would meet

the requirements with one gait cycle only.

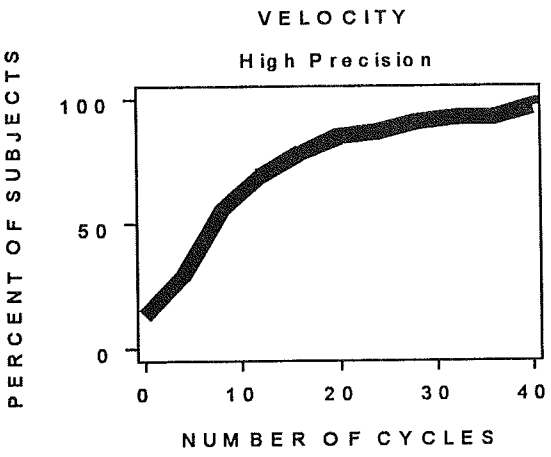

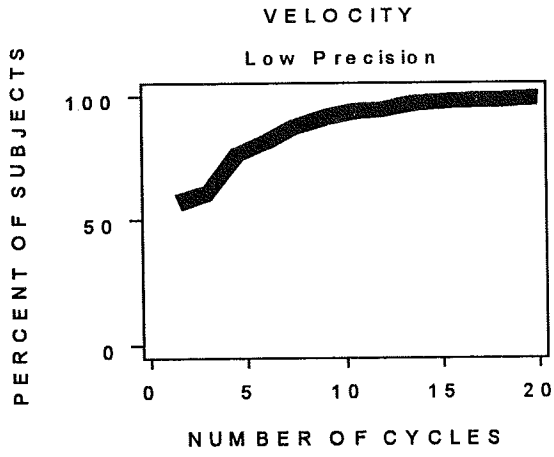

However, it would take 29 gait cycles to obtain highly precise data from greater than 90% of the subjects tested. Similarly, if lower precision was acceptable, 51% of the subjects tested would have obtained precise data if only one gait cycle was used. On average, at least 9 gait cycles were necessary to obtain data with acceptable limits from greater than 90% of the subjects. The conclusions for other time-distance gait parameters are similar. (Table 2).

Gait Parameter	Precision	
	High	Low
Stride Length (cm)	20	6
Cadence (steps/min)	21	7
Velocity (cm/sec)	29	9

Table 2. Number of Gait Cycles

DISCUSSION

Humans demonstrate movement variability. This variability may be increased in patients with pathological gait patterns, such as cerebral palsy, which comprised the majority of patients in this study. The tendency of human subjects to produce a variety of movement patterns on a given day adds an important source of variability that must be accommodated. Few studies have assessed the minimum number of walks needed to obtain a precise measurement. This study demonstrates that at least 6 to 9 gait cycles need to be averaged to obtain temporal-distance data which is low in precision, while at least 20-29 gait cycles are needed to obtain temporal-distance data which is more precise.

There are two potential sources of cycle-to-cycle variability. The patient could walk in a variable manner and/or there could be variability in the data reduction process. The variability of the data reduction process was checked by having three different individuals reduce data from the same patient. The rms error in the data reduction technique was 0.5 cycles for stride length and 0 cycles for cadence and velocity. Thus, the variability in the number of gait cycles reported in this study could be attributed to variability in the subject's gait pattern.

Studies on adult subjects during running indicate that 25 trials are required to produce reliable results (Devita et al., 1988). Kirkpatrick et al. studied variability in gait of children with cerebral palsy and reported no significant difference in variability whether the first three recordings or all five were used. The results of this study are similar to the Devita study. Knowledge of these requirements for obtaining reliable data are necessary to assure quality in clinical gait analysis.

REFERENCES

Devita P. et al. Intraday reliability of ground reaction force data. Hum Move Sci 7:73-85, 1988.
Kirkpatrick M. et al. Is the objective assessment of cerebral palsy gait reproducible? J Ped Orthop 14:705-708, 1994.

ACKNOWLEDGMENTS

Supported in part by NIH grants RO1-HD30150 and RO1-HD31476.

KNEE FUNCTION FOLLOWING ANTERIOR CRUCIATE LIGAMENT RECONSTRUCTION

D. E. Hurwitz, T.P. Andriacchi, P. Kopinski, C. Bush-Joseph, B. R. Bach Jr.,
Rush-Presbyterian-St. Luke's Medical Center
Department of Orthopedic Surgery, Chicago Illinois

INTRODUCTION

Subjects with anterior cruciate ligament deficiencies (ACLD) alter the manner in which they walk and perform athletic activities such as jogging, cutting and stopping (1, 2). More specifically decreases in the net external flexion moments during walking and jogging have been reported while increases in the net external extension moments during the more stressful athletic activities have been reported (1, 2). The objective of this study was to test the hypothesis that function during gait, jogging, cutting and stopping returns to normal following anterior cruciate ligament reconstruction (ACLR) with an autogenous patellar tendon reconstruction in patients with no patellofemoral pathology.

METHODS

Nineteen subjects with an autogenous patellar tendon reconstruction (age 27 $\pm$ 6 years) were tested along with 25 age matched normal subjects (25 $\pm$ 6 years). The knee kinematics and kinetics during gait, jogging, jogging and cutting and jogging and stopping on one leg were measured with an optoelectronic system and force plate (1, 2). All external moments were normalized to percent body weight multiplied by height (%BW * HT). At least 2 trials were collected on both sides for all activities and for walking 6 trials at self selected speeds of slow, normal and fast were collected.

To minimize the effect of walking and jogging speed on the associated kinetics, a representative trial at about the same speed for each of these activities was chosen. The average walking speed (1.1 $\pm$ 0.1 m/sec) and average jogging speed (2.8 $\pm$ 0.4) were not significantly different between the ACLR and normal groups ($p < 0.25, 0.94$).

The ACLR group was evaluated at a minimum of 8 months after reconstruction (22 $\pm$ 12 months) and all had less than 25% meniscal involvement at the time of surgery. At the time of the study none had significant patellofemoral complaints, evidence of knee flexion contractures or complaints of buckling or locking. The laxity of the ACLR side was similar to that of the contralateral side with an average side to side difference of 2 $\pm$ 2 mm. for 20 pounds and maximum manual (KT1000). The flexion and extension strength on the affected side was 94 $\pm$ 29% and 93 $\pm$ 32% of the unaffected side when measured at 60, 180 and 240 degrees/sec.(Cybex/KinCom).

Significant differences between the ACLR and normal group were identified using t-tests and a significance level of $\alpha = 0.05$.

RESULTS

During level walking the ACLR group did not have any of the abnormalities previously associated with subjects with an ACLD (1). The knee kinematics (minimum knee flexion, midstance knee flexion and knee range of motion) and peak external knee moments (flexion, extension, adduction,

internal rotation moments) were not significantly different between the normal and ACLR group (p>.05).

During jogging, however, the ACLR group did have significantly decreased knee flexion and internal rotation moments and a decreased midstance knee flexion angle as compared to normal group (p<.004, p<.034, p<.014) (Table I).

Table I: Peak Knee Flexion Moment During the Activities Tested (%BW * HT)

	Normal Group	ACLR Group	p value
Walking	2.6±1.3	2.4±1.6	0.64
Jogging	**14.3±2.4**	**11.0±3.5**	**.001**
Cutting	15.5±4.2	13.4±4.0	.145
Stopping	13.7±3.6	11.7±3.9	.114

Moreover, the ACLR subjects with at least a 10% loss of extension strength on the affected side as compared to the contralateral side had a significantly decreased knee flexion moment during jogging as compared to the ACLR subjects without a substantial extension strength deficit (p<.019) (figure 1).

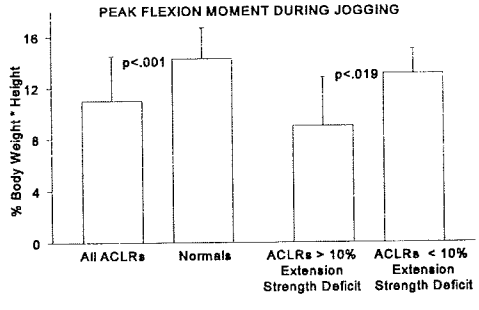

Figure 1: The flexion moment during jogging was significantly less in the ACLR group as compared to Normal. This moment was also significantly less among those ACLR subjects with at least a 10% loss in extension strength.

The increased knee extension moments seen in the ACLD subjects during athletic activities (2) were not present in the ACLR group. The external knee extension moments for the ACLR group were not significantly different from normal during jogging, cutting and stopping (p<.24, p<.47, p<.54).

DISCUSSION

Following ACL reconstruction gait returned to normal. The previously reported reduced knee flexion moments during gait (1) were no longer present in the ACLR group. This may be reflective of increased knee stability following ACLR. Following ACLR the need to minimize the anterior pull on the tibia through reduced quadriceps muscle activity would be lessened and thus the need for the reduced knee flexion moment during gait would be eliminated. This would also account for why the previously reported increased extension moments during the stressful athletic activities in the ACLD group (2) were not present in the ACLR group.

The knee flexion moment during jogging was still significantly less than normal and a similar trend was seen in the cutting and stopping activities. The decreased flexion moments during jogging reflected losses in extension strength.

REFERENCES

1. Berchuck, M. et al.: JBJS 72(A):871-77, 1990.
2. Andriacchi, T.P. Birac, D.: CORR 288:40-47, 1993.

ACKNOWLEDGMENTS

NIH AR39432

GAIT ADAPTATIONS BEFORE AND AFTER ACL RECONSTRUCTION SURGERY

P. DeVita[1], T. Hortobagyi[1], J. Money[1], M. Torry[2], K. Glover[2],
D. Speroni[2], J. Barrier[1], M. Mahar[1], J. Lochmann[2]
[1]Dept. of Exercise and Sport Science, East Carolina University, Greenville, NC
[2] Dept. of Physical Education, Southern Illinois University, Carbondale, Il

INTRODUCTION

Rehabilitated, ACL-injured individuals have increased hip extensor torque and hamstring EMG and decreased knee extensor torque and quadriceps EMG during stance in walking (2,4). The developmental process of these adaptations and factors that cause them are unknown. The purpose of the study was to compare kinematics and kinetics during walking as measured after injury but before surgery, one week after surgery, and three weeks after surgery in ACL-deficient and reconstructed individuals and healthy individuals.

REVIEW AND THEORY

It is the consensus that adaptations in ACL-injured gait are beneficial because they reduce anterior displacement of the tibia and therefore reduce stress on the knee joint while they also enable the subjects to perform the desired movement. (1,2,3,4,5). Although the final kinetic pattern for these people has been identified, neither the time course of its development nor the precise factors that cause or influence it are known. Consensus opinion is that the adaptations are caused by subconsciously learned, neuromuscular strategies due to the injury (1,2,4) but this hypothesis has not been directly tested. Other factors including rehabilitation protocol and use of a functional knee brace have been proposed as possible influences. To understand how various factors can influence the adaptations, it is necessary to know the developmental process of these learned movement strategies. The purpose of the study was to compare joint kinematics and kinetics during walking as measured 2 weeks after injury but before surgery, 1 week after surgery, and 3 weeks after surgery in ACL-injured and healthy individuals.

METHODS

Five ACL-injured (mean age: 19.2 yrs; mean mass: 72.3 kg) and 10 healthy (mean age: 20.9 yrs; mean mass: 65.8 kg) subjects were tested. Injured subjects had bone-patella-bone reconstruction using the central 1/3rd of the patellar tendon. All subjects gave informed consent according to University policy. AMTI force plate and 60 Hz video systems were used to measure the kinetics and kinematics of the stance phase of walking. ACL-injured subjects were tested three times: 2 weeks after injury but before surgery, 1 and 3 weeks after surgery. Joint position and velocity were calculated at the knee and hip joints of the injured limb. Magnitude of segmental masses and the mass center locations of the lower extremity along with their moments of inertia were estimated using a mathematical model and the individual subject's anthropometric data. Joint torques were calculated for each lower extremity through inverse dynamics. Extensor angular impulse during the initial half of stance was calculated from the knee and hip torque curves.

A quadratic trend analysis was used on the injured limbs to identify the developmental pattern in response to injury, surgery, and rehabilitation. Individual t-tests were performed between the control subjects and each of the three measurements of the injured limb to determine whether injured subjects' gait mechanics were different than those of healthy subjects. A .01 alpha level was used in both analyses.

RESULTS

The injured subjects' hip and knee were significantly more flexed at all test sessions compared to healthy controls (Table 1). Significant quadratic trends showed the surgical procedure increased flexion at both hip and knee joints and joint positions moved back toward presurgical values after 3 weeks.

Joint torques were different between the injured and healthy knees (Fig 1). The injured limb had extensor torque throughout stance before surgery and one week after surgery. The knee torque showed some recovery towards a normal pattern in midstance three weeks after surgery but the flexor phase was still absent. Significant trend for extensor impulse during the first half of stance indicated that the surgery initially caused the subjects to exert less impulse and the impulse was increased after three weeks. Extensor impulse at the hip was similar in injured and healthy limbs before surgery. A significant trend for impulse indicated that there was an initial decrease in impulse followed by a return toward presurgical values.

DISCUSSION

Primary result was the existence of an extensor torque in the injured knee throughout most of stance in pre- and post-surgical conditions. This pattern has not been previously identified in any self-selected walking gait and it is in contrast to the final adaptation of the net flexor torque during stance observed in fully rehabilitated ACL-deficient patients and termed, "quadriceps avoidance gait," (2). Present subjects were two weeks post injury on the first test indicating that the development of a quadriceps avoidance gait requires extensive time and occurs only after many gait cycles are completed. The lengthy developmental process of the adaptation to injury also suggests that factors other than innate, neuromuscular responses, may provide some impetus toward learning the new movement strategy. For example, rehabilitation programs emphasize strengthening the hamstrings which would lead to decreasing the extensor torque at the knee and so contribute to the adaptation. Current results present the first indication that the developmental period for these adaptations is relatively long and they therefore suggest that factors other than self-selected neuromuscular responses may influence the development of the adaptations.

The extensor torque past midstance in the injured knee was necessary to support the injured subjects. These people moved in a more flexed and crouched pattern than the healthy subjects which created an increased external flexor load on the knee. The existence of the extensor torque during most of stance in the pre-surgical and one week post surgical conditions indicated the patients were at increased risk of further injuring the knee or recently reconstructed ligament. This result suggests that rehabilitation programs include quadriceps strengthening before surgery to prepare for the increased, post-surgical demands on this muscle.

REFERENCES

1. Andriacchi, T. & Birac, D. Clin. Orthop. & Rel. Res. 288, 40-47, 1993.
2. Berchuck, M., et al. J. Bone Joint Surg. 72-A, 871-877, 1990.
3. DeVita, P., et al. Med. Sci. Sports & Exerc. 24, 797-806, 1992.
4. Shiavi, et al. J. Orthop. Res. 10, 226-236, 1992.
5. Sinkjaer, T. et al. J. Electromyo. Kines 1, 209-217, 1991.

ACKNOWLEDGMENTS

This work was supported by a grant from the School of Health and Human Performance, East Carolina University.

Table 1. Means values.

	Injured Limb			Healthy
	Before	1 wk.	3 wks	Controls
Average Position				
Hip	-9.6*	-14.8*	-12.0*†	-4.5
	(1.1)	(1.7)	(1.1)	(1.9)
Knee	-23.7*	-28.8*	-24.1*†	-17.8
	(3.0)	(1.6)	(3.2)	(2.0)
Extensor Angular Impulse				
Hip	8.7	7.2	10.1†	9.6
	(2.4)	(2.3)	(1.8)	(1.3)
Knee	4.5	3.8	4.2†	4.9
	(1.4)	(1.6)	(1.5)	(1.3)

Position in degrees; Impulse in N.s; Sd in (); * t-test $p<.01$; † trend analysis $p<.01$.

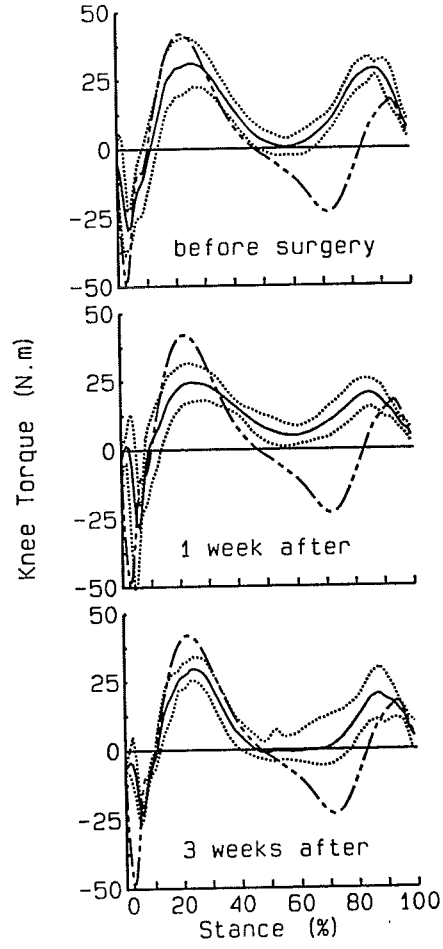

Fig 1. Knee torque during stance. Solid & dot are mean +/- sd from injured sample. Dash is mean of healthy sample. + values are extensor torques.

FATIGUE IN A SIMULATED BASKETBALL TASK ON TWO PLAYING SURFACES

J. Streepey[1], S. Sudarsan[2], M. Gross[1], B. Martin[2]
[1]Department of Movement Science, University of Michigan, Ann Arbor, MI 48109
[2]Department of Industrial and Operations Engineering, University of Michigan, Ann Arbor, MI 48109

INTRODUCTION

Overuse or overexertion phenomena resulting in tendinitis, sprain, strains and stress fractures of the lower extremity are common among basketball players (McClay et al., 1994). Differences in muscle activation patterns have been observed following fatigue in basketball movements (Nyland et al., 1994), and muscle fatigue may be a precursor to these traumatic disorders. Characteristics of the playing surface can affect musculoskeletal loading and muscle fatigue during a basketball game. Mechanical characteristics of sports surfaces may be associated with sports injuries (Nigg, 1993). In this study, we examined differences in muscle fatigue and perceived fatigue in subjects performing a simulated basketball task on a new playing ("smartcell") surface fabricated from recycled material and on a conventional wood floor. Preliminary results indicated that subjects perceived less fatigue in their legs and experienced less muscle fatigue in their ankle plantarflexors after performing the simulated basketball task on the new floor than on the conventional wood floor.

REVIEW AND THEORY

Objective measures are needed in order to differentiate the response of the human neuromuscular system to different playing surfaces. Muscle fatigue can provide physiological information about the cumulative effects of activities performed on playing surfaces and thus can be used as an indicator to characterize these surfaces. Electromyography (EMG) can be used to indicate fatigue during maximum contractions (Enoka and Stuart, 1992).

The purpose of this study was to determine the differences in muscle fatigue and perceived fatigue in subjects performing a simulated basketball task on two different playing surfaces, "smartcell" and a conventional wood floor.

PROCEDURES

Twenty-two male subjects with basketball experience were recruited from colleges and community centers in the Seattle area. All subjects were recreational basketball players, and some (n=6) participated on intercollegiate basketball teams. None of the subjects had experience running or jumping on the smartcell floor prior to the testing day. Each subject was tested on both the smartcell and wood floors. Each test was conducted on a different day, so subjects had a minimum of 24 hours of rest between tests. The order of testing was varied, so that about half of the subjects were first tested on the smartcell floor , and the other subjects were first tested on the wood floor. All subjects wore the same type of basketball shoe during the tests. Prior to each test, bipolar electrodes were placed on the skin above the vastus lateralis and soleus. Subjects sat in an instrumented chair in a standard position (knee and ankle angles at 90 deg) and performed knee extension and ankle plantarflexion maximum voluntary contractions (MVCs). Muscle activity and isometric force were recorded simultaneously. After the MVC tests, subjects completed a simulated basketball task on either the smartcell or wood floor. The task consisted of completing 20 laps of a 82.3 m course with a total of 80 cuts, 20 maximum height jumps, and a 1.02 mile run. Immediately after completing the course, subjects again performed the MVC tests and evaluated their perceived fatigue of lower back, upper legs, and lower legs using a visual 10 cm analog scale. Each anchor point corresponded to "no fatigue" and "extreme fatigue."

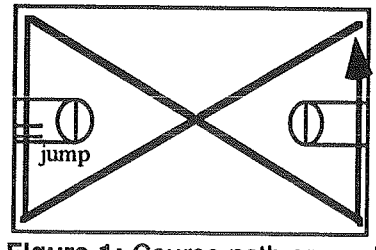

Figure 1: Course path on each playing surface.

Force and EMG data during MVC tests were amplified, filtered, and sampled at 1000 Hz. Maximum knee extension and ankle plantarflexion force and maximum vastus lateralis and soleus RMS EMG values were calculated. Perceived fatigue for each body part was scored as the distance marked between "no fatigue" and "extreme fatigue" on the visual analog scale. Repeated measures ANOVA was used to detect differences between floors with significance

level set at $p<0.05$. Preliminary results are reported here for 13 subjects.

RESULTS

Subjects were similar in age (20.6±3.0 yrs), height (1.8±0.05 m), and weight (760.5±76.4 N). Perceived fatigue on the smartcell floor was significantly less than on the wood floor for the lower legs ($p<0.011$) and the upper legs ($p<0.004$) (Fig. 1). Compared to the wood floor, perceived fatigue on the smartcell floor was reduced by 16% for the lower leg and 27% for the upper leg. Perceived fatigue also tended to be less for the lower back on the smartcell floor but the difference was marginally significant ($p<0.054$).

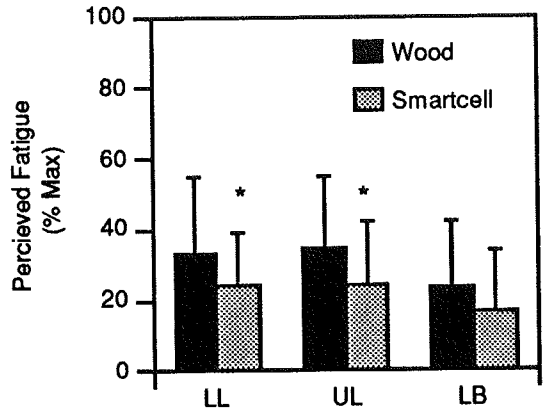

Figure 1: Perceived fatigue on each playing surface for the lower legs (LL), upper legs (UL), and lower back (LB).

Maximum ankle plantarflexion force did not change after running and jumping on the smartcell floor but was significantly reduced after running and jumping on the wood floor ($p<0.017$) (Fig. 2). Maximum knee extension force was not different after running and jumping on either the smartcell or wood floors.

The type of floor did not affect maximum RMS EMG activity for either muscle. However, maximum EMG activity was reduced at the ankle after the simulated basketball task on both smartcell ($p<0.014$) and wood ($p<0.002$) floors. Maximum vastus lateralis RMS EMG activity was reduced but did not depend on type of floor.

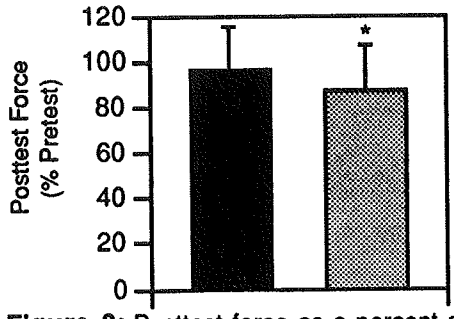

Figure 2: Posttest force as a percent of pretest force for ankle plantarflexion MVC.

DISCUSSION

The simulated basketball task in this study was sufficient to induce both perceived fatigue and muscle fatigue in the subjects. Compared with a professional basketball game (McClay et al., 1994), the distance run in the simulated task was about 50% of the distance run and the number of jumps was about 29% of the number of jumps in a professional basketball game.

Preliminary results indicate that subjects perceived less fatigue on the new playing surface than on the conventional wood floor. The objective measures of fatigue were consistent with the subjective data, since subjects were able to sustain force production in the ankle plantarflexors better after exercising on the new surface than on the conventional wood surface. These results suggest that the new surface may have beneficial characteristics for human performance during basketball-related activities. More studies are needed to determine if the reduction in fatigue experienced by subjects is associated with a decreased risk for fatigue-related injury.

REFERENCES

Enoka, R.M., Stuart, D.G. J. Appl. Physiol., 72, 1631-1648, 1992.

McClay, I.S. et al. J. Appl. Biomech.,10, 222-234, 1994.

Nigg, B.M. Aspects of Sports Shoes and Playing Surfaces, (pp. 11-23), University Printing, 1983.

Nyland, J.A. et al. J. Orthop Sports Phys. Ther., 20, 132-137, 1994.

ACKNOWLEDGMENTS

Support was provided by the Clean Washington Center and Satech Corp. Footwear was provided by Adidas.

MINIMIZATION OF A JOINT MOMENT COST FUNCTION AND THE PREFERRED CYCLING CADENCE

Anthony P. Marsh[1], Philip E. Martin[2], David J. Sanderson[3]
[1]Dept. of Health and Physical Education, California State University, Sacramento, CA 95819-6074
[2]Dept. of Exercise Science and Physical Education, Arizona State University, Tempe AZ 85287-0404
[3]School of Human Kinetics, University of British Columbia, Vancouver, Canada V6T 1Z1

INTRODUCTION

Eight experienced cyclists (C), eight well-trained runners (R) and eight less-trained noncyclists (LT) were selected based on a questionnaire and a bicycle VO_{2max} test to assess the influence of cycling experience, power output, and cadence on lower extremity joint moments. Manipulations of cadence [50, 65, 80, 95, 110 rpm, preferred cadence (PC)] at constant power output (C and R: 100, 150, 200, 250 W; LT: 100, 150 W) were conducted while video and pedal force data were collected. A 2-D inverse dynamics analysis was used to compute net joint moments at the hip, knee, and ankle. There was close agreement between the cadence at which the sum of the average absolute joint moments at the hip, knee, and ankle was minimized (mechanically optimal cadence) at each power output and the PC regardless of cycling experience. Further, the mechanically optimal cadence increased with increases in power output. Regardless of cycling experience the average absolute joint moments did not differ at any power output. The results of this experimental study corroborate earlier modeling work. Cursory examination of the data suggest that a mechanical variable may be associated with preferred cadence selection.

REVIEW AND THEORY

The results of studies reporting optimal cadences based on minimization of aerobic demand (55-65 rpm; e.g. Böning et al., 1984; Coast et al., 1985; Marsh et al., 1993; Seabury et al., 1977) have shown poor agreement with the cadences of 90-100 rpm generally preferred by experienced cyclists during steady-state submaximal cycling (Marsh et al., 1993). However, Hull et al. (1985) speculated that a cadence may exist at which the total hip joint moment is minimized and therefore that a cadence exists which minimizes the net joint moments of the lower extremity. Redfield et al. (1986) and Hull et al. (1988a), using a computer model, found that a cadence within the range of 95 to 105 rpm minimized the sum of the average absolute hip and knee moments during 200 W cycling. Thus, minimization of a mechanical variable, the net joint moment, may be associated with preferred cadence selection during cycling.

In their computer models, Hull and colleagues linearly scaled the normal and shear components of the pedal force so that power remained constant as cadence was manipulated. However, McLean et al. (1991) concluded that this technique did not accurately describe the changes in experimental pedal force profiles. This result raises the possibility that Hull and colleagues interpretations of the relationship between cadence and net joint moments may have been confounded.

The question of whether or not the lower extremity net joint moments are minimized at an individual's preferred cadence remains unresolved, particularly since previous modeling studies have not assessed preferred cadence. Further, direct comparisons of joint moment cost functions in cyclists and noncyclists may provide additional insight into the differences in cadence selection often observed between these groups. The purpose of this study was to test the hypotheses that: 1) the cadence at which the sum of the average absolute net hip, knee, and ankle joint moments is minimized is the same as the preferred cadence for all groups; 2) as power output increases the cadence at which the sum of the average absolute net hip, knee, and ankle joint moments is minimized increases; and 3) cyclists will exhibit lower average absolute net joint moments compared to runners and less-trained subjects. The cadence at which the moment-based cost function is minimized will be termed the "mechanically optimal" cadence.

PROCEDURES

Eight experienced cyclists (VO_{2max}=70.1±4.0 ml·kg^{-1}·min^{-1}), eight well-trained runners with no cycling experience (72.9±2.3 ml·kg^{-1}·min^{-1}) and eight less-trained noncyclists (45.4±2.5 ml·kg^{-1}·min^{-1}) were selected based on a questionnaire and a bicycle VO_{2max} test. Noncyclists were classified as individuals who did not use a bike as a training mode or for daily commutes longer than 15 min. A Velodyne trainer (Schwinn Corp., Chicago, IL) was used to control power output in all tests.

To determine preferred cadence, trained subjects rode for 8 min at 100, 150, 200, and 250 W, while the less-trained group rode at 100 and 150 W. Cadence was recorded every 15 s. Preferred cadence was calculated as the average cadence during the final 6 min at each power output.

Manipulations of cadence at constant power output were conducted while video (60 Hz) and pedal force data (120 Hz) were collected synchronously. A potentiometer and optical encoder were used to measure pedal and crank angle, respectively. Power outputs were the same as those used for preferred cadence determination. Subjects pedaled at six randomly presented cadences (50, 65, 80, 95, 110 rpm, and preferred cadence). Coordinate data corresponding to the 5 s of force sampling were

generated. After smoothing (Butterworth digital filter; film, 4-5 Hz; force, 10 Hz) the kinematic and kinetic data were combined in a standard 2-D inverse dynamics analysis to compute the net joint moments at the hip, knee, and ankle.

The joint moment cost function provided a single value that represented the sum of the average absolute joint moments at the hip, knee, and ankle for each cadence and power output. Based on previous research suggesting a quadratic relationship between the cost function and cadence (Redfield et al., 1986) the joint moment cost function for the five fixed cadences at a particular power output were fit with a 2nd order polynomial. This polynomial was then differentiated and set equal to zero to determine the mechanically optimal cadence.

Paired t-tests were used to compare the cadences at which the cost function was minimized to the preferred cadence at each power output. A 3 (group) x 2 (power output) x 5 (cadence) ANOVA with repeated measures on the last two factors was conducted to determine differences in the average absolute joint moment data.

RESULTS

There was close agreement between the mechanically optimal cadence at each power output and the preferred cadence regardless of cycling experience, supporting the first hypothesis (Table 1).

		Cyclists	Runners	Less-Trained
100 W	PC	95.6 (10.9)	92.0 (7.7)	78.2 (14.4)
	MO	85.8 (9.2)	86.9 (11.7)	86.3 (15.6)
150 W	PC	94.6 (10.6)	93.1 (7.0)	69.9 (10.9)
	MO	96.7 (9.6)	91.4 (9.4)	91.8 (12.4)
200 W	PC	93.6 (8.4)	92.1 (8.2)	
	MO	100.9 (7.2)	96.0 (8.5)	
250 W	PC	90.7 (10.2)	91.7 (10.2)	
	MO	94.4 (5.6)	97.8 (8.8)	

Table 1: Preferred (PC) vs. Mechanically Optimal (MO) cadences (rpm) for cyclists, runners and less-trained subjects. Mean (SD)

The second hypothesis, (i.e., that cadences which minimize the cost function increase with increases in power output), was also supported. In the three group analysis the mechanically optimal cadence was significantly higher at 150 W (93.3 ± 10.4 rpm) than at 100 W (86.3 ± 11.9 rpm) [F (1, 21 = 11.89, p = .002]. This response was common to all three groups [F (2, 21) = .12, p = .891]. Results were similar for the two-group analysis across the four common power outputs (cyclists vs. runners).

Hypothesis three, (i.e., the average absolute joint moments of cyclists are less than those of runners and less-trained subjects), was not supported. The average absolute joint moments did not differ at 100 and 150 W regardless of cycling experience [F (2, 21) = 1.07, p = .362]. This result was repeated in the analysis of the cyclists and runners at 100, 150, 200, and 250 W.

DISCUSSION

The data of the present study corroborate earlier work (Patterson et al., 1990; Sanderson, 1991; McLean et al., 1991) which showed that horizontal and vertical components of the pedal force do not scale linearly with changes in cadence at constant power. However, the cost function results of this study agree with previous modeling work and suggest that net moments about the ankle, knee, and hip are not especially sensitive to the linear scaling assumption.

The results suggest that a composite of the net joint moments is associated with the preferred cadence and thus, that a mechanical variable may play a role in preferred cadence selection. The notion that a mechanical variable may be given a higher priority than aerobic demand in the selection of a rate of movement as proposed by Redfield et al. (1986) has been strongly questioned (Kram, 1987). Kram, citing Hagberg et al. (1981) argued that mechanics were dictated by metabolic cost. While a strong relationship exists between the preferred and metabolically optimal rate of movement for gait, this does not appear to be the case in cycling. Marsh et al. (1993) showed that the most economical cadence was significantly less than the preferred cadence of experienced cyclists and highly fit runners.

While it is tempting to conclude that the body is attempting to minimize net joint moments during cycling other explanations should be considered. It is possible that the close match between the mechanically optimal cadence based on joint moments or muscle stresses and the preferred cycling cadence found in this study and by Hull et al. (1988a), Hull et al. (1988b) and Redfield et al. (1986) may simply be indicative of an underlying mechanism(s), e.g., mechanical properties of muscle under dynamic conditions, motor unit recruitment strategies.

REFERENCES

Böning, D. et al. Int. J. Sports Med, 5, 92-97, 1984.
Coast, J. R. et al. Eur. J. appl. Physiol. 53, 339-342, 1985.
Hagberg, J. M. et al. J. Appl. Physiol, 51, 447-451, 1981.
Hull, M. L. et al. J. Biomech, 21, 839-849, 1988a.
Hull, M. L. et al. Int. J. Sport Biomech, 1, 1-21, 1988b.
Hull, M. L. et al. J. Biomech, 18, 631-644, 1985.
Kram, R. J. Biomech, 20, 554, 1987.
Marsh, A. P. et al. MSSE, 25, 1269-1274, 1993.
McLean, B. D. et al. 13th ISB Congress, Perth, 1991.
Patterson, R. P. et al. MSSE, 22, 512-516, 1990.
Redfield, R. et al. J. Biomech, 19, 317-329, 1986.
Sanderson, D. J. J. Sports Sci, 9, 191-203, 1991.
Seabury, J. J. et al. Ergonomics 20, 491-498, 1977.

MODIFICATIONS IN JOINT KINETICS DURING STOP AND GO LANDING MOVEMENTS UNDER FATIGUED AND NON-FATIGUED CONDITIONS

J. L. McNitt-Gray, J. P. Eagle, S. Elkins, and B. A. Munkasy
Biomechanics Research Laboratory
University of Southern California
Los Angeles, CA 90089-0652

INTRODUCTION

The large reaction forces (3.5 to 14 times body weight) encountered during landings has been associated with the high incidence of injury associated with landing activities (NCAA, 1986, 1990). However, methodological limitations associated with load distribution and tolerance of anatomical structures, have prohibited development of a clear-cause effect relationship between load and injury (Nigg & Bobbert, 1990). Examination of mechanisms athletes use to attenuate the reaction forces experienced during landings under realistic practice and competitive conditions may assist in establishing a causal relationship between load and injury.

In this study, the intended movement following a landing and the level of fatigue were hypothesized to influence mechanics and loading characteristics of landings performed by female collegiate basketball players. This hypothesis was tested by examining reaction force characteristics, joint kinetics, and muscle activation patterns between three realistic rebounding movements: land and stop (LS), land and go (LG), and land and go under moderately fatigued conditions (LGF). All three tasks required visual interaction with a basketball suspended over head.

PROCEDURES

Collegiate female basketball players (n=7) volunteered to serve as subjects. During data collection, subjects were asked to land three different rebounding tasks (LS, LG, LGF) using their own self-selected landing strategy. LS and LG tasks were blocked and randomized between subjects. All LGF tasks were performed as the final task of the data collection session. The basketball players performed the LS task by jumping from a stationary position on the floor, palming the center of a suspended basketball located 0.41 m above their stand and reach height, and landing on a force plate. During LG tasks, each subject repeated the LS movement and then immediately performed a second vertical jump while reaching for a second ball located at 90% of the individual's preseason maximum vertical jump and reach height. During the LGF tasks, moderate fatigue specific to jumping was induced immediately prior to the performance of the LG task by requiring the subject to perform maximum vertical jumps once every three seconds, until they were unable to obtain 80% of their maximum vertical jump and reach height.

Reaction forces measured at the shoe-plate interface were quantified at 800 Hz (Kistler force plates). Sagittal plane kinematics were recorded simultaneously using high speed video (200 fps; NAC Motion Analysis System). Activity of the soleus (SO), medial gastrocnemius (MG), vastus medialis (VM), vastus lateralis (VL), rectus femoris (RF), gluteus maximus (GM), and semitendinosis (ST) were monitored using surface electrodes (1600 Hz, Beckman silver-silver chloride electrodes, Differential amps, Data, Inc.). Location of the center of pressure relative to the feet was determined by locating the force plate in the kinematic reference system. Each coordinate of the body landmarks (Zatsiorsky et al., 1987) were digitized (Peak Performance, Inc.) and filtered using a fourth order Butterworth Filter (Saito & Yokoi, 1982) using a cut-off frequency determined by Jackson (1979). The EMG signals from each muscle were processed as specified by the International Society of Electrokinesiology (ISEK, 1985) using high and low pass filters, rectified, normalized within muscle, and integrated during intervals prior to and during the landing. Synchronized kinematic and reaction force data were used to calculate the net joint forces and moments for the ankle, knee, and hip of the leg closest to the camera using Newtonian mechanics. Significant differences in normalized kinematics, reaction forces, joint kinetics, and EMG integrated over 25 ms bins (IEMG) were compared between tasks using within subject analysis of variance techniques ($p< 0.05$).

RESULTS AND DISCUSSION

The small variance and absence of significant differences in vertical velocity of the total body center of mass at contact between trials and subjects confirmed the experimental tasks constraints were successful in minimizing differences in vertical velocity at contact. Reaction force and net joint moment characteristics observed in this study were similar to those observed by Devita and Skelly (1992) and McNitt-Gray (1991). Within subject observations indicated, two of seven subjects demonstrated consistent increases in peak vertical force with fatigue and five of seven subjects demonstrated greater side-to-side differences in peak vertical reaction forces with fatigue. Significant differences in time to resultant peak vertical forces were also observed between LS and LG tasks. During the propulsive phase of the go movements (LG, LGF), the reaction force impulse and

integrated muscle activity were more pronounced than during the LS tasks (Figure 1).

Muscle activation patterns (IEMG) during landing tended to be consistent within subjects over the majority of trials. After accounting for a 50 ms electromechanical delay, the IEMG corresponded to the net joint moments (Figure 1). Activity of the MG was observed prior to contact. Activity of the RF, VM, VL were also observed together with knee extensor net joint moments. During the period when the knee and hip demonstrated extensor net joint moments, GM and RF activity were observed together and the ST tended to be more active in the LGF tasks than in the LS and LG tasks. Activation of biarticular muscles observed during periods where adjacent joints demonstrated opposite directions in net joint moment power, create the potential for energy transfer (Prilutsky & Zatsiorksy, 1994).

From these data, movements performed following landings do not significantly loading characteristics during the landing phase. Inducing moderate fatigue tended to increase the variability of loading characteristics. Effective coupling and loading implications during the transition between the landing phase and the initiation of the go movements requires further investigation.

REFERENCES

Devita, P. & Skelly. MSSE, 24, 108-15. 1992.

ISEK Standards, 1985.

Jackson, K, IEEE Trans Biomed. Eng, 26, 122-4, 1979.

McNitt-Gray, J., J of Biomech., 26, 1037-46, 1993.

NCAA Injury surveil. System, 1986, 1990.

Prilutsky, B.I. & Zatsiorsky, V. M., J. Biomech, 27(1), 25-34, 1994.

Saito, S., & Yokoi, T. Bull. of Hlth & Sport Sci, U of Tsukuba, 5, 201-206, 1982.

Zatsiorsky, V., Seluyanov, V., & Chugunova, L.G. Contemp. problems of biomech, 272-289, 1988.

ACKNOWLEDGMENTS

This project was funded in part by the NCAA. Basketball shoes were generously provided by Converse. The authors would like to thank members of the USC Basketball program, Michelle Welch, Jacki Heino, Terry Smith, Dawn Irvine, and the undergraduate research assistants in the USC Biomechanics lab for their assistance with this project.

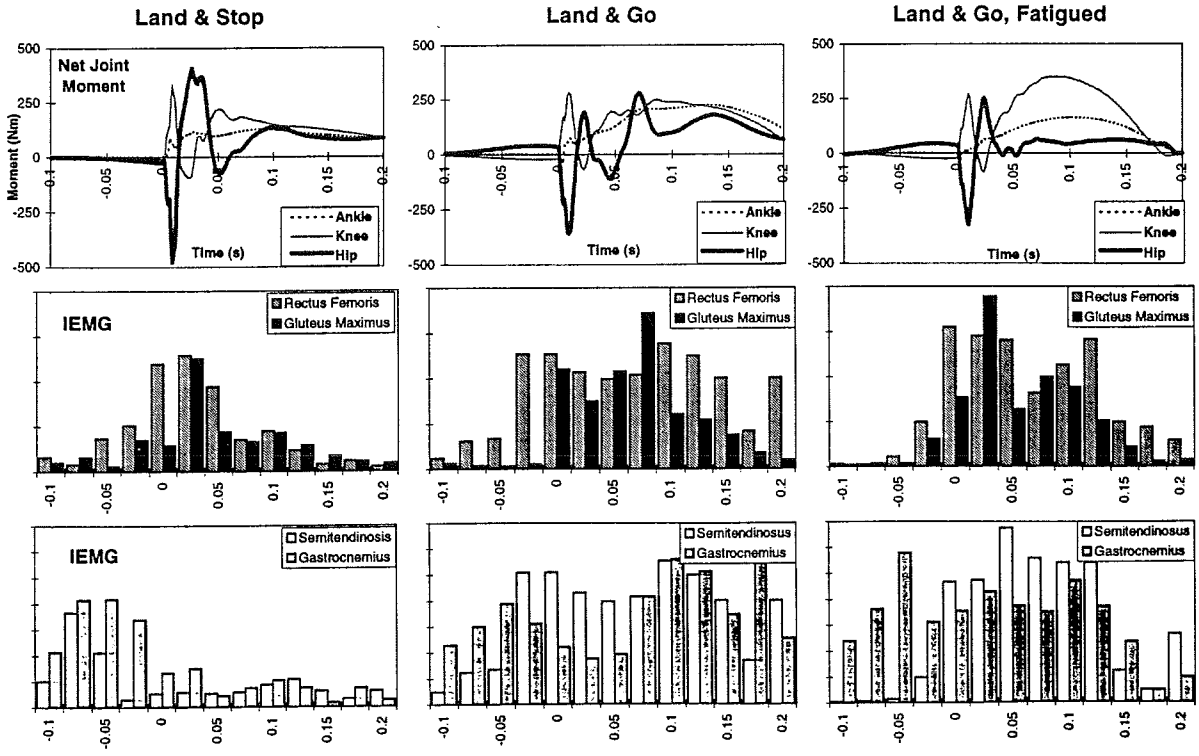

Figure 1. Representative ankle, knee, and hip net joint moments (+/- 500Nm) and IEMG of lower extremity muscles of a representative subject during Land and Stop (LS), Land and Go (LG), and Land and Go under moderately fatigued conditions (LGF).

MAXIMUM ANAEROBIC POWER AND GENDER DIFFERENCES IN RELATION TO THE SQUAT AND POWER CLEAN EXERCISES

J. Abendroth-Smith[1], Kim Sword[2]
[1]Department of HPER, Utah State University, Logan UT 84322
[2]Athletic Department, Utah State University, Logan UT 84322

INTRODUCTION

The purpose of this study was to determine whether isotonic back squats or isotonic power cleans were a better predictor of max. anaerobic power, as measured by vertical jump performance and vertical force measurements, and if differences existed between gender.

REVIEW AND THEORY

An athlete's ability to produce high amounts of power forcefully and quickly correlates highly with success in sport (Poidomoni, 1991). Anaerobic power is defined as the exertion of force through a given distance in as short a time as possible (Beckenholdt & Mayhew, 1983). Anaerobic power has become a key ingredient in successfully competing in sport (Kraemer & Fleck, 1987), so there is a need to find ways to improve anaerobic power safely and efficiently.

Two popular modes for increasing lower body strength and power are the isotonic parallel squat and the isotonic power clean (Chandler & Stone, 1991; Enoka, 1979). Although these training modes are of vital importance to trainers and coaches, both of these techniques have notable risks of injury even when being performed properly. It would be advantageous to find the best predictor of maximum anaerobic power (MAP), thereby limiting the injury problems many athletes face today.

The purpose of this research was to investigate slow isotonic back squat performance compared to fast isotonic power clean performance as predictors of the max. anaerobic power of 18-21 year-old female and male athletes.

PROCEDURES

The subjects in this research consisted of a convenience group of 18-21 year-old male and female Division One college athletes. All athletes were involved with varsity sports (gymnastics, track, volleyball, basketball, and football) but not in-season at the time of testing. All had been training for at least ten weeks with a collegiate strength staff on back squat and power clean lifts and had no previous injuries detrimental to performance on the lifts. Participants all signed informed consent forms.

Independent variables included the lift being performed (i.e., back squats or power cleans) and gender. The max. on each lift was determined using a three-repetition protocol. Proper form was used on all lifts (e.g., parallel back squats and the full catch on the power clean).

Participants performed 10 vertical counter-movement jumps, with height of jump, peak vertical force, and the time-to-peak vertical force, as measured via a force plate (Bertec force plate, Model 4060A) calibrated to standard specifications, being the variables recorded. Data were collected and filtered at a rate of 500 Hz. Multiple regressions were calculated between the subjects' normalized lift max. and their scores for peak force, height, and time-to-peak force. These analyses were conducted to determine the predictability of MAP by the power clean and back squat.

RESULTS AND DISCUSSION

For all subjects, multiple regression coefficients were strongest for associations between peak vertical force, time to peak vertical force, and jump height to the power clean scores (Table 1).

Table 1. Multiple Regression Coefficients for All Subjects: Squat or Power Cleans with Three Dependent Variables.

Lift	MR coefficient	Probability
PCleans	$r = .947$ * $r^2 = .897$	$F = 37.7$ $p < .0001$
Squats	$r = .354$ $r^2 = .125$	$F = .621$ $p < .613$

df = 17; * statistically significant at < .05 level

The correlation between lift performances (squats vs. power cleans) was fairly weak ($r = .291$). This served as an indication that good squat performance does not necessarily translate to good power clean performance (Figure 1).

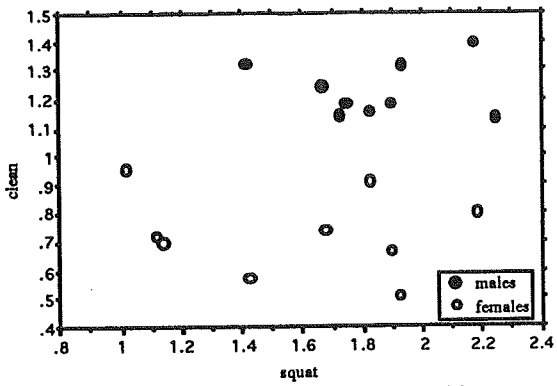

Figure 1. Squat-Power Clean Relationship (r = .291).

Although the better vertical jump performers were more proficient at performing the power clean lift, the strong correlation of r=.947 is misleading, as shown in Figure 2. The linearity of the scores come from the difference in jump performance between gender.

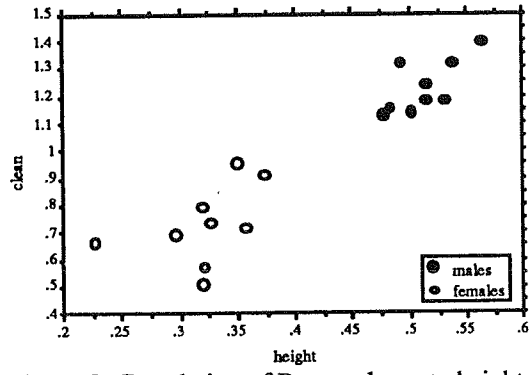

Figure 2. Correlation of Power cleans to height jumped (r = .932).

When examining the groups by gender, no significant differences were noted between the types of lifts and their correlation with the jump variables (Table 2). However, different trends were noted between gender. Women demonstrated much stronger correlations for the power clean scores and the jump variables, while the men demonstrated only slightly stronger correlations for the squat scores and the jump variables.

These research findings indicate that power clean performance is a better predictor of MAP than back squat performance for women, but not necessarily so for men. Hence, caution is urged when collapsing across gender. Replication is recommended to establish the reliability and generalizability of these findings.

Although the findings from one study do not provide evidence of causality, if the findings are replicable, coaches and trainers may have useful information regarding the strength/power modality yielding the best training adaptations needed for success in a highly anaerobic sport. The results of this research give coaches and trainers a better idea about utilizing back squats and power cleans for exercise prescriptions for their athletes and to not necessarily use the same prescription for men and women.

Table 2. Comparison of Multiple Regression Coefficients By Gender for Squat or Power Cleans with Three Dependent Variables.

Females		Males	
P.Cleans	r = .674	P.Cleans	r = .746
Squat	r = .450	Squat	r = .768

df = 7; no sig. differences found

REFERENCES

Beckenholdt, S.E., & Mayhew, J.L. (1983). Specificity among anaerobic power tests in male athletes. Journal of Sports Medicine, 23, 326-332.

Chandler,T.J., & Stone, M.H. (1991). The squat exercise in athletic conditioning: A review of the literature. National Strength and Conditioning Association Journal, 13(5), 52-29.

Enoka, R.M. (1979). The pull in Olympic weightlifting. Medicine and Science in Sports and Exercise, 11(2), 131-137.

Kraemer, W.J., & Fleck, S.J. (1987). Designing resistance training programs. Champaign, IL: Human Kinetics Books.

Poidomoni, M. (1991). Analysis of the countermovement vertical jump. Unpublished Masters Thesis: Western Michigan University.

ACKNOWLEDGMENTS

The authors wish to acknowledge and thank Bertec Force Plates for their support and also the Athletic Dept. and athletes of Utah State University for their help and support.

ELECTROMYOGRAPHIC ANALYSIS OF TWO RACING WHEELCHAIR PROPULSION TECHNIQUES

John W. Chow[1], Tim A. Millikan[2], Les G. Carlton[1], Martin I. Morse[2]

[1] Department of Kinesiology and [2] Division of Rehabilitation Education Services, University of Illinois at Urbana-Champaign, Urbana, IL 61801

INTRODUCTION

The purpose of this study was to quantify the activity of selected muscles during racing wheelchair stroking over a roller system using the conventional technique (CVT) and para-backhand technique (PBT) at two different resistance loads. Eight athletes of CVT and seven PBT users participated in this study. The electromyographic (EMG) signals of eight muscles were monitored using surface electrodes. Each subject performed maximum effort stroking for 30 s at two loads -- 30% and 50% of the maximum baking resistance provided by the roller system. Average values over three consecutive strokes were used for analysis. The results showed that large variations in muscle activation patterns existed in each technique group. No statistically significant differences between techniques were found in any of the EMG parameters. However, significant interactions between technique and load were found in several EMG parameters suggesting that the two techniques emphasized different muscles during the downward phase of the stroke cycle at different loads.

REVIEW AND THEORY

With the aim of reducing upper extremity injuries among wheelchair racing athletes, a new racing wheelchair propulsion technique -- the para-backhand technique (PBT) -- was proposed (Morse et al., 1994). The PBT is characterized by the contact along the distal surface of the fingers (fingertips) with base support provided by the thumb. This differs from the conventional stroke, where the contact occurs at the index and middle fingers and the base of the thumb. Theoretically, PBT enables an athlete to keep the elbows close to the body during stroking. This may help to decrease the stress placed on the rotator cuff muscles. Since previous EMG analyses of racing wheelchair stroking were mostly qualitative in nature, it was the purpose of this study to quantify the activities of selected muscles during racing wheelchair stroking over a roller system using PBT and CVT at two different resistance loads.

PROCEDURES

Subjects. The CT group consisted of eight males (33±5 yrs, injury level ranged from T5 to L1). The PBT group consisted of six males and one female (26±3 yrs, T8 to T12). All subjects were highly-trained experienced racers.

EMG Recordings. Eight pairs of surface electrodes with on-site preamplification circuitry (Liberty Technology MYO115) were attached to the right-hand side of the body to monitor the flexor carpi radialis (FCR), extensor carpi radialis (ECR), biceps brachii (BBR), triceps brachii (TBR), antero-middle (AMD), postero-middle deltoids (PMD), pectoralis major (PCM), and upper trapezius (UTR) muscles. To obtain maximum EMG levels of the selected muscles, maximum effort isometric contractions were performed before the experimental trials.

Trials. All stroking trials were performed on a computerized roller system with a maximum braking resistance of 15 Nm (roller dia. = 17.8 cm). A high-speed (120 Hz) video camera was stationed behind and to the left of the subject. As a result, a rear-side view of the subject's motion was recorded. An event synchronization unit was used to synchronize the video and EMG recordings.

Each subject performed a maximum effort trial for each of the two resistance loads -- 30% (30M) and 50% (50M) of the maximum resistance offered by the roller system. In each trial, the subject stroked for 30 s and was videotaped. The EMG signals were sampled at 1,000 Hz (10-500 Hz band pass) and collected for 5 s during the second half of the trial duration.

Data Reduction. The EMG signals were full-wave rectified and normalized to the maximum EMG levels observed during the isometric trials. Three stroke cycles of EMG and the corresponding video recordings were analyzed. Critical instances -- initial hand contact (HC), initial hand release (HR), and maximum elbow height (MH) -- were identified from the video images. For each stroke cycle, maximum and average EMG values (ME and AE, respectively) were determined for the contact (from HC to HR) phase (CT), ascending recovery (HR to MH) phase (AR), descending recovery (MH to HC) phase (DR), and recovery (HR to HC) phase (RC). Time duration (t) values for different phases of the stroke were also determined. For each temporal and EMG parameter in each trial, the average value over the three stroke cycles was used for subsequent analysis. A two way ANOVA was used to test for significant differences between the two techniques and two resistance loads.

RESULTS AND DISCUSSION

Among all temporal parameters, the only significant difference between the two techniques was the ascending recovery time expressed as a fraction of the stroke time (Table 1). The PBT group had shorter t_{AR} values at both loads. Significant differences between the two loads are found in the times for CT, RC, and DR. These results suggest that the subjects maintained the same stroke frequency at different loads by varying t_{CT} and t_{RC}.

Judging from the standard deviation (SD) values of the EMG parameters, it is concluded that large variations in muscle activation patterns existed in each technique group. In other words, the same stroking movement can be achieved by different combinations of muscle activation. The large SDs probably contribute to the fact that there was no statistically significant difference between techniques found in any of the EMG parameters. Although

statistically insignificant, FCR, ECR, and PCM seem to be more active for PBT while PMD and UTR are more active for CVT (Table 2). The activities of BBR and AMD are relatively low and insensitive to loads for both techniques.

	Conventional		Para-backhand	
Parameter	**30M**	**50M**	**30M**	**50M**
Speed[#] (mph)	20.5	16.7	21.4	16.8
	(2.0)	(2.0)	(2.7)	(2.4)
Stroke Time	0.539	0.539	0.527	0.522
	(0.068)	(0.067)	(0.026)	(0.052)
Stroke Frequency	1.882	1.880	1.904	1.930
(Hz)	(0.239)	(0.238)	(0.091)	(0.182)
Contact Time*	0.094	0.116	0.097	0.122
	(0.014)	(0.008)	(0.023)	(0.036)
%Contact Time*	17.7	21.7	18.4	23.2
	(3.5)	(2.8)	(4.1)	(6.2)
Recovery Time*	0.445	0.424	0.429	0.400
	(0.070)	(0.065)	(0.024)	(0.043)
%Recovery Time*	82.3	78.3	81.6	76.8
	(3.5)	(2.8)	(4.1)	(6.2)
Asc. Recy Time	0.337	0.335	0.315	0.310
	(0.047)	(0.042)	(0.017)	(0.032)
%Asc. Recy Time[¶]	62.6	62.2	59.7	59.3
	(4.1)	(2.5)	(1.8)	(3.8)
Desc. Recy Time*	0.108	0.088	0.115	0.091
	(0.033)	(0.031)	(0.023)	(0.021)
%Desc. Recy Time*	19.7	16.1	21.9	17.4
	(4.8)	(4.3)	(4.6)	(4.1)

[#] Speedometer reading
* Significant between loads ($p < .01$)
[¶] Significant between techniques ($p < .05$)

Table 1: Means and standard deviations of temporal parameters. Units in seconds unless specified.

	Conventional		Para-backhand	
Muscle	**30M**	**50M**	**30M**	**50M**
FCR*	32±13	27±11	55±45	27±9
ECR*	41±12	34±13	54±16	42±21
BBR	23±17	20±14	29±22	24±17
TBR	58±47	52±32	56±56	49±37
AMD	25±12	30±15	31±18	32±17
PMD*	57±20	39±18	44±18	32±13
PCM	54±16	50±22	76±50	72±55
UTR*	133±81	95±67	80±58	62±43

* Significant between loads ($p < .05$).

Table 2: Means and standard deviations of average EMG values over three strokes. Units in % maximum.

Significant differences between loads ($p < .05$) were found in ME_{CT} and AE_{AR} for FCR and in AE_{RC}, ME_{RC}, ME_{AR}, AE_{DR}, and ME_{DR} for ECR. Decreased activity with increasing load are observed in all cases. The AE_{CT} values for both techniques also decreased when there was an increase in load but the difference is not significant statistically. These results may suggest that the role of the wrist action changes from propulsion to stabilization as the load increase. A certain degree of wrist flexor-extensor co-contraction is presented throughout the stroke for most of the subjects (Fig. 1). It is not clear why they did not relax their wrist muscles during the recovery phase.

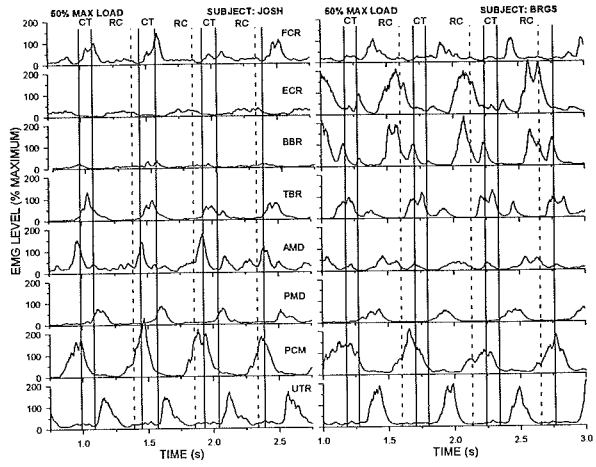

Figure 1: Rectified and normalized EMG curves of trials performed by subjects using CVT (left) and PBT (right) techniques. The dashed lines indicate the instances of maximum elbow height.

The excessive pronation and supination of the forearms during CT is considered a negative aspect of CVT. The "flicking" motion at the end of CT may lead to irritation of the musculotendinous tissues around the elbow. The forearm rotation is minimized in PBT and lesser stress on the forearm musculatures and elbow joints is expected. However, this supposition is not supported by the results of this study because there were no significant difference in EMG parameters for FCR, ECR, and BBR between the two techniques.

A significant interaction between technique and load ($p < .01$) was found in ME_{DR} for TBR -- a decrease for CVT and an increase for PBT with increasing load. Significant interactions with the opposite trend were found in ME_{DR} for AMD and in ME_{CT} for PCM. The same trends were also observed in the corresponding AE values but these were not significant statistically. Since these three EMG parameters are associated with the downward phase of the stroke cycle, it seems that the two techniques emphasize different muscles during this phase at different loads.

Significant differences between loads ($p < .05$) were found in most of the EMG values during RC, AR, and DR for UTR. It is speculated that UTR is less active at higher loads because of the shorter time for recovery (Table 1) or smaller range of motion during recovery.

In conclusion, the results of this study demonstrated some differences in muscle activation pattern between the two techniques and two resistance loads. However, the results do not provide sufficient information for determining the advantages of one technique over another in terms of injury prevention. To gain more insight into these two techniques, further studies on stroking kinematics and joint resultants are recommended.

REFERENCE

Morse, M. et al. *Sports 'n Spokes*, 20, 58-60, 1994.

ACKNOWLEDGEMENT

Funded by the University of Illinois at U-C Research Board.

NEUROPHYSIOLOGICAL CONSIDERATIONS OF PROPHYLACTIC ANKLE BRACING

Tetsuo Nishikawa, Mark D. Grabiner

Department of Biomedical Engineering, The Cleveland Clinic Foundation, Cleveland, OH 44195

INTRODUCTION

Ankle bracing is generally considered an effective means to reduce the frequency of ankle injuries. One of the mechanisms through which this prophylaxis occurs is by mechanically restricting undesired joint kinematics. A second mechanism is popularly purported to act through the neuromuscular system. This belief is founded in the thesis that ankle braces stimulate peripheral neural receptors that result in a change in the sensitivity of the nervous system to various stimuli.

REVIEW AND THEORY

The theme of this research is related to the ankle complex, specifically the influence of braces on athletic performance of gross motor tasks, and to lesser extent, the influence of braces on various "neuromuscular" variables including proprioception and postural steadiness. Improved proprioception (Feuerbach et al., 1994) and postural steadiness (Feuerbach et al., 1993) is often attributed to enhanced peripheral feedback associated with cutraneous receptors. Indeed, the neurophysiological literature (Moberg, 1983) demonstrates that stimulation of cutaneous afferents can have a profound effect on muscle activation. The contention that observed increases in activation latency 15 ms in the presence of ankle ligaments injury (Karlsson et al., 1992) may not have biomechanical significance gives impetus for the study of an alternative activation variable, i.e., activation amplitude. Activation amplitude is a variable that, unlike latency, has a direct influence on the contraction force that a muscle will generate. Presently, the results from two experiments in which the influence of ankle braces on reflexive activation of ankle complex muscles, particularly the peroneus longus muscle in normal subjects, are reported. The purposes of these experiments were to specifically test the hypothesis that the stimulation of cutaneous receptors by ankle braces would be manifested as increased reflexive activation amplitude. In one experiment, the influence of the ankle brace on the excitability of the motoneuron pool was measured directly and in a second experiment, the effect of the brace on the response to stretch was assessed.

METHODS (Experiment 1: H-reflex)

Eleven healthy subjects volunteered to participate in the study and provided informed consent. With the subjects comfortably seated with knee and ankle joint angles maintained at 120 and 90 deg, respectively, the right foot was secured to a modified foot plate of a Kin-Com dynamometer. Initially, each subject's maximum voluntary isometric eversion force was established as the mean of three trials. During the trials in which the H-reflex was elicited, subjects maintained 60 percent of the established maximum eversion force. Electrodes were placed over the bellies of the peroneus longus, lateral gastrocnemius and tibialis anterior muscles. The common peroneal nerve was stimulated at the point of the caput fibulae using a bipolar electrode (single rectangular pulses of 1ms duration). Five reflexes were collected at 12 stimulation voltages to establish a recruitment curve. At each stimulation voltage, the five trials were ensemble averaged, using the stimulus as the point of reference. Two randomly ordered conditions, with and without the semirigid AirCast Air-Stirrup (Aircast, Inc.) were collected.

Analysis consisted of extracting the peak-to-peak amplitudes of the M-wave and H-reflex to determine the recruitment curves. Recruitment curves were derived by plotting the amplitude of the M-wave and H-reflex as a function of the stimulus intensity. H-reflex was expressed as a percentage of the maximum M-wave. A Wilcoxon signed rank test was performed to compare the values of the maximum H-reflex for the two conditions.

METHODS (Experiment 2: Stretch reflex)

Fifteen healthy male and female subjects (mean age: 33.0 years) participated in the study. For the present study, a toes-up tilt of four degrees, with velocity of 61.2 (3.2) degree per second, was used to induce a stretch of the soleus and peroneal muscles. Two conditions were used in this experiment, one without and the second with the application of an ankle brace. Ankle braces used in this experiment were the semirigid AirCast Air-Stirrup and the lace-up cloth brace RocketSoc (DonJoy, Inc.). Reflexive activation was detected using surface EMG electrodes. For each condition, 10 trials were collected. In each trial, while the subject stood on the platform, the investigator manually enacted the data collection instrumentation and the perturbation platform. Processing consisted of quantifying the latencies and integrated EMG of the short and medium reflexes. Latencies were calculated as the difference between the onset of the platform movement and the muscle response, and integrated EMG were calculated from the averaged rectified EMG activities. Latencies and integrated EMGs of the short latency response (SLR) and median latency response (MLR) in the ankle braced conditions were compared with non braced conditions using a Wilcoxon signed rank test.

RESULTS (Experiment 1: H-reflex)

Of eleven subjects H-reflexes were collected in ten subjects. H-reflexes were evident only in the peroneus longus muscle. In contrast to the normalized M-wave curves, the H-reflex curve in the braced condition was shifted to the left on the stimulation axis and achieved a higher maximum than the non-braced condition. From recruitment curves the amplitude of maximum H-reflexes and M-waves were measured. The amplitude of the H-reflex was significantly (p=0.005) larger when measured during the braced condition compared in the non-braced condition. The mean maximum H-reflex amplitude in the non-braced condition was 13.6±8.6% (range 4.0-29.5) of maximum M-wave amplitude and in the braced condition was 21.0±16.1% (range 4.5-58.9) of maximum M-wave amplitude. (Fig.1)

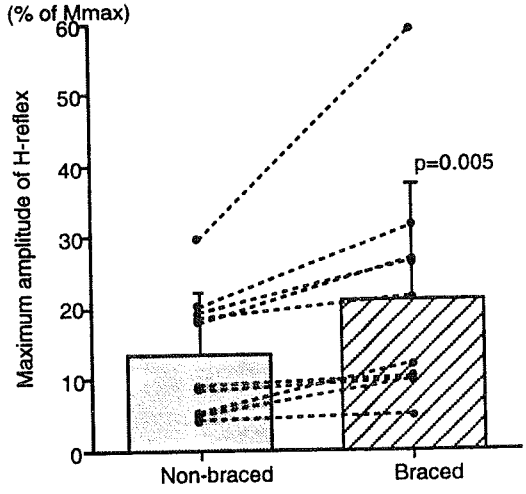

(Fig.1) Effects of brace on maximum H-reflex amplitude. Individual subject data are shown as solid circles. Bars illustrate the average (+standard deviation) across subjects.

RESULTS (Experiment 2: Stretch reflex)

In the soleus and peroneus longus muscle the reflex response was found to consist of two components, the first appearing about 60ms after the onset of displacement (SLR), the second appearing with a latency of about 100ms (MLR) after displacement onset. The integrated EMG of the SLR in the peroneus longus with semirigid and lace-up cloth ankle braces increased ($p<0.05$) by 25% and 26% respectively, and in the soleus increased by 23% ($p=0.011$) with semirigid braces and 15% with lace-up cloth braces when comparing with non-braced condition. Latencies of SLR and MLR remained unchanged with ankle braces compared to the non-braced condition. (Fig.2)

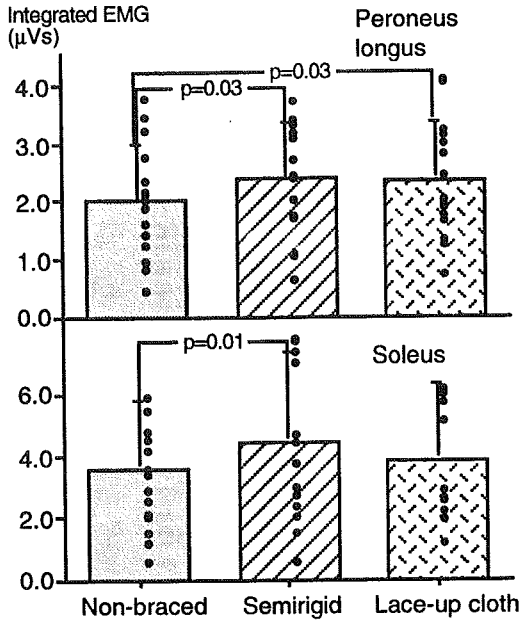

(Fig.2) Effects of ankle brace on short latency responses in the soleus and the peroneus longus muscle. Individual subject data are shown as solid circles. Bars illustrate the average (+standard deviation) across 15 subjects for three conditions (non braced, semirigid braced, lace-up cloth braced).

DISCUSSION

These findings of increased H-reflex and SLR amplitude provide further evidence that ankle brace application may increase the afferent feedback from cutaneous receptors, which may in turn lead to an increased motoneuron excitability of the peroneal and soleus muscles.

Based upon the importance of muscle contraction in preventing ankle joint injury and reinjury, this may be a motor control mechanism subserving the effectiveness of ankle braces.

REFERENCES

Feuerbach JW et al. J Orthop Sports Phys Ther 17, 149-154, 1993

Feuerbach JW et al. Am J Sports Med 22, 223-229, 1994

Karlsson J et al. Am J Sports Med 20, 257-261, 1992

Moberg E Brain 106, 1-19, 1983

ACKNOWLEDGMENTS

The authors gratefully acknowledge funding provided by Aircast, Inc. and Thomas Lundin for his assistance with the data collection and analysis.

ASSESSMENT OF ANTICIPATORY POSTURAL RESPONSES

W. Siler, R. Richter, A. Jorgensen
Department of Physical Therapy, Saint Louis University
1504 S. Grand, St. Louis, MO 63104-1395

INTRODUCTION

To determine if healthy young adults alter their posture in preparation for the jerks experienced during the Postural Stress Test (PST), the location of the center of pressure (COP) was assessed for the 3-s period prior to the subject being jerked from behind. Fifteen subjects experienced the PST on two separate occasions to determine if any adaptations which evolved during the first exposure to the PST were sustained over a period of at least one week.

REVIEW AND THEORY

The PST was introduced as an inexpensive method to identify individuals at greatest risk of falling (Wolfson et al., 1986). The PST is based on the premise that persons at greatest risk for falling will be less able to maintain or regain their balance when balance is disturbed. In the PST protocol, subjects are instructed to try not to move when jerked from behind. Weights corresponding to 1.5, 3.0, and 4.5% of the subject's body weight are then sequentially dropped from a height of approximately 0.6-m. Immediately prior to the weight striking the floor, the subject is jerked from behind.

In previous research (Duncan et al., 1990), the time lag between experiencing the jerk and the onset of muscle activity to counter the jerk decreased over the course of the three trials. Those investigators suggested that the decreased lag time was attributable to the increased weight dropped in each trial. They also suggested that the failure to control foot placement in the PST may have contributed to the reduced muscle latencies. We propose that the decreased lag times may reflect the development of strategies to combat the expected disturbances to balance. The purpose of this investigation was to determine if healthy young adults begin to form anticipatory postural responses in expectation of the jerks received in the PST. We hypothesized that postural preparations would evolve as subjects are exposed to the PST. We also hypothesized that the postural preparations would be evident when the PST was repeated one week later.

PROCEDURES

Fifteen healthy young volunteers were recruited from the university community. Subjects had no previous exposure to the PST and provided informed consent prior to participation in the investigation.

Volunteers reported for two separate data collection sessions, separated by at least 1-week. Upon arriving at the lab, shoes and socks were removed and body weight was recorded. Subjects then assumed a comfortable stance on the force platform and the outlines of the feet were traced on paper taped to the surface of the force platform. Subjects positioned their feet within the traced outlines for each of the remaining trials, thereby controlling foot position from one trial to the next.

Force plate data were sampled at a rate of 600-Hz. Initially, subjects stood quietly for a period of 3-s. These data provided baseline measures for later comparisons.

After determining the readiness of the subjects, the weight was raised to the required 0.6-m above the ground, the investigator paused for approximately 3-s, and the weight was dropped, jerking the subjects posteriorly. The 3-s of force plate data sampled prior to the drop of the weight was saved for subsequent analysis.

The mean location of the COP during quiet stance was subtracted from the mean location of the COP for the 3-s period preceding the drop of the weight to reflect adjustments relative to normal upright stance. The resulting data were analyzed statistically using a 2 x 3 (Day x Weight) ANOVA with repeated measures for the anteroposterior and mediolateral directions, respectively. All statistical comparisons were conducted with the level of significance set at $p \leq 0.05$.

RESULTS

The statistical analyses revealed only a significant main effect for weight when COP shifts in the anteroposterior direction were considered. The anterior shift of the COP prior to the 4.5% BW trial was significantly greater than either the 1.5 or 3.0% BW trials, [21.4 ± 19.7 (mean ± SD), 14.2 ± 18.7, and 15.8 ± 21.1 mm, respectively]. Figures 1 and 2 represent the means and standard deviations for the anteroposterior data from Sessions 1 and 2, respectively.

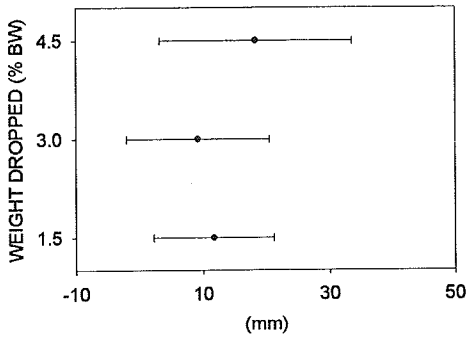

Figure 1: Anterior shift of COP - Session 1

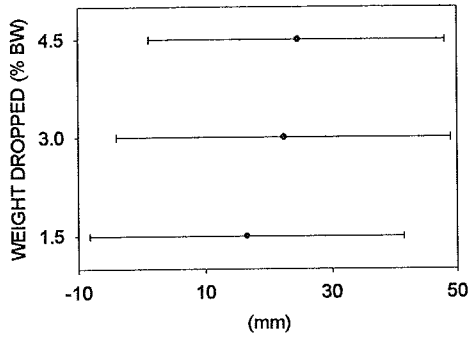

Figure 2: Anterior shift of COP - Session 2

DISCUSSION

This study shows that healthy young adults make preparatory postural adjustments in anticipation of the jerks received in the PST. Specifically, a significant shift of the COP in the anterior direction occurs after the being jerked posteriorly by the 3.0% BW weight. The absence of a significant main effect for session and a significant interaction term suggest that there is not a carry-over effect from Session 1 to Session 2.

Horak and Nashner (1986) investigated anticipatory postural responses in order to develop insights into central motor programs. In the scenario they presented, a central motor program would incorporate knowledge of previous experience and anticipation of external events in order to reduce the subjects' reliance on feedback for successfully managing a disturbance. Because our subjects had no previous experience with the PST, there was no basis for preparing a response in advance to a disturbance.

The amount of practice required before an effective anticipatory response evolves is unclear. Lacquiniti (1989) suggested that subjects form an internal model of the interaction between themselves and the expected disturbance and a single trial is sufficient to adapt the anticipatory response. Our interpretation of Lacquaniti's proposal is that the subjects in our investigation used the first jerk to create an internal representation the interaction. The second jerk provided the opportunity for subjects to revise their internal representation prior to receiving the final jerk. The absence of significant main effect for session or significant interaction term may then suggest the same process occurs each time.

Other investigators have found that the development of effective anticipatory responses requires several trials and is characterized by a great deal of inter-individual variation. Our data also revealed a great deal of variability in the manner in which subjects respond to novel disturbances. That variability was probably magnified by the inability of the subjects to anticipate the jerk (Lacquaniti & Maioli, 1989).

Regardless of the explanation of the data, the subjects in this investigation shifted the COP anteriorly in preparation for a posteriorly directed jerk. Consequently, the PST provides an opportunity to assess the development of anticipatory postural responses.

REFERENCES

Duncan, P. W. et al. Phys Ther, 70, 88-96, 1990.
Horak, F. B., & Nashner, L. M. J Neurophysiol, 55(6), 1369-1381, 1986.
Lacquaniti, F., & Maioli, C. J Neurosci, 9(1), 149-159, 1989.
Wolfson, L. I. et al. J Am Geriatr Soc, 34, 845-850, 1986.

ACKNOWLEDGEMENTS

Project supported by the Beaumont Faculty Development Fund, Saint Louis University

PRACTICE EFFECTS UPON ANTAGONIST CO-CONTRACTION DURING BALLISTIC ELBOW FLEXION TO A TARGET

D. A. Gabriel[1] and J. P. Boucher[2]
[1]Department of Orthopedics, Mayo Clinic/Mayo Foundation, Rochester, MN 55905
[2]Department of Kinanthropology, University of Quebec at Montreal, Montreal, PQ H3C 3P8

INTRODUCTION

This study examined changes in antagonist cocontraction (ANTCO) in response to ballistic elbow flexion practice. Sixteen male subjects performed 400 trials of ballistic elbow flexion to a target in the horizontal plane. A potentiometer and microswitch system at the elbow axis of rotation of a manipulandum recorded angular displacement and movement onset. Surface electrodes monitored the triceps brachii lateral head, and the electromyographic (EMG) signals were linear envelope detected with a 10 Hz cutoff frequency. The antagonist (ANT) EMG burst was divided in two: early low-level tonic activity (ANT1), and the large portion of the burst which occurs near target achievement (ANT2). As practice improved the speed of limb movement, onset of the first component remained unchanged while the second component started earlier. The magnitude of both portions of the ANT EMG burst increased from the first to last test day, but the change in ANT2 relative to ANT1 was more pronounced. These findings were used to explain the discrepant observations in the literature for learning induced changes in antagonist muscle activity.

REVIEW AND THEORY

Lagassé (1979) studied the effects of practice upon ANTCO during ballistic elbow flexion to a target. Antagonist cocontraction was defined temporally, and measured as the onset of triceps brachii lateral head EMG burst activity. Improvements in the speed of limb movement were found to be accompanied by a delay in ANT EMG burst onset. It was theorized that practice reduced ANTCO to allow the agonist to accelerate the limb unopposed and increase speed. In contrast, Darling and Cooke (1987) studied rapid elbow flexion and extension and showed that, as practice increased limb speed, the ANT EMG burst began earlier. If ANTCO is measured as an amplitude variable, the findings in the literature are still inconsistent. Moore and Marteniuk (1986) examined elbow extension but the learning task was time constrained to either 200 ms or 500 ms. These authors reported a reduction in ANT EMG amplitude. Corcos et al. (1993) recently showed that ANT EMG burst amplitude increases with the speed of limb movement. They also partitioned the ANT EMG burst in two: early low level tonic activity (ANT1) and the large portion of the burst which occurs near target achievement (ANT2). The second portion of the burst was used to determine EMG burst onset. The latency of ANT2 EMG burst activity was found to either decrease or remain unchanged with increases in the speed of limb movement, and one subject exhibited delayed onset as observed by Lagassé (1979). Thus, there are different EMG measures of ANTCO, and discrepant observations for how they change with ballistic elbow flexion practice. The purpose of this work was to examine learning induced changes in the different EMG measures of ANTCO, and determine how they relate to an increase in the speed of limb movement.

PROCEDURES

Sixteen right-handed males performed ballistic elbow flexion on a manipulandum to a target in the horizontal plane. With the arm in full extension at 0°, the target was an area between 75° and 90° of elbow flexion which was marked on the testing table as a 15° colored wedge. One hundred successful trials were required on each of four days of testing. There was twenty-four hours of rest between days 1 and 2 and days 3 and 4, with a one week interval between days 2 and 3. A potentiometer and microswitch system at the elbow axis of rotation of a manipulandum recorded angular displacement and movement onset. Standard Beckman Ag/AgCl surface electrodes were placed in line and 3 cm apart over the belly of the of triceps brachii lateral head (Delagi and Perotto, 1980). The reference electrode was secured on the clavicle. Electromyographic activity was amplified (Grass P-511) and digitized at 2000 Hz with the MDAS 7000 A/D and IBM PC. The displacement and event channels were also sampled at 2000 Hz. Electromyographic activity was linear envelope detected with a 10 Hz cutoff using a fourth-order Butterworth digital filter (Winter, 1990). Elbow angular velocity was obtained numerically by differentiating the displacement signal using finite differences.

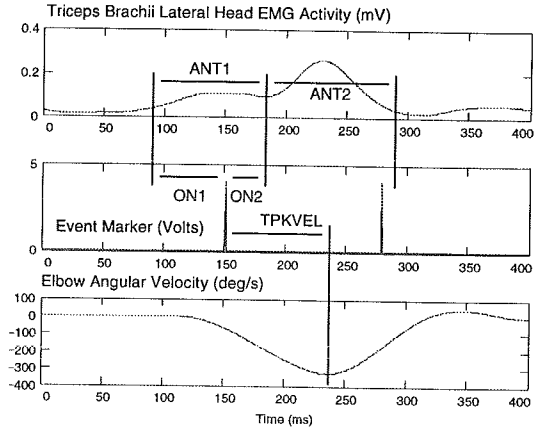

Figure 1. Temporal measures derived from the linear envelope detected EMG activity of the triceps brachii lateral head, event markers, and elbow angular velocity.

Figure 1 shows the temporal variables extracted from the electromyogram: ANT1 EMG burst onset relative to movement initiation (ON1), and ANT2 EMG burst onset relative to movement

initiation (ON2). The magnitude variables were ANT1 root-mean-square EMG amplitude (RMS1), ANT2 root-mean-square EMG amplitude (RMS2), and the ratio of ANT2-to-ANT1 root-mean-square EMG amplitude (RATIO). The kinematic measures included movement time (MT), peak velocity (PKV), and time to peak velocity (TPKV). The last five trials of each day of testing where subjected to a repeated measures analysis of variance, and post-hoc analysis was accomplished using the Tukey HSD (honestly significant difference) test.

RESULTS

The means and standard deviations of the measures are presented in Table 1 below. MT decreased (P <0.01) monotonically over the four test sessions for a total of 26 ms. PKV exhibited a linear increase (P <0.01) of 36 deg/s by the last day of testing. The TPKV had a small but significant reduction of 4 ms from the first to second week of testing (P <0.05). ON1 began an average of 59 ms before movement initiation and remained unchanged over the four test sessions. In contrast, ON2 began earlier (P <0.01) on the second session within each week, days two and four. RMS1 exhibited an increase (p <0.01) over the first three sessions, with no significant difference between the third and fourth test days. The same pattern of increase was observed for the RMS2. The RMS EMG amplitude of ANT2 exhibited a greater increase than ANT1 as measured by their ratio. The RATIO measure increased as a result of consecutive weeks of practice (P <0.05).

Table 1. Means (M) and standard deviations (SD) for the criterion measures. These values represent the last five trials of each test session from all sixteen subjects.

	DAY 1	DAY 2	DAY 3	DAY 4
	M(SD)	M(SD)	M(SD)	M(SD)
VARIABLES				
ON1 (ms)	-59(15)	-61(17)	-58(20)	-59(20)
ON2 (ms)	44(28)	36(24)	39(22)	35(21)
RMS1 (μV·s)	170(70)	210(90)	240(130)	230(80)
RMS2 (μV·s)	200(100)	250(130)	290(160)	280(130)
RATIO (units)	1.14(.19)	1.18(.23)	1.20(.33)	1.24(.37)
MT (ms)	148(26)	138(26)	128(22)	122(17)
PKVEL (deg/s)	303(40)	314(50)	328(45)	339(50)
TPKVEL (ms)	90(9)	87(13)	84(12)	84(12)

DISCUSSION

Motor learning was defined in the present study as an increase in the speed of limb movement for the same degree of accuracy. The kinematic adaptations exhibited by the sample were similar to those previously reported (Lagassé, 1979; Darling & Cooke, 1987; Corcos et al.,1993). Although ballistic elbow flexion is a simple skill, practice resulted in a significant improvement in motor performance as measured by MT. The ANT2 EMG burst began earlier in agreement with those authors who observed a decreased onset with a reduction in MT (Darling and Cooke, 1987; Moore and Marteniuk, 1986). In support of Corcos et al. (1993), practice also resulted in an increase in RMS EMG amplitude.

How then, do these findings resolve conflicting observations in the literature? The key to answering this question is the ratio of RMS EMG amplitude of ANT2-to-ANT1 which increased by 10%. The RMS EMG amplitude of ANT1 and ANT2 did not change proportionally over the four test sessions, ANT2 exhibited a greater increase. Lagassé (1979) fixed the threshold of ANT EMG burst onset to 10% of the signal peak, but the signal peak was located in ANT2. Before extended practice, it is possible that the algorithm detected ANT1. After practice, the amplitude of ANT2 increased relative to ANT2, and the detection algorithm ignored ANT1 and located ANT2, which was observed as a delayed onset. Cooke and Brown (1990) demonstrated that ANT2 functions as an agonist to actively "brake" limb movement while ANT1 represents "pure" antagonist cocontraction. If ANT2 is the "dynamic" portion of the EMG burst, as limb speed increases and larger decelerating forces are required, it is logical that RMS EMG amplitude of ANT2 should exhibit a greater increase than ANT1.

In terms of motor learning, the decrease in ANT2 EMG burst onset occurred for the second session within each week of testing and was not retained over the one-week rest period, while the reduction in MT progressed over the four test sessions. It is possible that ANT2 EMG burst onset responds only to intensive practice and is a short-term adaptation. An alternative is that the onset and magnitude of the ANT2 EMG burst interact to meet the force requirements of the task. The different adaptations observed in ANT EMG burst amplitude associated with learning a ballistic versus a time constrained movement supports this hypothesis. In the present study, the RMS EMG amplitude of ANT2 increased over the first three test sessions then plateaued on the last session, when the onset of ANT2 EMG activity again decreased. Moore and Marteniuk (1986) observed a reduction in ANT EMG amplitude for a time constrained task, because subjects were not required to continually improve movement speed. The force requirements for the faster time constrained task (200 ms) were met by an earlier onset of the antagonist muscle.

REFERENCES

Cooke, D., and Brown, S. J. Neurophysiol., 63, 465-472, 1990.
Corcos, D., et al. Exp. Brain Res., 94, 499-513, 1993.
Darling, W., and Cooke, D. J. Motor Behav., 19, 311-331., 1987.
Delagi, E., and Perotto, A. Anatomic guide for the electromyographer, (page 72), Charles C. Thomas, 1980.
Lagassé, P. (1979). Percept. Motor Skills, 49, 151-161.
Moore, S., and Marteniuk, R. Motor Behav., 18, 397-426, 1986.
Winter, D. Biomechanics and motor control of human movement, (pp 191-212), J. Wiley and Sons, 1990.

MODIFICATION OF MOTOR UNIT RECRUITMENT STRATEGY DUE TO SKILL ACQUISITION

M. Solomonow, M. Bernardi, R.V. Baratta
Bioengineering Laboratory, Louisiana State University Medical Center
New Orleans, LA 70112

INTRODUCTION

It is well established that specialized movement is manifested by pronounced changes in muscle properties. Certain types of strength training result in significant increases in force, modification of twitch properties, and changes in the aerobic capacity of muscle fibers (1). Very little is known, however, about the possible changes in motor unit recruitment strategy that may cause specialization in muscle function. The current understanding advocates that during increasing force contraction, all motor units are recruited by the time the force reaches 50–70% of maximal voluntary contraction (MVC), while the final force segment (up to 100% MVC) is generated by increase in firing rate only. Recent work in our laboratory (2,3,4) and elsewhere (5) suggests that during linear force increase, all motor units are recruited by the time 70–80% MVC is reached, whereas in stepwise-increasing force contraction (e.g. 0–10% MVC, 0–20% MVC, ...0–100% MVC) recruitment of motor units occurs only up to 50% MVC with the firing rate increase responsible for the final 50% of the force. Given the plasticity of the recruitment strategy established in these reports, it is reasonable to expect that skill acquisition over time may also be manifested from changes in the recruitment strategy.

It is the objective of this study to determine the possible changes in motor unit strategy during a six-week period of training in which adult human subjects practiced a 3-second linearly increasing force (elbow flexion), while attempting to track a 3-second ramp function display. The ramifications of such information is obvious for various sports and occupational applications.

METHODS

Six normal subjects, four males and two females, were instrumented with a pair of EMG electrodes (Ag-AgCl, 1 cm diameter, 4 cm interelectrode distance) after proper cleansing and gelling of the skin surface over the belly of the biceps. A single ground electrode was placed elsewhere. Subjects were seated in a chair with the elbow resting on an armrest and the wrist placed in a padded plastic brace attached to a metal rod which was connected to a load cell (Lebow Model 3132). Isometric contractions were practiced from rest up to 100% MVC (after MVC was determined). The subjects were instructed to track a 3-second ramp displayed on one channel of the oscilloscope with the actual force trace displayed on the second channel.

The EMG was amplified (100dB CMRR) and bandpass filtered (10–450 Hz) and stored in the computer at a sampling rate of 1024 Hz together with the corresponding force. The median frequency (MF) of the power spectra was calculated for each of 0.25 s epochs of the 3-second contraction with a 50% overlap of each new epoch relative to the previous one.

Subjects practiced linear elbow flexion force increase three times a week over six

consecutive weeks. Recordings of EMG and force were made in the initial visit and every two weeks thereafter. Over the six-week period, each subject practiced at least 360 times, i.e. a minimum of 20 times per visit.

RESULTS

The mean of the MVC of all six subjects increased by 9.3%, 6.2%, and 5.1% from the initial test to the second, third and fourth, to yield a 22% increase over the six weeks. T-test analysis shows that the increases were significant. T-test analysis of the force ramp relative to the displayed ramp shows significant improvement in accuracy over the six weeks. Similarly, the standard deviation decreased from test to test. Overall, a clear indication is present that skill acquisition indeed took place over the practice period.

The mean MF of the power density spectra of the EMG from the six subjects increased from 0 to 61% MVC in the initial test, from 0 to 76.4% MVC in the second, from 0 to 82% MVC in the third, and from 0 to 86.3% MVC in the fourth. The above increases in mean MF were significant ($p<0.5$) between tests.

CONCLUSIONS

The MF of the EMG power density spectra is linearly related to the mean conduction velocity of action potentials in the muscle, and therefore to the increase or decrease in the activity of larger motor units which have higher conduction velocity (6). The highest MF during the linear increase in elbow flexion over 0–100% MVC was recorded at 61.1% MVC in the pre-practice test, indicating that the largest motor units were fully active at that point. The increase in the %MVC at which the highest MF was recorded in the three consecutive trials indicate that motor units were recruited over a larger force range as skill acquisition took place. Over the six-week period, a significant increase of 25.2% MVC occured (from 0–61.1% MVC to 0–86.3% MVC). The elongation of the recruitment period allowed finer regulation of the forces and, therefore,

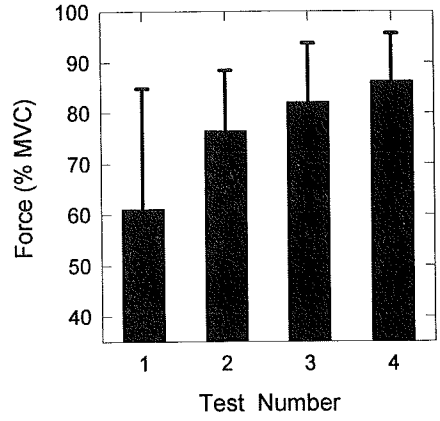

Figure 1: The percent MVC at which the maximal MF occurred in each test

improvement in accuracy of tracking the displayed ramp. The fact that the motor unit recruitment strategy can modify itself to allow for skill acquisition further confirms that this process of force control is not rigid, but rather a flexible central process that is tailored according to the function at hand.

Supported by U.S. NSF Grant BCS-9207007

REFERENCES

1. Moritani T.J. Biomech. 26:95–107, 1993.
2. Sanchez J., Solomonow M., Baratta R.V. J. EMG & Kinesiol. 3:33–40, 1993.
3. Bernardi M., Solomonow M., et al. Europ. J. Appl. Physiol. 70:493–501, 1995.
4. Bernardi M., Solomonow M., et al. EMG & Clin. Phsiol. In press.
5. Bilodeau M., Arsenault B., et al. Europ. J. Appl. Physiol. 63:24–28, 1991.
6. Solomonow M., Baten C., et al. J. Appl. Phsiol. 68:1177–1185, 1990.

GOAL-DIRECTED HEAD MOVEMENT CONTROL DURING TREADMILL LOCOMOTION

S.L. Smith[1], B.T. Peters[1], C.S. Layne[1], P.V. McDonald[1], J.J. Bloomberg[2]
Neuroscience Human Movement and Coordination Laboratory

[1]KRUG Life Sciences, 1290 Hercules Suite 120, Houston, TX 77058
[2]NASA-Johnson Space Center, Houston , TX 77058

INTRODUCTION

Are head movements during locomotion modified by goal-directed tasks? We will show changes in coordination patterns of the head and upper body which identify active modifications to maintain stable gaze at different visual target distances.

REVIEW AND THEORY

Effective gaze stabilization during locomotion requires complex coordination between eye, head, and trunk. During locomotion, the vestibuloocular reflex (VOR) functions in concert with compensatory pitch head movements in the sagittal plane to stabilize gaze. (Pozzo, T. et al., 1990) Previously we observed that these compensatory pitch head movements change in amplitude appropriately in response to alterations in target distance to the eyes. These data supported the hypothesis that such head movements are under goal-directed neural mediation (Bloomberg, J.J. et al., 1992). The aim of this investigation was to determine if additional modifications in head-trunk coordination strategies can be identified in a treadmill locomotion task involving visual fixation of targets that varied in distance from the eyes. These data are a subset of a larger investigation looking at the effects of space flight on eye, head, and trunk coordination during locomotion.

METHODS

Seven normal subjects participated in this study. The subjects walked at 6.4 km/h on a motorized treadmill while visually fixating an earth-fixed target (light emitting diode), positioned in the center of view either far (2 m) or near (30 cm) from the eyes. Passive retro-reflective markers were placed on the top of the head, at the neck (C7), and at the sacrum. The position of each marker in space was determined throughout each 20 second trial using a video-based motion analysis system, (Motion Analysis Corp. Santa Rosa, CA). The X, Y, and Z trajectories were extracted for further analysis. Prior to determining the peak to peak deviation in the medio-lateral (Y) axis the trajectories were low-pass filtered at 15 Hz. The peak to peak deviation for each marker, for each stride cycle, was obtained using the rising and falling edge of the signal and then averaged across the trial (approximately 18 strides). Temporal differences between the Y trajectories of the markers were obtained by calculating the difference between when the maximum peak occurred in the neck and sacral markers relative to the head marker maximum peak.

RESULTS AND DISCUSSION

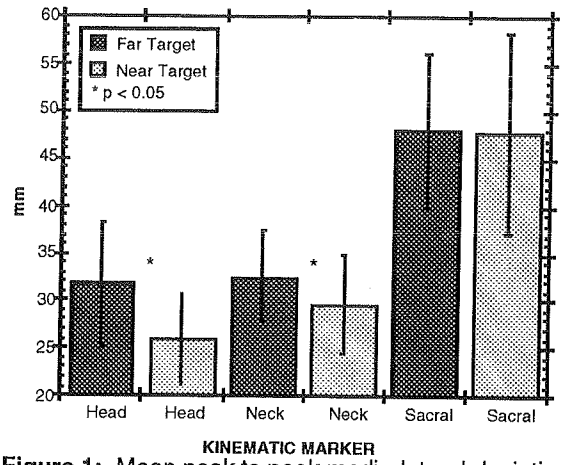

Figure 1: Mean peak to peak medio-lateral deviation: Near vs. far target.

For all subjects, there was a significant ($p < 0.05$) decrease in y peak to peak deviation of the head and neck markers with decreased target distance. There was no change in the sacral marker peak to peak deviation. Despite these changes in absolute deviations for the head and neck, there was no change associated with decreasing visual target distance in the temporal relationship between the maximum peaks of these two markers. The decrease in y axis displacement associated with the near target condition occurs in conjunction with the increase in pitch observed during this condition (Bloomberg, J.J. et al., 1992). The decrease in neck marker deviation suggests that the response to this goal-directed task is not limited to the head but involves a complex pattern of segmental coordination. This complex pattern of compensatory motion associated with changing visual target distance suggests the response is not solely resulting from the passive viscoelastic properties of the head-neck system, but rather, is a goal-directed response subject to neural influence.

REFERENCES

Pozzo, T et al. Head stabilization during various locomotor tasks in humans. I. Normal subjects. Exp. Brain Res, 82:97-106, 1990.
Bloomberg, J.J., et al 1992. The effects of target distance on eye and head movement during locomotion, Annals of the NYAS, 656: 699-707, 1992.

THE EXPLOITATION OF TASK CHARACTERISTICS DURING SKILL ACQUISITION AS REFLECTED BY TEMPORAL EMG CHANGES

G.D. Heise[1], L. Caillouet[2], A. Cornwell[2], and B. Sidaway[2]

[1]School of Kinesiology and Physical Education, University of Northern Colorado, Greeley, CO 80639

[2]Department of Kinesiology, Louisiana State University, Baton Rouge, LA 70803

INTRODUCTION

The purpose of this study was to examine if subjects learn to time the activation of muscles to take advantage of the spring characteristics of a ski simulator apparatus. Task performance improved as indicated by increased lateral displacement and cycle frequency. After considerable practice, durations of muscle activity in knee flexors and extensors and the duration of muscle coactivation decreased during knee flexion. The results suggest that subjects economize muscle activity by exploiting characteristics of the task.

REVIEW AND THEORY

Traditional skill acquisition research has focused on the outcome or goal of a movement as the primary dependent variable (e.g., Lee et al., 1990). Conclusions from these studies have implications for skill training concerns (e.g., training schedules, types of information feedback), however, little is added to our understanding of the underlying neuromuscular control processes. More recent research has focused on *how* the learner acquires control for a certain skill.

From a "dynamical systems" perspective, a learner will acquire the most economical coordination strategy available. That strategy incorporates principles such as mastering the redundant neuromuscular degrees of freedom and exploiting reactive forces present in the link-segment system (Bernstein, 1967). Vereijken (1991) suggested that learners discover the dynamical constraints imposed by the task and exploit them to their advantage. For example, she found that subjects altered the timing of their force application on a ski simulator apparatus as they became more proficient at the task. Subjects had to push the apparatus laterally against an elastic band that acted as a resistance (see Fig. 1). Vereijken suggested that learners began to exploit the elastic characteristics of the ski simulator apparatus and thus economized the timing of force application. The present study was designed to test this hypothesis from a neuromuscular level.

Presumably, subjects will learn to time the activation of muscles to take advantage of the spring characteristics of the ski simulator apparatus. Specifically, we hypothesized that, as subjects become more skilled and are able to displace the platform farther and at a higher frequency, the duration of muscle on-time of knee flexors and extensors and the coactivation between those muscle groups would decrease. We additionally hypothesized that this would be most noticeable during the time the apparatus springs back toward the center (i.e., during knee flexion of the right leg when the platform is moving right-to-left).

PROCEDURES

Six healthy men who were unfamiliar with the ski simulator volunteered as subjects (mean body mass = 78.5 ± 13.2 kg; mean body height = 179 ± 6 cm). Each subject attended four test sessions in which 25 trials were performed during each session. A trial consisted of a 30-sec attempt to go "as fast and as far as possible" on the ski simulator. Subjects applied force in a lateral direction against the movable platform which sat on curved rails (see Fig. 1). Once the platform reached the most lateral position, it sprang back towards the center because of elastic bands attached to it.

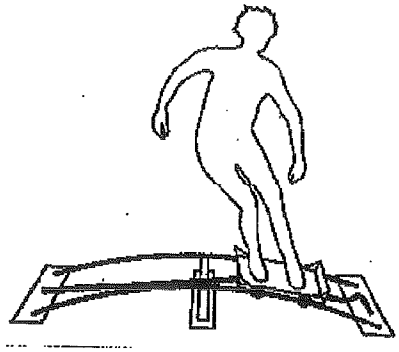

Fig. 1: Ski simulator apparatus (from Vereijken, 1991)

Prior to sessions 1 and 4, and after appropriate skin preparation, surface EMG electrodes were positioned over the bellies of muscles vastus lateralis (VL) and the long head of biceps femoris (lateral hamstrings - LH). A goniometer was placed over the right knee of each subject to monitor knee joint angle. A photoelectric cell was aimed at a reflector attached to the ski simulator platform so that an event signal was produced whenever the platform crossed top dead center (TDC). The goniometer signal, the event signal, and the EMG signals were digitized at 780 Hz for a duration of 3 s. All channels were then stored in digital format on a microcomputer.

Variables that assessed task performance were lateral platform displacement and cycle frequency. Maximum platform displacement from TDC was recorded with a video camcorder and subsequently quantified with a motion analysis system. Cycle frequency was determined from the photocell signal. A cycle was defined as the time it took a subject to go from TDC, to the far right, and back to TDC.

EMG data were full-wave rectified and low-pass filtered (f_{cutoff} = 15 Hz). Muscle onset and cessation were identified using an interactive, computer-graphics program that plotted the submaximal, linear envelope of each channel against time. Muscle on-time durations were calculated as a percent of knee flexion and extension depending on when the muscles were active during the simulated skiing cycle. Durations of coactivation were determined by calculating, as a percent of flexion and extension, the common durations of muscle on-time between VL and LH. For the above variables, the means of trials 3, 4, and 5 were compared to the means of trials 98, 99, and 100 using dependent t-tests.

RESULTS AND DISCUSSION

Task performance improved as represented by an increase in lateral platform displacement (mean [early in practice] = 60.2 cm; mean [late in practice] = 81.7 cm) and an increase in cycle frequency (mean [early] = 1.68 Hz; mean [late] = 2.09 Hz). Fig. 2 shows portions of knee flexion and extension and temporal EMG results from early and late practice trials. Knee extension took place as subjects pushed the apparatus laterally and flexion occurred when the platform came back toward TDC. As subjects became more proficient at the task, the duration of knee extension increased and flexion decreased, as a percent of cycle time (see Fig. 2).

It was during knee flexion that subjects appeared to economize their motion after considerable practice. This is evidenced by significant decreases in the duration of VL activity and VL-LH coactivation. Although not statistically significant, LH duration also decreased during flexion. This confirms Verijken's suggestion, that learners exploit the characteristics of the task. In other words, the elastic return of the ski simulator platform must aid knee flexion since the muscles are active for a shorter duration. The decrease in duration of knee flexion does not confound this finding because muscle activity durations are expressed as percents of flexion and extension, not as a function of cycle time.

Additionally, the increase in coactivation during extension suggests that subjects tuned the neuromuscular system to the characteristics of the ski simulator. Increased displacement requires knee extension against an increasing force in the elastic bands. An increase in stiffness through coactivation in knee flexors and extensors may be the mechanism of control late in the knee extension phase of the cycle.

REFERENCES

Bernstein, N. The Co-ordination and Regulation of Movements, Pergamon: Oxford, 1967

Lee, T.D. et al. J. Motor Behav., 22, 191-208, 1990.

Vereijken, B. The Dynamics of Skill Acquisition (thesis), Vrije Universiteit, 1991.

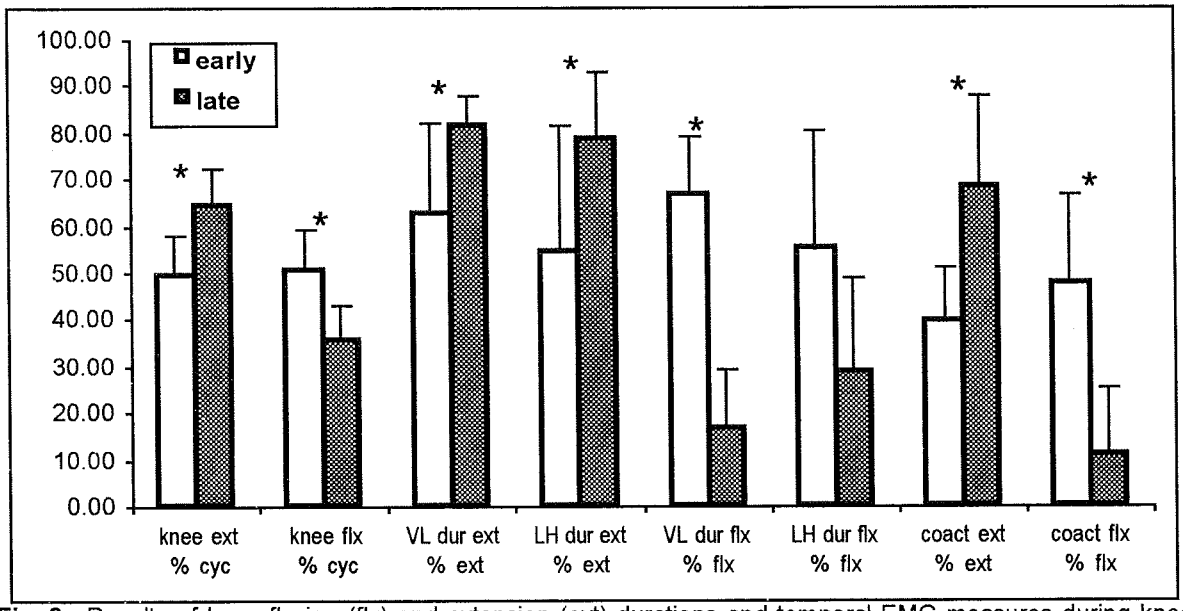

Fig. 2: Results of knee flexion (flx) and extension (ext) durations and temporal EMG measures during knee flx and ext. (VL - vastus lateralis; LH - lateral hamstrings; coact - duration of coactivation; *p <.05)

BENDING STRENGTH AND FAILURE MECHANISMS OF THE THUMB UCL

W.P. Smutz, W.P. Cooney, K.N. An
Orthopedic Biomechanics Laboratory, Mayo Clinic/Mayo Foundation, Rochester, MN

INTRODUCTION

To better understand the mechanisms of injury to the ulnar collateral ligament (UCL) of the thumb, bending strength, stiffness, and joint displacement at failure were measured. Acute injuries to the UCL are common and result from a wide variety recreational activities including skiing, wrestling, and football. Ten pairs of human cadaver specimens were tested to failure in abduction using a bi-axial servo-hydraulic test machine. Half the specimens were tested with the metacarpophalangeal (MP) joint extended while the other half were tested at 60 degrees of flexion. Results showed that the UCL was stronger, stiffer, and failed at a higher joint displacement with the MP joint extended and that the most common means of failure was a bony avulsion from the proximal phalanx.

REVIEW AND THEORY

Anatomically, the UCL of the thumb MP joint consists of two parts, a proper collateral ligament and an accessory collateral ligament. Both the proper and accessory collateral ligaments originate from the metacarpal head. The proper collateral ligament inserts into the base of the proximal phalanx while the accessory collateral ligament inserts in to volar plate. Acute injuries to the UCL are common and result from a wide variety activities. They are the most common upper extremity injury associated with downhill skiing and rank second among all downhill skiing injuries.[1] The injury is also common in wrestling, ice hockey, basketball, and football.[4] It is believed that the injury occurs when the thumb is forced into abduction, resulting in rupture of the UCL or avulsion of the distal end of the UCL from its attachment site on the proximal phalanx.[2] Moberg tested the strength of the proper UCL, in axial tension, in one human cadaver specimen.[3] To date, this is the only strength data available for the UCL. Therefore, the purposes of this study were to measure the torque and angular displacement required to produce failure of the UCL of the thumb MP joint in abduction and to examine the effect of joint position on failure strength, joint displacement, and the mechanism of failure.

PROCEDURES

Ten pairs of fresh frozen human cadaver thumbs (4 male and 6 female, mean age 75.9 years) were used in this study. After thawing, the specimens were disarticulated at the interphalangeal and carpalmetacarpal joints and the muscular soft tissue surrounding the MP joint capsule was removed. Care was taken to not disturb the joint capsule. The distal half of the proximal phalanx and the proximal half of the metacarpal were then embedded in plastic cylinders using dental plaster (Miles Dental Products, South Bend, IN). The specimen was then mounted in a specially designed test fixture attached to a bi-axial servo-hydraulic test machine (MTS 810, MTS Systems Corp., Minneapolis, MN). The center of the MP joint was positioned to coincide with the rotational axis of the hydraulic actuator. This technique allowed the MP joint to be loaded in pure torsion.

Before performing the failure tests, joint laxity was measured by loading each specimen to 0.5 N-m of torque in both abduction and adduction for 5 cycles. Joint laxity was measured for each specimen with the MP joint extended and at 60 degrees of flexion. The specimens were then tested to failure. The specimen was preconditioned to 0.5 N-m for 10 cycles and then tested to failure in abduction at a rate of 50 degrees per second. Torque and angular displacement were recorded at 120 Hz and stored on a computer. One thumb from each specimen pair was tested with the MP joint extended while the second thumb was tested with the MP joint at 60 degrees of flexion. After testing each specimen was radiographed and then dissected under 3.5x magnification to determine the structures that had failed. The differences in joint laxity, failure torque, angular displacement, and joint stiffness for specimens tested with the MP joint in extension or at 60 degrees of flexion were compared using paired T-tests. The differences in the mode of failure of the UCL, for specimens tested with the MP joint in extension or at 60 degrees of flexion, was compared using a Chi-squared test.

RESULTS

Joint laxity for a typical specimen is shown in Figure 1. For a torque of 0.3 N-m, mean joint laxity, for all ten specimens, was 27.4 $\pm$ 6.9 degrees when the MP joint was extended and 14.3 $\pm$ 4.6 degrees when it was flexed. Mean torque and angular displacement at failure and joint

stiffness are shown in Table 1. For the specimens tested with the MP joint extended, 6 of the 10 failed by bony avulsion of the proper UCL from the proximal phalanx. For the specimens tested with the MP joint in 60 degrees of flexion, 8 of the 10 failed by bony avulsion. The remainder of the specimens had midsubstance failures of the proper UCL. No statistically significant ($p>0.5$) differences were found for torque at failure or failure mode between the specimens tested with the MP joint in extension and those tested with the MP joint in 60 degrees of flexion. However, statistically significant ($p<0.5$) differences were found for joint laxity, angular displacement at failure, and stiffness between the specimens tested with the MP joint in extension and those tested with the MP joint in 60 degrees of flexion.

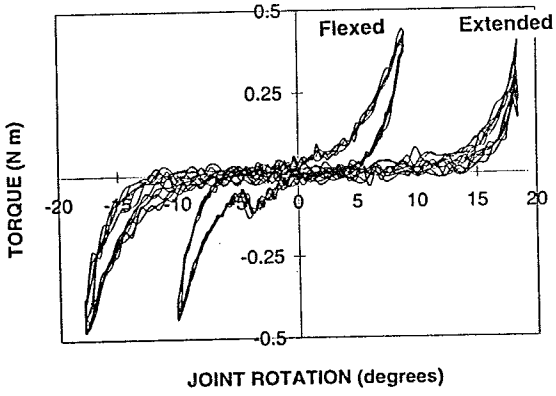

Figure 1. Comparison of joint laxity with the thumb MP joint in extension and at 60 degrees of flexion.

TABLE 1
MECHANICAL PROPERTIES OF UCL

MP Joint Position	Failure Torque (N-m)	Angular Displ at Failure (degees)	Stiffness (N-m/deg)
Extended	3.3 ± 1.2	32.8 ± 6.0	0.24 ± 0.08
60 Degees Flexion	2.8 ± 0.9	26.2 ± 5.4	0.18 ± 0.06

DISCUSSION

The laxity of the MP joint was found to be greater when the MP joint was extended than when it was flexed. This is consistent with anatomical findings that show the proper UCL is lax when the MP joint is extended and taut when the MP joint is flexed[3]. Results from this study are consistent with those reported by Moberg[3]. If it is assumed that during abduction, the MP joint pivots about a point close to the center of the joint (10 to 15 mm from the UCL), then the failure torque for the UCL measured in this study agrees closely with the 350 N tensile strength measured by Moberg[3]. Results from this study showed that the UCL was stiffer and failed at a higher angular displacement of the joint with the MP joint extended than when the MP joint was flexed to 60 degrees. The higher joint angular displacement at failure, when the joint is extended, is a result of the greater laxity of the MP joint when it is extended. Although not statistically significant, trends in the data also suggest that the UCL was stronger in extension than at 60 degrees of flexion. The increased strength and stiffness of the UCL, when the MP joint is extended, may be due to a greater contribution by the accessory UCL when the joint is extended. Anatomical studies of the MP joint have shown that the accessory UCL is taut when the MP joint is extended and lax when the MP joint is flexed.[3] The majority of the specimens in this study failed by bony avulsion of the proper UCL from the proximal phalanx. Clinically, the majority of acute UCL injuries are found to be midsubstance failures and not bony avulsions.[5] This difference in failure mechanisms may be because the normal mode of injury of the UCL is actually a combination of abduction and hyper-extension and/or torsion and not pure abduction as was modeled in this study. Also the loading rate for the actual injury may be much higher than the 50 degrees per second used in this study. Further work is needed before the mechanism of acute injuries to the UCL can be fully understood.

REFERENCES

1. Carr, D. et al. *Am J of Sports Med* 9(6): 378-383, 1981
2. Cooney, W.P. et al. *Ad in Ortho Surg* 13(6): 235-348, 1990
3. Moberg, E. et al. *Acta Chir Scand* 106:166-186, 1953
4. Newland, C.C. *Orthop Clin North Am* 23:41-48, 1992
5. Posner, M.A. et al. *Hand Clinics* 8(4):713-732, 1992

ACKNOWLEDGEMENTS

This study was supported in part by NIH Grant F32 AR08249

INDEX FINGER MUSCLE COORDINATION DURING AD-ABDUCTION FORCES MAY BE EXPLAINED BY THREE DEGREES OF FREEDOM AT MCP JOINT

F.J. Valero-Cuevas[†*], C. Burgar[†°], F.E. Zajac[†*°], V.R. Hentz[‡°], K. McGill[†], K.N. An[¥]

[†]Rehabilitation R&D Center and [‡]Hand Center, VA PAHCS, Palo Alto, CA 94306

[*]Dept. Mech. Eng. Stanford U. and [°]Dept. Functional Restoration, Stanford U. Medical Center. Stanford, CA 94305

[¥]Orthop. Biomech. Lab., Mayo Clinic, Rochester, MN 55905

INTRODUCTION

Identifying the muscle excitation patterns (MEPs) that produce finger forces is relevant to the restoration of hand function as they may reveal surgical and rehabilitation factors and principles that contribute to successful grasp outcomes. Our theoretical-experimental study of the static force generation capabilities of the index finger has identified the MEP which produces maximum abduction force (analogous to that used in key pinch). Production of this force requires control of the axial rotation degree-of-freedom (DOF) of the proximal phalanx at the MCP joint.

REVIEW AND THEORY

Due to the biomechanical complexity of the fingers, some finger forces which create grasps commonly targeted for rehabilitation (e.g., key and tip pinch) may be produced by different MEPs. Researchers have used biomechanical models to either find MEPs which optimize specific objective functions or graphically describe unique MEPs that maximize finger forces based on the natural limits of muscle forces, independently of objective functions (Chao et al, 1978). Using multidimensional computational geometry, we have generalized the latter approach to include the surgically relevant biomechanical characteristics of the index finger (e.g., strength, moment arms, DOFs, etc.) to understand how these parameters affect not only grasping MEPs, but also the bounds on their force generation capabilities.

The model is a four DOF kinematic chain consisting of a metacarpal and three phalanges, articulated by two orthogonal hinges at the MCP junction (ad-abduction and flexion-extension) and single hinges articulating the proximal and distal interphalangeal junctions (PIP and DIP flexion-extension, respectively). All seven muscles of the index finger are included in the model: *flexor digitorum profundus* (FDP), *flexor digitorum superficialis* (FDS), *extensor indices proprius* (EIP), *extensor digitorum communis* (EDC), *first lumbrical* (1LUM), *first palmar interosseous* (1PI) and *first dorsal interosseous* (1DI). A generic model of force production emulates specific muscles by setting pennation angle, physiological cross sectional area, muscle fiber length and excitation level. The excitation level, a value between zero and one, corresponds to muscle force magnitude between zero and maximum isometric. A MEP lists the excitation levels of the seven muscles at a given instant. We modeled the tendons and extensor complex as non-compliant mechanisms, based on measurements from a fresh cadaver, which define the moment arms of all muscles at all spanned joints as a function of joint angles (An et al, 1983). To our knowledge, this is the first 3D biomechanical model to consider all seven muscles of the index finger and the generation of distal phalanx torque (a consequence of having three flexion DOFs).

Briefly, all possible excitation levels of all muscles are biomechanically mapped into the bounds on achievable finger forces and torque. The functional constraints on a given grasping force (e.g., a specific direction) then define subsets of the bounds where its maximum biomechanically feasible magnitude is produced by a unique MEP. We now test our predictions for index finger key pinch force.

PROCEDURES

The model predicted the MEP which produces the theoretically maximum force originating at the midpoint of the distal phalanx subject to the following constraints: constant posture (i.e., static equilibrium, including zero torque at the distal phalanx) and force in the abduction direction (i.e., radial force). We studied two finger postures, extended (10° flexion at all joints) and flexed (45° flexion at MCP and PIP, 10° flexion at DIP joints), in neutral ad-abduction. Radial force in the flexed posture may be considered analogous to index finger force during key pinch. Peak force in adduction direction (ulnar force) was modeled and experimentally tested for completeness.

We estimated MEPs in eight healthy adults by simultaneously recording intramuscular EMG (iEMG) from all muscles of the index finger during the production of static, maximum voluntary radial force in both postures. All iEMGs were free from crosstalk and no significant discomfort was reported at the electrode sites. Concurrent visual feedback of force magnitude was provided. To present the subjects with the same constraints as those modeled, radial force was produced by pressing a 5 mm diameter brass ball—embedded in a custom thimble worn on the finger—against a rigid six axis force-sensing plate. The thimble ensured that the force was normal to the plate (i.e., in the desired direction) and that there was no distal phalanx torque, because the ball would slip or the finger flex otherwise. The subjects were instructed to produce and hold maximum force against the plate for 2-s. Three maximum forces were collected per posture and consistency of the posture was monitored by video recordings. Subjects performed a complete baseline experiment without

electrodes. Repeated measures analysis of variance (RM-ANOVA) found peak forces were not affected by the presence of the electrodes.

The envelope of the iEMG for each muscle was obtained by smoothing (τ=20 msec) the 100 Hz-20 KHz band pass amplified, full wave rectified signal. All iEMG envelopes were normalized by their corresponding reference maximum collected with the finger braced in place by the investigator during maximum isometric voluntary contractions of all muscles at each posture, immediately before and after radial force production. The normalized iEMGs present during maximum force were averaged across trials. RM-ANOVA tested for posture effect on mean excitation levels and peak force magnitudes.

RESULTS

Peak radial force at all postures is predicted to be the result of fully exciting 1DI (the principal MCP abductor) and not exciting 1PI, its ad-abduction antagonist. The strong MCP flexion torque 1DI produces must then be stabilized by maximal excitation of both extrinsic extensors, which have lower MCP torque capacity. The resulting extensor torques at the interphalangeal (IP) joints are then canceled by low level flexor excitation, due to their relatively larger IP torque capacities. 1LUM is predicted to be highly excited and to have little effect on peak force.

In the extended posture, RM-ANOVA post-hoc tests on average excitations showed that, in agreement with the model, 1DI, extensors and LUM were significantly higher than 1PI and flexors ($p<0.05$, Figure 1A). In the flexed posture (Figure 1B), 1DI excitation dropped ($p<0.05$) and 1PI was higher than 1DI to near statistical significance ($p<0.07$). Other muscle excitations and peak force did not change significantly with posture.

DISCUSSION

The observed 1PI activity in the flexed posture contradicts the model's prediction that maximum radial force requires zero antagonist excitation at all postures. We similarly found that maximum ulnar force also involved a decrease in agonist (1PI) and an increase in antagonist (1DI) excitation in the flexed posture ($p<0.05$). The reduction in agonist excitation can perhaps be explained by the fact that finger flexion shortens interossei muscle fibers and changes MCP flexion moment arms, but this does not explain the increased antagonist excitation.

This discrepancy can be resolved if we consider the torsion of the proximal phalanx at the MCP joint 1DI and 1PI can produce (a DOF not included in our or other published models). In the extended posture, radial force is mostly the product of abduction torque, as predicted by the model, and the slight pronation effects due to radial force and 1DI excitation are cancelled by low excitation of 1PI (Figure 1). In the flexed posture, however, the radial force produces greater pronation torsion and increased 1PI excitation is necessary to stabilize torsional posture. Note that, at 45° of MCP flexion, neutral MCP ad-abduction and torsion stabilization is not yet done passively by MCP collateral ligaments. The inverse of this complex muscle interaction applies to maximum ulnar force. The complex interactions at the extensor mechanism may explain the predicted and measured reduction in EIP excitation with increased 1PI excitation.

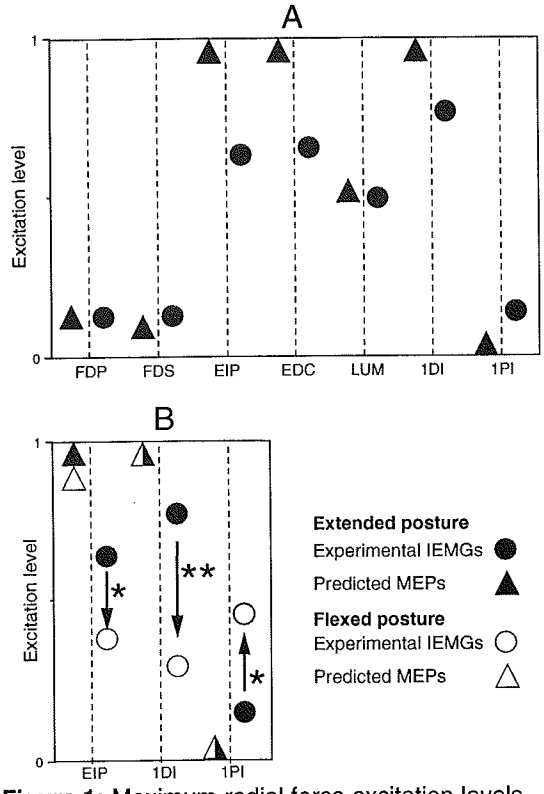

Figure 1: Maximum radial force excitation levels (n=8). Arrows indicate trends in mean excitation as posture changed from extension to flexion (**=significant at $p<0.05$; *=almost significant, $p<0.07$).

We conclude that understanding MCP joint control, in general, and maximum key pinch force, in particular, may require consideration of the MCP joint as a three DOF articulation.

REFERENCES

E.Y. Chao and K. An, J Biomech Eng. Graphical interpretation of the solution to the redundant problem in biomechanics, 100, 1978; K. An et al., J Biomech. Tendon excursion and moment arm of index finger muscles, 16(6), 1983.

ACKNOWLEDGMENTS

E.M. Johanson for placing the electrodes in some subjects; H.F.M. van der Loos and P. Lum for their assistance with the force sensing apparatus. Funding agency: Rehabilitation R&D Service, Department of Veterans Affairs.

MARKERLESS THREE DIMENSIONAL MEASUREMENT OF KNEE KINEMATICS USING SINGLE-PLANE FLUOROSCOPY

Scott A. Banks[1], Anne Z. Banks[1], Frank F. Cook[1,2], W. Andrew Hodge[1,2]
[1]Good Samaritan Medical Center, Orthopaedic Research Laboratory, West Palm Beach, Florida 33401
[2]Palm Beach Orthopaedic Institute, West Palm Beach, Florida 33401

INTRODUCTION

Kinematics of the normal, injured, or prosthetically replaced knee joint are a complex combination of rolling, gliding and rotational motions which are significantly influenced by activity, integrity of the ligaments and capsular structures, muscle activity, and articular geometry. Accurate kinematic information is critical to understanding the function and pathogenesis of the knee, particularly during weight bearing dynamic activities. The present study was undertaken to characterize the accuracy of a non-invasive fluoroscopic technique for measuring dynamic three-dimensional (3D) knee motions in individuals whose knees **have not** been prosthetically replaced. This technique utilizes orthogonal planar radiographic views of the knee to create a 3D contour model of consistently identifiable bony features for both the tibia/fibula and femur. The measurement technique is implemented by projecting the contour model onto digitized fluoroscopic images of the moving knee, and determining the translations and rotations which give the best correspondence between the projected contour model and the radiographic projection of the bone. Controlled *in vitro* assessment of the technique resulted in an average rotational accuracy of 1.1 degrees and a sagittal plane translational accuracy of 1.3 mm.

REVIEW AND THEORY

The functional motions of the normal human knee joint, although complex, are relatively constrained when the menisci, cruciate ligaments, and collateral ligaments are intact. Loss of any of these soft tissue constraints can increase the envelope of motion, and lead to knee instability, accelerated degenerative changes, and impaired functional capabilities. There continues to be great interest in accurate quantitative assessment of knee function in order to better understand normal knee mechanics, injury mechanisms, surgical and rehabilitative treatments, and the function of knee replacements.

Many techniques have been reported for the measurement of dynamic knee motion *in vivo*. However, most of these techniques suffer from one or more fundamental limitations: body surface mounted markers or fixtures which can move relative to the bones, insufficient frame rates, inability to measure dynamic weight bearing activities, and surgical or invasive attachment of markers to the bones.

Banks, *et al.*, (1996) recently reported a technique for the accurate 3D measurement of knee replacement motions using single-plane fluoroscopy. This technique provides a direct measurement of prosthesis motion at frame rates up to 200Hz using current video technology. The technique is based upon precise knowledge of the prosthesis surface geometry and the optical geometry of the fluoroscope, which are used to implement a shape matching technique for pose determination. However, this technique is not well suited for the measurement of anatomic (non-implanted) knee motions because precise individualized 3D bone models are not readily available, and would be cost prohibitive for all but the smallest of studies or clinical implementations.

This paper reports on the implementation and initial characterization of a simple technique for 3D kinematic measurement of the anatomic knee using single-plane fluoroscopy. We hypothesized for both the tibia/fibula and femur, that anatomic contours representing lines of maximum convexity or concavity could be identified and used to generate a 3D 'contour model', which could well represent the salient features of knee radiographs over a functional range of translations and rotations. The measurement procedure consists of two parts: model generation from orthogonal planar views of the knee, and matching projected model contours with fluoroscopic images of the moving knee.

PROCEDURES

Data Acquisition

An intact frozen knee specimen was rigidly mounted to the actuator of a biaxial (linear/rotary) servohydraulic testing machine (Instron model 8521, verified to ASTM E4, E74). The specimen was mounted so that the knee was in approximate alignment with the linear axis of the actuator. An orthogonal metal triad was fixed to the anterior aspect of the knee for alignment and absolute scale reference. A fluoroscope with 23cm diameter image intensifier was positioned to obtain a lateral view of the knee with the femoral condyles superimposed, and the knee center in the middle of the image. The knee was rotated 90 degrees about the long axis to obtain an anterior/posterior view of the joint centered in the image. The knee was again positioned in the lateral view, and images were recorded as the knee was rotated about the long axis from -16.0 degrees to +16.0 degrees in 2.0 degree increments. This procedure was repeated for ±2.54cm displacements of the linear axis of the actuator (superior/ inferior displacements). The knee was repositioned with the patella facing upward, and it was rotated about the anterior to posterior axis from -7.0 degrees to +7.0 degrees in 1.0 degree increments (abduction/ adduction of the knee). This procedure was also repeated

for ±2.54cm displacements of the linear actuator. The perspective projection parameters (principal distance and principal point) of the fluoroscope were determined using previously reported procedures (Banks, et al., 1996). All images were recorded on Hi-8mm videotape.

Image Processing, Model Generation, and Matching

Images were digitized and geometric distortions were corrected using bilinear interpolation. The femoral contour model was created by manually tracing the contours of the posterior and inferior aspects of the medial and lateral condyles, and a contour running from the anterior cortex, through the intercondylar notch, and up along the posterior cortex. The frontal plane view was used to determine the medial/lateral displacements of the sagittal contours. All contours were represented in 3D space through the appropriate inverse perspective scaling. The tibial contour model was similarly generated by tracing the contours of the superior fibular head, the posterior aspect of the medial tibial plateau, and the contour following the anterior tibial tubercle, the intercondylar eminence and the posterior cortical margin.

Matching and pose estimation were performed by projecting the contour model onto the fluoroscopic image of the knee in an unknown pose, and manually varying the model's 3D position and orientation until the best visual match between contours was achieved. The translations and rotations required to superimpose the contour model over the image were taken as the unknown 3D pose of the bones.

Analysis

The coordinate transformations between the reference frame of the knee and the actuator, and the actuator and the fluoroscope, were determined by minimizing the mean errors between the known actuator motions and the estimated knee motions (Banks, *et al.*, 1996, this procedure assumes that the measurement is unbiased). Given these transformations, it is possible to model the actuator motions in the measurement reference frame, and to compare these motions with the image matching based estimates. The calculated errors are zero mean, by definition, and therefore the standard deviation of these errors represents the error expected for a single measurement. The errors for the abduction/adduction tests were averaged with the long axis rotation and translation tests for the appropriate anatomical rotations and translations.

An alternative method to assess the errors is to compute the standard deviation of the 'motions' between the femur and tibia/fibula. Since the knee joint was frozen, the net motions were zero, and the standard deviation represents the error for measuring relative motions.

RESULTS

Table 1 gives the standard errors for the femur and tibia/fibula in the global reference frame. Matching results are consistently better for the femur than the tibia/fibula. Errors in relative motion estimates, which are approximately equal to the sum of the individual estimation errors, indicate that the measurement errors are uncorrelated.

Standard Errors	Femur	Tibia/Fibula	Relative Motion
Anterior/Posterior Translations (mm)	0.5	1.6	3.1
Superior/Inferior Translations (mm)	1.2	1.6	0.6
Medial/Lateral Translations (mm)	0.6	4.7	7.2
Ab/Adduction Rotations (deg)	0.8	1.8	1.6
Internal/External Rotations (deg)	0.7	1.3	1.9
Flexion/Extension (deg)	0.9	0.9	1.6

Table 1: Standard errors for the femur and tibia/fibula in the global reference frame, and their relative motions.

DISCUSSION

The initial experience with this measurement concept has been quite encouraging. The primitive, manual implementation of the matching technique provides knee kinematic estimates which have accuracy comparable to, or better than, many previously reported techniques. This technique provides a direct measurement of bone motion, thus the accuracy achieved for the calibration studies should also be realized for *in vivo* measurements.

The least accurate measurement using this technique is for translations perpendicular to the image plane, corresponding to medial/lateral displacements. This inaccuracy does not pose a serious limitation for the measurement of knee kinematics due to the very small magnitude of medial/lateral translations which occur in normal, pathological, and joint replaced knees.

The accuracy in tracking the femur was consistently better than that for tracking the tibia/fibula. This is due to differences in bony geometry, which affect both the ability of the 'contour model' to accurately represent the surface geometry of the bone(s), and the degree to which rotations and translations influence the shape of the bone's projection. We anticipate that with more complete models of the bony anatomy, and an optimization based automatic matching algorithm, we will be able to demonstrate significantly greater measurement accuracies than reported in this communication. We believe that this measurement concept has the potential to provide an accurate, clinically useful diagnostic tool using equipment which is already available in most hospitals.

REFERENCES

Banks, S.A., and Hodge, W.A., 1996, "Accurate measurement of three-dimensional knee replacement kinematics using single-plane fluoroscopy," *in press* IEEE Trans. Biomed. Eng., Vol. 43, No. 6.

PATELLOFEMORAL CENTER OF PRESSURE AND CENTROID OF CONTACT AREA: EFFECTS OF REMOVAL AND RECONSTRUCTION OF THE ANTERIOR CRUCIATE LIGAMENT

Yeou-Fang Hsieh, Louis F. Draganich, Sherwin Ho, and Bruce Reider
Section of Orthopaedic Surgery and Rehabilitation Medicine
Department of Surgery
The University of Chicago
Chicago, Illinois

INTRODUCTION

We investigated the effects of the removal and reconstruction of the anterior cruciate ligament (ACL) on the paths of the center of pressure and the centroid of the contact area on the retropatellar surface during physiologic levels of quadriceps loads in seven cadaveric knees. The knee was reconstructed with an intraarticular graft using the autogenous central one-third of the bone-patellar ligament-bone graft. Knee loading was produced by extending the knee with quadriceps forces based on one-third of reported maximum voluntary isometric extension moments. The three-dimensional positions of the patellofemoral and tibiofemoral joints were measured at 30°, 60°, and 90° of knee flexion with a six degree-of-freedom digitizer. Fuji Prescale film was used to record patellofemoral contact pressure. Pressure intensity was digitized using a high resolution optical scanner. Digital image processing techniques were applied to analyze the contact prints. Force and moment equilibrium of the patella under the actions of the quadriceps force, resultant contact force, and patellar ligament tension were performed to obtain the center of pressure. The centroid of the patellofemoral contact area was defined as the geometric center of the contact area.

REVIEW AND THEORY

Instability of the knee occurring with rupture of the ACL often results in functionally significant disability of the tibiofemoral joint and therefore of the patellofemoral joint. Despite the fact that reconstruction of the ACL enhances the stability of the tibiofemoral joint, frequently, even with good stability, patients have complained of pain in the anterior aspect of the knee[5,7]. Factors thought to contribute to patellar pain include malalignment between the patella and femur leading to abnormal patellofemoral contact. There have been no reports of studies performed on the effects of ACL deficiency or its reconstruction on patellofemoral center of pressure or centroid of the contact area. Such information would be important to further our understanding of the biomechanics of the patellofemoral joint, the causes of joint pathologic changes, and the surgical reconstruction of the ACL. Thus, the objectives of this in vitro study were to determine the effects of removal and intraarticular reconstruction (IAR) of the ACL on the paths of the center of pressure and of the centroid of the contact area on the retropatellar surface for physiologic levels of quadriceps loads.

PROCEDURES

The proximal and distal thirds of seven knees with a mean age of 51.4 years were obtained fresh at autopsy for testing. Tests were performed for three experimental states on each specimen, first on the intact knee, second following excision of the ACL, and finally following intraarticular reconstruction of the ACL for flexion angles of 30°, 60°, and 90°. An IAR was performed utilizing the central one-third of the patellar ligament with bone blocks attached. Patellofemoral contact areas and pressures were recorded using low-pressure Fuji Prescale film which was hermetically sealed in polyethylene sheets. A medial parapatellar incision was performed for insertion of the film packets. Prior to testing, four reference holes, 1 mm in diameter, were drilled in an anteroposterior direction through the patella to serve as reference positions for the coordinate transformation between the pixel and patellar coordinate systems. Testing consisted of applying external flexion moments equivalent to 1/3 of values reported in the literature for maximum isometric quadriceps moments[6], equilibrating the knee with quadriceps forces at a particular flexion angle, measuring patellofemoral and tibiofemoral joint motions, and digitizing attachment sites of the quadriceps tendon and patellar ligament with the 3Space digitizing and tracking system (Polhemus Navigation Sciences, Colchester, Vermont) having average and maximum inaccuracies of 0.57 mm and 1.01 mm, respectively. After the motion data were collected, the knee was disarticulated and bony landmarks of the femur, tibia, and patella were identified and digitized for construction of the anatomical coordinate systems[1,2].

The patellofemoral contact stain on the Fuji Prescale film was digitized with a high resolution (600 dpi X 600 dpi) scanner to obtain an image of size 640 X 480 pixels with an intensity (up to 256 levels) stored in each pixel. Before the contact stain could be analyzed, calibration of the scanning system and of the Fuji Prescale film was performed. Five scanning parameters [rotation (α), offsets (T_x,T_z), and scaling parameters (S_x,S_z)] were determined using the method of least-squares to establish a coordinate transformation between the pixel (u,v) and patellar (x,z) coordinate systems assuming the x-z plane to represent the posterior surface of the patella. A cubic polynomial was used to characterize the relationship between the magnitude of the pressure and the intensity of gray level. Patellofemoral contact pressure distribution maps were then established as $P_{u,v}=P(u,v)$, where (u,v) are the coordinates of a contact pixel with area of S_xS_z. Contact area (A_c) was defined as the locus of the contact pixels according to $A_c=\Sigma S_xS_z$. The resultant contact force (F_c) was obtained by integrating the pressure distribution over the entire contact area according to $F_c=\Sigma P_{u,v}S_xS_z$. Force and moment equilibrium of the patella under the actions of the quadriceps force $\left(F_q\vec{e}_q\right)$, patellofemoral contact force $\left(F_c\vec{e}_c\right)$,

and patellar ligament tension $\left(F_p\vec{e}_p\right)$ were performed to obtain the patellar ligament force (F_p), direction cosines ($\vec{e}_c$) of F_c, and center of pressure ($\vec{r}_c$) according to

$F_c\vec{e}_c + F_q\vec{e}_q + F_p\vec{e}_p = \vec{0}$ (1), $\sum_{i=1}^{3} e_{ci}^2 = 1$ (2), and

$(\vec{r}_q - \vec{r}_p) \times F_q\vec{e}_q + (\vec{r}_c - \vec{r}_p) \times F_c\vec{e}_c = \vec{0}$ (3), where

$\vec{r}_q$ and $\vec{r}_p$ were the attachment sites of the quadriceps tendon and patellar ligament. The centroid of the patellofemoral contact area was determined according to $x_{ca} = (\Sigma x S_x S_z)/A_c$ and $z_{ca} = (\Sigma z S_x S_z)/A_c$. Paired t-tests were performed to determine significant differences in the center of pressure and in the centroid of the contact area between the intact and ACL-excised knees and between the intact and IAR knees. Based on a Bonferroni adjustment for two comparisons at three flexion angles, an $\alpha = 0.008$ was considered significant.

RESULTS

In the intact, ACL-excised, or ACL-reconstructed knee, the patellofemoral contact zone consisted of a mediolaterally oriented band on the posterior surface of the patella which migrated from the distal one-third of the articular margin at 30° to the proximal margin at 90° of knee flexion. The center of pressure shifted proximally on the lateral facet of the patella as the knee flexed from 30° to 90° for the three states (Figure 1). The average amount of proximal and lateral shifts between 30° and 90° of knee flexion were 13.9 mm and 1.2 mm for the intact knee, 16.9 mm and -2.9 mm for the ACL-excised knee, and 15.1 mm and 2.7 mm for the ACL-reconstructed knee, respectively. Similar to the pathway of the center of pressure, the centroid of the contact area shifted proximally on the lateral facet of the patella as the knee flexed from 30° to 90° for the three states (Figure 2). The average amount of proximal and lateral shifts between 30° and 90° of knee flexion were 13.7 mm and 1.3 mm for the intact knee, 16.6 mm and -2.4 mm for the ACL-excised knee, and 15.1 mm and 3.0 mm for the ACL-reconstructed knee, respectively. However, neither removal nor reconstruction of the ACL resulted in significant differences in the path of the center of pressure or in the path of the centroid of the contact area on the retropatellar surface when compared to the intact knee. Furthermore, no significant differences were found between the center of pressure and the centroid of the contact area at 30°, 60°, and 90° of knee flexion for the three states.

DISCUSSION

In agreement with the results reported by Singerman et al.[8], the center of pressure shifted proximally on the lateral facet as the patella displaced distally on the femoral trochlea between 30° and 90° of knee flexion. The pathways of the centroid of contact area, which have not been reported previously, were found to be remarkably similar to those of the center of pressure from 30° to 90° of knee flexion. This finding is consistent with the result that the distribution of contact pressure was remarkably uniform over the entire contact surface[4]. Thus, for the three experimental states and loading conditions investigated, it appears that the centroid of the contact area can be used to predict the location of the center of pressure. This may be important in future studies of this nature because the determination of the centroid of the contact area is much less demanding. Although we did not discover patellofemoral center of pressure or the centroid of the contact area in the ACL-excised knee to be significantly different from those of the intact knee, there were some differences which might become significant with a larger number of samples since significant differences in tibiofemoral and patellofemoral kinematics were found[3]. However, the intraarticular reconstruction performed in this study was found to return normal tibiofemoral and patellofemoral kinematics to the ACL-excised knee[3]. Thus, significant differences in contact characteristics would not be expected between the intact and ACL-reconstructed knee. This suggests that factors other than patellofemoral center of pressure and centroid of contact area may be responsible for patellofemoral pain following IAR that returns normal kinematics to the patellofemoral joint.

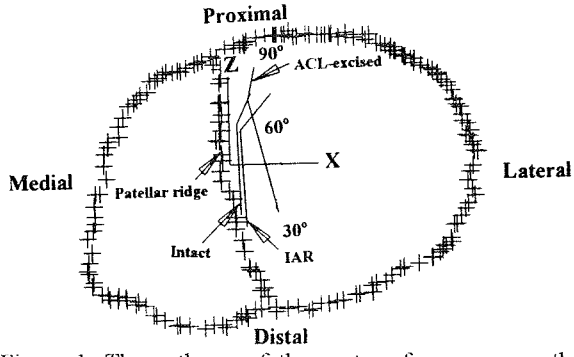

Figure 1. The pathway of the center of pressure on the retropatellar surface from 30° to 90° of knee flexion.

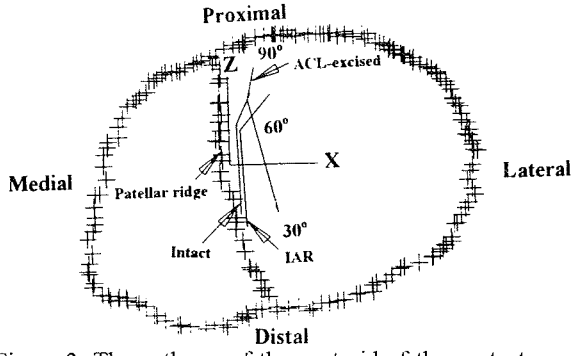

Figure 2. The pathway of the centroid of the contact area on the retropatellar surface from 30° to 90° of knee flexion.

REFERENCES

1. Grood et al: J Biomech Engng, 105: 136-144, 1983.
2. Hefzy et al: J Biomed Engng, 14: 329-343, 1992.
3. Hsieh et al: ASB 19th Annual Meeting: 251-252, 1995.
4. Huberti et al: J Bone Joint Surg, 66A: 715-724, 1984.
5. Noyes et al: Clin Ortho, 265: 241-252, 1991.
6. Lieb et al: J Bone Joint Surg, 53A: 749-758, 1971.
7. Sachs et al: Am J Sports Med, 17: 760-765, 1989.
8. Singerman et al: J Biomech, 27: 233-238, 1994.

BIOMECHANICAL EFFECT OF TENDON MEDIALIZATION IN ROTATOR CUFF REPAIRS

Jain Liu, Richard E. Hughes, Shawn W. O'Driscoll, and Kai-Nan An
Mayo Clinic/Mayo Foundation, Rochester, MN 55905

INTRODUCTION

Repair of rotator cuff tears may affect the mechanics of the shoulder abductor mechanism. Some repair methods require moving the insertion of the supraspinatus tendon medially from its normal location. The purpose of this study was to quantify the effect of medialization of the supraspinatus tendon on its moment arm for elevation in the scapular plane.

REVIEW AND THEORY

Many authors emphasized the importance of "watertight" closure of cuff tears to prevent "cuff-tear arthropathy". This can be easily achieved by direct repair in a tendon-to-tendon or tendon-to-bone fashion for small and medium tears, but not always in large/massive tears or revision repairs. In such cases, the tendons are mobilized and either transposed or sewn into a bony trough in the head as close as possible to the normal insertion (McLaughlin, 1944). After medialization, the line of action of a muscle changes due to the altered insertion; thus, the moment arm should change, altering the torque generated by the cuff. The change in moment arm after medialization can be used as an indicator of the effectiveness of the tendon in moving the joint.

PROCEDURES

Ten fresh frozen cadaveric shoulders free from rotator cuff pathology, arthritis, limited range of motion or bony deformity were used. There were five right shoulders and five left from four males and five females, and mean age was 67 (range 40 - 89). Specimens were prepared by attaching 50 lb test nylon line to the tendons of the supraspinatus, subscapularis, infraspinatus, and deltoid (anterior, middle, and posterior portions). The effect of medialization of the supraspinatus tendon was simulated by attaching 30 lb test nylon line to nine locations arranged in three anterior-posterior rows at three lateral positions beneath the supraspinatus tendon on the humeral head (Figure 1). The string for each simulated tendon insertion was affixed to the humeral head by an acrylic pin driven into pre-drilled holes in the bone. The first row of attachment sites was just inside the tendon, 3 mm medial to the synovial surface of the tendon insertion. The second row was 7 mm medial to the first row (i.e. 10 mm medialization), and the third row was 7 mm medial to the second row (i.e. 17 mm medialization). Weights (100 gm) were hung from the ends of the lines to remove slack from the system. The coracoacromial ligament was preserved.

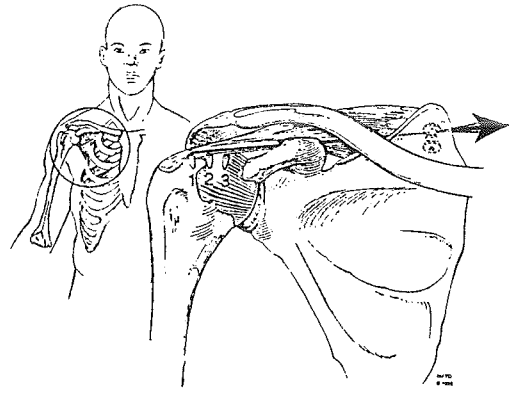

Figure 1. Location of simulated tendon insertions.

The scapula was rigidly attached to a Plexiglas test fixture, and an IM rod was inserted into the humerus so that elevation in the scapular plane could be controlled with a guide. The guide also prohibited internal or external rotation during elevation. The wires were routed through guides in the Plexiglas to pulleys attached to potentiometers (3500S-2-103, Bourns Corp., Riverside, CA), which were used to measure tendon excursion as the humerus was elevated. A magnetic tracking device (3Space Tracker, Polhemus; Colchester, Vermont) was used to measure the glenohumeral angles. Three humeral elevation trials were performed.

Moment arms were calculated from the tendon excursion and joint elevation angle data (An *et al.*, 1984). For each trial the tendon excursion-glenohumeral elevation angle relationship was modelled using polynomial regression. The lowest order polynomial such that the root mean square error was less than 0.5 mm was used. The moment arm was computed by analytically differentiating the polynomial.

The effect of tendon medialization was analyzed by normalizing the moment arms of the medialized insertion locations by the moment arm of the normal supraspinatus.

RESULTS

The average moment arm of the intact supraspinatus ranges between 25 to 30 mm through a range of 10 to 60 degrees of glenohumeral elevation (Figure 2), and it reaches a peak at 33 degrees.

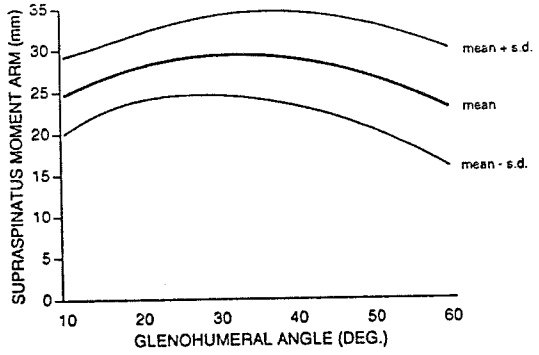

Figure 2. Abduction moment arm of the intact supraspinatus (Mean±S.D.) through the arc of motion.

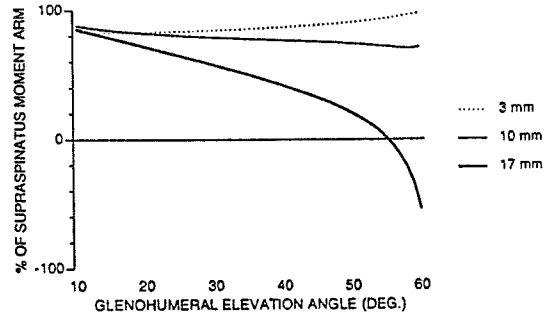

Figure 3. Normalized abduction moment arms for 3, 10, and 17 mm of medialization.

Normalized moment arms of the medialized tendon insertion (Figure 3) were affected by elevation angle ($P<0.0001$) and amount of medialization ($P<0.0001$). *Post-hoc* tests did not indicate that the 3 or 10 mm medialization conditions were significantly different from the normal supraspinatus; however, the moment arm for the 17 mm medialization condition was substantially less than the other conditions, especially in elevated postures.

DISCUSSION

Although medialization did affect moment arm, the effect was only present in the 17 mm medialization condition. That amount of medialization is not within the range of usual clinical practice. Therefore, it is reasonable to conclude that no evidence was found to support the hypothesis that medialization affects the abduction moment arm of the supraspinatus within clinically relevant ranges of tendon medialization.

This data supports the practice of medializing the insertion of the supraspinatus tendon when necessary. However, it should be noted that this analysis only considers the effect of medialization on abduction moment arm. The abductor mechanism is complicated, and other factors may also mediate the effect of medialization on abduction function. Medialization may also affect the length of the supraspinatus musculotendinous unit, which would affect the maximum force it could produce at any given glenohumeral angle.

REFERENCES

1. An, K-N *et al.*, *J. Biomech. Eng.*, 106, 280-282, 1984.
2. McLaughlin, H.L. *J. Bone Jt. Surg.*, 26, 31-51, 1944.

ACKNOWLEDGMENTS

Supported by NIH AR41171 and HD07447. J. Liu supported by the Rotary Foundation, Li Foundation, and National Science Council - Taiwan.

FORCES OF THE KNEE DURING OPEN AND CLOSED KINETIC CHAIN EXERCISES

N. Zheng, G. S. Fleisig, R. F. Escamilla, S. W. Barrentine, K. E. Wilk, J. R. Andrews
American Sports Medicine Institute, Birmingham, AL 35205

INTRODUCTION

Open kinetic chain (OKC) exercises, such as seated knee flexion and extension, are single joint and single muscle group exercises. Closed kinetic chain (CKC) exercises, such as squat and leg press, are multi-joint exercises and used as core exercises by athletes to enhance their performance in sport (Cahill and Griffith, 1978). Whether the OKC exercises or the CKC exercises should be used during rehabilitation of the knee has been controversial (Doucette and Child, 1996). The tibiofemoral force, patellofemoral force and the tensions of the cruciate ligaments are the key issues of the debate. This paper presents the cruciate ligament tensions, tibiofemoral force and patellofemoral force during knee extension, leg press and squat.

REVIEW AND THEORY

Tibiofemoral force and cruciate ligament forces at the knee in four men and one woman were compared during OKC and CKC exercises by Lutz et al (1993). The exercises were simulated by isometric contractions at 30, 60 and 90 degrees. The simulations of the exercises and measurement equipment mounted on the subjects may have had significant effects on their results. Steinkamp et al (1993) compared the patellofemoral forces during leg press and knee extension. Muscle activities, which have significant influence on the patellofemoral force, especially the co-contraction of the quadriceps and hamstring muscles, were not included in their study. In order to compare the forces at the knee and choose the appropriate exercise for strengthening or rehabilitation, data should be collected from normal exercises without influences from environment, such as the equipment mounted to subjects, and muscle activities should be included. In a previous work by these authors (Wilk et al, 1996) kinematic and kinetic data and muscle activities during OKC and CKC exercises were presented, but no cruciate ligament tension and patellofemoral compressive force were reported. The objective of this study was to calculate and compare the posterior cruciate ligament tension, tibiofemoral force and patellofemoral force during OKC and CKC exercises.

PROCEDURES

Synchronized data, kinematic, kinetic and electromyographic (EMG) were collected from the left knees of ten healthy male subjects. The EMG data were collected from the quadriceps, hamstring and the gastrocnemius muscle during knee extension, leg press, squat and maximum voluntary isometric contraction (MVIC). EMG data for each MVIC trial and exercise trial were rectified and integrated with a moving window of 0.1 sec width. EMG data for each exercise trail were then expressed as a percentage of the maximum value in the subject's corresponding MVIC trial. Resultant joint force and torque of the knee were determined by using 3-D rigid link models and principles of inverse dynamics. Resultant joint force and torque, and EMG data were then expressed as functions of knee angle, and averaged over the three repetitions per trial.

The model developed by Zheng et al (1996) was used to determine tibiofemoral force, patellofemoral force and tensions of the cruciate ligaments for each exercise. Two factor repeated measure ANOVA ($P<0.05$) (SigmaStat, Jandel Scientific Software, San Rafael, CA) was used to determine the differences among knee extension, leg press and squat and between phases (knee-flexing and knee-extending). Student-Newman-Keuls test was used to isolate the difference among different comparisons.

RESULTS

Tibiofemoral Force Table 1 lists the maximum mean values of the tibiofemoral compressive force during knee-flexing and knee-extending phases in the range of 15 to 95° knee angle. During the knee-flexing phase, the tibiofemoral force for knee extension was significantly greater than those for leg press and squat when the knee angle was less than 29° (Fig. 1). It was significantly less when the knee angle was greater than 71°. During knee-extending phase, the tibiofemoral force for knee extension was significantly greater than those for leg press and squat when the knee angle was less than 25°, and it was significantly smaller when the knee angle was greater than 81°. There was no significant difference between tibiofemoral forces for leg press and squat during both knee-flexing and extending phases. For knee extension the tibiofemoral force was significantly greater during knee-extending phase in the range of 57 to 83°. For leg press there was no significant difference between knee-flexing and extending. For squat the tibiofemoral force was significantly greater during knee-extending in the range of 33 to 53°.

Table 1. Maximum Mean Values of Tibiofemoral Forces (mean ±SD(N) at knee angle(deg))

phase	knee-flexing	knee-extending
knee ext.	3017 ±1511@39	3285 ±1927@57
leg press	3011 ±693@93	3155 ±725@91
squat	3192 ±930@81	3134 ±1040@53

PCL/ACL Force Table 2 lists the maximum mean values of PCL force. ACL force was produced only during knee extension exercise when the knee was near full extension (Fig. 1). During knee-flexing, the PCL force of leg press was significantly greater than that of knee extension when the knee angle was less than 33° and greater than 69°. No significant difference of the PCL force was found between leg press and squat in the range of 15 to 95°. The PCL force of squat was significantly greater than that of knee extension when the knee angle was less than 45° and greater than 61°. During knee extending, the PCL forces of

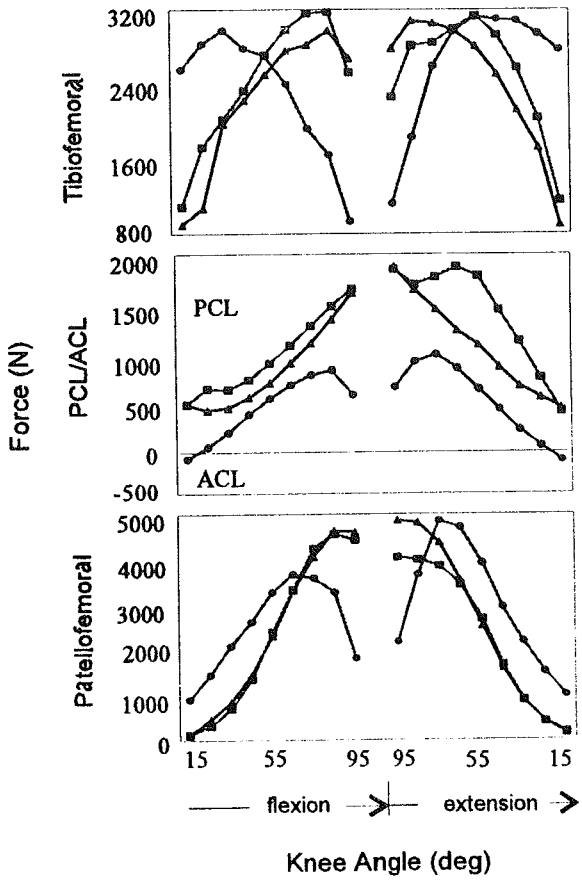

Fig. 1 Tibiofemoral (top), PCL/ACL (middle) and patellofemoral (bottom) forces vs knee angle during knee extension (circle), leg press (triangle) and squat (square).

squat and leg press were significantly greater than that of knee extension in the whole range of 15 to 95°. The PCL force of squat was significantly greater than that of leg press in the range of 27 to 79°. For all these three exercises, the PCL forces during knee-extending were greater than that during flexion at the same knee angle. The difference was significant in the range of 75 to 79° for knee extension, in the range of 25 to 90° for squat and in the range of 35 to 90° for leg press.

Table 2. Maximum Mean Values of PCL Forces (mean ±SD(N) at knee angle(deg))

phase	knee-flexing	knee-extending
knee ext.	801 ±220@83	959 ±299@79
leg press	1593 ±316@95	1866 ±383@95
squat	1635 ±369@95	1868 ±878@63

Patellofemoral Force Table 3 lists the maximum mean values of the patellofemoral compressive force. During knee-flexing the patellofemoral force for knee extension was significantly greater than those for leg press and squat when the knee angle was less than 47° and significantly less when the knee angle was greater than 85° (Fig. 1)

During knee-extending the patellofemoral force for knee extension was significantly greater than those for leg press and squat when the knee angle was less than 57°, and significantly less when the knee angle was greater than 89°. During knee-flexing and extending there was no significant difference between the patellofemoral force for leg press and squat. Also, patellofemoral force and knee angle relationships for the leg press and squat were also the same during knee-flexing. Compared to during knee-flexing, patellofemoral force during knee-extending was significantly greater in the range of 41 to 87° for knee extension in the range of 39 to 47° for squat, was not significantly different for leg press.

Table 3. Maximum Mean Values of Patellofemoral Forces (mean ±SD(N) at knee angle(deg))

phase	knee-flexing	knee-extending
knee ext.	3724 ±1940@67	4846 ±2454@75
leg press	4780 ±1194@91	4991 ±1352@91
squat	4548 ±1395@85	4042 ±1955@95

DISCUSSIONS

Tibiofemoral, patellofemoral and cruciate ligament forces were evaluated and compared among three commonly used exercises. The OKC exercise produced greater tibiofemoral and patellofemoral force when the knee angle was small and less force when it was about 90°. Tibiofemoral and patellofemoral forces during CKC exercises increased with the knee angle. No ACL force was observed during CKC exercises. ACL force was produced during the OKC exercise when the knee angle was small. Tibiofemoral force was about 10% less than that reported by Lutz et al (1993) during maximum isometric contraction. The maximum tibiofemoral force was generated during knee-extending for both CKC and OKC exercises. Tibiofemoral forces were significantly lower than those reported by Wilk et al (1996), who reported that the maximum occurred during the knee-flexing. The maximum patellofemoral force during leg press was much less than that reported by Steinkamp et al (1993), who reported that the maximum was over 12000 N at the knee angle of 90°. This paper presented three major forces at the knee during OKC and CKC exercises. The results are instructive for clinicians and athletes to chose appropriate exercise and the range of motion during exercise.

REFERENCES

Cahill, B. R. et al. Am J Sports Med 6:180-184, 1978
Doucette, S. A. and Child, D. D. J Orthop Sports Phys Ther 23(2):104-110, 1996
Lutz, G. E. et al. J Bone Joint Surg. 75A(5):732-739, 1993
Steinkamp, L. A. et al. Am J Sports Med 21:438-444, 1993
Wilk, K. E. et al. Am J Sports Med (in press), 1996
Zheng, N. et al. 20th ASB Annual Meeting (submitted) 1996

ACKNOWLEDGEMENTS

The authors would like to thank Andy DeMonia and Phillip Sutton for their assistance in data analysis.

Differences in Strain in the Anteromedial and Posterolateral Bundles of the ACL Under Application of Axial and Muscular Loads

J.M. Bach[1], M.L. Hull[2]
[1]UC Ergonomics Program, UC Berkeley/UC San Francisco, Richmond, CA 94804
[2]Department of Mechanical Engineering, University of California, Davis, CA 95616

INTRODUCTION

It is widely accepted that the ligaments of the knee do not behave as homogeneous structures. This is especially important to the study of ligament injury mechanics since failure will begin in the most highly strained fibers. If the location of the highest strain varies as the knee moves through it's range of motion, then the failure mechanics could be expected to vary also. The current research project was undertaken to determine the variation in strain between two bundles of the ACL under the application of axial moments and quadriceps force.

REVIEW AND THEORY

Axial rotations of the tibia on the femur have been implicated in ACL ruptures during Alpine skiing. Internal axial moment at high flexion angles (e.g., Ettlinger, 1989) and external axial moment near full extension (e.g., Fischer et al. 1994) may cause ACL failure. Axial moments may also occur in conjunction with quadriceps force in some falls.

Numerous studies have examined the effects of axial moment (e.g., Pope et al., 1990), and muscle loads (e.g., Renstrom et al., 1986) on ACL strain. Unfortunately the loads used in the majority of these studies were insufficient for generating an injury model. Berns et al. (1993) attempted to develop such a model and found that the load-strain relationships could not be extrapolated to loads beyond the levels applied in the experiments.

Another potential complication to an injury prediction model might be the need to include terms for the strain in multiple sites in the ACL. Several studies have shown that the anteromedial (AMB) and posterolateral (PLB) bundles reciprocate in function over the range of flexion/extension (F/E). Unfortunately none of these studies examined the effects of applied loads on ligament strain. It could be expected that the site of maximum strain, and therefore the onset of injury, varies with applied load.

The objective of this study was to experimentally test the hypothesis that AMB and PLB strains are significantly different from each other. If the hypothesis was true, then an injury model would have to consider strain in at least two sites in the ACL. If it was false, then a single model for the entire ACL might be adequate.

METHODS

Liquid mercury strain gages (LMSGs) were installed on the surface of both the AMB and PLB of 6 unembalmed cadaver knee specimens (mean age 46.8 ± 16.5 years). The specimens were installed and aligned in a six-degree-of-freedom load application system (LAS) (Bach and Hull, 1995). This apparatus was pneumatically actuated and under full closed loop control. Each degree of freedom was individually instrumented for load and displacement measurement.

The specimens were subjected to a detailed loading protocol to examine the effects of axial and quadriceps loads, and combinations thereof, on the strain in the ACL. For combined loadings the quadriceps force was applied to the desired level followed by the axial moment. Loads were applied at knee flexion angles of 15, 30, 60, 90, and 120 degrees.

The data from these experiments were subject to a repeated measures analysis of variance (RANOVA) procedure. For this analysis three within-subjects effects were modeled and all possible interactions were considered. The 25 load levels analyzed involved permutations of 5 levels each (-10, -5, 0, 5, 10 Nm) of I/E moment applied in conjunction with 5 levels (0, 250, 500, 750, and 1000 N) of quadriceps force.

RESULTS

From the RANOVA results for I/E loading, it could be seen that only the flexion angle and

load effects and their interaction were statistically significant (p=0.0005, p=0.0001, p=0.0008). The bundle effect was not significant (p=0.6080) nor was the flexion angle * load * bundle interaction (p=0.6732), although both the flexion angle * bundle (p=0.0853) and load * bundle (p=0.0986) interaction terms would have been significant at the α=0.10 level.

Though no significant differences between the two bundles were detected by the RANOVA, qualitative differences could be observed in the graphs of strain vs. internal and external axial moments (Figure 1 & Figure 2, respectively). Internal axial moment produced similar effects on strain relative to passive for both bundles (Figure 1). The effects of adding a quadriceps force produced similar effects on the strain due to an internal axial moment in the both bundles (Figure 1).

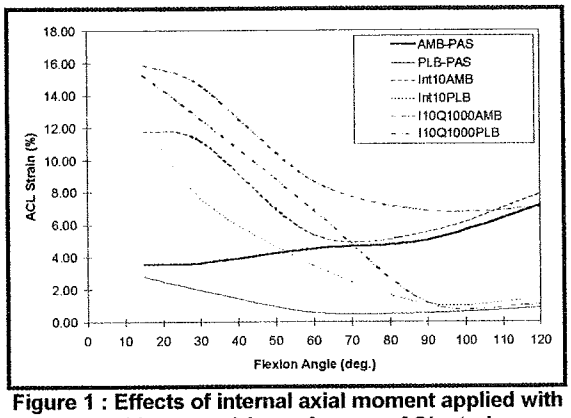

Figure 1 : Effects of internal axial moment applied with and without quadriceps force on ACL strain.

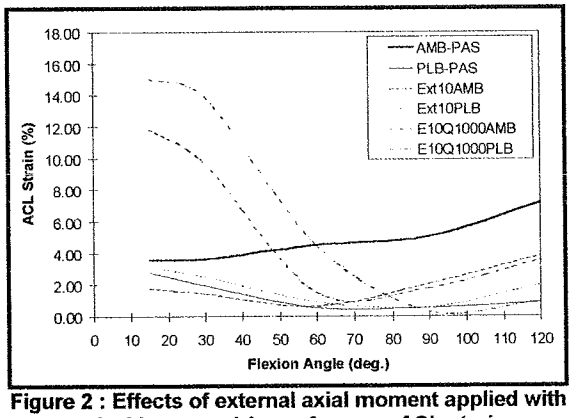

Figure 2 : Effects of external axial moment applied with and without quadriceps force on ACL strain.

External axial moment produced different results in the two bundles (Figure 2). For the AMB the application of an isolated 10 Nm external moment decreased the strain relative to passive for all flexion angles whereas for the PLB there was no effect on strain. For flexion angles of 15 to 60 degrees the external moment+quadriceps force combination increased strain in both bundles relative to passive strains (Figure 2).

DISCUSSION

Generating a model relating ligament strain to external and muscular loads as well as flexion angle is important to reducing the incidence of knee injuries in Alpine skiing. Such a model could be used in a programmable ski binding to monitor the state of strain based upon the state of these variables, and release the boot from the ski if the predicted strains approach injury levels. The ability to represent the ACL as a single structure rather than as multiple bundles would simplify both the experiments needed to generate the information for this model and the system which controls binding release.

The PLB strains due to the application of external moment + quadriceps force were visibly higher than those of the AMB. Between 15 and 30 degrees of flexion the PLB strain was up to 4% greater than the strain in the AMB. Although this difference was not statistically significantly, it can mean the difference between being injured or not being injured. This finding would indicate that although it might not be necessary to consider both bundles in an injury model, the model should be based upon the PLB.

REFERENCES

Bach, J.M.; Hull, M.L.; J. of Biomech. Eng., 117(4), 373-382, 1995.
Berns, G.S. et al. Skiing Trauma and Safety: Ninth Int. Symp., 89-110, 1993.
Ettlinger, C; Skiing, 85-121, 1989.
Fischer, J.F. et al., Acta Orth. Bel., 60(2), 194-203, 1994.
Pope, M.H. et al., Trans. of the First World Cong. of Biomech., 320, 1990.
Renstrom, P. et al., Am. J. .Sports Med., 14(1), 83-87, 1986.

ACKNOWLEDGEMENTS

The authors wish to thank the Tyrolia Corporation of Vienna, Austria for its continued support and Dr. Pat Patterson for his assistance with specimen preparation.

CORRELATION OF WRIST LIGAMENTOTAXIS WITH CARPAL DISTRACTION DURING EXTERNAL FIXATION

T. Loebig, A. Badia, M. Baratz, D. Anderson
Biomechanics Research Laboratory, Allegheny-Singer Research Institute
Pittsburgh, PA 15212

INTRODUCTION

Ligamentotaxis, a tightening of the juxtarticular soft tissues accompanying wrist distraction via external fixation, is used to effect and protect the reduction of distal radius fractures. Wrist and finger stiffness has been associated with overdistraction of the wrist (Kaempffe et al., 1993; Seitz, 1993). A decrease in the range of motion at the metacarpophalangeal and proximal interphalangeal joints occurs as distraction increases (Moran, 1992) . Empirically proposed guidelines for attaining adequate distraction (Agee et al., 1994; Seitz et al., 1993) have not been experimentally substantiated. We tested uninjured cadaver wrists to correlate progressive tension across the wrist with associated carpal distraction. To provide a clinically useful method to assess ligamentotaxis, we radiographically evaluated the relationships between joint spaces, applied distraction, and the tension carried across the wrist.

METHODS

Twelve cadaver forearms were stripped of skin and extrinsic musculature. They were mounted in an MTS machine for tensile testing by gripping half-pins (EBI/Pennig) inserted into the metacarpals and the radius. Load and actuator displacement were continuously recorded during controlled wrist distraction. Anteroposterior (AP) radiographs were obtained at applied distractions of 0, 1, 2, 4, 6, 8, 10, and 12 mm.

The apparent widths of the radiolunate (RLJ), radioscaphoid (RSJ), and midcarpal joint (MCJ) spaces parallel to the axis of the third metacarpal were measured from plain radiographs at each increment of distraction. Values for the carpal height ratio (CHR), revised carpal height ratio (RCHR) and carpal height index (CHI) were calculated (Nattrass et al., 1994).

Thirteen surgeons were asked to apply traction to a benchtop wrist model to simulate the amount of force they would apply while placing an external fixator on the wrist. The model contained a load sensor to quantify the applied force.

RESULTS

The observed relationship between carpal tension and applied distraction was typical of viscoelastic soft tissue behavior (Fig. 1). With applied wrist distraction of 2 mm, the carpus was lifted off of the radius, producing an increase in tension across the wrist averaging 8 N. The carpal ligaments were pulled to length at an average overall distraction of 4 mm, producing an average tension of 20 N. Transition of the load vs. distraction curve from low stiffness to a linear high stiffness region occurred at an average distraction of 6 mm (range 4-8 mm) and was associated with an average force of 40 N.

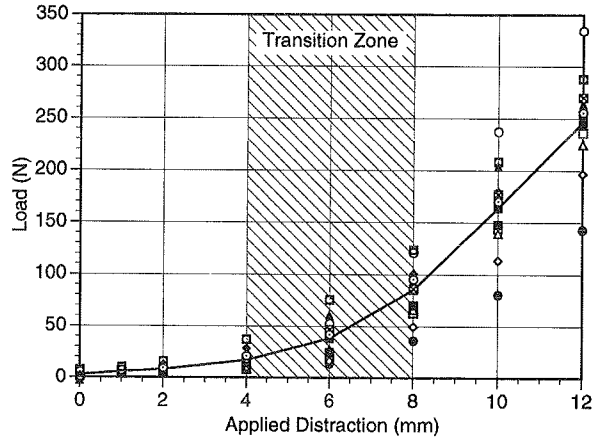

Figure 1: Load vs. applied distraction for individual specimens (symbols) and the average (line).

The average force generated by surgeons using the wrist simulator to effect wrist distraction was 49 ± 18 N. This corresponds to a range of experimentally applied distraction from 4 to 8 mm and lies within the transition zone on the load vs. distraction plot.

All carpal joint spaces as measured from radiographs were found to increase with applied distraction (Fig. 2). With overall distraction of 4 mm and above, a distal shift of the scaphoid relative to the lunate was observed, creating an apparent dissociation at the scapholunate joint. The average MCJ space was initially smaller than the RLJ,

but became larger as applied distraction increased. On average, the RSJ was wider than the MCJ, but ANOVA revealed no significant difference.

The average values of the carpal height parameters for undistracted wrists agreed with published values for normal wrists. Although highly variable, all parameters were found to increase linearly with wrist distraction. CHR had the highest variability of all parameters. ANOVA revealed no statistical difference between RCHR and CHI in assessing distraction. Relative changes in the carpal height parameters were independent of the values at 0 mm distraction and consistent for all specimens.

DISCUSSION

Use of the minimum amount of distraction that is necessary to protect reduction has been advocated when applying ligamentotaxis for distal radius fracture treatment, supplemented by limited internal fixation if necessary (Agee et al. 1994, Pennig et al.,1993). In this study, overall wrist distraction of 2 mm was observed to distract the carpus and unload the radiocarpal joint sufficiently to protect fracture reduction. Average overall distraction of 4 mm was sufficient to tighten the carpal ligaments. Assistive ligamentotaxis should be effective at or above this level of distraction. Further distraction will stretch the carpal ligaments and may be excessive, causing unnecessary loading of the soft tissue envelope of the wrist. Overdistraction has been linked to stiffness of the wrist and hand, but has not yet been clearly defined. We have found that carpal ligament tension required to produce effective ligamentotaxis in human cadaver wrists occurs within a range of applied distraction between 2 and 6 mm.

Dissociation of the proximal carpal row, appearing as a distal shift of the scaphoid relative to the lunate, was observed on radiographs for ten of the twelve specimens as the applied distraction increased. This was apparent at an average of 4 mm of applied distraction or 20 N of carpal tension.

The averages of the carpal height parameters that we evaluated (CHR, RCHR, and CHI) did not correlate well with applied distraction, and could produce errors as great as ±4 mm in assessing distraction. Relative carpal height measurements can be used to assess distraction when a baseline value is calculated for each patient. The amount of distraction applied to the uninjured wrist can then be directly calculated. The use of published "normal" values of any of the carpal height parameters as the baseline value for all patients may result in overdistraction due to their high variability. Distraction can be assessed effectively using comparative values of radiographic measurements of carpal height and carpal joint distraction.

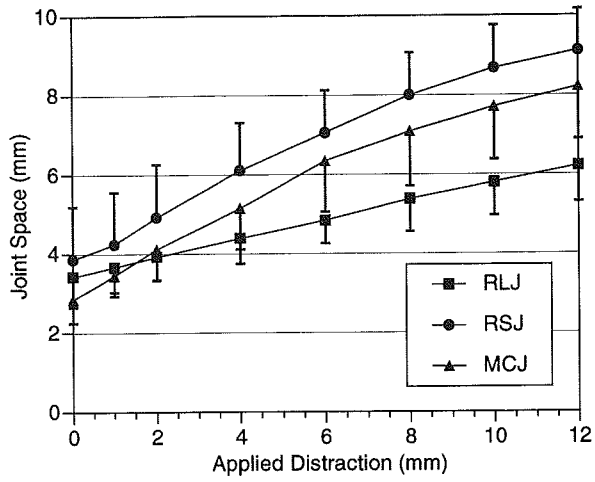

Figure 2: Magnitude of radiographically measured joint spaces vs. applied distraction (mean ± sd).

These results remain to be reproduced in specimens with an intact soft tissue envelope and a simulated distal radius fracture. If the experimental findings apply clinically, we may then be able to determine how much distraction is detrimental to final outcome.

REFERENCES

Agee J.M. et al. Orthopedics, 17, 1115-22, 1994.
Kaempffe F.A. et al. J Hand Surg, 18A, 33-41, 1993.
Moran J.P. M.Sc. Thesis in Mechanical Engineering, California State Univ., Sacramento, CA. 1992.
Nattrass G.R. et al. J Bone Joint Surg, 76A, 88-94, 1994.
Pennig, D.W. Hand Clinics, 9, 587-602, 1993.
Seitz W.H, Jr. Orthop Clin, 24, 255-64, 1993.

ACKNOWLEDGMENTS

The authors would like to thank Allegheny-Singer Research Institute for funding this project.

PRESSURE-VOLUME CHARACTERISTICS OF THE INTACT AND DISRUPTED PELVIC RETROPERITONEUM

M.R. Grimm, M.S. Vrahas, K.A. Thomas
Bioengineering Laboratory - Department of Orthopaedic Surgery
Louisiana State University Medical Center, New Orleans, LA 70112

INTRODUCTION

Severe pelvic fractures can lead to exsanguinating blood loss. Techniques to control bleeding include direct ligation, angiographic embolization, pelvic packing, and acute external fixation. With external fixation the pelvic volume is controlled, and possibly decreased; pressure in the retroperitoneum may increase and a tamponade may occur. A critical assumption is that the pelvic retroperitoneum is a closed space; anatomically this is not the case, but the pelvis may behave functionally as a closed space. *In vivo* the retroperitoneum is a potential space for bleeding; however given that there is adhesion between tissue planes, it seems reasonable that an opening pressure may be higher than the venous closing pressure. Therefore tamponade may occur before the opening of the retroperitoneal space.

REVIEW AND THEORY

Although it is widely accepted that pelvic stabilization helps to control hemorrhage, the concept has not been clearly proven. The vast majority of patients with pelvic fractures do not experience exsanguinating blood loss. Clinical series examining external fixation of the pelvis therefore exclude many patients, while other studies are not randomized with regard to treatment. Some patients exsanguinate even though a fixator has been applied. It is difficult to know whether the application of the fixator has a definite therapeutic benefit or whether other factors may also contribute to the control of blood loss (such as the use of general anesthesia to apply the fixator).

The purposes of this study were: (1) to develop a cadaveric model for pelvic fractures, by creating fractures that *in vivo* would have the potential for exsanguinating blood loss; and (2) to measure the pressure-volume characteristics of the intact and disrupted pelvic retroperitoneum, without and with external fixation. By comparing the pressures required for fluid to flow into the retroperitoneum under these conditions the effect of external fixation can be assessed. If fluid can flow at low pressure following a fracture, then external fixation to control the pelvic volume would have little effect on controlling blood loss. Conversely, if external fixation can raise the pressure required for fluid to flow into the retroperitoneum, then there would be a clear benefit for its use in these fractures.

PROCEDURES

Fluid Inflow and Pressure Measurements The femoral vein of unembalmed cadaveric specimens was dissected and cannulated, and the external iliac vein was disrupted. An arthroscopic irrigation pump, with a pressure transducer (CDIS™, Zimmer, Warsaw IN), was used to introduce the fluid (water) into the retroperitoneum. Radiopaque material was added to the fluid to document the extent of extravasation. After each liter of fluid inflow, the flow was stopped and pressure measurements were made. At the conclusion of the experiment, a laparotomy was performed and retroperitoneal pressure measurements were repeated. Dissection of the specimen verified placement of the catheter for fluid inflow, the retroperitoneal fluid collection, and the extent of the soft tissue injuries caused by the experimental fracture.

Experimental Pelvic Fractures Stainless steel rods (nominally 1/4" diameter, 16 inches in length) were placed through each pelvis, passing in a straight line entering through the ischial tuberosity and exiting through the anterior superior iliac spine; placed in this orientation the rods passed through the acetabulum and femoral

head. The pelvic fractures were created experimentally by application of a load that resulted in simultaneous rapid external rotation of the pelvis around the femoral heads. This mechanism of injury has been described by Tile and Hearn, and results in an open-book pelvic fracture. The test specimen was held fixed, in a horizontal orientation (i.e., supine), adjacent to the testing machine by a flexible cable attached to one of the pelvic rods. The contralateral pelvic rod was connected to the hydraulic actuator of a mechanical testing machine (858 Bionix Load Frame, MTS Systems Corporation, Minneapolis, MN) by a flexible cable passing over a pulley . The loading was applied at a constant displacement rate of 50 mm/minute. Control of the testing machine and the real-time data collection was performed using an integrated, computerized control system and software (TestStar and Testware-SX, MTS Systems Corporation, Minneapolis, MN).

RESULTS AND DISCUSSION

In the intact specimens, infusion pressures rapidly rose to approximately 40 mm Hg following inflow of 5 to 8 liters of fluid (Figure 1). Therefore in the intact pelvis, significant pressure is required to open the tissue planes to allow fluid to flow into the retroperitoneal space.

Open-book fractures (Tile type B-3) were created in 6 specimens. The mean force required to fracture to pelvis was 3481 N (standard deviation, 1143 N; range 2562 N to 5577 N). To our knowledge this represents the first time fractures of this type were experimentally created.

After fracture, large volumes of fluid (20 liters) could flow into the retroperitoneum at pressures ranging from 11 mm Hg to 38 mm Hg at the highest volumes. External fixation to control the pelvic volume has a moderate effect on raising the retroperitoneal pressure (Figure 2). The change in pressure depended upon the volume of fluid in the retroperitoneum. At low volumes, the external fixator increased the pressure approximately 3 mm Hg, and at the highest volumes the pressure increased approximately 11 mm Hg. This modest effect may provide tamponade for venous bleeding, and apposition of the fracture fragments may also help to control bony bleeding. These results indicate that even after acute external fixation, there exists a role for selective angiography, ligation, or pelvic packing for patients who do not respond to exernal fixation alone.

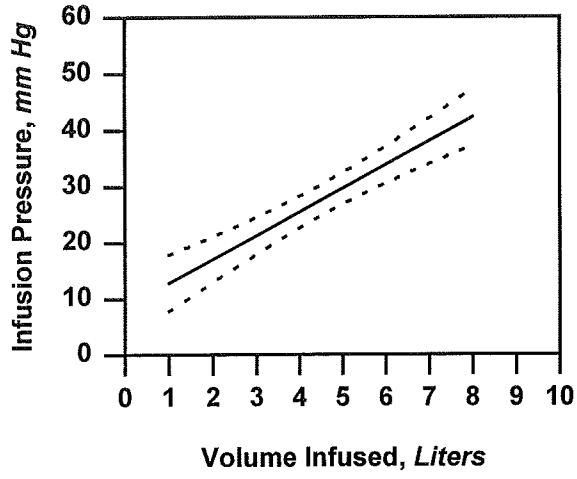

Figure 1: Pressure-volume characteristics of the intact pelvic retroperitoneum (4 specimens).

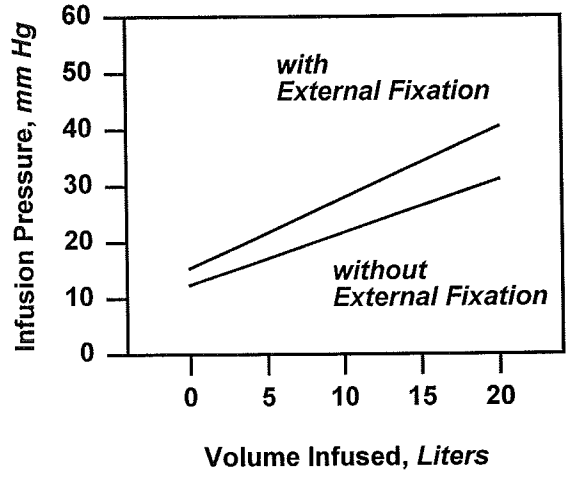

Figure 2: Effect of external fixation on retro-peritoneal pressure following an open-book pelvic fracture (6 specimens).

REFERENCE

Tile, M., Hearn, T. Fractures of the Pelvis and Acetabulum, 2nd Ed. (pp. 22-36), Williams and Wilkins, 1995.

The Mechanical and Histological Properties of Reharvested Patellar Tendon

F. Wentorf[1], R. LaPrade[1], C. Hamilton[1], D. Simmons[1], R. Montgomery[2]
[1]Department of Orthopaedic Surgery, University of Texas Medical Branch, TX 77551
[2]College of Veterinary Medicine, Auburn University, Alabama

INTRODUCTION

The purpose of this study was to assess the histologic, mechanical, and structural properties of the reharvested central third of the patellar tendon. A canine model was examined at six and twelve months after harvest of the central third with tensile failure and histological testing of the regenerated tendon.

REVIEW AND THEORY

An increasing number of anterior cruciate ligament (ACL) reconstructions, estimated at 50,000/year in United States (Johnson et. al., 1994), along with the rise of the number of failures, with the current estimate at 0.7 to 8 % (Karns et. al., 1994), has made the revision ACL reconstruction a more common clinical procedure. The "gold standard" for the initial reconstruction is the central third of the patellar tendon. It has been proposed that the repaired central third of the patellar tendon can be used for this revision. This study was performed to determine if the reharvested central third of the patellar tendon is a viable graft source for revision ACL reconstructions.

PROCEDURES

Twelve adult greyhounds were selected for this study. Preoperatively, all dogs had normal knees (stifles) both clinically and radiographically. One knee was randomly chosen for the operative procedure, while the contralateral limb served as the control. At time zero, all dogs had the central third of the patellar tendon (5 mm) removed with 5 X 10 mm bone blocks from the patella and tibia. The remaining tendon defect was loosely closed. Postoperatively, all dogs were ambulated 2.5 km three times/week on a motorized carousel. Six dogs each were euthanized at 6 and 12 months. The central third of the patella tendon was then reharvested from both the operative and the contralateral knee. Tendon cross-sectional area measurements were performed with calipers and a digital area micrometer. Mechanical properties were analyzed by load testing to failure on a MTS machine, while histological analysis of collagen structure and content were performed via haematoxylin and eosin staining and electron microscopy. Under electron microscopy, fibril size and distribution were calculated from a representative area.

RESULTS

No evidence of patellofemoral or tibiofemoral arthrosis or cartilage abnormalities were noted on gross examination of any knees. An analysis of the structural changes of the patellar tendons of the operative knees revealed a significant increase in thickness at both 6 and 12 months ($p < 0.01$) and a significant decrease in length at 12 months ($p < 0.05$) when compared to controls. Mechanical testing showed that the average ultimate tensile strength (Figure 1), failure load, elastic modulus, and strain to failure for the reharvested central third of the patellar tendon were significantly less than controls at both six and twelve months ($p < 0.05$, Table 1). Although all collagen fibers were noted to align with the long axis of the tendon (H&E stain, polarized light), tendons from the reharvested groups were hypercellular when compared to control tendons. Analysis of collagen fiber size by electron microscopy (Figure 2) revealed a significant

increase in mean collagen fiber diameter at six months (135 ± 40.6 nm for experimentals and 49.1 ± 4.45 nm for controls, $p < 0.01$). At twelve months, there was no significant difference between mean collagen fiber diameters. Collagen fiber packing, the amount of collagen fibers per unit area, was found to be decreased in the reharvested tendons at six months ($p < 0.01$). No significant change was seen in collagen fiber packing in the reharvested tendons at twelve months postoperatively with respect to their control tendons.

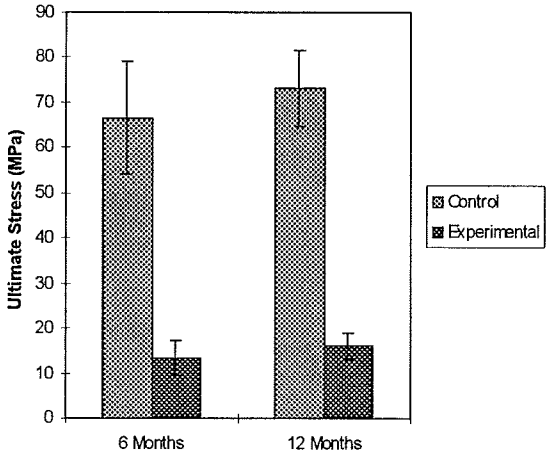

Figure 1: Ultimate Stress of the Reharvested Central Third of the Patellartendon

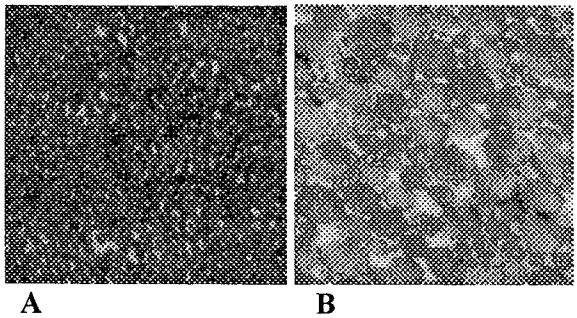

Figure 2: Electron microscopy of collagen fibers A) a six month control, B) a six month experimental (original magnification x 48,800).

Table 1: Mechanical Properties of the Reharvested Central Third of the Patellar tendon

	Failure Ld (N)	*Mod. (MPa)*	*Failure Strain*
6m: Cnt	1430±410	173±25	32.0±4.0
6m: Exp	760±240	83±24	17.9±5.8
12m: Cnt	1640±470	179±61	35.7±7.6
12m: Exp	890±350	72±31	22.2±7.2

DISCUSSION

This study demonstrates that the reharvested central third of the patella tendon does not have the same mechanical properties as the initial central third patellar tendon up to one year following harvest in a canine model. The hypertrophy of the patellar tendon seen after harvesting its central third following ACL reconstruction is due in part to a significant increase in the size of the collagen fibers. Material "flaws" in the healing tendon may be present that would directly effect the material properties of the structure (Shrive et. al., 1995). These findings suggest that the use of a reharvested patellar tendon as a source for revision ACL reconstruction must be carefully reexamined.

REFERENCES

Johnson D, et. al. Knee Surgery, (pp. 877-895), Williams and Wilkins, 1994.

Karns D, et. al. Case report: Revision ACL Reconstruction, Arthroscopy, 10, 148-151, 1994.

Shrive N, et. al. Soft-Tissue "Flaws" are Associated with the Material Properties of the Healing Rabbit Medial Collateral Ligament, J Orthop Res, 13, 923-929, 1995.

ACKNOWLEDGMENTS

Electron microscopy was done by Hal Hawkins, M.D., Ph. D. at the Shriners Burn Institute in Galveston, Texas.

BIOMECHANICAL CONSEQUENCES OF PLANTAR FASCIOTOMY: ALTERATIONS IN SECOND METATARSAL LOADING

S.Donahue[1], N. Sharkey[1,2], L. Ferris[2], T. Smith[3]
[1]Biomedical Engineering Graduate Group, University of California, Davis, Davis, CA 95616
[2]Department of Orthopaedic Surgery, University of California, Davis, Sacramento, CA 95817
[3]Department of Mechanical Engineering, University of California, Davis, Davis, CA 95616

INTRODUCTION

The plantar fascia is a syndesmotic structure originating on the tuberosity of the calcaneus and attaching distally to the plantar aspect of all five proximal phalanges. Inflammation of the plantar fascia, plantar fasciitis, frequently manifests near the calcaneal enthesis. The inflammation is thought to result from microtrauma to the collagen fibers of the fascia, caused by repeated mechanical overload. Intractable plantar fasciitis is frequently treated by plantar fasciotomy - the release of the plantar fascia from its calcaneal enthesis. The plantar fascia, particularly the central band, is believed to be an integral component of the medial longitudinal arch of the foot. We hypothesize that transection of the plantar fascia will disrupt the structural integrity of the arch, resulting in pernicious loading of the metatarsals.

REVIEW AND THEORY

The simple truss and windlass have been used as heuristic models to study the structure and function of the plantar fascia. In the truss model the tarsals and metatarsals comprise the compression members and the plantar fascia depicts the tension member. If loads are applied only to the joints of a truss its members experience no bending stresses (Lapidus, 1943). In this situation the axial loads borne by all members of the truss are inversely proportional to its height.

Dorsiflexion of the metatarsal-phalangeal joints increases the tension in the fascia as the height of the arch increases and its length decreases. This behavior has been modeled as a windlass mechanism (Hicks, 1954). The efficacy of the fascia in maintaining arch height and length has previously been demonstrated (Daly, 1992). The purpose of our study was to evaluate the role of the plantar fascia in maintaining physiologic loading of the metatarsals.

PROCEDURES

A cadaveric foot model was used to simulate the stance phase of gait and study the effects of plantar fascia release on the loading of the foot. Physiological muscle forces were applied to the tendons of the ankle plantar flexors to achieve vertical ground reaction forces representative of normal gait. Three axial strain gages were mounted on the mid-shaft of the second metatarsal to record metatarsal strains during loading. The foot was positioned to simulate two distinct periods of stance phase: heel-off (approximately 50 % stance) and the position corresponding to the second peak on the vertical ground reaction force curve (approximately 75 % stance). Repeated measures were made for each of these configurations for four conditions of the plantar fascia: (1) intact, (2) 50 % transection of the central band, (3) transection of the entire central band, and (4) complete transection of the fascia from its calcaneal enthesis.

The strain superposition principal of bending theory was employed to calculate the *in situ* axial load and bending moments in the second metatarsal using the *in situ* strains recorded during experimentation ([1]Carter, 1981). ANOVA's were used to asses seven dependent variables: strain from each of the three gages, plantar-to-dorsal and medial-to-lateral bending moments, second metatarsal axial load, and the Achilles tendon force required to attain the appropriate ground reaction force.

RESULTS

Values for the seven dependent variables for all treatment combinations are reported in Tables 1 and 2. No significant ($\alpha = 0.05$) changes were found in any of the measured parameters after the incision was made in the medial half of the central band of the fascia. Following transection of the full central band significant changes occurred in dorsal and medial strains at both positions, plantar-to-dorsal bending moment at 75 % stance, and second metatarsal axial load at 50 % stance. Following complete transection of the plantar fascia from the calcaneus the plantar-to dorsal bending moment in the 50 % stance position also became significantly different from the intact condition.

Table 1: Data for 50 % stance phase

	Plantar Fascia Condition			
Dependent Variable	**1**	**2**	**3**	**4**
Dorsal Strain ($\mu\varepsilon$)	-883^{a} (583)	-1010^{a} (455)	-1814^{b} (786)	-2075^{b} (849)
Medial Strain ($\mu\varepsilon$)	-40^{a} (562)	-82^{a} (369)	944^{b} (874)	905^{b} (1244)
Lateral Strain ($\mu\varepsilon$)	200^{a} (606)	513^{a} (686)	376^{a} (874)	646^{a} (1244)
P-D Moment (Nm)	1.42^{a} (1.21)	1.48^{a} (1.24)	2.78^{a} (1.42)	3.78^{b} (2.18)
M-L Moment (Nm)	-1.20^{a} (1.11)	-1.84^{a} (1.40)	-1.96^{a} (1.47)	-2.22^{a} (1.44)
Axial Load (N)	-299^{a} (74)	-277^{a} (107)	-187^{b} (53)	-187^{b} (94)
Achilles Load (N)	1081^{a} (129)	1072^{a} (87)	1036^{a} (97)	1035^{a} (123)

Mean values and (SD); n=5 for all cells.
Means, for a given variable, with the same superscript are not significantly different ($\alpha = 0.05$).

Table 2: Data for 75 % stance phase

	Plantar Fascia Condition			
Dependent Variable	**1**	**2**	**3**	**4**
Dorsal Strain (με)	-1235[a] (756)	-1504[a] (858)	-2981[b] (961)	-3361[b] (976)
Medial Strain (με)	-910[a] (806)	-791[a] (647)	943[b] (970)	1048[b] (1198)
Lateral Strain (με)	1011[a] (832)	1237[a] (1334)	892[a] (692)	1418[a] (902)
P-D Moment (Nm)	2.46[a] (3.15)	2.11[a] (2.04)	5.32[b] (2.53)	5.64[b] (2.51)
M-L Moment (Nm)	-3.11[a] (1.53)	-3.77[a] (2.59)	-3.45[a] (2.23)	-4.53[a] (2.77)
Axial Load (N)	-504[a] (149)	-480[a] (241)	-387[a] (189)	-372[a] (219)
Achilles Load (N)	1799[a] (195)	1690[a] (154)	1625[a] (181)	1596[a] (228)

Mean values and (SD); n=5 for all cells.
Means, for a given variable, with the same superscript are not significantly different ($\alpha = 0.05$).

A fatigue failure analysis, based on bone strain, was used to estimate the number of loading cycles to failure for the second metatarsal ([2]Carter,1981). Following total fasciotomy the estimated number of cycles to failure decreased three orders of magnitude from 1.01×10^8 in the intact feet to 4.81×10^5 post-surgically.

DISCUSSION

Although the two-dimensional truss is useful for conceptualizing the medial longitudinal arch of the foot it is not sufficient for structural analysis. Due to distributed loads and irregular geometries the compressive members (bones) are indeed subjected to bending stresses. For these same reasons it may not be safe to assume that the axial loads of the metatarsals and fascia are inversely proportional to the height of the arch. More accurately the arch could be modeled as a three-dimensional space truss, consisting of twelve compressive members (bones) and several tensile members (ligaments), subjected to distributed loading rather than loading at the joints only.

It appears that a primary function of the fascia is to maintain physiologic bending moments as well as axial loads in the metatarsals. Total plantar fasciotomy increased plantar-to-dorsal bending moments 167% and 129% for feet loaded at 50 and 75 % stance, respectively. Moreover, these bending moments have associated alterations in metatarsal strain. Both dorsal and medial strains were significantly altered following plantar fasciotomy. *In vivo* these alterations in strain are likely to initiate bone remodeling to repair fatigue damage and redistribute bone mass to accommodate the new loading environment. Following total fasciotomy medial strains reversed polarity and increased in magnitude. Dorsal strains increased from -883 με to -2075 με at 50% stance and from -1235 με to -3361 με at 75% stance. Animal studies suggest that peak physiologic bone strain for rigorous activity lies between 2000-3000 με (Rubin,1984). Following total plantar fasciotomy dorsal strain (-3361 microstrain) exceeded physiologic limits.

Numerous studies have documented the occurrence of lower limb stress fractures in soldiers and athletes. The etiology of stress fractures has been attributed to an accumulation of fatigue damage. Fatigue damage is a function of the frequency and magnitude of applied strain. An increase in either parameter will increase the rate of fatigue damage. These are the same mechanisms that are hypothesized to be responsible for the microtrauma to the collagen fibers of the plantar fascia. Because the plantar fascia and metatarsals are mechanically linked, plantar fasciitis may be a good indication that the metatarsals are experiencing fatigue damage. If this is the case, our results indicate that plantar fasciotomy may exacerbate metatarsal fatigue damage by increasing peak strains in the second metatarsal. Dorsal strain increased 135 % at 50% stance and 172 % at 75% stance following total plantar fasciotomy. Strain of this magnitude reduces the predicted number of loading cycles to failure by several orders of magnitude. *In vivo*, increases in strain magnitude may cause fatigue damage to accumulate faster than can be repaired by remodeling, resulting in stress fracture.

The central band of the fascia connects the calcaneus to the proximal phalanges. Of the three fascial bands the central appears to be the most instrumental in maintaining arch biomechanics. Not surprisingly, plantar fasciitis is commonly found in the central band near its calcaneal enthesis. Although plantar fasciotomy may be effective in reducing heel pain, the procedure may predispose the patient to other, perhaps more serious, complications in the foot. The results of this study contraindicate plantar fasciotomy. Since a large percentage of fasciotomy patients are athletes, who repetitively load their feet during the course of training, non-operative treatment is advocated as an alternative to surgery.

REFERENCES

[1]Carter, D.R. et al. *J. Biomech.*, 14(11), 739-745, 1981.
[2]Carter, D.R. et al. *Acta Orthop. Scand.*, 52, 481-490, 1981.
Daly, P.J. et al. *Foot Ankle,* 13(4), 188-195, 1992.
Hicks, J.H. *J. Anat.*, 88, 25-30, 1954.
Lapidus, P.W. *Arch. Surg.*, 46, 410-421, 1943.
Rubin, C.T. *Calcif. Tissue Int.*, 36, S11-S18, 1984.

FINITE ELEMENT MODELING OF THE SECOND RAY OF THE FOOT WITH FLEXOR MUSCLE LOADING

[1]David R. Lemmon, [2]Christopher R. Jacobs, and [1,2,3,4]Peter R. Cavanagh
[1]Center for Locomotion Studies and Departments of [2]Orthopaedics and Rehabilitation, [3]Kinesiology, and [4]Medicine, Penn State University, University Park, PA 16802 and Hershey, PA 17033

INTRODUCTION

Finite element models have previously been developed to study the relationship between plantar pressure, soft tissue thickness, and footwear geometry (Lemmon et al. 1996). Work is currently under way to develop a more comprehensive model that will include loading of flexor muscles to the distal phalanges and the effect of these loads on the metatarsal head. In the current work , a finite element model has been constructed to investigate the feasibility of some key features of the comprehensive model. This model is a sagittal section of the second ray from the proximal second metatarsal to the distal end of the proximal phalanx. The model is based on the existing finite element models and is designed to test the addition of joint rotation and flexor muscle tendons interacting with the tissue.

REVIEW AND THEORY

A biomechanical analysis of forces acting on the metatarsals during normal walking was performed by Stokes, et al. (1979). This was a two-dimensional, sagittal plane analytical model of a typical ray including the phalanges. Metatarsal loading included axial and shear loads and a moment at the proximal end, and ground reaction force and lateral tendon loads to the metatarsal head. Tendon loads were due to tension in the flexor digitorum longus (FDL) and flexor digitorum brevis (FDB) as they wrap around the metatarsal head. These flexors also applied a contact load at the metatarso-phalangeal joint due to their attachment to the phalanges. The finite element model in the current work applies these loads to the soft tissue continuum, and adds the proximal phalanx and corresponding joint forces.

Experiments have also been performed on cadaveric specimens to determine the loading of the metatarsal due to ground reaction forces and muscle loads. Sharkey, et al. (1995), applied simulated muscle loads in fresh cadaveric lower extremities. The specimens were rigidly mounted at the tibia such that the heel was elevated 10mm. An electric servo actuator applied tension to the Achilles tendon until measured vertical ground reaction force was 750N. This load was modulated as a 250N load was applied to the flexor digitorum longus (FDL), so that the ground reaction force remained 750N. Tests performed on nine feet yielded axial loads and plantar-dorsal moments in the second metatarsal of 450±303N, and 4.01±3.71N-m, respectively. These tests provide experimental data for validation of the current model.

PROCEDURES

The finite element model is a two-dimensional, plane strain sagittal section, and incorporates the second metatarsal, proximal phalanx, and plantar and dorsal soft tissue (Figure 1). The metatarso-phalangeal joint has been simplified by constructing a rigid body attached to the articular surface of the proximal phalanx, and to a node at the center of rotation. This center node is fixed in X- and Y-displacement to a coincident node of the metatarsal head, but is free to rotate about this node. In this way a hinge joint is formed that can transfer loads and produce reasonable kinematic motion in the joint.

In addition to the continuum of soft tissue used in previous studies, an exemplar flexor tendon has been added. Flexor tendons in the forefoot pass over the condyle of the metatarsal heads, with some intervening soft tissue. Essentially, the tendon passes through the soft tissue continuum, so it is reasonable to assume that, in a two dimensional model, the tendon is superimposed on the continuum of plantar soft tissue. The tendon was represented in this model by quadrilateral continuum elements. This interaction was modeled by a sliding interface between the top surface of the tendon elements and the bottom surface of a line of elements intervening between the metatarsal head and tendon. The flexor tendon thus wraps around the metatarsal head. It is attached to the distal end of the proximal phalanx. Note that the actual FDL and FDB flexor tendons attach to the distal and middle phalanges, respectively, and that this is simply a representative model to test the feasibility of flexor tendon modeling.

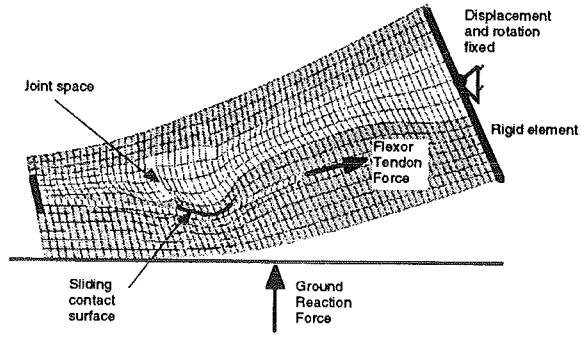

Figure 1 - Sagittal plane FE model of the second ray with added flexor tendon.

During solutions, nodes at the proximal end were tied to a rigid surface. This rigid surface was also tied to a node lying at the intersection of the proximal metatarsal and that metatarsal's neutral axis. This node was fixed by boundary conditions in displacement and rotation, which in turn fixed the rotation and displacement of all the nodes on the proximal end. The advantage of this arrangement over previous methods of restraining the proximal end is that both reaction forces and reaction moments can be determined from static solutions. These

reactions are similar to those borne by the cuneiform joint at the proximal end of the metatarsal.

Loading of the model was applied through a rigid surface in contact with the plantar surface. In this way known or measured ground reaction forces can be applied to the model and plantar pressures can be determined. In the model solutions, no friction was used in the contact surface, and the foot was allowed to make or break contact with the ground.

Material properties used in the model include a Young's modulus and Poisson's ratio obtained from published values for bone. The flexor tendon had stiffness one tenth the stiffness used for bone. The soft tissue continuum was given second order polynomial hyperelastic behavior as defined by the Abaqus "hyperelastic" material model. Coefficients obtained from compression of the heel plantar fat pad were used to approximate the sub-metatarsal material.

RESULTS AND DISCUSSION

The model was tested by applying loads and determining reaction forces measured by Sharkey, et al. (1995). A 188N ground reaction load to the second ray was determined by weighting the loads to the five rays as follows: 3-2-1-1-1 for the first through fifth rays, respectively. Loading to the flexor tendon was directed along a 10 degree angle from the X (horizontal) axis, and its magnitude was varied until the axial load and bending moment in the metatarsal was within the range measured by Sharkey, et al. (1995). Figure 2 shows Y direction normal stress contours in the soft tissue from two load cases: one with no load on the flexor tendon, an the other with a 250 N load at a 10 degree angle with the ground surface. Without the load in the flexor tendon, the phalanx is free to extend dorsally as the soft tissue beneath it is compressed.

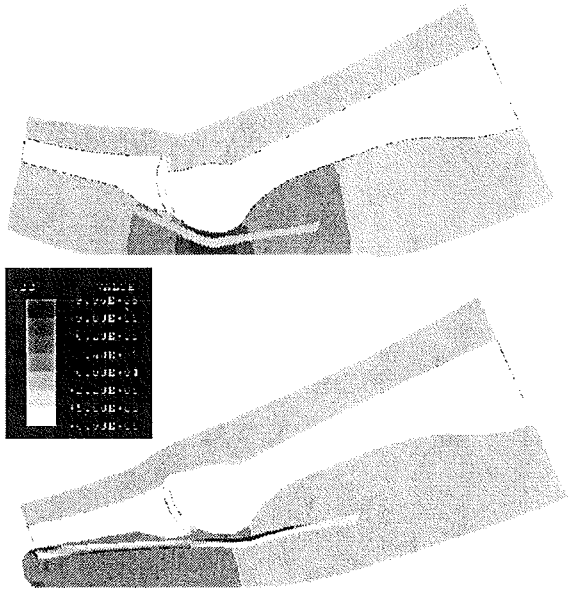

Figure 2 - Stress contours on deformed geometry for the two FDL loading conditions. Highest stress contours were 900 kPa in the unloaded flexor condition.

Peak normal interface stress (plantar pressure) is seen to be located near the metatarsal head. The normal reaction force in the metatarsal was 59 N and the moment was 10.34 Nm. When a 250 N load was applied to the flexor tendon, the axial reaction force in the metatarsal increased to 306 N and the bending moment decreased to 7.64 Nm, which correspond to the range of values obtained by Sharkey, et al. (1995). The tension in the flexor tendon served to counter the moment in the metatarsal created by the vertical load, and at the same time, to apply an additional axial load. The plantar pressure distribution shown in the figure reveals a shift in focal plantar pressure toward the proximal phalanx. It is believed that this shift in loading does occur during gait. There is also a dramatic reduction in the magnitude of the peak pressure - indicative of the load sharing between the sub-metatarsal head and sub-phalangeal regions as a result of muscle action. Additional refinement of the model, such as adding the middle and distal phalanges, should further improve the prediction of plantar pressure distribution.

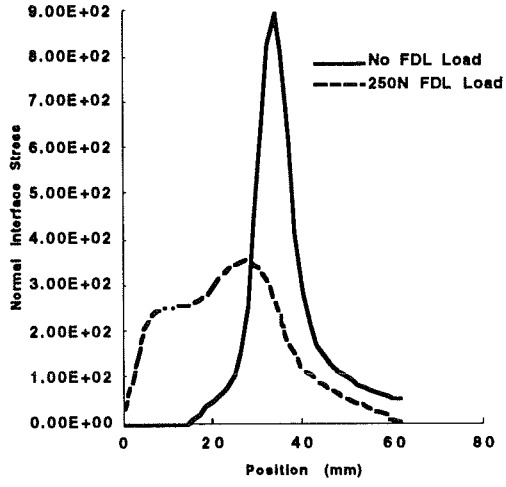

Figure 3 - Normal interface stress (plantar pressure) for the two FDL loading conditions. Stress is in kPa.

REFERENCES

Lemmon , D.R., Shiang, T.Y., Hashmi, A., Ulbrecht, J.S., Cavanagh, P.R., *J. Biomechanics, (In Review).*
Sharkey, N.A., Ferris, L., Smith, T.S., Matthews, D.K., *Journal of Bone and Joint Surgery, 77-A(7):1050-1057, 1995.*
Stokes, I.A.F., Hutton, W.C., Stott, J.R.R., *J. Anatomy, 129(3):579-590, 1979.*

ACKNOWLEDGMENT

The authors would like to acknowledge helpful discussions with Dr. Neil Sharkey which led to the refinement of this model.

A COMPUTATIONAL FORMULATION TO DETERMINE CONSTRUCT MECHANICAL OPTIMALITY FOR FIBULAR BONE GRAFTING IN FEMORAL HEAD NECROSIS

J. Sakamoto[2] and T.D. Brown[1]
[1]Department of Orthopaedic Surgery, University of Iowa, Iowa City IA 52242
[2]Dept. of Mechanical Systems Engineering, Kanazawa University, Kanazawa 920 JAPAN

INTRODUCTION

The disturbingly high rates of prosthesis failure in femoral head osteonecrosis have prompted a continuing search for head-preserving surgical alternatives. One very promising procedure is vascularized fibular bone grafting, in which a 12-15 cm vascularized fibular segment is anastomosed to the proximal femoral retinacular vessels, after insertion up into a core tract drilled superiomedially through an entry site on the lateral cortex (Urbaniak et al., 1995). Mechanically, the graft functions as a cantilever beam, uptaking some of the load that would otherwise pass through the weakened necrotic cancellous bone in the weight-bearing tract of the femoral head. To date, intra-operative placement of these grafts has relied upon intuition. However, recent finite element data have shown that the degree of structural protection provided depends sensitively upon the details of graft placement. Since three-dimensional characterization of lesion geometry is now routinely available from MRI, it has become plausible to entertain the possibility of patient-specific finite element analysis as a surgical planning vehicle for optimal graft placement. We here report a new computational formulation developed for that purpose. A key feature is that the structurally optimal graft configuration is determined automatically, thus avoiding the labor-intensive nature of manual finite element modelling of successive graft positioning refinements.

BACKGROUND

Clinical results from long-term follow-up of osteonecrosis patients have shown that vascularized fibular grafting has the potential to delay or arrest the process of head collapse in many patients having otherwise poor or guarded prognosis (Urbaniak, 1995). Recent finite element data (Brown et al., 1993; Yang and Chen, 1993) have shown that the risk of lesion collapse, as indexed in terms of the stress:strength ratio (SSR) in the involved bone, can be substantially reduced by a well-placed graft. However, not all graft placements reasonably approach ideal structural inforcement, and in some instances malpositioned grafts can even further elevate stresses in the lesion. Because each patient's lesion is unique, it is difficult to know intuitively what graft placement is most appropriate in a given case. Finite element analysis potentially could enhance the process of surgical planning in this circumstance, given appropriate strategies for orderly meshing of this complex three-dimensional structure (Rudert, 1994). However, to be of practical value in the clinical arena, it also is necessary that such a model make its determination of ideal graft positioning with little or no manual intervention. Algorithmic procedures developed in the field of structural optimization (Arora, 1984) lend themselves well to this problem.

PROCEDURES

Let the geometric position of the graft axis entry point on the femoral cortex be designated as point $\mathbf{P}_1$, and let the position of the graft tip be designated as point $\mathbf{P}_2$ (Figure 1).

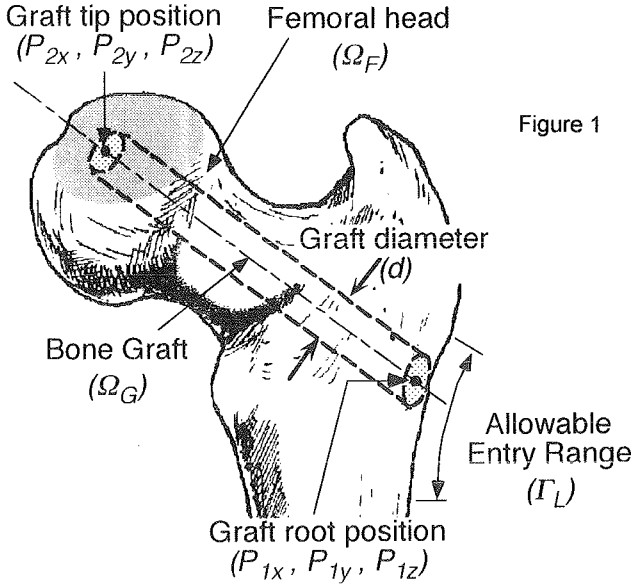

Figure 1

The graft is assumed to be straight and to have a diameter **d**. The parameters $\mathbf{P}_1$, $\mathbf{P}_2$, and **d**

constitute a set of design variables, upon which a to-be-optimized objective function $f(\mathbf{P}_1,\mathbf{P}_2,\mathbf{d})$ depends. Since previous patient-specific finite element modelling showed that the relative propensity for collapse correlated significantly with the peak local SSR (Baker et al., 1992), minimizing the peak SSR constitutes a reasonable design objective. Pertinent constraint conditions are that the graft tip not penetrate the subchondral plate ($\Omega_G \in \Omega_F$), and that the graft axis entry point be restricted to lie between the sites of gluteus maximus and vastus lateralis attachments on the lateral cortex ($\mathbf{P}_1 \in \Gamma_L$). From the SSR distribution emerging from the finite element solution for any starting set, **b**, of design variables, appropriate changes $\Delta\mathbf{b}$ are inferred from the direction of maximal change of the design sensitivity vector, $(\mathbf{D.S.} = \partial f/\partial\mathbf{P}_1, \partial f/\partial\mathbf{P}_2, \partial f/\partial\mathbf{d})$. The process of updating **b** to achieve ever-lower peak SSR values continues iteratively (Figure 2), until a

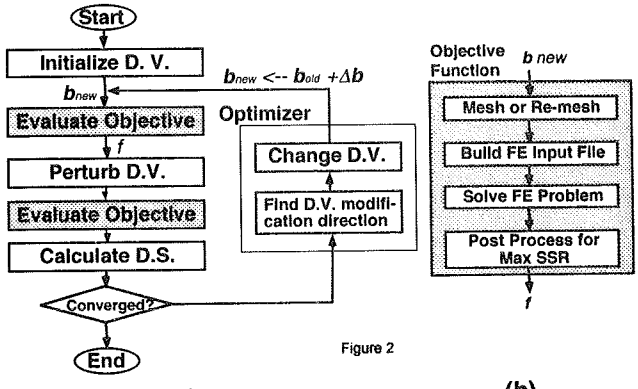

Figure 2

point is reached at which further perturbations of **b** fail to effect appreciable change, indicating solution convergence. During this iterative process, each perturbation of **b** changes the internal construct geometry, thus mandating automated re-meshing for the finite element analysis needed to compute the SSR distribution.

RESULTS

If begun from an initial graft tip position in the centro-medial region of the lesion, the algorithm identifies as structurally optimal a graft tip position flushly engaging the subchondral plate, in the centro-medial sector of the lesion, for the typical lesion involvement pattern and articular surface loading distribution shown in Figure 3. While no means currently exist for definitive validation, such a location is consistent with good surgical practice (Urbaniak et al.,1995; Brown et al., 1993). The structurally optimal lateral cortex entry point is identified to lie at the proximal margin of the surgically permissible domain. In this illustrative case, the optimal solution is reached in 15 iterations, and involves a reduction in peak SSR of 22 percent below the peak SSR value prevailing initially. The larger the graft diameter, the lower the peak SSR, approximately a 7% change being realizeable as the graft diameter changes over the clinically feasible range of from 6 to 10 mm.

DISCUSSION

Once an initial graft position is prescribed, no further manual intervention is required for computational determination of the optimal placement. However, systematic sampling of the available design variable space revealed that the optimization problem does not possess a unique solution. That is, there often exist several other "local" optima, typically involving graft tip positions below the distal border of the lesion, at the medial and lateral margins. Which of these local optima is settled upon by the algorithm depends on the initial choice of graft position. Attainment of a clinically useful local optimum requires a clinically and biomechanically informed judgement, initiating the graft tip in the superocentral substance of the lesion.

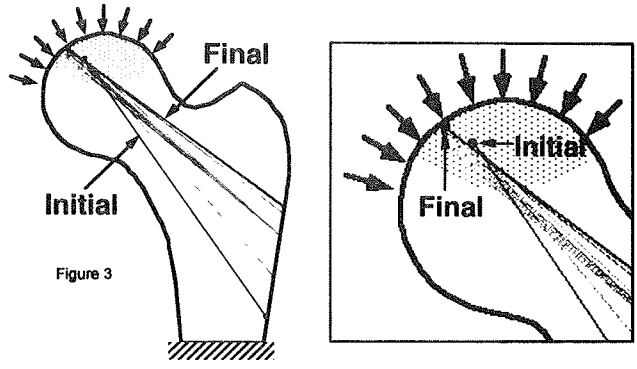

Figure 3

REFERENCES

Arora JS, In *New Directions in Optimal Structural Design*, E Atrek et al., eds, Wiley, 1984.
Baker KJ et al., *Proc. 2d NACOB*:361-362, 1992.
Brown TD et al., JBJS 75A: 1358-1367, 1993.
Rudert MJ, Ph.D. Thesis, Univ. of Iowa, 1994.
Urbaniak JR et al., JBJS 77A: 681-694, 1995.
Yang S & Chen JH, *1993 ASME Bioengineering Conf.*: 503-506, 1993

ACKNOWLEDGEMENTS: Financial support was provided by NIH Grant AR-35788, and by the Educational Ministry of Japan. Mr. D.R. Pedersen, Dr. M.J. Rudert, and Dr. R.A. Brand provided helpful advice.

THE EFFECT OF ACETABULAR COMPONENT ORIENTATION ON LOAD TRANSFER THROUGH THE CADAVER PELVIS

R. Klein, T. Loebig, D. Anderson, T. Mutschler, G. Ferguson
Biomechanics Research Laboratory, Allegheny-Singer Research Institute
Pittsburgh, Pennsylvania 15212

INTRODUCTION

The most common cause of failure in total hip arthroplasty (THA) is aseptic loosening of the femoral and acetabular components. The mechanical factors in femoral component loosening have been studied extensively, while the acetabular mechanics have received less attention (Oh and Harris, 1978; Huiskes et al., 1992).

Pelvic cortical bone strain and its relationship to the surgical parameters of THA has not been thoroughly investigated. Reis et al. (1989) studied the effects of oversized acetabular components and Massin et al. (1996) considered the contribution of prosthesis stiffness to the strain response. Siemon et al. (1991) investigated the effects of acetabular component orientation and found that it strongly influenced pelvic cortical strains, especially in the region around the acetabulum. Their method was limited, in that it involved applying photoelastic coatings to dried hemipelves.

The goal of this investigation is to characterize cortical strain patterns in cadaver pelves and to study how they are affected by the orientation of the acetabular component in THA.

PROCEDURES

Nine fresh-frozen cadaver pelves were dissected free of soft tissue, sparing the hip capsules, sacro-iliac ligaments, sacro-sciatic ligaments, and symphysis pubis. Radiographs were obtained to ensure freedom from orthopaedic deformities and osteoarthritis. The femurs were carefully disarticulated and stored for use during later testing.

Each hemipelvis was in turn prepared for strain gaging by scraping and sanding the cortical bone at the gage sites. All fascia and periosteum were removed producing a clean, smooth surface. The gage sites were scrubbed with a toluene solvent to remove oil-based contaminants and with isopropyl alcohol to displace water. Thirteen strain gage rosettes (Measurements Group WA-13-060WR-120) were affixed around the rim of the acetabulum, and on the medial and lateral surfaces of the hemipelvis. Lead wires were attached and the gages were sealed with acrylic. The specimens were stored for approximately 24 hours in a well hydrated environment allowing the cyanoacrylate glue and acrylic sealer to cure and ensuring that the bone was in a well hydrated condition for testing.

Mechanical testing was performed with the pelvis in a simulated single-leg stance (Figure 1). Each pelvis was fixtured for testing by potting its sacrum in a cylindrical block of PMMA. This block was then attached to the MTS actuator by a pin joint. The femur corresponding to the hemipelvis was potted in a cylinder of PMMA and mounted on a low-friction x-y table during testing. PMMA was used to imbed a wire

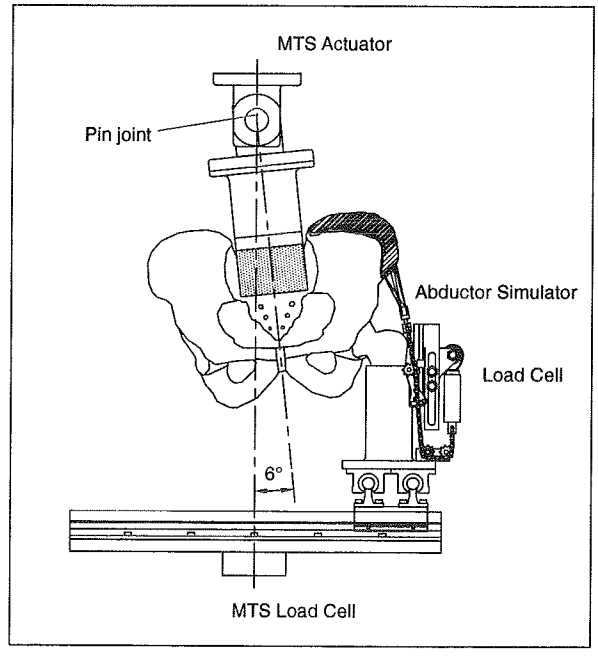

Figure 1: Pelvis in simulated single-leg stance.

mesh to the illiac crest. Steel cable connected the mesh to a specially designed abductor simulator. The simulator, via a special linkage and a built-in load cell, controlled the tension and direction of the cable to simulate abductor muscle force. Sacral load was monitored and controlled by the MTS load cell.

Prior to testing, each specimen was preconditioned to reduce viscoelastic effects (pelvis preloaded to 30

N, then cycled between 30 and 100 N for several minutes) and baseline strain readings were taken with the specimen loaded and unloaded. The sacral loading during data collection was 400 N. While sub-physiologic, this loading proved adequate to obtain useful strain information while not inducing material damage to the most fragile cadaver pelves.

Once the baseline information was gathered, a metal-backed, uncemented acetabular component was inserted in a preferred orientation by an orthopaedic surgeon. A femoral component, PMMA-potted in a metal cylinder, was substituted for the intact femur and the testing regimen was repeated. Next, the acetabular component was reoriented to a "neutral" position of 45° inclination - 15° anteversion and strain readings were recorded while the specimen was loaded. At this and each subsequent orientation considered, two loading trials were performed. The reorientation and testing routine was repeated, in 15° increments, until all possible orientations from 30° to 60° inclination and 0° to 30° anteversion were tested. Orientation of the acetabular component was controlled with a specially designed jig. After testing all orientations, the cup was again reoriented to 45°-15° and tested. Finally, a 2mm oversized acetabular component was inserted at a neutral orientation to study the effects of press-fitting an oversized acetabular component on pelvic cortical strains.

After assessing the initial results and finding little difference between trials, for each orientation, strain data were averaged across the two loading trials. The 45°-15° orientation was tested three times in each experiment, as a control, and these results were also averaged. After assembling the averaged data for each specimen, the strains were averaged across nine hemipelves for each periacetabular location.

RESULTS AND DISCUSSION

Figure 2 shows results of the maximum periacetabular principal strains measured at five locations around the acetabulum. The graph depicts the approximate location of each gage with respect to the geometry of the acetabulum. The maximum principal strain responses for three cup orientations was considered, along with the "Natural" case, which shows the strain response before acetabular component insertion. The cup orientations considered were for a constant anteversion of 15°, and 30°, 45°, and 60° inclinations.

As shown in Figure 2, the strain distribution around the acetabulum is not symmetric and neither are the apparent changes in the strain with varying cup orientation. The measured periacetabular cortical strains at all five locations were increased after component insertion. The greatest changes in strain during loading appear in the anterior portion of the

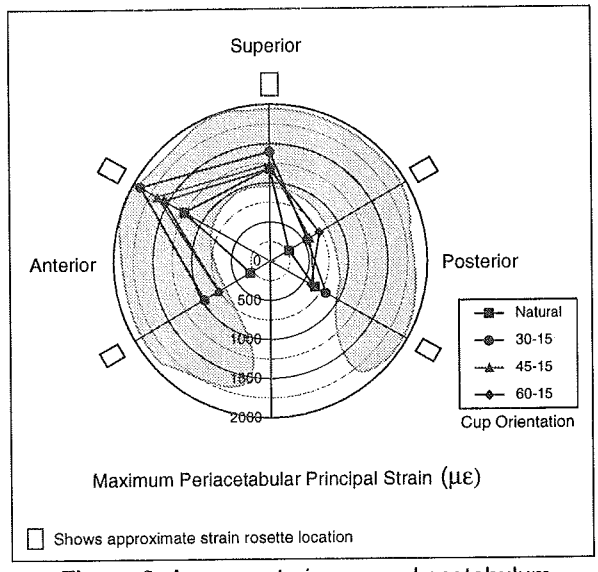

Figure 2: Average strains around acetabulum.

rim. The posterior strains, after insertion of the acetabular component, are relatively unchanged from the physiological state across the orientations considered.

The maximum principal strains represent one set of scalar measures which may be considered to describe the cortical strain distribution. Other measures have been proposed to predict yield in cortical bone, and our current efforts are focused on identifying at-risk regions of periacetabular bone near the acetabular component. Dynamic strain data collected during the press-fitting of oversized cups into the acetabula remain to be characterized, and they may provide further insight into damage associated with this procedure.

REFERENCES

Huiskes R, Weinans H, and Van Rietbergen B. Clin Orthop 274: 124-134, 1992.
Massin P, Vandenbussche E, Landjerit B, Augereau B. J Biomechanics 29(1): 53-61, 1996.
Oh I, and Harris W. J Bone Joint Surg 60A: 75-84, 1978.
Ries M, Pugh J, Au J, Gurtowski J, and Dee R. J Biomechanics 22(8/9): 775-780, 1989.
Siemon D, O'Donnell P, Little E. Strain 11/91:143-153, 1991.

ACKNOWLEDGMENTS

The financial support of the Albert B. Ferguson, Jr. M.D. Orthopaedic Foundation and the Allegheny-Singer Research Institute are gratefully acknowledged.

INFLUENCE OF THE ANNULAR INCISION TECHNIQUE ON THE BIOMECHANICAL CHARACTERISTICS OF A HERNIATED LUMBAR INTERVERTEBRAL DISC

R.N. Natarajan, G.B.J. Andersson
Department of Orthopedic Surgery
Rush-Presbyterian St.Luke's Medical Center, Chicago, IL 60612

INTRODUCTION

The technique used to incise the annulus fibrosus during lumbar discetomy may play a role in the subsequent healing process of the intervertebral disc and the stability of the motion segment. The organization and integrity of various components in a motion segment dictate the biomechanical properties of the disc. A surgical incision in the annulus, as necessary in the treatment of lumbar disc herniation, will change the biomechanical properties of the disc. Several methods of incision of the annulus are used such as removal of a full thickness rectangle, a straight transverse incision or a slit through the annulus (1). The reduction in the strength of disc after the surgical intervention has not been studied in detail and thus there is no biomechanical agreement on the technique that should be recommended. The aims of the current study were (1) to study if a box incision through the annulus has greater effect on the mechanical characteristics of the disc as compared to a slit incision. and (2) to study if flexion moment loading has the largest effect on the mechanical characteristics of a disc without nucleus and with annular incision.

MATERIALS AND METHOD

The geometrical shape of a lumbar motion segment was generated from a serial computed axial tomographic scan of an L3-L4 disc body unit. Using this CT scan a non-linear 3D finite element model was generated for the motion segment consisting of a vertebra-disc-vertebra unit. The annulus fibrosus was modeled as comprising 5 layers of fibrous materials with fibers inclined at both + 29 ^{0} and - 29 ^{0} and embedded in a ground matrix. The cross-section of the annular fibers was assumed to be largest at the inside surface of the annulus and least at the outer surface. The nucleus was modeled as inviscid incompressible fluid while the posterior elements were considered as elastic materials. The flat articulating facet surfaces were modeled as contact elements that can carry compressive load only. Ligaments were approximated as non-linear cable elements. Material properties for various elements of the motion segment were obtained from published literature. A full thickness rectangular incision (size 4 mm X 6 mm) in the right posterio-lateral quadrant at the mid-section of the anulus was modeled by appropriately removing elements through the entire thickness of the anulus. The slit incision was modeled in a similar fashion. Analyses were conducted for three different loading modes : compression, flexion combined with compression and torsion combined with compression. Biomechanical characteristics of an intact motion segment was compared with motion segment with annular incision in which the nucleus was either completely removed or remained intact.

RESULTS

Model validation : A compressive load of 400 Newton on an intact motion segment produced : average annulus compression of 0.35 mm, anterior disc bulge of 0.25 mm, posterior disc bulge of 0.60 mm. A flexion moment of 5 Nm combined with a pre-load of 400 Newton induced a flexibility of disc 0.5 ^{0}/ Nm, average annulus compression was 0.54 mm and anterior disc bulge of 0.75 mm. Torsional moment of 5 Nm combined with a compressive load of 400 Newton produced a flexibility of 0.15 ^{0}/ Nm, average annulus compression of 0.34 mm and posterior disc bulge of 0.52 mm. Maximum contact force occurred on the posterior edge of the facet surface.

The values predicted by the finite element

model agreed well with the corresponding values available in the literature.

Role of annular box incision and slit incision on disc biomechanical properties.

Effect of the two types of annular incisions on change in the biomechanical characteristics of the disc such as flexibility, disc bulge, and facet joint loads was similar. However, the type of incision did have an effect on the stresses in annulus and in annulus fibers. Both box and slit type of incisions increased the flexibility of the disc for all three modes of loading considered in this study (Figure 1). Annular incision alone did not increase the disc flexibility, but under compression loading mode a maximum of 174% increase in flexibility was calculated when the nucleus was also removed from the disc (Figure 1). A small decrease in anterior radial bulge (0.3%) was seen under all three types of loading when either type of incision was introduced in the annulus. Annular incisions reduced the posterior radial bulge by 2% under both compression as well as flexion moment loading. Torsional moment loading, however, increased the posterior radial bulge by 6%. Change in the maximum annular stress in the axial direction on the inside surface depended on the type of annular incision (Figure 2). Maximum change in the stress of 66% was observed under torsional moment loading (Figure 2). Annular fiber stress decreased due to the annular incisions and a maximum decrease of 85% was calculated under torsional moment loading. Facet loads increased after annular incisions. An increase of 8% and 15% was observed under flexion moment and torsional moment loading respectively. Both box as well as slit type annular openings was found to decrease in size due to compression and torsional moment loadings However, the size of the opening on the outer surface of the annulus increased under flexion moment loading.

DISCUSSION

Both box type and slit type of annular incisions produced similar changes in the biomechanical characteristics of the disc except the stresses in annular components. The largest effect due to annular incision was seen when the disc underwent compression loading. Annular incisions decreased the stability of the motion segment while reducing posterior bulge except under torsional loading mode. While the incisions did not have an adverse effect on the annular fiber stresses, they did have determental effects on annular stresses. Annular incisions transferred part of the load from the disc to facet joints. Thus the surgical intervention in the disc in the form of an annular incision followed by de-nucleation reduced the mechanical strength of the disc in addition to changing the pathway by which the external load is transferred in a lumbar motion segment. This study further shows that there is no preference between the two annular incisions as far as stability of the disc is concerned for the given loading conditions.

REFERENCE

(1) Ahlgren, BD et al., SPINE 19:1994, 948-954.

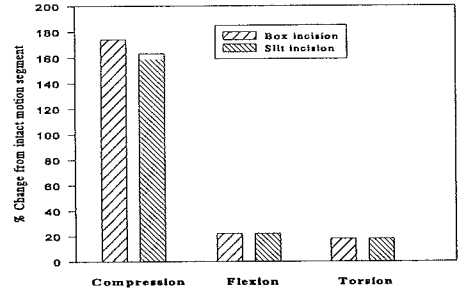

Figure 1. Changes in flexibility of disc due to annular incision

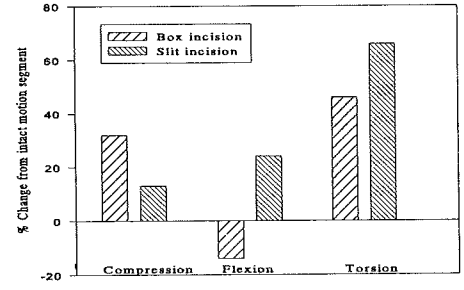

Figure 2. Changes in annular stresses due to annular incision

KINEMATIC ANALYSIS OF THE HUMAN EYE BLINK

*Rash, G., **Somia, N., *Phillips, H., **Sundine, M., ***Gossman, D. & **Barker, J.

*Gait & Biomechanics Laboratory, Frazier Rehab Center, Louisville, KY 40202.
**University of Louisville Dept of Plastic & Reconstructive Surgery, Louisville, LY 40292
***University of Louisville Dept of Opthamology & Visual Science, Louisville, LY 40292

INTRODUCTION & REVIEW

Several different types of facial disorders cause uneven blink responses. Numerous treatment protocols are used in order to attempt to achieve a more normal eye blink, or better closure on the affected side. Despite advances in technology, a subjective pre/post observation by the physician is the only means of quantifying the effectiveness of the treatment. Our goal was to use the unaffected eye kinematics as a control for the affected eye in measuring improvement of treatment. A review of the literature found a multitude of information regarding the rate of the human eye blink, however, nothing could be found regarding the bilateral kinematics of the human eye blink. Additionally, no objective information regarding bilateral synchronization of the eye blink was available. Therefore, the purpose of this study was to compare the bilateral kinematics and synchronization of the human eye blink in normal subjects.

METHODOLOGY

Ten healthy human subjects (7 male, 3 female) were used as subjects in this study. None of the subjects had previously undergone eye surgery nor had any of the subjects been diagnosed with a neurological disease. After identification of marker locations on the forehead and eyelids of the subjects by an plastic surgeon, 4mm diameter retroreflective markers were placed on the subject as shown in figure 1. A "T" bar with 3 reflective markers was used to establish a local coordinate system. The "T" bar was strategically placed such that the lower marker was 2 cm superior to the center of the bridge of the nose. Then the "T" bar was squared up by tilting the bar until the top markers measured the same distance from the nose bridge point. The markers on the upper eyelids were placed such that they were in the middle of the upper eyelid on the distal aspect of the eyelid above the lashes. The lower eyelid marker was placed at 1/3 the distance of the lower eyelid.

The subject sat in a pre-calibrated area such that they faced 3 cameras (60 Hz). A Qualisys motion analysis system was used to collect the multiple 15 second data collections until 5 spontaneous blinks were captured.

The 3D coordinate data were calculated from the three camera Qualisys motion analysis system via the DLT method and the 3D coordinate data were exported to a GX program for kinematic analysis. All data were digitally smoothed at 10 Hz. A 3D coordinate system was set up in the forehead using the "T" bar and all coordinates were rotated and translated into this system from the global system established by the calibration frame. The vertical and horizontal displacement, velocity and acceleration of the eyelids were then calculated with respect to the local coordinate system. The kinematics for the 5 blinks from each subject were averaged to establish a subject average, then the averaged subject data were averaged for an overall average.

Since kinematic data over time typically results in a graphic wave form and simple statistics do not yield a meaningful result when describing the similarity or variability of waveforms. A statistical measure called the adjusted coefficient of multiple correlation R_a (Winer, 1971) was used to evaluate the bilateral similarities of the kinematic data. When the wave forms are similar R_a tends to 1. If the wave forms are dissimilar R_a tends to 0. Thus, R_a yields a measure of synchronization between left and right eyelid kinematics.

RESULTS & DISCUSSION

The overall average peak displacement, velocity and acceleration magnitudes were 9.11 +/- 2.70 mm, 143.38 +/- 57.24 mm/s and 4010.38 +/- 2004.52 mm/s^2 respectively. Figure 2 shows a sample graph of the bilateral eyelid displacement plots which had an average R_a of 0.82. Figure 3 shows a sample graph of the bilateral eyelid velocity plots which had

an average R_a of 0.99. Figure 4 shows a sample graph of the bilateral eyelid acceleration plots which had an average R_a of 0.99. All subjects had small standard deviations with respect to individual kinematics, however, there was a large variability between subjects. The R_a for displacement was lower in all subjects as compared to velocity and acceleration. This is felt to be due mainly to marker placement on the eyelid, as well as normal bilateral asymmetries of the face. A small DC shift in the displacement plots could be seen for all subjects (typically 1-3mm).

From these results it was concluded: 1) Kinematics within subjects were very similar, but varied between subjects 2) Bilateral eye blinks are almost perfectly synchronized as shown by looking at the velocity and acceleration plots and averaged R_a values for these wave forms. Since there is superb symmetry bilaterally in normal subjects it is felt that this method of blink analysis will be a valuable tool for the physician. Further research is needed, but good results have been found using this technique on a single patient in regards to selecting the best mass of gold weight to use in a facial palsy patient. The study to assess it efficacy is now underway.

REFERENCES

Winer, B. Statistical Principles in Experimental Design, (pp. 261-288), McGraw-Hill, 1971.

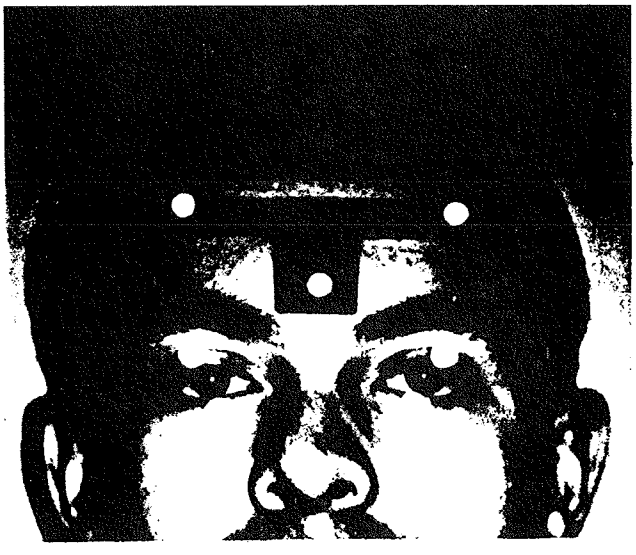

Fig 1. Marker Placement

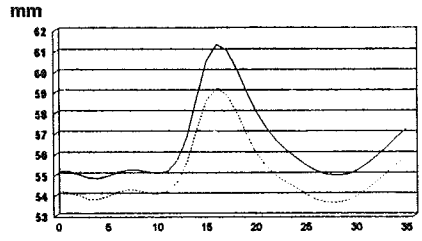

Fig 2. Normal Eye Lid Displacement

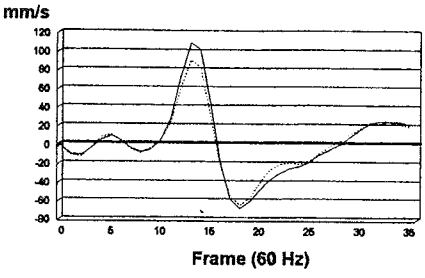

Fig 3. Normal Eye Lid Velocity

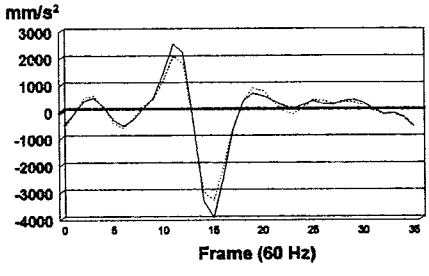

Fig 4. Normal Eye Lid Acceleration

RULid ——— LULid .....

WITHIN-DAY ACCOMMODATION AND HABITUATION EFFECTS ON VERTICAL IMPACT FORCES FOR TREADMILL RUNNING

Scott C. White, Kathryn A. Christina & Louise A. Gilchrist
Department of Physical Therapy & Exercise Science
SUNY at Buffalo, Buffalo, NY 14214

INTRODUCTION

Treadmills are a convenient medium for analyzing running mechanics. Subject experience or prior exposure to treadmill running may however, effect the reliability and validity of dependent measures. The present study reports changes in the impact peak of vertical reaction forces, and their variability over time, for eleven subjects running on a force measuring treadmill. Data are reported for the first thirty seconds and for every two minute interval up to twenty minutes. Inter-time interval differences were tested for significance via a repeated measures ANOVA. There were no significant differences in stride-to-stride variability over time intervals (accommodation). Relative to initial forces (t = 30 s) peak impact forces significantly increased after four and eight minutes. Within-day habituation but not accommodation may effect interpretation of impact forces with treadmill running.

REVIEW AND THEORY

Treadmills are often used to analyze sport shoe effects or shoe orthotics (Lafortune et al., 1994; Nigg et al., 1995) since steady state locomotion speeds can be maintained and successive, repetitive strides are easily documented. Within-day accommodation defined as no significant difference in stride-to-stride variability with running time, and habituation defined as a stable, normal gait with no significant differences in the averaged measurement parameter with exposure time, are two compounding factors that may influence the reliability and validity of dependent measures. Based on kinematics, some amount of time for subject adaptation to treadmill running is recommended (Shieb, 1986; Frost et al., 1994). To our knowledge, kinetic measures indicative of treadmill running accommodation and habituation have not been reported. Since the first passive vertical force peak after foot contact has been linked to impact measures (Miller, 1990; Perry et al., 1995), treadmill accommodation effects on this measure are of particular concern in sport shoe research. The present study reports foot-ground vertical force impact peaks, and their variability over time, for subjects running on a treadmill.

PROCEDURES

Vertical foot-ground reaction forces were collected on a treadmill housing force plates (Kistler Instruments Corp.) for eleven recreational runners. Six subjects were experienced treadmill runners and five had no prior experience. Subjects ran at a self-selected running speed (range = 2.25 to 3.0 m/s) for twenty minutes. Warm-up and stretching was done off the treadmill. Five seconds of force data were analog-to-digitally converted (600 Hz) and stored at 30 seconds, and at the end of every 2 minute interval up to a 20 minute running trial. The right step, peak vertical impact forces for the last five successive strides of each sample interval were normalized to subject body mass. Average initial (t = 30 s) force for each subject was subtracted from forces for successive time intervals to account for between subject, speed related differences in impact forces. Changes in force magnitude between time intervals were then tested for significance ($p < 0.05$) using a one-way, repeated measures ANOVA with contrast analysis. For each individual, the coefficient of variation (CV) was calculated for the right limb by dividing stride-to-stride (n=5) standard deviation values by their mean force. CV values were tested for significance differences in the same way.

RESULTS

There were no significant differences in CV values across time intervals for the 20 minute run. (Fig. 1). There were significant increases in average peak impact force changes relative to the initial values at four ($p = .047$) and eight ($p = .043$) minutes (Fig. 2). Peak impact forces tended to increase in the initial ten minutes of treadmill running and decrease over the last 16 to 20

minutes although individual responses were variable (Fig. 2).

DISCUSSION

Preliminary results show that treadmill running within-day habituation time (systematic magnitude changes) but not accommodation time (stride-to-stride variability) may effect the interpretation of peak vertical impact forces. Compared to CV values of about 12%, calculated from force data reported for overground running (Miller, 1995), CV results from the present study indicate that the stride patterns are more repeatable. Two factors, constant running velocity and environmental control (consistent surface, safety rails, etc.) probably contribute to reduced variability. Treadmill running may give more consistent results when repeated measures are used to evaluate experimental protocols in which shoe design effects (varus or valgus control) are the independent variables. When force magnitude comparisons are an issue (e.g. shoe material) habituation to treadmill running is an important consideration. The present results are consistent with kinematic data (Shieb, 1986) suggesting that running mechanics may change initially as the subject adapts to the treadmill. We saw an initial increase in peak impact force in the first 8 to 10 minutes. The changes may be related to increased stride lengths reported to occur with habituation (Schieb, 1986) since the lower limb strike angle relative to the running surface would change with an altered stride. We observed large individual differences in adaptability response consistent with conclusions based on kinematics (Frost et al., 1995; Nigg et al., 1995). Individual habituation considerations may be more important than utilizing an across group, rule-of-thumb habituation time. We also observed that the inexperienced runners exhibited greater habituation effects. Experience as an effect was not tested on the existing data set due to the small sample size. Others have concluded that running experience is not a factor based on kinematic changes (Nigg et al., 1995).

REFERENCES

Frost, G. et al. Ped. Exerc. Sci., 7, 162-175, 1995.

Lafortune, M.A. et al., 8th Biennial Conference, CSB, 90-91, 1994.

Miller, D.I. Biomechanics of Distance Running. Ed. P. Cavanagh, Human Kinetics Pub., 1990.

Nigg, B. M. et al. Med. Sci. Sport Exerc., 27, 98-105, 1995.

Perry, S.D. et al., Clin. Biomech. 10, 253-257, 1995.

Schieb, D.A. Res. Quart., 57, 1-7, 1986.

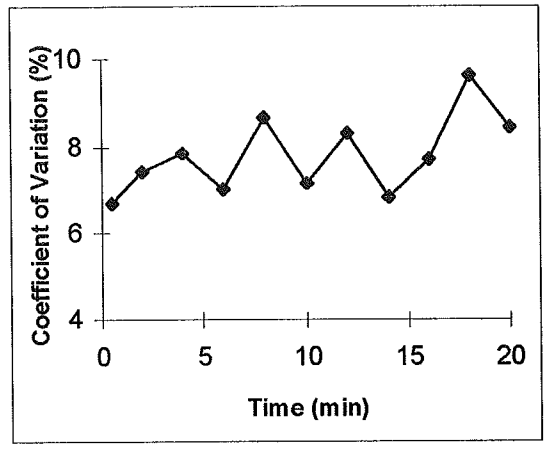

Fig. 1: Coefficient of variation for twenty minute, constant speed treadmill runs. Group mean is presented.

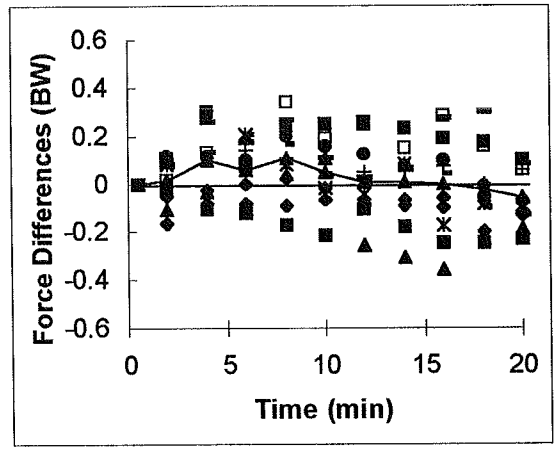

Fig. 2: Changes in peak impact force relative to initial value (t = 30s) over twenty minute, constant speed treadmill runs. Solid line represents group mean; individual data are represented as symbols.

GROUND REACTION FORCE CHARACTERISTICS AND RUNNING ECONOMY

G.D. Heise[1], P.E. Martin[2], and P.S. Carroll[1]

[1]School of Kinesiology and Physical Education, University of Northern Colorado, Greeley, CO 80631

[2]Exercise and Sport Research Institute, Arizona State Univerisity, Tempe, AZ 85287

INTRODUCTION

It was hypothesized that ground reaction force (GRF) characteristics that describe certain functional and mechanical requirements during stance would be positively correlated with the aerobic demand at a single speed of running (i.e., running economy). These characteristics describe potentially wasteful motion in terms of metabolic energy requirements. Recreational runners (n=16) ran on a treadmill at 3.35 $m \cdot s^{-1}$ for physiological measures and overground for biomechanical measures. Total vertical impulse, net impulses in three orthogonal directions, average vertical force, and descriptors of the free moment were correlated with $\dot{V}O_2$. Total vertical impulse was the only GRF characteristic significantly correlated to $\dot{V}O_2$ (r=0.62). This relationship suggests that the greater overall muscle support requirements during ground contact are responsible for greater aerobic demand.

REVIEW AND THEORY

For a given aerobic activity, such as distance running, some individuals are more economical than others. Biomechanists recently have hypothesized that variability in the aerobic demand of running can be partly explained by measures that describe runners' contact with the ground. For example, Kram & Taylor (1990) presented a simple inverse relationship between aerobic demand and stance time. They suggested that "it is primarily the cost of supporting the animal's weight and the time course of generating this force that determines the cost of running" (p. 265). They examined different animal species over a range of running speeds.

During ground contact, a runner activates muscles for purposes of stability and for the development of forward momentum. These functional and mechanical requirements during stance are described by characteristics of the ground reaction force (GRF). Linear momentum is produced in the vertical and mediolateral directions as well as the forward direction, and could be considered wasteful motion in terms of metabolic energy requirements. Linear impulse measures the change in momentum and quantifies "the time course" of the GRF. In the present study, it was hypothesized that less economical runners (i.e., those with a higher aerobic demand) would exhibit greater support requirements during foot contact, as indicated by the total vertical impulse, and greater changes in momentum, as indicated by the net impulse. It was reasoned that a greater net impulse, or a greater change in linear velocity of the center-of-mass, would be metabolically wasteful. It also was hypothesized that the average vertical GRF, the rate of vertical force application, and the free moment would be correlated positively with aerobic demand.

PROCEDURES

Sixteen well-trained men performed treadmill running for determination of running economy and overground running for which biomechanical measures were determined (running speed = 3.35 $m \cdot s^{-1}$). Specifically, time of contact (tc), average vertical ground reaction force (Favg), the rate of vertical force application, linear impulses for each of three orthogonal directions (vertical, Fz; anterior-posterior, Fap; medial-lateral, Fml), and descriptors of the free moment (Mz') applied to the force platform were calculated.

Five successful, right foot contacts with an AMTI force platform were chosen for analysis for each subject. Mean values of GRF characteristics were then calculated. The rate of vertical force application was the slope of the initial, linear portion of the Fz-time curve. This portion of the Fz-time curve was manually selected with the aid of an interactive, computer-graphics program.

Total vertical impulse was calculated as:

$$TVI = \int_0^{tc} \left\{ \frac{Fz}{BW} \right\} dt$$

Net impulses were calculated as:

$$NVI = \int_0^{tc} \left\{ |Fz - BW| \right\} dt$$

$$NAPI = \int_0^{tc} \left\{ \left| \frac{Fap}{BW} \right| \right\} dt$$

$$NMLI = \int_0^{tc} \left\{ \left| \frac{Fml}{BW} \right| \right\} dt$$

for vertical, anterior-posterior, and medial-lateral directions, respectively. The unit of measure for NVI was BW·s while other impulse measures were expressed in BW·ms.

Maximum and minimum values of the free moment applied to the force platform and the net angular impulse (NAIMz') associated with the free moment were determined and normalized based on calculations presented by Holden & Cavanagh (1991). Mean GRF characteristics were then correlated with submaximal $\dot{V}O_2$.

RESULTS AND DISCUSSION

Mean data and correlation coefficients between aerobic demand and GRF characteristics are shown in Table 1. The difference between the least and most economical subjects expressed as a percentage of the mean aerobic demand, 26.5%, agrees well with results of previous studies (see Martin & Morgan, 1992 for review). There existed no distinct pattern between subjects' $\dot{V}O_2$max and their submaximal aerobic demand as was verified by the poor correlation between these two variables ($r = -0.08$). The most economical runner used only 59% of his aerobic capacity, whereas the least economical subject used 83%.

Table 1: Mean data and correlation coefficients between $\dot{V}O_2$ and GRF characteristics (* $p < .05$).

Variable	MEAN	SD	r	
$\dot{V}O_2$max ($ml \cdot kg^{-1} \cdot min^{-1}$)	62.2	3.0	--	
$\dot{V}O_2$ ($ml \cdot kg^{-1} \cdot min^{-1}$)	44.6	3.3	--	
tc (ms)	243	17	.01	
Favg (BW)	1.58	0.1	.41	
Fz Rate ($BW \cdot s^{-1}$)	81.8	14.5	.17	
TVI (BW·ms)	382.5	17.5	.62	*
NVI (BW·s)	158.8	20.1	-.09	
NAPI (BW·ms)	42.8	3.5	.25	
NMLI (BW·ms)	10.2	2.9	.37	
Max Mz' (unitless)	4.9×10^{-3}	1.3×10^{-3}	-.08	
Min Mz'(unitless)	-3.5×10^{-3}	1.6×10^{-3}	-.04	
NAIMz'(s)	5.2×10^{-4}	1.0×10^{-4}	-.01	

The magnitudes of GRF characteristics were similar to previously reported values (Holden & Cavanagh, 1991; Munro et al., 1987, Williams, 1980). TVI was the only GRF characteristic to be significantly correlated with aerobic demand. More economical runners exhibited a lower TVI. Positive correlation coefficients, although not significant, were also noted between aerobic demand and Favg, Fz rate, NAPI, and NMLI.

In the present study, the combined influence of Fz and the "time course" of that force application, as represented by TVI, explains a significant amount of inter-individual variability in running economy. Kram & Taylor (1990) examined several speeds of running-type gait (e.g., trotting, galloping) in different species of animals and reported a significant relationship between tc and aerobic demand. In contrast, tc was not related to aerobic demand in the present study (see Table 1). Williams (1980) showed no trend between low, medium, and high economy groups and TVI. TVI can be considered an indication of overall muscular support during ground contact. Differences in muscle activation patterns during stance may help explain the significant relationship reported here. A recent study that examined this question found a trend that indicated economical runners exhibited more coactivation between two-joint muscles of the leg during stance (Heise et al., 1996). These neuromuscular differences in runners need to be examined further.

Of the impulse measures that reflected momentum changes, NAPI and NMLI exhibited the expected positive correlation coefficients with $\dot{V}O_2$, however, the relationships were not statistically significant. It is well documented that the mediolateral component of the GRF is quite variable (e.g., Miller, 1990).

The variables describing the free moment applied to the platform historically have not been examined by researchers examining GRF characteristics. Here it was hypothesized that any force application that detracted from forward motion may be metabolically wasteful. The free moment, thought of as a "twisting moment" applied by the foot to the ground does not influence aerobic demand. Its low magnitude prior to normalization (mean NAIMz' = 1.58 N·m·s) may partly explain the lack of a relationship.

In conclusion, only one of the GRF characteristics (TVI) exhibited a significant, positive correlation with aerobic demand. Several other correlation coefficients were positive as hypothesized, but tc, NVI, and descriptors of the free moment showed no correlation with $\dot{V}O_2$.

REFERENCES

Holden, J.P. & Cavanagh, P.R. J. Biomech, 24, 887-897, 1991.

Heise, G.D. et al. Int. J. Sports Med., 17, 128-133, 1996.

Heise, G.D. & Martin, P.E. ASB Proceedings, Palo Alto, CA, pp. 111-112, 1995.

Kram, R. & Taylor, C.R. Nature, 346, 265-267, 1990.

Martin, P.E. & Morgan, D.W. Med. Sci. Sports Exerc., 24, 467-474, 1992.

McMahon, T.A. & Cheng, G.C. J. Biomech., 23(Supp), 65-78, 1990.

Miller, D. In Biomechanics of Distance Running (Edited by P.R. Cavanagh), Human Kinetics, Champaign, IL, 1990.

Munro, C.F. et al. J. Biomech., 20, 147-155, 1987.

Williams, K. Ph.D. dissertation, The Pennsylvania State University, 1980.

THE INFLUENCE OF SIZE, SPEED, AND GRAVITY ON THE KINEMATICS OF HUMAN WALKING: A TEST OF THE DYNAMIC SIMILARITY THEORY FOR LOCOMOTION

J. Maxwell Donelan and Rodger Kram
Department of Human Biodynamics, University of California, Berkeley, CA 94720-4480
http://garnet.berkeley.edu/~hbbiomxl

INTRODUCTION

Alexander's theory of dynamic similarity (1977a, b) has been used to compare the locomotion of children, adults, various animal species and even to estimate the locomotion mechanics of dinosaurs. The theory depends on the assumption that gravity is the dominant factor that determines locomotion mechanics (Alexander, 1989). We tested the theory by varying gravity and speed while measuring the changes in the kinematics of human walking.

REVIEW AND THEORY

Two systems of moving bodies are dynamically similar if the motion of one can be made identical to the other by multiplying all linear dimensions, time intervals, and forces by constants (Duncan, 1953). For example, pendulums of different lengths moving through equal angles have dynamically similar motion.

Dynamic similarity in animal locomotion requires the same phase relationships, duty factors, relative stride lengths, and force records (Alexander, 1977a, b). A comparison of small and large animal species over a wide speed range indicates that animals move in a dynamically similar fashion when they travel at speeds that translate to equal values of the dimensionless Froude number (Alexander et al., 1983). The Froude number (Fr) is derived from the ratio of centripetal and gravitational force which reduces to:

$$Fr = v^2/g \cdot LL$$

where v is forward velocity, g is acceleration due to gravity and LL is leg length.

The purpose of this study was to determine the influences of size, speed, and gravity on the kinematics of human walking. We tested the hypothesis that humans walk in a dynamically similar fashion when walking at speeds and simulated gravities that provide equal values of the Froude number.

PROCEDURES

Five subjects were familiarized with treadmill locomotion and our reduced gravity simulator during preliminary sessions. We videotaped the subjects as they walked at normal gravity and at conditions simulating 0.75, 0.5 and 0.25G. At each level of simulated gravity, the subjects walked at speeds that equated to four Froude numbers (.1, .2, .3, and .4). At each level of gravity, they also walked at four fixed absolute speeds (.25, .5, .75, and 1.0 m/s) . Leg length was measured as the height to the greater trochanter. From the videotapes, we obtained the average stride time and duty factor for each trial and knowing the speed, converted stride time to stride length. Duty factor is the fraction of a stride that a foot is in contact with the ground. Relative stride length is stride length divided by leg length.

We simulated reduced gravity using a device that applied a nearly constant upward force to the body via a bicycle saddle. The upward force was provided by a series of compliant rubber spring elements, stretched to a length much greater than the subjects vertical oscillations. Force fluctuations were less than 0.03 G across all levels of gravity. Data obtained with our previous simulation device (He et al., 1991) are comparable to data obtained with other reduced gravity simulation techniques (Newman, 1994).

RESULTS

At all combinations of speed and gravity, subjects walked symmetrically, resulting in the same phase relationship. Thus, they met the first criteria for dynamic similarity. The second criteria, that subjects will have equal duty factors at equal values of the Froude number, was also met. That is, duty factors were not significantly different (ANOVA $p = 0.52$) (Figure 1). In contrast to the theory's predictions, at equal values of the Froude number the subjects did not have equal relative stride lengths ($p = 0.003$) (Figure 2). At the same Froude number, relative stride length differed by as much as 40%.

At all velocities, duty factors were slightly greater at higher gravities ($p < .001$) (Figure 3). Over a four fold range of gravity, the changes in relative stride length at a given velocity were significant ($p<.001$) but remarkably small (Figure 4).

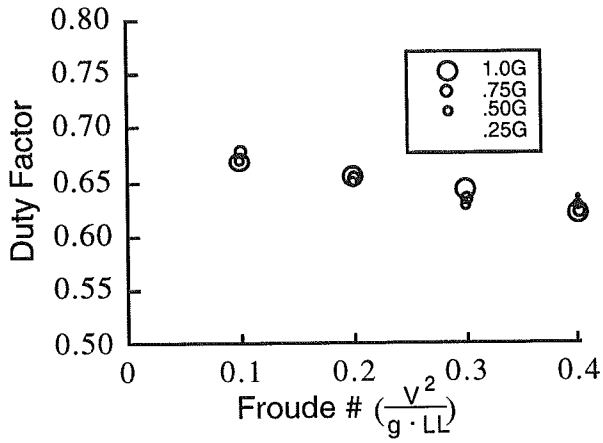

Figure 1.

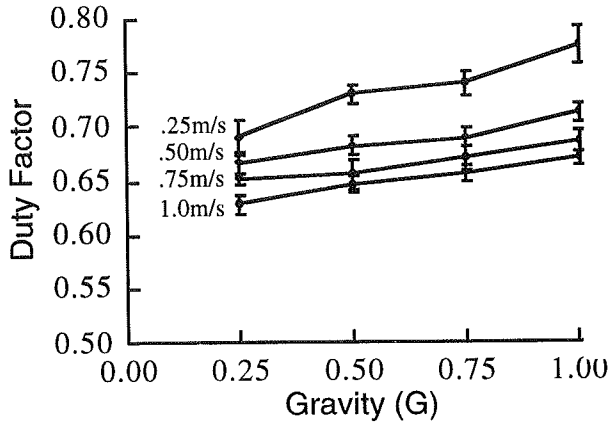

Figure 3.

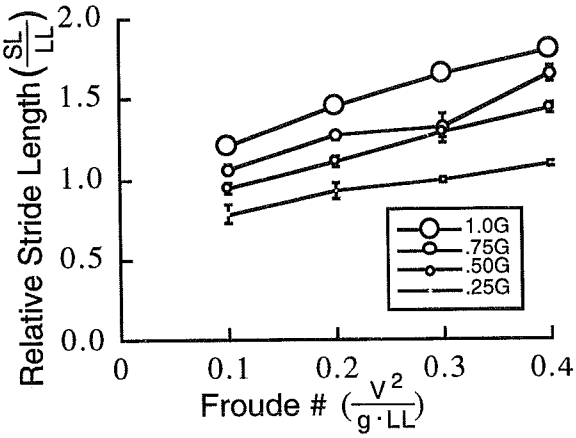

Figure 2.

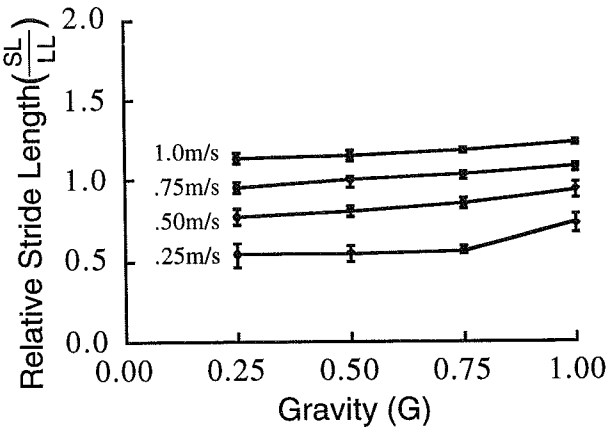

Figure 4.

DISCUSSION

We reject the hypothesis that humans walk in a dynamically similar way at equal Froude numbers. Alexander's dynamic similarity theory accurately predicts the kinematics of animal locomotion over a wide range of body sizes and speeds, but only at one gravity. As a practical matter, this theory can still be used, but a new theoretical construct is needed to interpret the underlying mechanisms of walking mechanics.

Walking and running are fundamentally different from a mechanical viewpoint. Walking is a series of vaults over relatively stiff legs. Running is a bouncing movement and the legs act like compliant springs (Cavagna et al., 1977). We found that stride length slightly shortens at lower gravities in walking but substantially lengthens at lower gravities in running (He et al., 1991). It seems likely that different hypothesis are needed to describe dynamic similarity in walking and running.

Our next experiments are designed to test the current dynamic similarity hypothesis in running under simulated reduced gravity and to investigate the possibility of alternate dynamic similarity hypotheses for both walking and running.

REFERENCES

Alexander, R. McN. Scale Effects in Animal Locomotion; (pp. 93-110), Academic Press, 1977a.
Alexander, R. McN. Mechanics and Energetics of Animal Locomotion; (pp. 168-203), Chapman and Hall, 1977b .
Alexander, R. McN. et al. J. Zoology, 201:135-152, 1983.
Alexander, R. McN. Physiol. Reviews. 69:1199-1227, 1989.
Cavagna, G.A. Am. J. Physiol. 233:R243-R261, 1977.
Duncan, W.J. Physical Similarity and Dimensional Analysis, Edwward Arnold, 1953.
Farley, C.T. et al. J. Appl. Physiol. 73:2709-2712, 1992.
He, J. et al. J. Appl. Physiol. 71:863-870, 1991.
Newman, D.J. et al. Aviat. Space. Environ. Med., 65:815-23, 1994.

ACKNOWLEDGMENTS

This research was supported by the Cal Space Institute.

Effect of Reduced Gravity on the Preferred Walk-Run Transition Speed

Rodger Kram, Antoinette Domingo, and Daniel Ferris
Department of Human Biodynamics, University of California, Berkeley, CA 94720
http://garnet.berkeley.edu/~hbbiomxl

INTRODUCTION

At speeds slower than ~2 m/sec, adult humans prefer to walk. It is possible to walk faster than 2 m/sec, but we prefer to run. The physiological or biomechanical reason for this preference is not yet clear. We investigated the effect of simulated reduced gravity on the preferred walk-run transition speed to try and understand the underlying mechanics of walking.

REVIEW AND THEORY

Some have argued that the walk-run transition occurs so as to minimize the metabolic energy expenditure (Alexander, 1989, Mercier et al., 1994), however, recent data disputes that idea (Hreljac, 1993a, Minetti et al., 1994). Various kinematic and mechanical triggers have also been suggested (Hreljac, 1995a, Minetti et al., 1994) but have not been convincingly supported by data. It is clear that the walk-run transition is not triggered by critical levels of ground reaction forces (Hreljac, 1993b) though force levels do explain some gait transitions in other animals (Farley & Taylor, 1991). Is there a simple mechanical reason for the walk-run transition?

A simple inverted pendulum model for a walking biped idealizes the body mass to a point mass on a rigid massless leg (Alexander, 1977). The major force that determines the movements of this pendulum is gravity. Gravity must be at least equal to the centripetal force needed to keep the center of mass traveling along a circular arc. The centripetal force needed is equal to mv^2/L where m is body mass, L is leg length, and v is forward speed. In this model, walking above a critical speed is impossible because the gravitational force would be less than the centripetal force required and the body would fly off the ground. The dimensionless ratio of the centripetal force needed and the gravitational force involved can be calculated for legged locomotion as v2/gL where v is forward speed, g is gravity and L is leg length. This dimensionless number is borrowed from fluid mechanics where it is called the Froude number (Fr). The Froude number can be thought of as a dimensionless speed. Above about 3 m/sec, Fr is greater than 1.0 and walking is impossible. At normal Earth gravity, humans and other bipedal animals prefer to switch from a walk to a run at Fr = 0.5 (Alexander, 1989, Gatesy & Biewener 1991, Hreljac, 1995b).

The purpose of this study was to better understand the mechanical determinants of the walk-run transition by changing gravity and observing the effects. We hypothesized that at lower levels of gravity, humans would prefer to switch from a walk to a run at a slower absolute speed, but at the same dimensionless speed or Froude number.

PROCEDURES

We studied nine volunteer subjects (average leg length (greater trochanteric height) = 0.89m, average mass = 63.8kg). They were familiarized with treadmill locomotion and our reduced gravity simulator during several preliminary sessions. The experimental session involved treadmill locomotion at a variety of speeds at normal gravity and at 5 levels of simulated gravity (0.8, 0.6, 0.4, 0.2, 0.1G). Reduced gravity was simulated by applying a nearly constant upward force to the body via a bicycle saddle.

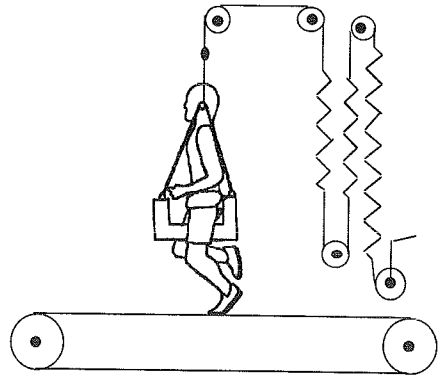

To create this constant upward force, a series of compliant rubber spring elements were stretched to a length much greater than the vertical oscillations of the person. Force fluctuations were less than $\pm$ 0.03G across all levels of gravity. See He, Kram & McMahon, (1991) for more details.

At each level of gravity we determined the preferred speed of transition from walking to

running. We increased the speed in 0.1 m/sec increments and allowed the subject to decide if they preferred to walk or to run at that speed as per Hreljac (1993a). We emphasized that we were looking for their *preferred* gait transition speed, as opposed to the maximum possible speed of walking.

RESULTS

At lower levels of gravity, the walk-run transition occurred at progressively slower absolute speeds At 1.0G, the average transition speed was 1.98 m s^{-1} which corresponded to an average Froude number of 0.45. We calculated the absolute speed that corresponds to a Fr =0.45 for each level of gravity and plotted this as a prediction. Above 0.2G, this prediction was within 11% of the actual preferred transition speed. At 0.2 and 0.1G, the preferred speeds were substantially higher than predicted. The table below indicates how the Froude number increased moderately down to 0.4G and then substantially increased at 0.2 and 0.1G.

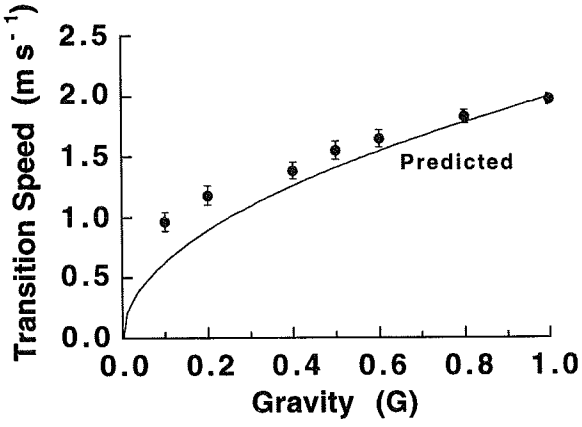

G	v ($m\ s^{-1}$)	Fr	predicted v ($m\ s^{-1}$)	% Diff. Actual - Predict.
1.0	1.98 (±0.038)	0.45 (±0.02)	1.98	-
0.8	1.84 (±0.049)	0.49 (±0.03)	1.77	4
0.6	1.65 (±0.066)	0.53 (±0.04)	1.54	7
0.5	1.55 (±0.067)	0.56 (±0.05)	1.40	11
0.4	1.39 (±0.062)	0.56 (±0.05)	1.25	11
0.2	1.18 (±0.073)	0.83 (±0.10)	0.89	34
0.1	0.97 (±0.075)	1.13 (±0.17)	0.63	54

DISCUSSION

In general, our data support the hypothesis that in reduced gravity, the walk-run transition occurs at a slower absolute speed but at a similar Froude number. However, at levels of gravity below 0.4G the Froude number was much greater. This appears to be due to the importance of arm and leg swing induced accelerations at very low levels of gravity. For example, we estimated that at a simulation of 0.2G, the limb acceleration force was equivalent to about 0.16G. The basis of the Froude number is the simple inverted pendulum model that has massless legs and no arms. Thus, the divergence of empirical data from the predicted values suggests that a model that includes arm and leg intertial forces would be useful.

The simple inverted pendulum model identifies the Froude number as an important variable, however, it only predicts the *maximum* walking speed (Fr = 1.0). Many investigators have noted that humans and bipedal birds *prefer* to switch from a walk to a run at a Froude number of about 0.5 (Alexander, 1977, Hreljac 1995b, Mochon & McMahon, 1980). Some have described this observation as a model prediction (Hreljac, 1995b). However, we are aware of no satisfactory model that predicts *a priori* that the transition should occur at Fr = 0.5. The most recent relevant modeling attempt was that of Alexander (1992) who included compliant legs with mass. This model could be forced to predict a transition at 0.5 but only with unreasonable assumptions. A simple mechanical model that *predicts* a transition at Fr = 0.5 remains elusive.

REFERENCES

Alexander, R. McN. Mechanics and energetics of animal locomotion, (pp. 168-203), Chapman & Hall, 1977.
Alexander, R. McN. Physiol. Reviews. 69:1199-1227, 1989.
Alexander, R.M. Phil. Trans. Roy. Soc. B. 338, 189-198, 1992.
Cavagna, G.A. et al. J. Physiol. 262, 639-657, 1976.
Gatesy S.M. & A.A. Biewener, J. Zool., 224, 127-147, 1991.
He, J. et al. J. Appl. Physiol. 71, 863-870, 1991.
Hreljac, A. Med. Sci. Sports Exerc. 25, 1158-1162, 1993a.
Hreljac, A. Gait & Posture. 1, 217-223, 1993b.
Hreljac, A. J. Biomech. 28, 669-677, 1995a.
Hreljac, A. Human Movmt. Sci. 14, 206-216, 1995b.
Margaria, R. Biomechanics and energetics of muscular exercise. Oxford Univ. Press, 1976.
Mercier, J. et al. Eur. J. Appl. Physiol. 69, 525-529, 1994.
Minetti, A.E. et al. Acta Physiol. Scand. 150, 315-323, 1994.
Mochon, S. & T.A. McMahon. J. Biomech. 13, 49-57, 1980.
Thorstensson, A. and H. Roberthon. Acta Physiol. Scand. 131, 211-214, 1987.

ACKNOWLEDGMENTS

Support for this project came from Cal Space Institute, NASA fellowship NGT-51416, UC Berkeley SROP, URAP and Biology Fellows Program.

SPASTICITY AND STRENGTH CHANGES AS A FUNCTION OF SELECTIVE DORSAL RHIZOTOMY

J.R. Engsberg[a,b], K.S. Olree[a], S.A. Ross[a], T.S. Park[a,b]
[a]Motion Analysis Laboratory, St. Louis Children's Hospital and [b]Washington University School of Medicine, St. Louis, MO 63110

INTRODUCTION

Selective dorsal rhizotomy (SDR) is performed on children with cerebral palsy to minimize or eliminate the influence of spasticity.[5] One contraindication and a limitation of SDR surgery is muscle weakness.[1] Currently objective measures to quantify spasticity and weakness are not used in the surgical decision making process or in outcome evaluation. This investigation quantified pre- and post-surgery spasticity and maximum active resultant joint torques in the hamstrings of children with cerebral palsy (CP group) undergoing a selective dorsal rhizotomy. Spasticity values were significantly greater than similar values for children with able bodies (AB controls) prior to surgery but not significantly different from AB controls after surgery. Maximum joint torques did not change as a function of surgery and were significantly less than the AB controls.

REVIEW AND THEORY

Recently, objective measures to quantify spasticity using 'velocity dependent resistance to stretch'[4] as its characterization and the maximum active resultant joint torque at the knee were developed.[2,3] The rationale for the development of the spasticity measure was due to the paucity of objective measures utilized in its quantification and the desire for the measure to be based upon sound mechanical principals. The chosen characterization permitted an objective measure based on simple mechanical constructs (i.e., angular velocity and a resistive torque through an angular range of motion). A similar process occurred for the maximum active joint torque measure. However, in addition, the maximum active torque protocol had to allow even the weakest child the opportunity to generate torque over a full range of motion. The purpose of this investigation was to quantify changes in spasticity and active joint torques as a function of SDR surgery. It was hypothesized that a significant decrease in both spasticity and active joint torques would occur as a result of the surgery.

PROCEDURES

Ten children (mean 11 years, range 4-16) with spastic diplegic cerebral palsy and undergoing SDR were tested the day prior, and approximately 8 months post-surgery. The AB controls consisted of 6 children (mean 9 years, range 4-17).

Each child sat on a dynamometer and had knee joint extension range of motion limits established. For the spasticity measure, the machine extended the leg passively through a range of motion at speeds of 10, 30, 60, and 90°/s while monitoring the resistive torque from the hamstrings.[2] For the active torque measure, the machine flexed the leg through a range of motion at 10°/s while the child performed a maximum contraction of the hamstrings.[3] Torque-angle data were processed to partial out effects of gravity and minimize acceleration and machine dynamic responses. Areas within the torque-angle curves were calculated for each speed and child, yielding work values (Fig 1).

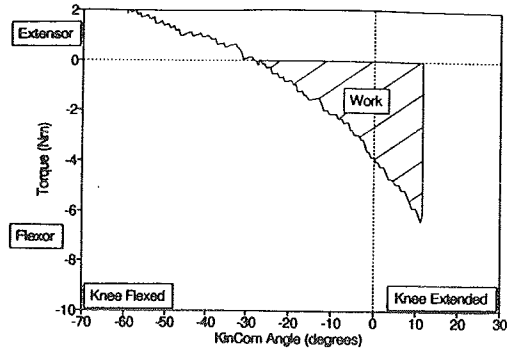

Fig 1. Work calculation of single child at a single speed for the spasticity measure.

For the spasticity measure, linear regression was used to derive the slope of the line of best fit for the work-velocity data. For the strength measure, work by the hamstrings was utilized. Paired and unpaired t-tests were used to test for significant differences pre- and post-surgery and between groups, respectively ($p<0.05$).

RESULTS

Pre-surgery, the hamstring spasticity in the CP group was significantly greater than that of the AB controls (Fig 2). Post-surgery values were significantly less than pre-surgery values and not significantly different than AB controls. Pre-surgery values for maximum flexion work of the hamstrings were not significantly different from post-surgery values. Both pre- and post-surgery work values were significantly less than similar values for the AB controls. The hypothesis that spasticity would be reduced was supported, while the hypothesis that active joint torques would be reduced was not.

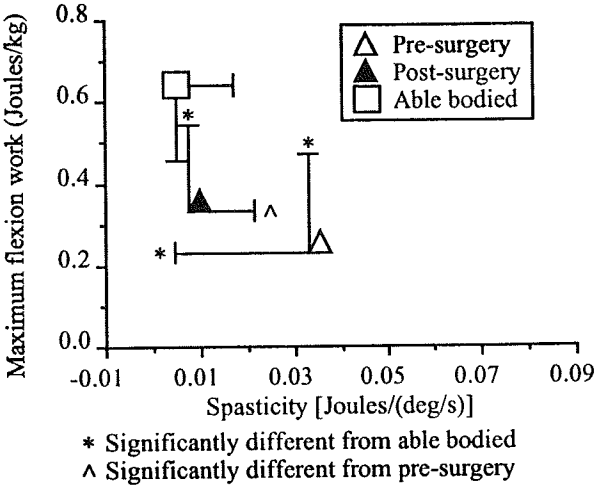

Fig 2. Mean values and standard deviations for spasticity and active torques in CP group (i.e., pre- and post-surgery) and AB controls

DISCUSSION

When determining whether an SDR should be performed, pre-surgery spasticity and weakness and post-surgery weakness are important concerns. Previous investigations have not simultaneously quantified spasticity and maximum active joint torque variables pre- and post-SDR. The present investigation indicated a reduction in hamstring spasticity, but not a reduction in active hamstring work. Whether this trend persists at the ankle and hip is presently unknown.

The standard deviation bars in Figure 2 illustrate the large amount of variation existing within the CP group. In 2 children, the pre-surgery spasticity measures were slightly less than the mean for the AB controls. For the active torque measure, 6 children displayed increases from pre- to post-surgery, but 3 children indicated decreases. This large variation seems to indicate the diversity of children that are undergoing the SDR surgery and leads to at least two considerations. The first is whether all of the children undergoing the SDR have the same degree of post-surgery functional outcome. It could be that those children with low spasticity and active torque values prior to surgery do not improve to the same degree as those with greater pre-surgery spasticity and active torques. The second is whether the measures quantified in this investigation could be used to aid in the selection process for children being considered for the SDR surgery. It is possible that children with spasticity and maximum active torques below a certain level are not candidates for the surgery. Current subjective methods of selecting the children do not appear to identify this subgroup. Investigations quantifying both spasticity and maximum active joint torques at the ankle, knee, and hip and functional measures (e.g., gait) could help clarify these issues.

REFERENCES

1. Cahan, L.D. et al. In Park (ed) Neurosurgery: State of the Art Reviews, 4(2) 477-484, 1989.
2. Engsberg, J.R. et al. Arch of Phys and Rehab Med, In Press, 1996.
3. Engsberg, J.R. et al. Dev Med Child Neuro, Supp 73, 42, 1995.
4. Lance, J.W. In Feldman (ed) Spasticity: Disordered Motor Control, 48, 1980.
5. Park, T.S. et al. Neurosurgery, 33(5), 929-934, 1993.

VARIATIONS IN NECK MUSCLE FASCICLE LENGTHS WITH HEAD POSITION

A. N. Vasavada[1,2], S. Li[1], S. L. Delp[1,2]
[1]Sensory Motor Performance Program, Rehabilitation Institute of Chicago
[2]Biomedical Engineering Department, Northwestern University
345 East Superior Street, Chicago, IL 60611

INTRODUCTION

The muscles of the neck generate head movements and maintain the stability of the cervical spine. The roles of individual neck muscles in this complex musculoskeletal system are not well understood. However, the unique features of cervical spine anatomy, kinematics and muscle architecture may influence neck muscle function at different postures. In this study, we found that neck muscle fascicles operate on different parts of the active muscle force-length curve during various movements and that muscles with similar functions may have very different fascicle operating ranges.

REVIEW AND THEORY

The head-neck system includes over 20 pairs of muscles. Many of these muscles can generate moments about more than one axis of rotation. The complex anatomy makes it difficult to use many common experimental techniques of musculoskeletal biomechanics, such as electromyography or measurement of moment arms. Thus, detailed, anatomically-based musculoskeletal models are important to understand neck muscle function.

Documenting the physiological operating ranges of muscle fascicles provides insight into the part of the force-length curve on which muscles operate, and therefore how force-generating capacity varies with head position. The objective of this study was to quantify neck muscle fascicle lengths over a range of head positions in three directions of motion.

PROCEDURES

A graphics-based musculoskeletal model of the head and neck was developed using Software for Interactive Musculoskeletal Modeling (Delp and Loan, 1995). Description of the head-neck model and preliminary results have been presented by Li and colleagues (1995).

The isometric force-generating properties of muscles were obtained by scaling a generic Hill-type model of muscle (Zajac, 1989). The four scaling parameters per musculotendon actuator are optimal fascicle length, tendon slack length, pennation angle and peak isometric force. Muscle architecture parameters were collected through a collaboration with Queen's University. The experimentally obtained parameters were muscle fascicle and sarcomere length at the neutral head position, physiological cross-sectional area and pennation angle. The muscles included in this analysis were sternocleidomastoid, longus capitis, scalenus (anterior, medius, and posterior), trapezius, splenius (capitis/cervicis), semispinalis (capitis/cervicis), rectus capitis posterior major, rectus capitis posterior minor, obliquus capitis superior and obliquus capitis inferior.

Cervical spine kinematics were defined based on data in the literature (White and Panjabi, 1990). The total angular range of motion of the head relative to the trunk was 136° in flexion/extension (pitch), 154° in axial rotation (yaw) and 122° in lateral bending (roll), and motions at the intervertebral levels were distributed as a percentage of the total head rotation angle.

Fascicle lengths at neutral were measured in anatomical studies. Changes in fascicle length were calculated in the model from muscle attachment sites and coordinate transforms defined by joint kinematics. Fascicle lengths were normalized to optimal length and superimposed on an active muscle force-length curve for analysis.

RESULTS

This analysis showed that the operating ranges of neck muscle fascicles vary considerably among muscles and movement directions. For example, fascicle lengths of sternocleidomastoid remain in the plateau region during pitch, enter the descending limb of the force-length curve during yaw, and encompass almost the entire active force-length curve during roll (Figure 1). Certain muscles which are commonly considered to have similar functions were found to operate on very different portions of the force-length curve. Splenius capitis and semispinalis capitis both generate an extension moment. However, splenius capitis fascicles act on the descending limb and plateau region during pitch, while semispinalis capitis fascicle lengths operate on the ascending limb and the plateau region (Figure 2). For all muscles studied, fascicle length variations were greatest for those directions with the largest moment arms.

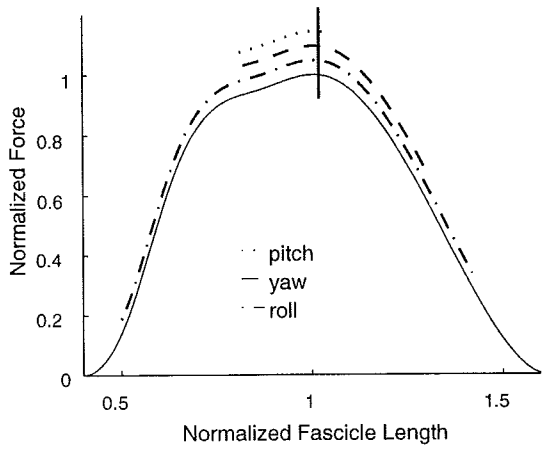

Figure 1: Fascicle operating ranges of sternocleidomastoid during head movements in pitch, yaw and roll. The vertical line indicates fascicle length at neutral head position.

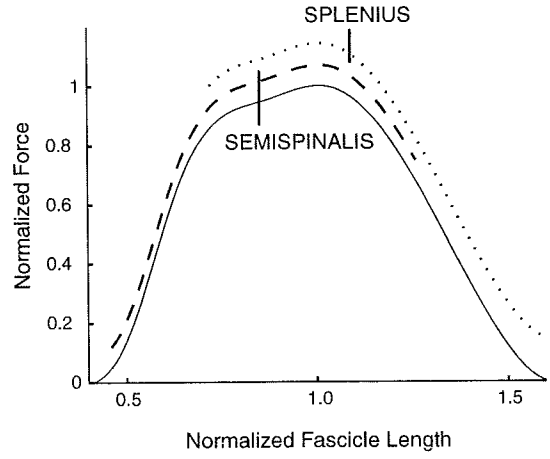

Figure 2: Fascicle operating ranges of splenius capitis (dotted) and semispinalis capitis (dashed) during pitch movements (head flexion and extension). Vertical lines indicate fascicle lengths at neutral head position.

DISCUSSION

The range of joint angles over which a muscle can generate active force is proportional to the ratio between optimal fascicle length and moment arm. A larger ratio indicates less variation in force-generating capacity with changes in head position. The ratio of optimal fascicle length to moment arm varies among neck muscles, more often because of differences in moment arm rather than fascicle length. For example, sternocleidomastoid has optimal fascicle length of 10.8 cm and flexion moment arm less than 1 cm. The optimal fascicle length of splenius capitis is 9.5 cm, but the extension moment arm is close to 5 cm. This explains why sternocleidomastoid remains on the plateau region during flexion-extension movements while splenius capitis undergoes large changes in fascicle length.

Differences in fascicle operating ranges in muscles with apparently similar functions may influence load sharing strategies. For example, splenius and semispinalis both have large extension moment arms. Splenius has greatest force-generating capacity at relatively shorter lengths (corresponding to head extension), while semispinalis can generate greater force at longer lengths (corresponding to head flexion).

The magnitude of the force decreases at the ends of the range of motion indicates that force-length effects can potentially play a large role in modulating muscle moment generating capacity. However, the extreme postures analyzed in this study may not occur during natural movements. In cats, fascicle lengths of most neck muscles remained on the plateau region during head and neck movements measured while tracking a drinker (Statler et al., 1995). Furthermore, the interaction of fascicle length and moment arm changes will influence the overall moment-generating capacity. The decreases in muscle force may be either offset or augmented by the changes in moment arm. Thus, characterizing the interaction of neck muscle architecture and musculoskeletal geometry is important to understanding muscle moment-generating and stabilizing capability at different head postures.

REFERENCES

Delp, S. and Loan, J. *Comput Biol Med*, 25, 21-34, 1995.

Hoy, M. et al. *J Biomech*, 23, 157-169, 1990.

Li, S. et al. Third Int Symp on the Head/Neck System, 1995.

Statler, K. et al. Third Int Symp on the Head/Neck System, 1995.

White, A. and Panjabi, M. Clinical Biomechanics of the Spine (p. 92-98), J. B. Lippincott, 1990.

Zajac, F. CRC Crit Rev in Biomed Eng, CRC Press, 1989.

ACKNOWLEDGMENTS

The authors gratefully acknowledge the work of Drs. Lynne Kamibayashi and Frances Richmond in collecting neck muscle architecture parameters. This study was supported by funding from NIDCD-NASA center grant for vestibular research and an NSF predoctoral fellowship.

THE EFFECT OF ELBOW FLEXION ANGLE ON SARCOMERE LENGTH IN HUMAN ELBOW MUSCLES

Wendy M. Murray, Thomas S. Buchanan, and Scott L. Delp
Department of Biomedical Engineering, Northwestern University, and
Sensory Motor Performance Program, Rehabilitation Institute of Chicago, Chicago Illinois

INTRODUCTION

The goal of this study was to investigate the variability of sarcomere lengths in human muscles and to determine the relationship between muscle sarcomere length and elbow flexion angle for the major elbow flexors and extensors. We measured sarcomere lengths of biceps, brachialis, brachioradialis, extensor carpi radialis longus, pronator teres, and triceps in eight fresh-frozen cadaver specimens in two different elbow positions. This data is essential for estimating the maximum forces of muscles at the elbow joint.

REVIEW AND THEORY

Muscle architecture parameters measured in cadaver specimens provide basic information about the functional capacity of muscles (Lieber et al., 1990). For example, optimal fascicle length (ℓ_o^M) is the length at which a muscle fascicle develops its maximum isometric force, and is one of four parameters used to characterize the force-length behavior of a musculotendon complex (Zajac, 1989). Estimating a muscle's optimal fascicle length involves measuring both the average fascicle length (ℓ_f) and the average sarcomere length (ℓ_s) of the muscle. ℓ_o^M is then calculated as

$$\ell_o^M = \left(\frac{2.8}{\ell_s}\right)\ell_f \qquad (1)$$

where 2.8μm is the optimal sarcomere length in human muscle (Lieber, 1994).

From Eq. (1), it is obvious that optimal fascicle length cannot be estimated without an accurate measure of average sarcomere length. The variability of sarcomere lengths within a muscle is an important consideration for obtaining an accurate estimate of ℓ_s.

Measurements of sarcomere length become even more useful if they can be correlated to a particular joint angle. Specifically, the portion of the isometric force-length curve over which a muscle operates can be estimated from the muscle's moment arm and the knowledge of ℓ_s at any joint angle.

Although sarcomere lengths of human muscles are commonly measured in anatomical studies (e.g., Lieber et al., 1990), little is known about the distribution of sarcomere lengths within human muscle. In addition, the relationship between sarcomere length and joint angle is not known for the elbow muscles. This study quantifies the variability in sarcomere lengths within individual muscles and between specimens in the elbow muscles.

PROCEDURES

Muscle parameters of the major elbow flexors and extensors were measured in eight fresh-frozen cadaver specimens using the methods of Sacks and Roy (1982). Three of the specimens were frozen at approximately 90° elbow flexion, the remaining five were frozen in full extension. After thawing, the specimens that were frozen in the flexed position remained flexed, and could not be extended without removing the elbow muscles from their attachment sites.

As a specimen was dissected, a segment of each muscle was removed and fixed in formalin for at least 48 hours. This segment included muscle fascicles extending from origin to insertion. Care was taken to remove the segment from the same location in each specimen. After the muscle segment was rinsed in phosphate buffer, ten muscle fascicles were dissected from each muscle segment. Each fascicle was then further dissected into smaller pieces at various locations along the length of the fascicle. These smaller pieces were mounted on a glass slide and sarcomere lengths were measured using the laser diffraction method (Lieber and Baskin, 1984). In each fascicle, twelve measurements of sarcomere length were taken, for a total of 120 measurements per muscle.

In the brachioradialis of one specimen, ℓ_s was measured in both the removed segment and throughout the remaining muscle to compare the distributions of sarcomere lengths in different areas of the muscle.

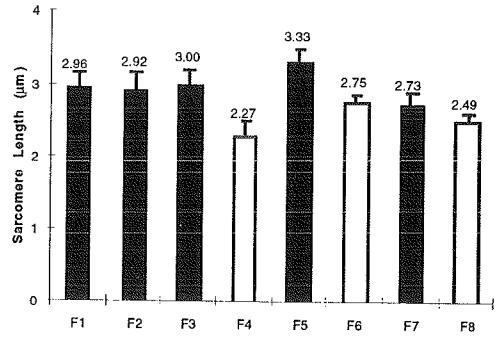

Figure 1. Average sarcomere lengths of the brachialis in 8 specimens. Black bars indicate specimens frozen in full extension. Variations in ℓ_s between specimens were observed in each muscle.

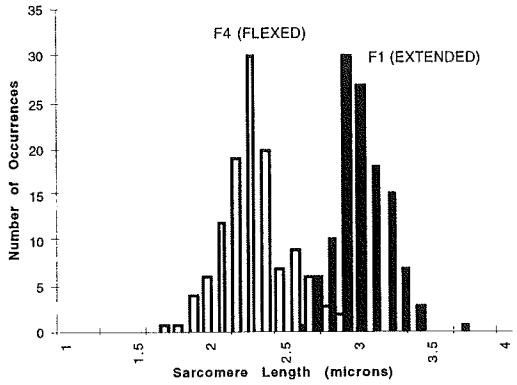

Figure 2. Distributions of sarcomere lengths measured in the brachialis in two specimens frozen at different positions.

RESULTS

In the brachialis, ℓ_s was greater than optimal sarcomere length in four of the five specimens frozen in extension (Fig. 1). In comparisons between individual specimens, ℓ_s of the brachialis was significantly shorter ($p<0.05$) in a specimen frozen in the flexed position than for a specimen frozen in full extension in every case except F6 *vs.* F7. However, there were also cases where two specimens frozen in the same position had significantly different average lengths (e.g., F5 *vs.* F7 in Fig. 1). For the brachialis, the average ℓ_s for the three flexed specimens (2.50μm, σ=0.24) was significantly shorter than the average ℓ_s for the five fully extended specimens (2.99μm, σ=0.22). A significant difference between groups was also observed in the brachioradialis (average ℓ_s was 2.45μm in flexed specimens, 2.90μm in extended).

Distributions of sarcomere lengths within the elbow muscles were approximately Gaussian, with standard deviations ranging between 5%-10% of the mean (Fig. 2). In a limited number of cases, we observed larger standard deviations and, upon examining the histograms, found the distribution of lengths to be bimodal. In general, the diffraction patterns observed in these particular cases were more diffuse and showed fewer diffraction orders than those of the other muscle segments. We concluded that these characteristics indicated the muscle had been damaged in some way.

Measurements from the entire brachioradialis indicate the sarcomere length distribution of a removed muscle segment is representative of the distribution for the whole muscle (Table I). This result also establishes the repeatability of our technique, and provides confidence that the variability observed between specimens is not due to the measurement method. Finally, the data from the brachioradialis shows the variation in ℓ_s along the length of the fascicles was greater than the variation in ℓ_s in fascicles of different lengths (Table I).

TABLE I
BRACHIORADIALIS SARCOMERE LENGTH MEASUREMENTS (F8)

	μ	σ
Removed Segment (n = 120)	2.38	0.15
Rest of Muscle (n = 120)	2.37	0.12
3 longest fibers (n = 36)	2.42	0.09
3 shortest fibers (n = 36)	2.39	0.18
middle of fiber (n = 120)	2.43	0.11
near origin (n = 60)	2.30	0.13
near insertion (n = 60)	2.34	0.13

DISCUSSION

We found a significant difference between the average ℓ_s of the group of specimens frozen in full extension and the group frozen in flexion in the brachialis and the brachioradialis. In the other muscles, the effect of elbow flexion angle was hidden by the variability of ℓ_s in specimens within the same group. While the muscle lengths of the brachialis and brachioradialis are primarily determined by elbow flexion angle, the other muscles that cross the elbow are also affected by the orientation of other joints. For example, the length of the biceps is determined by shoulder position, elbow flexion angle, and forearm rotation. Unfortunately, the joint configurations of the specimens were not under our control. We believe the variability of ℓ_s in specimens within the same group is partly explained by differences in orientations of the shoulder, wrist, and forearm. In addition, variability between specimens could have been introduced if the muscles were damaged through the freezing, dissecting, and fixation processes. However, only a small number of the muscles studied displayed characteristics that indicated substantial muscle damage. Finally, the variability in ℓ_s between specimens frozen at the same flexion angle could imply that muscles in different individuals operate over different portions of the force-length curves. At this point, however, it is not clear that the variability exists *in vivo*. In any case, these factors should be considered when making conclusions regarding the relationship between sarcomere length and joint angle.

REFERENCES

Lieber, R.L., and Baskin, R.J., J. Biophysics, **45**, 1009-1117, 1984.

Lieber R.L. et al., J. Hand Surg, **15A**, 244-250, 1990.

Lieber, R.L. et al., J. Neurophys., **71**, 874-881, 1994.

Sacks, R.D., and Roy, R.R., J. Morph., **173**, 185-195, 1982.

Zajac FE, CRC Reviews in BME, (pp. 359-411), CRC Press, 1989.

ACKNOWLEDGMENTS

This work supported, in part, by NSF BCS9110731 and NIH AR40408.

STRATEGY OF MUSCLE CO-ORDINATION DURING THE CONTROL OF AN EXTERNAL FORCE

B. I. Prilutsky*, R. J. Gregor
Department of Health and Performance Sciences, Georgia Institute of Technology, Atlanta, GA 30332
*Permanent address: Biomechanics Lab., Central Institute of Physical Culture, Moscow, Russia 105483

INTRODUCTION

The purpose of this study was to test the hypothesis that the stereotypical muscle activity during the control of an external force (Jacobs and van Ingen Schenau, 1992) corresponds to the strategy of muscle activation that allocates more force to muscles with a long moment arm. We simulated the following motor task: from three lower limb positions to exert the external force by pushing on the ground (or pulling a strap) in five different directions with two different force magnitudes. Forces of nine leg muscles were calculated using a standard, static optimization approach. Of three examined optimization criteria, the criterion that minimizes the sum of muscle stresses cubed predicted muscle forces for the pushing task that matched well the electromyographic (EMG) activity of the corresponding muscles reported in the literature for the same task. The results of this study suggest that during the control of the external force in pushing directions, the strategy of muscle co-ordination is characterized by the allocation of more force to muscles with a long moment arm and a large physiological cross-sectional area, and by an increased number of simultaneously active muscles. This strategy predicted the features of muscle co-ordination that were observed previously in experimental studies of walking, running, jumping, and cycling.

REVIEW AND THEORY

The performance of a motor task may require one to exert external force in different directions at the same limb position. Different directions of the external force are achieved by different distributions of the resultant moments among the joints (van Ingen Schenau et al., 1992). Based on an analysis of cycling, van Ingen Schenau et al. (1992) formulated a hypothesis that one- and two-joint leg muscles may have different roles in leg extension movements. According to this hypothesis, two-joint muscles (hamstrings and rectus femoris) are responsible for the controlling the distribution of resultant moments between the joints they cross (the knee and hip) and, as a consequence, for the control of the direction of the external force. The primary function of one-joint muscles was suggested to be the generation of mechanical energy. Jacobs and van Ingen Schenau (1992) tested the above hypothesis in the experiment where subjects trained to perform the task exerted a constant external force in five different directions from three limb positions. The recorded EMG activity of the main leg muscles demonstrated a linear relationship between the difference in EMG activity of rectus femoris and hamstrings and the difference in the resultant moment at the knee and hip (or the direction of the external force). Also, it was demonstrated that all muscles studied (except short head of biceps femoris, BFS) had increased EMG activity when they had a large virtual shortening. The authors concluded that the tested hypothesis was supported. The hypothesis about different roles of two- and one-joint muscles in controlling an external force does not explain why particular, stereotyped patterns of muscle activation are chosen by skilled subjects, since the same magnitude and direction of the external force (or the same combination of joint moments) may be provided by many different combinations of muscle activity. We hypothesized that the strategy of muscle activation observed by Jacobs and van Ingen Schenau (1992) corresponds to a strategy that allocates more force to muscles with a long moment arm, since a muscle length change is proportional to the muscle moment arm. In this study we tested our hypothesis.

PROCEDURES

The motor task investigated in this study corresponded exactly to the task studied by Jacobs and van Ingen Schenau, 1992: sitting in three limb positions to exert an external force on the ground by pushing in five different directions from -60 to -120° (Fig. 1) with two different force magnitudes -- 300 and 600 N. We assumed that the point of application of the external force coincided with the projection of the fifth metatarsophalangeal joint on the sagittal plane. In addition, we investigated exerting the external force of 300 and 600 N in five pulling directions from 60 to 120° (Fig. 1). The movement of the limb during pulling was prevented by an imaginary strap over the fifth metatarsophalangeal joint.

The resultant joint moments produced during exerting the external force in different directions were computed using a standard inverse dynamics analysis and a two-dimensional model of the leg consisting of four rigid-body segments (foot, shank, thigh, and pelvis) interconnected by three frictionless hinge joints (ankle (*a*), knee (*k*), and hip (*h*); Fig. 1). The rotation axis of the hip joint was assumed to be fixed. The length, mass, and center of mass location of each segment of the model were estimated from the total body length and mass of the subjects of Jacobs and van Ingen Schenau (1992) using the regression equations by Zatsiorsky et al., 1990. Moments that tended to extend the hip, knee, and ankle were defined as positive (Jacobs and van Ingen Schenau, 1992).

It was assumed that the resultant joint moments were produced by nine major two- and one-joint muscles of the lower limb. The equations relating the muscle length change and moment arm to joint angles were calculated using data from the literature. Virtual muscle length changes caused by a virtual displacement (10 mm) of the ankle from its original position in the directions of the external force (Jacobs and van Ingen Schenau, 1992) were calculated by determining the corresponding virtual changes in hip and knee joint angles and then computing the muscle length changes as the aforementioned functions of the joint angles.

Muscle forces producing the external force in different directions were calculated by solving numerically the following optimization problem:

minimize an objective function

$$F = f(F_1, F_2, \ldots, F_9), \quad (1)$$

subject to the equality constraints

$$M_j - \Sigma d_{ij} F_i = 0; \quad j=1, 2, 3; \quad i=1, 2, \ldots, 9 \quad (2)$$

and the inequality constraints

$$F_i \geq 0; \quad i=1, 2, \ldots, 9, \quad (3)$$

where F_i is the unknown force of the i-th muscle; M_j is the resultant moment at the j-th joint; d_{ij} is the moment arm of the i-th muscle relative to the j-th joint. Moments M_j and moment arms d_{ij} were calculated as described above. Three optimization criteria were examined: minimize the sum of muscle forces cubed, minimize the sum of the muscle stresses cubed (Crowninshield and Brand, 1981), and minimize the maximum of fatigue of the muscles (Dul et al., 1984). The first criterion allocates relatively more force to muscles with a long moment arm; the second criterion predicts more force in muscles with a long moment arm and a large physiological cross-sectional area; and the third criterion allocates more force to muscles with a long moment arm, large maximum force (or physiological cross-sectional area), and a high percentage of slow-twitch fibers. The percentage of slow-twitch fibers in the

studied muscles and their physiological cross-sectional area were estimated from the literature. The optimization problem (1) - (3) was solved using a sequential quadratic programming algorithm (Optimization ToolBox of MATLAB; The MathWorks Inc.) on a IBM PC computer.

RESULTS AND DISCUSSION

Of three examined optimization criteria, the criterion that minimizes the sum of muscle stresses cubed predicted relationships between muscle forces, joint moments, and muscle virtual length changes that were very similar to the corresponding EMG-moment-length relationships reported by Jacobs and van Ingen Schenau (their Figs 3, 4, and 5). In particular, a linear relationship between the difference in force of rectus femoris (RF) and long head of biceps femoris (BFL) and the difference in moment at the knee and hip was predicted (Fig. 2). Also, the increased force of BFS was predicted at the virtual muscle elongation. The latter result corresponds to the finding of Jacobs and van Ingen Schenau (1992), but contradicts their hypothesis that the main role of one-joint muscles in leg extensions is the generation of mechanical energy.

The features of the strategy of muscle co-ordination predicted in this study for the control of an external force in static leg extensions were also experimentally recorded in dynamic tasks. For example, straight line relationships between the EMG differences and the moment (M) differences -- (EMG_{RF} - EMG_{BFL}) vs (M_k - M_h) and EMG_{GA} vs (M_a - M_k), where subscripts *a*, *k*, *h* and *GA* denote the ankle, knee, hip, and gastrocnemius, respectively -- were found in lifting tasks (Toussaint et al., 1992; see also the corresponding force vs moment relationship found in this study, Fig. 2). The dependence of EMG magnitude of the two-functional muscles on moments about both degrees of freedom they serve was also reported for movements performed by the arm (Sergio and Ostry, 1994): muscle activity was substantially greater when muscles acted as agonists about both degrees of freedom they serve than when they had the antagonistic action about one or both degrees of freedom. Similar results were predicted in this study (Fig. 3).

The strategy of muscle co-ordination predicted in this study is also characterized by co-activation of certain one- and two-joint muscles crossing the joints from opposite sides: vastii (VA) and BFL (at flexion and extension knee moments, and extension hip moments) and GA and VA, and RF and gluteus maximus (GLM) (at extension ankle, knee, and hip moments). Similar patterns of muscle activity were observed in walking and running (Nilsson et al., 1985), jumping (Pandy and Zajac, 1991), and cycling (van Ingen Schenau et al., 1992).

The reciprocal activation of BFL and RF in walking, running, and cycling was reported in the studies cited above for the phases where the knee and hip moments do not tend to extend the two joints simultaneously. These facts correspond to the results of this study (Fig. 3). During the simultaneous production of extension moments at the knee and hip, co-activation of RF and BFL was reported in the literature and also predicted in this study (Fig. 3).

It was hypothesized (Jacobs and van Ingen Schenau, 1992; van Ingen Schenau et al., 1992) that one-joint muscles do not participate much in the control of the external force, and are activated when they are in a position to shorten and can contribute to the generation of mechanical energy. The predicted force production by BFS and iliacus (during pushing) and VA (during pulling) when they were in a position to elongate may suggest that one-joint muscles produce force when they can contribute to the joint moment irrespective of their virtual muscle length change. A strong correlation between the difference in force of VA and GLM and the difference in moment at the knee and hip (or direction of the external force) predicted in this study (Fig. 4) suggests that one-joint muscles may play an important part in the control of the direction of the external force. A similar relationship between the difference in EMG of VA and GLM and the difference in moment at the knee and hip can also be derived from Fig. 3 in Jacobs and van Ingen Schenau (1992).

REFERENCES

Crowninshield, R. D., Brand, R. A. *J. Biomech.*, 14, 793-801, 1981.
Dul, J. et al. *J. Biomech.*, 17, 675-684, 1984.
Jacobs, R., van Ingen Schenau, G.J. *J.Physiol.*, 457, 611-626, 1992.
Nilsson, J. et al. *Acta Physiol. Scand.*, 123, 457-475, 1985.
Pandy, M. G., Zajac, F. E. *J. Biomech.*, 24, 1-10, 1991.
Sergio, L. E., Ostry, D. J. *Exp. Brain Res.*, 97, 551-555, 1994.
Toussaint, H. M. et al. *J. Biomech.*, 25, 1279-1289, 1992.
van Ingen Schenau, G. J. et al. *Neuroscience*, 46, 197-207, 1992.
Zatsiorsky, V. M. et al. In *Contemporary Problems of Biomechanics* (pp. 272-291). Moscow: Mir Publishers, 1990.

ACKNOWLEDGMENTS

This study was supported by grant NSF IBN-9311398.

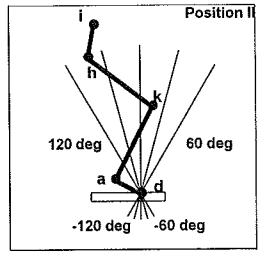

Figure 1: Leg position II during exerting external forces

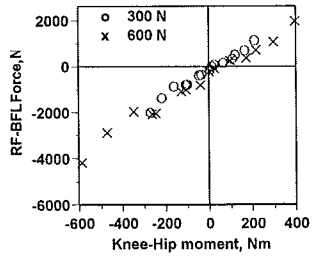

Figure 2: Difference in force of RF and BFL as a function of difference in moment at knee and hip during the pushing task

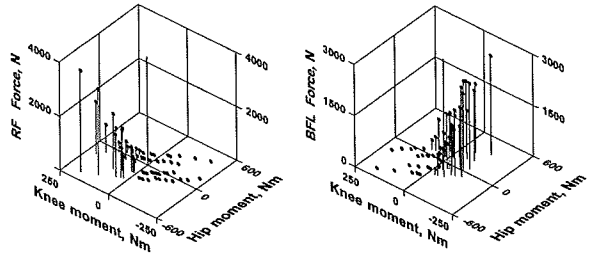

Figure 3: Forces of RF and BFL as a function of knee and hip moments during pushing and pulling tasks. Positive moments tend to extend the knee and hip.

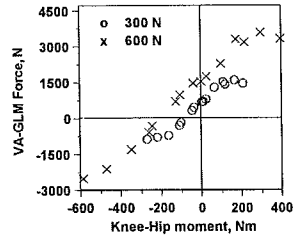

Figure 4: Difference in force of VA and GLM as a function of difference in moment at the knee and hip during pushing

A QUANTITATIVE TEST OF MUSCLE SPINDLE FUNCTION IN DIABETIC NEUROPATHY

Robert W. M. van Deursen, Maria Matilde Sanchez[1], Jan S. Ulbrecht, and Peter R. Cavanagh
Center for Locomotion Studies, Department of Kinesiology and
[1]Statistical Consulting Center, Penn State University, University Park, PA 16802

INTRODUCTION

Diabetic neuropathy is a very common complication of diabetes mellitus and involves progressive loss of peripheral nerve fibers secondary to prolonged hyperglycemia. Loss of plantar cutaneous sensation has been related to impaired postural control that is observed in diabetic neuropathy (Simoneau et al., 1994). Additionally, the muscle receptors, in particular the muscle spindles, play an important role in postural control. For example, muscles around the ankle joint play a critical role in the maintenance of balance (Pyykkö et. al., 1989). However, there is presently no quantitative test of muscle spindle function available in the literature. In this study, such a test was developed using muscle vibration to provide potentially confusing signals to intact muscle spindles (Gilhodes et al., 1986). Muscle vibration at a frequency of 80 Hz and with a small (0.5 mm) amplitude is known to specifically stimulate the muscle spindle primary endings. The effect of vibration is that a bias is introduced into the muscle spindle output, provided subjects are unable to see the area that is vibrated. The vibrated muscle is perceived to be longer than it actually is, leading to a perception of motion in excess of the actual movement (Sittig et al., 1987). The effect of muscle vibration only occurs when the muscle spindles and their nerve supplies are intact. Therefore, the illusory effects of muscle vibration would be reduced in individuals suffering damage to muscle spindles secondary to diabetic neuropathy.
We hypothesized that the adverse effects of vibration would be inversely related to the degree of nerve damage in diabetic neuropathy.

PROCEDURES

A total of 40 subjects, 10 young and healthy, 15 with diabetic neuropathy, and 15 age matched non-diabetic controls performed an ankle movement matching task with and without muscle vibration. The feet were placed in clamping devices which allowed actuator controlled movement of the right ankle (the "driven" side) and "free" movement of the left ankle (the "tracking" side) without stimulation of the plantar cutaneous mechanoreceptors. Ankle movement was measured by Penny & Giles goniometers attached to both ankles. To ensure muscle relaxation, electromyographic signals were measured in the lower leg on the driven side.
In each trial, subjects were instructed to continuously match the position of the tracking ankle to that of the driven ankle while it was moved through 3 cycles of dorsiflexion and plantar flexion at a velocity of 5°/s over a range of ± 25° (30 seconds total). The following conditions were presented in three (young, healthy) or four (matched groups) trials per condition:

1. Vibration: an inertial vibrator was attached to the Achilles tendon and to the Anterior Tibial tendon of the driven leg. A frequency of 80 Hz was used to add a potential bias signal to intact muscle spindles.
2. No vibration.

Additionally, seven of the neuropathic subjects and their matched control subjects returned on a subsequent day to repeat the procedure to allow the reliability of this test to be investigated.
The goniometer signals from the two ankles were analyzed for the time period that the driven ankle was moving. Gain was calculated as the quotient of the movement amplitude of the tracking over the driven side. The amplitude of the ankle movements

was expressed by the root mean square of the signals. Gain was 1 if both ankles were moved with exactly the same amplitude and was less than 1 if the tracking ankle was moved with a smaller amplitude.
The results of the young, healthy subjects were analyzed with a one-factor ANOVA to test the effect of muscle vibration.
A two-factor ANOVA was performed on the results of the neuropathic subjects and the matched controls to test the interaction between group and vibration.
The Intraclass Correlation for repetitions within days and between days was calculated as a measure of reliability.

RESULTS AND DISCUSSION

The one-factor ANOVA demonstrated that muscle vibration had a highly significant effect on the gain for the young, healthy subjects ($p<0.001$).
In the two-factor ANOVA the interaction between group and vibration was highly significant ($p<0.001$), indicating that the control subjects responded to a greater degree in the presence of vibration than the subjects with diabetic neuropathy.
The reliability of the test measured by the Intraclass Correlation was approximately 0.9 both within and between days.

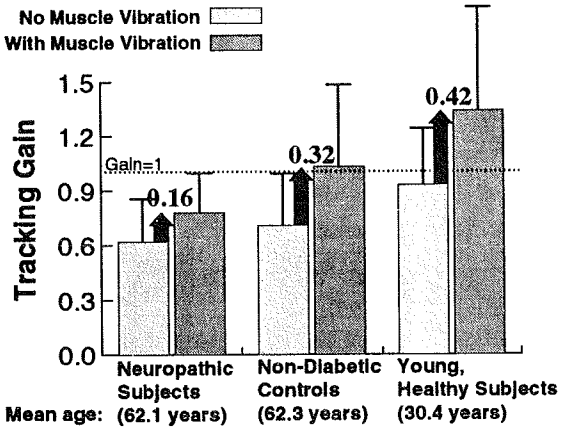

Figure 1: Mean gain of the tracking movement with and without muscle vibration for the neuropathic and control groups and the young, healthy group. The black arrows indicate the increase in gain (Δ gain) as a result of muscle vibration for each group.

The mean gains for the three groups with and without muscle vibration are shown in Figure 1. The young subjects (average age: 30.4) tracked the movement very well in the absence of vibration (average gain = 0.93). Muscle vibration caused a dramatic and significant increase in their movement amplitude (Δ gain: 0.42). The older control subjects (average age: 62.3) had some difficulty tracking the movement even without vibration (average gain = 0.71). However, muscle vibration caused a substantial increase in their movement amplitude as it had done in the young subjects (Δ gain: 0.32). The neuropathic subjects (average age: 62.1) had the most difficulty tracking the ankle movement in the absence of vibration (average gain = 0.62). More importantly, muscle vibration had much less effect on their performance (Δ gain: 0.16). The reduced effect of vibration indicates that diabetic neuropathy results in damage to the muscle spindles.
We conclude that: a) the change in tracking performance when vibration is added during an ankle movement matching task provides a test of muscle spindle function, and b) Diabetic neuropathy degrades muscle sensory function, presumably through the loss of either afferent or gamma efferent nerves to muscle spindles in the lower leg. This may contribute to the impaired balance and unsteadiness of gait that has been observed in diabetic neuropathy.

REFERENCES

Gilhodes, J. C. et al., *Exp. Brain Research*, 61: 395-402, 1986.
Pyykkö, I. et al., *Acta Otolaryngologia*, 468: 175-180, 1989.
Simoneau, G. G. et al. *Diabetes Care*, 17: 1411-1421, 1994.
Sittig, A. C. et al. *Exp. Brain Research*, 67: 35-40, 1987.

ACKNOWLEDGMENTS

This study was supported by NIH Grant 1R01 AG09345.
The authors wish to thank Mary B. Becker, David R. Lemmon, and Doug J. Tubbs for their contributions.

BIODYNAMICS OF HIP FRACTURES IN ELDERLY FEMALES

L. Cabell*, R. Shapiro*, D. Pienkowski**, R. Stine*

*Biodynamics Laboratory, University of Kentucky, Lexington, KY 40506-0070
**Division of Orthopaedic Surgery, University of Kentucky, Lexington, KY 40536-0284

INTRODUCTION

Falling is a common method of fracturing the hip, however, biomechanical and bone material studies have been unable to completely explain the mechanism of hip fracture and its relationship to falling in elderly females (Cummings, et al, 1985). It may be theorized that age related biodynamic changes of the lower extremity causing muscle generated overloading of the proximal femur could predispose the hip to fracture as a result of a single event. This study investigated the differences in joint angular displacement, moment, powers and muscle activity as a function of subjects' age. Age related differences may suggest the factors contributing significantly to hip fracture. Our preliminary data showed statistically significant differences in some of the biodynamic variables and also demonstrated some other interesting trends between the young and elderly women.

REVIEW AND THEORY

America's 250,000 hip fractures in post-menopausal women highly correlates to 50,000 deaths and cost approximately $7 billion each year (Phillips et al., 1988). Hayes et al. (1993) claimed that the mechanics of the fall rather than osteoporosis may well dominate the occurrence of the hip fractures. Other studies suggested that abnormal muscle coordination, or other internally generated mechanical forces, can overload the osteoporotic femur and cause fracture from falling (Klyver et al., 1995) or prior to falling (Yang et al, 1995). Repetitive excessive loading due to abnormal muscle activation patterns can, over a period of time, predispose the proximal femur to a spontaneous or low energy fracture from cumulative unrepaired fatigue damage (Cummings et al., 1985). In a review of studies of elderly gait, Winter (1991) reported the elderly have reduced mechanical power absorption at the knee and less hamstrings activity than a group of younger subjects. However, he did not characterize his subjects by gender.

The purpose of this study was to determine whether biomechanical and neuromuscular changes, associated with aging can change lower extremity loading patterns in a manner which predisposes elderly females to spontaneous, low energy hip fracture.

PROCEDURES

Six healthy female subjects volunteered to participate in this investigation and were divided into two groups:
Young (age 23.7 ± 0.6 yr., height 1.75 ± 0.08 m, mass 58.2 ± 7.3 kg, n = 3).
Elderly (age 66.4 ± 8.2 yr., height 1.57 ± 0.04 m, mass 51.8 ± 4.7 kg, n = 3).
Each subject was instrumented with Ag/Ag-Cl surface electrodes on the right side only. Muscles instrumented were: Gluteus medius, Adductor longus, Tensor fascia latae, Sartorius, Rectus femoris, Vastus lateralis, Lateral hamstrings, and Medial hamstrings. Data from EMG, synchronized with motion and force platform data provided information regarding muscle activation patterns for 3 sec. Retroreflective markers were placed on selected anatomical sites as described in the Simplified Helen Hayes marker set (Motion Analysis, Inc.) which enabled 3-D reconstruction of the lower extremity and pelvis from video data. Video data were collected from five video cameras at a sampling frequency of 60 Hz. After 3-D digitization, the data were low-pass filtered (6 Hz, Butterworth). Each instrumented subject was asked to walk at a self-selected pace over a piezoelectric force platform (Kistler Instrument, Inc.) while the ground reaction forces and EMG were collected at a nominal rate of 1000 Hz. The EMG signals were filtered with a high-pass filter at 40 Hz. A minimum of six trials was collected for each subject.

Kinematic and kinetic variables including joint moments and powers were calculated with the OrthoTrak II (Motion Analysis, Inc., Santa Rosa, CA) software package.

A three factorial repeated measures ANOVA was performed on the SAS statistical package to determine the statistical significance at 0.05 alpha level.

RESULTS

The results showed the statistically significant differences($p<.05$) between the two groups for the hip angle in all three planes at heel strike (HS), midstance (MS) and toe off (TO). The joint moment profiles were consistent for both groups during the stance phase, and were not statistically significant ($p>.05$) for the flexion/extension, abduction/adduction, and internal/external rotations (see Figure 1, 2, 3).

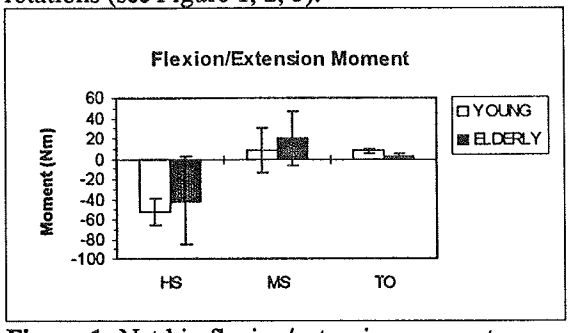

Figure 1: Net hip flexion/extension moments (using clinical angles, extension is negative)

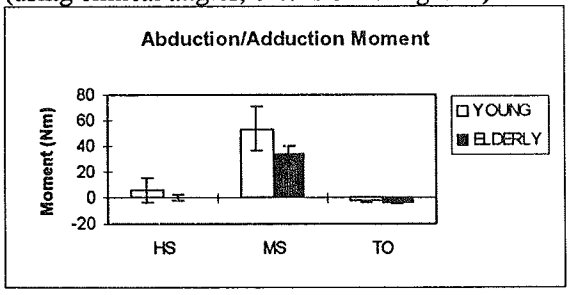

Figure 2: Net hip abduction/adduction moments (using clinical angles, abduction is positive)

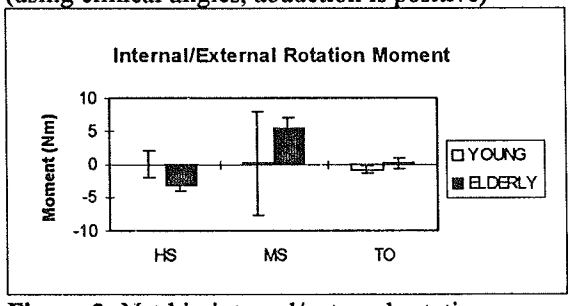

Figure 3: Net hip internal/external rotation moments (external rotation is negative)

The joint mechanical powers (generated and absorbed) did not present the significant statistical difference ($p>.05$) between the groups. The EMG profiles demonstrated the higher activity level in Sartorius at HS and Medial hamstrings at TO in the older group while the Adductor longus showed grater activity at TO in the younger group.

DISCUSSION

As expected, the results demonstrated decrease range of motion in the hip region in the elderly, mainly in flexion/extension of the joint. As seen in Figure 1. the hip extensor moments were dominant during the first half of the stance phase which generated the hip power to control the upper body, and the hip flexor moments were dominant during the second phase. These findings were similar to Winter's report (1991). The amplitude of the hip abductor moment was slightly larger in the young population (Fig.2) supported by larger muscle hip power absorption during the HS and better control during the MS. The larger external rotation moment observed in the elderly group at HS (Fig.3) may be related to the increased activity observed in the Sartorius. The elderly subjects also appeared to produce a much greater internal rotation moment at MS. This difference was masked by the small subject size and large variability in the young group. However, these differences suggest an altered hip loading strategy in the elderly subjects. As a result of the small subject population and the high activity level of the subjects it was not surprising to find very little difference in the biodynamic variables between the two age groups. From these preliminary results some potential differences supporting the altered loading hypothesis appeared to exist. Further investigation with a larger population divided by age and level of daily activity is needed for a larger population and the comparison between the active and sedentary subgroups is recommended.

REFERENCES

Cummings, SR et al., *Epidemiology Reviews*, 7, 178-208, 1985.

Hayes, WC et al. *Calcif Tiss Intl*, 52, 192-198, 1993.

Klyver, H et al., *Clinical Biomechanics*, 10, 268-270, 1995.

Phillips, S et al., *Bone*, 9, 271-279, 1988.

Motion Analysis, Inc. Manual. Santa Rosa, CA, 1990.

Winter, D., Biomechanics and Motor Control of Human Gait, University of Waterloo Press, 1991.

Yang, KH et al., *Transactions of the Orthopaedic Research Society*, 41, 238-239, 1995

THE RELATIONSHIP BETWEEN SWAY AMPLITUDE AND SWAY FREQUENCY AND ITS EFFECT ON POSTURAL STABILITY

J.E. Kasprisin and M.D. Grabiner

Department of Biomedical Engineering
The Cleveland Clinic Foundation, Cleveland, OH 44195

INTRODUCTION

Performance during postural stability tests is most often measured by the level of sway, such that larger values are indicative of greater instability. Visual feedback is most often manipulated using "eyes-open" and "eyes-closed" conditions and has been shown to be effective in decreasing postural sway (Ring et al. 1989).

Although it seems intuitive that reduced postural sway is affected by corrective responses (sway frequency), the relationship between sway amplitude and sway frequency has not been investigated.

In the present study visual feedback of center of pressure motion was provided during a unilateral postural stability test to examine the relationship between postural sway amplitude and sway frequency.

Visual feedback was shown to be associated with decreased sway amplitude and increased sway frequency in both anterior-posterior and medial-lateral directions. Results indicated a negative relationship between amplitude and frequency such that as frequency increases, sway amplitude decreases.

REVIEW AND THEORY

It is well known that vision plays a large role in maintaining postural stability. Processing the information provided by vision is also dependent upon vestibular and somatosensory cues. Enhanced visual feedback, such as with center of pressure motion, provides information regarding position and velocity from which postural corrections can be made.

The purpose of this study was to investigate a potential mechanism through which feedback improves postural sway.

It was hypothesized that the rate at which these corrections are made would affect sway amplitude, insofar as a decrease in sway amplitude is associated with an increased rate of correction. Visual feedback of center of pressure motion was expected to increase this rate.

PROCEDURES

Twenty subjects, ten males (28.5$\pm$4.88)yrs) and ten females (24.8$\pm$3.36)yrs) without ankle instability or dysfunction participated in this study.

A Balance System (Chattecx Corp., Chattanooga, TN) was used to investigate unilateral, static postural stability. The right leg was used for all of the subjects. Each subject stood erect with their arms relaxed at their sides on an adjustable foot plate made up of four load cells that measured the vertical reaction forces under the foot. Subjects wore low-top athletic shoes. Ten, fifteen second trials were collected in a no-feedback and a feedback condition. The feedback was provided by a computer monitor that displayed anterior-posterior and medial-lateral center of pressure motion. A rest period was given between trials and between conditions. The amplified signals were digitized synchronously at 68 Hz and stored for postprocessing.

Variables extracted for analysis included the sway amplitude (in cm) and sway frequency (median frequency of the power density spectrum in Hz) in both the anterior-posterior and medial-lateral and directions. Sway amplitude was calculated as the standard deviation of the instantaneous center of pressure positions about the mean value from the entire trial. Sway frequency represents the rate at which postural corrections were made.

A 2 x 2 (feedback by direction) repeated measures analysis of variance (ANOVA) was used to investigate the effect that feedback had on sway

amplitude and frequency in the anterior-posterior and medial-lateral directions.
Correlation analysis was performed for each subject using all ten trials to investigate the relationship between sway amplitude and sway frequency in both the anterior-posterior and medial-lateral directions.

RESULTS

The ANOVA revealed an significant direction (anterior-posterior vs. medial-lateral) by feedback (no-feedback vs. feedback) interaction ($p = 0.001$) which confirmed that expected influence of feedback on postural sway amplitude (decrease) and frequency (increase) (Table 1). Post hoc analysis revealed that feedback significantly decreased anterior-posterior sway amplitude ($p < 0.001$) but did not affect medial-lateral sway amplitude ($p = 0.759$). Significant increases in sway frequency were found in both the anterior-posterior ($p = 0.001$) and medial-lateral ($p = 0.030$) directions.

	AP	ML
SA(NF)	6.00(1.02)	4.08(.82)
SA(F)	5.11(1.17)	4.04(.87)
SF(NF)	.24(.10)	.42(.87)
SF(F)	.36(.15)	.47(.13)

Table 1: Mean and standard deviation for sway amplitude (SA) and sway frequency (SF) in the no-feedback (NF) and feedback (F) conditions in the anterior-posterior (AP) and medial-lateral (ML) directions.

The expected negative correlations between sway amplitude and sway frequency were found for both directions and feedback conditions but were only of moderate magnitude and not influenced by feedback. Paired t-tests revealed the difference between the feedback conditions was not significantly different from zero (Table 2).

	AP	ML
NF	-.57	-.43
F	-51	-.44

Table 2: Correlation matrix for the between sway amplitude and sway frequency in the no-feedback (NF) and feedback (F) conditions in the anterior-posterior (AP) and medial-lateral (ML) directions.

DISCUSSION

Although the correlation levels are moderate, they do suggest a functional relationship between increased sway frequency and reduced sway amplitude. The failure of the correlation to increase with feedback may reflect variability in the subject correlations. Subject correlations ranged from (.16 to -.91) and (.11 to -.94) in the anterior-posterior and medial-lateral directions respectively. This suggests that the rate of corrections may not positively influence sway amplitude unless they are appropriately performed in time and space. The median frequency does not reflect the spatial and temporal characteristics of the corrections.

In summary, the present study confirmed that decreased sway amplitude is in part, a function of the rate at which corrections are made.

REFERENCES

Ring C. et al. JAGS, 37, 745-749, 1989.

ACKNOWLEDGMENTS

This study was funded by the Aircast Corporation.

AGE-RELATED CHANGES IN THE ABILITY TO CHANGE DIRECTION DURING GAIT.

L. Gilchrist
Department of Physical Therapy and Exercise Science, S.U.N.Y. at Buffalo, Buffalo, NY 14214

INTRODUCTION

The focus of this study was on the ability of individuals to alter their gait path by shifting the plane of progression to one side. Two groups of women were studied to identify any age-related changes in the ability to perform this maneuver.

REVIEW AND THEORY

The ability to alter our intended direction of travel at relatively short notice is essential for full mobility in a complex environment. Stability, always an overriding concern in bipedal gait, is often placed at considerable risk when last-minute adjustments are made to the gait pattern. Such adjustments are required when obstacles suddenly appear (or are recognized). One option is to shift the plane of progression to one side and walk by the obstacle.

Patla and coworkers (1991) have studied the ability to turn the plane of progression by 30° or 60° in young adults. They found that such changes could not be made within one step and that considerable changes in the horizontal ground reaction forces occurred. They did not, however, test any older adults. Chen et al (1994) studied age-related changes in the ability to step over a virtual obstacle. They reported that older individuals were considerably less successful in making the step length adjustments required to avoid the obstacle at short notice. They did not, however, measure the ability to side-step, an alternative strategy for obstacle avoidance.

The purpose of this study was to identify age-related changes in the ability to incorporate a sideways shift of the plane of progression into a comfortable walking pattern. Of specific interest were: 1. Do elderly women accomplish such a shift in the same manner as do young women? 2. Do differences between the two groups seem to place the elderly at a greater risk for falling, either as the transition is made or in the steps immediately following?

METHODS

Sixteen young women (age=27 ± 6 yrs) and 16 older women (age=70 ± 3 yrs) were subjects for this study.

The given task was to walk down a 5 m walkway that was divided into three parallel lanes, delineated by brightly coloured tape on the floor. The subjects began each trial at one end of the center lane of the walkway, standing with both feet parallel. At a verbal cue from the investigator they began to walk down the center lane. On their third step a visual cue appeared which instructed the subject to move to the lane on the right, to move to the lane on the left, or to remain in the center lane. Subjects were told that in all cases they were to make any adjustments (i.e. change lanes) as quickly as possible, to continue walking forward to the end of the walkway, and to avoid stepping on any of the lines delineating the three lanes. A trial was complete when the subject reached the end of the walkway.

The three lanes were of identical width based on the feet-together stance width of each subject. The lane width was set as this stance width plus an additional 30%. Three footswitches were taped to each shoe and two infrared light beams were used to calculate the average velocity of the subject. Data collection began just before the subject's first heel strike and lasted for 5 s at a rate of 250 Hz. The appearance of the visual cue occurred 100 ms after the third heel contact.

The subjects performed 64 trials in total. Randomly spaced among these were 9 requiring a move to the right, and 9 requiring a move to the left. The visual cues consisted of the words "Right", "Left" or "Center" appearing in 4 cm high letters on a computer monitor. Trials were identified as either Ipsilateral, Contralateral or No Shift trials; e.g. if the signal appeared when the subject was on their right foot, an ipsilateral shift was to the right side.

A video camera placed at the end of the center lane of the walkway was used to record the subjects' footfalls. From this, the stepping strategies that the subjects used to shift their plane of progression (i.e. to change lanes), as well as the number of times they made an error (stepped on a line), could be discerned.

RESULTS

No subject was able to accomplish either shift within the same walking step as the visual cue. Most accomplished the ipsilateral shift within the next step; for the contralateral shift a 2-step strategy was most common (Table 1).

Table 1: Stepping Strategies

Extra Steps	Ipsilateral Trials		Contralateral Trials	
	Young	Older	Young	Older
1	**84.9**	**51.6**	31.2	1.5
2	11.5	27.8	**68.8**	**82.6**
3	3.6	19.0	0	8.3
4	0	1.6	0	6.1

Percentage of trials in which extra steps were used to move from the center lane to a side lane.

The older women walked with a slower average velocity than did the younger women, using longer stance times and shorter swing times (Table 2).

Table 2: Average Velocities (m/s)

	Ipsilateral Trials	No-Shift Trials	Contralateral Trials
older	1.17±.18*	1.22± .19	1.18 ± .18*
young	1.31±.12*	1.36± .13	1.36 ± .13

* = significantly different from the comparable no-shift trials. Age differences were significant for all conditions.

Analyses of the errors indicate that both groups were more likely to make errors on steps 5 and 6. The older women were more likely than were the young women to make an error on step 6.

To examine the temporal adjustments made to accommodate a shift in the plane of progression, only those trials in which the predominant strategies were used, were considered. For the 1-step ipsilateral strategy 183 trials (69%) were included. For the 2-step contralateral strategy 204 trials (76%) were included. The relative timing changes were similar for both groups (Figure 1). The exception was in the 2-step contralateral strategy: the young women spent less time on the second extra step (step 5) than did the older group.

DISCUSSION

The change in gait path studied here was not large; it involved simply taking a step to one side while continuing forward progression, a maneuver commonly used to avoid an obstacle. Although the direction of the shift was mandated, subjects were given the freedom to choose what stepping pattern and temporal adjustments they would use to accomplish the task.

The findings were consistent with those of Patla et al (1991) in that, for all subjects, no discernible alteration in the movement pattern was possible within the same step in which the visual cue appeared. Despite their slower velocity, the older women tended to choose the same stepping patterns as the young women although they were less consistent in their choice. More specifically, they were less likely to choose a rapid strategy. In a situation where such a change is required to avoid an obstacle, taking additional steps may increase the risk of contacting the obstacle. Chen et al (1994) demonstrated the reduced capacity of older individuals to step over an obstacle, particularly when there is little time available to make adjustments. The current study suggests that their result was not specific to alterations within the plane of progression (step length adjustments), but can be extended to include side-to-side alterations.

Although both groups had difficulty placing the foot accurately for step 5, the older group had difficulty on the subsequent step as well. This has implications for those situations where not only does an obstacle appear, but the options for alternate foot placement are limited. (Consider trying to avoid a large path of ice or pool of water in the center of a relatively narrow path.) Even if an older individual were able to respond rapidly enough to avoid running directly into the obstacle, their decreased ability to precisely place subsequent footfalls may also increase their risk of falling.

REFERENCES

Chen, H.-C..J Gerontol: Med Sci **49**(5): M227-M233, 1994.

Patla, A. E.. J Exp Psych **17**(3): 603-634, 1991.

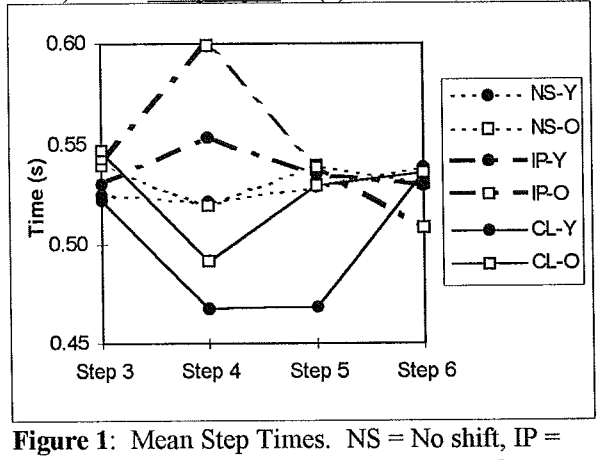

Figure 1: Mean Step Times. NS = No shift, IP = Ipsilateral, CL = Contralateral, Y = young, O = older. The visual cue appeared on step 3.

ANALYSIS OF MOVEMENT STRATEGIES DURING UNEXPECTED FALLS

S.N. Robinovitch, E. Hsiao, M. Kearns, and V. Frenk
Biomechanics Laboratory, Department of Orthopaedic Surgery, San Francisco General Hospital and University of California, San Francisco, San Francisco, CA 94110

INTRODUCTION

Falls rank among the chief causes of accidental injury in both young and elderly populations, the most important of which are hip and wrist fractures [1]. However, the vast majority of falls cause no injury, despite the fact that the energy available in a typical fall from standing height far exceeds that required to fracture the hip or wrist [3, 4]. This suggests that specific motor control strategies exist to ensure "safe landing" during a fall. However, no previous study has examined human body movements during unexpected falls, and thus little is known regarding how injury is avoided in this potentially disastrous event. To address this issue, we measured the 3-dimensional movements of various body segments as young, healthy subjects underwent unexpected falls from standing height onto a gymnasium mat. We focused particularly on determining the temporal sequence in contact to the upper extremities and pelvis, and the effect on pelvic impact velocity of initial contact to the upper extremity.

REVIEW AND THEORY

Despite the fact that over 90 percent of hip and wrist fractures are caused by falls, few studies exist on the biomechanics of falling. Such studies have been limited to examining body movements during parachutist landings [2] and self-launched falls in young athletes [5]. Since these studies involved voluntary rather than unexpected falls, it is likely that observed motions were governed by pre-planned strategies for executing safe landings. Questions therefore arise regarding how well these motions represent actual falls from standing, which most often result from sudden and unexpected slips, trips, or loss-of-balance, and allow little time for pre-planning of a landing strategy.

Of central interest in the present study was assessing whether, rather than being random and unpredictable, the motions of the body segments during an unexpected fall involve a common sequence of coordinated movements which are employed in an attempt to land safely. In particular, based on the predominance of upper extremity fractures and the scarcity of hip fractures in the young, we hypothesized that young fallers (1) commonly "break" the fall by impacting the ground with an outstretched hand before contact occurs to the pelvis or trunk, and (2) avoid impact to the hip.

PROCEDURES

Three healthy, young volunteers participated in the study (two males and one female; aged 23, 28, and 22 yrs; body weight 881, 739, and 525 N; body height 1.73, 1.77, and 1.52 m). During the experiments, subjects stood on a large gymnasium mattress, which suddenly translated by means of a spring-actuated platform (Figure 1), initiating an unexpected "slip". Throughout testing sessions, we randomly varied both the direction of the perturbation (achieved by having the subject stand forwards, backwards, or sideways with respect to the perturbation direction), and the strength of the perturbation applied to the platform (for each direction, two trials were conducted at horizontal accelerations of 4, 6, 8, and 9 m/s^2). In order to evoke natural protective responses, the only instructions to the subject were that the platform might move, and that they should "try to prevent themselves from falling".

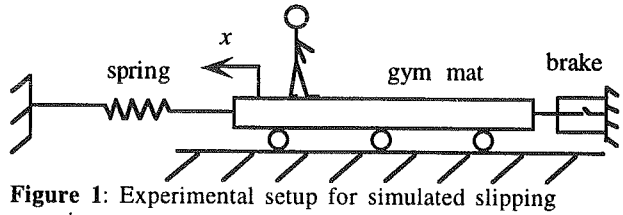

Figure 1: Experimental setup for simulated slipping experiments.

In all trials, a 6-camera, 60 Hertz motion analysis system (MacReflex, Qualisys Inc., Glastonbury, CT) was used to acquire the 3-dimensional positions of 20 soft foam, reflective markers located at the foot, ankle, shin, knee, thigh, anterior superior iliac spine (ASIS), sacrum, shoulder, elbow, wrist, and head. Custom routines written in MATLAB (The MathWorks, Natick, MA) were used to filter (recursive Butterworth filter, 10 Hz cut-off frequency) and differentiate position data.

In 73 percent of trials, subjects were able to regain balance through one or more steps. In four trials, subjects contacted the ground with one or both hands, but avoided impact to the trunk and knees. Fifteen trials resulted in "falls", defined as contact to a body part other than the feet and hands (distribution between subjects: 4, 3, and 8; direction of falls: 12 posterior, 3 lateral, 0 anterior), and were the subject of further analysis. Through close examination of stick figure animations and position-time graphs, we found that a reasonable criteria for the occurrence of ground contact to a given body part was passage of the corresponding body marker below a horizontal plane located 140 mm above the gym mattress. Contact velocities were then taken to equal the vertical velocity of the given marker at this instant.

RESULTS

In all falls, impact occurred to one or both wrists, consistently before impact to the ipsilateral elbow or shoulder. The average time for wrist impact after initiation of platform acceleration was 647±110 (s.d.) ms. In all falls, impact also occurred to at least one pelvic marker (right ASIS, left ASIS, or sacrum), at an average time of 732±166 ms. In all but one fall, pelvic impact occurred after impact to the wrist. However, the

average time of 732±166 ms. In all but one fall, pelvic impact occurred after impact to the wrist. However, the time difference between wrist and pelvic impacts was small, averaging 85±86 ms. In 47 percent of falls, the left or right ASIS was observed to impact before the sacrum, suggesting posteriolateral or laterally-directed impact towards the hip.

Wrist contact velocities were found to average 2.69±0.9 m/s, while pelvic contact velocities averaged 2.52±0.9 m/s. The time interval between wrist and pelvis contact was found to significantly affect pelvis contact velocity (Figure 2): as this time increased, the contact velocity of the pelvis decreased (r^2=0.54; $p<0.05$).

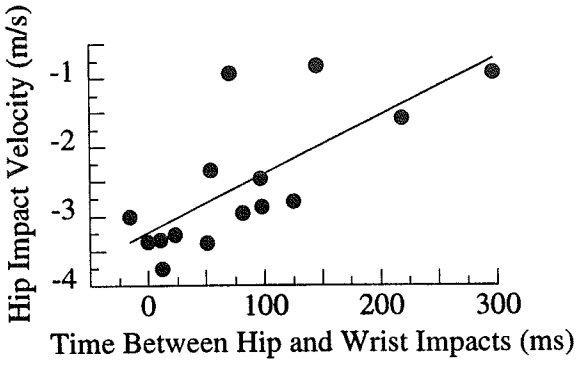

Figure 2: Hip impact velocity as a function of the time interval between contact to the wrist and pelvis. Positive x-axis values reflect the wrist impacting before the pelvis.

Trajectories observed from the various falls showed strong similarity, involving steady downward movement of the pelvis, and a considerably more complex pattern for upper extremity movement (Figure 3). This involved an initial upwards movement of the wrist immediately following application of the perturbation (perhaps reflecting a startle response), followed by a rapid downward movement, and ending with another upward movement just prior to impact.

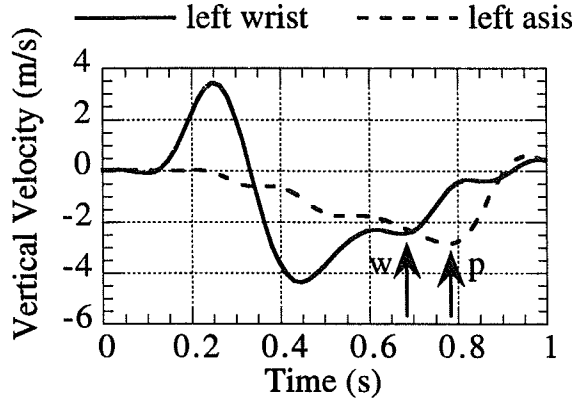

Figure 3: Variation in wrist and pelvic markers as functions of time after application of the perturbation to balance. w = time of wrist impact; p = time of pelvic impact.

DISCUSSION

In this study, we hypothesized that in the event of an unexpected fall, young, healthy individuals "break" their fall by contacting the ground with the upper extremity before the trunk or pelvis. Our experimental data suggest this to be true, since all but one fall involved impact to the wrist before the trunk or pelvis. We also hypothesized that young individuals avoid impact to the hip during a fall (thereby minimizing their risk for hip fracture). We found this to be untrue, based on the regular occurrence of impact to the pelvis, which was often oriented to predispose towards hip impact. It appears that rather than selecting for avoidance of hip impact, the motor control strategy governing falling seeks to reduce the likelihood of injury to any body part by: (1) distributing impact energy over several body regions through near-simultaneous impacts to the upper extremity, lower extremity, and pelvis; (2) imparting a relative upward motion to the distal upper extremity in the latter stages of the descent process, thereby reducing its kinetic energy at impact; and (3) reducing the velocity and kinetic energy of the pelvis at impact by ensuring the upper extremity contacts just prior to the pelvis.

This study appears to represent the first measures of movement strategies during unexpected falls. Limitations of the study include the possibility that subjects may have been less fearful of falling on a gymnasium mattress than on a hard surface. Furthermore, due to safety concerns, elderly subjects were not included. Whether elderly individuals exhibit similar falling patterns to those observed here is therefore unknown. However, it is interesting to consider our results in light of the fact that fall-related hip fractures are much more common in the elderly than the young, while upper extremity fractures are similar between the two populations. It may be that age-related changes in sensory and motor function cause deviations in falling behavior from those observed here, and that such deviations largely dictate hip fracture risk.

REFERENCES

(1) National Research Council. Injury in America, National Academic Press, 1985. (2) Henderson, J. M. et al. Military Med., 158: 810-816, 1993. (3) Lotz, J. C. et al. J, Bone Joint Surg., 72-A: 689-700, 1990. (4) Myers, E. R. et al. Calcif. Tissue Int., 52: 199-204, 1993. (5) van den Kroonenberg, A. et al. Trans. 39th ORS, Vol. 18, p. 24, 1993.

ACKNOWLEDGMENTS

This study was supported by a grant from the Academic Senate of the University of California, San Francisco.

THE PRESENCE OF THE BILATERAL DEFICIT IN ELDERLY DOES NOT SUPPORT SELECTIVE RESTRICTION OF MOTOR UNIT ACTIVATION

T.M. Owings and M.D. Grabiner

Department of Biomedical Engineering, The Cleveland Clinic Foundation, Cleveland, OH 44195

INTRODUCTION

The central nervous system seems to normally limit the neural drive to skeletal muscle during conditions in which bilateral, homologous muscle are intended to be maximally activated at the same time. This phenomenon has been referred to as the *bilateral deficit*. To date, the neural basis for the bilateral deficit has yet to be described. Although it is broadly accepted that the central nervous system imposes a restriction on the extent to which the motor unit pool may be activated, the question of whether there is a selective restriction of specific motor units or whether the entire motor pool is affected remains unanswered.

Currently, there has been only one published report of the bilateral deficit in the elderly. Häkkinen et al. (1996) failed to demonstrate the presence of the bilateral deficit for an isometric knee extension task in middle-aged (44-57 years) and elderly (59-75 years) men and women. Since the normal aging process is generally associated with selective atrophy of high threshold motor units, these motor units would not contribute to force generation during unilateral or bilateral conditions, thus causing an absence of the bilateral deficit. Therefore, these results support the contention that an inability to fully activate high threshold motor units is the cause of the bilateral deficit.

Previous studies support the hypothesis that the limited activation of high threshold motor units is the cause of the bilateral deficit (Vandervoort et al., 1984), while other studies indicate it is caused by a restricted activation of the low threshold motor units (Secher et al., 1978). Unpublished observations from our laboratory tend to support the hypothesis that a restriction of the entire motor pool is the cause of the bilateral deficit. The present study was undertaken to further investigate the bilateral deficit in a sample of healthy elderly male and female subjects.

PROCEDURES

Thirty-five healthy elderly subjects (ages: 56-83 years) performed maximum voluntary contractions during isometric unilateral and bilateral knee extensions (group I: n=9; group II: n=26) on a customized KIN-COM isokinetic dynamometer (Chattanooga Corporation, Chattanooga, TN). The dynamometer allowed simultaneous measurements of knee extension force of each leg. A knee flexion angle of 45 degrees was used for group I. For group II the knee joint angle was positioned with the shank vertical to the floor (approximately 90 degrees of knee flexion).

Subjects performed three trials of maximum voluntary isometric knee extension at each of the three knee extension conditions (right leg only, left leg only, and both legs). The collection order for the conditions was randomized between subjects. Once the subject felt they had reached their maximal value, force data from the KIN-COM was collected for one second.

The digitized force data was smoothed using a recursive Butterworth filter (cut-off frequency = 10.0 Hz). The smoothed forces were converted to moments and averaged over the one second duration. The value for each condition was determined by averaging the three trials. The bilateral index was calculated as:
$[100 \times (\text{bilateral value/unilateral value})] - 100$
(Howard and Enoka, 1991), where the bilateral and unilateral values represented the knee extension moments for each leg. A negative

value indicated a bilateral deficit while a positive value indicated a bilateral facilitation.

Paired sample t-tests were used to compare the unilateral to the bilateral conditions. T-distribution comparisons were used to indicate if the bilateral index was different from zero. A probability level of 0.05 was used as the maximum acceptable value indication significant differences.

RESULTS

The results showed that a bilateral deficit was present in both groups of subjects (Table 1). The moment generated during the bilateral condition was significantly less than during the unilateral condition for both legs and both groups (group I: left leg ($p = 0.001$), right leg ($p=0.008$); group II: left leg ($p=0.005$), right leg ($p=0.04$)). Similarly, the bilateral index was significantly less than zero for the four comparisons ($p < 0.05$).

Table 1: The calculated bilateral index and the maximum voluntary moments of the right and left leg during unilateral and bilateral knee extensions. (A) Averaged data for Group I - knee angle 45 degrees. (B) Averaged data for Group II - knee angle 90 degrees.

(A) Group I	Bilateral Index	Unilateral Condition (Nm)	Bilateral Condition (Nm)
Left	-12.9 ± 5.3 *	82.3 ± 18.4 †	71.6 ± 15.8
Right	-11.1 ± 6.8 *	94.7 ± 24.8 †	83.0 ± 17.3

(B) Group II	Bilateral Index	Unilateral Condition (Nm)	Bilateral Condition (Nm)
Left	-8.9 ± 15.4 *	76.1 ± 29.9 †	68.3 ± 25.7
Right	-6.5 ± 13.7 *	85.0 ± 35.2 ‡	77.7 ± 29.0

* Statistically different than zero ($p < 0.05$)

† Statistically greater than corresponding bilateral condition ($p < 0.01$)

‡ Statistically greater than corresponding bilateral condition ($p < 0.05$)

DISCUSSION

This investigation confirmed the presence of a bilateral deficit in a group of elderly subjects, which is a direct contradiction of the data reported by Häkkinen et al. (1996). The observation of a bilateral deficit, combined with the reported age-related atrophy of high threshold motor units, tends to refute the contingency that the inability to fully activate high threshold motor units is the cause of the bilateral deficit. Furthermore, the degree of the bilateral deficit was comparable to that of young, healthy subjects (Owings, 1994). Based on these two observations, we conclude that the bilateral deficit is not caused by a restriction of the high threshold units. One possible explanation for the bilateral deficit which can account for similar observations across a wide age range is a central nervous system mechanism that reduces the maximum discharge rate of all motor units of a motor pool.

REFERENCES

HÄKKINEN, K. et al. *J. Gerontology*, 51A, B21-B29, 1996.

HOWARD, J.D. et al. *J. Appl. Physiol.*, 70, 306-316, 1991.

OWINGS, T.M. et al. *Conf. Proc. ASB at OSU*, 199, 1994.

SECHER, N.H. et al. *Acta Physiol. Scand.*, 103, 456-462, 1978.

VANDERVOORT, A.A. et al. *J. Appl. Physiol.*, 56, 46-51, 1984.

ACKNOWLEDGMENTS

This work was supported by the Chattanooga Corporation. The authors would like to acknowledge Thomas Lundin, Julee Kasprisin, and Julie Perry for their assistance with the data collection.

SLOW FINGER MOVEMENTS ARE LESS STEADY IN ELDERLY ADULTS

D. H. Laidlaw, M. Bilodeau and R. M. Enoka

Department of Biomedical Engineering
The Cleveland Clinic Foundation
Cleveland, OH 44195

INTRODUCTION

There is accumulating evidence that age-related changes in the human neuromuscular system decrease the ability to perform precise movements, especially those requiring dexterity of the hand. For example, when older adults lift an object with a pinch grip, the force is more variable than for young adults (Cole & Beck, 1994). Further, older adults have greater difficulty than younger adults maintaining a constant force during submaximal isometric contractions. This is evident by an increase in the normalized fluctuations about the target force (Galganski et al., 1993; Keen et al., 1994), especially at low force levels (2.5% and 5% of the maximal force; MVC). In healthy adults, slow finger movements are characterized by oscillations that are manifested as 8-10 Hz cycles in the acceleration-time record and are more pronounced during lengthening (eccentric) compared with shortening (concentric) contractions (Vallbo & Wessberg, 1993). The purpose of this study was to determine the effect of age on the ability of subjects to perform slow concentric and eccentric contractions.

PROCEDURES

Fourteen healthy subjects were assigned to one of two age groups, an elderly group (n = 9; average 73.1 yrs; range 67-84) and a young group (n = 5; average 26.6 yrs; range 25-28). All subjects were carefully screened for neuromuscular disorders. Each subject participated in a familiarization and four experimental sessions. This allowed for the averaging of many trials performed by each subject. The tasks performed by the subjects involved the index finger of the left were: (1) isometric abduction MVC; and (2) non-isometric constant-load contractions with loads of 2.5% and 5% MVC.

The isometric contractions were performed with the index finger abducted 5 deg. The non-isometric trials (3-5 with each load) were performed with the index finger moving through a 10-deg range of motion from the initial position (0 deg abducted). For the non-isometric trials, a weight (2.5%, 5% MVC) was attached to the subject's index finger at the proximal interphalangeal joint to provide a load in the adduction direction. The subjects raised and lowered the weight during 6 s of abduction and 6 s of adduction, respectively. A triangular movement template was displayed on an oscilloscope and the subjects were given several practice trials to become familiar with the timing and amplitude of the task. Index finger position was recorded with a low friction linear displacement transducer. The subjects were encouraged to match the desired finger-displacement template as closely as possible.

The smoothness of the movement was determined by measuring the variations about the average velocity. A least-squares regression was used to determine the average movement velocity. The slope of the regression line was subtracted from the data to remove the trend (slope) from the position data. The standard deviation (SD) about the mean was calculated from the detrended data for the entire abduction and adduction phases (~6 s each) and the middle 4 s of each phase.

RESULTS

Older subjects were unable to perform slow concentric and eccentric contractions as smoothly as younger subjects (Figure 1). For each comparison, the standard deviation of the position fluctuations was greater for the elderly subjects compared with

the young. The largest differences between groups were observed during the eccentric phase (2.5% - elderly = 0.66 deg, young = 0.31 deg, p = 0.001; 5% - elderly = 0.62 deg, young = 0.28 deg, p = 0.001). There were no differences between young and elderly subjects in the amplitude (peak position) or the slope (average velocity) of the movements in both phases and with either load. Data for the whole phases (Figure 2A) revealed that elderly subjects had equal difficulty during the concentric and eccentric phases, while the young subjects had greater difficulty with the concentric phase compared with the eccentric. For the middle 4 s of each phase (Figure 2B), the elderly subjects had more variability during the eccentric contraction while the young subjects had lower but similar variability during the two phases.

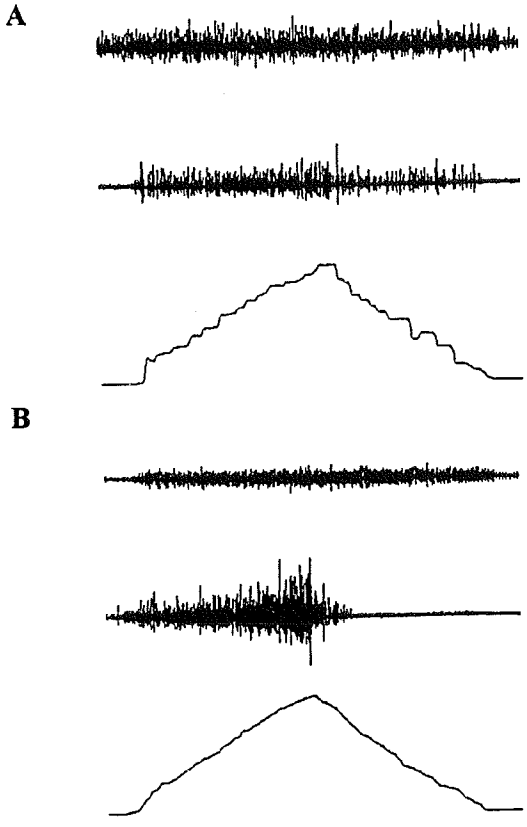

Figure 1. Position data from an elderly (A) and a young (B) subject performing the non-isometric constant-load task with a load of 5% MVC. The surface electromygraphic records are from first dorsal interosseous (FDI, middle trace) and adductor pollicis (AP, upper trace).

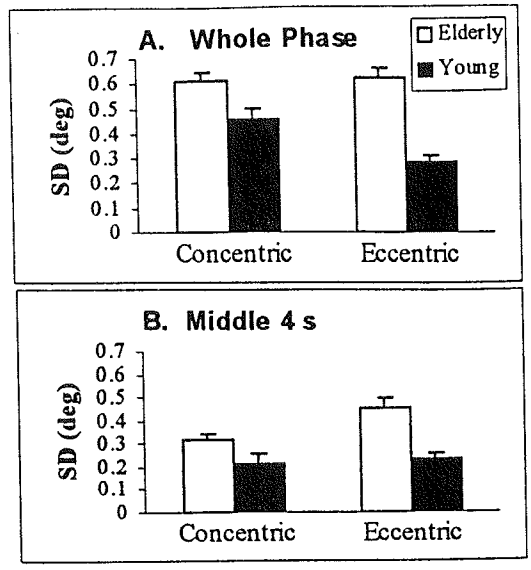

Figure 2. Effect of age on the ability to perform steady concentric and eccentric contractions with a load of 5% MVC. Position fluctuations during the whole (6 s) concentric and eccentric phases (A) and during the middle 4 s of each phase (B) are shown as the standard deviation (SD) in degrees.

DISCUSSION

The main finding of this study was that elderly subjects had greater difficulty than young subjects performing steady, slow non-isometric contractions. This was most obvious at the movement transitions, from rest to the concentric phase and from the concentric to the eccentric phase (Figure 1). When these end effects were removed, however, the elderly subjects still exhibited greater position fluctuations (Figure 2B). Furthermore, this effect was greater for the eccentric contractions. These results suggest that age has a more pronounced effect on the steadiness of slow movements than on the steadiness of submaximal isometric contractions.

REFERENCES

Cole KJ, Beck CL: *J Motor Behav* 26: 171-177, 1994.
Galganski ME et al.: *J Neurophysiol* 69: 2108-2115, 1993.
Keen DA et al.: *J Appl Physiol* 77: 2648-2658, 1994.
Vallbo ÅB et al.: *J Physiol (Lond)* 469: 673-691, 1993.
Supported by NIH grant AG 09000 to RME.

THE EFFECTS OF AGING AND FATIGUE ON LOWER EXTREMITY STIFFNESS

T. Hortobágyi, P. DeVita, J. Barrier, J. Money, T. McLuckie
Biomechanics Laboratory, East Carolina University, Greenville, NC 27858

INTRODUCTION

Aging-related reductions in movement capabilities have been linked to motor accidents. When a perturbation occurs during gait or stair descent, stiffness offers the body's first reaction to the challenge. Thus, it is important to determine the effects of aging on stiffness. In addition to possible changes in stiffness during aging, fatigue may also affect muscle stiffness. Even during daily activities muscle fatigue can set in rapidly and could interfere with stiffness regulation. In a step-down paradigm, we examined lower extremity stiffness in young and old men before and after lower extremity fatigue. Lower extremity stiffness was about 2.5 times less in the young than in the elderly. Fatigue of the lower extremity muscle increased stiffness in the young and decreased stiffness in the old.

REVIEW AND THEORY

Although the 30-40 N per decade decline of maximal strength after age 40 is well documented, recent studies suggest that a loss of maximal strength may not be as critical in the aging related decline in movement capabilities. For example, a few reports (Hortobágyi et al., 1995) suggest a relative maintenance of lengthening (eccentric) muscle forces with aging. These forces occur in the critical phase of human movement such as the loading phase of gait or stair descent. Thus it appears that not the magnitude of force but its control (Galganski et al., 1993) may be related the cause of reduced movement capabilities in the elderly.

One aim of the present pilot study was to determine the effect of aging on force control by examining lower extremity stiffness during stepping. Based on animal data (Alnaqeeb et al., 1984), the prediction was that lower extremity stiffness is greater in the aged due to a decrease in muscle mass and an increase in connective tissue mass and an increase in stiffness of connective tissue.

A second aim of the study was to examine the effect of fatigue on lower extremity stiffness. Previous human studies showed that although stiffness was excepted to decrease after fatigue in proportion to voluntary force (Kirsch & Rymer, 1992), there was only a slight reduction in stiffness. It was postulated that some force regulation mechanism compensated for fatigue and maintained stiffness. Because aging is associated with impairment of various neural control mechanisms (Horak et al., 1989), we expected differences in the stiffness responses to fatigue between young as compared to old subjects. The purpose of this pilot study was to determine the effects of aging and fatigue on lower extremity stiffness.

PROCEDURES

Pilot data were collected in apparently healthy young (n=3, age=22±2.6 SD) and old (n=3, age=66±1.7) men. Subjects were asked to step down with the right leg from a platform set at 10% and 20% of body height to a force plate. Subjects were wearing a protective harness suspended from the ceiling through a pulley. Three trials were done under the following conditions: (1) 10% height with and (2) without vision; (3) 20% height with and (4) without vision before and after fatigue induced by cycling. Reflective markers were placed on the centers of the lateral malleolus and hip and subjects were videotaped at 200 Hz with a NAC camera placed at 10 m perpendicular in relation to the plane of stepping. Lower extremity stiffness coefficient was computed as the quotient of the maximal vertical ground reaction force to the total linear displacement between the hip and ankle joints. Fatigue was induced by cycling for 3 minutes at each load of 1, 2, and 3 kg.

Surface EMG electrodes were placed on the vastus lateralis, biceps femoris, tibialis anterior, and lateral gastrocnemius. Peak EMG amplitude and its latency in relation to ground contact were determined for the vastus lateralis and lateral gastrocnemius. To quantify fatigue, maximal isometric knee extension strength was measured before, 1 minute after cycling, and after the 12 stepping trials.

RESULTS AND DISCUSSION

Figure 1 shows that lower extremity stiffness (data pooled for the vision and an no vision conditions) during step down was 2.7 times greater in the elderly. Fatigue, as measured 1 minute after cycling with maximal voluntary isometric knee extension, was 28% in the young and 24% in the old. Fatigue measured after the completion of the last stepping trial was still 20%. Fatigue decreased stiffness in the elderly by 19% and increased stiffness by 16% in the young (Figure 1). In relation to baseline, vastus lateralis and gastrocnemius peak EMG amplitude decreased by 24% in the old after fatigue and increased by 60% in the young. The latency of these EMG peaks was 100 ms in both groups and fatigue lengthened latency in both groups by 10%.

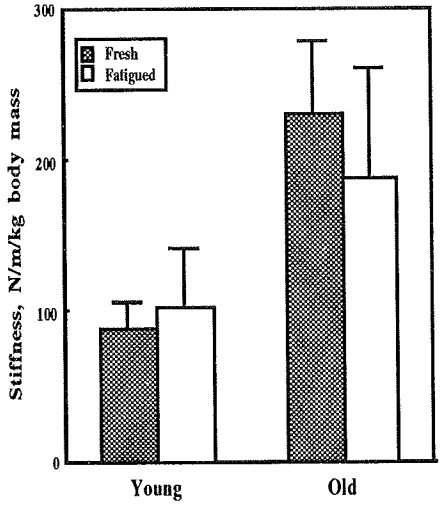

Figure 1. Effects of aging and fatigue on lower extremity stiffness during stepping.

These pilot data suggest that aging increases lower extremity stiffness. A substantially greater stiffness in the aged may result in inadequate adjustments to large or unexpected perturbations leading to motor accidents. Perhaps increased stiffness in the aged is not only an expression of the muscle-tendon-connective tissue system becoming more stiff as demonstrated in rats (Alnaqeeb et al., 1984), but also an expression of impaired force regulation. That a force regulation problem may emerge with aging is also illustrated by the differences in the responses to fatigue by young and old. While in the young medium-latency reflex augmentation may have compensated for fatigue and increased stiffness (Kirsch & Rymer, 1992), in the elderly reflex down-regulation occurred in conjunction with a decrease in stiffness. In conclusion, aging has a profound effect on lower extremity stiffness possibly due to a combination of changes in tissue properties and force regulation.

REFERENCES

Alnaqeeb, M. A. et al. Connective tissue changes and physical properties of developing and ageing skeletal muscle. J. Anat. 139, 677-689, 1984.

Galganski, M. E. et al. Reduced control of motor output in a human hand muscle of elderly subjects during submaximal contractions. J. Neurophysiol, 69, 2108-2115, 1993.

Horak, F. B. et al. Components of postural dyscontrol in the elderly: A review. Neurobiol. Aging, 10, 727-738, 1989.

Hortobágyi, T. et al. The effects of aging on muscle strength and muscle fiber characteristics with special reference to eccentric strength. J. Gerontol., 50A, B399-B406, 1995.

Kirsch, B. F. & Rymer, W. Z. Neural compensation for fatigue-induced changes in muscle stiffness during perturbations of elbow angle in human. J. Neurophysiol., 68, 449-470, 1992.

ACKNOWLEDGMENTS

Supported in part by an NIHCD-30422 (T.H.) and a Research/Creative Activity grant from East Carolina University's Faculty Senate (P.D.).

THE EFFECTS OF POSTURAL STABILITY ON ANTICIPATORY POSTURAL ADJUSTMENTS

Alexander S. Aruin and Mark L. Latash

Department of Kinesiology, The Pennsylvania State University,
University Park, PA 16802, USA

INTRODUCTION

We compared anticipatory postural adjustments (APAs) in standing subjects who dropped a standard load by a standard motor action while the stability of the vertical posture was manipulated. The instabilities were induced either by the subjects themselves or by balancing on special boards. Different planes and levels of instability were used. APAs showed a dependence on both plane and degree of instability. We conclude that APAs depend on all three major factors associated with the task: perturbation, action, and posture.

REVIEW AND THEORY

APAs are seen prior to voluntary movements that are expected to lead to a postural perturbation. APAs have been shown to depend on the magnitude of the motor action by the subject and on the magnitude of the expected perturbation (Aruin, Latash, 1995). The influence of posture on APAs was studied during rising onto toe tips, rocking on heels, when the trunk was initially inclined towards its final position, and while standing on one foot (Lipshits et al., 1981, Nardone, Schieppati, 1988, Nouillot et al, 1992). It has been suggested that APAs are absent when the posture is unstable (Nouillot et al, 1992). However, the effects of the plane and level of instability have not been studied. We decided to study these effects using an earlier paradigm (Aruin, Latash, 1995) which includes dropping a standard load from the extended arms with a standard motor action. This paradigm allows to eliminate possible effects of the magnitudes of the action and of the perturbation on APAs.

PROCEDURES

Subjects stood on a biomechanical platform (OR-65 AMTI) and hold a 2.2 kg load in the extended arms. At the computer tone signal, they were required to release the load by a low-amplitude, fast bilateral shoulder abduction.

Displacements of the center of pressure (CP) were calculated from the platform signals. Surface electromyograms (EMGs) of the following muscles from the right side of the body were recorded: erector spinae (ES), rectus abdominis (RA), rectus femoris (RF), biceps femoris (BF), tibialis (TA), and soleus (SOL). A miniature accelerometer (Sensotec) was taped to the left wrist. All the signals were sampled at 500 Hz with a 12-bit resolution. A Mac-IIci computer with a customized software based on the LabView-3 package was used to control the experiment, collect the data, and perform most of the analyses. The trials were aligned according to the first visible change in the acceleration signal. APAs were quantitatively assessed as EMG integrals during a 150 ms interval ($\int$EMG) corrected for the background activity.

Six subjects participated in Experiment-1 where one stable (regular, bipedal) and two unstable (inclined forward and unipedal) postures were used. Thirteen subjects took part in Experiment-2 with one stable and four unstable postures. The subjects stood on a wooden board (0.45 x 0.45 m) whose other side rested on a plank providing contact with the platform. The plank was 0.45 m long and either 0.04 m or 0.08 m wide.

RESULTS

Anticipatory changes in the activity of postural muscles were seen in all the series as a decrease in the activity of ES, BF, and SOL and an increase in the activity of ES, RF, and TA (Fig. 1). APAs were smaller when the posture was unstable in a sagittal plane (both experiments) and when the posture was unstable in a frontal plane (Experiment-2). Standing on one foot did not lead to significant changes in APAs. Within Experiment-2, instability in a sagittal plane had higher effects on APAs than instability in a frontal plane. Standing on a board with the smaller area of support produced higher effects on the APA magnitude. The effects of the plane of instability were statistically significant for RA, RF, BF, and SOL, while the effects of the support area were significant for ES, RF, BF, and SOL as

demonstrated by three-factor ANOVAs. Figure 1 shows averaged across the subjects values of ∫EMG for RA and ES with standard error bars. Note considerable changes in the RA ∫EMG activity in experiments with postural instability.

DISCUSSION

We have demonstrated that the magnitude of APAs in conditions of a standard perturbation induced by a standard motor action by the subject depends on two factors related to the postural task, namely, the plane of postural instability and the area of support. The last factor may be considered an inverse measure of the degree of instability. Note that the purpose of APAs is to generate joint torques whose effects on the position of the center of gravity should be opposite to the expected effects of a perturbation. As such, APAs lead to shifts of the center of gravity and may by themselves be sources of postural perturbations. In conditions of postural instability, the central nervous system may be "unwilling" to generate strong APAs in order not to subject the fragile equilibrium to another source of perturbations. The present study shows that APAs can indeed be graded with respect to the degree of postural instability. The effects of the plane of instability may be related to the fact that most of the major postural joints rotate in a sagittal plane, and therefore, APAs are more sensitive to instabilities in this plane.

REFERENCES

Aruin AS, Latash ML. Exp Brain Res, 106:291-300, 1995.

Lipshits ML, Mauritz K, Popov KE Human Physiology, 7: 411-419, 1981.

Nardone A, Schieppati M. Exp Brain Res, 69: 469-480, 1988.

Nouillot P, Bouisset S, Do MC. Neurosci Lett, 147: 1-4, 1992.

ACKNOWLEDGMENTS

The study was supported by an NIH grant HD-30128

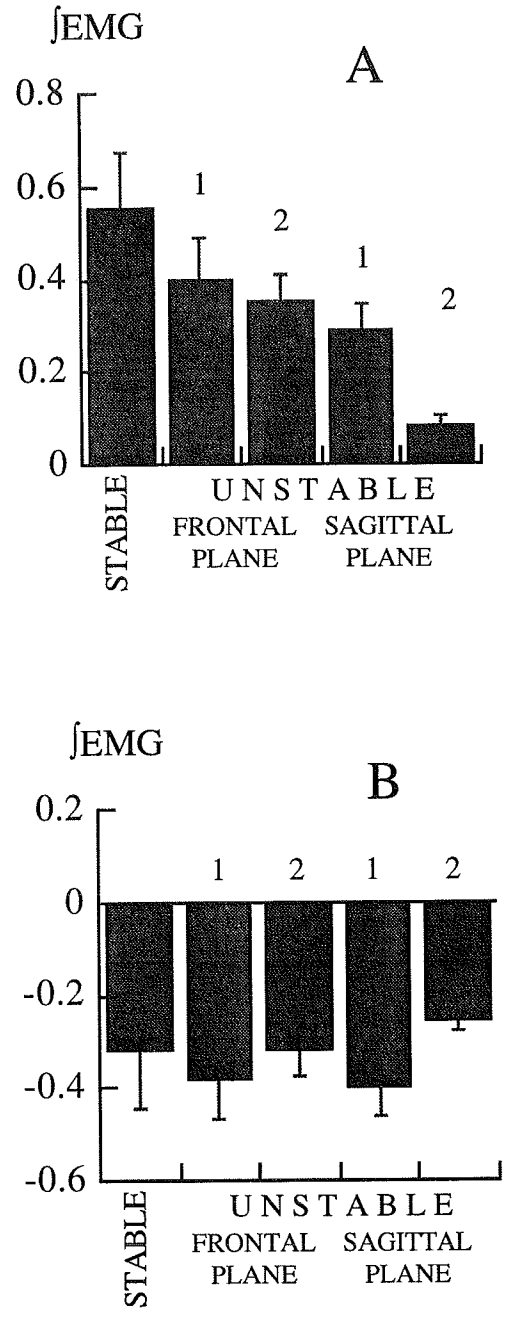

Fig. 1. Averaged across 13 subjects normalized anticipatory changes in the background activity of rectus abdominis (A) and erector spinae (B) during dropping the load from when the subjects stood in a regular, stable posture or were balancing on different boards.

STEPPING MECHANICS UTILIZED IN BALANCE RECOVERY: SWING AND CONTACT PHASE MODELING

Elizabeth T. Hsiao, Vladislav Frenk, Stephen N. Robinovitch

Department of Orthopaedic Surgery, San Francisco General Hospital and University of California San Francisco, San Francisco, CA 94110

INTRODUCTION

When upright posture is perturbed in humans, two mechanisms exist for balance recovery: sway (standing balance maneuvers) and stepping. While numerous studies have investigated balance control through sway, few have focused on the stepping response. Particularly lacking are studies examining *how* balance recovery is achieved by stepping, a process which occurs not in the initiation or swing phases of the step, but rather in the final contact stage of the step. Therefore, the purpose of this study was to develop a mathematical model of balance recovery by stepping, and compare model predictions of optimal stepping behavior to experimental data.

REVIEW AND THEORY

Falls due to slips, trips, and loss of balance are a major source of morbidity, particularly in the elderly [5]. Characterization of postural control mechanisms is essential for identifying individuals at risk for falls and fall-related injuries, and designing therapies for the prevention of such injuries.

While the great majority of biomechanical studies in this area have focused on control of balance via sway [3, 6], studies have also assessed the initiation and swing phases of the stepping response for balance recovery [1, 2, 4]. No study, however, has extended these analyses to examine the step contact phase, where the downward motion of the body is arrested, thereby preventing a fall.

To address this issue, we used a combination of experimental and mathematical models to explore how balance recovery is achieved by stepping. Specific hypotheses motivating this study were that step mechanics are chosen: (1) in an attempt to recover balance with a single step; and (2) to minimize the contact force and energy required to be absorbed in the stepping leg in order to achieve balance recovery.

PROCEDURES

Balance recovery experiments were conducted on three healthy young females and three healthy young males (age range 22-30 years, mean body mass 67±15 kg, mean height 166±11 cm) who had no previous falling history or fall training. The experimental protocol was similar to that used by Do and co-workers [1], and involved using an electro-magnetic brake and inextensible tether to instantly release subjects from an initially inclined position (Figure 1a). Each subject was randomly cycled twice through nine different initial lean angles, θ_o, for a total of 18 measurements. The only instruction given to subjects was to "prevent themselves from falling". Three-dimensional position data were recorded using a 6-camera, 60-Hz motion analysis system (MacReflex, Qualisys Inc., Glastonbury, CT) and 20 soft foam retro-reflective markers on the subject. Kinematic data (lean angle, step angle, and leg lengths) were computed after filtering position data (recursive Butterworth filter, 10 Hz cut-off frequency), using custom routines written in MATLAB (The MathWorks, Natick, MA).

A two-dimensional mathematical model was developed to interpret the functional significance of sagittal plane dynamics during the first step. This model consisted of a single link inverted pendulum, representing the head, torso, upper extremities, and rear pivot leg, and a massless linear spring, representing the stepping leg (Figure 1b).

During the swing or pre-contact phase, the equation of motion governing the pendulum-spring model is

$$I\ddot{\theta} - mg\,l/2\sin\theta = 0.$$

The equation of motion for the contact phase is

$$I\ddot{\theta} - mg\,l/2\sin\theta + \frac{kx_cC}{2\sqrt{B - C\sin\theta}}\cos\theta - kC/2\cos\theta = 0,$$

where l is the total length of the pendulum, $a = \sqrt{l^2/4 + x_c^2 - lx_c\cos\alpha_c}$ is the distance between the feet at contact, $B = l^2/4 + a^2$, and $C = al$. The input variables to the model are the initial body lean angle θ_o, leg stiffness k, stepping angle at contact α_c, and length of the stepping leg at the instant of contact x_c. From numerical integration of this equation, peak contact force $F_{max} = kx$ and peak energy $E = 1/2\,kx^2$ absorbed in the leg spring were computed.

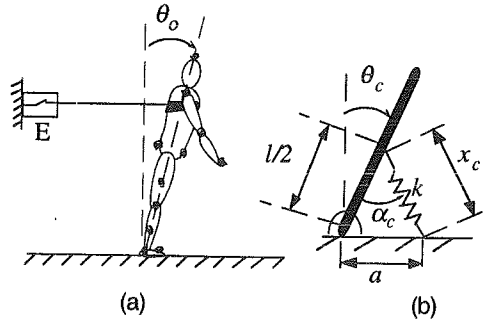

Figure 1: (a) Setup for balance perturbation experiments. E = electromagnetic brake. (b) Model of stepping response incorporating an inverted pendulum with moment of inertia I and massless linear leg spring with stiffness k.

RESULTS

In all but the slightest perturbations to balance, stepping represented the primary means for balance recovery. Twenty percent of the trials involved balance correction through sway alone, 66% involved a single step, and 14% involved multiple steps. Pooling together the latter two categories (based on ANCOVA analysis revealing no significant difference in α_c (p = 0.23) and θ_c (p = 0.25) between the two), we found that both the stepping angle (α_c) and lean angle (θ_c) at the instant of foot contact increased as the strength of the perturbation increased (Figure 2). Mean values were 35°±13°s.d. for α_c, 17°±4° for θ_c, and 1.4±0.3 for α_c/θ_c.

Model simulations based on average experimental values of θ_o = 15°, x_c = 761 mm, $l = 1.655$ m, and $m = 67$ kg suggested that the minimum (or critical) value of α_c allowing balance recovery increased from 12° for high leg stiffness ($k = 90$ kN/m) to 28° for low leg stiffness ($k = 10$ kN/m). Simulations also showed that, regardless of the magnitude of leg stiffness, minimal contact force and energy absorption in the leg spring is obtained for α_c between 30° and 40° (Figure 3), values similar to the experimentally observed average of α_c = 35°.

Modifying θ_o had little effect on model predictions of optimal stepping angles, while increasing x_c (greater knee extension at contact) reduced both the critical value of α_c for balance recovery and the optimal value of α_c for minimizing E and F_{max} (α_c = 20° to 30°).

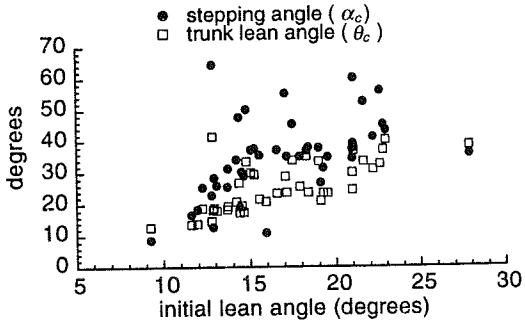

Figure 2: Measured body configuration at the instant the stepping foot contacts the ground.

DISCUSSION

The validity of our first hypothesis, that step mechanics are chosen in an attempt to recover balance through a single step, appears to be confirmed by the observation that a single step was used to regain balance in 82% of trials involving a stepping response. Further support for this hypothesis is provided by the results of ANCOVA analysis showing that both α_c (p = 0.23) and θ_c (p = 0.25) were not significantly different between single and multiple step responses, after accounting for the effect of θ_o, which was greater in multiple step trials (θ_o = 22°±4° for multiple steps vs. 15°±4° for single steps).

Comparison between model predictions and experimental results also appears to verify the reasonableness of our second hypothesis, that step mechanics are selected to ensure balance recovery while minimizing the energy absorbed and contact force generated in the stepping leg. The model predicts that minimal E and F_{max} will occur for stepping angles within 30° and 40°, while experimentally observed stepping angles averaged 35°±13°.

From Figure 3, it can be seen that the critical, or minimum, value of α_c for successful balance recovery increases with decreasing leg stiffness k. This indicates that for lower leg stiffness (due, for example, to impaired strength), larger steps are required to maintain balance; placing additional demands on lower extremity joint ranges of motion and reaction time. Such interactions between motor capacity and functional demand may play an important role in the epidemiology of falls in the elderly, and the design of exercise therapies for fall prevention.

REFERENCES

[1] Do et al. *J. Biomechanics*, 15, 933-939, 1982.
[2] Grabiner et al. *J Gerontol*, 48,77-83, 1993.
[3] Gu et al. *J. Biomechanics*, 29, 319-329, 1996.
[4] Maki et al. *J. Biomechanics*, 29, 343-353,1996.
[5] US Public Health Service. *Health People 2000*, 1993.
[6] Winter et al. *Med Progress Tech*, 16, 31-51, 1990.

ACKNOWLEDGMENTS

This study was supported by a grant from the Academic Senate of the University of California, San Francisco.

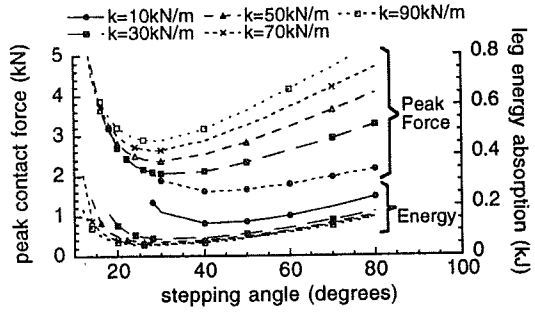

Figure 3: Influence of leg stiffness and stepping angle on peak contact force and energy absorbed in the stepping leg. Simulations are based on θ_o = 15°, x_c = 761 mm, $l = 1.655$m, and $m = 67$ kg. Lines correspond to constant stiffness, with smallest stepping angle representing the critical minimum α_c required for balance recovery.

EFFECTS OF OBSTACLE HEIGHT AND PROXIMITY ON TEMPORAL-DISTANCE MEASUREMENTS AND ON KINEMATICS OF THE TRAILING LIMB

Li-Shan Chou and Louis F. Draganich

Section of Orthopaedic Surgery and Rehabilitation Medicine, Department of Surgery
The University of Chicago, Chicago, Illinois 60637

INTRODUCTION

Falling is a significant problem for the elderly and tripping over obstacles with the trailing limb (limb crossing the obstacle last) occurs. We thought it important to first investigate the biomechanics of the trailing limb of young healthy adults to obtain base-line data before proceeding to studies on the elderly. We studied the effects of obstacle height and location on temporal-distance measurements and on kinematics of the trailing limb in seven healthy young adults stepping over obstacles of 51, 102, and 204 mm heights positioned at distances from the trailing foot of 10, 20, 30, and 40% of the step length measured during unobstructed level walking. An optical-electronic digitizing system and force platform were used.

REVIEW AND THEORY

Tripping over obstacles is the most frequently mentioned causes of falls in the elderly (Blake et al., 1988; Tinetti and Speechley, 1989; Campbell et al., 1990). Laboratory studies have been performed to investigate the effects of obstacle height and width on the motion of the leading limb (Chen et al., 1991; Patla and Rietdyk, 1993) and on the motion of the trailing limb (McFadyen and Winter, 1991; Chou and Draganich, 1996). The former studies demonstrated that the trajectory of the leading limb was substantially modulated for obstacle height but minimally for obstacle width and also demonstrated that hip, knee, and ankle flexion increased with obstacle height. The latter studies found that a strategy favoring knee flexion of the trailing limb was adopted when stepping over obstacles. Studies of the effects of limb-obstacle proximity have not been reported. Thus, the purpose of this study was to investigate the effects of obstacle height and location on temporal-distance measurements and on kinematics of the trailing limb.

PROCEDURES

Gait analysis was performed on seven healthy young adults (5 males, 2 females) having a mean age of 24 years (range, 20 to 32 years). Their average height was 174 cm (range, 167 cm to 184 cm), and their average weight was 705 N (range, 637 N to 881 N). Subjects wore their own low-heel shoes. Three sets of experiments were performed. For each experiment subjects walked along a 9.5 m walkway at their comfortable, self-selected speeds. In the first experiment, each subject's average step length over several strides was measured. In the second experiment, the subject was instructed to walk along the walkway and step over an obstacle (white elastic band 1 mm thick and 6 mm wide) of 51, 102, or 204 mm height in his/her usual self-selected manner. To do this, the obstacle was placed beyond the force plate at a fixed location. The subject's beginning position was adjusted until with practice the subject had established a comfortable gait and the toe of the trailing foot landed within ±5 cm of a marker on the force plate before lifting the trailing foot to step over the obstacle. This beginning position was used in the third experiment. For the third experiment the average step length for the subject found in the first experiment was used to compute lengths of 10, 20, 30, and 40% of step length. The obstacle of each height was randomly placed at these distances from the marker on the force plate. The subject was instructed to maintain the stride attained in the second experiment until heel-strike of the trailing foot just prior to stepping over the obstacle. Thus, the distance from the toe of the trailing foot (during stance just prior to stepping over the obstacle) to the obstacle was controlled. Trials were accepted only if the toe of the trailing foot was within ±5 cm of the marker on the force plate.

Ground reaction forces were measured with a force platform in the center of walkway. Clusters of six or eight infrared light-emitting diodes were attached to the foot, shank, and thigh of the left lower limb and pelvis of the subject with elastic straps. Kinematic parameters were collected with the optoelectronic, 3-D digitizing system. Kinematic and force parameters were sampled at a rate of 100 Hz. The overall accuracy of the system was better than 5 mm for a volume 2 m long, 1.5 m high, and 0.7 m wide. The kinematic data were analyzed for the trailing limb period beginning with heel-contact just before crossing the obstacle to the next heel-contact just after crossing the obstacle. We termed this the crossing stride. Stride length was normalized to lower limb length.

The effects of obstacle height and location on crossing speed, stride time, stride length, stance time, toe-obstacle

clearance, and 3-D angles of the joints of the trailing limb were tested using two-way ANOVA with repeated measures. An α=0.0056 level of significance was used based on a Bonferroni adjustment for nine comparisons. If a significant difference was detected, the polynomial test was performed at the α=0.05 level of significance to determine if a linear trend existed. One trial per obstacle height and distance were used in formulating the results. The temporodistance parameters and 3-D angles of the knee joint are reported.

RESULTS

When stepping over an obstacle in the subject's usual self-selected manner (i.e., without controlling the distance from the toe of the trailing foot to the obstacle) the distances between the obstacle and the toe of the trailing foot ranged from 42.5% to 44.4% of the step length measured during unobstructed level walking (Fig. 1). This distance was not found to be affected by obstacle height. Crossing speed decreased significantly as obstacle height increased (p=0.00004) and as limb-obstacle proximity decreased (p=0.002) (Fig. 2). Linear trends were found between crossing speed and obstacle height and between obstacle height and limb-obstacle proximity (p=0.0008 and p=0.008, respectively). The normalized stride length decreased significantly (p=0.001) as limb-obstacle proximity decreased. A linear relationship between the normalized stride length and limb-obstacle proximity was found (p=0.011). The time required for the crossing stride increased significantly as obstacle height increased (p<0.00001) and decreased significantly as limb-obstacle proximity decreased (p=0.005). A linear relationship between stride time and obstacle height was found (p<0.00001). Stance time of the trailing limb during the crossing stride was affected significantly only by obstacle height (p=0.00001). Stance time increased linearly as obstacle height increased (p=0.0006). Toe-obstacle clearance decreased as limb-obstacle proximity decreased. However, significant differences were not found.

When the toe of the trailing limb was over the obstacle flexion of the knee increased significantly (p=0.00001) as obstacle height increased and decreased significantly (p=0.0013) as limb-obstacle proximity decreased (Fig. 3). Linear relationships were found between knee flexion angle and obstacle height (p=0.00016) and between knee flexion angle and limb-obstacle proximity (p=0.012). Obstacle height or limb-obstacle proximity was not found to affect the abduction-adduction or internal-external rotation of the knee.

DISCUSSION

When stepping over obstacles of various heights in a self-selected manner the subjects consistently placed their trailing feet at the same distance from the obstacle in agreement with that reported previously (Chen et al., 1991). Obstacle-trailing foot proximity affected not only the temporodistance parameters of gait but also knee flexion. The reduction in knee flexion found when the toe was over the obstacle may decrease the clearance between the toe of the trailing foot and the obstacle. This may in turn affect the propensity to trip. We are currently investigating this possibility.

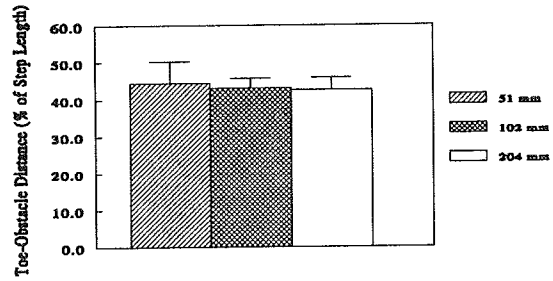

Figure 1. Average distance between the toe of the trailing foot during the crossing stride and the obstacles of 51, 102, and 204 mm heights when crossing the obstacles at self-selected toe-obstacle distances.

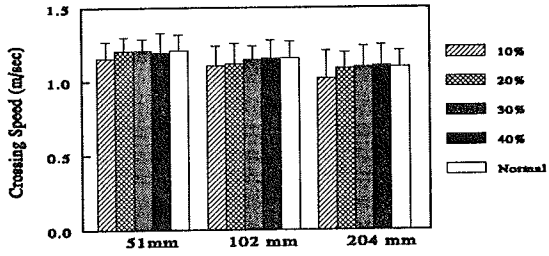

Figure 2. Average crossing speeds when stepping over the obstacles of 51, 102, and 204 mm heights positioned at the different locations.

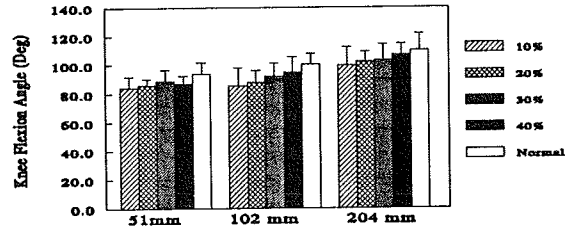

Figure 3. Average knee flexion angle when the toe was over the obstacle of 51, 102, and 204 mm heights and the obstacle was positioned at the different locations.

REFERENCES

1. Blake et al., *Age and Ageing* 17: 365-372, 1988,
2. Campbell et al., *Age and Ageing* 19: 136-141, 1990.
3. Chen et al.,*J Gerontology* 46, M196-203, 1991.
4. Chou et al., submitted to *J. Biomechanics.*, 1996
5. McFadyen et al., *Neurosci. Res. Comm.* 9: 37-44, 1991.
6. Patla et al.,*Gait & Posture* 1, 45-60, 1993.
7. Tinetti et al., *New Eng. J. Med.* 320: 1055-1059, 1989.

THE CONTROL OF SPATIAL BODY ORIENTATION IN HUMAN UPRIGHT STANCE

G. Wu[1] and W. Zhao

[1]Department of Exercise and Sport Science
Department of Mechanical Engineering and Center for Locomotion Studies
The Pennsylvania State University, University Park, PA 16802

INTRODUCTION AND BACKGROUND

The maintenance of upright balance represents a major goal of human postural control. Although it has been well accepted that the upright balance is controlled by the central nervous system which integrates the information provided by the peripheral sensory systems, the specific nature of the controlled variable(s) is not clear yet.

Researches on pattern generators in control of locomotion have suggested that there exists an elaborate neural circuitry in the spinal cord (at least in animals) that is responsible for automatic execution of basic locomotion patterns (Marsden, 1982). Similarly in the control of human upright balance, a set of automatic postural reflexes has been observed in leg muscles when a person stands on a platform that suddenly moves (Woolacott et al., 1986). Although these reflexes are found to either decrease its magnitude with consecutive movements of the supporting surface when it destabilized the posture, or increase its magnitude when it stabilized the posture (Nashner, 1976), their timings are relatively invariable.

In this study, the peak magnitude and the peak time of body orientations were measured when subjects' postural balance was unexpectedly disturbed. The variations of these two variables with respect to the number of trials were examined. We hypothesized that the human upright balance is controlled by a pattern generator which regulates the timing of body movement.

METHODOLOGY

Postural perturbation was applied to the subject through an unexpected platform movement in the anterior-posterior direction of the subject. The maximum acceleration was $8m/s^2$, speed $40cm/s$ and total displacement $8cm$. The spatial orientation (or angular displacement) of the head, trunk and arms, thigh, and shank in the sagittal plane was determined based on the measurements of multiple marker positions by a video-based motion analysis system (Peak Performance) with two cameras. An accelerometer was attached to the movable platform to measure its acceleration in the moving direction. The output from the accelerometer was synchronized with the video data and collected at $120Hz$.

A total of 10 healthy subjects (ages ranged from 19 to 28 years, with a mean of 23.8 years) participated in this experiment. During the experiment, each subject was tested for a total of 12 conditions, 4 times each. They included: vision/no vision, moving forward/backward, and standing on hard/soft/reduced surfaces. All these conditions were provided in a random, but blocked order.

Before each trial, the subject was instructed to stand quietly on the movable platform, with feet comfortably separated in the lateral direction, arms folded across the chest, and eyes looking at a target $25m$ in front of the subject. The subject was given a random number between 50 and 100, and was asked to continuously subtract by 3 as quickly and accurately as possible until the platform movement started. In response to the platform movement, the subject was instructed to try to maintain the upright balance by moving any part of the body except for the arms.

The perturbation onset time was first determined based on the first point at which the platform acceleration was above the mean plus three times the standard deviation of the baseline level. Two parameters were calculated: first maximum peak magnitude (P_{max}); first peak time (T_p) defined as the time at which the magnitude reached to a maximum for the first time. Data were analyzed using Analysis of Variance (ANOVA) to identify differences among the four trials of all the conditions. If the test proved to be significant, Least Squares Means analysis was made to detect which differences among the trials were significant ($p < 0.05$).

RESULTS

The means of all four trials of both peak magnitude and the peak time of the orientation angles are shown

in Fig. 1. Those trials that are statistically significant are summarized in Table 1.

First maximum peak amplitude (P_{max}): The results (Table 1) showed that the difference in P_{max} between the first and the later trials was significant for the shank, thigh and trunk segments. In general, the significant difference occurred at about the second trial. In all cases, no significant difference was found between the third and the fourth trial. In addition, these differences were independent of surface, vision, and movement direction conditions.

First peak time (T_p): For most of the cases the ANOVA test determined that there was not enough evidence to suggest a difference among the mean of the trials except for the thigh angle between the first and the last trials. The results of all the other variables were not affected by factors such as surface, visual condition, and movement direction.

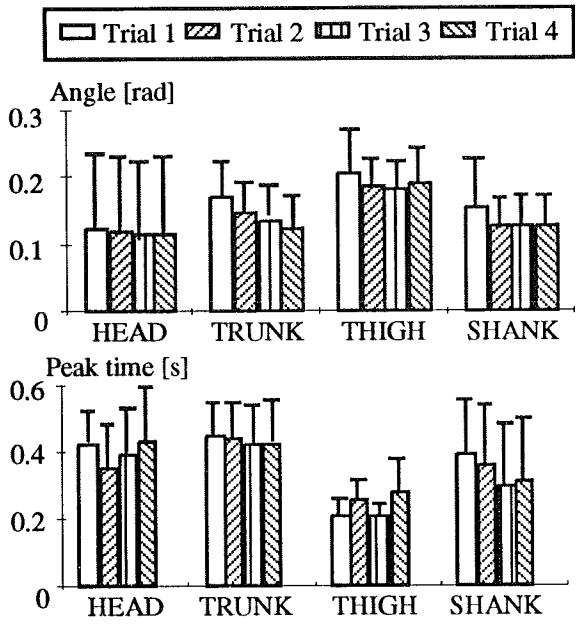

Fig. 1. Means+stds. of maximum peak orientation angles and the first peak time of four body segments.

	Head	Trunk	Thigh	Shank
P_{max}	NS[a]	1-2 1-3 1-4	1-2 1-3 1-4	1-2 1-3 1-4
T_p	NS	NS	1-4	NS

Table 1: Statistically significant difference between trials for the maximum peak amplitude and peak time. All the results are not affected by surface, vision and movement direction. (NS: not significant among trials.)

DISCUSSION AND CONCLUSIONS

It is observed in this study that both the first maximum peak magnitude and the first peak time of the head orientation angle in space do not show any sign of adaptation. This suggests that the control of the stability of the head has a stable pattern which regulates both the magnitude and the timing. The fact that these characteristics of the head movement are not effected by vision and surface conditions further suggests that the pattern generator for head stabilization is probably controlled by other mechanisms than visual and somatosensory systems in the foot. Early studies by others (Roberts, 1973) have suggested that the orientation of the head in space is stabilized by means of vestibular and neck reflexes.

Differently from the head, it is interesting to find in this study that the magnitude of the spatial orientations of the trunk and legs are adapted when multiple trials with similar conditions are experienced by the subject, although the timing at which the first peak value occurs does not seem to be adaptive. This finding establishes the fact that the timing and the amplitude of body movement are independently controlled. In fact, this is consistent with the results in an indirectly related study by Radin et al. (1991) on the effect of knee pain on general gait patterns: that the timing of the peak ground reaction force was significantly altered in the knee pain group compared to the normal subjects while the magnitude was kept the same.

REFERENCES

Marsden, C.D. The mysterious motor function of the basal ganglia. Neurology. 32:514-39, 1982

Nashner, L.M. Adapting reflexes controlling the human posture. Exp Brain Res. 26: 59-72,1976 .

Radin, E.L. et al. Relationship between lower dynamics and knee joint pain. J Ortho Res. 9: 398-405, 1991

Roberts, T.D.M. Reflex balance. Nature, 244:156-158, 1973

Woolacott, M. et al., Aging and postural control: changes in sensory organization and muscular coordination. Int J Aging Hum Dev. 23:97-114, 1986

ACKNOWLEDGMENT

The authors would like to thank Mary Becker for recruiting subjects. This work was supported by a grant from the Whitaker Foundation and by a National Institute of Health grant No. 1R29AG11602-01A2.

RELATION BETWEEN ANKLE MOVEMENT AND POSTURAL REFLEXES

G. Wu[1] and J. Chiang[2]

[1]Department of Exercise and Sport Science
[2]Bioengineering Program
Center for Locomotion Studies
The Pennsylvania State University, University Park, PA 16802

INTRODUCTION AND BACKGROUND

The control of human upright posture involves the integration of sensory information from the somatosensory, vestibular, and visual systems. In the past, the contribution of these sensory systems to postural control has been studied extensively except for the specific role of each of the somatosensory receptors. The reason is not only due to the complexity of the somatosensory system but also due to the difficulty in separating each of these receptors.

In particular, the precise role of joint receptors in postural control is still under discussion. While it is generally accepted at present that joint receptors provide position information only at the extremes of joint rotation (Ferell, 1988), it has been shown that joint sensations are critical during low frequency platform movement (Diener et al. 1986).

The purpose of this study was to investigate the relation between the ankle movement and the postural reflexes in the leg muscles during a rapid, toes-up rotation of the supporting base. The ankle joint was either free to move or immobilized to alter the range of the ankle motion. The latencies of the leg muscle responses were recorded and correlated to the ankle movement.

METHODOLOGY

Fifteen male subjects were included in this study with mean weight of 66±3kg, mean age of 25±4 years. During testing, subjects stood barefoot on a rotational platform with eyes closed. The ankle joints were either allowed to move freely or constrained in the sagittal plane by a pair of ankle immobilizers that were firmly placed around both ankle joints (Chiang, 1995). The platform was rotated in the toes-up direction with an amplitude of 8°, and velocity of 60°/s. In response to the platform movement, subjects were instructed to keep their body as still as possible and not to move their feet unless they absolutely had to. A total of 10 trials was repeated, 5 for each ankle condition.

The following biomechanical variables were directly measured: ankle rotation in the sagittal plane by a strain gauge goniometer (Penny & Giles Inc.), EMG signals from the lateral gastrocnemius and tibialis anterior muscles of the right leg by a pair of EMG electrodes (Therapeutics Unlimited), pressure distribution under the feet by a pair of pressure detector insoles (Pedar system, Novel), and platform acceleration by a linear accelerometer (Kistler Instrument Ltd.). Pressure data were collected at 50 Hz for 4 seconds, and the signals from the goniometer, the EMG electrodes and the accelerometer were collected at 1000 Hz for 4 seconds.

The peak pressures were determined in forefoot, midfoot and rearfoot regions. The dynamic change and the maximum range of ankle rotation during the platform movement were calculated. In addition, the angular velocity of the ankle joint movement was calculated using numerical differentiation. Both angular displacement and velocity data were then low-pass filtered by a 4th order numerical Butterworth filter with a cut-off frequency of 25 Hz. The muscle latencies were calculated according to the time between the perturbation onset time and the rising burst of muscle response. They were then categorized into short latency (30 to 69 ms post perturbation onset), medium latency (70 to 119 ms post) for the gastrocnemius muscle, and long latency (120 to 200 ms post) for the tibialis anterior muscle.

Analysis of variance (ANOVA) was used to identify differences between two ankle conditions for three muscle latencies, regional peak pressures and maximum range of ankle joint rotation. This analysis was followed by a Least Squares Means test when significant main effect differences were found. These effects were considered significant at $p < 0.05$.

RESULTS

Ankle joint rotation: During the entire perturbation period the ankle movement increased monotonously with time (Fig. 1). When the ankle joints were free to move, they changed about 1.2° at 50*ms* and up to

8° at 300*ms*. When both ankles were constrained with the immobilizer, they changed very little (about 1° maximum) throughout the entire perturbation period.

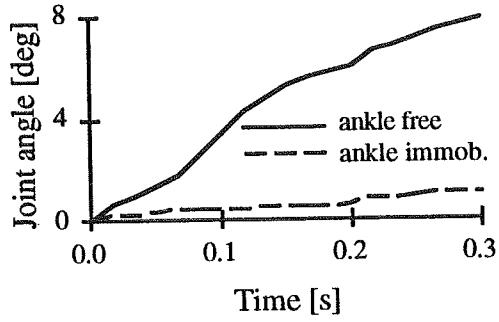

Fig. 1. Ankle angle after onset of the platform movement for both ankle conditions.

Pressure: The regional peak pressures for both ankle conditions were remarkably similar (Fig. 2). Statistical analysis revealed that the peak pressures between the two ankle conditions were not significantly different ($p>0.05$).

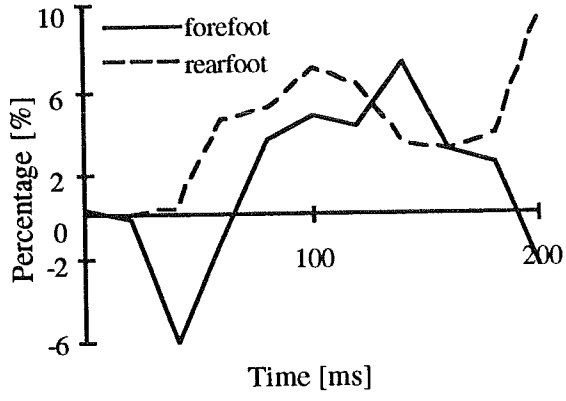

Fig. 2. Percent differences of plantar pressures between two ankle conditions.

Muscle latencies: The means and standard deviations of latencies of leg muscle responses for both ankle conditions are shown in Fig. 3. Statistical analysis revealed that the short latencies were not significantly different between ankle conditions ($p = 0.39$). However, when the ankle joints were immobilized, both medium and long latencies were significantly delayed compared to those without having the ankles fixed ($p < 0.044$).

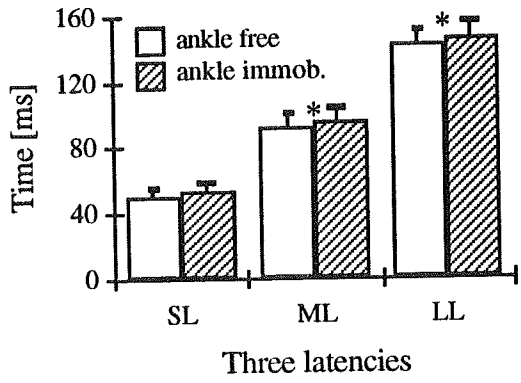

Fig. 3. Mean+std. of short, medium and long latencies for both ankle conditions. Symbol * indicates significant difference between two conditions ($p<0.05$).

DISCUSSIONS

In this study, three variable, namely, ankle joint movement, plantar pressure under the feet and postural reflexes in the leg muscles were monitored during a fast, toes-up rotation of a supporting base. Comparing to the condition when the ankles were allowed to move freely, it is found that when both ankle joints were immobilized both medium and long latency responses in the leg muscles were significantly delayed. Furthermore, the ankle movements were found to be greatly limited while the plantar pressures were not altered. Therefore, it can be concluded that the input of joint receptors could affect the medium and long latency muscle responses.

REFERENCES

Ferell, W.R. Discharge characteristics of joint receptors in relation to their proprioceptive role. In: Soukoup, T. et al. (Eds), Mechanoreceptors: dev struc func, Plenum NY, 1988

Diener et al. Role of visual and static vestibular influences on dynamic posture control. Human Neurobiol. 5:105-113, 1986

Chiang, J. The effect of plantar cutaneous mechanoreceptor input on dynamic upright posture. M.S. Thesis, Penn State University, 1995

ACKNOWLEDGMENT

This work was supported by a grant from the Whitaker Foundation and by a National Institute of Health grant No. 1R29AG11602-01A2.

Exploring Human Adaptation using Optimized, Dynamic Human Models

S. McGuan
Mechanical Dynamics Inc., Ann Arbor, MI 48105

INTRODUCTION

Classic inverse/dynamics methods fall short in providing a methodology which allows the human model to adapt to a change in environment or equipment. This paper introduces a dynamic human model with joint torques governed by coupled feedback controllers and optimized to a specific objective to allow for a structured approach in human adaptation simulation.

REVIEW AND THEORY

Inverse/dynamics methods for human simulation include methods of calculating the joint torques necessary for the human model to emulate the recorded motion [Allard 1995]. One problem analysts using these methods often encounter is in replicating the recorded motion with a high degree of accuracy [Li 1993]. This is in part due to the fact that various motions in the joints of the multi-segment chain representing the human, may be highly non-linear and discontinuous, resulting in high torque spikes which do not translate to exactly emulating the recorded motion. This is combined with the fact that the motion data is not acutely accurate to begin with, due to unwanted movement of the motion targets attached to the skin of the human subject. Using standard methods, these models are also unable to adapt to changes in environment or equipment.

This paper introduces a method of accurately replicating the recorded motion with a dynamic human model. It also accounts for data error of the motion targets and introduces an adaptation scheme for adjusting the torques to allow for the human to accommodate small changes in the environment.

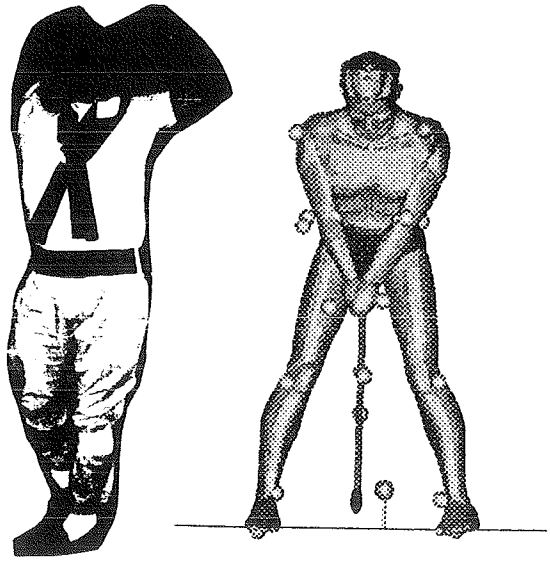

Fig. 1 Data Collection and Simulation for Full Body Motion.

PROCEDURES

Motion data from a data collection source (i.e., video, sensors, etc.) consists of 3D position histories of markers placed at various locations on the human subject. These markers are electronically tracked through time for the duration of the activity. This approach can be used to model the full body with large joint motion as in figure 1, or a specific limb with small articulations as in figure 2 [McGuan 1994].

Fig. 2 Data Collection and Simulation for Partial Body Simulation.

The ADAMS® (Mechanical Dynamics Inc.) mechanical simulation system is used to process these data into a dynamic human model. The process begins by positioning "motion agents" on the multi-segmented human model at the same relative locations as in the experiment. The motion agents, displayed as spheres (figures 1 and 2), are driven with the experiment motion data. The agents are physically attached to the corresponding human segment using a 6 degree-of-freedom (DOF) spring elements (bushings). The stiffness of this connection is normalized to the relative accuracy rating of the specific target marker in the experiment (available from the motion analysis equipment/software). This allows for the marker with a higher degree of accuracy to contribute more to the motion in the model changing the nature of the motion data to motion influencing rather that motion governing.

A kinematic analysis is performed with this arrangement to retrieve the joint rotation histories for the human model emulating the motion. In the case of the model in figure 1, the joint motion is retrieved for the major joints in the body, in figure 2 it is for the equivalent joints throughout the articulating foot.

Adaptable, Dynamic Human Simulation

To perform a dynamic simulation with this model the motion agents are removed and torque elements are positioned at each DOF. The joint torque functions are implemented using the rotations from the proceeding kinematic analysis in a feedback controller of the form displayed in figure 3.

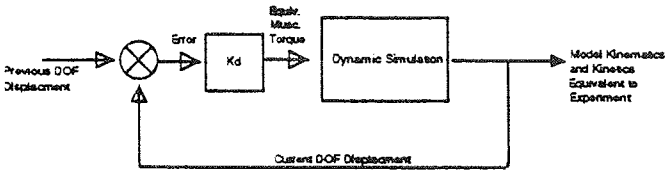

Fig. 3 Feedback Controller for Torque Functions in the Dynamic Human Model.

This controller produces the torques necessary for the human model to follow the motion from the proceeding kinematic analysis. The controller gains, K_d, for each DOF may be coupled with the gains from other areas in the body in such a way to systematically adjust the motion tracking ability of the dynamic human model. By adjusting these coupled coefficients, the human model will track the motion differently. By introducing an optimization scheme to adjust these coupled coefficients to achieve a specified goal, the human model will react to changes in the environment.

RESULTS

Motion data was collected for the golfer in figure 1. The simulation was performed using a dynamic human model and a golf club with a flexible shaft (Young's modulus = 2.68 x 10^6 N/cm^2). The procedure outlined above was used for the dynamic simulation of the golf swing. This resulted in an acceptable swing with a loft (face-angle with the vertical) of 9.7° and a club head velocity of 59.8 m/s at impact [Jorgensen 1994].

A second simulation was performed to display the effects of a change in equipment to the human model without any adaptation. For this test, the golf club shaft stiffness was increased by 30%. Without any adaptation, the human model swings the club using the same force as if it were the club from the proceeding analysis. With the differing mechanical characteristics of the club the human model's timing will be off. During the swing, the club is still bent backwards at contact and the loft is decreased to -6.6° and a club head velocity of 39.8 m/s at impact, indicating that the shaft has not fully straightened out.

Adaptation was then implemented in the model with the goal being to adjust the timing of the swing action to utilize the energy of the stiffer club. The optimization process [Pike 1986] consists of maximizing an objective function by iterating on variables under some system constraint. The objective in this golf simulation was the club head speed at ball contact. The constraints were the limits for the head face and loft angle at contact, and the variables were the controller gains for the torque functions. Coupling was introduced to the gains, grouping the arms, trunk, and legs into 5 variables, decreasing the number of gains from 34 and the greatly speed up the optimization process.

The results of the adaptation simulation yield a respectable 8.5° loft and a head speed of 51.8 m/s. Figure 3 displays a comparison between the three simulations.

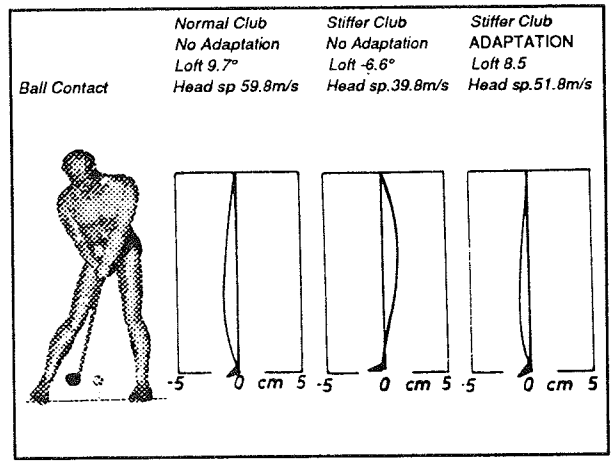

Fig. 3 Results: 1. Normal club, 2. Stiffer Club 3. Stiffer Club (Adaptation).

DISCUSSION

The next step in this research is to simulate the golf swings (or other activities) of several subjects with clubs of variable stiffness. From this sampling, trends may be identified to aid in the K_d coupling, bounding and heuristics to allow for statistically viable human models with a higher degree of biofidelic adaptation. This system promises much utility in muscle control and coordination research, as well as practical applications of sports simulations, gait analysis, etc.

REFERENCES

Allard, P., et al (1995) Three-Dimensional Analysis of Human Movement, Human Kinetics Publishers.

Jorgensen, T. (1994) The Physics of Golf, AIP Press Publishers.

Li, J. et al (1993) "An Integrated Procedure to Assess Knee-Joint Kinematics and Kinetics During Gait using an Optoelectric System and Standardized X-Rays"., J. Bio
9

McGuan, S., et al (1994) "An Approach for a Detailed Analytical Model of the Human Lower Extremity During a Drop Landing", 1994 ASB Columbus, Ohio.

Pike R. (1986) Optimization for Engineering Systems, Van Nostrand Reinhold Publishers.

AN INVESTIGATION OF ADDING A STEP-UP APPROACH TO A SWIMMING RELAY START

S.P. McLean[1], K.D. Beckett[2], P.F. Vint[3], and E. Kendrick[1]
[1]Department of Health and Human Performance, Iowa State University, Ames, IA 50011
[2]Department of Physical Education and Athletics, The College of Wooster, Wooster, OH 44691
[3]Department of Exercise Science and Physical Education, Arizona State University, Tempe, AZ 85287

INTRODUCTION

The addition of an approach to a vertical jump has been shown to increase the height of the jump. Because of this, a trend in competitive swimming has developed in which a single or double-step approach is added to the traditional relay start. This is thought to increase the swimmer's forward velocity prior to beginning the traditional starting movement using only an arm swing. Thus total momentum will increase such that the swimmer will achieve a higher forward takeoff velocity. The effectiveness of this technique remains in question as evidenced by the continued use of the traditional relay start in national and international competition. This may be in part due to the lack of systematic, scientific study of this technique. This study was undertaken with the intent of comparing the ability of the traditional relay start and the new step-up approach to achieve forward takeoff velocity.

REVIEW AND THEORY

The movements performed in a swimming start are closely related to those of a vertical jump with the difference being the direction of motion. A flat start in swimming may be likened to a squat jump since the swimmer moves only forward during the start. A relay start more closely resembles a counter-movement jump. In addition a relay start provides a swimmer with an advantage because forward movement of the body begins prior to the finish of the incoming swimmer. Maglischo (1993) suggests that this may provide the swimmer with an advantage of 0.6 to 1.0 s over a flat start.

It is reasonable to assume that the performance of the start can be enhanced using the principles applicable to vertical jumping given the similarities between these activities. Kayambashi (1977) and Enoka (1971) found that the inclusion of an approach to a vertical jump improved performance. Therefore, the addition of a step-up approach to a swimming start should enable the swimmer to increase forward takeoff velocity.

The purpose of this study was to compare the performance of a traditional arm swing (AS) relay start to that of a relay start incorporating a single-step (SS) and double-step (DS) approach. The hypotheses proposed for this study were:
1) horizontal takeoff velocity will be highest for the DS start, 2nd highest for the SS start, and lowest for the AS start, and 2) the arms will contribute a greater proportion of forward lift to the AS start than either step-up start.

METHODS

Ten collegiate swimmers (five males, five females) provided informed consent to participate in this study. All subjects had received prior instruction and practice in the performance of the three relay starting techniques. Each subject completed two maximal effort relay starts using each technique. A flat start condition was included as a baseline.

Two-dimensional video data were collected at 60 Hz in the sagittal plane. One trial from each condition was chosen for analysis. Twenty-one points were used to define a 14 segment model of the body. Whole body CM location during the trial was computed using segmental masses and center of mass locations obtained from the mean data of De Leva (in press). Data were smoothed using a quintic spline algorithm.

The CM velocity at takeoff was computed using a finite difference differentiation of the smoothed position data. Forward lift was defined as the change in horizontal relative momentum between the initiation of forward movement and the instant of takeoff from the starting block. Forward lift was computed using the method of Ae and Shibukawa (1980). The contributions of the head and trunk, arms, and legs to forward lift were defined as the proportion of whole body relative momentum during the propulsion phase. Net forward lift was defined as the difference in relative momentum at the instant of takeoff and the start of the propulsive phase. Peak forward lift was defined as the maximum difference in relative momentum between the instant of takeoff and the instant of peak forward velocity. Statistical comparisons were made using matched-pairs t-tests. To control type II errors the alpha level was adjusted using the Bonferroni procedure to 0.004.

RESULTS

The mean horizontal velocity of the center of mass at takeoff for the AS start was 0.3 m/s slower than both the SS and DS starts (see Table 1). These differences were not statistically different but were characterized by moderate effect sizes (ES=0.53 and 0.54, respectively for SS and DS).

The net forward lift values for the legs, were greater than 100% at the instant of takeoff for each starting condition (see Table 1). No significant differences between conditions were found. With the exception of the SS start the head and trunk, and arms had negative

contributions to net forward lift. This difference was characterized by moderate effect sizes (0.4-0.6).

Table 1 - Comparison of mean horizontal CM velocity and percent of net forward lift. (SD)

Start	V_X (m/s)	P_{TRUNK} (%)	P_{ARMS} (%)	P_{LEGS} (%)
flat	3.5	-2.3	-0.2	102.7
	(0.6)	(6.8)	(1.1)	(7.0)
arm	3.4	-2.2	-1.0	103.4
swing	(0.4)	(6.0)	(1.7)	(7.1)
single	3.7	0.5	-0.7	100.4
step	(0.5)	(5.4)	(1.8)	(4.8)
double	3.7	-1.2	-1.5	102.8
step	(0.5)	(4.1)	(1.2)	(3.7)

Investigation of the change in forward lift of the arms throughout the propulsive phase of the start indicated that the peak forward lift was reduced only for the arms in flat starts (see Table 2 and Figure 1).

Table 2 - Peak forward lift of the arm and time of peak during the propulsive phase. (SD)

Start	Arms (N·s)	Time of Peak (%)
flat	13.6	63.3
	(2.8)	(16.9)
arm swing	18.9	69.1
	(4.8)	(5.7)
single step	19.0	71.3
	(5.3)	(8.0)
double	19.1	72.6
step	(4.8)	(5.9)

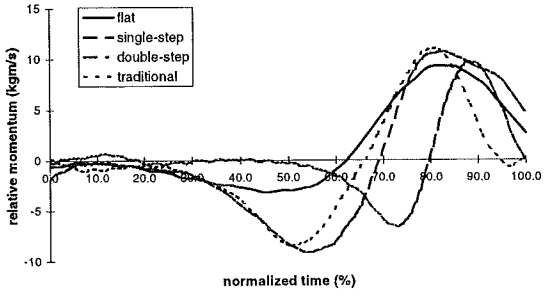

Figure 1 - Representative graph of forward lift throughout the propulsive phase of a start.

DISCUSSION

The data supported hypothesis #1. The horizontal velocity of takeoff was increased in the starts which incorporated the use of a step-up approach. However, the overwhelming contribution to net forward lift from the legs did not support hypothesis #2. All starts received similar contributions to net forward lift from the arms. It was believed that the inclusion of a step-up approach would increase the contribution to net forward lift from the trunk and head to compensate for an inability to fully use the arm swing as in the traditional relay start. The lack of difference in the percent of net forward lift from each segment did not support this (see Table 1). However, a limitation of the relative momentum approach is that it represents a finite difference in momentum values. It does not provide an assessment of the changes in momentum throughout the movement.

An alternative to using net forward lift was considered. This technique examined the momentum relative to the initial point as it changed throughout the propulsive phase. These data for the arms indicated that they generated a higher peak forward lift contribution in the relay starts than in the flat start. The lack of an arm swing in the flat start was responsible for its inability to match the relay starts in peak forward lift contribution. However, assuming that the arm swing was not compromised during the step-up approach, the peak forward lift contribution should have been greater for the arms because the body was moving forward during either step-up approach. This forward velocity of the body should have added to the forward velocity of the arm center of mass caused by its radial motion. This would have increased the resultant velocity of the arm and thus increased its forward lift contribution. The similar peak values for the arm forward lift (see Table 2) in each relay start suggested that the arm swing was compromised when using a step-up approach.

The incorporation of a step-up approach in a swimming relay start resulted in a greater forward takeoff velocity. This suggested that it had advantages over the traditional arm swing relay start. The lack of increase in the contribution to forward lift from the arms when using a step-up approach suggested that future development of this technique should focus on an enhanced arm swing.

REFERENCES

Ae, M., & Shibukawa, K. (1980). *Japanese J. Phys. Ed.*

De Leva, P. (in press). *J. Biomechanics*

Enoka, R.M. (1971). *New Zealand J. Health, Phys. Ed. and Rec.*

Kayambashi, K. (1977). Unpublished Masters Thesis, Western Illinois University.

Maglischo, E.W. (1993). *Swimming Faster.*

A Three Dimensional Analysis of Flat, Slice and Topspin Serves in Tennis

Robert Schleihauf*, Deborah Lee, Aida Martinez, and Geraldine Ahern
*San Francisco State University, Kinesiology Department, S.F. CA 94132

Introduction

The service motion is purposefully varied by skilled performers in order to impart various degrees of spin and velocity to the ball. The coaching literature (i.e., Braden and Burns, 1977) indicates that three distinct types of serves are used to generate different types of spin on the ball: the *flat* serve involves minimal spin but maximal velocity; the *slice* serve involves sidespin; and the *topspin* serve involves a combination of topspin and sidespin. The scientific literature includes numerous three dimensional analyses of the flat serve (i.e., Elliott et al., 1995) but no studies were found which compare flat, slice and topspin serves for elite competitors. The purpose of this study is to compare 225 trails of flat, slice and topspin serve techniques across a sampling of 15 male and 10 female professional competitors and coaches. Further, the results obtained in this study are provided for use as a initial biomechanical database of tennis serves. This database is intended for use in the analysis of developing tennis performers.

Procedures

Data was collected on outdoor hard courts during normal daytime practice sessions. Each player was asked to perform ten flat, five slice and five topspin serves. The players were asked to hit the serves into a 1 meter wide by 2 meter long target area adjacent to the deuce court center line and service line but to otherwise perform the serves as they would under singles match conditions. The best three serves (as measured by depth and up the middle ball placement) of all types for each subject were selected for analysis.

Three dimensional video data was collected with a two camera setup. Each data trial was manually digitized on computers equipped with Targa 16 video digitizer boards. The video digitizing process involved data collection on 21 points: a background reference mark; 5 points on the racket (racket head, frame bottom, right side frame, left side frame, and grip); the ball; and 14 points on the body (toes, ankles, knees, hips, shoulders, elbows, and wrists).

Racket angle, impact vector, and arm joint angle data were collected as described in Schleihauf, 1996 (this volume). An extended action phase (EAP) was defined as beginning at the instant 5 video fields before the back scratch event and ending at the instant when the racket head advanced below the level of the shoulder. The range of motion (Rom) during the extended action phase was computed for all joints on the racket arm. The peak joint velocity (Jtv - peak rate of change of joint angle with respect to time) during the extended action phase was also computed for each joint.

Results and Discussion

The mean (M) and standard deviation (SD) data for the peak ball velocity magnitude and the peak racket head velocity magnitude are shown in table 1:

Table 1

	Ball Velocity (mps)				**Racket Velocity** (mps)			
	Male		Female		Male		Female	
	M	SD	M	SD	M	SD	M	SD
Flat	46.8	4.5	37.0	3.9	35.8	2.6	29.8	2.4
Slice	41.6	6.0	33.2	2.8	36.1	2.4	29.2	2.6
Topspin	37.6	4.5	30.7	3.6	36.4	2.7	28.9	2.3

An ANOVA analysis (2 x 3 gender by serve type with repeated measures on the second factor) for the racket head velocity data revealed that there is no significant difference between the racket speeds employed with flat, slice and topspin serves within the male and female groups.

The racket angle data (table 2) accounts for the differences in ball velocity across serve types. The direction of spin is given by the impact vector sidespin and topspin components (tables 3 and 4).

Table 2 - Racket Angle

	Male		Female		Both			
	M	SD	M	SD	M	SD	ANOVA	p
Flat	27	6	28	7	28	6	Type:	.000
Slice	40	6	40	6	40	6	Gender:	.916
Topspin	48	6	46	7	47	7	Interact:	.299

Note. Descriptive statistics are shown on the left side of the table; the ANOVA section (right side) shows the significance level for comparisons by type, by gender and for a type - gender interaction.

Table 3 - Impact Sidespin

	Male		Female		Both			
	M	SD	M	SD	M	SD	ANOVA	p
Flat	4.6	2.0	5.0	1.4	4.8	1.8	Type:	.000
Slice	9.7	2.2	9.3	1.3	9.6	1.9	Gender:	.495
Topspin	11.5	3.4	9.9	1.2	10.9	2.8	Interact:	.144

Table 4 - Impact Topspin

	Male		Female		Both			
	M	SD	M	SD	M	SD	ANOVA	p
Flat	6.9	2.1	5.4	2.3	6.3	2.3	Type:	.000
Slice	8.3	2.0	5.6	2.1	7.3	2.4	Gender:	.007
Topspin	11.4	2.3	7.8	2.3	10.0	2.9	Interact:	.005

Figure 1 shows a comparison of flat, slice, topspin and twist serve racket head patterns of motion and the spin vector components.

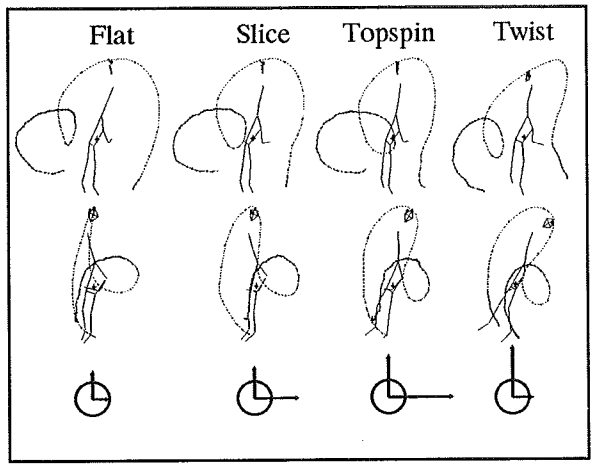

Figure 1. The top row shows the side view ; the second row shows the front view; the bottom row illustrates a rear view of the ball and the spin vector data. The columns for Flat, Slice and Topspin show data for a single subject. The column labeled Twist shows data for a second subject who had the most extreme topspin serve in the sample. The racket head pattern of motion is shown as a dotted line in the stick figure diagrams. The stick figure is shown at the moment of ball impact.

The location of the racket center point with respect to the body center of gravity at the moment of impact provides additional insight into differences in service techniques. The data for the ball impact distance in front of the body, and to the side of the body are shown in tables 5 and 6. All measures are normalized to express distances with respect to a 6 foot tall subject.

Table 5 - Ball Impact Distance - Side (cm)

	Male		Female		Both			
	M	SD	M	SD	M	SD	ANOVA	p
Flat	5.4	10	5.2	1.4	4.8	1.8	Type:	.000
Slice	7.1	11	10	1.3	9.6	1.9	Gender:	.217
Topspin	-16	20	0.3	1.2	10.9	2.8	Interact:	.008

Table 6 - Ball Impact Distance - Front (cm)

	Male		Female		Both			
	M	SD	M	SD	M	SD	ANOVA	p
Flat	23	9.6	24	8.3	23	8.9	Type:	.000
Slice	19	8.3	21	8.5	20	8.3	Gender:	.853
Topspin	13	8.0	12	6.8	13	7.4	Interact:	.457

Joint angle data for wrist extension-flexion (WExtFlx), radial-ulnar flexion (RadUln), supination-pronation (SupPro), elbow, shoulder horizontal abduction-adduction (SHAbAd), shoulder abduction-adduction (SAbAd) and shoulder external-internal rotation (SExtInt) were computed for each trial (table 7).

Table 7 - Joint Angle ROM and JTV

	Flat		Slice		Topspin	
Joint Angles	Rom	Jtv	Rom	Jtv	Rom	Jtv
WExtFlx	75	17	86	18	97	21
RadUln	103	33	103	31	110	36
SupPro	135	35	124	33	140	35
Elbow	114	22	113	22	121	23
ShAbAd	59	11	54	11	52	11
SAbAd	74	12	12	12	12	12

Note. Rom data is shown in degrees. Jtv data is shown in radians / sec. All data is for the combined male-female sample (no significant differences by gender were found for any Rom or Jtv measure).

The timing of the JTV data was measured with respect to the ball impact event. The absolute timing measures were normalized with respect to racket speed, and all timing values were expressed with respect to a 100 mile per hour serve. The sample average JTV sequence timing measures (in milli-seconds) for all serve types is shown in table 8.

Table 8. Peak JTV timing

JTV time (millisec)	Flat	Slice	Topspin
SAbAd	-103	-105	-100
Elbow	-50	-45	-45
RadUln	-25	-20	-38
SupPro	-12	-13	-27
WExtFlx	-2	2	2

The sequence of joint velocity peaks is the same for all serve types: SAbAd peaks first, followed by elbow, RadUln, SupPro and WExtFlx. Given the invariance of this joint sequencing pattern, it seems that the timing data on these five joints is a critical element in skillful service technique.

References

Braden, V. and Burns, B. (1977). *Vic Braden's tennis for the future*. Boston: Little, Brown.

Elliot, B., Marshall, R., and Guillermo, J.N.. (1995). Contributions of upper limb segment rotations during the power serve in tennis. *Journal of Applied Biomechanics*. 11: 433-442.

Acknowledgment

This research was supported by a grant from the United States Tennis Association. The researchers are also indebted to the players and coaches who made the project possible.

KINEMATIC AND KINETIC COMPARISON OF FULL-EFFORT AND PARTIAL-EFFORT BASEBALL PITCHING

G.S. Fleisig, N. Zheng, S.W. Barrentine, R.F. Escamilla, J.R. Andrews, L.J. Lemak
American Sports Medicine Institute, Birmingham, AL 35205

INTRODUCTION

The kinematics and kinetics of full-effort and partial-effort baseball pitching were compared. Differences may help determine the best use of partial-effort pitching in training, warm-up, and rehabilitation of baseball pitchers.

REVIEW AND THEORY

Partial-effort pitching is often used by baseball pitchers during training, warm-up, and rehabilitation. The intent of these throws is to progressively increase the loads on the athlete's body to the high levels produced in full-effort pitching while reinforcing proper timing, coordination, and movement patterns (Wilk et al., 1994). While the biomechanics of full-effort pitching has been well-documented (Dillman et al., 1993; Feltner et al., 1986; Fleisig et al., 1995; Fleisig et al., 1996; Sakurai et al., 1993; Werner et al., 1993), the biomechanics of partial-effort pitching has not been published. Although it has not be scientifically verified, many baseball experts believe that compared to full-effort pitching, partial-effort pitching has similar kinematics and decreased kinetics. The purpose of this study was to evaluate this hypothesis.

PROCEDURES

Twenty-seven healthy college baseball pitchers were tested. Their height was 1.84±0.07 m, and their mass was 81.6±8.8 kg. After providing informed consent, history, and physical information, each pitcher was tested in an indoor laboratory. Reflective markers were attached to 14 bony landmarks. After stretching, the subject threw three balls from seven different conditions (i.e. 21 total trials). The conditions were: 100% effort from a standard-height 10" mound, 75% effort from a 10" mound, 50% effort from a 10" mound, 180' crow-hop throw, 120' crow-hop throw, 60' crow-hop throw, 100% effort from a 13" mound. Only data from the first three conditions listed were used for this study. The order of conditions was randomized for each subject, and warm-up time was provided before testing each condition. For all trials on a mound, the subject pitched from a portable pitching mound (B&P Sports Products Inc., Amelia, OH) towards a strike zone ribbon located over a home plate at a distance of 18.4 m (60.5 ft) from the pitching rubber. Ball velocity was recorded with a Tribar Sport radar gun (Jugs Pitching Machine Company, Tualatin, OR).

Three dimensional coordinates during the second trial of each condition was determined with a four-camera 200 Hz automatic digitizing system (Motion Analysis Corporation, Santa Rosa, CA). Root mean-square error in calculating three-dimensional location was 1.0 cm. Using the digitized data, and published anthropometric data, 23 kinematic (Figure 1) and kinetic (Figure 2) parameters were calculated as previously described (Dillman et al., 1993; Fleisig et al., 1995; Fleisig et al., 1996). A one way repeated measures Analysis of Variance was performed, using a Bonferroni t-test to identify significant ($p<0.05$) differences between full-effort pitching (i.e. control group) and the other conditions.

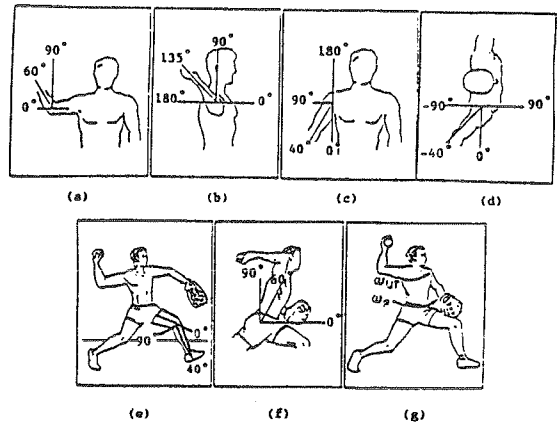

Figure 1. Kinematic parameters: (a) elbow flexion; (b) shoulder external; (c) shoulder abduction; (d) shoulder horizontal adduction; (e) lead knee flexion; (f) forward trunk tilt; and (g) pelvis angular velocity (ω_P) and upper torso angular velocity (ω_{UT}).

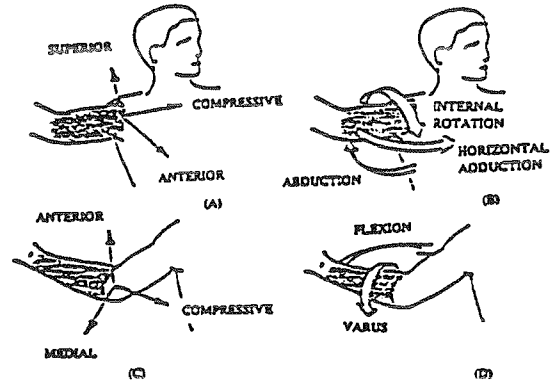

Figure 2. Kinetic parameters: (a) shoulder forces; (b) shoulder torques; (c) elbow forces; and (d) elbow torques.

RESULTS

Means and standard deviations for all parameters are presented in Table 1. Significant differences between partial-effort (75%, 50%) and full-effort (100%) pitches are indicated. In order to simplify interpretation of the results reported in Table 1, mean values for 75% and 50% effort pitches were expressed as percentages of values for 100% pitching. A summary of these percentages, approximated within 5%, is shown in Table 2.

DISCUSSION

Coaches, therapists, trainers, and pitchers often discuss pitching at "75%" or "50%." However, what 75% or 50% means is not well-defined. In this study, pitchers were given similar vague instructions, and their kinematics and

Table 1. Kinematic and kinetic parameters for 100%, 75%, and 50% effort pitching

	100% effort	75% effort	50% effort
Instant of foot contact			
Stride length between ankles (%height)	71±4	70±4	69±4
External rotation	42±26	36±30	36±28
Elbow flexion	90±18	86±17	84±17*
Knee flexion	47±10	41±10*	40±9*
Arm cocking phase			
Pelvis velocity	620±70	570±70*	540±80*
Upper torso vel.	1170±80	1080±80*	1030±100*
Max. elbow flexion	105±10	102±10	101±11*
Max. horizontal adduction	20±8	22±8*	24±7*
Max. external rotation	172±12	169±12*	167±11*
Elbow varus torque	54±7	44±7*	41±7*
Shoulder internal rotation torque	55±10	46±8*	42±8*
Shoulder anterior force	330±40	310±50	280±50*
Arm acceleration phase			
Elbow extension velocity	2350±250	2130±280*	1940±270*
Shoulder internal rotation velocity	7290±1090	6400±1050*	5820±1110*
Elbow flexion torque	52±7	47±8*	44±8*
Instant of ball release			
Elbow flexion	25±7	29±8*	30±7*
Horiz. adduction	9±10	13±10*	15±9*
Trunk angle above horizontal	59±8	64±9*	66±9*
Knee flexion	36±12	44±10*	49±10*
Ball speed (mph)	79±4	73±5*	68±6*
Arm deceleration phase			
Elbow compressive force	800±90	680±100*	590±100*
Shoulder compressive force	910±110	790±130*	700±130*
Shoulder posterior force	360±200	280±120	270±160

* Significantly different ($p<0.05$) from 100% effort.

Table 2. General description of 75% and 50% effort pitching, relative to 100% effort pitching.

	75% effort	50% effort
Ball speed	90%	85%
Arm and trunk speed	90%	85%
Mechanics	Increased horizontal adduction. Reduced arm rotation, knee flexion, and trunk lean.	
Forces and torques	85%	75%

kinetics were quantified. At 75% effort, pitchers produced approximately 90% of the velocity and 85% of the force and torque as produced during full-effort. At 50% effort, pitchers produced approximately 85% velocity and 75% force/torque. Reduced effort pitching also corresponded with reduced arm rotation during cocking, increased horizontal adduction, and a more upright trunk (less knee flexion and less trunk lean) at ball release.

These results were similar to a previous study of partial golf swings which found that compared to a full golf swing, a 50% effort swing generated less backswing rotation, 75% as much torque (based upon angular acceleration), and 87% as much velocity (Lemak et al., 1994). Standard deviations were noticeably greater during partial golf swings, compared to during full swings. In the present study, standard deviations were fairly consistent among the different effort throws. This implies that while golfers had varied interpretations of partial-effort, pitchers had fairly consistent interpretation of partial effort.

In summary, reduced force/torque and reduced rotation were produced during partial-effort pitching. As a result, reduced body and ball velocity were generated. Although there were some differences in mechanics, pitching with reduced effort appears to be useful for a pitcher in training or rehabilitation who does not want to overload his arm.

REFERENCES

Dillman, C.J. et al. J Orthop Sports Phys Ther, 18(2), 402-408, 1993.

Feltner, M. et al. Int J Sport Biomech, 2(4), 235-259, 1986.

Fleisig, G.S. et al. Am J Sports Med, 23(2), 233-239, 1995.

Fleisig, G. S. et al. J Appl Biomech, 12(2), 207-224, 1996.

Lemak, L.J. et al. Science and Golf II, (pp. 14-19),E&FN Spon, 1994.

Werner, S.L. et al. J Orthop Sports Phys Ther, 17(6), 274-278, 1993.

Wilk, K.E. et al. The Athlete's Shoulder, (pp. 669-678), Churchill Livingstone, 1994.

ACKNOWLEDGEMENTS

The authors would like to thank B&P Sports Products for donating the mounds. The assistance in data collection and analysis provided by Andy DeMonia and Phillip Sutton is also greatly appreciated.

KINEMATIC AND KINETIC COMPARISON OF BASEBALL PITCHING FROM A MOUND AND THROWING FROM FLAT GROUND

G.S. Fleisig, R.F. Escamilla, S.W. Barrentine, N. Zheng, J.R. Andrews
American Sports Medicine Institute, Birmingham, AL 35205

INTRODUCTION

The kinematics and kinetics of baseball throwing were compared between pitching from a mound and throwing from flat ground. Differences may help explain why most baseball throwing injuries involve pitchers. Results may also help determine the appropriateness of flat-ground throwing drills (such as long toss) for pitchers, as well as considerations for changing players between pitching and non-pitching positions.

REVIEW AND THEORY

Most overuse throwing injuries in baseball involve the pitcher. Consequently, previous motion analysis research in baseball throwing has focussed on the pitcher (Dillman et al., 1993; Elliott et al., 1986; Feltner et al., 1986; Fleisig et al., 1995; Fleisig et al., 1996; Pappas et al., 1995; Pappas et al., 1985; Sakurai et al., 1993; Vaughn, 1985; Werner et al., 1993). Conversely, minimal research has been published on baseball throwing mechanics utilized by non-pitchers (Atwater, 1979; Elliott et al., 1990; Hay, 1985), and no research has reported mechanics used by pitchers during flat ground drills. Although minimal scientific data are available, many baseball experts believe that throwing mechanics from a mound and from flat ground are similar; therefore, throwing from flat ground (in competition or practice) is appropriate training for a pitcher. The purpose of this study was to evaluate the hypothesis that minimal kinematic and kinetic differences exist between pitching from a mound and throwing from flat ground.

PROCEDURES

Twenty-seven healthy college baseball pitchers were tested. Their height was 1.84±0.07 m, and their mass was 81.6±8.8 kg. After providing informed consent, history, and physical information, each pitcher was tested in an indoor laboratory. Reflective markers were attached bilaterally to the distal end of the mid-toe, lateral malleolus, lateral femoral epicondyle, greater trochanter, lateral tip of the acromion, and lateral humeral epicondyle. A reflective band was wrapped around the wrist on the throwing arm and a reflective marker was attached to the ulnar styloid of the non-throwing arm. After stretching, the subject threw three balls from seven different conditions (i.e. 21 total trials). The conditions were: 100% effort from a standard-height 10° mound, 180° crow-hop throw, 120° crow-hop throw, 60° crow-hop throw, 75% effort from a 10° mound, 50% effort from a 10° mound, 100% effort from a 13° mound. Only data from the first four conditions listed were used for this study. The order of conditions was randomized for each subject, and warm-up time was provided before testing each condition. For all trials on a mound, the subject pitched from a portable pitching mound (B&P Sports Products Inc., Amelia, OH) towards a strike zone ribbon located over a home plate at a distance of 18.4 m (60.5 ft) from the pitching rubber. Velocity of the ball as it left the pitcher's hand was recorded with a Tribar Sport radar gun (Jugs Pitching Machine Company, Tualatin, OR).

Three dimensional coordinates during the second trial of each condition was determined with a four-camera 200 Hz automatic digitizing system (Motion Analysis Corporation, Santa Rosa, CA). Root mean-square error in calculating the three-dimensional location of markers randomly placed within the calibrated space was 1.0 cm. Using the digitized data, and published anthropometric data, 23 kinematic (Figure 1) and kinetic (Figure 2) parameters were calculated as previously described (Dillman et al., 1993; Fleisig et al., 1995; Fleisig et al., 1996). A one way repeated measures Analysis of Variance was performed, using a Bonferroni t-test to identify significant ($p<0.05$) differences between pitching from a mound (i.e. control group) and the other conditions.

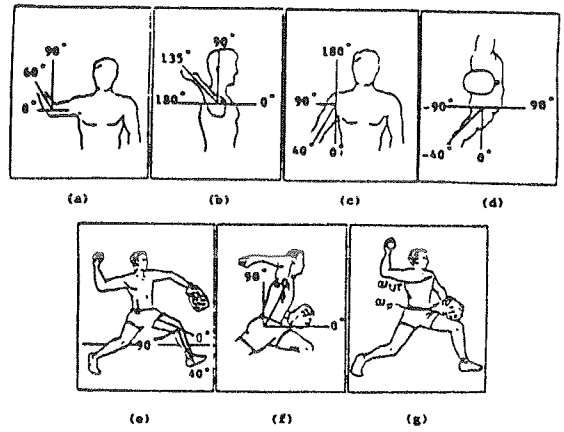

Figure 1. Kinematic parameters: (a) elbow flexion; (b) shoulder external; (c) shoulder abduction; (d) shoulder horizontal adduction; (e) lead knee flexion; (f) forward trunk tilt; and (g) pelvis angular velocity (ω_p) and upper torso angular velocity (ω_{UT}).

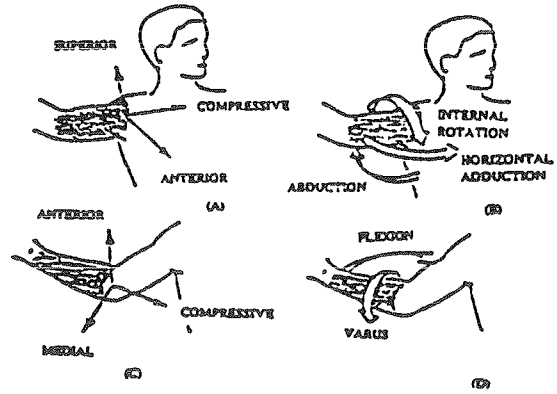

Figure 2. Kinetic parameters: (a) shoulder forces; (b) shoulder torques; (c) elbow forces; and (d) elbow torques

Table 1: Mound pitching and flat ground throwing parameters. Angles, velocities, forces, and torques in °, °/s, N, and Nm, respectively, except where indicated.

	Mound	180' Flat	120' Flat	60' Flat
Instant of foot contact				
Stride length between ankles (%height)	71±4	66±5*	66±4*	67±4*
External rotation	42±26	30±31*	28±30*	27±32*
Elbow flexion	90±18	87±19	88±19	89±18
Knee flexion	47±10	39±10*	37±12*	39±12*
Arm cocking phase				
Pelvis velocity	620±70	620±70	620±100	630±70
Upper torso vel.	1170±80	1120±90*	1110±110*	1150±100
Max. elbow flexion	105±10	108±10	106±10	108±9
Max. horizontal adduction	20±8	22±8*	22±8*	21±8
Max. external rotation	172±12	170±12	167±11*	170±12
Elbow varus torque	54±7	59±15*	54±12	51±8
Shoulder internal rotation torque	55±10	59±16	53±11	54±10
Shoulder anterior force	330±40	350±80	330±70	340±70
Arm acceleration phase				
Elbow extension velocity	2350±250	2340±290	2290±320	2330±270
Shoulder internal rotation velocity	7290±1090	6830±1150	6740±1240*	7060±1240
Elbow flexion torque	52±7	49±8	50±8	52±8
Instant of ball release				
Elbow flexion	25±7	25±7	27±8	26±8
Horiz. adduction	9±10	9±10	11±9	9±11
Trunk angle above horizontal	59±8	67±10*	67±10*	64±10*
Knee flexion	36±12	36±12	34±14	34±13
Ball speed (mph)	79±4	N/A	N/A	76±4
Arm deceleration phase				
Elbow compressive force	800±90	720±100*	710±120*	780±100
Shoulder compressive force	910±110	830±120*	820±130*	890±110
Shoulder posterior force	360±200	310±100	320±150	350±150

* Significantly different ($p<0.05$) from pitching.

RESULTS AND DISCUSSION

Contrary to the belief that pitching and flat ground throwing mechanics are the same, several significant differences were found (Table 1). Throwing from flat ground corresponded with a shorter stride and less shoulder external rotation at foot contact. The drop of the mound appears to give the pitcher more time to stride forward a greater distance, and more time to externally rotate the shoulder. Arm and body motions and kinetics during arm cocking and acceleration were similar between mound and flat ground throwing.At the instant of ball release, a pitcher's trunk was more vertical when throwing from flat ground. However, relative to the throwing surface, the trunk angle was the same for 60' throwing from flat ground and pitching from a mound. This is because the trunk was 5° less upright for pitching from the mound, but the mound was sloped 5° downward. The trunk was 3° more upright for the longer distance throws, which may help the athlete throw the ball with a slightly more upward trajectory in order to get more distance.

During arm deceleration, compressive forces generated at the elbow and shoulder to resist distraction were less in long distance flat throws than in 60' mound or flat throws. This may be related to the low incidence of throwing injuries in non-pitchers.

Reduced deceleration forces in long toss support the concept that these are good training drills for pitchers. The biomechanics of these throws are similar to pitching; however, when converting from other positions or from flat ground training to pitching from a mound, an athlete should lengthen his stride and tilt his trunk forward.

REFERENCES

Atwater, A.E. et al. Exer Sport Sci Rev, 7, 43-85, 1979.
Dillman, C.J. et al. J Orthop Sports Phys Ther, 18(2), 402-408, 1993.
Elliott, B. et al. J Human Mov Stud, 18(1), 1-23, 1990.
Elliott, B. et al. Int J Sport Biomech, 2(1), 20-28, 1986.
Feltner, M. et al. Int J Sport Biomech, 2(4), 235-259, 1986.
Fleisig, G.S. et al. Am J Sports Med, 23(2), 233-239, 1995.
Fleisig, G. S. et al. J Appl Biomech, 12(2), 207-224, 1996.
Hay, J.G. Biomechanics of Sport Techniques, Prentice-Hall, 1985.
McLeod, W.D. et al. Phys Ther, 66(12), 1901-1904, 1986.
Pappas, A.M. et al. Am J Sports Med, 23(3), 312-315,1995.
Pappas, A.M. et al. Am J Sports Med, 13(4), 216-222,1985.
Sakurai, S. et al. J Appl Biomech, 9(1), 47-65, 1993.
Werner, S.L. et al. J Orthop Sports Phys Ther, 17(6), 274-278, 1993.

ACKNOWLEDGEMENTS

The authors would like to thank B&P Sports Products for donating the mounds. The assistance in data collection and analysis provided by Andy DeMonia and Phillip Sutton is also greatly appreciated. In addition, the authors wish to thank the pitchers and coaches from the University of Alabama, the University of Alabama at Birmingham, and Samford University for their participation in this study.

THE MECHANICS OF CATTING IN HIGH JUMPING

J. Dapena

Department of Kinesiology, Indiana University, Bloomington, IN 47405.

INTRODUCTION

The forces exerted on the ground during the high jump takeoff determine the maximum height that the center of mass (c.m.) will reach and the angular momentum of the body. In the air, the athlete makes a twisting somersault rotation which leads to a supine layout position over the bar (Figure 1). A defective twist rotation can lead to a tilted position at the peak of the jump, with one hip lower than the other, and this can reduce the effectiveness of the bar clearance. To find solutions for this problem, it is first necessary to understand how the twist rotation is produced in normal jumps. Previous work has shown that about half of the twist rotation is produced by angular momentum, and the other half by action-and-reaction rotations, or "catting" (Dapena, 1995). The purpose of this project was to analyze the mechanics of catting in high jumping.

THEORETICAL CONSIDERATIONS

The angular momentum of a system is $\mathbf{H} = \sum m_i (\mathbf{r}_i \times \mathbf{v}_i)$, where m_i is the mass, and $\mathbf{r}_i$ and $\mathbf{v}_i$ the location and velocity vectors of each particle of the system relative to a reference point, typically the system c.m. The equation implies that the angular momentum of each particle is proportional to the rate at which it sweeps area about the c.m. (Hopper, 1973). This concept can facilitate the analysis of catting. Consider a person that stands initially motionless on a turntable supported by a frictionless vertical axle, with the right arm pointing forward (Figure 2, image a). The subject then rotates the arm clockwise (b), brings it closer to the trunk (c), rotates it counterclockwise (d), and finally extends it forward again (e). At the end, the body-plus-turntable system has the same configuration as in image a, but it is positioned more counterclockwise, even though the total angular momentum of the system was zero throughout the maneuver. Between images a and b, the particles that make up the right arm swept large clockwise areas about the vertical axis that passes through the middle of the turntable. (See the bottom row of images in Figure 2.) Between b and c the arm moved directly toward the c.m., and did not sweep any area. Between c and d the particles of the arm swept counterclockwise areas, but the flexed configuration of the arm made them smaller than the clockwise areas previously swept between a and b. The area swept by the arm between d and e was zero, since the arm moved directly away from the c.m. Thus, over the entire catting maneuver the right arm swept a net clockwise area. Since the angular momentum of the whole system was zero, the turntable and the rest of the body swept counterclockwise areas in compensation. The result was the final counterclockwise orientation shown in image e.

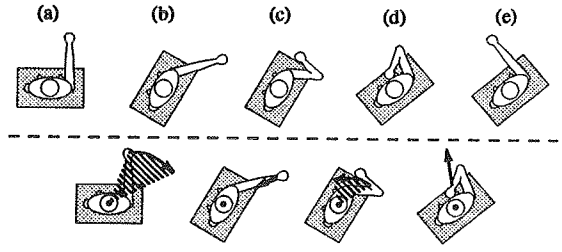

Figure 2: Catting maneuver on a turntable.

The rotation produced by catting is more difficult to see in high jumping than in the turntable example, because in the high jump it is masked by the somersault and twist rotations produced by the angular momentum. To understand how catting works in high jumping, we need to visualize it in isolation from the other motions of the body. It will also be useful to quantify the contributions to catting by the various parts of the body.

PROCEDURES

Ten normal high jumps were studied: five trials by men, and five by women. Body landmark locations were calculated using 3D film analysis. The body was modeled as a 16-segment system. (See Dapena, 1995.) Center of mass location and angular momentum were calculated following a method based on Dapena (1978). The

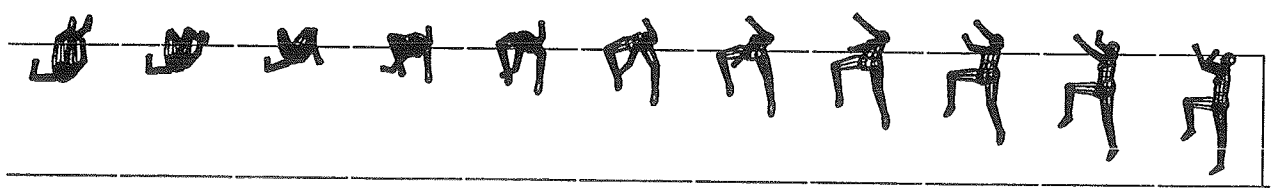

Figure 1: Sequence of a normal high jump, viewed from a direction perpendicular to the plane of the bar and the standards. The sequence runs from right to left.

orientation of the longitudinal principal axis was computed following Hinrichs (1978).

To separate the catting from the rotations produced by the angular momentum, the jump needs to be viewed from a rotating reference frame R_H. R_H somersaults with the longitudinal axis of the athlete, and twists about the longitudinal axis at the angular velocity ω_{TH} associated with the twisting component of angular momentum. In each frame, the angular momentum vector **H** was projected on the longitudinal principal axis to compute its twisting component, H_T. The value of ω_{TH} for each frame was computed using the equation $\omega_{TH} = H_T / I_L$, where I_L was the moment of inertia of the body about its longitudinal axis. The cumulative twist rotation of R_H was computed by integration of ω_{TH} over time. The view of the jump from reference frame R_H was produced using computer graphics.

The angular velocity of catting ω_C is the difference between ω_{TH} and the angular velocity of twisting of the hip axis. It can be shown that $\omega_C = {}^PH / I_L$, where ${}^PH$ is the apparent twisting angular momentum of the body relative to a rotating reference frame R_P that somersaults with the longitudinal axis and twists with the hip axis. (Note: The term "apparent" is used because this angular momentum was measured relative to a rotating reference frame, which negates some of the properties of true angular momentum.) In turn, ${}^PH / I_L = (\sum {}^PH_i) / I_L = \sum ({}^PH_i / I_L)$, where ${}^PH_i$ is the apparent twisting angular momentum of each segment with respect to R_P. Thus, the contribution of each segment to ω_C can be expressed by ${}^PH_i / I_L$. The cumulative contributions of each arm, of each leg, and of the head-plus-trunk to catting between takeoff and the peak of the jump were calculated by integrating the corresponding ${}^PH_i / I_L$ values over time.

RESULTS AND DISCUSSION

Table 1 shows that the total amount of catting was larger in the women than in the men. This was consistent with previous results (Dapena, 1995). The separation of catting into contributions by the various body parts shows that the right arm generally favored catting, while the left arm hindered it; the combined contribution of the arms to catting was quite small. In contrast, both legs made clear positive contributions to catting, especially the right leg; the legs were responsible for almost all of the catting.

Table 1: Contributions to catting between takeoff and the peak. (N = 5 men, 5 women; mean ± s.d., in degrees)

	r.arm	l.arm	r.leg	l.leg	hd+tk	arms	legs	total
men	7±3	-7±4	16±3	5±2	2±1	0±3	21±4	23±6
women	6±5	-3±2	22±6	8±6	1±2	2±4	30±4	34±5

Figure 3 shows a high jump, viewed from rotating reference frame R_H. In this view, the apparent twisting component of angular momentum is zero, but the orientation of the body in the last image seems clearly more counterclockwise than in the initial one. This is the result of catting. The sequence shows how the legs produced the catting. At takeoff, the right leg was in front of the body, and the left leg was directly below the body. After takeoff, the right leg moved outward toward the right, and then backward. The left leg was first moved behind the body through flexion at the knee; then it opened out toward the left. The motions of both legs involved the sweeping of clockwise areas, and made the rest of the body rotate counterclockwise. This is what produced the markedly counterclockwise orientation of the hips at the end of the sequence.

The dominant role of the legs in the production of catting has important implications for the diagnosis and correction of problems in the twist rotation.

REFERENCES

Dapena, J. *J. Biomech.* 11:251-256, 1978.

Dapena, J. *Conf. Proc. ASB* :35-36, 1995.

Hinrichs, R. *Principal axes and moments of inertia of the human body: an investigation of the stability of rotary motions.* M.A. Thesis, University of Iowa, 1978.

Hopper, B.J. *The mechanics of human movement*, American Elsevier, 1973.

ACKNOWLEDGEMENTS

This project was funded by grants from the U. S. Olympic Committee and U.S.A. Track & Field.

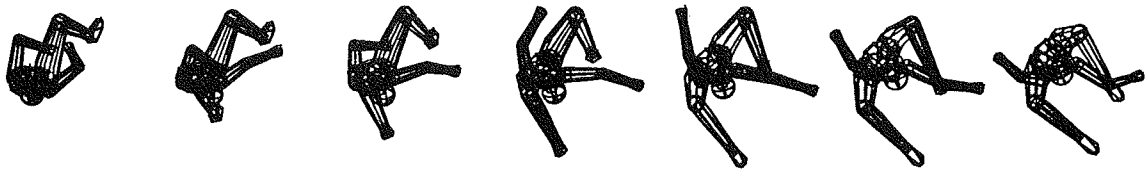

Figure 3: Sequence of a normal high jump, between takeoff and the peak of the jump, viewed from a rotating reference frame R_H which somersaults with the longitudinal axis and twists with the angular velocity due to the angular momentum of the system. The sequence runs from left to right, and it shows the rotation due to catting, isolated from the other rotations.

GENERATION AND TRANSFER OF ANGULAR MOMENTUM IN THE JAVELIN THROW

M.K. LeBlanc and J. Dapena
Department of Kinesiology, Indiana University, Bloomington, IN 47405.

INTRODUCTION

At the instant of release in a right-handed javelin throw, the center of mass (c.m.) of the javelin is located in a high position to the right of the thrower, and it is traveling forward and upward at high speed. These conditions require rather large amounts of angular momentum in the javelin and throwing arm, as well as appropriate ratios among the three-dimensional components of the angular momentum. The angular impulses of the forces exerted by the ground on the athlete's feet during the throw generate angular momentum for the combined thrower-plus-javelin system. This angular momentum can be separated into two parts, associated respectively with the motions of the body-minus-throwing arm ("body-minus-arm") and of the throwing arm-plus-javelin ("arm-plus-javelin") subsystems. The purpose of this project was to study the changes in the system angular momentum in the course of the throw, and the transmission of angular momentum to the arm-plus-javelin.

METHODS

At the end of the run-up, a right-handed thrower makes a cross-over step, lands on the right foot (RTD), plants the left foot (LTD), and releases the javelin. (See the sequences in Figure 1.) The athlete is in single-support (SS) between RTD and LTD, and generally in double-support (DS) between LTD and release. A period including the SS and DS phases of eight of the finalists in the men's javelin throw competition at the 1995 USA Track and Field National Championships was filmed using standard three-dimensional (3D) film analysis procedures.

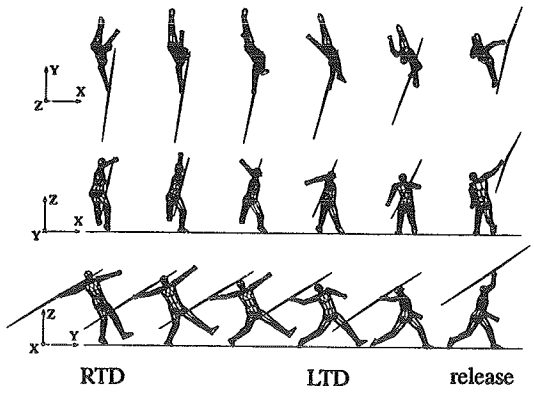

Figure 1: Sequences of a javelin throw.

Two throws were analyzed for each subject. Digitized data from the film images were used to calculate the coordinates of 21 body landmarks and three javelin landmarks. The 3D coordinates were expressed in an orthogonal reference frame in which the X axis pointed toward the right (normal to the runway), the Y axis pointed forward, and the Z axis pointed upward. The coordinate data were smoothed using quintic spline. Center of mass locations and the angular momentum values of the body segments and of the javelin were calculated following a method based on Dapena (1978). The location of the javelin c.m. was computed using information from Hubbard and Bergman (1989).

The SS and DS phases were each divided into two equal time periods. An inverse dynamics approach was used to calculate the average forces made by the ground on the system in each of the four periods. The 3D angular momentum values of the body-minus-arm, arm-plus-javelin and complete system, all relative to the whole-system c.m., were calculated for five instants: (1) RTD, (2) the mid-point of SS, (3) LTD, (4) the mid-point of DS, and (5) release.

RESULTS AND DISCUSSION

Average angular momentum values for the 16 throws are shown in Table 1. To facilitate this discussion, the terms "clockwise" (CW) and "counterclockwise" (CCW) will replace the signs of the X, Y and Z angular momentum components; the directions will correspond to views from the right, from behind and from overhead for the H_X, H_Y and H_Z angular momentum components, respectively.

At RTD the system had a CCW H_X of 13 kg·m²/s. Ground reaction forces in the YZ plane changed this to a CW value at LTD (35 kg·m²/s), and to an even larger CW value at release (67 kg·m²/s). During the first half of SS, the average ground reaction force exerted on the system pointed backward and upward (F_Y = -480 ± 200 N; F_Z = 1230 ± 190 N). Since the right foot was almost directly below the c.m. during this period, the horizontal force was mainly responsible for the CW angular impulse (28 N·m·s) received by the system. During the second half of SS, the foot was clearly behind the c.m., and the ground reaction force was near vertical (F_Y =20 ± 200 N; F_Z = 1010 ± 180 N). Therefore the CW angular impulse received by the system during this period (20 N·m·s) was produced mainly by the vertical force. During DS the system received large backward and upward ground reaction forces (F_Y = -1850 ± 320 N and F_Z = 2200 ± 230 N during the 1st half of DS; F_Y = -1540 ± 480 N and F_Z = 2400 ± 320 N during the 2nd half of DS). The resultant must have passed below the system c.m. to produce the CW angular

impulses observed during both halves of the DS (14 N·m·s and 18 N·m·s, respectively) which increased the CW angular momentum of the system to its final value at release.

At RTD, the H_Y of the system had a CW value of 8 kg·m²/s. During SS the average ground reaction forces in the XZ plane pointed upward and slightly toward the left (F_X = -50 ± 140 N and F_Z = 1230 ± 190 N during the 1st half of SS; F_X = -110 ± 120 N and F_Z = 1010 ± 180 N during the 2nd half of SS). The angular impulses were CCW (13 N·m·s and 17 N·m·s in the 1st and 2nd halves of SS, respectively), implying that the resultant force passed to the right of the system c.m. This must be attributed to the position of the support foot, which was located to the right of the c.m. The angular impulses changed the system H_Y to 23 kg·m²/s CCW at LTD. The overall change in H_Y between LTD and release was small. The average ground reaction forces pointed upward and moderately toward the right during this period (F_X = 380 ± 290 N and F_Z = 2200 ± 230 N during the 1st half of DS; F_X = 430 ± 280 N and F_Z = 2400 ± 320 N during the 2nd half of DS). The left foot was planted clearly to the left of the c.m., and data from Deporte & Van Gheluwe (1988) has shown that most of the ground reaction force is exerted through the left foot during DS. This strongly suggests that the combination of the left foot position and the direction of the resultant force is what made the force pass near the system c.m., and led to the rather small changes in H_Y during DS.

The system H_Z was very small during SS; at LTD, it had a CCW value of 3 kg·m²/s. During DS the average ground reaction forces in the XY plane pointed backward and moderately toward the right (F_X = 380 ± 290 N and F_Y = -1850 ± 320 N during the 1st half of DS; F_X = 430 ± 280 N and F_Y = -1540 ± 480 N during the 2nd half of DS). The angular impulses were CCW (14 N·m·s and 6 N·m·s in the 1st and 2nd halves of DS, respectively), implying that the resultant force passed to the left of the system c.m. The angular impulses changed the system H_Z to 23 kg·m²/s CCW at release.

Table 1. Angular momentum (kg·m²/s). (Means ± s.d.)

Times:	1 (RTD)	2	3 (LTD)	4	5 (release)
H_X					
body-minus-arm	13 ± 4	-15 ± 4	-30 ± 7	-30 ± 6	-26 ± 9
arm-plus-javelin	0 ± 1	0 ± 1	-5 ± 1	-19 ± 2	-41 ± 5
system	13 ± 4	-15 ± 5	-35 ± 7	-49 ± 5	-67 ± 9
H_Y					
body-minus-arm	7 ± 4	-6 ± 5	-24 ± 6	-18 ± 7	-8 ± 7
arm-plus-javelin	0 ± 0	0 ± 0	1 ± 1	2 ± 3	-13 ± 5
system	8 ± 4	-6 ± 5	-23 ± 6	-16 ± 7	-21 ± 6
H_Z					
body-minus-arm	2 ± 3	0 ± 4	-1 ± 2	5 ± 4	5 ± 6
arm-plus-javelin	1 ± 1	0 ± 1	4 ± 2	12 ± 2	19 ± 5
system	3 ± 4	0 ± 3	3 ± 3	17 ± 5	23 ± 9

Having determined how the system obtains angular momentum, we will now examine how angular momentum was transmitted to the arm-plus-javelin in order to produce a large velocity of the javelin at release. At RTD, all the H_X of the system was in the body-minus-arm, and most of the changes produced in H_X during SS by the ground reaction forces also went into the body-minus arm; only a small CW amount of H_X was transmitted to the arm-plus-javelin, in the 2nd half of SS. During DS the system received a large CW angular impulse, but the H_X of the body-minus-arm did not change much; in essence, all the additional H_X obtained from the ground during DS was transmitted through the body to the arm-plus-javelin.

At RTD, all the H_Y of the system was in the body-minus-arm, and during SS practically all of the CCW changes in H_Y produced by the ground reaction forces also went into the body-minus arm. Between LTD and release there was only a small overall change in the system H_Y, but during the 2nd half of DS there was a marked transfer of CCW H_Y from the body-minus-arm to the arm-plus javelin.

During most of the SS, the system H_Z was close to zero. At LTD, the system had a small amount of CCW H_Z, and essentially all of it was in the arm-plus javelin. During DS the ground reaction forces increased the CCW H_Z of the system. Part of the H_Z obtained during the first half of DS stayed in the body-minus-arm, and part was transmitted to the arm-plus-javelin; all the additional H_Z obtained during the 2nd half of DS was transmitted through the body to the arm-plus-javelin.

CONCLUSIONS

The angular momentum of the throwing arm-plus-javelin at release is closely related to the velocity of the javelin, one of the most important factors affecting the result of the throw. The results of this project have improved our understanding of the mechanisms through which the ground reaction forces exerted on the feet of the thrower generate the angular momentum of the thrower-plus-javelin system. The results have also shown that the angular momentum of the system is produced during both single-support and double-support, while the transmission of angular momentum to the throwing arm-plus-javelin occurs almost exclusively during double-support.

REFERENCES

Dapena, J. *J. Biomech.* 11:251-256, 1978.

Deporte, E. and B. Van Gheluwe. *Biomechanics XI-B* (pp.575-581). Free University Press, 1988.

Hubbard, M. and C.D. Bergman. *Int. J. Sport Biomech.* 5:40-59, 1989.

KINEMATICS PRIOR TO CONTACT IN LANDINGS PRECEDED BY ROTATION

Barry A. Munkasy, Jill L. McNitt-Gray and Michele D. Welch
USC Biomechanics Research Laboratory, Department of Exercise Sciences
University of Southern California, Los Angeles, CA 90089-0652

INTRODUCTION

Evaluation of gymnastics performance is largely defined by a gymnast's ability to successfully land complex forward and backward rotating skills. Unfortunately, a high incidence of injury has been associated with load experienced during the landing phase of these skills (Linder & Caine, 1990). During optional competition, gymnasts have chosen to perform backward rotating skills more often than forward rotating ones. Preference towards backward rotating skills may be attributable to the higher landing success rate for backward rotating skills than for forward rotating skills (McNitt-Gray, 1992). In addition, this preference towards performance of backward rotating skills may also be associated with the ability of the gymnast to generate momentum prior to the skill while facing backward, the ability of the gymnast to view the surface for a longer period when preparing for contact, or may be associated with the differences in load distribution within the lower extremity during contact observed between landings of forward and backward rotating skills (Nigg 1985; McNitt-Gray & Nelson, 1988; McNitt-Gray et al., 1991; Sidaway, McNitt-Gray, & Davis, 1989; McNitt-Gray, 1992; Wilkerson & Smith, 1992).

The purpose of this study was to examine mechanisms gymnasts use to prepare for landings preceded by forward and backward rotation. We hypothesized the ability of the gymnast to prepare for contact may be compromised by the differences in visual conditions and segment between landings preceded by forward rotation as compared to backward rotation. Since critical actions for attenuation of forces experienced within 20 to 40 ms after contact must occur prior to contact (Lees 1981; Melvill-Jones et al., 1971; Viitasalo et al., 1987) we've chosen to examine absolute joint angular velocities and relative segment velocities of the lower extremity during front and back salto landings. This approach has proven to be useful in providing insight regarding preparation for contact strategies used during simple drop landings (McKinley, 1992; McKinley et al., 1992) and reduced force landings (Munkasy et al., 1992).

PROCEDURES

Twelve healthy male gymnasts, who were members of the US Men's Junior National Team, volunteered to serve as subjects (mean (SD) mass 61.3 (9.4) kg., height 1.67 (0.05) m, age 15.75 (0.87) yr., experience 8.9 (1.9) yr.., practice time 19.6 (5.1) hr./week). During data collection, each subject successfully landed two front tucked saltos and two back tucked saltos using their normal competitive landing style. Both tasks were initiated from a height of 0.72 meter above the top surface of a regulation gymnastics landing mat (0.1 m thick, 100 ILD) fully supported by a Kistler force plate (0.6 x 0.9 m). A successful landing was one in which the gymnast landed without taking a step. Segment kinematics were recorded using high speed video (200 fps; NAC Motion Analysis). Segment end points were digitized using a video based data acquisition system (Peak Performance, Inc.). Each coordinate of the digitized body landmarks were digitally filtered using a fourth order Butterworth filter with a cut-off frequency derived by the method of Jackson (1979). Segment centers of mass were computed using the data of Zatsiorsky et al., (1983). Data analyzed were relative segment velocities of the thigh, shank, and foot and joint angular velocities of the hip, knee, and ankle observed 10 ms prior to contact during front and back salto landings. Relative segment velocities were calculated as follows:

$$v_{T/H} = v_T - v_H$$
$$v_{S/K} = v_S - v_H - v_{K/H}$$
$$v_{F/A} = v_F - v_H - v_{K/H} - v_{A/K}$$

where v represents vertical velocity; / means with respect to; T, S, and F represent thigh, shank, and foot centers of mass; and H, K, and A represent the hip, knee, and ankle joints.

RESULTS AND DISCUSSION

In contrast to drops (Munkasy et al., 1992) the lower extremity center of mass fell at a faster rate than the total body center of mass for both front and back saltos. Intuitively, this must occur because the legs must be brought underneath the trunk prior to contact.

For back salto landings absolute joint angular velocity data indicated that the ankle, knee, and hip

were all flexing prior to contact. However, in front saltos the knee and hip were extending (see Figure 1). In terms of relative segment velocity the foot was falling slower than the ankle and the shank was falling slower than the knee for both movements. However, in front saltos the thigh was falling faster than the hip while the antithesis was true for back saltos (see Figure 2).

Rotation had a differential effect on preparation for landing. While strategies for drop landings and back saltos are similar in terms of absolute joint angular velocity (McKinley, 1992; McKinley et al., 1992) and relative segment vertical velocity (Munkasy et al., 1992) it appears that fronts are different. The uniqueness of front rotation landings from the kinematic perspective presented here and the kinetic perspectives presented elsewhere (McNitt-Gray et al., 1991; McNitt-Gray, 1992; Wilkerson & Smith, 1992) may partially explain the gymnasts' avoidance of and lack of success with forward rotating skills (McNitt-Gray, 1992). While avoidance may also in part explain the noted kinetic variability (McNitt-Gray et al., 1993; Wilkerson & Smith, 1992), a difference in variability for the kinematics examined was not found.

Vision is thought to play a major role in preparation for contact (Lee et al., 1981). During activities involving rotation (especially in the forward direction) time to view the landing surface may be reduced due to the anatomical orientation of the head and eyes and the need to complete rotations with limited angular momentum and flight time (McNitt-Gray, 1992). The differences found here may be associated with differences in viewing time or biomechanical constraints associated with the need to stop the linear and angular momentum present at contact with the landing surface without stepping.

These results indicate that landing forward rotation skills pose a different challenge and may require a different landing strategy than do drop landings and back saltos. To overcome these differences and the lack of success associated with forward rotation skills landing drills may need to be emphasized.

REFERENCES

Jackson. *IEEE Trans. Bio. Eng.*, 26, 122-124, 1979.
Lee et al., Nature (London) 293, 293-294, 1981.
Lees. *Eng. Med.*, 10, 204-211, 1981.
Linder & Caine (1990). *CJSS*, 15(4), 254-261.
McKinley, P. *Tutorials in Motor Behavior II*, (pp. 713-723), 1992.
McKinley et al., *Exp. Brain Res.*, 90, 427-440, 1992.
McNitt-Gray, *Int. J. Sport Biomech*, 7, 201-204, 1991.
McNitt-Gray, (1992). *USGF Sport Science Congress.*
McNitt-Gray, *J Biomech.*, 26, 1037-1046, 1993.
McNitt-Gray & Nelson, (1988). *MSSE* Sup, 1988.
McNitt-Gray et al., (1991). *Proceedings of the ASB*
McNitt-Gray et al., (1993). *Proceedings of the ASB.*
Melvill Jones et al. *J. Physiol.*, 219, 709-727, 1971.
Munkasy et al. *ASB Proceedings.*, 1992.
Nigg (1985). *Sprts Med.* 2, 367-379.
Sidaway et al., (1989). *Eco. Psy.* 1(3) 253-264.
Viitasalo et al. *Biomechanics X-B,* (pp. 695-700), 1987.
Wilkerson & Smith (1992). *USGF Sport Science Congress.*
Zatsiorsky et al. *Biomechanics VIII-B*, 1152-1159, 1983.

ACKNOWLEDGMENTS

The authors wish to acknowledge the support of the US Olympic Committee, the Division of Sports Science at the US Olympic Training Center in Colorado Springs, CO, USA Gymnastics, and the work of the members of the USC Biomechanics Laboratory.

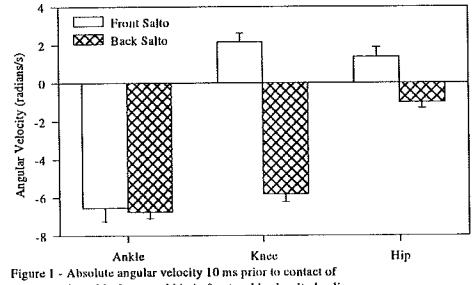

Figure 1 - Absolute angular velocity 10 ms prior to contact of the ankle, knee, and hip in front and back salto landings.

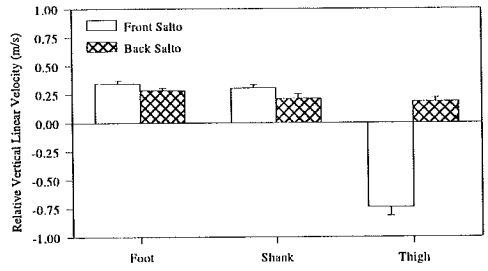

Figure 2 - Relative vertical velocity 10 ms prior to contact of the foot, shank, and thigh in front and back salto landings.

ESTIMATED EFFECTS OF CARPAL MALALIGNMENT IN JUVENILE RHEUMATIOD ARTHRITIS ON WRIST JOINT MOMENTS

Roger V. Gonzalez[1], Marianne K. Nieuwenhuis[2], Paul J.M. Helders[2], and Thomas S. Buchanan[1]

[1]Departments of Biomedical Engineering and Physical Medicine & Rehabilitation, Northwestern University, and Sensory Motor Performance Program, Rehabilitation Institute of Chicago, 345 East Superior St., Chicago, IL 60611
[2] Department of Pediatric Physiotherapy, University Hospital for Children and Youth, the Wilhelmina Children's Hospital, Utrecht, The Netherlands

INTRODUCTION

A muscle's performance as it spans the wrist is critical. In Juvenile Rheumatoid Arthritis (JRA), displacement of the carpal bones in an ulnar direction affects the movement and configuration of the joint and, most certainly, the paths of the muscles. These altered paths in turn affect the joint's strength. The resulting muscle pathokinesiology probably intensifies the condition, as restoration of the carpal alignment at the wrist is rarely observed. The role of muscle path and force during the progression of JRA at the wrist joint is rarely considered. When so, only a superficial qualitative perspective is attempted and discussed. To more effectively understand the role of wrist muscle function in the malalignment process of the wrist, a detailed representation of the bone and muscle geometry is needed.

REVIEW AND THEORY

Juvenile Rheumatoid Arthritis generally affects more than one joint. Wrist involvement is quite common and is only second to the knee in occurrence (Ansell and Kent, 1977). Functionality of patients is quite limited during the acute/sub-acute phase of the disease and joint movement limitations can remain even after the disease has remitted. Since wrist deformity can also be an important cause of more distal deformities (Evans *et al.*, 1991), factors that can potentially worsen the deformity of the joint should be studied.

The development of carpal ulnar displacement is believed to be the result of a loss of ligamentous constraint in combination with the compressive forces of the muscles acting across the wrist and the inclination angle of the radius (Linscheid, 1986). Relative ulnar shortening and/or slanting of the radius spiphysis, typical in children with JRA, *may* be an additional factor. Interestingly, the progression of wrist malalignment cannot be fully explained by current muscle pathokinesiological concepts (Nieuwenhuis *et al.*, 1995). The lack of a quantitative JRA wrist investigation is probably due to the shortage of appropriate analysis tools which are needed for such an examination. Advancements in musculoskeletal analysis tools (Delp et al., 1995) and the current state of knowledge on normal wrist function (Gonzalez *et al.*, 1996; Delp *et al.*, 1996) make a quantitative analysis of the JRA wrist possible.

PROCEDURES

This preliminary JRA wrist model is a modified version of the normal wrist model developed by Gonzalez *et al.* (1996). This model represents the three-dimensional geometry of the bones (ulna, radius, carpal, and metacarpals), kinematics of the joints, and the lines of action and force-generating properties of the 15 muscles that span the wrist joint. The model was implemented using the musculoskeletal modeling software (SIMM) described by Delp et al. (1990). With the use of SIMM, we have developed two JRA wrist models (Figure 1).

Since the normal wrist model accurately represents normal function of wrist strength and its individual muscle contributions (Gonzalez *et al.*, 1996), modifications were made to the model to represent JRA carpal displacement. Part of the challenge at this stage of ulnar displacement is to investigate the contribution of altered muscle paths to joint moment as they relate to the modified skeletal geometry.

For two patients posterior-anterior x-ray images of the forearm and hand at different radial-ulnar deviation angles were used to modify the normal wrist model. They provided the location of the carpal and metacarpal bones with respect to the radius and ulna. Model modifications were based on existing x-ray images from current patient populations at Wilhelmina Children's Hospital in Utrecht, The Netherlands. By using multiple x-ray images we were able to adequately describe the alignment of the radius, ulna, carpus, and metacarpals in the model. The axes of rotation for flexion-extension and

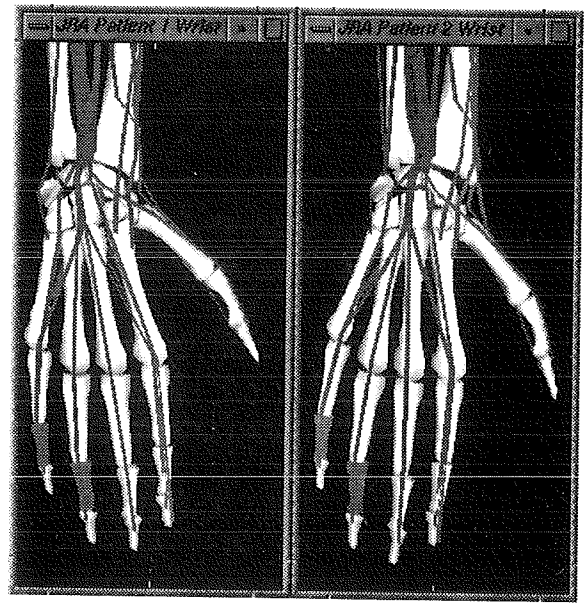

Figure 1. Graphical models of two maligned wrists developed from anterior-posterior x-ray images of children with juvenile rheumatoid arthritis. Left wrist is JRA patient 1 and right wrist is JRA patient 2. Graphical models were develop on SIMM (Delp et al., 1995).

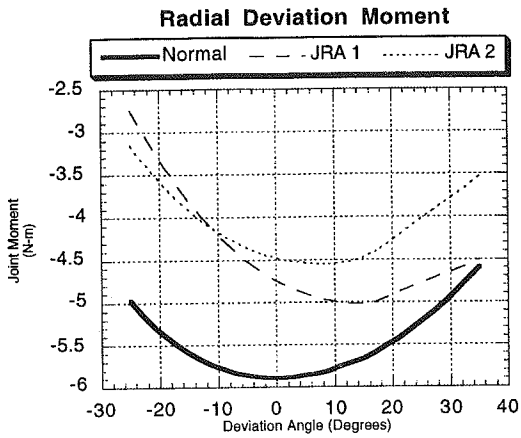

Figure 2. Maximum isometric radial deviation moments estimated by the model for a normal and that of patients JRA 1 and JRA 2.

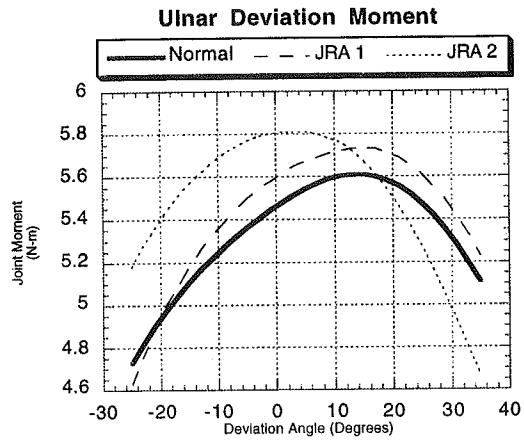

Figure 3. Maximum isometric ulnar deviation moments estimated by the model for a normal and that of patients JRA 1 and JRA 2.

radial-ulnar deviation were not modified from the normal model, that is, they remained in the same location relative to the ulna.

RESULTS

The model estimated the maximum isometric wrist moments in both radial-ulnar deviation and flexion-extension. The largest moment changes were estimated in radial (Figure 2) and ulnar (Figure 3) deviation while negligible effects were estimated in flexion. Radial deviation moments were decreased throughout the range of motion by an average of 1.5 and 1.1 N-m for JRA Patients 1 and 2, respectively. An increase in ulnar deviation moment was estimated for both patients with the exception of the estimation for Patient 2 at large ulnar deviated positions. On average, the increase in ulnar deviation moment was approximately 0.1 N-m for both patients. Extension moments decreased on average 0.4 and 0.2 N-m for JRA Patients 1 and 2, respectively. Changes in the flexion moment were negligible. Figure 4 shows the average percent change in the moments for both degrees-of-freedom. The model estimated a 2 to 3% increase in ulnar moments and a 19 to 26% decrease in radial deviation moments. For flexion-extension moments, the model also estimated very little change in flexion moments (1 to 2%) and a decrease of 3 to 8% in extension moments.

DISCUSSION

The larger changes in maximal isometric moments in the radial deviation direction estimated by the model were due to the translation of the carpal bones in the ulnar direction. This ulnar translocation of the entire hand moved the insertion points for the wrist muscles in an ulnar direction and decreased the magnitude of the radial moment arms, thus decreasing the net joint moment. A similar increase was expected in the ulnar deviation moment yet was not estimated by the model, likely because the largest contributors to radial deviation did not have substantial ulnar deviation moment arms. The kinesiological changes in musculotendon paths as depicted by the model in JRA wrists need verification by means of MRI data before changes in joint moment, solely due to the realignment of the carpus, can be estimated.

REFERENCES

Ansell B.M. *et al. Skel Radiology*, 1, 129-44, 1977

Delp S.L. *et al. Comp Bio Med,* 25, 21-34, 1995

Delp S.L. *et al. J Biomech*, 1996 (in press)

Evans D.M. *et al. J Hand Surg*, 16, 293-304, 1991

Gonzalez R.V. *et al. J Biomech*, 1996 (accepted)

Linscheid R.L. *Clin Orthop Rel Res,* 202, 27-38, 1986

Nieuwenhuis M.K. *et al. Physio Theo Prac*, 1996 (in press)

ACKNOWLEDGMENTS

This work is supported, in part, by NIH F32AR08389 and a grant from the Arthritis Foundation.

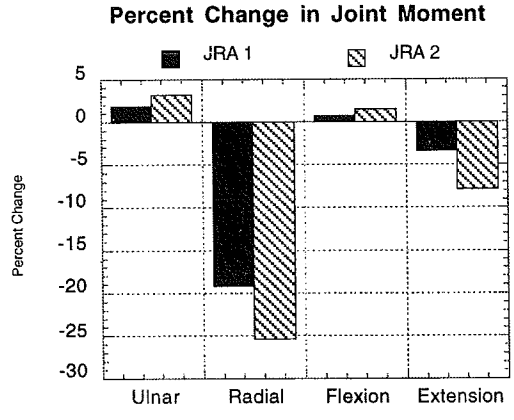

Figure 4. Average percent change in joint moment between a normal wrist and that of patients JRA 1 and JRA 2.

A PROTOCOL FOR AUTOMATED GENERATION OF A CT-BASED FINITE ELEMENT MODEL OF THE DISTAL RADIUS

C. Puttlitz[1], B. Adams[2], V. K. Goel[1]
[1]Department of Biomedical Engineering, University of Iowa, Iowa City, IA 52242
[2]Department of Orthopaedic Surgery, University of Iowa Hospitals and Clinics, Iowa City, IA 52242

INTRODUCTION

A protocol was developed that allows for automated creation of finite element (FE) models of the distal radius. The geometry and material properties of the model are generated from computed tomography (CT) data and result in an accurate replication of the peri-articular region. The model was subjected to loads that have been reported by previous in vitro studies. The resulting stress distributions are consistent with previous findings, however, the location of the maximum stress is more distal than found previously.

REVIEW AND THEORY

Fully three-dimensional FE models of the distal radius are not commonly found in the literature. This is surprising considering the unusually high incidence of orthopaedic challenges that are associated with this area. Many of these challenges involve the distal metaphysis and/or articular surface regions. Thus, accurate replication of the articular surface and the metaphysis in the FE model is essential if the predicted stresses and strains are to have clinical validity. Modeling of these areas is difficult due to the highly irregular articular geometry and varying thickness of the cortical shell in the metaphysis. To date, CT data has been used to generate models of the distal radius. However, these models are either two-dimensional and/or do not attempt to replicate the peri-articular geometry. Described herein is a method for automated creation of FE models of the distal radius wherein the geometry of the articular surface and the metaphysis is closely replicated. The model has been used to predict where the peak stresses and strains occur under neutral flexion loading conditions.

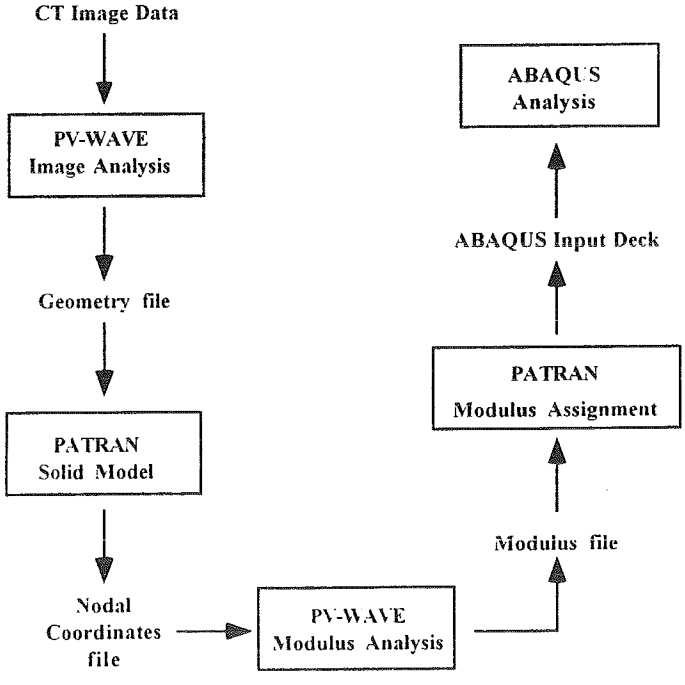

Figure 1: Flow Chart of Mesh Generation

PROCEDURES

The geometry of the distal radius was obtained from CT data. The scan was performed on a fresh frozen cadaver radius (64 year old white male) using a Siemans Somatom DR/H scanner (Siemens Medical Systems, Iselin, NJ) with a previously-described protocol[1] (scanner settings: 125 kV, 286.48 mA, 2ms pulses, 1.0 mm slice thickness, 10 pixels/mm).

Each CT slice was analyzed using code written in PV-WAVE (Precision Visuals, Boulder, CO). The goal of this analysis was to automatically determine the endosteal and periosteal borders of the slice. These borders were easily determined after applying a greyscale threshold and a Sobel filter (3x3 mask). Rays were sent radially inwards towards the area centroid of the slice and the bony borders were detected by gray scale differences. The coordinates of the points and other commands for creation of the solid model were written out to a "geometry" file.

The geometry file was used as an input deck by PATRAN (PDA Engineering, Costa Mesa, CA). The solid model was meshed and the elements, their nodes,

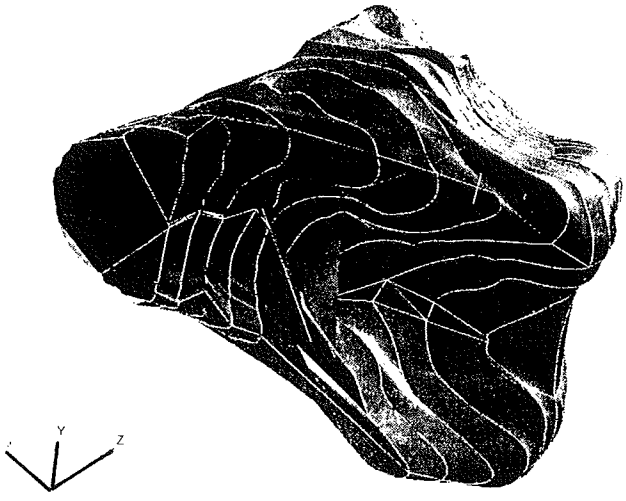

Figure 2: PATRAN Solid Model of Distal Articular Surface

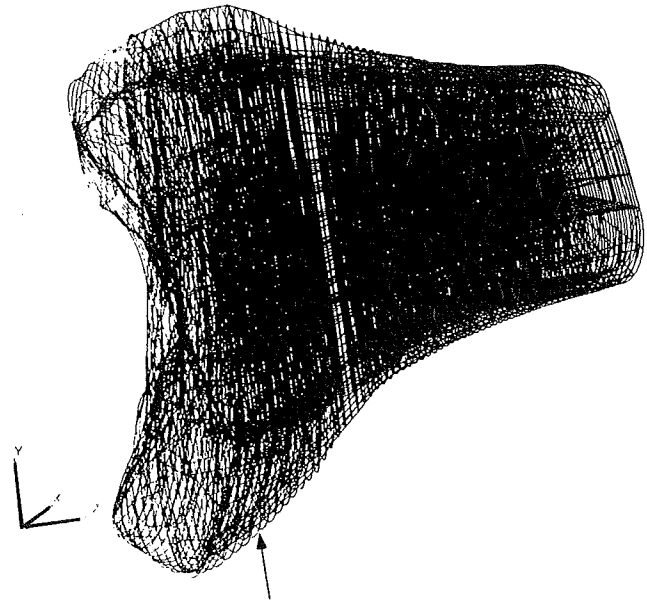

Figure3: Resulting FE Mesh Showing Point of Highest von Mises Stress (arrow)

and the nodal coordinates were then written out to a "nodal coordinates" file. This file was read by another PV-WAVE program that computed the elastic moduli for each element from the CT data. Pixel gray scale values were converted to elastic modulus values via a gray scale to density conversion and the Carter-Hayes[2] elastic modulus-density relation. The elastic modulus of the element was obtained from the average of these calculated moduli. The elemental elastic moduli were then inputted into the PATRAN FE model and the resulting ABAQUS input deck was generated. All analyses were performed using ABAQUS (Hibbitt, Karlsson and Sorenson, Pawtucket, RI).

A 100 N load was applied such that 80% was transmitted through the scaphoid fossa and 20% through the lunate fossa, with the direction of the load being perpendicular to the articular surface. The proximal end of the model was constrained against displacement.

RESULTS

The resulting FE model consisted of 12870 hexahedral elements with 13307 nodes. Under neutral loading conditions, the model predicts that the highest von Mises stresses are experienced in the dorsal metaphyseal shell (Fig. 2).

DISCUSSION

The predictions made with this model are consistent with those found by a previous model[3]. However, our model predicts the maximum intraosseous stresses are located more distally than has been reported by the earlier model. This is consistent with clinical findings. Colles' fractures commonly involve the distal metaphyseal cortical shell due to the highly reduced thickness of the shell in this area. The modeling protocol allows for accurate reproduction of both the geometry and thickness of the distal metaphyseal shell, resulting in more accurate replication of the peri-articular geometry and cortical thickness.

A protocol has been developed such that automated cadaver-specific FE models can be generated. The protocol could be applied to produce patient-specific FE models, thus allowing for clinical fracture risk determination. Future work includes validation of the protocol via physical experiments and mesh convergence refinement study.

REFERENCES

1) Adams et al., *JOR* 13, 690-9, 1995.
2) Carter and Hayes, *JBJS* 59, 954-62, 1977.
3) Viegas et al., *J Hand Surg* 14A, 458-65, 1989.

ACKNOWLEDGMENTS

This work is supported by a grant from Johnson and Johnson Orthopaedics, Raynham, MA.

FORCE SHARING AMONG FINGERS ACTING IN PARALLEL AS A MODEL OF THE REDUNDANCY PROBLEM

Zong-Ming Li, Mark L. Latash, Vladimir M. Zatsiorsky
Biomechanics Laboratory, The Pennsylvania State University, University Park, PA 16802

INTRODUCTION

Since the work by N. Bernstein (1935), the problem of how the large number of muscles in the skeletomotor system are controlled to produce a required common output has received considerable attention (Theeuwen, et al., 1994; Maier, et al., 1995). We studied the human hand as an example of such a redundancy system (Gurram, et al., 1995; Kinoshita, et al., 1995; Radwin, et al., 1992).

PROCEDURES

Four quartz force transducers were used to measure individual finger forces in various tasks. Ten university students, who gave informed consent, participated in the experiment. The subjects had no previous history of trauma to the upper limbs. The subjects were asked to press as hard as possible with the index (I), middle (M), ring (R), and small (S) fingers separately and, then, in combination of IM, IMR, and IMRS. The subjects performed 10 trials for each of the IM, IMR, and IMRS tasks, trying to follow a target ramp total force that was presented on a monitor screen.

RESULTS

Figure 1 shows the force production in the tasks for a typical subject. The force-force correlation coefficients among fingers in the IM, IMR and IMRS tasks showed a strong linear relationship among fingers when they worked in concert to produce the force. The force-force curves and corresponding regression lines in the IMRS task for a subject are displayed in Figure 2.

The intercepts for the regression lines were negligibly small for each series of trials for each subject. The regression lines were expressed as

$$F_k = \alpha_k F_{Index}$$
$$k = Middle,\ Ring,\ or\ Small\ fingers$$

where F_k is the force for the involved fingers in the task. The force-force ratio was I:M = 1:1.02 for the IM task. In the IMR and IMRS tasks, the ratio values were I:M:R = 1:1.22:0.65, and I:M:R:S = 1:1.08:0.72:0.39, respectively.

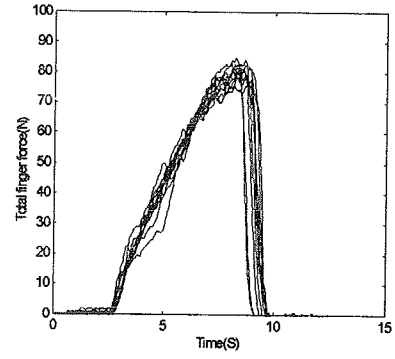

(a)

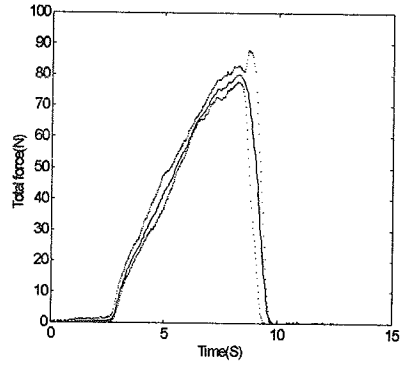

(b)

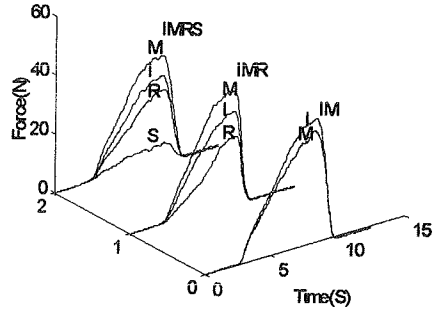

(c)

Figure 1. Force curves for a typical subject. (a) Total force produced in the IM task for ten attempts. (b) Average total force (±SD) from the ten attempts in the IM task; (c) Average individual finger forces in the IM, IMR and IMRS tasks.

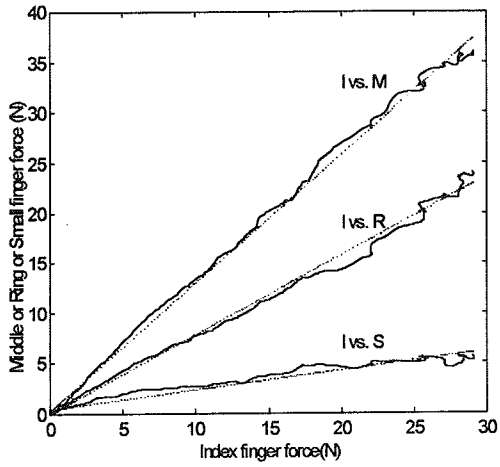

Figure 2. Finger force-force curves and their linear approximation in the ramp period in the IMRS task. (The straight dotted lines are linear regression lines for the force-force curves.)

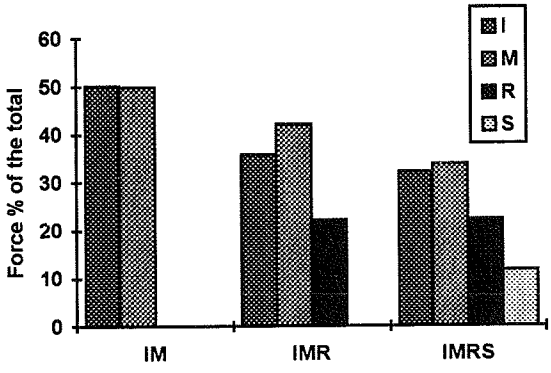

Figure 3. Force sharing of the involved fingers in the tasks, % of the total force.

The force sharing among fingers was calculated as

$$S_{Index} = 1 / \Sigma(1+\alpha_k)$$

$$S_k = \alpha_k / \Sigma(1+\alpha_k)$$

The force sharing among fingers in different tasks is shown in Figure 3.

Each finger could only generate its own maximal force when it pressed independently. The *force actualization* was defined as a percentage of maximal force produced by an individual finger in a multi-finger task compared to the maximal force generated by the same finger in the single-finger task, the maximal force, F_{mm}. As the task changed from the IM to IMR, the force actualization of the index finger decreased significantly, while the value for the middle finger maintained. As the task changed from the IMR to IMRS, the force actualization of the index and middle fingers decreased significantly, while the value for the ring finger was constant. The added finger helped the force actualization of the neighboring finger significantly (Figure 4).

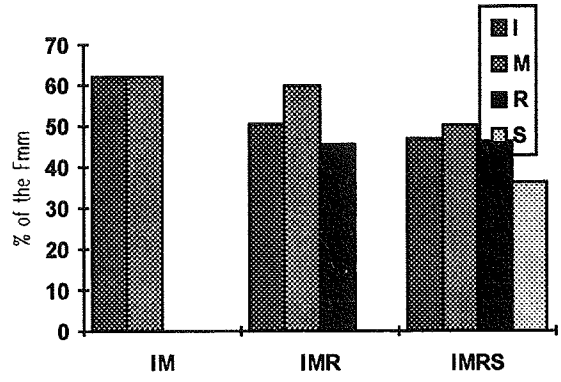

Figure 4. Force actualization of the involved fingers in the tasks, % of the single-finger maximal force, F_{mm}.

SUMMARY

1. A simple force sharing pattern exists among fingers in the force production tasks. The forces produced by individual fingers are linearly related to each other. The central nervous system scales the forces of the involved fingers at the starting of force production.
2. Sharing among the fingers is dependent on the number of fingers involved.
3. There is a finger interaction. Adding a finger to a task leads to a drop of force produced by individual fingers. This drop is typically not seen in the immediate neighbor fingers.
4. Each finger can only produce its maximal force when pressing independently. A portion of the single-finger maximal force, F_{mm}, can only be realized when fingers are combined to do the press task.
5. Coordinating factors (neural and/or biomechanical) exist which help solve the problem of redundancy.

REFERENCES

Gurram R, et al., Ergonomics, 38(4): 684-699, 1995

Kinoshita H, et al., Ergonomics, 38(6): 1212-1230, 1995

Maier MA et al., Exp Brain Res, 103:108-122, 1995

Maier MA, et al., Exp Brain Res, 103:123-136, 1995

Radwin R, et al., Ergonomics, 35(3): 275-288, 1992

Theeuwen M, et al., Exp Brain Res, 101:493-505, 1994

MORPHOLOGY AND KINEMATICS OF THE METACARPOPHALANGEAL JOINT

H. Nägerl[1], D. Kubein-Meesenburg[2], J. Fanghänel[3], C. Ziehn[2]

[1]IV. Phys. Institute, University of Göttingen, D-37073 Göttingen
[2]Department of Orthodontics, University of Göttingen, D-37085 Göttingen
[3]Institute of Anatomy, University of Greifswald, D-17489 Greifswald

INTRODUCTION

The aim is to develop outlines of a kinematical theory of the human finger based on the curvature morphology of the articulating surfaces.

REVIEW AND THEORY

Generally advanced models of finger kinematics presuppose that the MCP has a hinge axis which is stationary in the os metacarpale (e.g. Leinsje et al., 1995). This implies that the articular surfaces of caput metacarpale and basis phalangis have congruent radii of curvature. But there are some papers (e.g. Tamai et al., 1974) which do not agree with this assumption. Literature review suggests the following hypotheses:

a) The articular surface of the caput metacarpale is egg-shaped.
b) The concave surface of the basis phalangis is spherical.
c) The radii of curvature of these two articulating surfaces differ from one another: The caput has significantly smaller radii.

If hypothesis c) was true the kinematics of the MCP would be determined by an overlapping dimeric link chain whose one pivot is stationary in relation to the os metacarpale while the second is fixed in reference to the phalanx.

PROCEDURE

The study was performed on human autopsy material which was stabilized by a specific solution that largely preserves the osseous and articular structures (Schultz & Fanghänel, 1962). 40 MCPs from five right and left hands of female corpses were analysed. By methods from dentistry precise superhard plaster copies were produced. They served for the production of negatives out of elastomer, which could easily sectioned in sagittal or horizontal planes. The section surfaces were copied by stamp ink onto a sheet of paper. The articular contours were thus visible and precisely measurable (fig. 1).

RESULTS AND DISCUSSION

The sagittal and the transversal contour of the fossa phalangis and the transversal contour of the caput could be fitted by circles in their entire functional range. The sagittal contour of the caput, however, evidently differs from a circle. Functionally, two regions must be distinguished which are often separated by an eyecatching groove G (40% of the specimens): a dorsal region, on which the extensor tendon lies and that does not articulate with the fossa, and the articulation region, whose curvature increases continuously palmarly. Dividing this part in half, the sagittal articular contour was approximated by two circular arcs that have a common tangent t at the point of transition T. Thus, we measured four sagittal radii of contours K_{s1-4} (fig. 1). These data were evaluated by a threefold variance analysis with the categorial variables: K = the four contours, F = the type of finger, H = right or left hand. The radii only differed significantly with respect to K (step $\alpha < 0.001$). Type of finger, right or left hand as well as all interactions (K*F, K*H, F*H, K*F*H) do not have any significant effects. For category K, the average radii (and SDs) are:
r_{ds} = 3.9mm (0.9mm), r_{cs1} = 6.9mm (0.9mm), r_{cs2} = 5.8mm (0.9mm) and r_{bs} = 10.3mm (3.3mm).
Regarding the hypotheses:
a) The caput is egg-shaped. The mere fact that the sagittal contour had to be divided up into three pieces K_{s1}, K_{s2}, K_{s3} in order

to determine the morphology of curvature confirms the hypothesis.
Hypothesis b) is proven wrong, since the sagittal radius is on average 1.4mm greater than the transversal one.
Hypothesis c) is clearly confirmed: The differences in radii between the articulating surfaces, sagittally ($<r_{bs} - r_{cs1}>$ = 3.4mm and $<r_{bs} - r_{cs2}>$ = 4.5mm) and also transversally ($<r_{bt} - r_{ct}>$ = 1.6mm) emerge to be highly significant. Thus, it is proven that the MCP cannot be a simple "ball-in-socket" joint with three degrees of freedom. In main sagittal function the MCP has <u>two</u> degrees of freedom. It can structurally be modelled a dimeric link chain: the phalanx can rotate around the center of the caput M_C and simultaneously around the center M_B of its basis (fig. 2). Resulting angle $\alpha = \alpha_C + \alpha_B$. The link R is the difference in radii of curvature. R coincides with the line of the compressive joint force. In an equilibrium without external forces the force line of the extensor and that of the flexors must meet line R in the same point. This conditions that the set of possible equilibria is characterized by an functional relation between the rotations α_C and α_B (fig. 3). Since $d\alpha_C$ and $d\alpha_B$ have the same direction the momentary rotational center P_S lies on R between M_C and M_B. During flexion the contact point K moves dorsally on the fossa and the joint space C_V must open at the <u>palmar</u> side of the MCP.

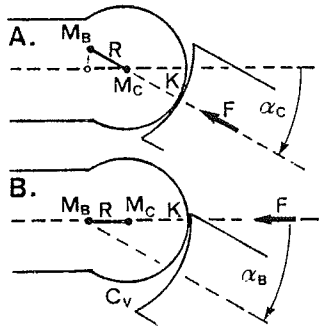

Fig. 2: Fundamental rotations of the MCP.
A. Rotation of phalanx, link R and force line F around M_C. Controlled by force.
B. Rotation of phalanx around M_B. Link R and force are stationary. Palmarwards the joint space C_V is opened. Controlled by torque.

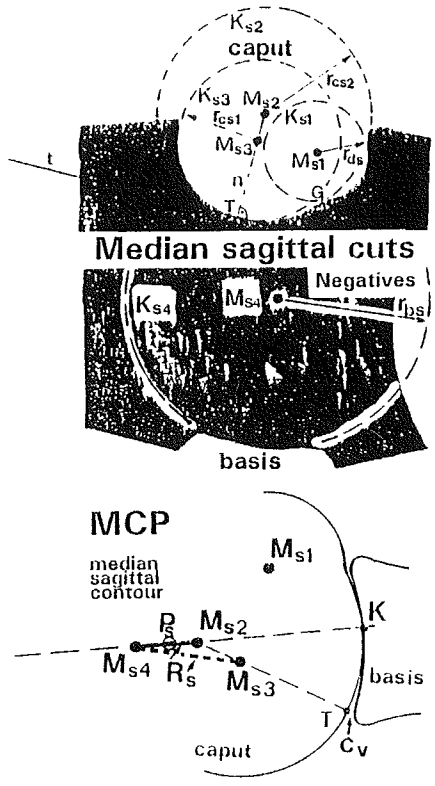

Fig. 1: Negatives of median sagittal contours: caput, basis. Reconstruction of stretched MCP.

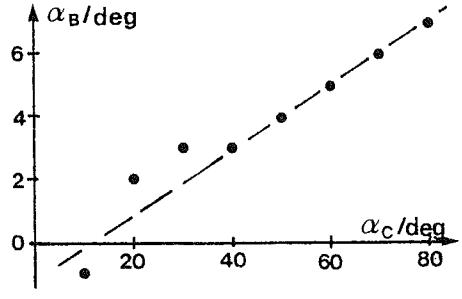

Fig. 3: Static equilibria yield a functional relation between the two fundamental rotations α_C and α_B. The inclination $d\alpha_B/d\alpha_C$ determines the position of mamentary rotational axis.

REFERENCES

Leijnse JNAL et al. J. Biomechanics, 28, 237-249, 1995.
Tamai K et al., J Hand Surg [Am] 13, 521-529, 1988.
Schultz E. & Fanghänel J., Z med Lab 3 329-332, 1962.

CARPAL TUNNEL PRESSURE: EFFECTS OF WRIST FLEXION/EXTENSION

P.J. Keir[1], J.M. Bach[1], J.W. Engstrom[2] and D.M. Rempel[1]
[1] Ergonomics Program, Department of Medicine, University of California, San Francisco, Richmond, CA 94804
[2] Department of Neurology, University of California, San Francisco, San Francisco, CA, 94143

INTRODUCTION

The relationship between wrist angle and elevated carpal tunnel pressure (CTP) has been reported for the end ranges of flexion and extension as far back as 1947 (Brain *et al.* 1947). However, the dose-response relationship of wrist angle to CTP has not yet been determined. This study examined, in detail, the relationship between wrist flexion-extension angle and CTP by simultaneous measurement in 20 healthy volunteers.

REVIEW AND THEORY

Carpal tunnel syndrome (CTS), the most common upper extremity neuropathy in the workplace, has been strongly associated with a sustained elevation of carpal tunnel pressure (Szabo & Gelberman, 1987). Awkward work postures are commonly reported in the workplace and may lead to sustained elevated CTP.

The relationship between wrist posture and CTP has typically been examined using a minimum of data points, i.e. neutral wrist posture, end range flexion, and end range extension. These postures are not often reached in daily activities and do not allow determination of a dose-response relationship.

There are several factors which have the potential to increase CTP. Cadaveric research has demonstrated that the movement of the lumbricals can increase pressure by occupying space within the carpal tunnel (Cobb *et al.*, 1994) and that muscles of the forearm have a large effect on carpal tunnel pressure by acting on and within the carpal tunnel (Keir *et al.*, 1995). Static fingertip loading has also been shown to increase CTP (Rempel *et al.*, 1994).

From our external view point , one can not ascertain the cause of a given increase in CTP, the pressure may be elevated from its minimum or baseline level due to muscle activity above and beyond the increase due solely to postural changes. In this paper, we address the response of CTP to a simple active wrist flexion-extension task and discuss the nature of the response.

PROCEDURES

Twenty subjects who had no signs, symptoms or electrodiagnostic evidence of CTS took part in this study. An 18 gauge needle was inserted at a 45° angle about 5 mm proximal to the distal wrist crease. A saline-solution-filled 20-gauge catheter with 3 side holes was threaded through the needle into the carpal tunnel, the needle was removed, and the catheter was secured with a suture. A biaxial wrist goniometer (Penny & Giles, Santa Monica, CA) was used to collect simultaneous wrist angle data. For all motions, the metacarpophalangeal joints were flexed to 45° as previous research in our lab determined that the lowest CTPs were found in that posture. After determining the wrist posture of lowest CTP (*cf.* Weiss *et al.*, 1995), the subject moved their wrist through a comfortable range of flexion-extension motion, keeping the motion in the other planes constant. Each test started from the position of lowest CTP, then the subject slowly flexed the wrist, slowly extended the wrist, and then the cycle was repeated, finishing at the posture of lowest CTP.

The data were analyzed at increments in wrist angle of ten degrees. Based on previous studies evaluating the goniometer, the data were averaged for each wrist angle plus or minus two degrees. Only cycles that were continuous from full flexion to full extension, and vice versa, were included in the analysis (three values at each angle for each subject). For each subject, the minimum, mean, and maximum pressures at each wrist angle were calculated from the three passes of each angle. Group means and standard errors of the mean of each of these values (minimum, mean, and maximum) were subsequently calculated.

RESULTS

The curves from individual subjects indicated that some subjects had substantial differences in CTP within the same trial (see Figure 1). These increases typically occurred at the end of the range of motion of flexion and/or extension and were, in some instances, up to 50 mmHg.

Figure 2 shows the study grand means of the minimum and maximum pressures seen for each subject at each wrist angle, as well as the mean of all three trials per subject. Thus the "minimum" curve on Figure 2 represents the mean of the each subject's lowest CTP at each wrist angle. These values are on the order of 10-15 mmHg lower than the "maximum" data points which reflect the CTPs of highest contamination of other factors.

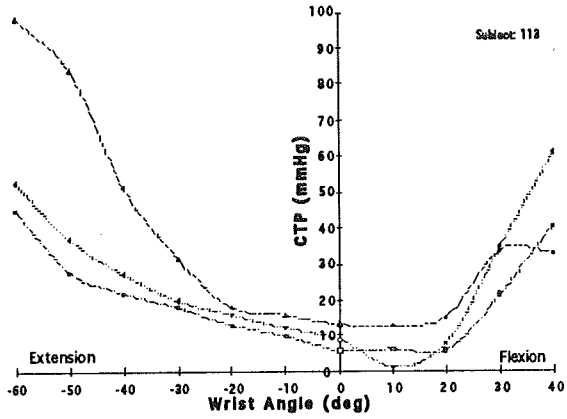

Figure 1. Data for an individual subject showing the differences in the three passes in a single trial. (Each trial took approximately 30 seconds to complete)

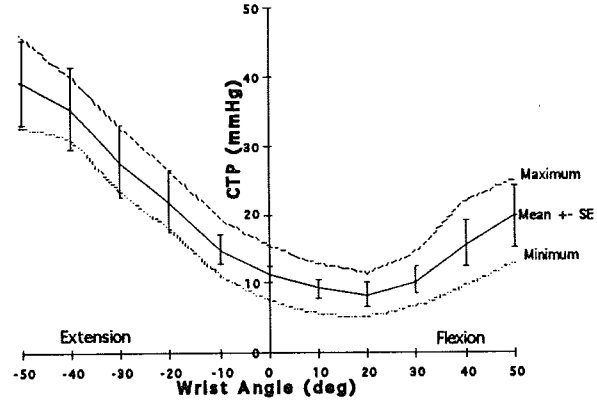

Figure 2. Grand means of the minimum, mean and maximum CTPs found at each posture. (n= 20). Standard error bars have been included for the mean CTP data.

DISCUSSION

This study sheds new light on the relationship between posture and pressure. During the analysis of the data it became apparent that the CTPs were not identical when measured at the same wrist angle at different times. Our technique of simultaneous posture and CTP measurement allowed us to examine the differences found in successive wrist movements which have not been reported previously.

The curve in Figure 2, identified as "minimum" represents what we consider to be the best estimate of the posture-CTP relationship. Because we know of only pressure elevating mechanisms intrinsic to the hand/wrist system, we must attribute these minimal pressures to posture alone. The increase above the minimum can be attributed to other factors within the tunnel (e.g. muscle/tendon tension). Thus the mean and maximum represent the combined effects of posture and muscle tension.

The time course of the pressure changes (as seen in Figure 1) was a matter of seconds, thus factors which may alter pressure over time cannot be deemed as plausible for explaining the changes. As the changes occurred typically near the end of the subject's unresisted range of motion or as the direction of wrist motion changed, it is plausible that changes in muscle activity and thus force may be responsible for the large changes in CTP. Okutsu *et al.* (1989) demonstrated that CTP is increased by grip force, extension force, and flexion force, the latter two being corroborative to our data. The increases in CTP variance were found to be greatest at the end ranges of motion (as seen in Fig. 1 for an individual and in Figure 2 for between subjects). This could be caused by a cocontraction associated with the change in direction of wrist motion.

The carpal tunnel pressures in Figure 2 appear lower than previous studies. The range of motion seen in this study was much less than in other studies thus the data are not directly comparable. The nature of the protocol used here was to elicit the lowest pressures possible, that is, to limit the activity of the musculature beyond that required to move the wrist in order to characterize the pressure changes in functional wrist postures.

This study has used a large number of healthy wrists to examine the effects of posture on CTP. We have determined a dose-response profile that we feel just in attributing to posture alone. We have also demonstrated what can be considered typical contamination due to intervening factors by also quantifying the highest CTPs found in each trial.

REFERENCES

Brain *et al., The Lancet,* 1, 277-282, 1947

Cobb, T.K. *et al.., J. Hand Surg.* 19B, 434-438, 1994.

Okutsu, I. *et al., J. Bone Joint Surg.* 71A, 679-683, 1989.

Keir, P.J. & Wells, R.P. *ASB 1995,* pp. 129-130, 1995.

Rempel, D. *et al.* In: Proceedings of the 40th Annual Meeting of the Orthopaedic Research Society, 1994.

Szabo, R.M. and Gelberman,R.H., *J. Hand Surgery,* 12A(5), 880-884, 1987

Weiss, N.D. *et al, J. Bone Joint Surg*, 77A(11), 1695-1699, 1995.

INFLUENCE OF THUMB POSTURE ON CARPAL TUNNEL PRESSURE

[1]J.M. Bach, [2]J.W. Engstrom, [1]D.M. Rempel
[1]Ergonomics Program, Department of Medicine, University of California San Francisco, Richmond, CA, 94804
[2]Department of Neurology, University of California San Francisco, San Francisco, CA, 94143

INTRODUCTION

Sustained elevated carpal tunnel pressure may lead to the development of carpal tunnel syndrome. The following laboratory experiment was performed in an effort to correlate carpal tunnel pressure with thumb posture.

REVIEW AND THEORY

Carpal tunnel syndrome (CTS) is the most common work-related entrapment neuropathy. There is indirect evidence that the pathophysiologic mechanism of activity-related CTS involves repeated and prolonged elevations of carpal tunnel pressure (CTP)(Szabo & Gelberman, 1987; Fuchs et al., 1991). Elevated pressure leads to ischemia, flexor tendon synovial tissue edema, further elevations in CTP, and slowed nerve conduction.

It has been shown that CTP varies with wrist flexion/extension, ulnar/radial deviation (Weiss et al., 1995), forearm pronation/supination, and metacarpophalangeal angle (Rempel et al., 1995). The current study examines the relationship of CTP to thumb posture.

METHODS

Sixteen volunteers who demonstrated no evidence of carpal tunnel syndrome based on history, examination, and nerve conduction testing participated in this study. Carpal tunnel pressure measurement was accomplished via a saline-filled catheter inserted percutaneously into the carpal tunnel, and attached at the proximal end to an in-line pressure transducer (Rempel et al., 1994). CTP was measured continuously on a digital computer. The transducer was secured to the mid forearm at the same elevation as the carpal tunnel.

After catheter insertion, the subject was methodically directed through a range of wrist and forearm motions to determine the position of lowest CTP (defined as the rest position). The rest position provided the starting and ending point for all subsequent maneuvers.

Beginning in the neutral wrist and forearm position the subject positioned their fingers until an MP angle of 45 degrees was reached. The subject then adducted the thumb and held the posture for 5 seconds. The subject then extended, abducted, opposed, and flexed the thumb sequentially pausing for 5 seconds at each posture. The CTP value stabilized within 1 to 2 seconds after each new position was achieved. The experimenter continuously observed the subject's thumb position and time stamped the data at the beginning and end of each 5 second pause.

A repeated measures ANOVA was performed on the data with a single factor, thumb position, with five levels. Tukey's method of multiple comparisons was performed using the repeated measures results to determine significant differences between the various levels of the factors.

RESULTS

The CTP means and standard errors can be seen in Figure 1. The repeated measures ANOVA revealed that the thumb posture had a significant effect on CTP ($p=0.0001$). Tukey's method detected significant differences in the CTP for several of the positions (Figure 1).

DISCUSSION

Carpal tunnel pressure is known to vary with wrist, forearm, and metacarpophalangeal postures (Weiss et al., 1995; Rempel et al., 1995). The results of the current study reveal that thumb posture influences CTP as well. If CTP plays a role in the development of

activity-related CTS, then redesigning tools and tasks to minimize CTP should decrease the risk of developing CTS. Based upon the results of this study, tasks requiring prolonged thumb opposition or flexion should be minimized.

REFERENCES

Szabo R.M. and Gelberman R.H., J. Hand Surg., 12a, 880-884, 1987.

Fuchs P.C. et al., J. Hand Surg., 16a, 753-758, 1991.

Rempel D.M. et al., J. Hand Surg., 19a, 106-110, 1994.

Rempel D.M. et al., Proceedings of the 50th Annual Meeting of the Amer. Soc. for Surg. of the Hand, 1995.

Weiss, N. et al., J. Bone Joint. Surg., 77-A(11), 1695-1699, 1995.

ACKNOWLEDGMENTS

Thanks to Ron Tal for his contributions to this research project. This study was supported in part by grant K01OH--121-01 the National Institution of Occupational Safety and Health of the Centers for Disease Control.

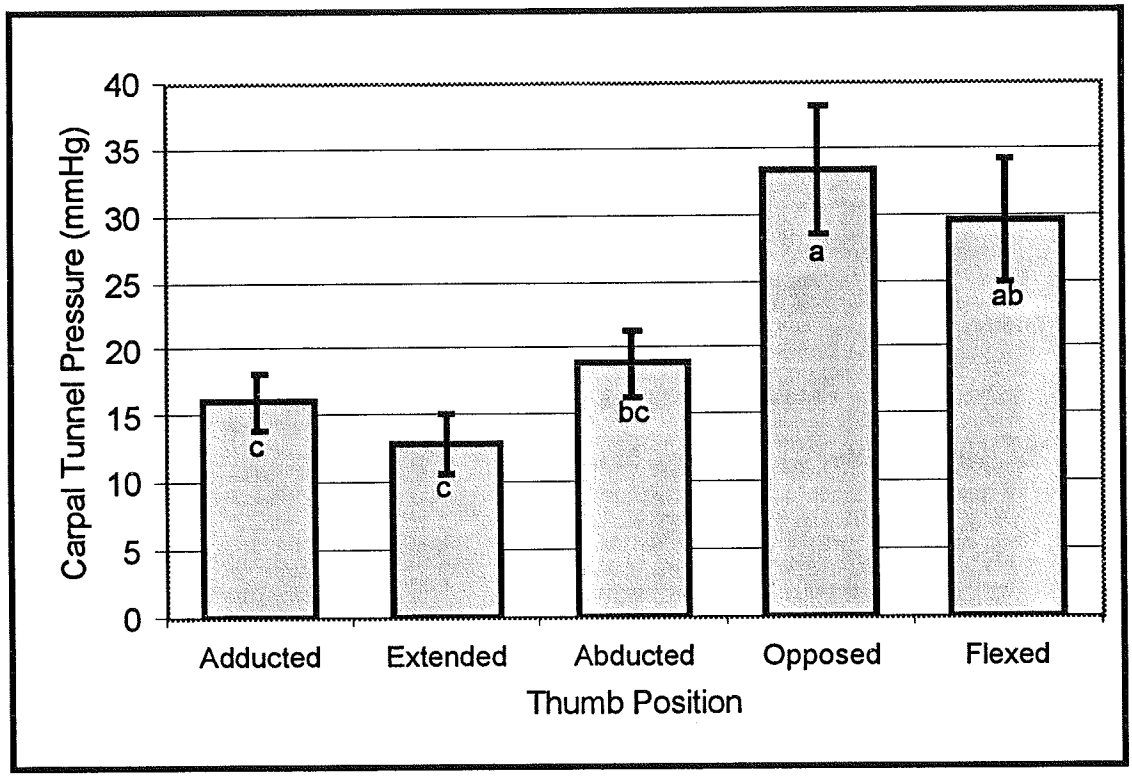

Figure 1 : CTP means and standard errors. Positions with a common letter (a, b, c) were not significantly different.

A FINITE ELEMENT ANALYSIS OF A FRACTURED HUMAN TIBIA THROUGH HEALING WITH DCP AND IM INTERNAL FIXATION DEVICES

P. Neale*, K. Baker, M. Finnegan*
*The University of Texas Southwestern Medical Center at Dallas, Dallas, TX 75235
Texas Scottish Rite Hospital for Children, Dallas, TX 75219

INTRODUCTION

Selecting a method of internal fixation for spiral fractures of the tibial diaphysis remains an enigma for orthopaedic surgeons. To secure proper healing, it was necessary to determine the device that closely imitated the response of normal bone to loading. A 3-D finite element model (FEM) was developed to compare the stresses in normal bone to those induced in a spiral fracture following fixation with a dynamic compression plate (DCP) or an interlocking intramedullary (IM) nail.

REVIEW AND THEORY

The two types of fixation devices recommended for fixation of a spiral tibial fracture are based upon different principles. Interlocking IM rods traverse the length of the bone and are attached at the metaphyses, thereby acting as a splint to protect the fracture ends under axial compression, but without providing torsional and bending stability at the fracture site. A DCP is attached to the bone in multiple locations throughout the diaphysis, thus rigidly protecting the fracture ends from excessive motion and forces under all loading types. However, with the plate diverting stresses away from the bone over a long period of time, resorption will occur according to Wolff's Law which could lead to refracture upon implant removal because of reduced bone density and thickness[1,2].

Ideally, a fixation device should be supportive early in the healing process for more efficient healing, yet it should allow the bone to carry loads once the fracture has begun to heal. Clinical reports on the effectiveness of various types of internal fixation offer conflicting results [3,4]. Additionally, other experimental or analytical comparisons of commercial devices have not been well documented. Therefore, the purpose of this study was to compare the stress distributions imposed on bone by fixation with these devices, and to provide clinical recommendations based on these comparisons.

PROCEDURES

A 3-D FEM of a whole normal human tibia was developed using PATRAN (PDA Engineering, Santa Ana, CA) based upon CT scan data using linear brick and wedge solid elements (15798 degrees of freedom). A simple spiral fracture with a 2 mm axially displaced fracture gap was created in the lower diaphyseal region (Figure 1). To fix the fracture, the model was adapted to include a DCP and an IM nail, with locations based upon surgical specifications [5], and represented by equivalent 3-D beam elements. Using ABAQUS (HKS, Pawtucket, RI), the model was loaded under combinations of axial compression, torsion, and four-point bending, and supported using physiological constraints. Variations of the models were created that simulated four advancing stages of healing within the fracture gap, with material properties based on published literature [6,7,8]. The stages that were represented simulated immediately post-fixation; after granulation tissue had formed within the gap; once the tissues had matured to callus tissue; and at full healing, with the fixation devices still intact.

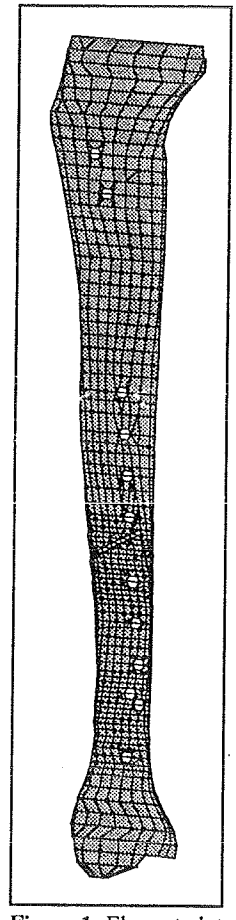

Figure 1: Element plot of tibia, M-L view; Screws and fracture shown in white.

Validation of the model was accomplished by mechanical testing of strain-gauged cadaveric tibias with spiral fractures and an IM nail or a DCP. The bones were tested under several loading conditions with strain vs. load data recorded. The strains were then compared to strain values in the analytical model. Additionally, results of the analytical model were compared with other reports in literature. The normal variation was primarily used for these comparisons due to the lack of similar studies with fixation devices or a spiral fracture.

RESULTS AND DISCUSSION

Contour plots of the principal stresses were obtained for the loading and geometric variations. The analysis

focused on three areas: the drilled holes for the transverse screws as an indication instrumentation loads; a cross-sectional slice through the fracture region; and overall stress patterns occurring with the fixation devices and advancing stages of healing.

The presence of drill holes for implantation of the devices did not significantly alter the normal diaphyseal stress distribution, although small stress concentrations were noted around the transcortical screw holes, particularly under axial compression.

Once the fixation devices were implanted, significant differences in the cortical stress patterns and magnitudes were noted for both devices. Immediately after fixation, the diaphysis of the nailed bone did not show a normal stress pattern. Large stress concentrations at the metaphyseal transverse screws suggested that the nail was supporting a majority of the load. The area surrounding the fracture for the plated bone was similarly protected, although the stress pattern was closer to normal bone. Significant stress concentrations were also seen around the screws of the plate, particularly the most proximal and distal screws.

Once initial healing tissues had formed within the fracture gap, the stress distribution across the fracture gap was notably more similar to that of the normal bone for both the nailed and the plated bone cases. This suggested that although the tissues had not fully healed, the bone could support a transfer of loads across the fracture so the surrounding bone was less likely to undergo resorption. However, although the stress distribution was more similar, the stress magnitudes still showed evidence of stress shielding by the fixation devices. Upon full healing, in all of the loading cases, the nailed bone stress magnitudes through the fracture area were closer to the normal values than the plated bone stresses were.

The results of the analytical model generally concurred with those of the experimental validation testing, with most experimental results within one order of magnitude of the analytical results. For all load types, the plated bone recorded larger strains than the nailed bone, suggesting that upon initial implantation, the plate was supporting a larger portion of the load, as was indicated in the analytical model. Additionally, analytical results of the normal, unfractured bone showed many similarities to mechanical tests and FEM of normal tibia in literature.

A finite element model was created to compare the stresses imposed by fixation of a spiral diaphyseal tibial fracture with an interlocking IM nail and a DCP. Immediately after fixation, the plated bone fracture ends were more stable than in the nailed bone. However, after full healing had occurred, the magnitudes and the contour patterns of the nailed bone returned to levels closer to normal than did those of the plated bone (Figure 2). The plated bone tended to show significant levels of unwanted stress protection of the diaphysis throughout all stages of healing. This was particularly evidenced under the M-L bending and axial compressive loadings.

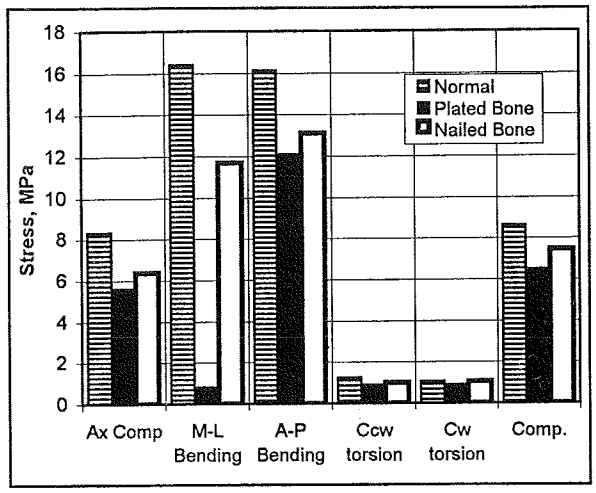

Figure 2: Maximum compressive stress comparison through mid-fracture cross section for normal, plated, and nailed bones.

Therefore, in an attempt to avoid this stress protection and resorption of the diaphysis, it is recommended that a spiral tibial fracture be fixed with an interlocking intramedullary rod, and supported with additional external fixation early in the healing process to provide greater stability until tissues within the fracture gap have developed.

REFERENCES

1. Carter DR, et al. Acta Orth. Scand., 52, 241-8, 1981.
2. Woo SL-Y, et al. J Biomech., 10, 87-95, 1977.
3. Brown PW and Urban JG. J Bone Joint Surg., 51-A, 59-75, 1969.
4. Bostman O, et al. J Trauma, 29, 639-45,1989.
5. Schatzker Jand Tile M. The Rationale of Operative Fracture Care. Springer-Verlag, 1987.
6. Reilly DT and Burstein AH. J Bone Joint Surg.,56-A, 1001-2, 1974.
7. Hayes WC, et al. J Biomech., 11, 21-33, 1978.
8. Blenman PR, et al. J Orth Res, 7, 398-407,1989.

STRESS-BASED MODEL FOR DENTAL ROOT RESORPTION

L. Lutterotti[1] and M. Ferrari[2]
[1]Dipartimento di Ingegneria dei Materiali, Università di Trento, 38050 Mesiano (TN), Italy
[2]Biomedical Microdevices Center, Department of Civil Engineering and Department of Material Science and Mineral Engineering, University of California, Berkeley, CA 94720

INTRODUCTION

The area of tissue remodeling has attracted considerable research interest (Fung, 1990), with primary emphasis on the remodeling of bone (Cowin, 1986; Fyhrie et al., 1985). In this case, the controlling variables appear to be the services stress and consequent strain cycles, and thus purely mechanical in nature. By comparison with the attention dedicated to the microstructural variations in cortical and cancellous bone tissue at remodeling equilibrium, research in the analogous phenomena in the dental arena has been more limited. This is associated in part with a relative scarcity of clinical and experimental data, and in part with the additional complexity deriving from the fact that the mechanical factors alone are not sufficient to trigger the remodeling process. A dominant mode of dental remodeling is resorption - a phenomenon that is associated with prosthetic implants, trauma, dentition, and endodonthic intervention - and generally results in the loss of the involved tooth. In this paper, we offer a theoretical framework for the analysis of root resorption, and validate it by comparison with clinical evidence. Conclusions are offered that may be of significance for the practicing orthodontist, endodontist, and oral surgeon.

REVIEW AND THEORY

There are several types of resorption affecting teeth: internal, external, invasive, pressure and idiopathic (Bakland, 1992). Trauma are recognized has the principal factor associated with the event and more than one experiment has shown the correlation between the appearance of resorption and tooth movement (Sismanidou et al., 1995) or dentition (Beck et a., 1994). Also the application of mechanical loads has been proved to stimulate cementogenesis in laboratory animals (Brudvik et al., 1995). By comparison with the resorption in bone, it is possible to recognize (Hammarstrom et al., 1992) that the root resorption needs one more condition, that is the damage of the cementoblastic layer that normally shield the osteoclasts from responding to hormones and cytokines that stimulate the bone resorption. Following this, the removal of the hyanilized tissue can start in the zone interested by the resorption (Brudvik et al., 1993).
Following the suggestion of comparing resorption in tooth with the similar process in bone we can formulate the hypothesis that also in the dental case the resorption can happen when the service stress field in a part of the tooth root drops down to a lower value as a consequences of tooth movement or traumatic events. The dentition and in particular the artificial repairing of tooth can change dramatically the stress field in the root if a dental alloy with different stiffness from the tooth is used.
In this paper, we postulate that there is a minimum service stress threshold, below which the process of resorption is activated, resulting in loss of density. Consequently, a loss in elastic modulus is recorded, which is here modeled in accordance with the poly-inclusion theory (Ferrari, 1994). In the absence of external intervention, this triggers a yet larger stress-reduction based tendency towards resorption. Complete resorption is here modeled by postulating a critical density threshold, below which the tissue is unstable (Ferrari et al., 1996).

PROCEDURES

After the novel theoretical approach is reviewed, in this paper we address its clinical validation. In particular, the Finite Element implementation of the theory is adopted to analyze a case of resorption induced by endodontic intervention in an adjacent tooth (Figure 1, 2).

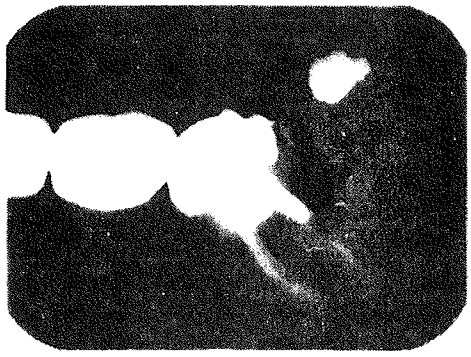

Figure 1: X-ray image

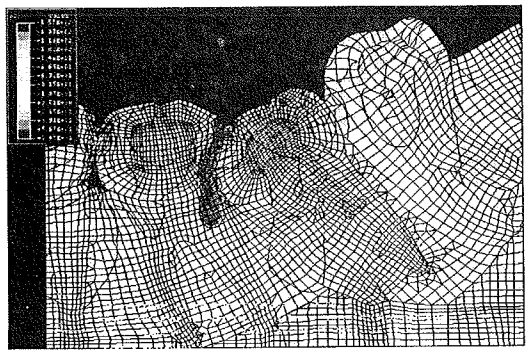

Figure 2: σ_{22} contour stresses by FEM

RESULTS

In the studied clinical case, it is shown that the phenomenon of resorption, if modeled by stress-reduction to modulus-reduction mechanism, has increasing amplitude and necessarily terminates in dental loss. The theory is calibrated as to predict resorption amplitude and morphology that are consistent with clinical evidence.

DISCUSSION

The clinical study seems to validate the approach of (Ferrari et al. 1996). The associated analysis indicates that the trigger of the resorption phenomenon in this case was the root-canal performed on the adjacent tooth, which acts as a reducing mechanical support for the tooth experiencing resorption. For this case, the use of a lower-modulus dental composite would arguably have avoided the triggering of resorption.

REFERENCES

Bakland, L.K., Dent. Clinic N. Amer., 36 (2), 491-507, 1992.

Beck, B. W., Harris, E. F., Am. J. Orthod. Dent. Orthop., 105 (4), 350-361, 1994.

Brudvik, C., Rygh, P., Eur. J. Orthod., 15 (4), 249-263, 1993.

Brudvik, C., Rygh, P., Eur. J. Orthod., 17 (3), 189-198, 1995.

Cowin, S.C., J. Biomech. Eng., 108, 83-88, 1986.

Ferrari, M., Composites Eng., 4 (1), 37-45, 1994.

Ferrari, M.and Lutterotti, L., in preparation.

Fung, Y.C., Biomechanics - Motion,flow, stress, and growth, Springer-Verlag, New York, 1990.

Fyhrie, D.P. and Carter, D.R., Trans. Orthop. Res. Soc., 31, 337, 1985.

Hammarstrom, L., Lindskog S., Proc. Finn. Dent. Soc., 88 suppl. 1, 115-123, 1992.

Sismanidou, C., Lindskog, S., J. Oral Sci., 103 (5), 292-298, 1995.

COMPUTER SIMULATIONS OF SUBCHONDRAL BONE REMODELING: THE ROLE OF JOINT INCONGRUITY

C. Jacobs[1], F. Eckstein[2], B. Mertz3
[1]Musculoskeletal Research Laboratory, Pennsylvania State University
[2]Anatomiche Anstalt, Lubwig Maximilians Universitat, Muchen, Germany
[3]Institut Straumann, Waldenburg, Switzerland

INTRODUCTION

The subchondral bone plate is a thin layer of dense bone tissue situated between articular cartilage and epiphyseal cancellous bone. Although it is commonly acknowledged that much of the bone in the skeleton is able to alter its structure to become well suited to its mechanical environment, the mechanically adaptive nature of subchondral bone has received little study. Subchondral bone density in the human elbow joint typically exhibits a bicentric distribution with two maxima located dorsal and ventral to a central minima (Eckstein et al., 1995). Furthermore, this bicentric pattern seems to coincide with a naturally occurring incongruity of the joint whereby the trochlear notch is deeper than would be required for an exact fit with the trochlea. In this work we intend to show that a theoretical model of bone adaptation can successfully explain the observed density bicentricity in terms of joint incongruity.

REVIEW AND THEORY

Finite element modeling allows the computation of the mechanical stresses and strains in bones with complex geometries and inhomogeneous material properties. Significant advances have been made over the last two decades resulting in theoretical mathematical relationships between the local tissue mechanical environment and the biological response of bone apposition or resorption. Although the details of this biologic response are still unclear, these models have been shown to be capable of phenomenological predictions that are consistent with clinical and animal experiments (Hart et al., 1984). Finite element computer simulations have been conducted in a wide variety of applications including normal cancellous and cortical bone adaptation as well as the remodeling response to the presence of orthopaedic implants. However, this work represents the first application of these methods to the subchondral bone plate.

In this study we have adopted the bone remodeling theory of Beaupré et al. (1990). Bone is assumed to respond to changes in a measure of the local mechanical load intensity know as the "tissue level daily stress stimulus" which allows multiple load cases to be considered. Simulations were conducted using the node-based numerical implementation of Jacobs et al. (1995) due to its enhanced numerical performance and advantageous spatial stability properties.

METHODS

Five plain stress finite element models were created with differing degrees of incongruity (20%, 10%, 5% deeper, congruous, and 10% wider) (Figure 1). Frictionless sliding contact was allowed at the articular surface, and a uniform 1mm thick cartilage layer was included on each side of the joint. Rotation of the trochlea within the trochlear notch was prevented. Five load cases were studied, one central load, two directed 22.5° laterally, and two directed 45° laterally. Each load was assumed to be 70N in magnitude and applied for 2,000 cycles per day. A dead-zone response was incorporated and simulations .

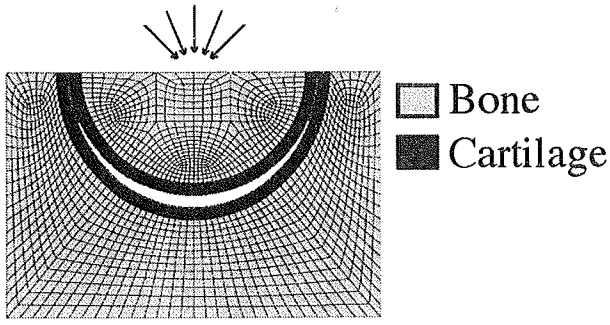

Figure 1 Mesh used for the 10% deeper socket model with the five assumed load cases.

were carried out for 300, 10-day time steps. In all cases the solutions had reached a converged configuration

RESUTLS

The simulation results display a strong dependence on the type and degree of joint incongruity. In the case of deeper sockets, a thin layer of dense subchondral bone was predicted to form (Figure 2). In the case of a congruous or wider socket, subchondral densities were dramatically lower (Figure 3). Deeper sockets lead to progressively higher densities and more pronounced bicentricities.

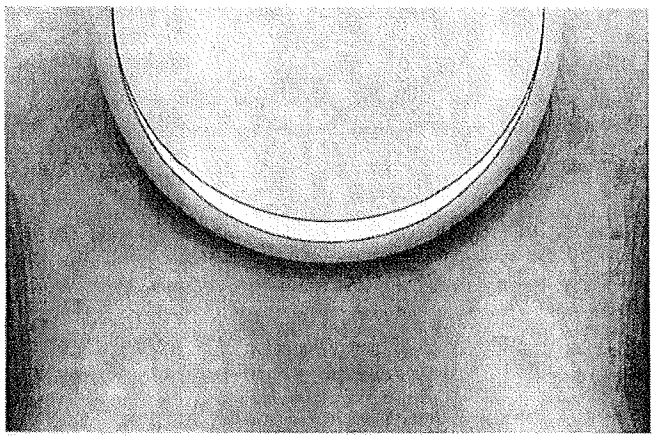

Figure 2 A plot of the predicted bone density for the 10% deeper socket model, higher density being darker. Note the dense subchondral bone layer and its bicentric nature

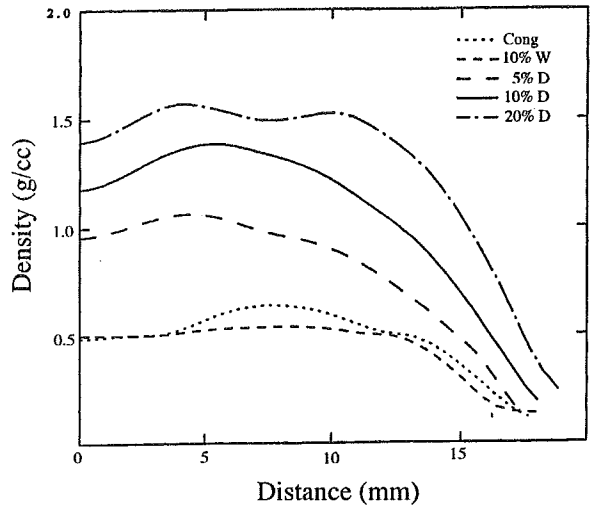

Figure 3 A plot of the subchondral bone density at the bone/cartilage interface as a function of distance from bottom dead center of the joint to the joint margin. Note that the density distribution is symmetric, thus only half of the results are depicted.

CONCLUSION

A theoretical computational model of subchondral bone adaptation has shown that subchondral bone density patterns in the humeroulnar joint can be understood to be a result of adaptive remodeling in the presence of joint incongruity. Future models of this type will be anatomically accurate and are anticipated to reveal more details of this relationship, and in particular the relationship between density patterns and joint contact pressures.

REFERENCES

Eckstein, F. et al. J Orthop Res, 13, 268-178, 1995.
Hart, R.T. et al. J Biomech Eng, 106, 342-350, 1984.
Beaupré, G.S. et al. J Orthop Res, 8, 651-670, 1990.
Jacobs, C.R. et al. J Biomech, 28, 449-459, 1995.

Correspondence: C Jacobs, Dept. of Orthopaedics, P.O. Box 850, Hershey, PA, 17033.

COMPARISON OF SCREW PULL-OUT STRENGTH FROM WEIGHT-BEARING AND NON-WEIGHT-BEARING DIRECTIONS IN BOVINE CANCELLOUS BONE

Y. H. An[1], Q. Kang[1], J. H. Zhang[1], R. J. Friedman[1], F. A. Young[2]
[1]Department of Orthopaedic Surgery and [2]Department of Materials Science
Medical University of South Carolina, Charleston, SC

INTRODUCTION

Screw fixation is used very commonly in orthopedic surgery to hold bone pieces together or fix tendon or ligaments to the bone. Since bone trabeculae lay in a certain direction depending on the functional requirement, when choices exist of more than two directions from a given point for screw placement, is there a better or best direction for a ultimate holding power?

The hypothesis from the above question is that the holding power of a screw placed in cancellous bone depends on the relation between the direction of the screw and the direction of oriented trabeculae (or major trabeculae direction which is the weight-bearing direction), i.e. the strength would be the strongest if the two are in a same direction, be the weakest if the two have a 90° intersection angle, and be in between the strongest and weakest if the angle of the two is in between 0° and 90°.

The purpose of this study is to verify the above hypothesis by testing the holding strength of screws placed at three different angles (0°, 45°, and 90°) referenced to the major trabeculae direction in bovine cancellous bones.

PROCEDURES

Five distal femoral condyles of adult cow were obtained from a local slaughter house and used as the bone samples for this study. The bones were fresh frozen at -20°C. in a laboratory freezer for 1-4 weeks before mechanical testing. The medial or lateral condyle was cut into two rectangular blocks (at least 2.5×2.5×4.0 cm) and named as level 1 and level 2 (Figure 1A). Four distal femurs were used for screw pull-out testing. And four blocks from one distal femur were cut into serial 3-mm thick sections horizontal, sagittal, and coronary planes, which were x-rayed on a Faxitron radiographic machine (Field Emission Corporation, McMinnville, OR) to obtain high resolution radiographic images.

A 40 mm long 3.5 mm thread diameter self-tapping cortical screw was chosen for this testing since it is a standard screw size which is commonly used in clinical setting and it has been often used by other investigators for screw pull-out tests. Pilot holes were drilled with a 2.5 mm drill bit at the directions illustrated in Fig. 1C, and D. The above mentioned screw was then hand driven into the bone to a depth of 15 mm. Three holes were drilled on each bone block from the three angles and care was paid to ensure no intersection between any two holes.

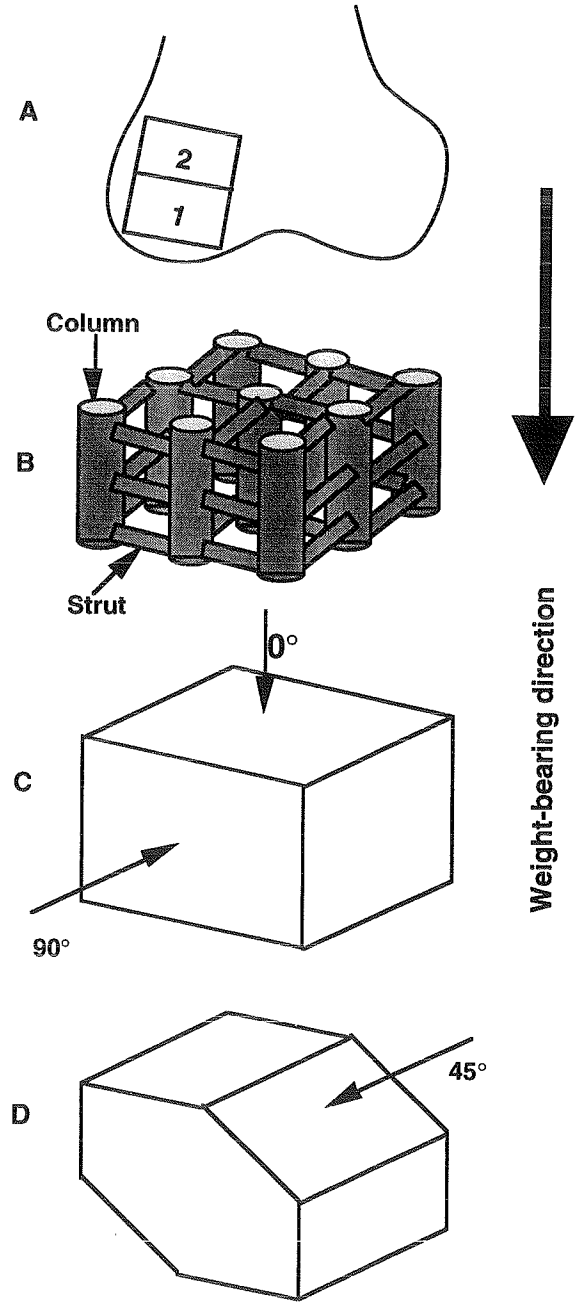

Figure 1. A. The location where the bone blocks were taken from bovine femoral condyle; B. The idealized structural model of the bone block; C and D. Directions for screw insertion. Corners were cut off the D block for inserting the screw at a 45° angle to the major trabeculae direction.

A mechanical testing machine (MTS System 810, Minneapolis, MN) was operated in a displacement control mode. The machine displacement transducer had been previously calibrated using an extensometer. A stainless steel fixture was used, consisted of a upper screw gripping bar (connected to the load cell) and a lower specimen holding frame (Fig. 2). After the specimen was positioned on the fixture the lower part of the fixture was pulled down (away from the load cell) at a constant rate of 1 mm/min. Loading was stopped when the curve passed the ultimate load (the highest point of the curve). The curve of load-displacement was recorded using a chart recorder. A stiffness measurement was obtained by measuring the slope of the linear portion on the load-displacement curves. Since the test machine was controlled with a linear displacement rate (monitored by a built-in LVDT), the time base of the recorder could be converted to displacement. Ultimate strength σ (MPa) was calculated using the following formulae:

$$\sigma = P/\pi dh \qquad (1)$$

where P was the ultimate pull-out load (Newton), d (mm) was the major diameter of the screw (3.5 mm), and h was the length of effective threads (13.5 mm) in the cancellous bone. Since the three measures were taken from the same bone block and only difference was the directions of the screw (different conditions), an ANOVA test for repeated measures was used to determine the differences between the holding strengths from the three directions.

After mechanical testing, the bone blocks were cut along or transverse to the screw hole to create 3 mm thick bone slices which were x-rayed to obtain high resolution radiographic images. The directions of screw hole and of trabeculae were determined.

RESULTS AND DISCUSSION

According to the X-ray images, it was apparent that on sagittal and coronary planes contained highly oriented trabeculae lying vertically, which basically was the direction of weight bearing. On the horizontal plane, a honey-comb-like image was seen. These findings were confirmed by the post-testing X-rays. The structure of the bone block was idealized into a column-strut model (Fig. 1B). The columns indicate the major trabeculae direction and the struts represent the trabecular connections between columns (column trabeculae).

Investigations have shown that bone strength is significantly higher along the weight-bearing direction, or proximal-distal direction than the side directions (Vahey and Lewis 1987; Galante et al., 1970). This phenomenon may be explained by the structural model proposed in this study (Figure 1 B).

According to the ANOVA analysis, the pull-out strengths of the screws inserted from different directions were significantly different from each other (Table 1, and Figure 2). The new structural model may be used to explain these differences. The strongest one was in the 0° direction or weight-bearing direction (in the direction of columns, mainly affected by column trabeculae). The weakest was in the 90° direction or side direction (in the direction of struts, mainly affected by strut trabeculae). The strength in 45° direction was in between the above two (affected by both column and strut trabeculae).

Table 1. Pull-out parameters (Means±SEM, N=16).

Direction	Ultimate load (Newton)	Stiffness (N/mm)	Strength (MPa)
0°	818±82	2833±297	54.9±5.4
45°	649±59	2237±196	42.8±3.9
90°	563±76	1955±219	37.1±5.0
P value	<0.0001	<0.001	<0.0001

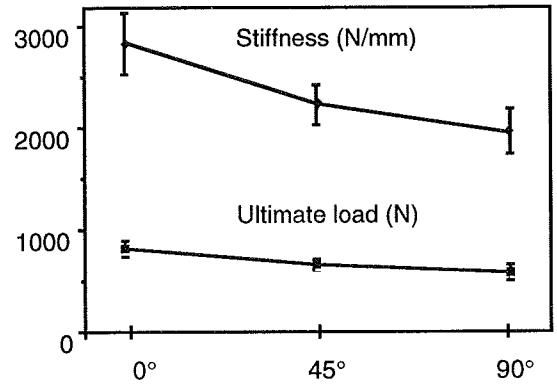

Figure 2. The relationship between the mechanical parameters and the degree of angle between screw shaft and main steam of bone trabeculae

REFERENCES

Vahey, J. W. and Lewis, J. L. J. Biomechanics, 20,29-33, 1987.

Galante, J. et al. Cal. Tiss. Res., 5, 236-246, 1970.

ACKNOWLEDGMENT

The authors thank Dr. R. Draughn of the Dept. of Materials Science, MUSC for technical consultation on mechanical testing. No financial support was received for this project.

Tri-axial Testing of Human Morselized Cancellous Bone

M.D. Brodt[2], C.C. Swan[3], T.D. Brown[1]
[1] Departments of Orthopaedic Surgery, [2] Mechanical Engineering, & [3] Civil/Environmental Engineering,
University of Iowa, Iowa City IA 52242

Introduction

A tri-axial compression testing protocol was used to study the mechanical properties of morselized human cancellous bone. For various levels of compressive radial stress, recordings of stress versus deformation (axial) were used to calculate the apparent elastic modulus, the cohesion, and the Mohr-Coulomb shear failure envelope.

Review and Theory

Morselized cancellous bone is used in many orthopaedic reconstructive applications, including curettage for neoplasms/ infections/osteonecrosis, trauma, and total joint revision. While obviously not intended as a robust structural material, morselized graft is a bona fide element in these constructs, and therefore merits representation in quantitative structural analyses, especially by finite element models.

Currently, very little is known about the mechanical properties of morselized bone. Because of the analogy to packed granular soils, we hypothesized that tri-axial compression tests could be applied to characterize samples of morselized human cancellous bone. The tri-axial compression test (Figure 1) is widely used in the field of soil mechanics to determine the shear strengths of granular soils (Das, 1994). In this testing mode, a cylindrical specimen is subjected to a hydrostatic confining pressure while it is axially compressed. This test is different than confined uni-axial compression tests, as the specimen is allowed to yield along the 'natural' (shear) failure plane. By measuring the axial stress at shear failure and knowing the hydrostatic pressure, the shear strength can be determined.

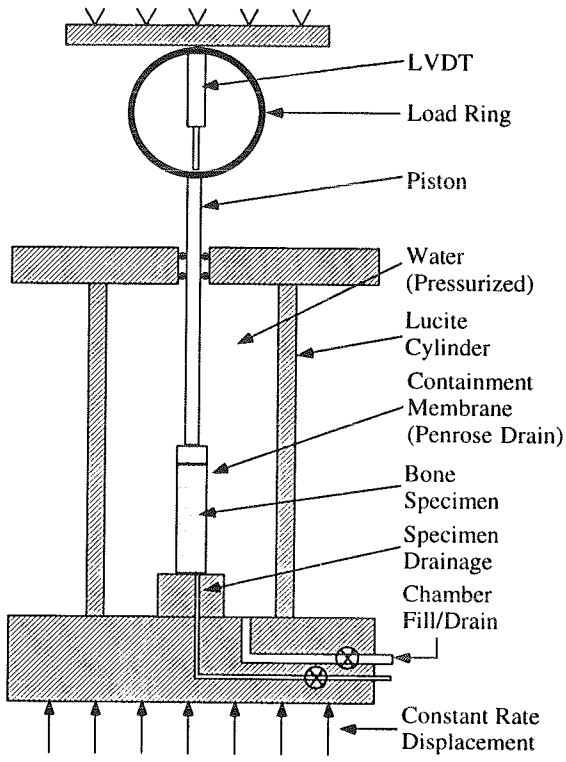

Figure 1- Tri-axial testing chamber.

Procedures

Cancellous bone was obtained from one fresh-frozen cadaver distal femur. A Tracer bone mill was turned by hand to morselize the cancellous bone, yielding irregularly shaped particles in the size range of less than 1 mm up to 5 mm.

Specimens were hand packed into a thin cylindrical rubber containment membrane (Penrose drain tube, thickness =0.32 mm, inner diameter =27.2 mm) which was attached at the base to the apparatus, and sealed with a PMMA cap. A vacuum line communicating with the pore space of the morselized bone (inside the Penrose drain) and connected to a valve maintained the cylindrical shape of the specimen. Specimen tare dimensions were measured, and then the testing chamber was sealed, filled with water, and pressurized.

After pressurization of the water, the vacuum on the specimen was released, and the pore space of the specimen was left open to atmosphere. This allowed fluid exudation from the specimen, since the hydrostatic pressure of the water was above atmospheric.

The loading platen was then driven upward at a constant rate (0.127 mm/sec). Axial force measurements were obtained with a load ring, while axial displacement of the chamber (and thus of the specimen) were recorded with an LVDT. Parametric tests were conducted to determine the effect of increasing the hydrostatic pressure.

Results

Preliminary uni-axial test data had shown that, provided free egress of interstitial fluid was permitted, load uptake by morselized bone was nearly independent of imposed strain rate, over three orders of magnitude spanning the physiologic range (0.0001 s^{-1} to 0.1 s^{-1}). Therefore, only one strain rate (0.004 s^{-1}) was used in this series of tri-axial experiments.

The axial stress at shear failure was nearly independent of increasing hydrostatic confining pressure (upper four curves, Figure 2). An average tangent modulus value was 3.97 MPa (at 5% strain).

An additional result of increasing the confining pressure is the amount of pre-strain in the specimen. When the chamber water is pressurized, it acts to pre-compress the specimen. This results in isotropic pre-strain values of 10-20%, depending on the pressure level. Trials conducted at zero hydrostatic pressure showed a consistent axial failure stress of less than 0.1 MPa. Similar behavior is observed for non-zero hydrostatic pressure if the membrane is inadvertently punctured by a bony spicule, since the differential between interstitial and chamber pressures falls to zero.

In soil mechanics, cohesion is defined as the stress required to fail a specimen in shear under zero hydrostatic pressure. The axial stress at shear failure of the specimens under zero hydrostatic pressure in this series was very near zero, thus suggesting that the cohesion is negligible in this material.

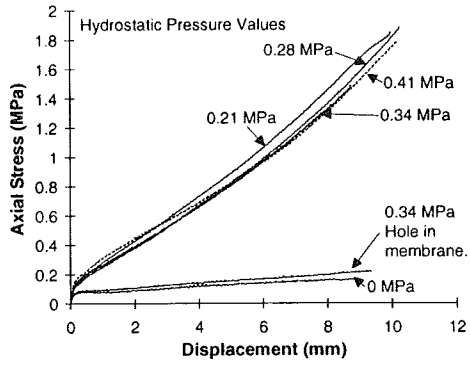

Figure 2-Displacement verses axial stress at four hydrostatic pressure levels.

Discussion

The present results demonstrate that the tri-axial testing technique can be applied to morselized cancellous bone to estimate material properties. Two caveats, however, merit note. First, when testing morselized bone, the ratio of particle size to containment tube diameter (O(5-10%)) is much greater than that customarily used for soils (O(0.1%), or less), so non-continuum effects may come into play. Second, because of the propensity of bony spicules to puncture the containment membrane (not an issue with soils), it is not feasible to use membranes as thin and complaint as might otherwise be desired.

References

Principle of Geotechnical Engineering 3rd ed.; Das, 1994

Acknowledgments

Tracer Designs generously provided the surgical bone mill used in specimen preparation. R.A. Brand and D.R. Pederson kindly assisted. Financial support was provided by NIH Grant AR-35788.

EFFECTS OF MULTIPLE FREEZING AND THAWING ON THE INDENTATION STRENGTH OF BOVINE CANCELLOUS BONE

Y. H. An, Q. Kang, R. J. Friedman
Department of Orthopaedic Surgery, Medical University of South Carolina, Charleston, SC 29425

INTRODUCTION

It is well accepted that freezing bones at -20°C for storage and thawing at room temperature will produce little change of their mechanical properties. But, due to complexity of an experiment or unforeseen circumstances, sometimes a specimen must be thawed and frozen several times. The question arises if multiple freezing and thawing is harmful to the mechanical properties of bone samples. This question has been partially answered by Linde and Sørensen (1993). They found that freezing and thawing five times did not alter the compressive properties of human tibial cancellous bones, but no freezing conditions were given. The purpose of this study was to study the effects of multiple freezing and thawing on the indentation strength of bovine tibial cancellous bone, with attention paid to the effects of freezing conditions (in saline or not) and methods of thawing (in saline or air).

PROCEDURES

Two proximal tibiae from adult cows were obtained from a local slaughter house and used as the bone samples in this study because of their size and the successful studies conducted by other investigators. After harvesting, the bone was stripped of all soft tissues and cut on a bandsaw 10 mm below the upper joint surface. A second cut was made 10 mm below the surface to make a bone slice (level 1). Another cut was then made to produce a second slice (level 2). The cut surfaces were ground with a 240 grit silicon carbide metallographic paper on a grinding wheel.

Indentation test using a flat-ended cylindrical indentor has been used successfully in this laboratory and by other researchers (An et al, 1995; Aitken et al., 1985; Sumner et al., 1994). A MTS machine (System 810) was used. The platform holding the specimen should be leveled to ensure that the loading was perpendicular to the specimen surface. A cylindrical stainless steel indentor 4.25 mm in diameter with a flat bone-contacting surface was used. After the specimen was positioned on the platform a transparent plastic sheet with a drawn 6.5 mm × 6.5 mm grid (with a 5.0 mm diameter hole punched in each square) was adhered to the sectioned surface by normal saline.

The indentor was adjusted close enough to the specimen surface within defined squares according to the experimental plan and then driven into the bone surface at a constant rate of 1 mm/min. The loading was stopped manually when the curve turned downward after having reached the ultimate load. The distance between any two indentations was 2.25 mm. Half of the squares in the grid were tested (the black squares in Fig 1). Incomplete squares around the periphery of the sample were not tested.

After testing, the slice "level 1" was wrapped in paper towels, soaked with normal saline, and placed in a airtight plastic bag. The slice "level 2" was placed in a plastic bag without paper towel wrapping and saline soaking. Both bone slices were then frozen at -20°C. in a laboratory freezer. After 5 days, the bone samples were thawed on each day at room temperature in normal saline (slice level 1) and in the air (slice level 2) for three hours and then frozen again in the same way mentioned above. After the fifth thawing, the bone slices were indentation tested again in the designated squares (the white squares in Fig 1).

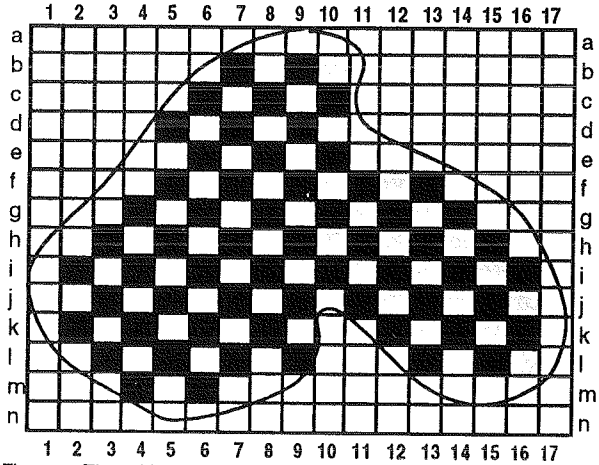

Figure 1. The grid and the contour of the bone surface to be tested. The black squares were tested before freezing and the shaded squares were tested after 5 cycles of freezing and thawing. Because of the edge-effect, no test was done to the circumfrancial squares (the white squares on the specimen surface).

Very importantly, before collection and calculation of the testing results a significant machine compliance (10 to 15 percent) was determined by loading the system without a specimen, which were deducted from the total compliance or deformation. The ultimate load from each load-deformation curve was divided by the indentor end-face area to obtain ultimate bone strength as shown by the following formulae (Nakabayashi et al., 1994):

$$\sigma = 4\,P/\pi d^2 \qquad (1)$$

where P is the ultimate indentation load and d is the diameter of the indentor. Using the formulae developed by Timoshenko and Goodier (1970) and

validated recently by Sumner et al. (1994), the local elastic modulus for each test site was calculated with the following formula:

$$E = S(1-\nu^2)/d \qquad (2)$$

where S is the indentation stiffness and d is the diameter of the indentor. Like the way of Sumner et al. (1994) and Aitken et al. (1985), the Poisson ratio (v) is assumed to be 0.2 according to Vasu et al (1982). Also, variation in the value for ν has a minor effect on the calculation of Young's modulus (Sumner et al., 1994).

RESULTS AND DISCUSSION

Using paired student T test, comparisons were made for each mechanical parameter between designated pairs (51-57 pairs) of indentations adjacent to each other in either mediolateral (ML) or ventrodorsal (VD) directions. No statistical difference was found for either the sample frozen and thawed in saline or the sample frozen without saline and thawed in air (Table 1).

It has been verified that multiple thawing and freezing makes no difference in the compressive mechanical properties of cancellous bone (Linde and Sørensen, 1993). Our results are in accordance with theirs, since indentation testing is a kind of constrained compression test and the data from indentation testing correlates well with that from conventional compression test (Sumner et al.,1994). It is thought that the experimental design is desirable for our purpose since the comparison between before and after multiple freezing and thawing fits the paired student T test and also the specimen number is large.

Although no statistical difference was found between the two treatments of each indentation parameter, a potential difference, or trend, may in fact exist. The actual elastic moduli after multiple freezing and thawing cycles are lower than those before treatment, especially for level 2 samples (freezing without saline and thawing in air), 452±356 MPa compared to 533±411 MPa or 441±358 MPa compared to 535±414 MPa with a P value of 0.078 (Table 1). A similar pattern is also found for the stiffness data. A possible explanation for this phenomenon may be that trabeculae were damaged by the freezing and subsequent expansion of interstitial fluids, which was postulated by Sonstegard et al. (1977), and Brown and Gruess (1982). Sonstegard et al. (1977) found a 10% decrease in stiffness by freezing.

It should be noted that the effects of storage at -20°C for short periods of time are minor. The maximum effect is a 4.6 percent reduction of torsional strength of a dog long bone (Strömberg et al., 1976). However, after bone thawing, enzymes such as collagenases and proteases may become active and degrade the tissue. Also, enzymatic degradation is not completely arrested at - 20°C (Tomford et al., 1983). This may be a possible explanation for the potential reduction of stiffness and elastic modulus in our study.

With concerns about the effects of evaporation and enzymatic degradation, a question arises if there are any effects of long term storage at -20°C. Panjabi et al. (1985) found no significant effects of freezing (for a period of 7 to 8 months) on the mechanical properties of human vertebrae bone. Roe et al. (1988) found that bones frozen at -20°C for eight months did not become significantly weaker than control bones, but had significantly lower compressive loads than the bones frozen for one week, indicating that structural properties of the bone may have degenerated slightly with time. Since time periods longer than 8 months have not been reported for frozen storage at -20°, storage at this temperature for more than 8 months is not recommended. Alternatively, -70°C, -80°C, or even lower temperatures or liquid nitrogen are suggested for long term bone storage, since these temperatures may minimize evaporation (Brown and Gruess, 1982) and markedly reduce enzyme activity (Tomford et al., 1983).

REFERENCES

Aitken, G. K. et al. Clin. Orthop., 201,264-270, 1985.
Linde, F. et al. J. Biomech., 26,1249-1252,1993.
Malinin, T. I. et al. Clin. Orthop., 196,44-57, 1985.
Nakabayashi, Y. et al. J. Arthroplasty, 9,307-315, 1994.
Panjabi, M. M. et al. J. Orthop. Res., 3, 292-300, 1985.
Pelker, R. R. et al. J. Orthop. Res., 1:405-411, 1984.
Roe, S. C. et al. Am. J. Vet. Res., 49,873-877, 1988.
Sedlin, E. Acta Orthop. Scand., 36 (suppl 83),1-77, 1965.
Sedlin, E. D. et al. Acta Orthop. Scand., 37,29-48, 1966.
Sonstegard, D. A. et al. Trans. Orthop. Res. Soc., 2, 283, 1977.
Strömberg, L. et al. Acta Orthop. Scand., 37, 254-256, 1976.
Sumner, D. R.et al. J. Biomech., 27,1095-1099, 1994.
Tomford, W. W. et al. Clin. Orthop., 174,15-21, 1983.

AKNOWLEDGMENTS

The authors thank Drs. RA Draughn and RA Young of the Dept. of Materials Science, MUSC for technical consultation.

Table 1. Mechanical values of indentation test of bovine cancellous bone in the upper tibia before and after multiple freezing and thawing (5 times) (Mean±SD, n= 51-57 pairs of indentation points).

Bone level		Ultimate load (N)	Stiffness (N/mm)	Ultimate strength (MPa)	Elastic modulus (MPa)
Level 1-ML	fresh	492±345	2305±1729	35±24	522±391
	after 5 freezing/thawing	492±313	2084±1306	35±22	471±296
Level 1-VD	fresh	489±330	2257±1502	35±23	511±340
	after 5 freezing/thawing	495±315	2133±1356	35±22	483±307
Level 2-ML	fresh	575±326	2356±1817	41±23	533±411
	after 5 freezing/thawing	578±358	1995±1573	41±25	452±356
Level 2-VD	fresh	576±327	2358±1830	41±23	534±414
	after 5 freezing/thawing	558±361	1948±1580	40±26	441±358

P > 0.1 for all paired comparison between values of fresh bone and after 5 times of freezing and thawing cycles

THE MECHANICAL SYMMETRY OF RABBIT LONG BONES STUDIED BY BENDING AND INDENTATION TEST

Y. H. AN, Q. Kang, R. J. Friedman
Department of Orthopaedic Surgery, Medical University of South Carolina, Charleston, SC 29425

INTRODUCTION

Bilateral animal models are used extensively (95% overall) for evaluating compatibility and functionality of biomaterials in bones (LaBerge et al., 1991). Implicit in such an approach in biomechanical studies is the assumption that in the same animal a pair of corresponding right and left bones have similar mechanical properties. There is little published data, however, that verify this assumption (Bak et al., 1992; Kersey et al,,1993; Mather, 1967). One report on the mechanical symmetry of rabbit long bones addressed only the torsional properties of the femur and tibia (White et al., 1974). Also, unlike the number of reports on the mechanical properties of human, canine, and bovine bones, there have been very few reports with comparable data of rabbit bones. One reported on the elastic modulus of the rabbit tibiae tested by an ultrasonic method (Lees et al., 1992). Simple parameters such as yield strength (Wootton et al., 1990) or peak load (Nash et al., 1994) for rabbit tibiae were used, but the data cannot be extrapolated for other studies. This study was aimed to determine if the bending and indentation parameters of rabbit long bones are symmetrical bilaterally, and to generate a comparable mechanical data set of rabbit long bones.

PROCEDURES

Seventeen pairs of fresh frozen (-20°C in saline) femurs, tibiae and humeri of adult New Zealand white rabbits (4.0±0.5 kg) used as healthy controls from other studies were used. At the time of testing, the bones were thawed in saline and kept moist during the testing. A mechanical test machine (MTS System 810) was operated in a displacement control (calibrated using an extensometer) for both three point bending and indentation tests. A significant machine compliance (10-15%) was determined by loading the system without a specimen, which were deducted from the total.

For 3-point bending test, loading point was chosen at the mid shaft of the femur, junction of middle and distal one thirds of tibia, and junction of the proximal three fifths and distal two fifths of the humerus. The specimen aspect ratios in this were 6.25 for the femur, 8.67 for the tibia and 7.62 for the humerus. After the bone was positioned on the two supports (steel rods, 6mm diam) with a 50 mm span, the striker (6mm diam.) was driven to the bone surface at a constant rate of 1 mm/min. until the bone fractured. The following equation was used to calculate the ultimate bending strength (Jørgensen etal., 1991; Martin et al., 1993):

$$\sigma_b = P_b L a / 8I \quad (1)$$

where P_b is the ultimate load, L is the distance between the supporting bars, a is the average value of the external anteroposterior diameters of the cross sections at the loading point, and I is the area moment of inertia. The area moment of inertia was calculated assuming the bone to be elliptical tubular:

$$I = \pi (a^3b - a'^3b')/64 \quad \text{(femur and tibia)} \quad (2)$$

$$I = \pi (ab^3 - a'b'^3)/64 \quad \text{(humerus)} \quad (3)$$

The values chosen for a, a', b, and b' were the average values of the external and internal anteroposterior and mediolateral diameters of the cross-sections at the loading points of the bone. The rest part of the tested portion of the bone was assumed to be consistent in cross-sectional size and shape. For the humerus, equation (3) was used since the surface of bone facing the loading striker was lateral for humerus. The external diameters (a and b) were measured before testing using a digital caliper. After testing, the pieces were glued together and cut transversely at the break point. The dimension of the medullary canal (a' and b') was then measured. The following equation was used to calculate bending elastic modulus (Kasra et al. 1994):

$$E_b = SL^3/48I \quad (4)$$

where S is the stiffness and L is the distance between the two supporting bars.

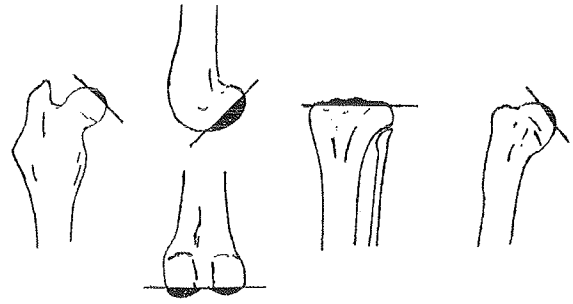

(1) (2) (3) (4)

Figure1. (1) The femoral head was ground perpendicular to the center line of the femoral neck from the center of femoral head to a depth of 2 mm. (2) The distal femoral condyle was ground from weight-bearing surface of the condyles to a depth of 2.0 to 2.5 mm (This surface had a 20 degree angle with the distal femoral diaphysis). (3) The tibial plateau was ground from the upper joint surface to a depth of 2 mm. (4) The humeral head was ground perpendicular to the center line of the humeral neck from the center of humeral head to a depth of 2.0 to 2.5 mm. The bones were then embedded in dental stone with the surfaces to be tested at a horizontal position.

For indentation test, selected sample bones were cut and ground to a certain depth in the cancellous bone at the epiphysis (Fig 1). The surfaces to be tested were on a plane perpendicular to the line of weight-bearing. The platform holding the specimen was leveled to ensure that all loading was perpendicular to the surface to be tested. A cylindrical steel indentor with a flat end surface (2.32 mm diam.) was driven into the bone surface at a constant rate of 1 mm/min. The loading was stopped manually when the curve dropped down obviously after the ultimate load. Ultimate strength was calculated using the formulae (Nakabayashi et al., 1994):

$$\sigma_i = 4 P_i/\pi d^2 \quad (5)$$

where P_i is the ultimate load and d is the diameter of the indentor.

RESULTS

There were no statistically significant differences (by student T test) between the mean values of each bending property for the right femoral, tibial or humeral diaphyses and the mean values of the same property for the left ones, except the elastic modulus of the femurs (P = 0.02) (Table 1). There was also no statistically significant differences between the mean values of each indentation property for the right femoral, tibial or humeral epiphyses and the mean values of the same property for the left ones (Table 1). The ultimate strength was 81-86 MPa for the femoral head, 45-64 MPa for the distal femoral condyles, 55-76 MPa for the tibial plateau, and 32-35 MPa for the humeral head.

DISCUSSION

This study utilized a standard 3-point bending test on rabbit long bones. The elastic modulus of rabbit femur and tibia are 13-15 and 20-21 GPa respectively, which is in the average range (5-21 GPa) of diaphyseal bones from other species (Currey et al., 1988). It is interesting to notice that the ultimate load for femur and tibia are basically the same (320 to 350 N), but the ultimate strength (140 and 190 MPa respectively) and elastic modulus (14 and 20 GPa respectively) are very different. This could be explained by their different geometric structure, since the femur is bigger in overall diameter than the tibia. According to the results no significant differences were found between the right and left femur, tibia, or humerus for all of the parameters except the elastic modulus of the femurs, indicating mechanical symmetry of the bones in terms of mean value (Table 1). Although the elastic modulus of the femurs was different statistically (P = 0.020), the actual difference was minor (13.0 vs 14.9 GPa).

Although indentation test has not been used widely, several advantages of this test have been shown. It is simpler than compression test. Only a flat surface of a sample is needed for testing. There has been no report on testing rabbit cancellous bones using compression tests or any other methods, likely because the bone size is too small. Since the structure of cancellous bone is anisotropic and is more obvious for smaller bones, indentation test could be an alternative for compression test. In this study, there was no significant differences between the mean values of each indentation property for the right femoral, tibial or humeral epiphyses and the mean values of the same property for the left ones. Obvious differences were found between different epiphyseal bones, which is resulted from different functions of different locations (Goldstein et al., 1987). There have been no reports on the mechanical symmetry of rabbit long bones using bending and indentation test. White et al. (1974) found no evidence of right or left dominance in torsional properties of rabbit long bones, but considerable variation between pairs. This is in accordance with our study. Although no difference was found between the mean values of the mechanical parameters of the left and right side bones, significant variations indeed existed between both sides for a certain number of animals. The current study also showed that the variation in the mechanical properties of a given long bone of different animals was much greater then between paired bones of the same animal. So, a "paired left-right" comparison in one animal is a much better than comparison between two animals. "Paired" designs are based on the assumption that the mechanical properties between left and right limbs are symmetrical. If the condition is well controlled the number of animals in each group can be reduced significantly. The mechanical symmetry of some human and other animal bones has been verified (Bak et al., 1992; Kersey et al., 1993; Mather, 1967; White et al., 1974). When using an animal of which the mechanical symmetry has not been experimentally verified, a better design is that a given variable be employed to the left or right side randomly and then all the treated sides and the untreated sides can be compared using a paired student T test. By doing this a potentially existing asymmetry between the two sides can be eliminated.

REFERENCES

Aitken, G.K. et al. Clin. Orthop., 201,264-270,1985.
Bak, B. et al. Bone, 13,289-295,1992.
Currey, J.D. et al. J. Biomech., 21,131-139,1988.
Goldstein, S.A. J. Biomech., 20:1055-1061,1987.
Jørgensen, P.H. et al. Bone, 12,353-359,1991.
Kasra, M. et al. Bone,15,557-561,1994.
Kersey, R.C. et al. Trans Soc Biomater, 16,119,1993.
LaBerge, M. et al. J. Invest. Surg., 4,109-110,1991.
Lees, S. et al. Calcif.Tiss. Int., 50,88-92,1992.
Mather, B.S. J. Trauma, 7,633-638, 1967.
Martin, R.B. et al. J. Biomech., 26,1047-1054,1993.
Nakabayashi Y. et al. J. Arthropl., 9,307-315,1994.
Nash, T.J. et al. Bone,15,203-208,1994.
White, A.A. et al. Acta Orthop Scand 45,328-336,1974
Wootton, R. et al. Int. Orthop., 14,189-193,1990.

ACKNOWLEDGMENTS

The authors thank Drs. RA Draughn and RA Young of the Department of Materials Science, MUSC for technical consultation.

Table 1. Mechanical parameters (Mean±SD, n=17 pairs of each diaphyseal bone or each epiphyseal bone).

Mechanical test	Ultimate load (N)		Stiffness (N/mm)		Ultimate strength (MPa)		Elastic modulus (GPa)	
Bones or epiphyses	Left	Right	Left	Right	Left	Right	Left	Right
Three point bending								
Femoral diaphysis	352±54	353±53	393±58	413±80	122±23	137±34	13.0±1.8	14.9±2.6*
Tibial diaphysis	320±49	320±53	304±52	301±63	187±23	198±33	20.4±2.5	21.5±4.6
Humeral diaphysis	289±36	284±33	363±53	367±72	181±29	165±19	14.4±2.4	13.6±2.7
Indentation test								
Femoral head	344±88	362±92	1259±379	1497±455	81±21	86±22		
Med. femoral condyle	266±78	271±72	1526±716	1586±791	63±18	64±17		
Lat. femoral condyle	190±52	190±53	1048±558	1066±563	45±12	45±13		
Med. tibial plateau	247±86	244±79	1336±620	1041±438	58±20	55±21		
Lat. tibial plateau	338±101	320±104	1693±635	1510±643	77±21	76±25		
Humeral head	146±39	136± 21	806±326	609±225	35±9	32±5		

* P=0.020 (It was the only one with P value less than 0.05. For all others, P value was larger than 0.05).

ETHANOL FIXATION VS. FRESH FREEZING: EFFECTS ON TORSIONAL PROPERTIES OF OVINE TIBIAE

H. Reichel[1], M. Fagan[2], A. Turner[3], K. Ohland[2], H. Aberman[2]
[1]Klinik für Orthopädie, Martin-Luther-Universität Halle-Wittenberg, Halle, Germany
[2]Howmedica Worldwide R&D, Howmedica Inc., Rutherford, NJ 07070
[3]Department of Clinical Science, Colorado State University, Fort Collins, CO 80523

INTRODUCTION

When investigators from several facilities collaborate, specimens may be tested at sites far from where they are harvested. Often, the specimens are fresh frozen and shipped overnight with dry ice. However, when the collaborations are international the specimens may need to be fixed prior to shipping due to international shipping requirements. While it has been shown that freezing has little effect on the mechanical properties of bone (Sedlin et al., 1966), the effect of fixation on the properties of whole cortical bone, is inconclusive (Sedlin et al., 1966; Linde et al., 1993; Hayes et al., 1979). This study was performed to quantify the changes in the torsional properties of ovine tibiae due to fixation in 70% ethanol.

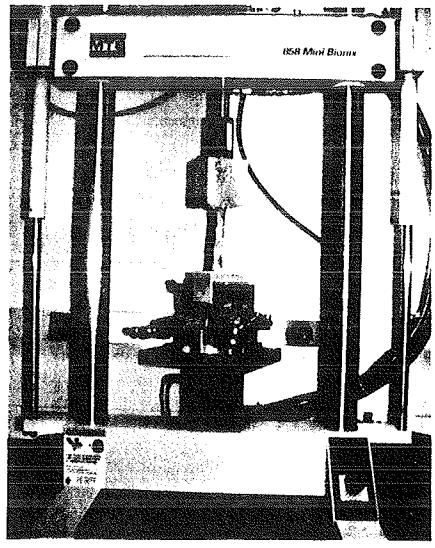

Figure 1: Mechanical testing apparatus

PROCEDURES

Ten pairs of tibiae were harvested from skeletally mature sheep of the same breed, sex and age. One tibia from each pair was placed in 70% ethanol at room temperature for four weeks. The contralateral tibiae were kept fresh frozen for the same time period at -20°C. Prior to testing, the frozen tibiae were thawed to room temperature and all tibiae were dissected free of soft tissue. The tibiae were then trimmed and each end potted in bone cement using a fixture specially designed to maintain alignment. The testing was performed using a MTS 838 Bionix test machine (Figure 1).

Figure 2: Mode of failure for tested specimen

A compressive load of 10N was applied and then the vertical displacement was fixed. The tibiae were tested to failure in torsion by rotating the distal end internally at 15°/min. The maximum torque and angle at maximum torque were recorded. The energy of absorption and the torsional stiffness up to 65% of the maximum torque were calculated using the trapezoidal rule and linear regression, respectively. Paired Student's *t*-tests, for normal distributions, and Wilcoxon's signed-ranks tests, for skewed distributions, were performed to determine significance between groups.

RESULTS

All tibiae failed by spiral fracture in the diaphysis (Figure 2). Normal distributions were found for maximum torque and torsional stiffness, but not for angle at maximum torque or energy of absorption (Table 1). The maximum torque, angle at maximum torque, and energy of absorption for the ethanol-fixed tibiae were significantly larger than those for the fresh frozen tibiae ($p<0.001$ in all cases). The torsional stiffness for the fresh frozen tibiae were significantly larger than those for the ethanol-fixed tibiae ($p<0.0001$). Although the ethanol-fixed tibiae were only ~15% less stiff than the fresh frozen tibiae, the ethanol-fixed tibiae absorbed more than twice as much energy.

Table 1: Torsional Properties of Ovine Tibiae

Property	Ethanol Fixed	Fresh Frozen
Maximum Torque (N-m)	68.8±10.3	52.5±7.3
Angle at Max. Torque (deg)	14.3±1.8	9.0±0.9
Torsional Stiffness (N-m/rad)	314.7±33.3	363.0±36.6
Energy of Absorption (J)	8.7±2.5	4.0±0.8

DISCUSSION

While it is preferable to test specimens that are fresh or have been fresh frozen, it is not always possible. Comparison of the torsional properties between ethanol-fixed and fresh frozen specimens indicates that ethanol fixation increases the compliance of the ovine tibia. This may be due to dehydration of the bone with the resultant loss of fluid stiffening (Ochoa et al., 1991), and/or crosslinking of proteins within the bone matrix. Therefore, storage conditions should be taken into consideration when performing mechanical testing of bones. Furthermore, the use of paired contralateral controls is recommended to limit the effect of storage and handling, as well as inter-subject variability, that could confound the results of the study.

REFERENCES

Hayes, W.C. et al. in Skeletal Research, (p. 267), ed DJ Simmons et al., Academic Press, NY, 1979.

Linde F et al. J Biomech, 26, 1249-52, 1993.

Ochoa JA et al. J Biomech Eng, 113, 259-62, 1991.

Sedlin ED et al. Acta Orthop Scand, 37, 29-48, 1966.

APPLICATION OF INDENTATION TEST ON RAT TRABECULAR BONE

Y. H. An, J.H. Zhang, Q. Kang, R. J. Friedman
Department of Orthopaedic Surgery, Medical University of South Carolina, Charleston, SC 29425

INTRODUCTION

Indentation testing is a kind of compression test of driving an indentor into a sectional surface of a bone specimen. Although the failure mechanisms are more complicated and less clear than the conventional compression test, it has been used for examining the mechanical properties of different cancellous bones of different species (Aitken et al., 1985; Behrens et al., 1974; Finlay et al., 1989; Josefchak et al., 1987; Saitoh et al., 1993; Sumner et al., 1994). While different parameters have been drawn from this test, very few comparable data set could be found in the literature. So far, no applications of the indentation test to smaller animals such as rabbits, which are widely used as models for bone growth, fracture healing, or osteoporosis, have been published. It is apparent, therefore, that further exploration is needed to provide a better experimental design, so that comparable data can be obtained, especially for small bones. In this study, the application of this indentation method on rat cancellous bone was described and the simplicity and usefulness of this method were analyzed. Also using this indentation test a mechanical data set for rabbit diaphyseal cancellous bones was reported.

PROCEDURES

Fifteen pairs of femurs, tibiae and humeri of adult female Sprag-Dawley rat (500±50 gm) used as healthy controls from other protocols were studied. The bones were collected within one hour of sacrifice, stripped of all soft tissues, wrapped in normal saline soaked paper towel, and frozen in airtight plastic bags at -20°C until mechanical testing. At the time of testing, the bones were thawed in normal saline and kept moist. The rat bones were potted in dental stone and ground on a rotating grinder to a certain depth (roughly one-third of the thickness of the sample bone) in the cancellous bone at the level of the epiphysis (Table 2). The surfaces to be tested were in a plane perpendicular to the line of weight-bearing considering the loading direction during the in vivo loading situation.

A mechanical test machine (MST System 810) was operated in a displacement control mode with a ramp function. The machine displacement transducer had been previously calibrated using an extensometer. The platform holding the specimen was leveled to ensure that the loading was perpendicular to the specimen surface to be tested. A cylindrical stainless steel indentor which was 1.31 mm in diameter with a flat bone-contacting surface was used. After the specimen was positioned on the platform and the indentor adjusted close to the specimen surface, the indentor was driven into the bone at a constant rate of 1 mm/min. The loading was stopped when the curve obviously dropped down after the ultimate load (the highest point of the curve). The curve of load-displacement was recorded using a chart recorder. No preloading was used, which was basically the initial part of the load-displacement curve. A stiffness measurement was obtained by measuring the slope of the linear portion on the load-displacement curves. A significant machine compliance (10-15 %) was determined by loading the system without a specimen, which were deducted from the total compliance. Since the test machine was controlled with a linear displacement rate (monitored by a built-in LVDT), the time base of the recorder could be converted to displacement. Indentation depth (or deformation) (μm) at 50 N was measured from the load displacement curve. Ultimate strength was calculated using the formulae (Nakabayashi et al., 1994):

$\sigma = 4P/\pi d^2$ (P is the ultimate indentation load and d is the diameter of the indentor).

ANOVA method was used to determine if any differences existed between different locations. Pearson correlation coefficients were calculated between indentation depth and elastic modulus or ultimate strength.

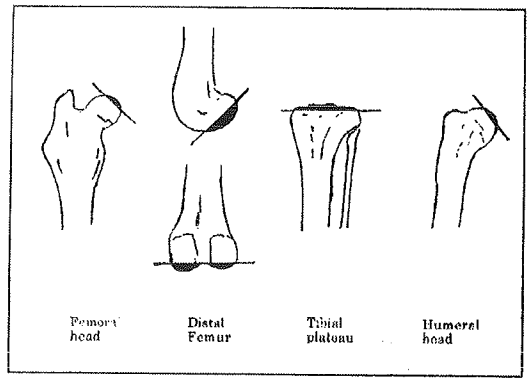

Figure1. The surfaces to be tested were in a plane perpendicular to the line of weight-bearing. The femoral head was ground perpendicular to the center line of the femoral neck from the center of femoral head to a depth of 1 mm. The distal femoral condyle was ground from weight-bearing surface of the condyles to a depth of 1 mm (This surface had a 20 degree angle with the distal femoral diaphysis). The tibial plateau was ground from the upper joint surface to a depth of 1 mm. The humeral head was ground perpendicular to the center line of the humeral neck from the center of humeral head to a depth of 1.0 to 1.5 mm. The bones were then embedded in dental stone with the surfaces to be tested at a horizontal position.

RESULTS

The ultimate load, stiffness, ultimate strength (ultimate stress), and indentation depth (at 50 N load) of the rabbit bones were obtained directly or calculated from the load-deformation curve (Table 1).

The ultimate strength were 71±15 MPa for the femoral head, 45±9 MPa for the medial distal femoral condyle, 39±11 MPa for the lateral distal femoral condyle, 50±10 MPa for the medial tibial plateau,38±9 MPa for the lateral tibial plateau, and 44±9 MPa for the humeral head. Good correlation have been obtained between indentation depth (at 50 N load) and ultimate strength (r^2 = -0.878, P<0.05), which mean that with the increase of ultimate strength the indentation depth or deformation decreased proportionally.

DISCUSSION

To the best of our knowledge, this is the first report on measuring mechanical properties of rabbit cancellous bones using indentation test. A useful mechanical data set has been generated. Differences were found between epiphyseal cancellous bones at different locations. The reason for this phenomenon is the functional difference between different locations of the tested cancellous bones (Goldstein, 1987). For example, the humeral head bears less load comparing to the femoral head, so the ultimate strength of the cancellous bones of humeral head is smaller than that of femoral head. Good correlations have been obtained between indentation depth (at 50 N load) and ultimate strength (r^2 = -0.878, P<0.05), which mean that with the increase of ultimate strength the indentation depth or deformation decreased proportionally.

Summer et al. (1994) has verified that the data obtained from the indentation test correlated well with that from the conventional compressive test. Although the ultimate strength and elastic modulus of different cancellous bones from different subjects are different, they generally fall into a certain range, like that of compression tests. According to the data pooled from the literature (Aitken et al., 1985; Behrens et al., 1974; Finlay et al., 1989; Josefchak et al., 1987; Sumner et al., 1994). and the data generated from this study, the ultimate strength of cancellous bones by the indentation test ranges from 38 to 71 Mpa. The wide ranges of these values are not surprising and are obviously due to different subjects and different locations. Even with the conventional compressive test, the range of elastic modulus was even much larger, such as from several MPa to 3000 MPa (Goldstein, 1987). Trabecular bone modulus can vary 100-fold from one location to another even within the same metaphysis (Goldstein, 1987).

Indentation testing is more suitable to the in vivo condition (a constrained compression test). The mechanical properties (mostly obtained from compression test) of a cube or cylinder bone sample separated from the bone such as femur or tibia are not the same as when the cube or cylinder are in the bone tissue, which can be only obtained by indentation testing. Indentation test is simpler than compression testing. Only a flat surface of the sample is needed for testing. It is less invasive than the conventional compression test. The indentation test makes testing on smaller bones such as the rat bones feasible since the diameter of the indentor can be designed as small as 1.31 mm. There have been no reports of attempts to test rat bones, using compression testing or any other methods, possibly because the bone size is too small. Since the structure of cancellous bone is anisotropic and is more apparent for smaller bones, indentation test may be an alternative for the conventional compression test. Also, fewer variables are involved with indentation testing compared to compression test. When the conditions of the test machine are set the same, with indentation test only the specimen deformation and the surface area of the indentor are needed, while using compression test with a cylindrical sample the length (which can not be controlled easily), end surface area, and the deformation have to be known.

In conclusion, the ultimate load, stiffness, and ultimate strength of the rat epiphyseal bones were obtained by using the indentation test. A useful mechanical data set has been generated. Differences were found between the cancellous bones at different locations. Based on the results and the comparison with the conventional compression test, the simplicity and usefulness of this indentation test for smal bone samples are apparent.

REFERENCES

Aitken, G.K. et al. Clin. Orthop., 201,264-270, 1985.
Behrens, J.C. et al. J. Biomechanics, 7,201-207, 1974.
Finlay JB. et al. Clin Orthop 247,193-201,1989.
Goldstein SA. J. Biomech., 20,1055-1061, 1987.
Josefchak, R.G. et al. Clin. Orthop., 220,192-199, 1987.
Nakabayashi, Y. et al. J. Arthroplasty, 9,307-315, 1994.
Saitoh, S. et al. Skeletal Radiol., 22,425-431, 1993.
Sumner D.R. et al. J. Biomech. 27,1095-1099, 1994.

ACKNOWLEDGMENTS

The authors thank Drs. R. A. Draughn and R. A. Young of the Dept. of Materials Science, MUSC for technical consultation.

TABLE 1. The results of indentation testing (Mean±SD, n=30 each epiphyseal location).

Bones	Ultimate load (N)	Stiffness (N/mm)	Ultimate strength (MPa)	Indentation depth (μm) at 50 N load
Femoral head	95±21	490±230	71±15	125±54
Med. fem. condyle	61±13	223±96	45±9	263±98
Lat. fem. condyle	52±14	249±81	39±11	216±70
Med. tibial plateau	67±14	239±65	50±10	223±64
Lat. tibial plateau	52±12	259±77	38±9	209±67
Humeral head	60±12	242±75	44±9	223±64

MECHANICAL PROPERTIES OF CANINE TRABECULAR BONES TESTED BY INDENTATION AND COMPRESSION TEST

Y. H. An, Q. Kang, R. J. Friedman
Department of Orthopaedic Surgery, Medical University of South Carolina, Charleston, SC 29425

INTRODUCTION

An indentation test was use to evaluate the mechanical properties of canine trabecular bones and compared to compression test. Samples from eight pairs of canine femoral heads, femoral condyles, tibial plateau, and humeral heads were tested. Ultimate load, stiffness, ultimate strength, and elastic modulus were obtained and calculated. Based on the results and compared to compression test, the simplicity and usefulness of the indentation test for testing compressive properties of the cancellous bone are apparent.

REVIEW AND THEORY

Indentation test has been used for examining the mechanical properties of different cancellous bones, such as human proximal femur (Saitoh et al., 1993), distal femur (Behrens et al., 1974; Nakabayashi et al., 1994), upper tibia (Behrens et al., 1974; Finlay et al., 1989), distal tibia (Aitken et al., 1985), proximal humerus (Saitoh et al., 1993), patellae (Josefchak et al., 1987), dog distal femur (Søballe et al., 1991). Since different parameters have been drawn from this test by different groups, very few comparable data sets could be found for inter-study comparison. Since dogs are popular for bone related research, the mechanical properties of their cancellous bones are important, which have not been well characterized. In this study, both indentation and compression test were used to evaluate the mechanical properties of canine epiphyseal cancellous bones. Also the correlation between the two tests and correlation between these tests and bone densities were analyzed.

PROCEDURES

Eight pairs of each femoral, tibial, and humeral bones (fresh frozen) of adult dogs (mixed bred, 18-23 kg) used as controls of other studies were used. The bones were kept moist during sample preparation and testing. The bones were ground and cut to obtain slices from the epiphyseal area (Fig 1). Identical slices from left or right limbs were randomly chosen for indentation or compression test. A total of 64 slices (5-mm thick) were harvested from the bones on one side, containing a total of 80 points for indentation test (3 points on tibial plateau). On the contralateral side at the identical points 80 4-mm diameter cylinders (5mm length) were made using a trephine for compression test. A mechanical test system (MTS 810) was operated under displacement control. After the specimen was positioned on the lower platen and the surface of the indentor (4.24 mm diam.) or the upper platen (polished steel) adjusted close enough to the sample surface, loading was started at a constant rate of 1 mm/min (monitored by a LVDT) and stopped when the curve dropped down obviously after the ultimate load. A stiffness measure was obtained from the linear portion of the curve. A significant (10-15 %) machine compliance was determined by loading the system without a specimen, which was deducted.

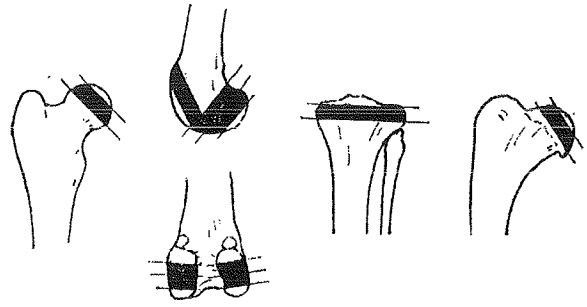

Figure 1. The surfaces and slices created for indentation and compression test.

Ultimate indentation strength (Nakabayashi et al., 1994) were calculated with the equation: $\sigma = 4\,P/\pi d^2$ (P is the ultimate load and d is the diameter of the indentor or the bone cylinder). Using the formulae of Timoshenko et al. (1970) and validated recently by Sumner et al. (1994), the elastic modulus by indentation test was calculated with the following equation: $E_I = S_i(1-\nu^2)/d$ (S_i is the indentation stiffness and d is the diameter of the indentor). Like the way of Sumner et al. (1994), the Poisson's ratio ν is assumed to be 0.2. The elastic modulus by compression test was calculated using the following equation (Martens et al., 1983; Mosekilde et al.,1987): $E_c = S_c L/A$ (S_c is the compression stiffness, L is the length of the cylinder, and A is the end-face area of the cylinder).

The tested cylinders were put into 1 % sodium hypochlorite for 18 hrs to remove the marrow, defatting for 4 hrs in 1:1 ethanol/acetone, rehydrated in water under vacuum, and followed by centrifugation at 3,700 rpm for 30 min to remove excess water. The samples were then weighed for wet weight. Apparent density was calculated by dividing the wet weight by the sample volume. Then, the samples were ashed in a furnace at 500°C for 48 hrs. The Ash density was calculated by dividing the ash weight by the sample volume. Pearson correlation coefficients were calculated between the two mechanical tests and between the two tests and the bone densities.

RESULTS AND DISCUSSION

For different bone locations, the elastic modulus by both indentation test and compression test were different, with the highest values for the femoral head

and the lowest for the humeral head (Table 1). The mechanical parameters by indentation test were higher than those obtained by compression test. Correlation analysis showed the two sets of mechanical values by indentation and compression test correlated very well (r^2>0.08). Also, bone densities (Table 2) correlated very well with the mechanical values by both mechanical tests (r^2>0.8).

Table 1. Mechanical properties (MPa) of canine cancellous bones (Mean±SD, n=8 pairs of each part of the bone).

Bones	Test	Ultimate strength	Elastic modulus
Femoral head	Comp	29±4	428±237
	Indent	85±15	1111±284
Med. fem. condyle level 1	Comp	28±7	354±13
	Indent	67±11	945±342
Lat. fem. condyle level 1	Comp	24±4	394±105
	Indent	56±9	924±129
Med. fem. condyle level 2	Comp	19±5	317±98
	Indent	40±7	636±212
Lat. fem. condyle level 2	Comp	14±4	279±185
	Indent	37±4	517±156
Fem. intercondylar groove	Comp	13±3	210±47
	Indent	41±9	585±187
Medial tibial plateau	Comp	10±3	215±153
	Indent	26±9	346±63
Lateral tibial plateau	Comp	24±6	426±208
	Indent	44±11	572±259
Anterior tibial plateau	Comp	5±2	106±51
	Indent	17±7	232±101
Humeral head	Comp	18±6	350±171
	Indent	43±8	667±70

Table 2. Appearant density and ash density of canine epiphyseal trabecular bones (Mean±SD, n=8).

Bones	Apperant density (mg/mm^3)	Ash weight (mg/mm^3)
Femoral head	1.17±0.17	0.65±0.09
Med. fem. condyle level 1	0.98±0.07	0.56±0.07
Lat. fem. condyle level 1	0.89±0.12	0.50±0.08
Med. fem. condyle level 2	0.77±0.17	0.44±0.10
Lat. femoral condyle level 2	0.69±0.13	0.41±0.10
Intercondylar groove	0.69±0.12	0.40±0.05
Medial tibial plateau	0.52±0.11	0.31±0.09
Lateral tibial plateau	0.83±0.20	0.44±0.13
Anterior tibial plateau	0.41±0.11	0.22±0.04
Humeral head	0.84±0.17	0.43±0.06
Mean±SD	0.78±0.22	0.44±0.12

There are very few reports on the mechanical properties of canine epiphyseal bones. In this study, a data set was generated using the conventional compression test. For the same locations (distal femur, proximal tibia), the values of ultimate strength and elastic modulus are basically in accordance with that reported by others (Vahey et al.,1987; Kuhn et al., 1989). Comparing the values of the distal femur and tibial plateau, the ultimate strength of human bones (4 MPa) (Linde et al., 1992) is much weaker than that of canine bones (17 MPa). Sumner et al. (1994), Aitken et al. (1985), Nakayabashi et al. (1994) were the few groups reported comparable data of trabecular bones using indentation test. The elastic modulus based on the stiffness data by Finlay et al. (1989) is also comparable (300-400 MPa for human upper tibia). From the present study, a comparable data set was generated by using indentation test. Compared to human bones, canine bones are stronger (ultimate strength 37-67 MPa vs 5-40 MPa for distal femur) (Nakayabashi et al., 1994). The values by indentation test are higher than that by compression test. The reasons may be 1) that the column of bone tissue under the indentor is under the constraint of the surrounding bone and 2) a strong shearing resistance arises around the edge of the indentor while the indentor is being pressed in.

The correlation analysis is in accordance with that of Summer et al (1994), in which the mechanical values by the indentation test correlated very well with those by compression test. Several advantages of this test have been shown. Presumably, indentation test is more suitable to the in vivo condition, a constrained compression test. It is simpler and less invasive than compression test. Since the structure of cancellous bone is anisotropic and is more apparent for smaller bones, indentation test may be more useful. Fewer variables are involved with indentation test. Using indentation test, only the indentation depth and the surface area of the indentor are needed. Due to the error during specimen preparation the final dimension of bone cylinder will differ to a certain degree. In this study, for example, the planned length of the bone cylinder was 5mm, while the final length was 4.95±0.45mm, with the minimum being 3.65mm and maximum 5.84mm.

The correlation between bone densities and compression test have been well documented (Carter et al., 1977; Rice et al., 1988; Linde, 1994). Rice et al. (1988) found that both of the modulus and strength are proportional to the square of apparent density and therefore proportional to one another. There were very few reports on the correlation between indentation values and bone densities. The present study verified that the correlation between the indentation test and bone densities are very significant. One explanation for the stronger and stiffer nature of canine trabecular bones may be that the values of apparent density are much higher in dog bones (0.78 gm/cm^3) than human bones (0.05-0.60 gm/cm^3) (Keaveny et al., 1993).

REFERENCES

Aitken, G.K. et al. Clin. Orthop., 201:264-270, 1985.
Carter, D.R. et al. J. Bone Joint Surg., 59A,954-962, 1977.
Finlay, J.B. et al. Clin. Orthop., 247,193-201, 1989.
Josefchak, R.G. et al. Clin. Orthop., 220,192-199, 1987.
Linde, F. et al. J. Biomech., 25,359-368, 1992.
Keaveny, T.M. et al. J. Biomech. Eng., 115,534-542, 1993.
Martens, M. et al. J. Biomechanics, 16,971-983, 1983.
Mosekilde, L. et al. Bone 8,79-85, 1987.
Nakabayashi, Y. et al. J. Arthropl., 9,307-315, 1994.
Rice, J.C. et al. J. Biomechanics 21,155-168, 1988.
Saitoh, S.et al. Skeletal Radiol. 22,425-431, 1993.
Saitoh, S. et al. J. Shoulder Elbow Surg., 2,78-84, 191993.
Søballe, K. et al. Skeletal Radiol. 20,345-352, 1991.
Sumner, D.R. et al. J. Biomech., 27,1095-1099, 1994.
Timoshenko, S.P. et al. Theory of Elasticity (pp. 380-409), McGraw-Hill, 1970

ACKNOWLEDGMENTS

The authors thank Drs. R. A. Draughn and R. A. Young of the Dept. of Materials Science, MUSC for technical consultation.

EFFECTS OF A CARRAGEENAN INDUCED ARTHRITIC KNEE ON THE PERIARTICULAR BONE IN THE RABBIT

Y. H. An, Q. Kang, R. J. Friedman
Department of Orthopaedic Surgery, Medical University of South Carolina, Charleston, SC 29425

INTRODUCTION

Bogoch et al. (1988) reported that carrageenan-induced knee arthritis caused juxtaarticular osteopenia to the femoral metaphyseal and diaphyseal bone in a rabbit model. However, the morphologic changes have not been well documented. Many questions remain unanswered, such as structural and morphological changes in bone volume, any effects in the proximal femur and distal tibia. The mechanical properties of osteopenic bone are very important parameters to consider in issues such as fracture mechanics or bone ingrowth to prosthetic surfaces under osteopenic conditions. There has been only one report characterizing the mechanical properties of osteopenic bones, that being in the distal femoral condyle by indentation testing only (Søballe et al., 1991). To answer these questions, inflammatory knee arthritis was induced by carrageenan injection in adult rabbits to evaluate the effects of inflammatory arthritis on the structural and mechanical properties of the adjacent long bones.

METHODS

Thirty six adult male NZW rabbits (4.0±0.5 kg) were used. All the right knees were injected with 0.3 ml 1% carrageenan (Gardner 1960) twice a week for 6 weeks. Two weeks after the first injection cylindrical implants were implanted bilaterally into the distal femoral condyle as part of another study. The animals were sacrificed 6 weeks after surgery. Six pairs of femurs, tibiae, and humeri were used to evaluate the effects of the arthritis on long bone structure. Ten pairs of these bones were used to evaluate the effects on mechanical properties of the bone using three point bending and indentation test (An et al., 1996)

The following structural and morphological parameters were studied: 1) bone density by X-ray image analysis; 2) long bone geometry and morphology measured by direct measurement and SEM; 3) cancellous bone structure based on SEM images, including trabecular bone volume (TBV), trabecular number (Tb.N) and continuous marrow space number (Ho.N), trabecular thickness (Tb.Th), trabecular spacing (Tb.Sp), trabecular node (Nd), trabecular free ends (Tm) (Parfitt et al., 1983), and the thickness of subchondral bone plate (SCBP).

A MTS machine (System 810) was operated in a displacement control mode with a ramp function for both three point bending and indentation tests. The machine displacement transducer had been calibrated using an extensometer. Since the machine was controlled with a linear displacement rate (monitored by the built-in LVDT), the time base of the recorder could be converted to displacement.

For the bending test, the point to be tested was located and marked and dimensions at that point were measured with a sliding electronic caliper. After the bone was positioned on the two supports of the testing gear (6 mm diameter each and a 50 mm span), a striker (6 mm diameter) was driven to the bone surface at a constant rate of 1.0 mm/min. until the bone fractured. The specimen aspect ratios in this setting was 6.25 for the femur, 8.67 for the tibia and 7.62 for the humerus. The following equation was used for calculating the ultimate bending strength (Jørgensen et al., 1991, Martin et al., 1993):

$$\sigma_b = P_b L a / 8I \quad (1)$$

where P_b is the ultimate load, a is the average value of the external anteroposterior diameters of the cross-sections at the loading point of the tested bone, L is the distance between the supporting bars, and I is the area moment of inertia (assuming the long bone cross-sections to be elliptical tubular):

$$I = \pi (a^3 b - a'^3 b')/64 \text{ (femur and tibia)} \quad (2)$$

$$I = \pi (ab^3 - a'b'^3)/64 \text{ (humerus)} \quad (3)$$

The values chosen for a, a', b and b' are the average values of the external and internal anteroposterior and mediolateral diameters of the cross-sections at the loading points. The remainder of the tested portion of the bone was assumed to be consistent in cross-sectional size and shape. For the humerus, equation (3) was used since the surface of bone facing the loading striker was lateral for humerus. The following equation was used for calculating elastic modulus of the diaphyseal bones (Kasra et al., 1994):

$$E_b = SL^3 / 48I \quad (4)$$

where S is the bending stiffness and L is the distance between the supporting bars.

(1) (2) (3)

Figure 1. (1) Bone surfaces created for indentation test. Femoral head: ground from anterior side to a depth of 30 percent of the whole thickness; (3) Tibial plateau: ground from anterior side to a depth of one third of the whole thickness. (3) Humeral head: ground from posterior side to a depth of 30 percent of the whole thickness.

For indentation test, selected sample bones were rough cut on a bandsaw and then ground on a rotating grinder to a certain point in the cancellous bone in the

epiphysis (Fig.1). A cylindrical stainless steel indentor (2.8 mm diam) with a flat end-surface was used. The indentor was driven into the bone at a constant rate of 1 mm/min. The loading was stopped manually when the curve turned downward after the ultimate load. The ultimate load from each curve was divided by the indentor face area to obtain ultimate strength (Nakabayashi et al., 1994):

$$\sigma_i = 4\,P_i/\pi d^2 \qquad (5)$$

where P_i is the ultimate indentation load and d is the diameter of the indentor.

Since the data were obtained from paired samples, student T test was used. The correlation between structural and mechanical parameters were analyzed.

RESULTS AND DISCUSSION

At necropsy, all the right knees developed inflammatory arthritis by maro- and micro-evaluation. Significant differences of bone density were found between the left and right side for the femur and tibia by X-ray. The femur and tibia showed obvious differences in cortical thickness, cross-sectional cortical bone area, and cross-sectional medullary canal area (MCA) between right and left legs as shown by direct measurement. SEM showed that on the arthritic side of the proximal femoral diaphyseal region the trabecular portion of the cortex was diminished and looked more porous, with obvious thinner trabeculae compared to the control side. In the distal one third of the femur the endosteal surfaces were more porous than the control side. Many cavities were seen on the cortical sectional surface, which indicated subendosteal cavitation.

For cancellous bone, image analysis showed that the TBV was significantly decreased for the right femur and tibia (Table 1.). The trabeculae on the right side were thinner and had wider marrow space. The subchondral bone plate was also much thinner on the arthritic side. The indices of cancellous connectivity, Euler number (Tb.N-Ho.N) and Nd/Tm ratio showed less connectivity on the arthritic side for the femur and tibia compared to normal.

Compared to the control side, the ultimate load, stiffness, ultimate strength, and elastic modulus by three point bending of the femoral and tibial diaphysis and the ultimate load, stiffness, and ultimate strength by indentation test of the right (arthritis side) femoral head and tibial epiphysis, and , were all significantly diminished (Table 2). No differences in structural or mechanical properties were found in the humerus. Using Pearson correlation analysis significant correlation was found between mechanical changes and most morphological parameters (r>0.8).

Carrageenan-induced knee arthritis resulted in osteopenic changes to the entire ipsilateral femur and tibia, including the femoral head and distal tibia. No differences were found in the bones of the humerus. These results demonstrate that this rabbit model can be used as a model for studying localized osteopenia.

The causes of the osteopenia may include the lack of stimulation from gravity or weight-bearing ambulation, and changes in local blood flow due to increased intraarticular pressure. The carrageenan arthritis caused a dramatic decrease of bone strength in both epiphyseal and diaphyseal regions of this rabbit model. The structural changes, both in bone volume and quality, are the basis for this reduced mechanical strength.

Table 1. Comparison of TBV (Mean±SD, N=6).

Bone	Control (left)	Arthritic (right)	P
Femoral head	48±11	28±3	0.003
Medial femoral condyle	35±7	19±6	0.001
Upper tibia	30±6	16±6	<0.001
Distal tibia (lat. trochlea)	45±11	26±10	0.023
Humeral head	37±10	33±3	0.429

REFERENCES

An, Y.H. et al. Application of indentation test on rabbit cancellous bone. J. Orthop. Res., submitted, 1996.
Bogoch, E. et al. J. Orthop. Res., 6,648-656, 1988.
Jørgensen, P.H. et al. Bone, 12,353-359, 1991.
Gardner, D.L. et al. Ann. Rheum., 19,369-376, 1960.
Kasra, M. et al. Bone, 15,557-561, 1994.
Martin, R.B. et al. J. Biomech., 26,1047-1054, 1993.
Nakabayashi, Y. et al. J. Arthropl., 9,307-315, 1994.
Parfitt, A.M. et al. J. Clin. Invest., 72,13961409,1983
Søballe, K. et al. Skeletal Radiol., 20,345-352, 1991.

ACKNOWLEDGMENTS

The authors thank Drs. RA Draughn and RA Young of the Dept. of Materials Science, MUSC for technical consultation.

Table2. Effect of carrageenan-arthritis on mechanical properties of rabbits bones (Mean±SD, n=10 pairs).

Mechanical test	Ultimate load (N)		Stiffness (N/mm)		Ultimate strength (MPa)		Elastic modulus (GPa)	
Bones or epiphyses	Left	Right	Left	Right	Left	Right	Left	Right
Three point bending								
Femoral diaphysis	380±65	227±33**	604±83	370±51**	97±21	80±16*	8.3±1.5	7.1±1.4*
Tibial diaphysis	395±39	299±41**	474±72	353±70**	186±26	173±19*	15.9±2.9	14.9±2.2†
Humeral diaphysis	350±39	349±33†	461±76	473±48†	158±25	157±26†	11.9±2.7	12.4±2.4†
Indentation test								
Femoral head	419±9	159±48**	2296±1041	1038±704**	68±15	26±8**		
Upper tibia	207±50	100±45**	1232±469	565±298**	34±8	16±7**		
Humeral head	183±47	184±52†	1397±724	1179±849†	30±8	30±8†		

* P<0.05; ** P<0.01; † P>0.05.

THE EFFECT OF INTERLOCKED STRESSES ON CARTILAGE MECHANICS: A FINITE ELEMENT STUDY

Thomas E. Daniel and Donald D. Anderson
Biomechanics Research Laboratory, Allegheny-Singer Research Institute
Pittsburgh, Pennsylvania 15212

INTRODUCTION

Finite element (FE) analyses were performed to study the effect of experimentally observed cartilage swelling/curling on joint mechanics. Residual pre-stress was introduced to an axisymmetric model of a cartilage-on-bone cylindrical plug to examine joint stresses during compressive loading. In addition, an axisymmetric layered model of joint articulation (validated against an analytical solution) was used to quantitate the stress/strain field local to deformable contact with and without interlocked residual stresses.

REVIEW AND THEORY

Cartilage swelling and curling, upon release from its anchorage to subchondral bone, has been documented in *in vitro* experimental preparations (Fry, 1974, Setton et al., 1994). While these findings strongly suggest the existence of residual stress in the intact joint, the mechanical parameters used to describe these shape changes in cartilage have only recently begun to be quantified. Kaufmann et al. (1995) implemented a porohyperelastic transport/ swelling theory in FE modeling of soft tissues. Using an analytical model, Setton et al (1992) calculated pre-stress in spherical and cylindrical layer models of articular cartilage, and found maximum radial stress at the cartilage-bone junction and maximum circumferential stress at the cartilage surface. While these models use sophisticated formulations, they do not easily lend themselves for use in large deformation contact analyses.

We intend to develop a computational model, first using simplistic material formulations, to investigate the role of residual stresses in the normal loading environment of articular cartilage. Such an implentation will lend itself to more sophisticated material modeling of specific three dimensional joint contact behavior. Two FE models were developed to achieve this purpose. The first was of a cartilage-bone plug to develop the technique of including cartilage pre-stress. The second model, more representative of joint contact, was based on an analytical formulation developed by Eberhardt et al (1991). Using an axisymmetric model of two layered elastic spheres, localized stresses and strains can be studied in the presence and absence of simulated pre-stress. Our hypothesis is that the predicted stress/strain field at the cartilage-bone interface of a loaded joint will be reduced in the presence of residual cartilage pre-stress.

PROCEDURES

In the first model, a cylindrical region (radius=5mm, thickness =1mm) was modeled with 1190 isotropic continuum elements and 12 finite sliding contact elements across the cartilage surface. The 2610 degree-of-freedom (DOF) axisymmetric FE model initially consisted of one linear elastic material region (cartilage). The nodes lying on the axis of symmetry were fixed radially and a pre-stress field, varying linearly with cartilage depth was supplied as an initial condition. The magnitude of radial and circumferential pre-stress corresponded to the elastic stress components derived by Setton et al. (1992). This model was run to verify actual curling phenomenon as observed in experiments where cartilage was separated from the underlying bone. The model was then halved to include a subchondral bone layer. In this two layer configuration, an additional constraint was supplied to constrain the inferior nodes of the bone in the vertical direction. To examine the effect of pre-stress in a normal loading environment, a curved rigid surface was brought into contact with the cartilage surface while pre-stress was included in the cartilage elements.

Lastly, a 2422 DOF axisymmetric contact model (Figure 1) of two elastic spheres was created using the geometry and material properties of an analytical model developed by Eberhardt et al. Two spheres were modeled with 1153 isotropic continuum elements and 20 finite sliding contact elements. Both bodies consisted of three linear elastic material regions: cartilage, subchondral bone, and cancellous bone. With and without cartilage pre-stress, equal and opposing loads were applied to the bodies. Both models were run under large deformation analysis using the ABAQUS standard FE code.

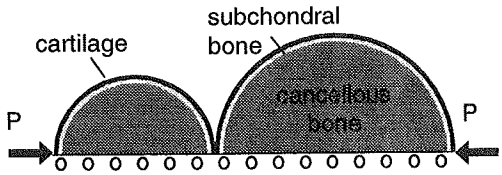

Figure 1

RESULTS

The curling behavior of cartilage, simulating its removal from its bony attachment, is depicted in a von Mises strain/deformation plot shown in Figure 2. The darkest region corresponds to strain values approaching 22%.

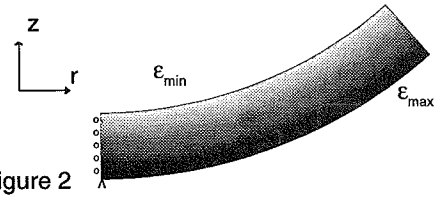

Figure 2

Including the supporting subchondral bone and contact loading with a rigid spherical indentor, a plot of principal stresses through cartilage depth at the model's center is given in Figure 3.

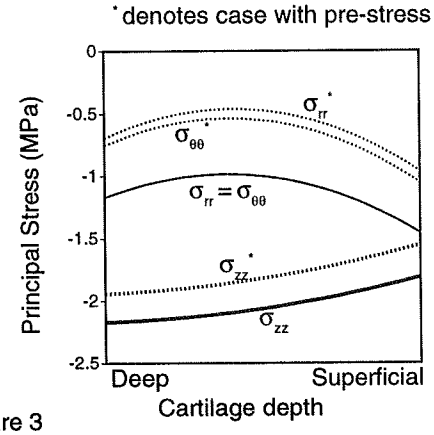

Figure 3

The FE solution of two spheres in deformable contact (without pre-stress) agreed with the analytical solution (in terms of surface contact stress and contact area) to within 1%. In the presence of an applied radial and tangential pre-stress (corresponding to the pre-stress in spherical layers calculated by Setton et al.), the resulting maximum axial compressive stresss decreased by 8%. Figure 4 shows a deformation plot of axial stresses in the contacting cartilage layers for the two cases.

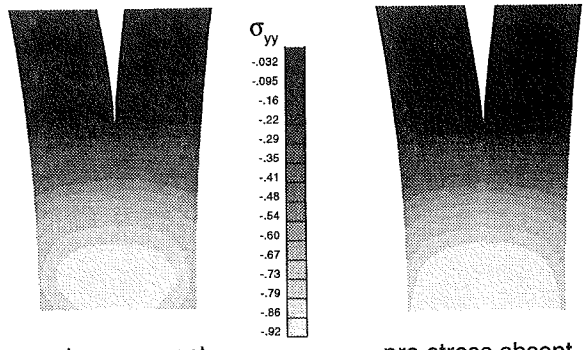

Figure 4 Axial compressive stress (MPa)

DISCUSSION

The main limitation of the two models is the simplistic property definition of cartilage. While specific stress information on the solid matrix and interstitial fluid components of cartilage are not derived from our analyses, the finding of decreased stresses during compressive loading in the presence of pre-stress is consistent with the postulated hypothesis (Setton et al). Furthermore, we have demonstrated a technique that can easily be implemented in large deformation, contact analyses.

Finite element models used to study articular contact must incorporate experimental observations of sophisticated material behavior and loading environment. While FE models of articular joints have incorporated non-linear, viscoelastic formulations of experimental material behavior and the phenomenon of contact, the analytical and experimentally observed behavior of cartilage pre-stress has not received much mention in FE analyses. With future inclusion of full three-dimensional geometry and more accurate material formulation of cartilage, the role residual pre-stress plays in a specific joint under complex loading can be studied.

REFERENCES

Eberhardt AW et al., J Biomechanical Engineering, Vol 113:410-417, 1991.
Fry JH, J Plastic Surgery (Br), Vol 27:363-364, 1974.
Kaufmann MV et al., Advances in Bioengineering, ASME/BED,Vol 29:315-316, 1995.
Setton LA et al., Advances in Bioengineering, ASME/BED, Vol 22: 485-488, 1992.
Setton LA et al., Advances in Bioengineering, ASME/BED, Vol 28: 135-136, 1994.

ACKNOWLEDGMENTS

Financial support from the Albert B. Ferguson, Jr. M.D. Orthopaedic Foundation is gratefully acknowledged.

Load sharing between the solid and fluid in cartilage during in situ loading

N. Mukherjee, J.S.Wayne
Orthopaedic Research Laboratory
Medical College of Virginia, Virginia Commonwealth University
Richmond, VA 23298-0694

INTRODUCTION

Articular cartilage must function in the demanding environment of diarthrodial joints which impose large loads over millions of cycles. This ability has been attributed to many features of diarthrodial joints including the structural makeup and bio-mechanical behavior of cartilage and the mechanism of lubrication between opposing articular surfaces.

The biomechanical behavior of articular cartilage has been successfully modeled with the biphasic theory (Mow et al., 1980). By virtue of incorporating both solid and fluid phase contributions to the overall biomechanical behavior, a given load/stress imposed on cartilage is shared by both phases. For the experimental configurations of confined compression and indentation, the free draining condition at the surface specifies the fluid pressure to be zero at the surface. This partitioning of the applied stress would be 0% for the fluid and 100% to the solid at the surface. However, when cartilage is loaded in situ, it has been suggested (Hou et al, 1989) that the stress is partitioned to both phases at the surface. Partitioning the applied stress to different levels between the two phases has a dramatic influence on the behavior of the cartilage layer (Wayne, 1995). The actual level of partitioning in situ is not well known, however.

This study sought to determine the load partitioning at the surface between the two phases of cartilage under in-situ loading conditions. It combines both experimental and theoretical approaches to appropriately describe cartilage behavior in a joint environment.

PROCEDURES

The purpose of the experimental approach was to measure different parameters for cartilage in the in situ environment of a loaded joint. A static compressive load of 450 N was applied to the porcine knee in the maximally extended position over a ramp time of 60 s and then held constant. During this time, the fluid pressure at the cartilage surface on the lateral femoral condyle was monitored by two miniature fiber optic pressure transducers (Brodrick et al.,1996). The initial and deformed thickness of the cartilage layer were measured without disarticulation (Brodrick et al.,1995) at various times during loading. Thus cartilage deformations at those time points under the given loading conditions were calculated.

The purpose of the theoretical approach was to model the experimental setup incorporating boundary conditions of the applied stresses determined and the anatomic features of the cartilage layer. The u-p finite element model (Wayne et al., 1991) was used to model cartilage behavior in this setup. Points defining the boundary of the cartilage on the lateral femoral condyle were obtained from a digitized roentgenographic image of the unloaded cartilage surface where both the bone-cartilage interface and the cartilage surface were clearly visible (Brodrick et al, 1995). A finite element mesh was created based on these points using PATRAN, a commercially available finite element package.

The boundary conditions applied to the u-p model were: 1) at the bone-cartilage interface, the cartilage was rigidly attached to the bone; 2) at the surface of the cartilage, the total applied pressure was based on the pressure readings obtained from the two pressure transducers used in the experiment. The distribution of this pressure across the surface for a given instant of time was assumed to be linear. Material properties of the cartilage layer were obtained from indentation experiments on the porcine lateral femoral condyle and were found to be : aggregate modulus = 0.92 MPa, permeability = 0.005 mm^4 /Ns and Poisson's ratio = 0.14.

For each knee examined, four finite element cases were considered based on the percent of partitioning of the applied stress between the solid and fluid phases at the cartilage surface. 1) 30%

of the total stress was partitioned to the fluid; 2) 50%; 3) 70%; and 4) 90%. The load partitioning was assumed to be constant across the cartilage surface and over the duration of the experiment.

Each of the finite element predictions of cartilage deformation normal to the cartilage-bone interface were compared with that obtained experimentally. Only two time points (60 s, i.e. at the end of ramp loading, and 120 s after the start of loading) for each experiment were used in conjunction with the finite element predictions to maintain cartilage behavior in the linear region. This combination of experimental measurements and finite element predictions was completed for two porcine knees.

RESULTS AND DISCUSSION

From both experimental and finite element observations, the linear distribution of pressure produced increasing deformations consistent with the direction of pressure increase, i.e. from lateral to medial edge of condyle (Figure 1). The u-p finite element predictions for the four cases showed expected trends when a larger partitioning of the load by the fluid at the surface was specified: 1) smaller deformations of the cartilage layer were incurred (Figure 2); and 2) progression toward equilibrium proceeded more rapidly.

The comparison between the experimental measurements of cartilage deformation and the predictions of the finite element model indicated that the best correlation was obtained when 70% of the applied pressure was supported by the fluid at the surface (Figure 3). This indicated that the fluid supports a major amount of the applied stress during normal cartilage function under a static compressive axial load. The same behavior was observed in both specimens examined, suggesting that the fluid phase has a significant role in load transmission in the diarthrodial joints. The percent of this load partitioning is consistent with theoretical reasoning that the percent should be related to the volume fraction of fluid within cartilage (Hou et al., 1989). This number characteristically lies in the 70-80% range for normal cartilage.

This study has provided both experimental and theoretical support for the concept that an applied stress to a cartilage layer is partitioned between the solid and fluid phases of the tissue at the surface. This may serve as one mechanism by which the solid component in normal cartilage is protected from large stresses during joint function.

REFERENCES

Brodrick et al., Fall Meeting BMES, Boston, 1995
Brodrick et al., Trans ORS, 21(2):737, 1996
Hou et al., J Biomech Eng, 111:78-87, 1989
Mow et al., J Biomech Eng, 102:73-84, 1980
Wayne et al., J Biomech Eng, 113:397-403, 1991
Wayne, Ann Biomed Eng, 23:40-47, 1995

ACKNOWLEDGMENTS

This work was made possible by the generous support of the Whitaker Foundation.

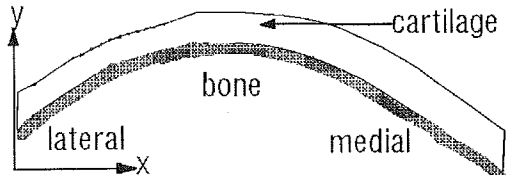

Figure 1: Outline of the cartilage surface and cartilage-bone interface obtained from digitizing the roentgenogram of the lateral femoral condyle.

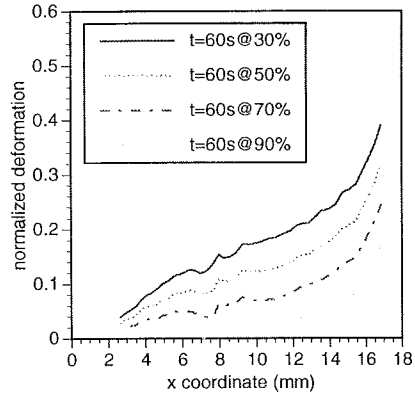

Figure 2: Cartilage deformation normalized to the undeformed thickness across the surface for different load partitioning cases. The x coordinate corresponds with that depicted in Figure 1.

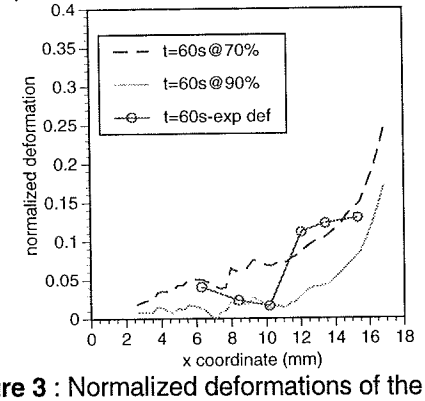

Figure 3 : Normalized deformations of the cartilage surface as predicted by the u-p finite element model for two partitioning cases. Experimental data points are superimposed.

MATHEMATICAL MODEL FOR THE DETERMINATION OF ZERO STRAIN REFERENCE

Yeou-Fang Hsieh and Louis F. Draganich
Section of Orthopaedic Surgery and Rehabilitation Medicine
Department of Surgery
The University of Chicago
Chicago, Illinois

INTRODUCTION

A mathematical model is developed for determining the zero strain reference (ZSR; i.e., the slack-taut transition length) of a ligament fiber for a given range of joint motion. The ZSR is necessary for determining engineering strain of the fiber. The model is based on the optimal elastic strain energy generated in the fiber. The determination of the ZSR consisted of three steps: first, determining the length pattern of the fiber, second, formulating the total elastic strain energy function, and third, formulating a nonlinear equation, representing optimization of the total elastic strain energy. This new non-contact method was validated by performing an experiment to determine the ZSR of a band composed of natural pure gum rubber. The application of this method is demonstrated for the anterior cruciate ligament (ACL) of the human knee although it may be applied to other ligaments in the knee or in other synovial joints.

REVIEW AND THEORY

Measurement of length change[6,7] or relative strain[1,3] as a function of joint position of the knee have been used to assess the biomechanical function of ligaments under various loading conditions. However, the engineering strains (absolute strains) of the ligaments in these studies could not be determined since the ZSRs, the lengths at which the ligaments begin to carry loads, were unknown. Therefore, the exact range of motion through which a ligament was restraining motion of the joint was unknown. Thus, determination of the ZSR for the calculation of engineering strain is necessary for precisely evaluating the stabilizing roles of the ligaments in the knee or other joints. Such information is needed for developing prosthetic ligaments and for surgically reconstructing ligaments. The objective of the present study was to develop a mathematical model for determining the ZSR of a given ligament fiber of the knee for a given range of knee motion and loading.

PROCEDURES

The determination of the ZSR (L_o) of the ligament fiber of interest consisted of three steps: first, determining the length pattern of the ligament fiber, second, formulating the total elastic strain energy function, and third, formulating a nonlinear equation to represent the optimization of the total elastic strain energy. In formulating this model two assumptions were made: (1) the ligament fiber is an incompressible material and (2) strain in the ligament fiber is uniform and stationary when the joint is in equilibrium.

Mathematical model

(A) The length pattern (L_m) of a ligament fiber over a range of motion can be expressed in terms of the tibial ($\bar{r}_T$) and femoral ($\bar{R}_F$) points of insertion of a fiber and the position of the tibia with respect to the femur (represented as $[B_{F,T}]_m$, a transformation between the tibial and femoral coordinate systems at the mth joint position) according to the equation

$$L_m = \left| \bar{R}_F - [B_{F,T}]_m \bar{r}_T \right| = \sqrt{(R_{xF} - r_{xF})^2 + (R_{yF} - r_{yF})^2 + (R_{zF} - r_{zF})^2} \quad (1)$$

(B) The total elastic strain energy function (U) for a fiber of a ligament for a range of flexion of the knee can be determined according to

$$U = U(L_o) = \sum_m U_m = \sum_m {A_o}/{\lambda_m}\, \sigma(\varepsilon_m)\,(L_m - L_o) \quad (2)$$

where U_m is the elastic strain energy stored in a ligament fiber at the mth joint position and is formulated as $(A_o/\lambda_m)\sigma(\varepsilon_m)(L_m\text{-}L_o)$. A_o is the initial cross-sectional area, which decreases during extension of the fiber by the ratio $1/\lambda_m$ (λ_m is defined as L_m/L_o), assuming that the ligament fiber is composed of an incompressible material[4]. σ_m is the time-independent elastic stress which is a nonlinear function of the strain, ε_m, and is formulated as[8]

$$\sigma_m = \sigma(\varepsilon_m) = C_1\left(e^{C_2 \varepsilon_m} - 1\right) \quad (3)$$

where C_1 and C_2 are constants describing the material properties of the ligament fiber. These constants can be determined using a nonlinear least-square method to curve-fit the experimental stress-strain data obtained from tensile testing of the ligament fiber. ε_m is the elastic strain defined according to the engineering strain equation as

$$\varepsilon_m = \frac{L_m - L_o}{L_o} \times 100\% \quad (4)$$

Hence, U is simply a function of L_o as long as the ligament fiber, knee motion, and loading conditions are specified.
(C) Based on assumption 2 and since the length of the ligament fiber can be determined for each angle of flexion tested in which the knee is in equilibrium, the ZSR of the fiber may be determined by applying an optimization technique to equation 2 to maintain the total elastic strain energy generated in the fiber over the range of motion of the knee to a stationary value. The optimization approach applied for the determination of L_o (ZSR) of a ligament fiber is according to ${\partial U}/{\partial L_o} = 0$ when U is expressed in a Taylor's series for small value of changes in L_o and higher order terms are neglected. Accordingly, we obtain

$$\sum_m \left(e^{C_2\left(\frac{L_m - L_o}{L_o}\right)} \left(1 + C_2 - 2\frac{L_o}{L_m} - C_2\frac{L_m}{L_o}\right) + \left(2\frac{L_o}{L_m} - 1\right) \right) = 0 \quad (5)$$

Knowing the values of C_2 and L_m, equation 5 is used to numerically determine the ZSR, for the ligament fiber over the desired range of flexion of the knee and under the desired loading conditions. Strain as a function of flexion angle is then determined using equations 1 and 4.

Validation The method was validated by performing tensile tests to determine the ZSR of a band composed of natural pure gum rubber. Dial calipers accurate to 0.025 mm were used to measure the distance between the ends of the band as it was brought from a state of slack to a state of tension. Tension in the band was measured with a load cell simultaneously. A stress-strain relationship for the band was then created to determine the two constants in equation 3 using a nonlinear least-square method. The length pattern of the band was determined using the 3Space Fastrak system (Polhemus Navigation Sciences, Colchester, Vermont) and applying equation 1. The ZSR of the band was then determined with equation 5.

Application The application of the model was demonstrated using a knee obtained fresh at autopsy from a 57 year old donor. The three-dimensional position of the tibiofemoral joint and anatomic geometry of the knee was determined with the Fastrak system. The knee was passively extended from 90° to 0° in 2° increments without imposing internal or external rotations. After all of the position data were collected, a medial parapatellar incision was made on the knee to expose the ACL. A fiber of the ACLam inserting into the tibia was identified through dissection. The path of the fiber was followed to its insertion into the femur and that insertion point was digitized. The knee was then disarticulated and bony landmarks of the femur and tibia were identified and digitized for construction of the anatomical coordinate systems. With this data, reported techniques[5] were used for determining the three-dimensional kinematics of the tibiofemoral joint. The length pattern of the ACLam fiber was determined using equation 1. Experimental stress-strain data obtained from the literature[2] for the ACLam were used to determine C_1 and C_2 in equation 3. The ZSR and strain levels were then determined with equations 4 and 5.

Results of validation and application The mean (standard deviation) cross-sectional area of the band was 2.674 mm^2 (0.064 mm^2) and the resting length of the band was 72.009 mm as measured with the dial calipers. The ZSR of the band computed with the model was 73.152 mm. Thus, the error in ZSR for the band was 1.59% of the resting length. The length of the ACLam fiber increased with knee flexion angle from a minimum of 19.0 mm at 0° to a maximum of 21.5 mm at 90° of knee flexion (Figure 1). The strain pattern was similar to that of the length pattern (Figure 2). The ZSR of the ACLam fiber for passive loading was predicted to occur between 54° and 56° of flexion. The strain of the ACLam fiber increased with knee flexion to a maximum of 5.5% at 90°.

DISCUSSION

This mathematical model has three advantages. First, it is a non-contact method. Second, this method is not limited to a single flexion angle or loading condition. Third, this method may be used to determine the ZSR of a single ligament fiber. Although this new method was demonstrated for the ACLam fiber of the knee, it may be applied to other ligaments in the knee or in other synovial joints. The determination of the ZSR was based on the optimization of the total elastic strain energy stored in the ligament fiber. Two assumptions were made in developing the analytical model in this study. First, the ligament fiber was assumed to be incompressible as the fiber elongated under tension[4]. This assumption made it possible to formulate the elastic strain energy in terms of A_o, which was conveniently eliminated during the differentiation process when optimizing the total elastic strain energy. Second, it was assumed that the strain in the ligament fiber was uniform and stationary when the knee was in equilibrium. This allowed the application of the optimization procedure to determine the ZSR of the fiber. The mathematical model was validated by performing tensile tests to determine the ZSR of a pure gum rubber band. The ZSR computed with the model was in error by 1.59% from the measured resting length of the band, demonstrating good agreement. The model was demonstrated by applying it to a fiber of the ACLam. The length pattern found for the selected fiber was in agreement with that reported previously for passive flexion of the knee[7]. The mean maximum strain to failure of the ACLam found in a study on specimens from seven cadaveric knees has been reported as 19.1%[2]. Thus, the maximum strain predicted with the model for passive flexion, 5.5%, was of reasonable magnitude.

Figure 1.

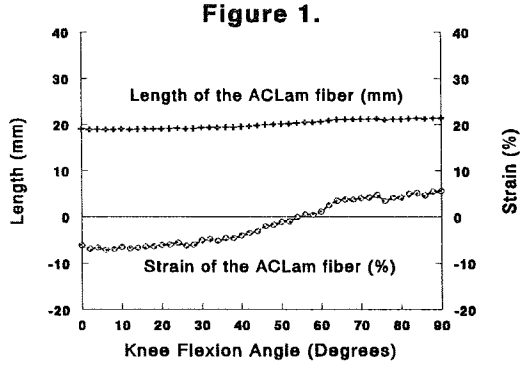

REFERENCES

1. Arms et al: Am J Sports Med 12: 8-18, 1984.
2. Butler et al: J Biomech 25: 511-518, 1992.
3. Draganich et al: J Orthop Res 8: 57-63, 1990.
4. Fung: Am J Physiol 23: 1532-1544, 1967.
5. Grood et al: J Biomech Engng, 105: 136-144, 1983.
6. Hefzy et al: J Biomech Engng 108: 74-82, 1986.
7. Hollis et al: J Biomech Engng 22: 208-214, 1991.
8. Woo et al: J Biomech Engng 103: 293-298, 1981.

OVERALL MICROMOTION OF CEMENTLESS ACETABULAR COMPONENTS USING ELECTRONIC IMAGING

A. Brantley[1], T. Hansen[1], C. Beardsley[2]
[1]Harrington Arthritis Research Center, Phoenix, AZ 85006
[2]Howmedica Inc., Worldwide R&D, Rutherford, NJ

INTRODUCTION

A new technique for measuring and presenting overall three dimensional (3D) micromotion of implanted cementless acetabular components was developed. The method utilizes electronically processed images of acetabular cups and surrounding bone during *in vitro* non-destructive loading. Relative motion was determined using rigid body motion analysis. The migratory and elastic motion of two cup sizes were evaluated and presented in terms of tangential (shear) and radial (normal) motion.

REVIEW AND THEORY

Migration of cementless acetabular cups *in vivo* can inhibit bony ingrowth and lead to implant failures. Various techniques have been used to measure relative micromotions between acetabular cups and bone *in vitro* [Clarke *et al.*, 1991, Kamaric *et al.*, 1996, Pavlovic *et al.*, 1994]. All of these studies have involved measurements and presentations of data that are site-specific. The amount of motion that occurs at the bone-implant interface has been shown to vary over the surface of the implant [Kamaric *et al.*, 1996]. Therefore, multiple sensors are needed to fully characterize the 3D interfacial motion, and to find the site and magnitude of the maximum amount of relative motion. Attachment of multiple sensors can alter the interfacial properties and cause inaccurate results. The objective of this study was to develop a new technique that could be used to determine the magnitude and site of the maximum amount of relative motion that occurs between an implanted acetabular cup and surrounding bone.

PROCEDURES

Six time-zero canine pelves with porous coated acetabular implants inserted by line-to-line reaming were included. Left and right acetabulae were implanted with 15x26mm and 15x28mm size cups, respectively, with the larger cups considered oversized. Small reflective markers were attached to the rim of the metal implants and the surrounding bone. Three-dimensional tracking of the reflective markers during loading was done using two CIDTEC® cameras, a frame grabber and the ExpertVision® system (Motion Analysis Corp.). Video recording was not used to eliminate tape noise. A total of 5 tests were studied, representing 5 different combinations of A/P and M/L loading configurations (see Table 1) (Hansen *et al.*, 1995). A kinematic algorithm based on a method by Spoor et al. [1980] was modified and used to determine finite screw axis parameters (FSAPs) for each rigid body (i.e., implant and bone). A solid computer model (ANSYS®) incorporating spherical layers of elements defining each rigid body was used with the FSAPs to replicate the measured motion. Relative motion between the cup and surrounding bone was determined by analyzing relative displacements at each of 101 nodal points connecting the two rigid bodies, with the nodes representing 101 equally spaced points on the outside surface of each size acetabular cup. Motion was analyzed in a spherical coordinate system, with components representing radial gap (normal) and shear (tangential) motion. Data was analyzed using paired Student's t-tests (two-tailed, $P=0.05$), comparing motion of right vs. left side cups (26 vs. 28 mm cups, respectively).

RESULTS AND DISCUSSION

Image noise of the motion data was found to be less than 9 microns (0.0104% field of resolution). A 2D vector plot (with latitudinal contours distorted into equal segments along the longitude) was used to aid visualization of relative tangential motion over the whole hemisphere (see Fig. 1). Maximum motion parameters (tangential motion and radial gap motion) are summarized in Table 1 (migratory and elastic motion). The average magnitude of motion (elastic or migration, tangential or radial) was greater for the larger (i.e. 28 mm) cup in all cases but one. However, the increased motion for the larger cup was statistically significant ($P<0.05$) in only one case. Grouping all the tests together (i.e., ignoring loading angles and increasing the sample population) made the increase in average motion for the larger cup statistically significant for all types of motion (see Table 1). The elastic component of tangential motion was, in the majority of cases, larger than the corresponding migratory component.

The elastic components of relative motion can be compared to site-specific values of motion reported by previous investigators using other measurement techniques. For instance, Pavlovic, et al [1994], measured interfacial motion of cementless acetabular cups in human acetabulae, *in vitro*, and reported translation vector

magnitudes (in a rectangular coordinate system) ranging from 0 mm to 3.14 mm (or 3140 microns). The accuracy of their measurement technique, involving a six degree-of-freedom instrumented spatial linkage (ISL), was ±50 microns. In comparison, Kamaric, et al [1996], who measured micromotion of time-zero plasma-sprayed acetabular components at three different sites per cup in human bone using eddy current transducers, reported average shear (tangential) and normal (radial gap) motions of around 50 microns. Stiehl et al [1991], who measured cup-peripheral micromotion of time-zero acetabular components in human bone using LVDTs, have reported micromotions of around 100 microns (elastic). The differences in the magnitude of the elastic motion among the reported studies may be related to bone quality, bone fixation techniques and test methods. In addition, our reported values are based on a maximum value of elastic motion, which occurred at some point away from the reflective marker sites. It is also possible that the value is somewhat magnified due to the assumption of rigid body motion. This assumption may be inappropriate since bone is elastic. However, it is believed that the technique is more descriptive than other methods in terms of incorporating interfacial motion over the whole surface of the cup. The method will be utilized and improved in future studies comparing the stability of different designs of acetabular cups and/or cups with longer implantation times.

REFERENCES

Clarke H et al., *J Arthropl*, Vol. 6. No. 4, p 335, 1991.

Hansen T et al., *Proc. CORS*, p , San Diego, CA, 1995.

Kamaric E et al., *Proc. ORS*, p 528, Atlanta, GA, Feb, 1996.

Pavlovic J et al., *18th Proc. ASB*, p 99, Columbus, OH, Oct. 1994.

Spoor et al., *J Biomech* Vol 13, p 391, 1980.

Stiehl J et al., *J Arthropl*, Vol.6 No. 4, p 295, 1991.

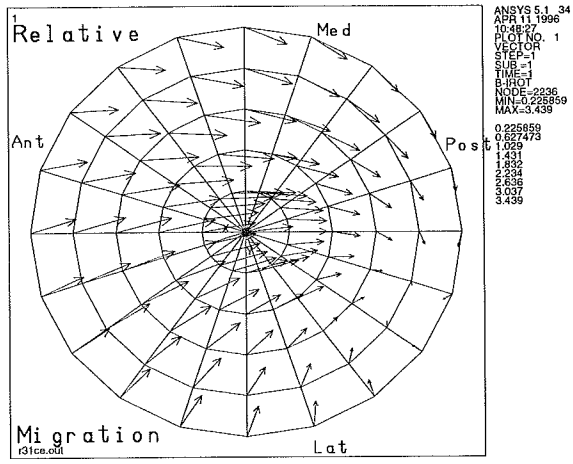

Figure 1 2D polar vector plot illustrating relative tangential motion at each of 101 nodes for one case. (Anterior-Cranial, Posterior-Caudal)

ACKNOWLEDMENTS

This study was funded by Howmedica. The authors thank Mike Kuzel for assistance during testing.

Table 1 Summary of Results (Bold faced indicates P<0.05)

Test	1	2	3	4	5	All Combined
A/P (°)	0	0	0	15	-15	-
M/L (°)	45	35	55	45	45	-
Elastic Tangential Motion (avg ± st.dev. [μm])						
26 mm cup	489±211	869±483	467±351	346±211	850±683	604±239
28 mm cup	1024±738	2453±2141	583±337	751±548	1640±776	**1290±764**
Elastic Radial Motion (avg ± st.dev. [μm])						
26 mm cup	190±196	550±645	233±353	206±255	231±462	282±151
28 mm cup	628±533	1381±1731	294±152	374±352	415±628	**618±444**
Migratory Tangential Motion (avg ± st.dev. [μm])						
26 mm cup	221±173	317±146	184±106	189±116	510±439	284±137
28 mm cup	**506±260**	601±396	312±195	356±285	1411±941	**637±448**
Migratory Radial Motion (avg ± st.dev. [μm])						
26 mm cup	153±139	187±102	148±97	98±84	254±271	168±57
28 mm cup	1106±2037	362±216	139±77	239±210	908±966	**551±429**

BIOMECHANICAL CONSEQUENCES OF MALREDUCTION OF TRANSVERSE ACETABULAR FRACTURES

A.J. Hamel, D.J. Hak, B.K. Bay, and S.A. Olson
Orthopaedic Research Laboratories, University of California, Davis

INTRODUCTION

Fractures of the acetabulum result in a disruption of the acetabular articular surface. The goals of surgical intervention are to reduce the fracture and provide stable internal fixation. Malreductions occur when the fractured surfaces are not restored anatomically and an articular discontinuity results. These malreductions can be classified generically as a step: where the discontinuity is perpendicular to the articular surface (Figure 1a), or as a gap: where the discontinuity is parallel to the articular surface (Figure 1b). This study was undertaken in order to understand the effects of different malreductions of transverse acetabular fractures on the contact characteristics of the hip joint.

REVIEW AND THEORY

Malreduction of the acetabular articular surface has been found to increase the rate of degenerative arthritis fivefold, therefore making it a clinically relevant problem. Increased articular contact pressures are hypothesized to result in the accelerated degeneration of the articular cartilage and thus the development of osteoarthritis. The effects of acetabular malreduction on contact pressures have not previously been studied. Therefore this study was undertaken to ascertain how fracture reduction and fracture type affect contact pressure and area in the hip joint.

The interaction of the fracture with the superior articular portion of the joint was varied between two transverse fracture types. It is hypothesized that increasing superior involvement will result in greater alteration of joint biomechanics following malreduction. It is also hypothesized that malreductions will result in localized increases in contact pressure, with the largest pressure increase in the step displacement.

PROCEDURES

Six intact pelves were excised from fresh cadavers and cleaned of excess tissue, leaving the joint capsules intact. Four hips were tested in each of the two transverse fractures: a juxtatectal fracture where the fracture line intersected the superior aspect of the fovea (Figure 2a), and a transtectal fracture where the fracture line bisected the articular surface of the superior acetabulum (Figure 2b). For both fractures four conditions were tested: intact, anatomic reduction, step malreduction and gap malreduction.

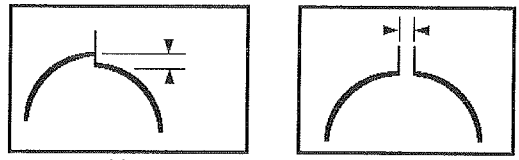

Figure 1:(a) Step malreduction (b) Gap malreduction

Each whole pelvis was instrumented for testing, placed in the loading apparatus, and loaded using the methodology described by Bay *et al.* First the intact joint was loaded. The particular fracture was then created, reduced anatomically and loaded, malreduced with a gap discontinuity and loaded, and malreduced with a step discontinuity and loaded. The induced step and gap malreductions resulted in approximately 4 millimeters of displacement at the articular surface.

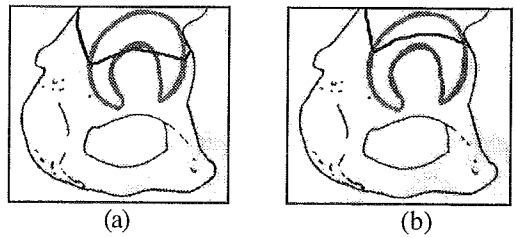

Figure2:(a) Juxtatectal acetabular fracture location, (b) Transtectal acetabular fracture location.

Fuji Pressensor Low Film (2.5-10MPa) was inserted into the joint space before each loading run in order to transduce the articular contact pressure and area. Two runs were performed at each condition to ensure repeatability. For those conditions which elicited a pressure response that saturated the Low Film, Medium Film (10-50MPa) was then inserted into the joint to attain maximum pressure resolution.

Two small holes were drilled in the acetabulum and blunt probes inserted. These reference marks were used to align the patterns consistently and define the different regions of the joint. The Fuji film patterns were digitized on a flat bed scanner and analyzed using NIH Image software (W.Rasband).

RESULTS

The intact condition demonstrates a peripheral distribution of load. Following anatomic reduction of both the transtectal and juxtatectal fractures, more superior loading occurs. Gap and step malreductions in the juxtatectal fracture result in no significant difference from the anatomic condition. In the transtectal fracture, however, maximum pressure in the superior acetabulum increased markedly. Maximum pressures of 25-30 MPa were recorded in both malreductions along the fracture line.

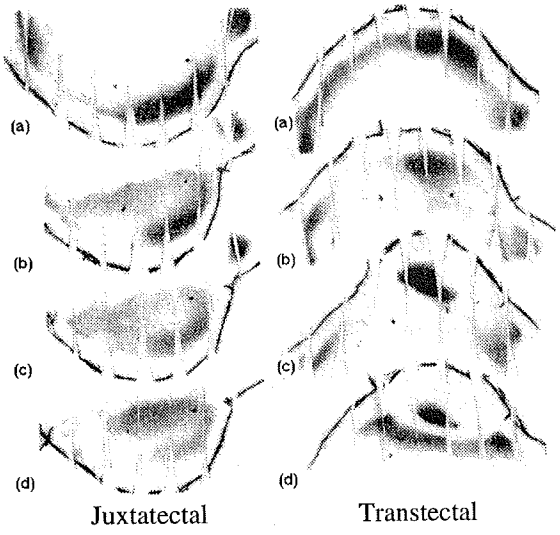

Figure 3: (a) Intact, (b) Anatomic, (c) Step, (d) Gap

The maximum pressure in the transtectal fracture for each region and condition is plotted in Figure 4. None of these changes are statistically significant due to limited sample size and specimen variability, however an increasing trend can be seen in the superior region. Contact area did not significantly change for either fracture in all four conditions. In the transtectal fracture, mean pressure showed a trend similar to max pressure in the superior region, but this was not statistically significant.

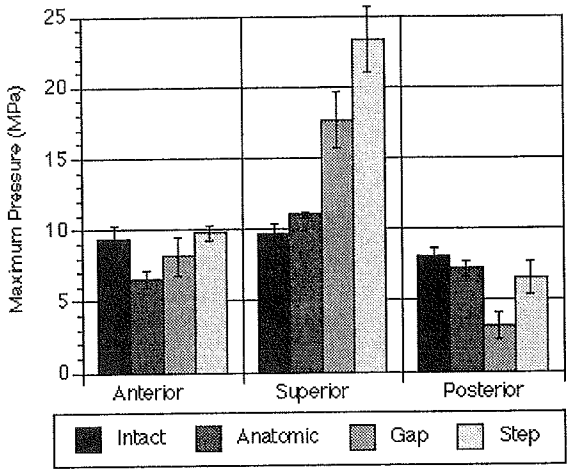

Figure 4: Maximum pressure for the four different conditions grouped by region. Error bars represent standard error.

DISCUSSION

In the juxtatectal fracture, less of the articular surface is bisected by the fracture line. This limited articular involvement in the superior portion of the joint results in minor changes to the load transmission characteristics. This may indicate that a precise anatomic reduction of a juxtatectal fracture is not critical to good joint outcome. However, when the fracture line crosses directly through the articular cartilage of the superior acetabulum, as in the transtectal fracture, it is very important that anatomic reduction occur. Both the step and gap malreductions resulted in very high maximum contact pressures which could result in accelerated degeneration and eventual joint dysfunction.

REFERENCES

Bay, B.K., Olson, S.A., Hamel, A.J. *Experimental Technique has an Effect on Measured Contact Characteristics of the Human Hip Joint.* Proceedings of the ASB, 1995.

Biomechanical Evaluation of Knee Braces During Level Walking by Motion Analysis System

F.C. Su, C.H. Lin, C.Y. Yang*
Institute of Biomedical Engineering and Department of Orthopedics*
National Cheng Kung University, Tainan, TAIWAN

INTRODUCTION

Since the anterior cruciate ligament (ACL) is necessary for maintaining the normal biomechanical function of the knee, the knee joint will become unstable after rupture of the ACL. Rehabilitative brace is frequently prescribed for immobilization and controlled motion during early phase and for provision of external stabilization during training in late phase of rehabilitation. What are the effects of various braces on knee motion? Therefore, the purpose of this study was to measure *six degrees of freedom* of knee movement, with and without using brace, during level walking by using a video-based motion analysis system and thus to evaluate the influence of braces on knee motion and their ability of protection for the injured or post-operative tissue.

REVIEW AND THEORY

Do knee braces help to stabilize the knee joint and reduce the strain on the injured or post-operative tissue? From literature available, few studies are related to the function of postoperative braces, despite the apparent popularity of these braces. A working knowledge of the capabilities and limitations of specific braces in these different categories is required of the physician to properly prescribe these orthotics. One of the principal problems that confronts the investigator interested in functional comparison of knee braces is the selection of the appropriate test specimen and the method of instrumentation. Medical-legal aspect must be considered with *in vivo* studies.

Clinically, arthrometers have been used to measure applied loads, translations, and angular displacements of the knee joint for diagnosis of pathologic anterior (Cawley et al., 1989). Although anterior drawer laxity can correlate functional instability in many cases, these studies are constrained to static testing and the information provided if of limited value. For dynamic measurement, electrogoniometers have widely used for three-dimensional measurement of flexion-extension, varus-valgus, and internal-external rotation, but not for translations (Chao, 1980, Cawley et al., 1989). However, the anterior translation of the tibia is an essential measurement of how well the braces contained the limb. Due to its inherent limitations: weight, bulk, and soft tissue interface, the electrogoniometer is not appropriate for functional evaluation studies.

Cawley et al. (1991) recommended that future investigations must address the physiologic aspects of functional bracing. In order to evaluate knee braces under physiologic load, such as running and level walking, an analytic model to determine three-dimensional motion (3 rotations and 3 translations) between two body segments from noisy markers' trajectories placed on segments was developed in this study. This model utilizes the least square measurement errors to reduce the artefacts from at least 4 markers on each segment to determine the rotation matrix and translations or helical axis-for two body segments (Spoor and Veldpaus, 1980).

To determine the total motion of knee joint, the movement of the shank and thigh with respect to laboratory coordinate system was determined first. Then, the relative movement of the shank with respect to thigh was further derived and expressed in the local moving coordinate system of the thigh. For representation of knee joint motion, an orthogonal joint coordinate was defined on the joint center. Through the coordinate transformation, the knee joint motion was determined from the rotation matrix and translation vector of the tibia relative to the shank. Finally, the knee joint motion was expressed based on "floating" coordinate system of the knee joint.

PROCEDURES

Seven left ACL-deficient patients (ages 23-37), 6 with ligament reconstruction and 1 with partial rupture of ACL only, were recruited for this study. The interval between previous operation and this testing was 18.9 months. Six normal subjects, free of pathological changes on the back or lower limbs that might possibly affect their gait, comprised the control group. Motion analysis system (Expert Vision^{TM}, Santa Rosa, CA) was used to measure the motion of lower limb with 8 markers each on the thigh and shank during level walking. Four combinations, (1) injured limb, (2) control limb, (3) injured limb with Don Joy ROM splint (Don Joy, Carlsbad, CA), (4) injured limb with Don Joy 4-Point brace, were investigated. Six trials were collected for each combination. Finally, the finite helical axes and Eulerian angles of knee joint were calculated to represent its 6 degrees of freedom of motion, 3 translations and 3 rotations.

RESULTS

Table 1 demonstrated that the difference of the range of motion of knee joint was not significant between unbraced patients and controls. However, the ROM splint reduced 16.5% flexion/extension, 33.0% abduction/ adduction and 32.4% internal/external rotation of knee motion while compared to that without the brace. For 4-point brace, the reduction of knee motion was 10.8% in flexion/extension, 19.4% in abduction/adduction, and 25.8% in internal/ external rotation.

The translation of knee was 12.8±2.6 mm in anterior/posterior direction and 2.6±0.8 mm in medial/lateral direction for ACL injured patients (Table 2). While bearing the ROM splint, the knee reduced 19% anterior/ posterior, 19% superior/inferior, and 23.4% medial/lateral translations. For 4-point brace, the translation reduction was 14.7%, 10.6%, and 15.6%, individually.

DISCUSSION

There has been little biomechanical or clinical investigation on the function of the knee braces and most of them are static in nature. By placing 8 markers each on the thigh and using least square error technique, the reliable in-vivo translational evaluation of knee braces become possible. Compared to Marans's (1989) study by a spatial linkage system, the translation of knee joint is within clinical allowance.

The reason why the reduction is more distinguishable using ROM splint might be the same as Cawley's description. We conclude that ROM splint restricts the knee motion more pronounced than 4 point brace. The straps, which interlock with the side bars to create a strong single functional unit, may contribute the effectiveness at controlling rotations and translations at the knee. There were no significant differences in knee motion between injured and control limbs without bearing the brace because the injured limbs had been operated 18.9 months prior to experiment. This is compatible with the clinical evaluation that no patients complain the pain or discomfort during level walking.

Table 1: Range of motion of the knee joint

Subject	Flexion/ Extension (degree)	Abduction/ Adduction (degree)	Axial Rotation (degree)
unbraced	62.6±6.3	12.5±5.6	16.0±5.8
ROM Splint	52.3±4.1	8.4±3.1	10.8±3.5
4-Point Brace	55.9±5.1	10.1±3.7	11.8±4.6
Control	60.6±5.2	11.4±4.5	15.6±5.5

Table 2: Translations of the knee joint

Subject	anterior/ posterior draw (mm)	superior/ inferior translation (mm)	lateral/ medial shift (mm)
unbraced	12.8±2.7	11.8±3.0	2.6±0.8
ROM Splint	10.4±1.9	9.5±2.5	2.0±0.6
4-Point Brace	10.9±2.5	10.5±2.9	2.2±0.6
Control	12.3±2.5	11.4±3.0	2.4±0.6

REFERENCES

Cawley, P.W. et al. *Am. J. Sports Med.*, 17, 141-146, 1989.

Cawley, P.W., et al. *Am. J. Sports Med.*, 19, 226-233, 1991.

Chao, E.Y.S. *J. Biomech.*, 13, 989-1006,1980.

Spoor C.W. et al. *J. Biomech.*, 13, 391-393,1980.

Marans, H. J. et al. *Am. J. Sports Med.*, 17, 325-333, 1989.

ACKNOWLEDGEMENT

This work was supported by National Science Council, NSC84-2213-E-006-081, Taiwan, ROC.

INVESTIGATIONS ON THE SENSORY FUNCTION OF LIGAMENTS IN THE KNEE

J. Fanghänel[1], B. Miehe[1], H. Nägerl[2], D. Kubein-Meesenburg[3],
M. Hanschke[1], U. Kraatz[1], and A. Blümel[1]

[1]Institute of Anatomy, University of Greifswald, D-17487 Greifswald
[2]IV. Phys. Institute, University of Göttingen, D-37073 Göttingen
[3]Department of Orthodontics, University of Göttingen, D-37085 Göttingen

INTRODUCTION

Using the knee joint as an example, it will be shown that ligaments possess an important sensory function. To this end, qualitative histological and histochemical investigations were undertaken, and quantitative analyses of the findings were conducted.

REVIEW AND THEORY

Aside from a biomechanical function, ligaments also have sensory functions. Sporadic and empirical histological analyses have been conducted on some ligaments (Zimny 1988). Sensitive terminal bodies (mechanical-sensory bodies: Vater-Pacini lamellar bodies, Ruffini bodies) reflect the existence of a *sensory system.*

PROCEDURES

The investigations were conducted on the knee-joint ligaments of 25 male domestic pigs (Sus scrofa domestica).

The ligaments (Lig. collaterale med.et lat., Lig. cruciatum ant. et post., Lig. patellae, ligament suspensors of the menisci, Lig. transversum genus) were dissected out and usually cut into three sections (bone insertions, center). They were either frozen in liquid nitrogen and then kept at -25 °C until histologically/histochemically examined, or they were fixed in Bouin's solution or 4 % formalin, then rinsed, dehydrated, and embedded in paraffin.

6 µm-thick sections taken every 150 µm were prepared from the tissue embedded in paraffin. Using the HE stained sections, the number of superficial and interfascicular Vater-Pacini lamellar bodies and Ruffini bodies was determined by counting out the entire tissue block.

From the frozen tissue blocks, 10 µm-thick cryostat sections were taken every 150 µm for use in HE staining, an enzyme-histochemical test for acetylcholinesterase, an immunohistochemical visualization of protein S 100 (PAP technique) and neurofilament (APAAP technique), and a gold-chloride representation.

The number of Vater-Pacini lamellar bodies and Ruffini bodies in the cryostat sections stained with different methods was also determined and identified as either superficial or interfascicular.

RESULTS AND DISCUSSION

Vater-Pacini lamellar bodies and Ruffini bodies occur throughout the ligaments of the joint. They are easily seen in HE-stained sections; the nerve fibers within them are Ach-E-, neurofilament-, and protein S 100-positive, and are markable with gold chloride.

Ruffini bodies are found both superficially and interfascicularly. Their regional distribution within the ligaments studied varies according to ligament. In collateral ligaments, they are more frequently found in the bone insertions and less frequently in the central areas. The distribution of Ruffini bodies in the cruciate ligaments is more even; here, in comparison to the other ligaments, they are more numerous. Ruffini bodies are also found in the meniscus attachments, which has not been previously described in the literature. Obvious regional differences in their distribution could not be found.

On the whole, *Vater-Pacini lamellar bodies* are less frequent. They settle primarily superficially, hardly interfascicularly. Obvious regional differences in their distribution within one and the same ligament could not be determined.

The existence of mechanical-sensory bodies leads to the assumption that, using the tibia as a reference, the cruciate ligaments exercise control on the sagittal plane, the lateral ligaments on the frontal plane, and the menisci on the horizontal plane (Fanghänel et al. 1996).

REFERENCES

Fanghänel, J. et al. Ann Anat 178, Suppl. 162 - 163, 1996.

Zymny, M. L. et al. Am. J. Anat. 188, 16 - 26, 1988

THE EFFECTS OF TOTAL KNEE ARTHROPLASTY UPON MUSCLE MOMENT ARM BALANCE AT THE KNEE

W.L. Buford, Jr., F.M. Ivey, D.J. Malone, R.M. Patterson, D. Nguyen
Orthopaedic Biomechanics Lab, The University of Texas Medical Branch,
Galveston, TX 77555-0892; (409) 772-9072; fax 747-4223;
e-mail: william.buford@utmb.edu

INTRODUCTION

The purpose of this study is to investigate the effect on the muscle balance at the knee after total knee arthroplasty with posterior cruciate ligament (PCL) sparing and sacrificing prostheses. The muscle balance of the knee is the relationship of all the muscle moment arms throughout a full range of motion. For purposes of comparison in this study we form a global moment arm (average total excursion divided by average total angular range of motion) for the flexors and the extensors. The effects of the ACL deficient knee, the PCL sparing, and PCL sacrificing prostheses upon the global moment arm are reported relative to the same for the normal knee.

REVIEW AND THEORY

An improved, more accurate description of normal muscle moment arms will help to more precisely define design parameters for TKA. Also, the effect of TKA upon the balance of muscles at the knee will assist in the clarification of arthroplasty success. The extent to which moment arms at the knee have been studied is summarized by Spoor, et al [1993]. Studies to date have been limited in the use of preserved specimens, static positioning, exclusion of certain muscles, few specimens, and limiting assumptions. Also, to our knowledge, the moment arms of knees with TKA have not been studied.

PROCEDURES

Nine fresh-frozen, hemi-pelvis specimens were skinned and the muscle-tendon units instrumented to measure the muscle travel (excursion) and knee joint angle during dynamic motion of the leg. The leg was manually rotated between full flexion and full extension, in smooth sweeping motions, approximate to a slow walk. Potentiometers measured motion about the flexion/extension axis described in [Hollister, et al, 1993]. The instantaneous moment arm was calculated as the derivative of the tendon travel with respect to the joint angular motion as described in [An, et al, 1984]. Each leg was then mounted into the test apparatus and passively rotated through the full range of motion. The ACL ligament was then severed and data acquisition was repeated for this condition. PCL sparing and sacrificing prostheses were implanted into the leg, respectively, following the surgical technique of the implant manufacturer. Each of the knees had a different model of prosthesis. A five point smoothing technique was used on the flexion/extension angle, internal/external rotation angle, muscle-tendon excursions and moment arms. Data from every cycle of the leg was averaged together using a natural cubic spline routine, for each of the four conditions.

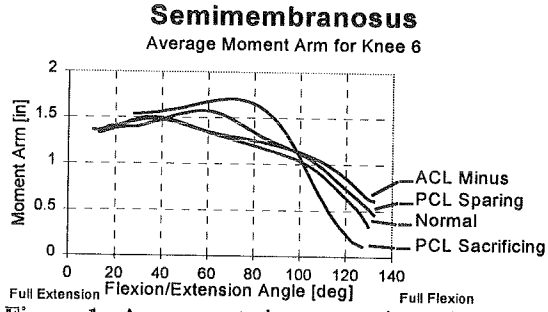

Figure 1. A representative comparison chart of moment arms for one muscle for each of the four test conditions of one specimen in the study.

RESULTS

An example of the instantaneous moment arm for one muscle in each condition of one of the knees in the study is depicted in **Fig. 1.**

The muscle-tendon excursions and instantaneous moment arms for the thirteen muscles and the patellar tendon were analyzed for each of the four conditions of all seven knees. Since the moment arm is the change in excursion over the change in angle, a global moment arm can be inferred from the total excursion over the total range of motion. **Fig. 2** shows a balance comparison by a grouping of the flexor and extensor muscles.

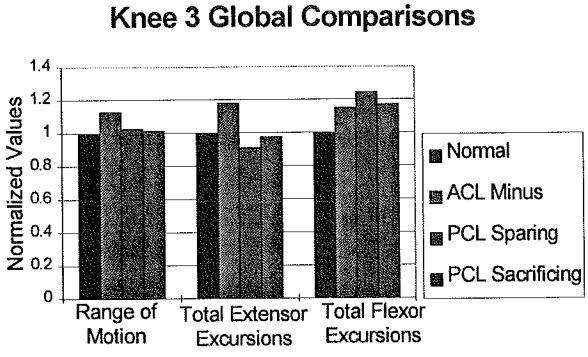

Figure 2. Comparisons of range of motion and maximum excursions for the extensor and flexor muscles of one specimen (Normal, ACL min., PCL Spar., PCL sac., left to right). All values have been normalized to the normal knee condition.

Statistical T-tests were used to compare the three conditions to the normal condition. The increased total excursions for the flexors and extensors of the ACL deficient condition were due to the greater total range of motion for this condition. The prostheses had ranges of motion that were not significantly different than the normal knee. However, the total excursion for the flexor muscles was significantly greater than that of the normal knee ($P<.01$). The total excursion for the extensor muscles was not significantly different from the normal case. This resulted in an increased moment arm for the flexor muscles without a corresponding increase for the extensors. This demonstrates a dramatic shift in the balance of the knee favoring the flexors for these particular two prostheses.

With the preceding analysis as background, the global moment arm was formed to compare the effect of the three conditions relative to the normal flexion-extension balance of muscles at the knee. This comparison is depicted in **Fig. 3**.

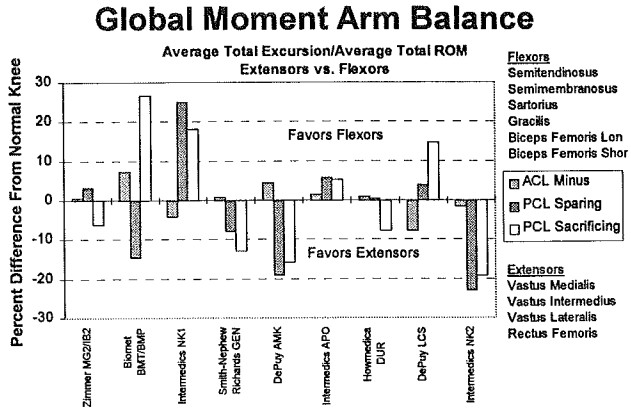

Figure 3. The comparison of the ACL deficient condition and two types of arthroplasty upon muscle balance at the knee (depicted as % change from the normal knee).

DISCUSSION

As shown in **Figure 3**, the ACL minus condition had minimal effect upon the changes in muscle balance. Some prostheses produced dramatic effects upon muscle balance. Certain prostheses produced a balance that increased the moment arm balance for the flexors, while others increased the moment arm balance for the extensors. Five PCL sparing TKA's unbalanced favoring flexion (ranging from 1% - 24%) and four unbalanced favoring extension (ranging from 8% - 22%). Four PCL sacrificing TKA's unbalanced toward flexion (range 5% - 27%) and five unbalanced toward extension (range 6% - 19%).

REFERENCES

An, K.N., et. al.,*J. of Biomechanical Eng*, 106:280-282, 1984.

Hollister, A.M., et. al.,*Clin Ortho & Rel Res*, 290:259-268, 1993.

Spoor, C.W., and VanLeeuwen, J.L., *J. of Biomechanics*, 25:201-206, 1992.

ACKNOWLEDGEMENTS

Primary funding for this project was provided by Intermedics Orthopedics, Inc., with supplemental funding provided by Zimmer-Jones, Inc. and Biomet-Omni, Inc.

MOMENT ARMS OF MUSCLES AT THE KNEE FOR THE NORMAL KNEE AND THE ACL-MINUS KNEE

W.L. Buford, Jr., F.M. Ivey, D.J. Malone, R.M. Patterson, D. Nguyen
Orthopaedic Biomechanics Lab, The University of Texas Medical Branch,
Galveston, TX 77555-0892; (409) 772-9072; fax 747-4223;
e-mail: william.buford@utmb.edu

INTRODUCTION

This study seeks an understanding of the normal muscle balance at the knee and the effect on that balance when the anterior cruciate ligament (ACL) is resected. The objectives are to define the normal moment arms for all of the muscles of the knee throughout the flexion-extension range of motion, and to describe any changes to these moment arms (muscle balance) when the ACL is absent.

REVIEW AND THEORY

An accurate model of the muscle moment arms is necessary in order to predict the forces generated in the knee during motion. Since the muscle moment arms change during knee flexion, an instantaneous moment arm is used to describe the mechanical advantage of each muscle during motion. Spoor, et al (1993) summarizes the work to date in attempts to characterize moment arms at the knee. Historically, limitations have been in the use of preserved specimens, static positioning, exclusion of certain muscles, few specimens, and limiting assumptions.

PROCEDURES

Nine fresh-frozen, hemi-pelvis specimens were skinned and the muscle-tendon units instrumented to measure the excursions and joint angular motion during dynamic rotation of the knee. Excursions were measured for thirteen muscles that cross the knee (plus the patellar tendon). Potentiometers measured motion about the flexion/extension and internal/external axes described in [Hollister, et al, 1993]. The instantaneous moment arm was calculated as the derivative of the tendon travel with respect to the joint angular motion as described in [An, et al, 1984].

Legs were mounted into the test apparatus (each muscle was tensioned with 2 lb. weights) and passively rotated through the full range of flexion/extension and internal/external motion. The ACL ligament was then severed and data acquisition was repeated for this condition.

A five point smoothing technique was used on the flexion/extension angle, internal/external rotation angle, muscle-tendon excursions and moment arms. Data from every cycle of motion (full E to full F for the flexors and full F to E for the extensors) was averaged together using a natural cubic spline routine, for the normal and ACL-minus knees.

RESULTS

The excursions and moment arms for all major muscle-tendon units crossing the knee are described for both the normal knee and the ACL-minus knee. **Figure 1** depicts a typical record of the calculated moment arm for one muscle from 13 flexion-extension cycles. Although there exists wide variation between specimens (see **Figures 2** and **3**), each muscles moment arm has it's own unique shape consistent between specimens. The average moment arms for nine normal knees are depicted in **Figure 4**.

There was no significant difference between the normal moment arms and those for the ACL deficient condition. The differences between the moment arms for each condition were analyzed at 2.5 degree intervals using the SAS GLM procedure (the null hypothesis of no difference was accepted at $p<.01$).

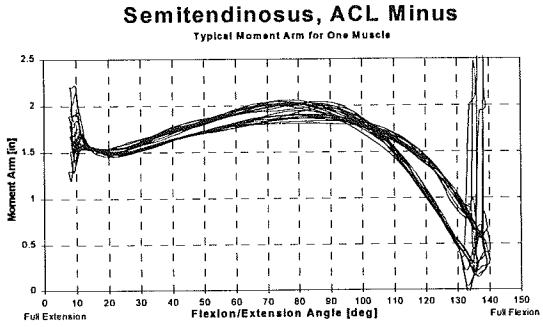

Figure 1. A typical moment arm curve for one ACL minus knee calculated from the excursion record of a muscle during several cycles of flexion/extension motion.

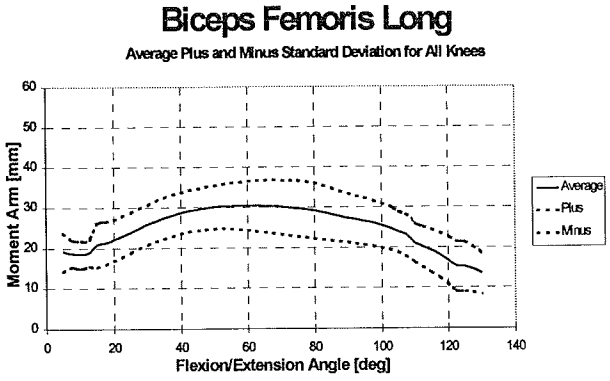

Figure 2. The average moment arm curve (+/- 1 S.D.) over nine specimens for the biceps femoris muscle (normal knee).

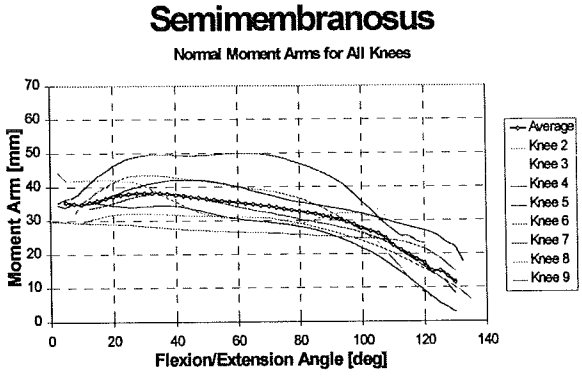

Figure 3. The moment arms of the SM muscle averaged over all flexion-extension sweeps for each knee and the average for all knees highlighted.

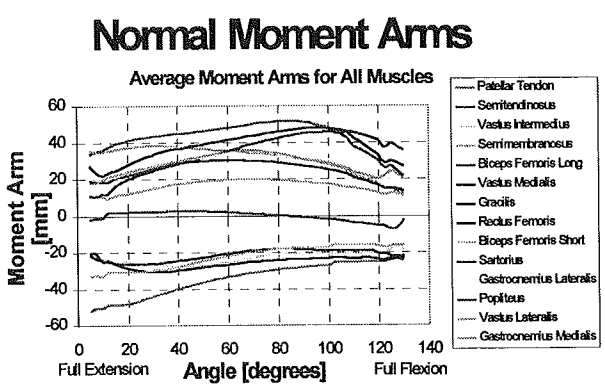

Figure 4. Average moment arms for the normal knee (9 specimens). Extensor muscles and the patellar tendon are on the negative side. The popliteus exhibits a negligible moment arm for either flexion or extension. Of the flexors, the biceps femoris has the smallest moment arm and the semitendonosis the largest (to nearly 100° flexion).

DISCUSSION

The normal moment arms resulting from this study provide improved knowledge of knee structure from which more valid models and predictions can be made for joint reaction forces. The results also provide a clearer understanding of muscle balance in the normal knee.

The fact that the ACL minus condition did not significantly effect the moment arms might be attributed to our experimental method. We surmise that by loading the muscles and moving the lower leg in slow sweeping motions (approximate to a walk) the joint maintained congruence and possible ACL deficient effects upon the moment arms did not occur.

REFERENCES

An, K.N., et. al.,*J. of Biomechanical Eng*, 106:280-282, 1984.

Hollister, A.M., et. al.,*Clin Ortho & Rel Res*, 290:259-268, 1993.

Spoor, C.W., and VanLeeuwen, J.L., *J. of Biomechanics*, 25:201-206, 1992.

ACKNOWLEDGMENTS

Primary funding for this project was provided by Intermedics Orthopedics, Inc., with supplemental funding provided by Zimmer-Jones, Inc. and Biomet-Omni, Inc.

THE EFFECTS OF CYCLIC LOADING ON WEAR OF THE UHMWPE COMPONENT OF TOTAL KNEE REPLACEMENTS A THREE-DIMENSIONAL FINITE ELEMENT STUDY

Bonnie J. Beard*, Raghu N. Natarajan, Thomas P. Andriacchi, and Farid M.L. Amirouche*
Department of Orthopedic Surgery
Rush-Presbyterian-St.-Luke's Medical Center, Chicago, Illinois
*Department of Mechanical Engineering
University of Illinois at Chicago, Chicago, Illinois

INTRODUCTION

Wear of the Ultra High Molecular Weight Polyethylene (UHMWPE) tibial component is one of the primary mechanical factors limiting the life of total knee replacements. Numerous studies of retrieved tibial components have demonstrated severe wear (1,2,3). The tibial component is subjected to fatigue loading due to the cyclic nature of the loads that are applied to the component during the stance phase of gait from heelstrike to toe-off. The purpose of this study was first, to examine the effect of this cyclic loading on the stress distributions in the UHMWPE component through the use of three-dimensional finite element analysis. Secondly, to examine the possibility of fatigue due to cyclic stressing of the component.

THEORY AND PROCEDURE

A three-dimensional, non-linear, finite element model was developed of the medial compartment of an average size Miller/Galante I prosthesis, as shown in Figure 1. The tibial component was modeled using non-linear material properties of UHMWPE through a plastic multi-linear model. A compressive elastic modulus of 572 MPa, a yield strength of 12.7 MPa and a Poisson's ratio of 0.45 were used based on the study by DeHeer (4). A von Mises yield criterion was applied with isotropic hardening of the component. The tibial component is flat in the sagittal plane, consistent with this prostheses. Boundary conditions simulating the presence of a metal support tray were adopted.

A Co-Cr femoral component was modeled with an elastic modulus of 120,000 MPa and a Poisson's ratio of 0.3. The femoral radius of curvature used in the analysis was 35 mm, consistent with the medial compartment of an average Miller/Galante I prosthesis. The medial compartment was modeled since the majority of the load is transmitted through this compartment in a neutrally aligned knee and because it has a smaller radius of curvature than the lateral compartment it represents a worst case stress situation. The movement of the load through the various contact points during the stance phase of gait was modeled using prescribed displacements which were applied to the top surface of the femoral component. The finite element analysis was performed using ADINA (5).

The external loading at the knee joint was obtained through standard gait analysis of a patient with a Miller/Galante I prosthesis. The internal normal loads and the contact locations during level walking were subsequently obtained from an analytical knee model developed by Wimmer et al (6). Loads at the knee joint corresponding to six specific contact points during the stance phase of gait were taken as input for the finite element model. These loads were distributed along the line of nodes at the midplane of the femoral component for each case. Seventy percent of each of the total normal loads obtained from Wimmer's model were applied to this medial compartment model, consistent with a neutrally aligned knee (7).

RESULTS AND DISCUSSION

The yield stress of the UHMWPE component was exceeded at two of the six load cases analyzed. As a result, residual stresses were present in the UHMWPE after all six loads were applied. The magnitude of the residual stresses were less than 1 MPa, however, this value would be expected to increase as subsequent cycles are added. As a result, plastic deformation of the component is expected.

The contact stress (σ_x) contours demonstrated a zone of large compressive stresses surrounded by tensile stresses, thus providing a fatigue environment as the contact point is shifted during gait. The normal stress component in both the anterior-posterior (σ_z), and medial-lateral (σ_y), directions also displayed a similar stress distribution. Figure 2 shows the fluctuations in the contact stress (σ_x) plotted along a line of points from the anterior-most aspect of the tibial component to the posterior-most aspect at the middle of the component surface for all six cases considered here. This figure shows the extensive stress fluctuations that occur in the component.

The contact stress (σ_x) fluctuated due to femoral rollback at a location 32 mm from the anterior-most aspect of the tibial component from +2.3 MPa during load case 3 to -14.8 MPa during load case 4. This fluctuation yielded a tensile to compressive load ratio of 6.4. Compressive to compressive cycling also occurs in the component, however, the maximum fluctuation is highly dependent on the minimum compressive stress being approximately zero and thus, magnitudes will not be reported here. At the same location, the normal stress component in the medial-lateral direction (σ_y) also showed extensive cycling. The stress fluctuated from +2.8 MPa to -11.6 MPa, yielding a tensile to compressive load ratio of 4.1. The normal stress component in the anterior-posterior direction (σ_z), at the same tibial location, showed a tensile to compressive range of +2.3 MPa to -11.3 MPa, for a load ratio of 4.9.

Fatigue failure has been observed in both experimental studies of UHMWPE and retrieved tibial components (8, 9). An experimental study by Pruitt et al., (9) has shown that fatigue crack propagation occurs in UHMWPE for tensile to compressive load ratios greater than 3 and for compressive to compressive load ratios greater than 25. All of the tensile to compressive load ratios reported here exceeded 3. Additionally, as shown in Figure 2, compressive to compressive load ratios in excess of 25 are observed in the component although numerical values were not reported here.

The analysis shows that the posterior contact region of the component is more subject to fatigue than the anterior contact region due to femoral rollback, as shown in Figure 2. Also, this analysis demonstrates that the component is subjected to fatigue due to not only the contact stress (σ_x), but also the normal stress component in both the medial-lateral (σ_y), and anterior-posterior (σ_z), directions. Thus, based on this stress analysis, fatigue crack propagation is a predominate factor that should be considered in future knee prosthesis designs. Also, efforts should be taken to reduce the number of material defects in UHMWPE, since fatigue crack propagation is highly dependent on the presence of a defect for crack initiation.

REFERENCES

(1) Wright et al. Clin. Orthop. Rel. Res. 276:126-134, 1990.
(2) Hood et al. J. Biomed. Matr. Res. 17:829-842, 1983.
(3) Collier et al. Clin. Orthop. Rel. Res. 273:232-242, 1991
(4) DeHeer, M.S. Thesis, Purdue University, 1992.
(5) ADINA R & D, Inc. 71 Elton Ave. Watertown, MA 02172
(6) Wimmer et al., ORS, 20:735, 1995.
(7) Andriacchi et al. J Arthrop 1:3, 211-219, 1986.
(8) Weightman et al. J. Biomed Matr. Res. 13:669-672, 1979.
(9) Pruitt et al. JOR, 13:143-146, 1995.

ACKNOWLEDGEMENTS

Rush Arthritis and Orthopedics Foundation
NIH Grant AR 20702
University of Illinois Fellowship

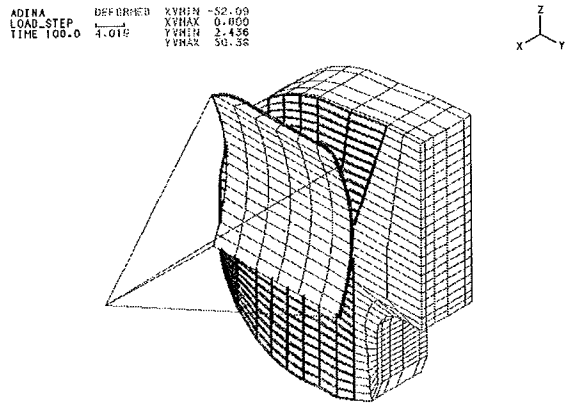

Figure 1. Three-Dimensional Finite Element Model

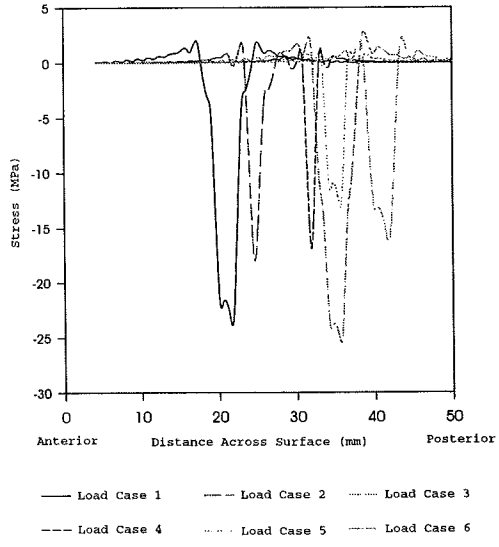

Figure 2. Contact Stress (σ_x) Fluctuations Across Tibial Component Surface for Six Load Cases

ROLL OF CONTACT GEOMETRY AND STRESS IN WEAR OF UHMWPE IN TOTAL KNEE JOINT

S. Pal & A. Roychowdhury

School of Bioscience & Engineering
Jadavpur University, Calcutta-700032, India.

INTRODUCTION

Excessive wear and also subsurface crack of the polyethylene liner in condyler type total knee joint replacement is a matter of great concern to the orthopaedic surgeons and implant designers over the past decade(1). The wear debris causes osteolysis at the bone prosthesis junction leading aspectic loosening of the prosthesis pair and subsequent failure(2) . The objective was to analyze the contact stress and other relevant stresses to investigate the causes of such failure and suggest remedies from design point of view.

REVIEW AND THEORY

The lubrication regime in TKR is boundary lubrication and the surface of contact of the metal condyles of the femoral component has some specific kinematic compulsions, e.g. flexion extension, 0 - 120°, and rotation about the knee axis of 5 - 10° some gliding motion of 10 - 12 mm. The loading also varies from 0 to 6 times the body weight during various activities, including sports.

Some early designs showed comparatively flatter P.E. tibial liner and some recent designs indicated more conforming congruent contact surface which restricts the functional movement. It was also noted that UHMWPE used as a liner was of variable grades depending on its molecular weight. The mechanical strength depends on the molecular weight range. This material has high strength and great wear resistance, still wear debris production and subsurface crack and catastrophic failure were not uncommon. The magnitude of the stress at the contact area is a significant parameter which determines the wear behaviour in invivo situation to a great extent.

Friction wear and lubrication, the three aspects of tribological science should be studied to address the problem in totality. Both friction and wear are very much depended on surface finish and normal force in contact area of the pair in touch. Normal stress depend on contact area, which is depdended on geometry of contact of the two mating surfaces.

PROCEDURE

In this study, we have considered the geometrical parameters which affects the contact stress i.e. radii of curvature of femoral component of the knee that of mating PE liner and its thickness t, Fig(1). We have tried to search the optimum geometry for minimum contact stress and shear stress in contact area. For that we have analyzed from simple Hertzian contact models to complex 3-D model using FEM. We have used, for 2-D analysis, isoparametric 6 noded trianglur element, point to point contact element, and for 3-D, 10 - noded tetrahedral solid and surface to surface contact element as given in ANSYS 5.0. In knee joint two radii of curvature of femoral and tibial part in sagittal plane was considered, Fig1. So first, for sagittal plane we analyzed the simple Hertzian contact 2-D model,using a solid cylinder of radius(r) on a hollow cylinder of radius(R), by changing the magnitude of these two radii of curvature and thickness(t) of PE liner.

RESULT AND DISCUSSION

After analyzing fortytwo such type of geometries, we have obtained optimum two set of geometrical parameters in mm.

R = 35, r = 25, t = 8.
R = 30, r = 25, t = 8.

Where t is the minimum thickness of the polyethylene (UHMWPE) liner, at the middle.

Same way we have found the optimum radii of curvature for frontal plane parameters remembering conformity and flexiability of movement of knee joint.

Results from these analyses have been used in an actual TKR model at two typical posture, namely,

1) at fully extended position.
2) 30° flexion of the knee.

For each case we applied four times the body weight considering a man with weight 70 kg. At fully exstended position, stress generated at contact point in UHMWPE liner was 3.08 MPa. It is allowable as 2% proof stress of UHMWPE varies between 20 to 25 MPa. At 30° flexion we observed, compressive stress of 3.9 MPa and shear stress of 1.95 MPa. The matter of concern was not the magnitude but it's position as it was developed quite below the contact surface. The load on knee joint due to sudden jerk or impact may cause high shear stress, reaching plastic yielding which may lead to subsurface crack or excessive wear after prolonged use.

To avoid that we suggest a new type of design, inserting a metallic circular Tee inside UHMWPE tibial partFig2, in this case the shear stress at metallic Tee and in UHMWPE came down to 1.6MPa as shown in Fig(3). This part need to fabricated and tested. The fixation will be with a thin layer of bone cement. But the design is to some extend complicated to manufacture.

To overcome the limitations of two dimensional analyses we have decided for 3-D analyses with help of the results from 2-D analyses.It should be noted that, we have taken radii in the range of 8 to 12mm for the frontal plane of the femoral condyles. Then we have optimized the contact stress, and also the shear stress in contact area Among all the geometrical analyses, the lowest compressive stress observed was, -14.7MPa and other stresses were low, so insignificant..On the other hand, deformation was 0.074 mm at the contact area. The developed compressive stress was very close to permissible limit but the deformation was quite allowable. We found the improved values of model parameters, those magnitude may be the main guidelines for knee prosthesis development in future.

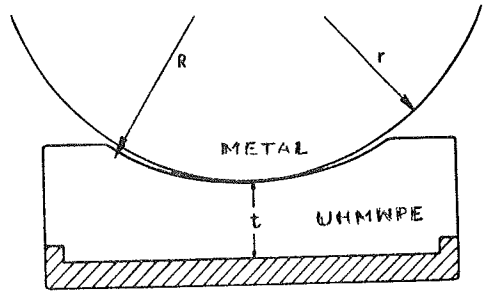

Fig. 1 Simple Hertzion contact model for sogittal plone.

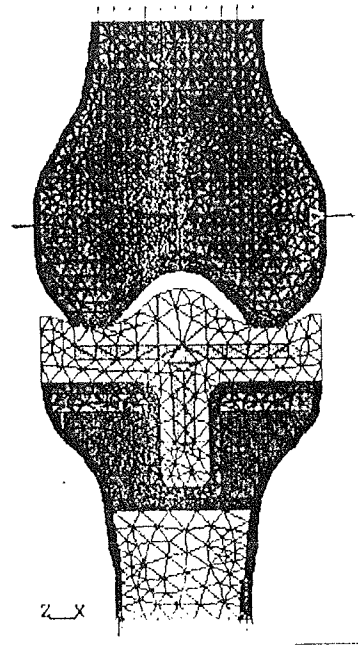
Fig 2. The FE-structure of Femoral and Tibial part with Tee-insert

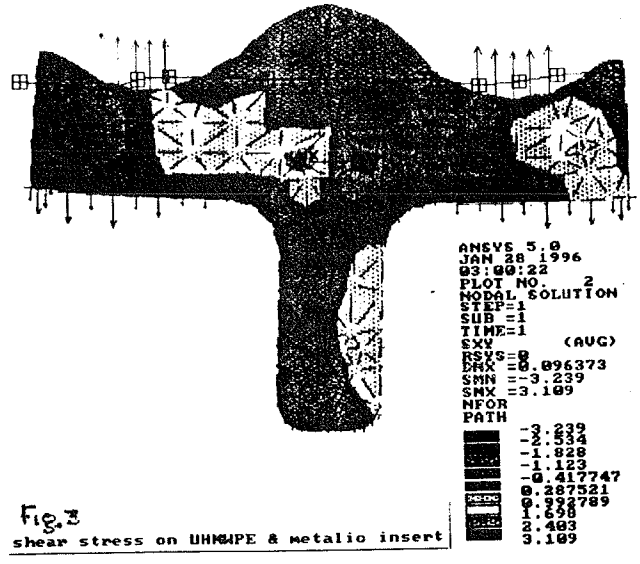

Fig.3
shear stress on UHMWPE & metalic insert

REFERENCE

1) Goodman S, Lidgren L. (1992) polyethylene wear in knee arthoplasty a review - Acta orthop Scand. 63(3) 358-364,
2) Knutson, K et al. (1986) Survival of knee arthoplastics. A nation wide multicentre investigation of 8000 cases, JBJS (B) 68(5),795-803

ACKNOWLEDGEMENT

This work was partially funded by the CSIR, and also the University Grants Commission, India.

EVALUATION OF A NEW SWELLING TYPE COMPOSITE MATERIAL FOR FIXATION IN BONE

A. Abusafieh[1], A. Vemuganti[2], S.Siegler[3], and S. R. Kalidindi[1]
[1]Department of Materials Engineering
[2]Biomedical Engineering and Science Institute
[3]Department of Mechanical Engineering
Drexel University, Philadelphia, PA 19104

INTRODUCTION

A new swelling type composite material system capable of self-fixation in bone has been recently developed for bioimplant applications (Greenberg and Kamel, 1978; Sharda and Kamel, 1993; Ahmad and Kalidindi, 1994; Abusafieh et al., 1996). Self-fixation is achieved after implantation by swelling of the implant material through the absorption of body fluids; this results in an expansion-fit mechanism. The proposed material system comprises of a cross-linked hydrophobic/hydrophilic copolymer matrix reinforced by three-dimensionally braided graphite fibers. The copolymer matrix is designed to be slightly hydrophilic thereby providing the desired swelling characteristics to the material whereas the 3-D braided graphite fibers provide excellent mechanical properties (i.e. modulus, strength, fracture toughness, fatigue strength, and impact resistance).

A detailed experimental study was conducted to investigate the swelling and self-fixation characteristics in bone of this new class of composites. The major goal of the study was to evaluate the mechanical properties of the developed composite material and measure the fixation levels achieved in bone.

REVIEW AND THEORY

The desired swelling levels of the proposed composite can be controlled by varying the ratio of methylmethacrylate (hydrophobic component) to acrylic acid (hydrophilic component) as well as the amount of cross linking agent in the copolymer matrix. In this study, we examined the influence of the relative amount of the hydrophilic component in the matrix on the mechanical properties and fixation levels achieved in bovine cortical bone. Specifically, we examined five ratios of MMA/AA: 100/0, 90/10, 80/20, 70/30, 60/40.

PROCEDURES

A series of push-out tests were performed on cylindrical plugs of the synthesized composite with varying hydrophobic/hydrophilic ratios. These plugs were slip-fit into thick plates of cortical bovine bone which were then immersed in excess saline solution (see Fig. 1).

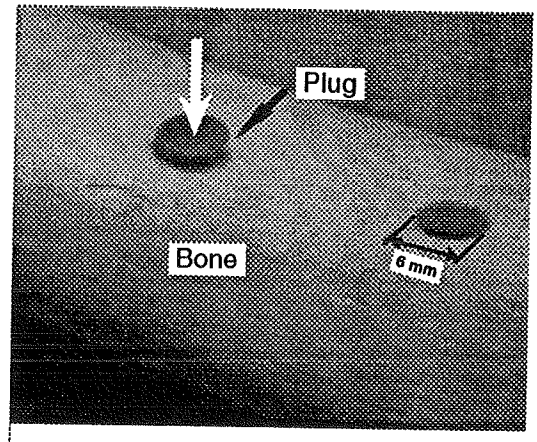

Figure 1: Photo-image of composite plug slip-fit into bovine cortical bone.

The plugs were pushed out of the bone after one week of immersion and the maximum push-out loads were recorded. A typical push-out load-displacement curve is shown in Fig. 2.

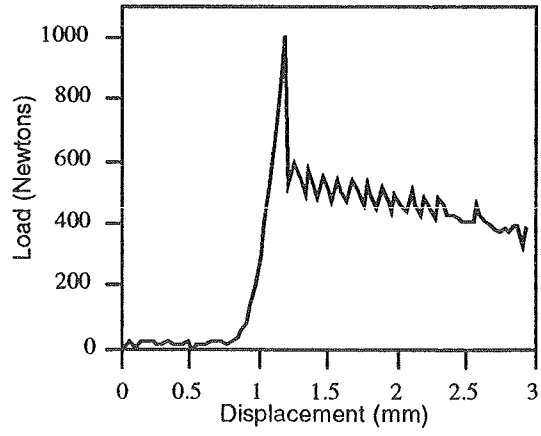

Figure 2: Typical push-out load-displacement curve of composite plugs.

Compression tests were performed on the same plugs immediately following the push-out tests and the stress-strain curves similar to Fig. 3 were generated.

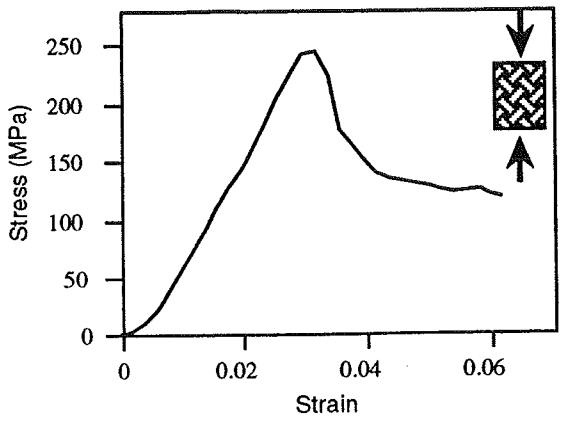

Figure 3: Typical stress-strain curve of composite plug tested in compression after implantation.

RESULTS AND DISCUSSION

The push-out loads of plugs of various matrix compositions are shown in Fig. 4.

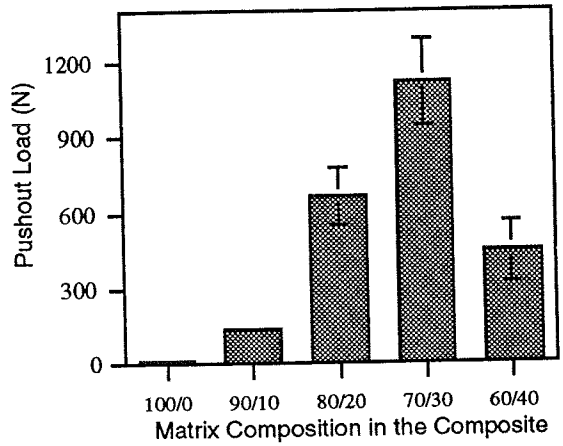

Figure 4: Push-out load of composite plugs with varying matrix compositions.

The results indicate that the fixation levels increase with the hydrophilic ratio in the matrix and reaches a maximum with samples containing 30% acrylic acid (70/30 composition). Further increase in the relative amount of the hydrophilic component did not show any improvement in the fixation levels. In general, these push-out strengths indicate good promise for the use of these composites for soft tissue fixation applications.

The compressive yield strength of the pushed-out composite plugs are presented in Fig. 5.

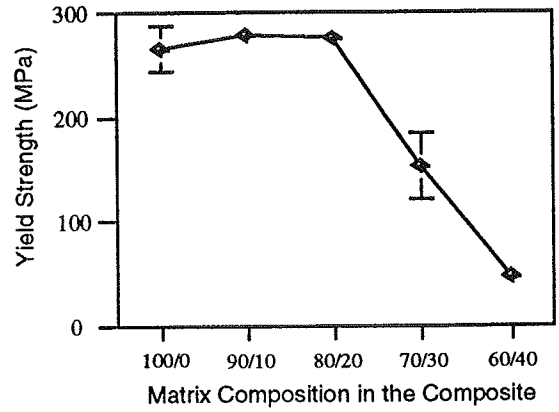

Figure 5: Compressive yield strength of composite plugs tested after implantation.

As indicated by the yield strength values, it can be observed that a significant decrease in the mechanical properties (due to swelling) occurs in samples containing relatively high amounts of acrylic acid (> 20%).

In conclusion, a matrix composition ranging from 80/20 to 70/30 is found to yield high fixation levels without a significant loss in mechanical properties. The obtained results show that the composite with the proposed composition has a compressive yield strength of about 200 - 230 MPa and a modulus of elasticity of 40 - 50 GPa.

REFERENCES

Abusafieh, A. et. al. (1996) submitted to J. of Appl. Polymer Science.
Ahmad, P and Kalidindi, S, Thirteenth Southern Biomedical Engineering Conference, (pp. 171-173), University of District of Columbia, Washington, DC, 1994.
Greenberg, A. R. et. al., J. of Biomed. Mat. Res., 12, 922-924, 1978.
Sharda, A.N. and Kamel, I, (1993) Ph.D. Thesis, Drexel University.

ACKNOWLEDGMENTS

The authors gratefully acknowledge support for this work through a grant from the Whitaker Foundation.

COMPARISON OF PULLOUT CHARACTERISTICS FOR TWO TAPERED BONE SCREWS

J. E. Hale, D. V. Carmines, C. L. Baker
Department of Orthopaedics, University of Virginia, Charlottesville, VA 22908

INTRODUCTION

Screw fixation is one of the most widely used means of affecting internal stabilization. However, implant related complications, such as screw loosening, compromise the usefulness of such procedures. To improve the screw/bone interface strength, a self-tapping bone screw with a tapered minor diameter and a buttress thread was developed. Compared with constant minor diameter screws, a tapered design increases the interface area and cancellous bone volume between the distal screw threads.

Although previous studies have reported a "small but significant effect" of major/minor diameter on pullout strength [DeCoster, 1990], the effect of tapered minor diameter screws has not been widely studied. The purpose of this study was to compare the screw/bone interface strength of a new tapered screw with that of a similar, commercially-available device.

PROCEDURES

The strength of the screw/bone interface was investigated in the pedicle of lumbar vertebrae. Fifteen lumbar specimens (L1-L5) were obtained from four human cadaveric lumbar spines (3 male, 1 female), dissected down to the ligamentous tissues, and subjected to non-invasive bone density measurement (DEXA). Prior to testing, the pedicle dimensions were measured and a pedicle screw was inserted while measuring insertion torque. Specimens with screws inserted were mounted in the test fixture and a monotonic tensile load was applied along the axis of the screw through a circular opening (1.25 cm diameter) in the fixture. Loading to failure was performed using a materials test system(MTS Model 858 Bionix, Eden Prairie, MN) under a controlled displacement rate of 1 mm/sec. Specimens were randomly X-rayed with screws inserted and then sectioned following pullout testing to inspect screw purchase and alignment.

Two self-tapping, cannulated screws were evaluated, each with major diameter=7 mm, thread length=40 mm, and pitch=2.8 mm. One screw (Danek, Cannulated bolt: P/N 823-131) featured a proximal taper (PT) reducing the minor diameter from 6 mm to 5 mm within 4 threads, followed by a constant diameter of 5 mm to its distal tip. The second screw provided a full taper (FT), with minor diameter decreasing from 6 mm proximally to 4.2 mm distally. Insertion was performed according to the standard surgical procedure. Pilot holes were drilled using a straight drillbit (PT screw) or a drillbit with matched taper (FT screw), each undersized by 0.3 mm diameter, respectively. To obtain paired data for the two screw designs, one screw of each type was inserted into the right and left pedicles of each vertebral body tested. Assignment of the screws to the right or left pedicle was reversed in adjacent levels to minimize the effect of specimen asymmetry.

RESULTS

Mechanical characteristics were computed from the load-displacement curve for each screw test, including: pullout force (maximum load), loading stiffness (slope of load-displacement curve over linear region), and loading energy (area under load-displacement curve up to maximum load) (Figure 1).

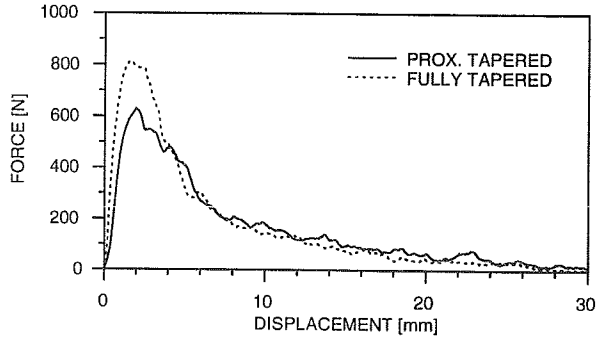

Figure 1. Representative load-displacement data for pullout tests of two tapered screws (PT vs. FT) inserted in the same vertebral body.

The FT screw provided greater pullout forces than the PT screw in 12 of 15 vertebrae tested (range: 6% to 80%, p=0.083 for paired t-test). The loading energy was also higher for the FT screw in 10 of 15 vertebrae, while comparable loading stiffnesses were observed for the two screws. Means and standard deviations were computed for population test data concerning pullout force, loading stiffness, and energy to failure (Table 1).

Table 1. Population mean (standard deviation) for pullout characteristics of two tapered screws.

	SCREW TYPE	
	PT (n=15)	FT (n=15)
PULLOUT FORCE [N]	766.2 (240)	894.8 (172)
STIFFNESS [N/mm]	742.9 (274)	753.2 (202)
ENERGY [N-mm]	1013 (382)	1249 (461)

Bone mineral density measurements for the fifteen specimens ranged from 0.672 - 0.904 gm/cm^2 (mean = 0.761).

DISCUSSION

Commonality of the proximal screw design standardized the purchase of the two screws within the posterior cortical bone and pedicle isthmus, thereby providing a comparison of the effect of the major/minor diameter ratios within the vertebral body. The increased major/minor diameter ratio of the FT screw provided increased holding strength in cancellous bone compared with the PT screw.

Correlation analysis revealed a weak positive correlation between pullout force and bone mineral density (CORR=0.25, both screws). However, the pullout force correlated more strongly to insertion torque for the PT screw (CORR=0.65) as compared to the FT screw (CORR=0.37), indicating that the FT screw may be less sensitive to insertion torque errors.

Direct comparison of the pullout force results with those of previous studies is complicated by differences in bone density, screw diameter, insertion torque, etc. Soshi et al. [1991] presented a linear correlation between bone mineral density and pull-out force for a 7.0 mm major diameter screw with a constant minor diameter. Based on the mean bone mineral density for specimens in this study, a pullout force of 720.2 N is obtained, less than that of either tapered screw. Prior evaluation of a tapered screw (major diameter=6.0 mm, minor diameter=3.9-5.0 mm) by Yamagata et al. [1992] demonstrated improved endurance limit in bending fatigue tests, but did not report pullout strength.

Results of this study indicate that the full tapered pedicle screw design provides comparable, if not improved, pullout strength when compared to the proximally tapered screw. It also provides comparable mean stiffness and loading energy up to ultimate load. Based on these findings, additional testing and design development may lead to an improved screw design based upon minor diameter thread taper.

REFERENCES

DeCoster, T.A. et al., J Orthop Trauma 4(2):169-74, 1990.
Soshi, S. et al., Spine 16(11):1335-41, 1991.
Yamagata, M. et al., Spine 17(3S):51-4, 1992.

ACKNOWLEDGMENTS

This work was supported by a grant from the Sofamor-Danek Corporation (Memphis, TN). The authors also gratefully acknowledge the contributions of E. Jang, S. Thanapipatsiri, C. McLaurin and G. Wang to this work.

STRAIN DISTRIBUTION NEAR TRANSCORTICAL IMPLANTS

Mark J. Hiatt[1], Yuan Lin[2], Dennis L. Powers[1] and Vasanti M. Gharpuray[1]
[1]Department of Bioengineering, Clemson University, Clemson, SC 29630
[2]Department of Mechanical Engineering, Clemson University, Clemson, SC 29630

INTRODUCTION

Transcortical implants have been used by numerous investigators to evaluate the response of cortical bone to various implant materials. The experimental model involves placing cylindrical implants of the test material in holes which have been drilled through the cortex of a long bone. The implants are retrieved after a predetermined period of time and the bone/implant interface is assessed to determine the response of bone to the material. However, different researchers have reported a wide range of results from experiments designed to measure the response to apparently similar implant materials (Black, 1989).

Although there are several factors that influence the result of the transcortical test (e.g., species, sex, age, diet, etc.), one potentially important factor that has been consistently overlooked is the strain field in bone surrounding the implant. Wolff's law states that adaptive bone remodeling occurs when bone is strained differently from its natural state. Therefore, any variable that affects the strain state around the implant will affect remodeling around the implant, and thus may affect the results of a transcortical osseocompatibility test.

REVIEW AND THEORY

Peelan et al. (1977) showed bone apposition to tricalcium phosphate implants at regions of the bone-implant interface that were in compression, but fibrous tissue formation in areas of debonding. Based on these results, Heimke et al. (1981), suggested that the reaction of bone to an implant may be influenced by biomechanics as well as by chemical compatibility, and that the results of a compatibility test may be interpreted differently depending on the location of histological sections used to assess the interface.

The effect of implant location on the results of a transcortical test was studied by Dalton and Cook (1995) using the push out test. They showed that the push out strength depended on the location of the implant and cautioned that bilateral paired comparisons were necessary for un-biased results. However, several other investigators have also suggested that the location of the implant does not affect the results of the transcortical test (e.g., Hayashi et al., 1993).

In this study, we hypothesized that the strain state in bone will vary with location and stiffness of the implant. To verify this hypothesis, strains in bone were measured *in vivo* around implants of two different stiffnesses and in three different locations.

PROCEDURES

Nine skeletally mature Nubian goats received three transcortical implants in each femur, placed at 35%, 50% and 65% of the femoral length. Implants were made of one of two biocompatible materials: i) Ultra-high molecular weight polyethylene, (UHMWPE) (elastic modulus one tenth that of cortical bone); and ii) Tantalum (modulus ten times that of cortical bone). In addition to the UHMWPE and tantalum implants, a control treatment (no holes or implants) was also included to determine the natural strain state at the implant sites. Treatments were placed within the three locations in each femur according to a randomized block design.

A lateral surgical approach was used, and four single axis strain gages and two tri-axial stacked rosette gages were attached to the lateral aspect of the femur (Figure 1) using the procedure described by Szivek and Magee (1989). Holes were then drilled through the lateral cortex and cylindrical implants were placed in the holes.

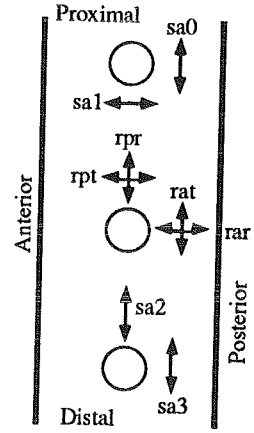

Figure 1: Schematic diagram of lateral aspect of the femur showing implant and strain gage placement, and strain gage nomenclature.

In vivo strains were measured twice weekly for each animal. Dynamic data was obtained by walking the animals on a treadmill at speeds of 1 m/s and 2 m/s. For comparisons between different treatments, a "strain amplitude" was computed as the algebraic difference between the strain at mid-stance and the strain during the swing phase. In order to compare data obtained from the single axis gages and the rosettes, data from

the rosette gages were transformed into radial and tangential components of strain with respect to the implant. The data collection was discontinued when failure of the gage or the adhesive was evident as indicated by abnormal strain patterns during gait. Except for five gages which were damaged during placement, gages remained active for one to four weeks.

RESULTS AND DISCUSSION

Figure 2 illustrates a strain pattern obtained dynamically during level walking at 2 m/s. The plot indicates that strains in the femur exhibit peaks that correspond to heel strike and toe off during a gait cycle. For these data, it can be seen that the strain amplitude recorded by gage sa0 is approximately +225 microstrain (με), while that by gage sa1 is -90με.

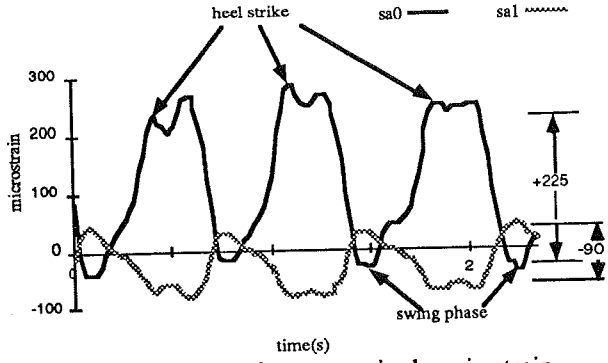

Figure 2: Strain data from two single axis strain gages near a tantalum implant.

Figure 3 summarizes the strain amplitudes measured for each implant material and gage. Statistical examination using one way analysis of variance showed that strains parallel to the long axis of the bone were significantly different ($p<0.05$) from strains perpendicular to the long axis. There were no significant differences between implants in different locations (e.g., no differences between sa0, rat, and sa3 for the same material implant), nor were there differences between strains around implants of different moduli.

We believe that differences may exist but that they were not large enough to be detected in the present study due to the large variability in the data and to the sensitivity of the data acquisition system (smallest detectable difference of 14με). A closer examination of Figure 3 shows a trend in mean strain amplitudes and suggests that the implant may act as a strain riser. For example, the mean strain amplitude measured for gage sa0 showed increasing strain with increasing modulus; for the UHMWPE implant the strain was +98με, for no implant (and no hole) the strain was +107με and for tantalum implant, the strain was +126με. A recently reported mathematical model (Gharpuray, 1996) shows similar trends. The model predicted that the magnitude of strains will increase as the elastic modulus of the implant increases.

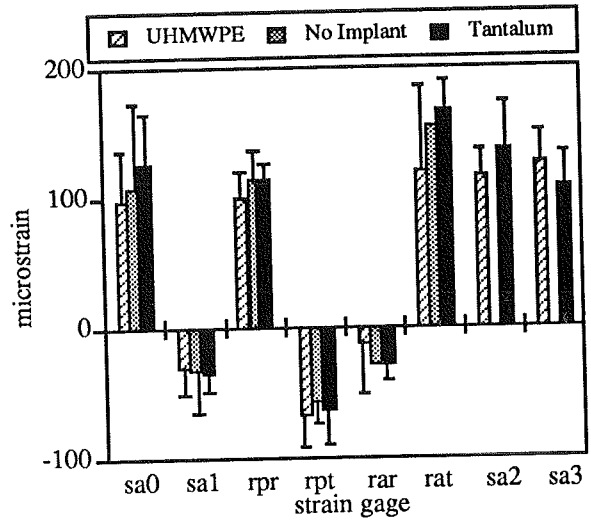

Figure 3: Strain amplitudes for each gage and material. Error bars show standard deviations.

Finally, it is important to note that proximal to the implant, radial tensile strains were measured at the bone/implant interface. These strains may actually pull the bone away from the implant creating a region of debonding which may lead to formation of fibrous tissue at the interface. Anterior to the implant, however, radial compressive strains are developed creating an area which will likely develop closely apposed bone tissue and thus create a stronger interface. This finding reinforces the suggestion of Heimke, et. al., that orientation and location of a histological section may be extremely important when assessing the suitability of an implant material when using the transcortical method.

REFERENCES

Black JB, J Biomed Mat Res, 23, 1243-1245, 1989.
Dalton J and Cook S, J Biomed Mat Res, 29, 133-136, 1995.
Gharpuray VM et al., accepted, J Biomed Mat Res.
Hayashi K et al., Biomaterials, 14, 1173-1179, 1993.
Heimke G, et al., J Biomed Eng, 3, 209-213, 1981.
Peelan JG et al., Sci Ceram, 9, 226-236, 1977.
Szivek J and Magee F, J Invest Surg, 2, 195-206, 1989.

ACKNOWLEDGMENTS

This study was supported by the National Institutes of Health (Grant No. 1 R15 AR42726-01). We would also like to thank Implex, Inc., West Lake Plastics, and Zimmer, Inc.

STRESS REDUCTION OF AMPUTEE SOCKET DUE TO CHANGE OF PREFLEXION ANGLES

Saiwei Yang and Hsin-Ji Tsai
Institute of Biomedical Engineering
Yang-Ming University, Taipei, Taiwan

INTRODUCTION

A well fit socket with proper alignment highly affects the wear willing of an amputee and make one's gait efficiency. Although the CAD/CAM system is efficient in manufacturing of prosthetic socket, a proper socket modification for stress reduction and alignment are still counted on the expert prosthetics. This study applied the finite element method to characterize the stress distribution of residual limb in different preflexion angles, materials and size of modification in order to establish a template database for socket modification and to design a better custom made socket.

REVIEW AND THEORY

A successful prosthesis depends on three factors: well fit socket, right alignment, and a suitable prosthetic foot. The stress distribution between socket and residual limb is an index of a well fit socket since abnormal stresses contribute not only skin breakage and ulceration but also affect an efficient gait. The shear stresses on a residual limb are thought to cause tissue breakage, however, there are no quantitative studies to evident the above conclusion. The interface resultant shear magnitudes were measured higher at anterolateral distal , posterodistal, and posteroproximal end by special design transducers (Sander et al , 1992) and the compatible results were simulated by his finite element analysis (Sander,1993). An amputee usually feels most uncomforted at the late heel strike phase of a gait cycle. Quesada and Skinner (1991) parametrically analyzed the stress distribution of a PTB socket at heel strike condition and concluded that the highest normal stress and shear stress were at the distal anterior tip of socket/stump. Higher normal stresses were found at the posteromedial proximal and higher shear stress were at posteroproximal anterior distal end; 14% reduction of maxima pressure resulted from changing the socket material 10 times lower than the original one. The present study applied the finite element analysis to investigate the stress distribution of socket/stump interface stress in different preflexion angle, material properties, size of modification in order to locate the exact areas of weight bearing and stress concentration. This quantitative analysis will suggest a prosthetics the way of modification with minimizing interface stress in order to fabricate a comfort prosthetic socket.

PROCEDURES

A negative stump model was cast from an experienced amputee. The dimension of model was digitized and used to manufacture a socket by a CASD/CAM system (Seattle Shape Maker) . The digitized geometric data in Macintosh format was first transferred to IBM compatible PC AUTOCAD format as the nodal points to construct the liner shell of the socket in finite element modeling. The shell of socket, thickness of liner were constructed by measuring the finished product made by CASD/CAM system. The geometries of soft tissue and bone were reconstructed according to the images of CT scan of the amputee. The geometries of socket, liner (Pelite), soft tissues, tibia bone, wooden base were meshed and analyzed by ANSYS5.0. The complete finite element model consisted of 3964 nodes and 3665 elements excluded the tibia bone since the mechanical properties of bone is much stiffer than others. The material properties of socket shell, liner, wooden base were obtained from experimental material test by a MTS machine. Two types of socket material: polypropylene (Young's modulus E=1000Mpa, Poisson's ratio v=0.3), Polyester resin (E=14000Mpa, v=0.13) were used to fabricate the socket.

A 750Nt force with equivalent flexion and internal rotation moments were applied to the bottom of socket to simulate the ground reaction force 1.5 times of a person weighted 50kgs at the heel strike phase of gait cycle. The degree freedom of internal nodes of the soft tissue layer were fully constrained due to the properties of bone being much stiffer. Three sizes of anterior tibia crest modification (cut out 10 cm^2, 16cm^2, and 20cm^2) were analyzed in

three preflexion angle conditions: 0, 10, and 20 degrees

RESULTS

The reliability of FE results was validated first by comparing with the experimental data of the socket in six strain gages under the same analytical condition. The results were compatible with deviation ranged under 5%. The variation was mainly due to the non-uniform thickness between the experimental and FEA sockets. The results showed that the interface stresses were concentrated in the regions of anterior distal end (AD), patella tendon (PT) and posterior proximal (PP) (Table 1) When the preflexion angle increased from 0 to 20 degrees, the effective stress at the patella tendon area decreased 34%, but increased 30% at other locations. As preflexion angle increased from 0 to 10 degrees the location of maximum effective stress shifted from PT to AD. And stresses increased 1.39 times while the angle reached to 20 degrees. By removing 16cm^2 patch at the anterior distal end along the tibial crest it resulted in 35% decrease of the equivalent stress. The stress level at the other locations were either slightly decrease or no change. With larger removing size the stress level had no further decrease. By changing the elastic modulus of socket 14 times higher resulted in normal stresses decreased up to 2.5% at AD, 5% at TE, 2% at LD, 3% at PD, 3.5% at PP, 6% at MD, and 8% at PT. The maximum shear stresses were at PP regardless the preflexion angles. The AMP, ALP, ALD only produced small shear stresses. This results confirmed the experimental measurements done by Sanders (1992) (Figure 1, Table 2).

DISCUSSION

A higher elastic modular material did not significant decrease the normal stress level . This result is similar to that of Quesada (1991). The normal stresses increased with increased of preflexion angle except the stress locate at patellar tendon region. By removing the anterior distal end with size of 16 cm^2 will effectively relief the high stress level and shift the concentration area upward. To combine with an effective prosthesis alignment technique an optimal design of prosthesis could be achieved through this study.

	RM 0			RM 20			RM42			RM51		
	0	10	20	0	10	20	0	10	20	0	10	20
AD	191	214	266	180	211	257	80	130	150	110	124	150
TE	24	27	33	24	27	32	13	19	25	24	18	19
LD	48	54	65	47	53	64	50	56	74	60	60	86
PD	48	54	65	48	53	64	50	65	80	50	65	85
PP	72	85	98	71	82	97	80	90	100	94	90	100
MD	52	59	65	50	58	64	52	60	74	55	60	74
PT	215	161	140	190	150	135	190	152	147	190	148	150

Table1: Stress distribution at different preflexion angles and modification

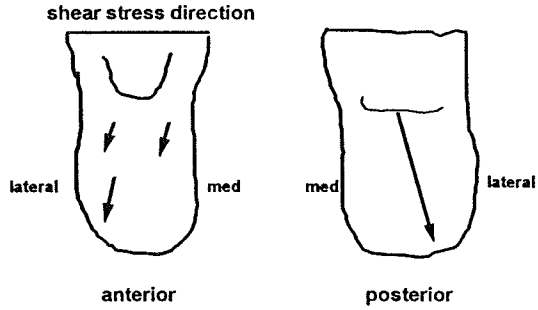

Figure 1: Shear Stresses directions

SHEAR STRESS (kPa)		AMP	PP	ALD	ALP
RM 0	0	3.2	38	4.2	1.7
	10	2.4	42	7.7	2.7
	20	2.3	44.5	11	2.5
RM 20	0	2.3	40.7	4.2	1.07
	10	2.5	42	7.8	2.66
	20	3.3	45	11.5	3.68
RM 42	0	2.5	41	5.4	1.15
	10	3.4	46.1	9.5	3.26
	20	4.7	49.4	13.1	4.6
RM 51	0	2.7	41.7	5	1.12
	10	4.1	46.5	9.25	1.9
	20	5.8	49.6	13.4	4.68
Sanders 1992	Exp.	5	45	30	6

Table2: Comparison the FEA results of shear stresses and Sander's experimental data

REFERENCES

Quesada, P. J. of Reh. Res. Dev., 28, 1-12, 1991
Sander J. J. of Reh. Res. Dev., 29, 1-8, 1992
Sander J. J. of Reh. Res. Dev., 30, 191-204

ACKNOWLEDGMENTS

This work was supported by National Science Council of R.O.C. NSC83-0420-B-075-047

Failure Strength of Patellar Tendon, Quadriceps Tendon, and Hamstring Tendon Grafts in Anterior Cruciate Ligament Reconstruction: A Biomechanical and Histologic Analysis

T. R. Stapleton[1], D. T. Curd[2], C. L. Baker, Jr.[1]
[1]The Hughston Clinic, P.C., Columbus, GA, 31908-9517
[2]Hughston Sports Medicine Foundation, Inc., Columbus, GA, 31908-9517

INTRODUCTION

Reconstruction of the anterior cruciate ligament (ACL) is a commonly performed procedure in sports medicine. The orthopaedic literature has many reports comparing the viability of the patellar tendon, the quadriceps tendon, and various hamstring tendon combinations as graft materials. The purpose of this study was to compare these methods biomechanically and histologically, which has not previously been accomplished.

REVIEW AND THEORY

Previous studies in this area (Noyes, F.R. et al., 1984, Howe, J.G. et al., 1991) have suggested that patellar tendon grafts are the strongest available tissue for this reconstruction. However, this work did not represent a clinical method of fixation or a physiologic manner of testing. Current clinical methods of doubling, tripling, or quadrupling the hamstring and gracilis tissues were also not examined. Another study (Fulkerson, et al., 1995) suggests the advantages of the central quadriceps tendon as graft material but fails to compare it to the hamstrings or patella tendon graft. Although these are excellent biomechanical studies, they do not fully represent current concepts in clinical fixation and graft preparation.

PROCEDURES

Seven each of the following grafts were harvested from young cadaver knees: 9-mm patellar tendon graft (PTG), 10-mm PTG, 11-mm PTG, doubled semitendinosus, tripled semitendinosus, woven quadrupled semitendinosus with gracilis, nonwoven semitendinosus with gracilis, and 10-mm quadriceps tendon graft. Cadaver knees were reconstructed using these grafts and stressed to failure on a materials testing system using a special jig designed to mimic the pivot shift maneuver. Failure strengths were recorded. Failed grafts were sectioned and preserved for histomorphometric analysis.

RESULTS

The strongest graft was the woven quadrupled semitendinosus with gracilis graft, followed by the nonwoven quadrupled semitendinosus with gracilis, the tripled semitendinosus, the 11-mm PTG, the doubled semitendinosus, the 10-mm PTG, the quadriceps tendon, and the 9-mm PTG (Figure 1). Most patellar tendons and quadriceps tendons failed at their respective bone plugs, whereas the semitendinosus grafts generally failed at midsubstance. In order to obtain graft failure instead of fixation failure, interference screws were used for the patellar and quadriceps tendon grafts, and the semitendinosus grafts were fixed with a screw and washer on the tibial end and three sutures tied around and AO screw on the femoral end.

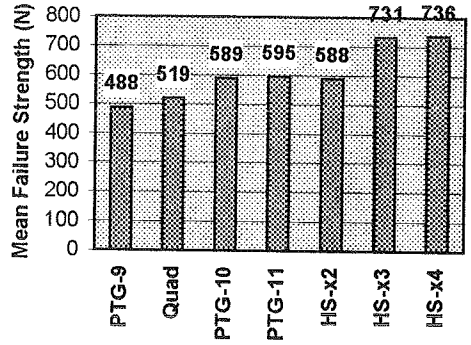

Figure 1: Graft Failure Strengths

DISCUSSION

The results of the biomechanical analysis may be partially explained from the histologic analysis. Examination of the failed grafts indicated that the type I collagen fibrils are much more densely packed in the semitendinosus grafts than in either the patellar or quadriceps tendon grafts. The transition zone between tendon and bone is much larger on the quadriceps side than on the patellar side, making the quadriceps tendon an even weaker graft than the patellar tendon.

CONCLUSIONS

We conclude that the strongest ACL graft tested was the quadrupled semitendinosus with gracilis graft and the weakest graft was the 9-mm PTG. Histology can help to explain the differences in these graft strengths. The method of fixation plays a significant role in graft failure strength.

REFERENCES

Cooper, D.E. et al. Am. J. Sports Med., 21(6), 818-824, 1993.
Fulkerson, J.P., et al. Arthoscopy, 11(2), 252-254, 1995.
Howe, J.G. et al. Am. J. Sports Med., 19(5), 447-457, 1991.
Marshall, J.L. et al. Clin. Orthop., 143, 1979.
Noyes, F.R. et al. J. Bone Joint Surg., 66-A, 344-352, 1984.
Staubli, H.U. The Knee and the Cruciate Ligaments. Berlin: Springer-Verlag, 1992.
Woo, S.L-Y. et al. Am. J. Sports Med., 19(3), 217-225, 1991.
Yasuda, K. et al. Am. J. Sports Med., 20(4), 471-475, 1992.

ACKNOWLEDGMENTS

This work was funded in part by Mitek Products, Westwood, MA, and the Hughston Sports Medicine Foundation.

COMBINED EFFECTS OF LASER PHOTOSTIMULATION AND EARLY MECHANICAL STRESS ON REGENERATING FUNCTIONALLY LOADED ACHILLES TENDON

G. K. Reddy, S. Gum, L. Stehno-Bittel, C.S. Enwemeka
Department of Physical Therapy, University of Kansas Medical Center, Kansas City, KS 66160

INTRODUCTION

Unlike other soft tissues, primary healing of tendons takes several weeks during which they are protected in immobilization casts. The long period of protective immobilization required to prevent re-rupture of the tissue predisposes muscle atrophy, infection, tendo cutaneous adhesion, and joint stiffness. These complications retard post-operative rehabilitation because full restoration of function cannot be attained unless they are overcome. Accumulating evidence suggests that various therapeutic physical modalities such as functional loading, electrical stimulation-induced mechanical stress, and laser photostimulation independently promote healing of experimentally tenotomized tendons.

REVIEW AND THEORY

Laser modalities are extensively used in dermatology and plastic surgery, particularly for treatment of wounds and other vascular lesions. Laser photostimulation appears to have numerous biological effects at the cellular level including the modulation of connective tissue metabolism in a selective and non-destructive manner. The evidence indicates that low intensity laser photostimulation promotes collagen biosynthesis in skin wounds and fractures (1). Additionally, favorable results have been obtained with use of electrical stimulation on chronic wounds (2) and promotes the gliding function in repaired tendons. In earlier studies we demonstrated that early functional loading alone augments the healing process of repaired tendons. Given our earlier results indicating that functional loading promotes tendon healing, and the reported positive effects of laser photostimulation on repaired tendons and other connective tissues, we hypothesized that healing of repaired functionally-loaded tendons would be accelerated further when treated with a combination of laser photostimulation and early mechanical loading. Thus, the purpose of this study was to compare the biomechanical and biochemical effects of functional loading alone with that of a combination of laser photostimulation and early mechanical stress superimposed on functional loading. Specifically, we measured and compared the load, energy absorption, Young's modulus of elasticity, stress, strain, total collagen and collagen crosslinks of both groups of tendons.

PROCEDURES

Forty two white male New Zealand rabbits, aged 10 weeks, were weighed, anesthetized and tenotomy was performed according to our standard protocol (3). Animals were divided randomly into control and experimental groups. The animals in the experimental group received electrical stimulation for five consecutive days beginning from the first post-operative day. An interrupted galvanic current (with 3 seconds ramp and a duty cycle of 12 seconds on: 30 seconds off, delivered at a frequency of 120 pulses per second) was used to impose mechanical stress on the repaired tendon via artificial contraction of the triceps surae. In addition, the tendons were treated with 1.0 J cm^{-2} doses of He:Ne laser photostimulation beginning from the first post-operative day. On the fifth post-surgical day immobilization casts were removed from the surgical limbs of rabbits to allow functional loading in both control and treatment groups. Thus, the animals were allowed to weight bear to tolerance. Electrical stimulation was halted at that point, and treatments continued with daily laser photostimulation. Two weeks after tenotomy, the tendons from each rabbit were excised for biomechanical and biochemical studies.

Biomechanical analysis: The cross-sectional area was determined by measuring the radius of each tendon. The biomechanical characteristics of each tendon was then determined using an Instron device as described by An et al (4).

Biochemical Analyses: Total collagen was determined by measuring the hydroxyproline content in each tissue as previously described (5). The hydroxypyridinum crosslinks in neotendon were determined using high performance liquid chromatography as described previously (6).

Statistics: A multivariate analysis of variance (MANOVA) was used. Statistical differences were defined as $P < 0.05$.

RESULTS

There were no significant changes detected in the cross-sectional area of tendons in modality-treated animals compared to controls. A comparison of the strength of the control tendons and those receiving modalities demonstrated no statistically significant differences between the two groups in terms of maximum load, Young's modulus of elasticity and energy absorption capacity (Fig. 1). Maximum stress was 2.02 ± 0.20 MPa for control tendons and 2.62 ± 0.39 MPa for experimental tendons showing modest improvement. Similarly, strain measurements increased slightly with treatment but did not reach statistical significance (51 ± 3% for controls and 58 ± 3% for the modality-treated group). In summary the biomechanical data revealed little or no difference in the strength, elasticity, and resilience between control

tendons and those receiving modality-treatment with laser phototherapy and early mechanical stress.

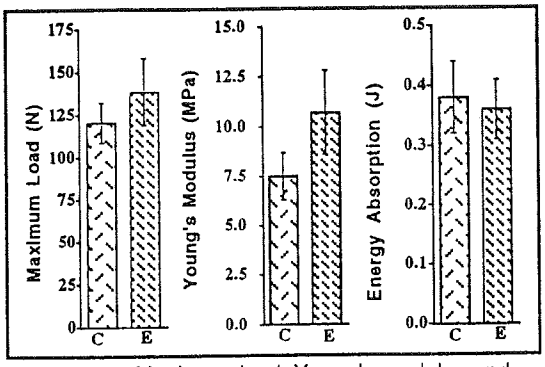

Figure 1. Maximum load, Young's modulus and Energy absorption in control (C) and modality-treated (E) tendons.

In contrast to the biomechanical data, the biochemical assays showed a significant increase in collagen production with daily modality treatments ($P<0.03$; Fig. 2). Measurement of hydroxypyridinium crosslinks revealed that control tendons had slightly more crosslinks than the modality-treated tendons (Fig. 2).

DISCUSSION

In the present investigation, we examined the combined biological effects of laser photostimulation with early mechanical stress on the tissue repair process using surgically tenotomized rabbit Achilles tendons. It was anticipated that a combination of laser photostimulation and early mechanical stress would have greater beneficial effects and quicken the repair process of tenotomized tendons. However, the combined effects of these modalities as reported here show marginal to no effect on the biomechanical characteristics of regenerating tendons. These results contradict our earlier studies (3) demonstrating improved tendon healing with laser treatment determined biomechanically. It is our postulate that several factors may be the cause of these apparently contradictory findings. In earlier studies, rigid plaster of Paris casts immobilized the repaired tendons whereas in the present study, re-usable polyurethane casts were used while maintaining the same design as the rigid plaster casts. Although the design of the casts was identical, the mean weight of polyurethane casts was three fold lower than that of plaster cast. Moreover, it is worth noting that the animals used in this study were from a source different from those used in our earlier studies. Animal variation, health, and nutrition could have played a role in the results of this study.

Unlike the biomechanical results, the biochemical assays show that the total content of collagen is increased significantly in modality-treated group. However, the hydroxypyridinium crosslinks of collagen were decreased, but not significantly, in the modality-treated group. These biochemical findings may appear to contradicts the biomechanical results. However, it is quite possible that these two modalities have the therapeutic effects of enhancing synthesis more new collagen molecules that may not have formed stable crosslinks. Although there is not enough evidence available with regard to the direct relationship between collagen crosslinks and biomechanical properties, evidence suggest that the biomechanical properties of the tissue primarily depend on the nature of the collagen crosslinks.

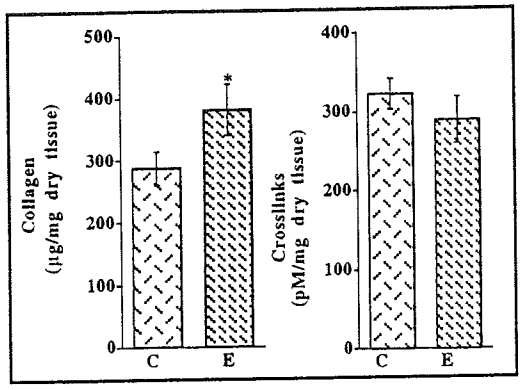

Figure 2. Collagen content and hydroxy-pyridinium crosslinks in control (C) and modality-treated (E) tendons. The mean collagen content values in modality-treated tendons were significantly higher than that of control tendons ($P = 0.03$)

The clinically important finding of the present study is that the combined modalities of laser stimulation with early mechanical stress induced by electrical stimulation did not significantly enhance the healing of repaired tendons. Since these modalities are used currently in many hospitals and clinics for tendon repair, their employment and reimbursement should be re-examined.

REFERENCES

1. Abergel, R.P. et al: J. Am. Acad. Dermatol. 11: 1142-1150, 1984.
2. Davis, S.C. and Ovington, L.G: Dermatol. Clin. 11: 775-781, 1993.
3. Enwemeka, C.S: J. Orthop. Sports. Phys.Ther. 14:198-212, 1991.
4. An K-N, et al: J. Biomech. 19: 399-404, 1986.
5. Reddy, G.K.and Enwemeka, C.S: Clin. Biochem. (In press, 1996).
6. Eyre, D.R. et al : Anal. Biochem. 137:380-388, 1984.

ACKNOWLEDGMENT

This work was supported by VA RR&D grant number A534-RA.

EFFECTS OF TARGET LOCATION ON TORSO KINEMATICS DURING SEATED DISCRETE REACHING MOVEMENTS IN THREE-DIMENSIONS

Xudong Zhang, Don B. Chaffin, and Qing Shen
Center for Ergonomics, The University of Michigan, Ann Arbor, MI 48109-2117

INTRODUCTION

Reaching movements require the participation of the torso when the target is located beyond one's arm length. Sometimes, significant torso assistive motions may also be involved when the target is located closer than an arm length away (Kaminski et al., 1994). These types of movements occur in many vehicle driving tasks as well as other manual workplace tasks. To further improve the design of these tasks requires an accurate model of the movements with a realistic description of the torso kinematics. This latter description helps reducing the kinematic indeterminacy and complexity associated with multi-segment reaching movements involving torso motions. It also facilitates a clearer understanding of human postural control and movement coordination mechanisms. The present study is an attempt to develop statistical models to predict the effects of target location on selected torso kinematic characteristics during seated reaching movements in three-dimensions (3D). Regression models that quantify 1) the amount of torso flexion and 2) the direction of the torso motion are presented. The seated reaching movements studied are discrete, volitional, and right-handed.

REVIEW AND THEORY

Although arm reaching has received extensive attention in the field of motor control research, the majority of previous investigations have focused on reaching involving only the upper limb without torso assistance allowed (Morasso, 1983; Abend et al., 1982; Lacquaniti et al., 1982; Flash et al., 1985; Kaminski et al., 1986). Recent studies by Ma et al. (1995), and Kaminski et al. (1994) have considered torso assistive motions, but both studies were restricted to a simplified experimental paradigm with reaching tasks performed either on a horizontal table or within the sagittal plane. There appears to be a need to study reaching motions in a more diverse or realistic context for biomechanical modeling and ergonomics analysis purposes. Additionally, these types of studies normally do not produce any quantitative results that specify the kinematics of the torso.

A quantitative model of torso kinematics derived from empirical results is vital to the modeling of normal human reaching movements. The lack of such a model has degraded the performance of this type of modeling efforts in the past (Ryan, 1969; Kilpatrick, 1970) in which heuristics and rough estimates of torso kinematics were used. Predictive models have been proposed to resolve the kinematic redundancy inherent to modeling multi-segment movements; many rely on the theory that human beings follow an optimal strategy with respect to some biomechanical measure (e.g., minimal energy expenditure) in controlling dynamic postures (Ayoub et al., 1974; Marshall et al., 1985). These models, however, have yet to be validated for arm reaching movements involving the torso.

PROCEDURES

An experiment with seated reaching tasks was conducted in a vehicle driving simulator developed by the Center for Ergonomics at the University of Michigan. Three young healthy volunteers, anthropometrically categorized as a small female (SF), a small male (SM), and a large male (LM), served as subjects. Figure 1 illustrates the experimental setup along with the laboratory coordinate system. Ten targets (numbered 1-10 in the figure) were evenly positioned as a 2×5 matrix in the dash area. Within each row (1-5 or 6-10) the distance from a target to the subject increased with the target number. The closest target was located such that, once the preferred seat adjustment was made, it was just beyond the extended arm reach without torso motion regardless of individual anthropometry; the farthest target was positioned such that it simulated reaching to the opposite side of a large passenger vehicle.

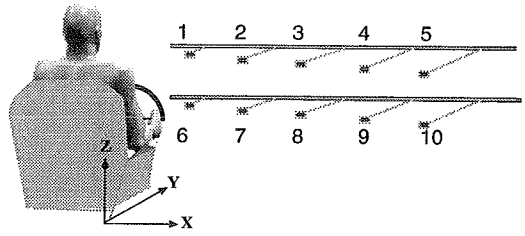

Figure 1. A simulated vehicle where reaching motions were performed towards ten targets in the dash area.

A MacReflex™ motion analysis system with four cameras was employed to capture the motions of six reflective markers placed over the body landmarks identifying the right wrist, right elbow, right acromion, suprasternale, and left and right anterior superior iliac spines (ASIS). Torso motions are represented by the triangle formed by the suprasternale and two ASIS markers. A sampling rate of 25 Hz was used. At the start of each reaching movement, the subjects assumed a posture with both hands on the steering wheel in the typical 10:00 and 2:00 positions. Light-emitting-diodes (LED) embedded in the targets provided a visual cue for the subjects to identify which target to reach. Three repetitions for each target reach motion were obtained. Thus each subject performed a total of 30 trials, the order of which was randomized.

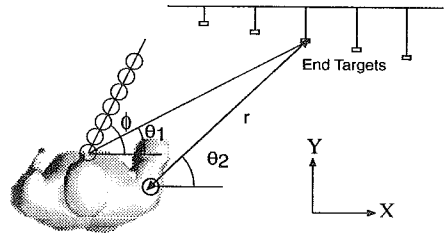

Figure 2. An overhead view of three variables that quantify a target location, and the torso motion direction angle.

As depicted in Figure 2, three variables were derived to quantify the location of a target with respect to the initial posture: 1) r—the ratio of the distance between the target and the right shoulder marker relative to the individual's

Table 1.
Derived values of three independent variables that quantify the target locations with respect to individual subject.

	Target 1			Target 2			Target 3			Target 4			Target 5		
Subject	r	θ_1	θ_2	r	θ_1	θ_2	r	θ_1	θ_2	r	θ_1	θ_2	r	θ_1	θ_2
SF	1.05	55	72	1.15	44	55	1.34	35	47	1.48	24	31	1.69	14	20
SM	1.02	50	67	1.13	44	57	1.30	36	46	1.43	27	35	1.58	20	28
LM	1.09	62	78	1.14	55	69	1.22	48	59	1.28	40	50	1.34	33	43
	Target 6			Target 7			Target 8			Target 9			Target 10		
Subject	r	θ_1	θ_2	r	θ_1	θ_2	r	θ_1	θ_2	r	θ_1	θ_2	r	θ_1	θ_2
SF	1.24	54	72	1.34	45	59	1.52	32	43	1.68	24	31	1.80	13	17
SM	1.17	54	70	1.26	45	57	1.41	36	46	1.58	28	37	1.71	21	29
LM	1.21	62	77	1.25	54	68	1.32	46	59	1.39	39	51	1.44	32	43

* Subject stature: SF-154 cm; SM-164 cm; LM-195 cm. Angles are in degrees.

arm length; 2) θ_1—the angle subtended by the projection of a line connecting the target and the suprasternale marker projected onto the horizontal plane and measure from the X-axis; and 3) θ_2—the angle between the projection of a line connecting the target and the shoulder marker projected onto the horizontal plane and measured from the X-axis. The ratio r was used rather than the absolute distance to account for individual anthropometry as well as preferred seat placement. Table 1 presents the subject-specific values of these three variables for the 10 targets.

Two dependent measures were used to characterize the torso kinematics: 1) δ—the amount of torso flexion, which is the angular displacement of the torso projected onto the mid-sagittal plane; and 2) ϕ—the direction angle of torso motion towards each target, as estimated from the projection of the suprasternale marker's trajectory projected onto the horizontal plane (Figure 2).

RESULTS AND DISCUSSION

Figure 3 shows the means of sagittal plane torso flexion incurred by each subject when reaching to the ten targets. Both the target and subject effects were statistically significant at a $P<0.01$ level. Inspection of the graphed results indicates, 1) the amount of torso flexion increased with the target distance; 2) the far targets (3-5, 8-10) required a substantial or even extreme (>45 deg) torso flexion; and 3) the amount of flexion was affected by subject stature.

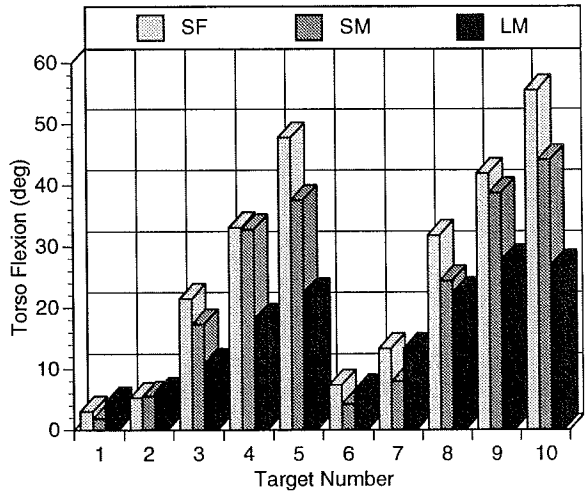

Figure 3. Amount of torso flexion incurred during reaching movements towards the ten targets for the three subjects.

As the ratio r was adopted as a predictor to "cancel-out" the confounded effects of anthropometry and preferred seat position, a strong linear relationship between δ and r was revealed (for $r > 1$ only) and modeled as:

$$\delta = -76.3 + 72r \quad (R^2=0.95)$$

When the direction angle of the torso motion ϕ was determined from the trajectory of the suprasternale marker onto the horizontal plane, a high degree of linearity in the trajectory was identified for all reaches to the far targets (3-5, 8-10). Less linearity was exhibited by the trajectories for the closer reaches. In other words, as the value of r approached 1 there was less consistency in the trajectory patterns with an increased rate of nonlinear or erratic ones. Statistical analyses concluded that ϕ can be best predicted by θ_1 using the following quadratic regression model:

$$\phi = 44 - 0.65\theta_1 + 0.027\theta_1^2 - 1.65ID \quad (R^2=0.88)$$

where ID is an indicator (-1 for SF & SM; 1 for LM) to account for individual differences. An alternative model using θ_2 as the predictor had a similar form but with a slightly lower R^2. A large scale study underway will allow us to identify one or more individual attributes to replace the indicator variable ID and generate a more robust population model.

Collectively, the above findings suggest that the torso is an adept prime mover for common arm reaches, though constrained by its biomechanical construct as well as the specific seating conditions. It is proposed that future studies of arm reaches need to consider the torso as an integral part of the normal kinematic linkage. Studies should be designed to challenge subjects to move their hands to a variety of specified locations in 3D space. By doing so not only will realistic human motion patterns be statistically revealed for scientific reference, but the results will be useful for both ergonomic design and patient diagnosis as well as treatment purposes.

REFERENCES

Abend, W. et al. Brain, 119, 331-348, 1982.
Ayoub et al. Human Factors, 16, 585-594, 1974.
Flash, T. et al. J. Neuroscience, 5, 1688-1703, 1985.
Kaminski, T.R. et al. Exp Brain Res, 106, 457-466, 1995.
Kilpatrick, K.E. Ph.D. Thesis, Univ. of Michigan, 1970.
Lacquaniti, F. et al. J. Neuroscience, 2, 399-408, 1982.
Ma, S. et al. J . Neurophysiology, 73-5, 2120-2122, 1994.
Marshall et al. Proc. of ASB, 1985.
Morasso, P. Biol. Cybern., 48, 187-194, 1983.
Ryan, P.W. JANAIR Report, 700202, 1969.

ACKNOWLEDGMENT

This work was supported by the Challenge Fund from Chrysler Corporation.

ACUTE EFFECTS OF EXERCISE ON PASSIVE JOINT STIFFNESS

M. Ricard, D. Butterfield, D. Draper, S. Schulthies, W. Myrer
Physical Education Department, Brigham Young University, Provo, UT 84602

INTRODUCTION

The purpose of the study was to compare the effects of exercise on passive knee joint stiffness. Passive knee joint stiffness was measured prior to and following a weight training exercise bout.

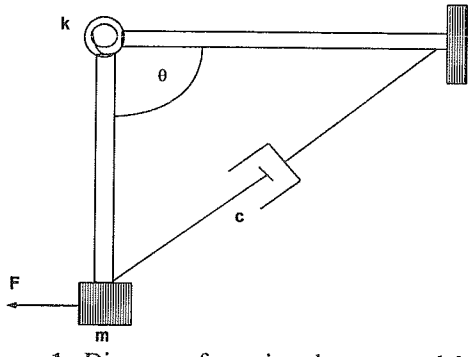

Figure 1. Diagram of a spring-damper model used to describe the stiffness (k) and damping coefficient (c) of the knee.

Passive stiffness in a human joint is due muscular factors attributed to actin-myosin filaments and connective tissue factors which can be attributed to fascia, ligaments and friction in the joint. The viscoelastic behavior of a human joint can be modeled using a spring-damper model as shown in Figure 1. A torsional spring with linear stiffness can be used to represent the elastic response of the actin-myosin filaments and connective tissue in the knee joint. The time-dependent behavior of connective tissue can be modeled using a viscous damping element as shown in Figure 1. The immediate effects of an exercise bout such as weight lifting are known to increase the stiffness of the joint involved. High specific tensions in the muscle may disrupt the sarcolemma and sarcoplasmic reticulum resulting in subcellular microtrauma to tissue (Armstrong, et al., 1983; Friden, et al., 1983; and Kuipers, et al., 1983). Lakie, et al. (1988) found that joint stiffness increases following active or passive movements. However, little is known about the acute effects exercise on joint stiffness immediately following an exercise bout.

PROCEDURES

Twenty three subjects with normal knees were selected for this study. Passive knee joint stiffness was measured prior to and following a weight training exercise bout. The exercise bout involved 10 sets of 10 single knee extension/flexions at 75% of 1 RM, followed by 10 sets of 10 eccentric contractions. The stiffness of the relaxed knee was measured using a Penny & Giles electrogoniometer. The position of the right knee was sampled for 6 s at 500 Hz.

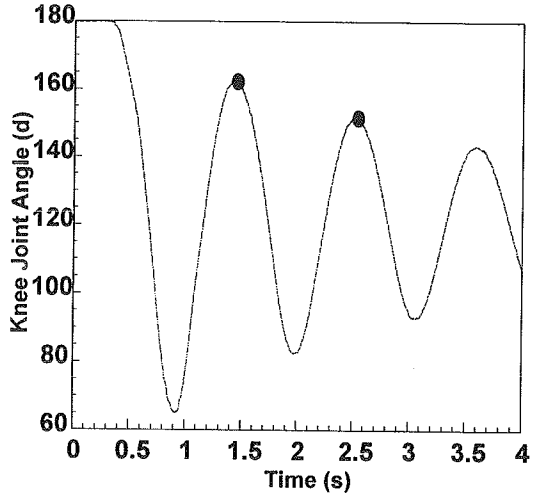

Figure 2. Typical damped oscillation resulting from allowing the lower leg to swing freely about the knee joint.

The stiffness and damping coefficients of the relaxed knee was determined with the subjects seated on a table. The lower extremity was supported by the researcher with the knee completely extended. Once the subject was completely relaxed the leg-foot system was released allowing the lower limb to freely oscillate until the lower leg comes to rest in the vertical position. Five good trials were obtained prior and after exercise. A typical damped oscillation of the knee is shown in Figure 2. Stiffness was calculated from the first two complete cycles of oscillation using the methods presented by Meirovitch (1975). The logarithmic decrement (δ) of the oscillation was calculated by

$$\delta = \ln(\theta_1 - \theta_2)$$

where θ_1 and θ_2 are the knee joint angles for the first two peaks in the oscillation (Figure 2). The viscous damping factor (ξ) was calculated as follows.

$$\xi = \frac{\delta}{\sqrt{(2\pi)^2 + \delta^2}}$$

where δ is the logarithmic decrement of the damped oscillation. The natural frequency of the oscillation (ω) was determined from the following equation.

$$\omega = \frac{\delta}{\xi \times T}$$

where δ is the logarithmic decrement, ξ is the viscous damping factor and T is the time between oscillation peaks. The damping coefficient (c) was obtained as follows.

$$c = 2\,\xi\,\omega\,I$$

where ξ is the viscous damping factor, ω is the natural frequency and I is the moment of inertia of the lower leg and foot about the knee joint. The passive stiffness (k) of the knee joint was obtained using the following equation.

$$k = I\omega^2$$

where I is the moment of inertia of the leg-foot and the ω is the natural frequency. All five trials for stiffness (k) and damping coefficients (c) were averaged. Dependent t-tests were used to test for significant differences in stiffness and damping after exercise.

RESULTS

The acute effects of exercise on passive knee joint stiffness, damping coefficient and natural frequency are shown in Table 1. Significant increases in passive knee joint stiffness, damping coefficient and natural frequency were observed following exercise ($p < .05$). Mean passive knee joint stiffness increased by 1.56 N•m/rad immediately following the exercise regime. Single knee extension strength decreased significantly from 37.8 ± 14.87 kg prior to exercise to 14.28 ± 2.42 kg following the exercise bout.

Table 1: Mean and SD for Knee Joint Stiffness and Damping Before and After Exercise

	Before Exercise	After Exercise
Joint Stiffness (N•m/rad)	4.59 (1.23)	6.15 (2.32)
Damping Coefficient (N•m/s/rad)	-.014 (.006)	-.017 (.009)
Natural Frequency (Hz)	5.98 (.33)	6.88 (.94)

DISCUSSION

Passive knee joint stiffness arises from the combined effects elastic structures including muscle, tendon, articular surface, ligament and skin. In a relaxed joint a considerable portion of joint stiffness can be attributed to passive resistance offered by actin-myosin filaments. Mechanically induced micro-trauma to the myofibrils can be quantified immediately after the exercise based upon morphological changes (Newham, et al., 1983; Brooks, et al., 1995). In the current study knee joint stiffness and damping significantly increased immediately after an exercise. Joint stiffness may increase following exercise as a result of mechanically induced disruption of sarcomeres. The increased damping in the knee joint following exercise may be due to trauma to the myofibrils and inflammation of the joint caused by an increase in extracellular proteins (Armstrong, 1990). In conclusion, the immediate effects of exercise resulted in an increase in damping and passive stiffness in the human knee joint.

REFERENCES

Armstrong, R.B. et al. J. Appl. Physiol. 54, 80-93, 1983.

Armstrong, R.B. Med. Sci. Sports Exer. 22, 429-435, 1990.

Brooks, S.V. et al. J. Physiol. 488, 459-469, 1995.

Friden, J. et al. Int. J. Sports Med. 4, 170-176, 1983.

Kuipers, H. et al. Int. J. Sports Med. 4, 45-51, 1983.

Lakie, M. et al. J. Exp. Physiol. 73, 487-500, 1988.

Meirovitch, L. Elements of Vibration Analysis. McGraw-Hill, 1975.

Newham, D.J. et al. J. Neurol. Sci. 61, 109-122, 1983.

SUBJECT LOAD-HARNESS INTERACTION DURING ZERO-GRAVITY TREADMILL EXERCISE

Jean L. McCrory, Heidi A. Baron, [1]Janice A. Derr, [2]Brian L. Davis, and Peter R. Cavanagh
Center for Locomotion Studies, Department of Kinesiology and [1]Statistical Consulting Center
Penn State University, University Park, PA 16802
[2]Department of Biomedical Engineering, The Cleveland Clinic Foundation, Cleveland, OH

INTRODUCTION

When astronauts exercise on orbit, a subject load device (SLD) must be used to return the subject back to the supporting surface. The load in the SLD needs to be transferred to the body by a harness which typically distributes this load between the pelvis and the shoulders. Through the use of a zero-gravity simulator, this research compared subject comfort and ground reaction forces during treadmill running at three levels of subject load (60%, 80%, and 100% of body weight) in two harness designs ("shoulder only" and "waist and shoulder ").

REVIEW AND THEORY

Exercise will almost certainly play an integral part in minimizing the adverse effects of space travel on the body, particularly bone mineral loss and muscular atrophy. It is hypothesized that an effective exercise regimen would elicit loads on the lower extremities that resemble those encountered on Earth (Cavanagh, 1986; Convertino and Sandler, 1995). No testing has been done in space to quantify the ground reaction forces to which the lower extremities are exposed, but it is believed that these forces are much less than those experienced in 1-G (Cavanagh, 1987).

The Penn State Zero-Gravity Simulator (PSZS Davis et al. 1996), is a device which suspends subjects horizontally from multiple latex cords, with each cord negating the weight of a different limb segment. A treadmill mounted on the wall under the PSZS enables subjects to run in simulated zero-gravity. The SLD has, in the past, consisted of a set of 4 springs attached to a harness, with the waist of the subject feeling the entire pull of the SLD. With this system, the subjects could only tolerate an artificial gravity of 60% of 1-G (Davis et al. 1996). Astronauts currently wear a harness system in which the SLD pulls both at the waist and shoulders (Greenisen and Edgerton, 1994), although the tension in these springs has not been quantified. However, it is likely that previous SLDs have only provided loads less than Earth gravity (Cavanagh 1986, 1987).

The purpose of this study was to quantify ground reaction forces, subject load, and subjective ratings of comfort from subjects wearing one of two harness designs under loads of 60%, 80%, and 100% of body weight while running in the PSZS. The objective was to gain insight into the effectiveness of the present countermeasures against bone mineral loss and muscular atrophy in space.

PROCEDURES

Eight subjects (mean age 29.4 ±4.5 years, mean height 176.6 ±9.0 cm and mean mass 73.3±5.3 kg) participated in this study. Two harness configurations were assessed: a "shoulder only" design, in which 4 springs were attached to shoulder pads worn by the subject, and "waist and shoulder " design, in which 4 springs were attached to the shoulder pads and 4 to a waist harness. Three levels of load (60%, 80%, and 100% of body weight) were randomly administered in each harness design. Ground reaction forces were measured via a Kistler force plate mounted within the treadmill belt. Load cells measured tension in the SLD. A modified Borg scale was used to assess the levels of discomfort. Subjects ran at a speed of 1.96 m/s for 3 minutes during each condition. A period of 3 minutes rest was given between conditions. Data were collected at 500 Hz.

RESULTS

The level of discomfort increased significantly ($p<0.05$) as the subject load increased from 60% to 80% to 100% body weight. Also, on a scale from 0 (no discomfort) to 10 (excruciating pain), the maximum levels of discomfort at 100% BW load averaged 2.3 ± 0.6 in the "shoulder only" condition and 2.5 ± 0.8 in the "waist and shoulder " condition ($p<0.05$).

The following subject load variables were measured: maximum load, time to maximum load, minimum load, time to minimum load, average load, and load fluctuation. By definition, the subject loads were significantly different between the loading conditions of 60%, 80%, and 100% of body weight ($p<0.05$). When comparing the two harness designs, the "waist and shoulder " design resulted in a lower minimum load and average load, while the load fluctuation was greater ($p<0.05$). Selected load variables for the full body weight loading conditions are shown in Table 1.

Table 1: Subject Load variables during a 100% BW load.

Load Variables (% BW)	Shoulder Only	Waist & Shoulder
Maximum	112.6 ± 2.6	110.5 ± 3.0
Minimum	90.0 ± 2.5	70.8 ± 2.8
Average	101.4 ± 2.3	91.7 ± 2.7
Fluctuation	22.5 ± 1.3	39.7 ± 1.4

The following ground reaction force variables were measured: contact time, maximum impact force, time to maximum impact force, maximum propulsive force, time to maximum propulsive force, impulse, and loading rate. In both harness designs, the maximum impact force, maximum propulsive force, impulse, and loading rate were significantly different between loading conditions ($p<0.05$). Results for the "waist and shoulder " conditions are shown in Figure 1.

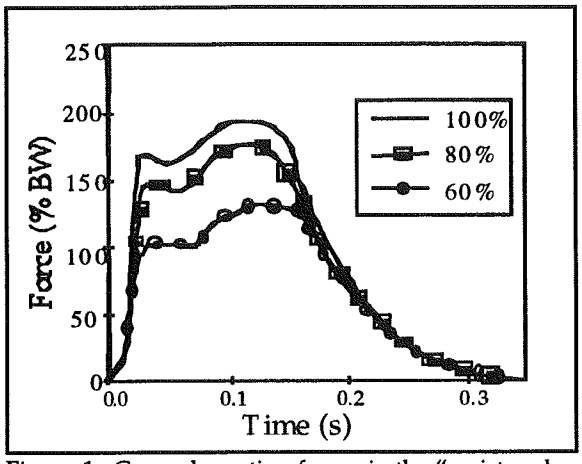

Figure 1: Ground reaction forces in the "waist and shoulder " condition in each of the subject loads.

When comparing the two harness designs, the maximum propulsive peak and the impulse were significantly greater in the "shoulder only " harness configuration ($p<0.05$). The ground reaction force curves at 100% load are shown in Figure 2.

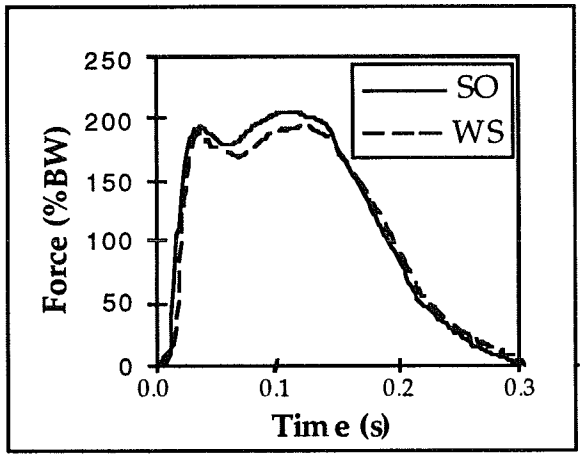

Figure 2: Ground reaction force curves at a load of 100% BW. (Harness design: SO= shoulder only, WS= waist and shoulder)

DISCUSSION

The clear dependence of peak reaction force on subject load is apparent from Figure 1. This highlights the importance of maximizing subject load if countermeasures are to generate 1-G like loads on the lower extremity. At 100% load, the peak ground reaction force was significantly greater for the "shoulder only" harness configuration. The amount of discomfort from the SLD and harness was perceived to be in the slight to moderate range at 100% loading. However, in both harness configurations, the shapes of the ground reaction force curves of subjects running in the PSZS were characteristic of the "groucho running" force curves reported by McMahon et al. (1987), indicating that the subjects were running in a slightly crouched (hips and knees flexed) position. This was most likely an attempt to reduce the discomfort caused by the SLD pulling on the body.

The effectiveness of tethering running as a countermeasure against bone mineral loss and muscle atrophy is believed to be dependent upon the presence of 1-G type forces. Unless a harness can be designed which will alleviate pressure felt at the SLD attachment sites, astronauts will tend to do "groucho running" to lessen the pain of the harness, thereby also attenuating the ground reaction forces. Another possibility is that the altered gait patterns result from subject loads which are locally applied (at the hips and shoulders) compared to the more global action of gravitation force.

REFERENCES

Borg, G.V. MSSE, 14, 377-387,1982.

Cavanagh, P.R. et al. A Final Report to Krug International, 1-126, 1987.

Cavanagh, P.R. Workshop on Exercise Prescription for Long-Duration Space Flight, NASA Conference Publication 3051, 61-67, 1986.

Cavanagh, P.R. and Lafortune, M.A. J. Biom., 13, 397-406, 1980.

Convertino, V.A., and Sandler, H. Acta Astro., 35, 253-270, 1995.

Davis, B.L. et al. Av. Space Env. Med. 67, 235-242, 1996.

Greenisen, M.C. and Edgerton, V.R. In: Space Physiology and Medicine, (pp. 194- 210), Lea & Febiger, 1994.

McMahon, T.A. et al. J. App. Phys., 62, 2326-2337, 1987.

ACKNOWLEDGMENTS

This research was supported by NASA grant NAGW-4421 and by a STIR award under the Pennsylvania Space Grant Consortium.

FINGERTIP PULP RESPONSE DURING KEYSTRIKES

E.R. Serina and D.M. Rempel
Department of Mechanical Engineering, University of California, Berkeley
UC Ergonomics Program, Berkeley and San Francisco

INTRODUCTION

High fingertip forces have been cited as a contributor to musculoskeletal disorders during typing (Bergqvist et al., 1995). Applied fingertip forces are 3-5 times higher than required to activate the keyswitch (Armstrong et al., 1994). The keystroke force history (Fig. 1) possess a peak impact force when the key reaches its mechanical stop and a second maxima at the end of fingertip pulp compression (Rempel et al., 1994). Transmission of the applied force to the musculoskeletal system is dictated by the response of the fingertip pulp to the force. During simulated tapping against a flat, rigid surface without impact, the pulp attenuated high frequency forces less than 1 N and transmitted high frequency forces of higher magnitudes (Serina et al., 1996). However, the transmission of forces by the pulp during a keystrike when typing remains unknown. This information is essential to identifying the force components contributing to musculoskeletal injuries.

Effects of keyswitch design characteristics such as key landing on keying force has not been investigated. The key landing is the stiffness of the keyswitch before the end of key travel. Keyswitches are currently not damped and a force of impact occurs when the end of key travel is reached (Rempel et al., 1994). Hence, modification of key landing characteristics may reduce the impulsive forces. No specifications for key landing design are indicated by current standards (ANSI/HFS 100-1988).

The objectives of this study of simulated typing are to determine the force transmission of the fingertip pulp during keying and the effects of key landing on the transmitted force.

METHODS

Five subjects (3 male, 2 female; age=24±2 years) tapped on a keyswitch (KCM type, Alps Electric Co., Ltd.) repeatedly with the right index finger while the applied force and pulp displacement were measured simultaneously. Subjects assumed a typing posture with a 45° fingertip contact angle and rapidly struck the keyswitch in a manner similar to typing. Three key landing configurations were used, randomly ordered: soft, medium, and stiff (Fig. 2). Key landing was modified with foam strips placed underneath the keycap. The 'stiff' configuration was the keyswitch without padding. All other keyswitch design parameters were identical between configurations.

A high-speed motion analysis system (Kodak SP2000) continuously tracked index fingertip and keycap motion during keying (fov: 10X15 mm) while a force plate (Bertec Corp., OH) under the keyswitch measured the applied force. The fingernail and keycap were marked to facilitate tracking of their motions. Force and position data were collected at 1000 Hz simultaneously. Position data were manually digitized. Data were filtered by a low-pass, 4th order Butterworth filter with a 300 Hz cutoff frequency. Contact force and position data were synchronized for each keystroke.

RESULTS

Fingertip pulp displacement was a nonlinear and increasing function of force during a keystroke (Fig. 3). The pulp force-displacement curve can be separated into three sections: before, during, and after impact of the keyswitch with the mechanical stop. Pulp displacement was very sensitive to force magnitude before impact. When the mechanical stop was reached, the peak impact force was F_I = 3.18±1.11 N for the stiff keyswitch. No equivalent sharp increase occurred in pulp compression, so a force spike was present in the pulp force-displacement curve. After impact, pulp stiffness is markedly increased. The finger continued to load the keycap to a second maxima of F_{max} =2.65±0.57 N and displacing the pulp to a maximum

compression of x_{max} =2.0±0.5 mm. Mean force duration for the stiff keyswitch was 118±29 ms.

Tapping on the keyswitch with a soft landing resulted in smaller F_I (2.94±0.53, 3.25±1.59, and 3.18 N for soft, medium, and stiff, respectively) but greater F_{max} than on the other keyswitch configurations (2.95±0.41, 2.62±0.64, and 2.65 N for soft, medium, and stiff, respectively). Similar maximum pulp displacement and force duration were found between the different key landing configurations.

DISCUSSION

In this simulated typing experiment, subjects struck the key with force magnitudes, time histories, and durations similar to typing (Rempel et al., 1994). Force-displacement curves of the fingertip pulp during a keystroke resembled the those curves obtained during tapping without impact (Serina et al., 1996), especially in the region when the key was stationary. Because the pulp is compliant at the lower forces, the sensing of tactile information at the fingertips is not limited by the mechanical properties of the pulp. It is possible that, because a force spike is present in pulp force-displacement curves, the pulp does not dissipate completely the force of impact.

Key landing appears to influence the relative maxima of the applied keystroke force history. Maximum forces while tapping on the keyswitch with the soft key landing configuration differed from those from the other key landing configurations. The stiff and medium key landings may have been too similar to cause detectable differences in the applied force. Pulp displacement and force duration did not seem to be strongly affected by this keyswitch design parameter.

REFERENCES

Armstrong *et al., Am. Ind. Hyg. Assoc. J.*, 55, 30-35, 1994.

Bergqvist *et al., Ergonomics*, 38, 763-776, 1995.

Rempel *et al., J. Biomech.*, 27, 1101-1104, 1994

Serina *et al., J. Biomech.* (in review) 1996.

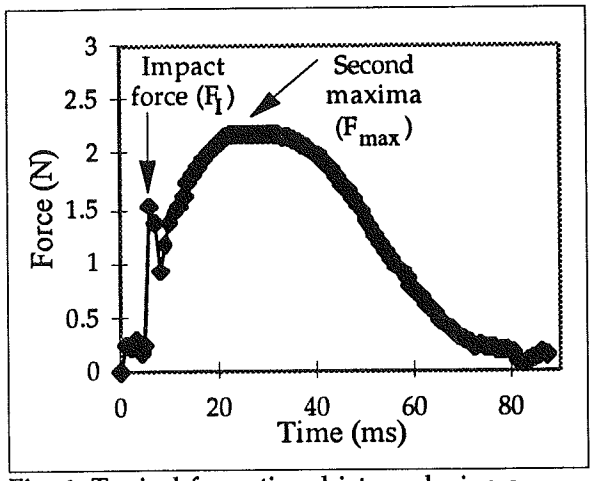

Fig. 1: Typical force-time history during a keystroke.

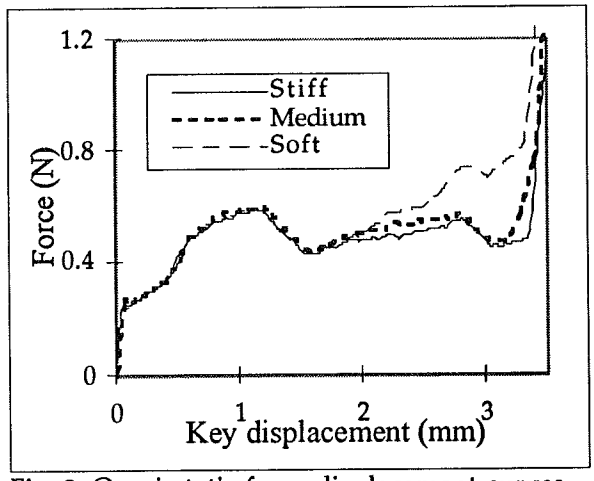

Fig. 2: Quasi-static force-displacement curves of the keyswitch configurations used (loading portion only). Keyswitches differed only in key landing stiffness.

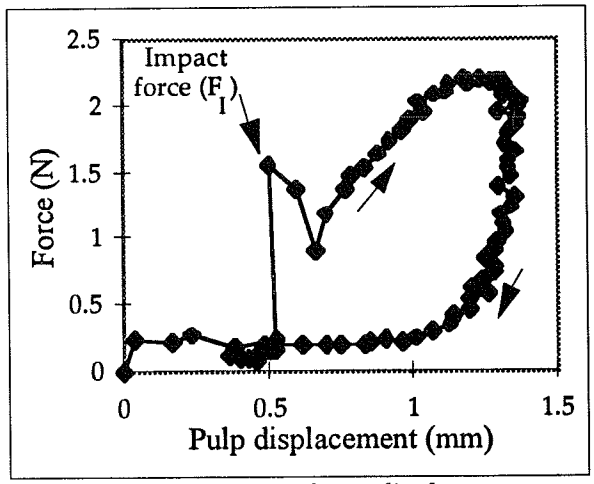

Fig. 3: Typical dynamic force-displacement curve of the fingertip pulp during a keystroke.

RANGE OF MOTION, BODY CONFIGURATION, AND INDIVIDUAL DIFFERENCES AFFECT PREDICTIONS OF FUNCTIONAL CAPACITY BASED ON KNEE STRENGTH MEASUREMENTS

M.J. Pavol[1], M.D. Grabiner[2]
[1]Biomedical Engineering Center, The Ohio State University, Columbus OH 43210
[2]Dept. of Biomedical Engineering, The Cleveland Clinic Foundation, Cleveland OH 44195

INTRODUCTION

In many applications in ergonomics and rehabilitation, it is desired to know the proportion of an individual's strength capabilities that are employed during a task or, alternately, whether the performance of a task is within the capabilities of an individual. For either such evaluation, a model of the subject's maximal functional capacity is necessary.

Minimally, a model of functional capacity must describe the variations in strength at a joint as a function of joint position and velocity, as both variables significantly affect muscle strength. Such a model, consisting of a moment-angle-velocity surface representing maximum functional capacity, may be constructed from experimental isokinetic measures of joint strength at different velocities. However, these models are normally based on data from a single range of motion and body configuration. In addition, data is often averaged across subjects to produce a standard model of functional capacity which is then applied to the evaluation of individual subjects or tasks.

One purpose of this study was to determine whether, for knee extension, isokinetic maximum voluntary moment-angle (M-θ) relationships determined for a single velocity, range of motion, and body configuration would accurately describe the relationships observed at that velocity over different body configurations and ranges of motion. In addition, the relative errors associated with approximating the strength characteristics of a single individual by a group-average relationship were to be determined.

PROCEDURES

Ten healthy young subjects (22-33 yrs, 5 female) performed maximum voluntary isokinetic knee extensions with their dominant leg on a KIN-COM dynamometer. Contractions were performed at 30°/s to a knee flexion angle of 10° from 5 different starting knee flexion angles: 90, 75, 60, 45, and 30° (0° = maximal knee extension). Subjects were tested in both seated and supine positions (hip flexion angles of 90 and 0° respectively). The initial hip position was balanced between subjects, the order of starting knee angle testing randomized. Three maximum voluntary contractions (MVCs) were performed at each hip/ start angle combination, separated by at least 1 minute rest. Subjects were instructed to reach their maximum force output as rapidly as possible at the start of each exertion. The KIN-COM movement threshold was 11-17 lb.; acceleration was at the device's high rate.

Knee flexion angle and extension velocity and force were measured at 300Hz and knee extension moment computed. Filtered, interpolated data from the 3 MVCs at each hip/ start combination were combined by selecting, at each integer angle, the maximum moment measured at a velocity between 27 and 33°/s. The resulting M-θ relationship was smoothed using an averaging filter and corrected for the effects of the passive knee moments measured by the KIN-COM at 30°/s over the tested range of motion in each hip position.

Isokinetic MVC M-θ relationships were normalized by subject by the maximum moment generated during the 90°hip/ 90°start trials. Average normalized moments were extracted from each MVC curve over 10 knee angle ranges: 85-80, 80-75, 70-65, 65-60, 55-50, 50-45, 40-35, 35-30, 25-20, and 20-15° of flexion. A group-average normalized isokinetic MVC M-θ relationship was computed across subjects for each hip/ start combination. The root-mean-square (RMS) errors, as percentages of the group-average moment, between the group-average M-θ relationships and those of each subject were computed. Within-subject RMS error was estimated based on the percentage variation about the mean, by hip and knee angle, of the moments over the range of 65-30° for each individual, neglecting data from the first 10° of any MVC.

2-way (hip by start angle) repeated measures ANOVAs were performed for the average normalized moments over each of the joint angle ranges of interest, the normalized moments at 85, 70, 55, 40, and 25° of knee flexion, as well as the individual versus group-average RMS errors. Appropriate post hoc analysis was performed. Effects were considered significant at an $\alpha<0.05$.

RESULTS

Significant effects of hip position and start angle on isokinetic MVC knee extension moment were found over selected ranges of knee flexion (Tables 1 and 2). An interaction between hip position and start angle on moment occurred only at 70°. Figure 1 illustrates the group-average normalized isokinetic MVC M-θ relationships determined for each of the hip/ start angle combinations.

When computed across all subjects, hip/ start combinations, and knee angles, the overall RMS error of approximating an individual normalized isokinetic MVC M-θ relationship with the group-average relationship was 15.4% of the group-average moment, a value significantly greater than the corresponding within-subject RMS error of 5.3% of average moment. The RMS errors observed between the individual subject and group-average normalized isokinetic MVC M-θ relationships were unaffected by hip position and starting knee angle. Maximum errors of approximating the subject-specific moments by the group average ranged from 4.0 to 49.9% of the group-average moment across the individual relationships, with a mean (S.D.) maximum error of 23.4% (11.4%).

DISCUSSION

The results indicate that isokinetic MVC M-θ relationships can be significantly affected by the range of motion and the body configuration under which a contraction is performed,

Table 1 : Mean knee extension moment over selected knee flexion angles as a function of hip flexion angle (moments in % of the 90°hip/90°start peak moment)

Hip flexion angle	Knee flexion angle(s) 85°	85-80°	80-75°	70-65°	65-60°	55°	55-50°	50-45°	40-35°
0°	66.5 *	71.8 *	78.4 *	84.5 *	87.4 **	85.5 **	82.2 *	78.8 *	67.4 *
90°	70.8	78.0	87.4	90.9	95.3	88.2	88.3	85.2	72.4

Moment significantly different from that at 90° of hip flexion: * = p<0.05, ** = p<0.01

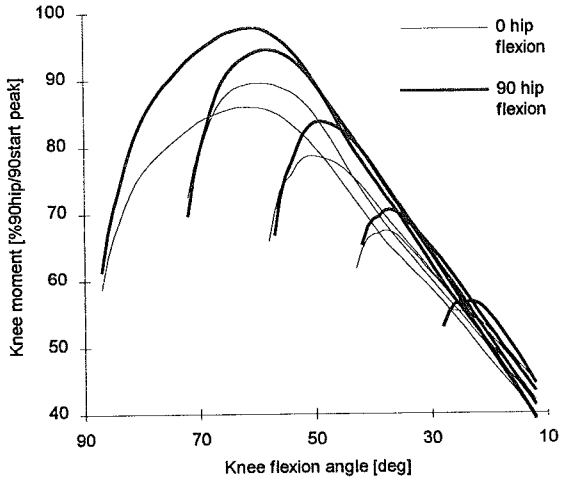

Figure 1 : Group-average normalized isokinetic MVC moment-angle relationships

leading to significant over- or under-estimation of the functional capacity of an individual.

Body configuration, as given by hip flexion angle, affected the isokinetic MVC moments over every range of knee flexion angles from 85 to 35°. This can be attributed to the change in length of the biarticular rectus femoris between hip positions, as the muscle operates in different regions of its length-tension relationship for similar knee motions under each hip condition.

For starting knee angles above 30°, the moments observed 5° into the motion were consistently less than those seen in the MVCs that were further into their range of motion at that angle, despite identical knee angular velocities. Joint angles less than 5° into the motion displayed even greater relative depression of the isokinetic MVC moments. This can be attributed to the finite time required for a muscle to attain its maximal active state following activation, as well as the damping action of tendon on musculotendon force development.

Beyond the first 5° of motion (10° for the 60° start angle), the isokinetic MVC M-θ relationships at a given hip angle converged to a single steady-state relationship over the range of 70 to 30° of knee flexion. Such a steady-state convergence was expected based on the force-velocity properties of muscle. However, at knee flexion angles of less than 25°, isokinetic MVC moment decreased linearly with increasing start angle of the exertion. This most likely reflects the effects of fatigue or an inability to maintain a maximal activation over a sustained isokinetic MVC.

Table 2 : Mean knee extension moment over selected flexion angles for different initial knee angles (moments in % of the 90°hip/90°start peak moment)

Knee angle(s)	Initial knee flexion angle 90°	75°	60°	45°	30°
70° (90° hip)	94.4	79.1*			
55°	89.7	91.1	75.2*†		
55-50°	87.5	89.4	78.8*†		
40°	71.7	73.9	74.5	67.9†‡	
25-20°	51.9	52.8	53.9	55.1	55.3
20-15°	46.1	46.8	48.0	49.6	51.0

Moment significantly different from that for initial angle of 90° (*) 75°(†) and 60° (‡) at p<0.05. Significant (p<0.05) linear trends between initial angle and moment at 25-20° and 20-15°.

These results indicate that an isokinetic MVC M-θ relationship will significantly over-estimate the functional capacity of an individual during transient changes in muscle activation, with at least the first 160msec of a knee extension MVC from rest so affected. Overpredictions as great as 45% of the true moment were observed in our group average relationships over this transient period. This is significant in that most activities of biomechanical interest are dominated by transiently altering levels of muscle activation.

Approximation of the M-θ relationships of specific individuals by a scaled set of group-average relationships was associated with large RMS errors that were significantly greater than the within-subject variation in the measured MVCs. This error must be attributed to large individual differences in the M-θ relationships of the subjects studied.

These results argue against the use of simple moment-angle-velocity surfaces in the prediction of functional capacity, as well as against the use of scaled group-average musculoskeletal strength models or relationships. Accurate prediction of functional capacity requires a musculoskeletal model that incorporates the finite rate of muscle activation. The model may require inclusion of the effects of biarticular muscles. Finally, evaluations of the capabilities of specific individuals should employ a model tailored to the strength characteristics of the individual.

ACKNOWLEDGMENTS

This research was partially funded by NIH R01AG10557. The authors wish to thank Dr. A. Al-Johar for his assistance in data collection.

WRIST AND FOREARM POSITION DURING A TYPING TASK USING VARIOUS KEYBOARD MODELS

G. Simoneau[1], R. Marklin[2], J. Monroe[2], J. Zabors[2]
[1]Program in Physical Therapy, Marquette University, Milwaukee, WI 53201
[2]Dept. of Mechanical and Industrial Eng., Marquette University, Milwaukee, WI 53201

INTRODUCTION

In this study, the wrist and forearm position of clerical workers using commercially available "alternative" keyboards was investigated using electromechanical goniometric devices. The purpose of this study was to determine the effectiveness of these keyboards in placing the forearm and wrist in a more neutral position, as compared to the wrist and forearm position seen when a conventional keyboard is used.

REVIEW AND THEORY

While the exact cause of occupationally induced cumulative trauma disorders (CTDs) in keyboard users is not known, the ulnar deviation of the wrist and the fully pronated position of the forearm dictated by the design of the standard flat keyboard are often implicated in the etiology of hand and wrist CTDs. Over the past few years, several keyboards with design features aimed at reducing wrist ulnar deviation and excessive forearm pronation when typing have been introduced into the marketplace. These new keyboards are referred to as "alternative" because they differ fundamentally in their overall structural shape when compared to the conventional computer keyboard. All keyboards used in this study featured the conventional QWERTY key layout.

The specific aim of this study was to determine whether the fundamental design of three types of "alternative" keyboards actually placed the wrist and forearm in a more neutral posture than the conventional computer keyboard.

PROCEDURES

Subjects: Each of the 30 subjects who participated in this study met the following criteria:

1. Worked in a clerical position and typed at least two hours per day in the office.
2. Typed at least 45 words per minute.
3. At the time of testing, was asymptomatic of any musculoskeletal pain or discomfort that would interfere with typing on a computer keyboard.
4. Was between 21 and 55 years of age.
5. Had been typing for more than 5 years.
6. At the time of testing, used a standard keyboard.

Keyboards: Three commercially available keyboards were used in the study:

A. A fixed-angle split keyboard.
B. An adjustable-angle split keyboard.
C. A vertically inclined keyboard, which resembles a drawbridge when both halves are raised.

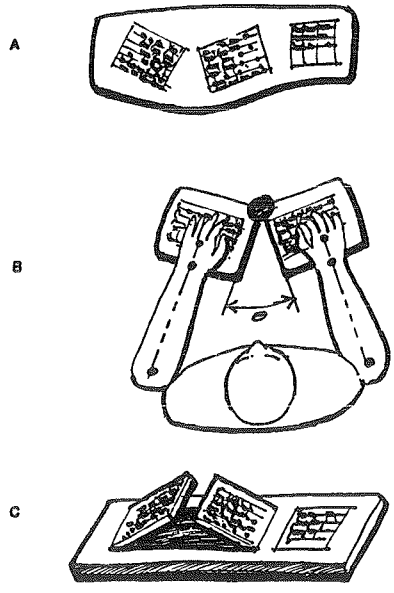

Figure 1. Alternative keyboards

Apparatus: Radio-ulnar and flexion-extension position of the wrists as well as pronation of the forearms were monitored with electromechanical goniometers (Schoenmarklin and Marras, 1993; Marras and Schoenmarklin, 1994). Both upper extremities were monitored simultaneously.

Experimental procedures: After a subject agreed to participate in the study, one of the three alternative keyboards listed above was randomly assigned to the subject. The keyboard was then set up in the subject's office by a member of the research team.

Each subject used the assigned keyboard in his/her office to perform her/his regular work activities for a minimum of 20 hours over a one- to two-week period. Then the subject participated in a half day of testing at Marquette University's Human Motion Laboratory.

In the lab, the goniometric instrumentation was attached to the subject's left and right wrists and forearms. The subject was then instructed to type (at a comfortable speed) a text that appeared on the VDT screen. Ten samples of 30 seconds of data were collected as the subject was typing over a 16-minute period. The subject was not aware of the time when the 30-second windows of data were collected.

Each subject was tested using their assigned alternative keyboard and the conventional keyboard (in order to serve as their own control). The order of testing was randomized.

RESULTS

Table 1. Mean wrist radial (positive) and ulnar (negative) deviation angle with the three alternative keyboards. (n=10 for each keyboard comparison)

Standard Keyboard	Alternative Keyboards	
-8.4 ± 8.0	0.3 ± 9.1	(Keyboard A users)
-9.0 ± 12.8	-2.9 ± 8.8	(Keyboard B users)
-8.5 ± 5.8	5.1 ± 5.0	(Keyboard C users)

Keyboard A: Fixed-angle split keyboard
Keyboard B: Adjustable-angle split keyboard
Keyboard C: Vertically inclined keyboard

Table 2. Mean wrist extension angle with the three alternative keyboards. (n=10)

Standard Keyboard	Alternative Keyboards	
19.3 ± 6.6	15.1 ± 6.7	(Keyboard A users)
18.0 ± 16.2	15.3 ± 14.6	(Keyboard B users)
15.7 ± 6.9	12.5 ± 8.1	(Keyboard C users)

Table 3. Mean forearm pronation angle with the three alternative keyboards. (n=10)

Standard Keyboard	Alternative Keyboards	
59.8 ± 7.4	55.8 ± 4.4	(Keyboard A users)
61.5 ± 3.6	62.7± 6.7	(Keyboard B users)
61.6 ± 7.2	39.8 ± 9.8	(Keyboard C users)

DISCUSSION

All three alternative keyboards placed at least one component of wrist and forearm posture in a more neutral position than the conventional keyboard.

The split keyboards significantly reduced ulnar deviation ($p < .02$) and placed the wrist in a more neutral position. The inclined keyboard significantly ($p < .01$) reduced forearm pronation. Only small differences were noted for changes in wrist extension angle with the alternative keyboards.

Although only a small number of subjects have been studied, it appears that alternative keyboards (of the type used in this study) place the wrist and forearm in a more neutral posture than a conventional keyboard. The effect of this change of wrist and forearm position on the incidence of CTDs is unknown.

REFERENCES

Marras W.S., et al. Ergonomics, 33(4), 341-351, 1993.
Schoenmarklin R., et al. Ergonomics, 37(9), 1449-1460, 1994.

ACKNOWLEDGMENTS

The authors would like to thank the National Institute for Occupational Safety and Health (NIOSH) for sponsoring this study (#1 RO3 OH03 184-01A1).

CALCULATING CENTER OF GRAVITY DISPLACEMENT DURING STANDING TASKS

D.L. King and V.M. Zatsiorsky
Biomechanics Laboratory, The Pennsylvania State University, University Park, PA 16802

INTRODUCTION

Center of gravity (COG) displacement is an important variable to studying postural stability. Traditionally, however, center of pressure (COP) is used instead of COG, primarily due to the simplicity with which COP can be measured and calculated. In this project a method to calculate COG displacement directly from force platform recordings was developed and results were compared to two traditional posturographic variables, COP and horizontal force (Fh).

REVIEW AND THEORY

Several proposals to estimate COG displacement from force platform recordings have been presented in the past. Shimba (1984) used the horizontal ground reaction force to estimate the anterior/posterior displacement of the COG. The horizontal ground reaction force is directly proportional to the horizontal acceleration of the COG, and thus its second integral is proportional to COG horizontal displacement. The two constants of integration, initial position and initial velocity, needed to perform this integration are unknown. Shimba proposed estimating these constants with a linear curve fit of two functions E(t) and S(t). The function S(t) is the second integral of the horizontal ground reaction force and $E(t) = x_p + z_G F_{ox}/F_{oz}$, where x_p is the point of application of the ground reaction force, z_G is the vertical component of the COG position vector, and F_{ox} and F_{oz} are the horizontal and vertical components of the ground reaction force respectively. Alternatively, Benda, et al. (1994) proposed filtering COP time history records to estimate COG horizontal displacement based on the hypothesis that COP displacement is a summation of two processes: a low frequency component representing COG displacement and a higher frequency component representing inertial forces. This method, however is unable to accommodate for any phase differences between COP and horizontal COG displacement.

The purposes of this project were 1) to calculate horizontal COG displacement from horizontal ground reaction force, Fh, with a new method for determining the necessary initial constants of integration and 2) to compare the horizontal COG displacement results with the traditional measurements of COP and horizontal force.

PROCEDURES

The proposed method to calculate the horizontal displacement of the center of gravity, hereafter called CGD, from F_h is based on the postulation that the CGD and COP coincide when Fh is zero. Accordingly, the procedure requires knowledge of the COP and Fh as obtained from a force platform.

Step 1. Determine COP when $F_h=0$ ($x_{cop}|F_h=0$)

Step 2. Calculate $a(t) = F_h/m$ (a(t) is acceleration, m is body mass)

Step 3. Integrate a(t) twice from $t_0|F_h=0$ to $t_1|F_h=0$. Use $x_{cop}(t_0)$ as initial position and $v(t_0)=0$ as initial velocity.

Step 4. Subtract $x_{cop}(t_1)$ from the calculated integration value, $x_{cal}(t_1)$.

Step 5. Divide the result from Step 4 by $(t_1 - t_0)$. This is the real initial velocity, $v_{real}(t_0)$.

Step 6. Integrate a(t) twice from $t_0|F_h=0$ to $t_1|F_h=0$. Use $x_{cop}(t_0)$ as initial position and $v_{real}(t_0)$ as initial velocity.

Step 7. Continue this procedure from $t_{n-1}|F_h=0$ to $t_n|F_h=0$ for the entire recording.

Force platform data were collected on 5 subjects. The subjects were students at Penn State University and gave their written informed consent prior to participating in this study. Each subject performed 4 standing tasks in a self selected comfortable standing posture for either 1 minute or 30 seconds. The tasks were: quiet standing (1 minute), quiet standing eyes closed (1 minute), slow intentional sway (1 minute), and fast intentional sway (30 seconds). A Bertec force platform (Bertec Inc., Ohio) and a pentium P5-100 personal computer with a 12 bit National Instruments (National Instruments, Corp., Texas) data acquisition board were used for data collection at a sampling frequency of 10 Hz.

RESULTS AND DISCUSSION

Sample data from 1 subject are presented for one of the tasks - quiet standing eyes closed in Figure 1.

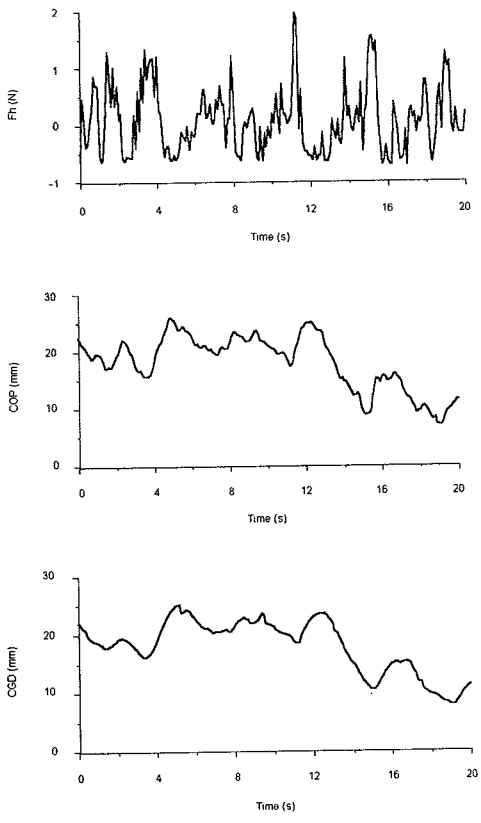

Figure 1. Time history plots of Fh, COP and CGD during quiet standing eyes closed.

While the median frequencies of the COP and CGD for the presented data were similar at 0.12 Hz, a closer inspection reveals that the COP contains a higher frequency component superimposed on the lower frequency CGD. This is more easily discerned by subtracting CGD from COP. Figure 2 shows this subtraction, henceforth called delta.

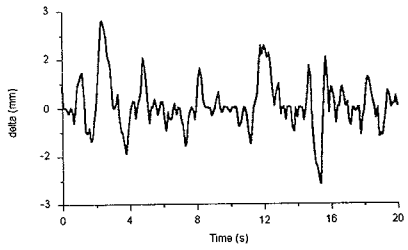

Figure 2. Time history plot of delta (COP–CGD) during quiet standing eyes closed.

For the sample data illustrated in Figure 1, the correlation between COP and CGD is 0.97. Similarly high correlations were seen for all quiet standing and slow sway tasks. The root mean square difference (RMD) for the presented data was .79 mm and the RMD normalized to COP standard deviation (nRMD) was 15%. There was a consistent peak negative correlation between either COP or CGD and F_h for all standing tasks. This peak correlation occurred at zero lag. Thus, there was no time delay between the horizontal force and the system response, indicating that the system response was due to mechanical properties of the system. The findings of this study suggest 1) the proposed algorithm may be an appropriate technique to calculate CGD from force platform recordings and 2) additional information can be gained by studying COP, CGD, and F_h during standing tasks.

REFERENCES

Benda, B.J. et al. IEEE Trans. Rehab. Engng., 2, 3-10, 1994.

Shimba, T. J. Biomechanics, 17,53-60, 1984.

COMPARISON OF TWO METHODS FOR COMPUTING ABDUCTION MOMENT ARMS OF THE ROTATOR CUFF

Richard E. Hughes, Jain Liu, Glen Niebur, and Kai-Nan An
Mayo Clinic/Mayo Foundation, Rochester, MN 55905

INTRODUCTION

Muscle moment arms are a critical component of models used for estimating muscle forces from net intersegmental moments. The purpose of this study was to compare two methods for estimating moment arms of the rotator cuff muscles during humeral abduction in the scapular plane.

REVIEW AND THEORY

Thee-dimensional models of the shoulder have used an idealized mathematical model of muscles where muscles are modeled as strings that take the shortest distance from origin to insertion (van der Helm, 1994; Ḧgfors *et al.*). Simple geometric assumptions are made about the skeletal structure in cases where a straight line from origin to insertion would cross through a bony structure (e.g. the humeral head is assumed to be spherical constraint for muscles crossing the glenohumeral joint). In this approach, the moment generated by a muscle is the cross product of a vector joining the joint center to the muscle line of action and the force vector acting along the line of action. Although there may be no formal moment arm calculated in this approach, an estimate of it can be estimated by computing the moment generated by a unit of force. The abduction moment arm is the dot product of the moment vector and a unit vector along the axis of rotation.

An alternative approach is to use the principle of virtual work, e.g. the moment arm is the slope of the tendon displacement vs. joint angle curve (An *et al.*, 1984).

PROCEDURES

Ten fresh frozen cadaveric shoulders free from rotator cuff pathology, arthritis, limited range of motion or bony deformity were used. There were five right shoulders and five left from four males and five females, and mean age was 67 (range 40 - 89). Specimens were prepared by attaching 50 lb test nylon line to the tendons of the supraspinatus, subscapularis, infraspinatus, and deltoid (anterior, middle, and posterior portions). Muscle origins were simulated by placing eyehooks in the center of the respective muscle origins. Weights (100 gm) were hung from the ends of the lines to remove slack from the system. The coracoacromial ligament was preserved. The scapula was rigidly attached to a Plexiglas test fixture, and an intramedullary rod was inserted into the humerus so that elevation in the scapular plane could be controlled with a guide. The guide also prohibited internal or external rotation during elevation. The wires were routed from the tendons through the eyehooks to cylinders attached to potentiometer shafts (3500S-2-103, Bourns Corp., Riverside, CA), which were used to measure tendon excursion as the humerus was elevated. A magnetic tracking device (3Space Tracker, Polhemus; Colchester, Vermont) was used to measure the glenohumeral angles. Three humeral elevation trials were performed. The locations of the muscle origins (the eyehooks) and insertions were digitized using the 3Space device. Points on the articular surface of the humeral head and glenoid were also digitized after disarticulation of the joint.

The principle of virtual work was used to estimate abduction moment arms from tendon excursion data. For each trial the tendon excursion-glenohumeral elevation angle relationship was modelled using polynomial regression. The lowest order polynomial such that the root mean square error was less than 0.5 mm was used. The moment arm was computed by analytically differentiating the polynomial.

The method described in van der Helm (1994) was used to compute abduction moment arms using the minimum distance origin-insertion approach. The geometry of the humeral head

was assumed to be a sphere, and the radius (r^{hum}) of the sphere was estimated from the digitized points on the articular surface. The center of rotation was estimated by fitting a sphere of radius r^{hum} to the points digitized on the glenoid. Each muscle was assumed to take the shortest distance from origin to insertion, wrapping around a spherical humeral head if needed. The 3D moments generated by a unit of force in each muscle was computed. The abduction moment arm was the projection of the moment vector onto the axis of rotation during abduction.

Differences in moment arms for each muscle were analyzed using a repeated measures ANOVA model (angle and method are non-repeated factors; specimen is repeated).

RESULTS

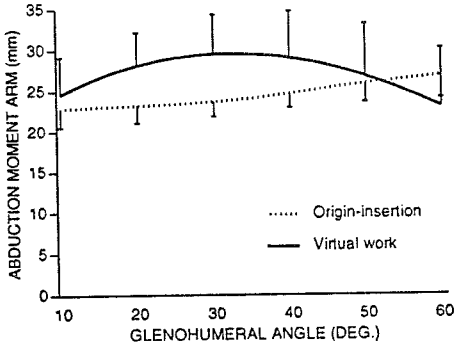

Figure 1. Supraspinatus moment arm.

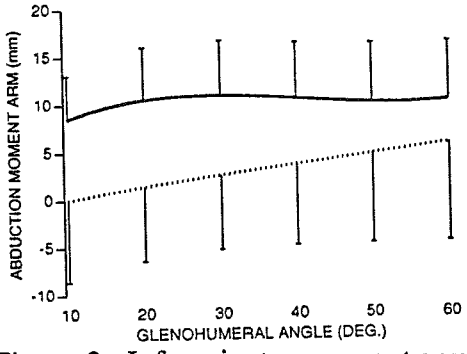

Figure 2. Infraspinatus moment arm.

Abduction moment arm was affected by glenohumeral angle and estimation method (virtual work vs. origin-insertion) at the $P<0.0001$ level of significance. Figures 1 through 3 illustrate the supraspinatus, infraspinatus, and subscapularis abduction moment arms through the arc of elevation for both methods (one-sided standard deviation bars are included). Solid lines represent the average moment arm computed by the virtual work method; dotted lines show the origin-insertion method mean.

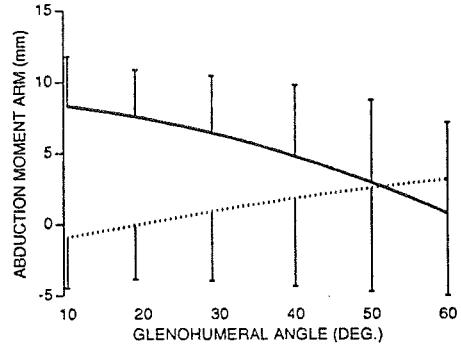

Figure 3. Subscapularis moment arm.

DISCUSSION

These results indicate that there may be substantial differences in abduction moment arm estimates computed by the origin-insertion and virtual work methods. Since muscle force estimates are especially sensitive to muscle moment arm magnitudes, these results suggest that biomechanical models of the shoulder that use the origin-insertion method are likely to produce very different muscle force estimates than models based on the virtual work method.

Future development of shoulder models should carefully evaluate the merits of available moment arm estimation methods. The origin-insertion approach may benefit from a more sophisticated geometric description of the humeral head.

REFERENCES

1. An ,K-N *et al.*, *J. Biomech. Eng.*, 106, 280-282, 1984.
2. H'ögfors, C. *et al.*, *J. Biomech.*, 20, 157-166.
3. van der Helm, F.C.T., *J. Biomech.*, 27, 551-569.

ACKNOWLEDGMENTS

Supported by NIH AR41171 and HD07447. J. Liu supported by the Rotary Foundation, Li Foundation, and National Science Council - Taiwan.

CRITERION VALIDITY OF THE ARIEL PERFORMANCE ANALYSIS SYSTEM™ (APAS™) FOR THE CALCULATION OF JOINT ANGLES USING APAS™ AND GAITLAB™ SOFTWARE

Marcus Besser,PhD[1,2], Negda Anton[2], Michael Denny[2], and Scott Quaile[2]
[1]Human Performance Laboratory, [2] Department of Physical Therapy, Thomas Jefferson University, Philadelphia, PA 19107

INTRODUCTION

Computer assisted motion analysis systems provide an objective tool for recording and evaluating human movement. It is important that the validity of motion analysis systems be established in order to consider the data of value to clinicians. Various sources of error exist with camera-based systems, but the contributions of each depend upon which system is being used. Previous research has quantified single sources of error; however, clinicians are concerned with the total errorin the calculated joint angle. This study was conducted to examine the total error associated with joint angle calculations using computer assisted motion analysis.

The objective of this study is to determine the criterion reference validity of the APAS™ and GaitLab™ software systems for the calculation of lower extremity joint angles.

REVIEW AND THEORY

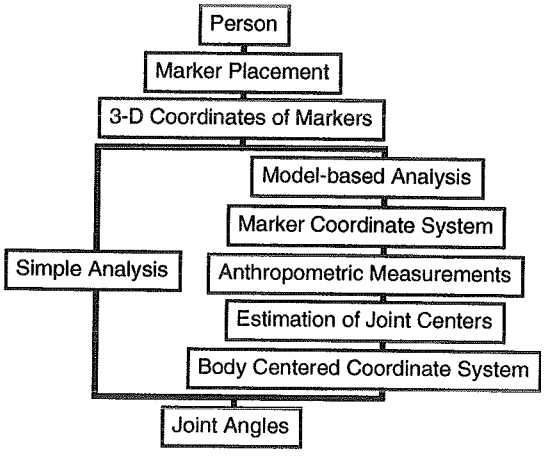

Figure 1: Flowchart for Joint Angle Calculation

Figure 1 is a flow chart of the steps for camera-based analysis of joint angles. At each level of this flowchart, error may be introduced into the process. Errors are introduced due to marker misplacement or soft tissue movement over bony prominences[2,5,6,8,11]. Soft tissue error in the lower extremities of 10-20 mm[2], and soft tissue error in the ankle of 8.8-12.8 mm[11] have been reported. Subject motion is recorded using cameras, and the two-dimensional camera recordings of marker locations are transformed into three-dimensional coordinates of the markers in the laboratory space. Errors introduced at this point may be due to associated hardware (cameras, lenses, calibration frame), or due to the direct linear transformation[7,12,15]. RMS error of 5.7 mm in a calibration field 3.5 meters long, 2.5 meters high, and 1.5 meters wide has been reported with direct linear transformation[15].

The coordinates of the markers may be analyzed using a simple point-to-point method, or using a model. The simple analysis connects marker locations using vectors, and then calculates angles between these vectors (Fig. 1, left branch of flowchart). Calculation errors related to the inverse trigonometric functions increase as the angle approaches 180°[7,13]. A major limitation of this simple analysis is that motions out of the plane of the markers cannot be measured. In order to measure out of plane motion, a model must be used.

A more complex model incorporates a segmental coordinate system and anthropometric measurements to estimate joint centers, or a body-centered coordinate system can be imbedded at a body segment's center of mass to calculate three dimensional joint angles. Errors may arise from inaccurate anthropometric measurements, or when extrapolating beyond the limits of the data from which the model was created. In addition, errors may occur with joint center estimation, especially at the hip[1,3,4,6,9]. When the joint angle approaches 180°, the cosine algorithm again introduces error[13].

While these researchers have looked at each of the individual errors, clinicians are more interested in the total error. Stanhope developed a test procedure that was effective in quantifying the magnitudes of angular kinematic inaccuracies associated with unilateral lower extremity gait analysis[12]. A series of tests were performed on an idealized lower extremity model, to estimate errors in calculated knee and ankle angles. This test allowed for evaluation of a composite error from sources including hardware, direct linear transformation, segmental coordinate systems, and estimation of joint centers. Kinematic inaccuracies were quantified as the mean and range of knee and ankle angular displacement. Joint displacement error including sources such as camera obstruction and model motion were found to be 3.6°. However, this composite error did not account for errors due to soft tissue movement, marker misplacement, joint motion in the multiple planes, and motion at multiple joints. In addition, the lower extremity model used did not allow for articulation at the knee, nor did it include the hip joint.

In this study, the left lower extremity of a plastic skeleton was fixed in various positions using clamps and rods. Each position combined hip and knee flexion and extension, and hip ab/adduction. Kinematic data were collected and joint angles were calculated using two methods: the software

provided with the Ariel Performance Analysis System™ and GaitLab™ gait analysis software[14]. These were compared to direct angular measurements taken with an electronic inclinometer to evaluate total composite error.

PROCEDURES

Data were collected using the Ariel Performance Analysis System™ *, a video based three-dimensional motion analysis system. A calibration device consisting of six steel cables and twenty-four reflextive markers was used to define a control volume 1.2 m wide x 2.0 m long x 1.7 m high. Nine retroreflective markers were placed on the pelvis and left lower extremity of a plastic skeleton. The skeleton was fixed, in approximately 10° increments, from 13° of hip extension to 40° of hip flexion and in approximately 5° increments from 22° of abduction to 11° of adduction. The knee joint angle was fixed from 4° to 83° of flexion in approximately 10° increments. After the skeleton was fixed in a position, the joint angles were measured by three researchers using an electronic inclinometer. This process was repeated three times to yield a total of nine measurements per joint in order to establish intra- and interrater reliability. The skeleton was videotaped while moving through the calibrated field, then the joint angles were remeasured by one researcher to assure that there was no change in position.

The images from each videotape were grabbed and, automatically or manually digitized using the APAS™. Manual digitization was performed only when the system misidentified markers. The direct linear transformation was used to calculate 3-D marker locations. The marker data was downloaded from APAS™, then analyzed using the APAS™ software and GaitLab™ to calculate the joint angles.

RESULTS

Intraclass correlation coefficients (3,1) were calculated for each joint motion to establish intrarater reliability for each researcher, and to establish interrater reliability of measurements obtained with the electronic inclinometer for each joint motion. All values were greater than .995.

Errors were calculated for each method throughout the range of angles (Table 1).

Table 1: Ranges of error for specific joint angles

Error range	GaitLab™	APAS™
Hip Flexion/Extension	0.1° - 18.6°	0.6° - 17.8°
Hip Ab/Adduction	0.2° - 7.2°	32.0° - 97.5°
Knee Flexion/Extension	1.2° - 11.9°	1.3° - 6.1°

DISCUSSION

For most trials, the APAS™ and GaitLab™ hip and knee flexion and extension angle measurements both agree with the inclinometer; however, occasionally, there are large, non-systematic disagreements of up to 18.6°. between the inclinometer, as the standard, and the video analysis software interpretations of joint angles. This occurred near neutral hip flexion/ extension, as measured by the inclinometer. As only two data points were collected in this position, conclusions cannot be drawn.

When the error for each plane of motion for both software programs was plotted against the range of motions that were tested, no systematic error among the joint positions tested could be ascertained. The only consistent error among the calculated joint angles occurred with hip abduction and adduction using the APAS™ software. These errors range from 32.0° to 97.4°. This was not unexpected, since APAS™ calculates angles using marker to marker vectors, and no marker can be placed on the actual hip center.

In this study, we found a larger errors than has been published in previous studies. These studies, not based on an anthropometric structure, have shown video based analysis systems to be accurate to within a few degrees. An under estimation of 2.4° was reported at 180° by Vander Linden et al.[13] Mean angular error of 0.26° was reported by Klein[7] , and error of 2.1° was reported by Scholz[10]. All of these studies used retroreflective markers attached to goniometers under static conditions. This does not simulate the human structure to a large degree, and lacks applicability to clinical situations. Our study depicts the accuracy of these systems as they are routinely used, and has more clinical relevance and validity. Future studies should continue to address total error, possibly incorporating an estimate for soft tissue movement.

REFERENCES

1. Campbell KR, et al. *J Biom*, 21:860. 1988.
2. Cappozzo A., et al. Proc. ISB XIVth Cong, 238-9, 1993.
3. Duke RP, et al. *J Biom,*; 10:781-786, 1977.
4. Grood ES, et al. *J Biomech Eng.*,105:136-144, 1983.
5. Kadaba MP, et al. *J Orthop Res.* 7(6):849-860, 1989.
6. Kadaba MP, et al. *J Orthop Res.* 8:383-392, 1990.
7. Klien PJ, et al. *Arch Phys Med Rehab.* 76:183-189, 1995.
8. O'Connor PD, et al. *Phys Ther.* 73(7): 478-483, 1993.
9. Ramakrishnan HK, et al. *J Biomech,* 10: 969-977, 1991.
10. Sholtz JP. *Phys Ther,* 69(8): 679-689, 1989.
11. Stanhope SJ. *Gait & Posture,* 2 (1): 58, 1994.
12. Stanhope SJ. *Proc. 13th Southern Biomed. Eng. Conf.*, Wash. D.C., 1030-1034, 1994.
13. Vander Linden DW, et al. *Phys Ther.*, 72(4):300-305, 1992.
14. Vaughan CL, et al. *Gait Analysis Laboratory.* Human Kinetics Publishers, 1992.
15. Wood GA, et al. *J Biom.* 19:781-785, 1988.

ACKNOWLEDGMENTS

We would like to acknowledge Dr. Stephen Stanhope, Ms. Christine DelMarcelle, Dr. Theodore Bross, Mr. Michael Hopwood and Mr. Peter Guzzetti for their assistance with this research.

* Ariel Dynamics, Inc., Trabuco Canyon, CA 92679

CALIBRATING INSTANTANEOUS HELICAL AXES TO IDENTIFY THE ELBOW AND SHOULDER JOINT CENTERS FOR MOVEMENT STUDIES

Xudong Zhang, Maury A. Nussbaum, and Don B. Chaffin
Center for Ergonomics, The University of Michigan, Ann Arbor, MI 48109

INTRODUCTION

A linkage representation used to model a human musculoskeletal system or subsystem is a collection of rigid segments interconnected by the centers of hypothetical smooth ball or hinge joints. In movement studies, very often surface markers are placed over the anatomical landmarks to achieve a 'stick-figure' representation that best approximates the linkage. There is a need to transform the collected motion data of surface markers into those of joint centers by quantifying the spatial relationship (or the discrepancy) between the two entities. Despite the availability of general guidelines for palpating body landmarks and placing surface markers to ensure the 'rigidity' of the above relationship, it is under possible influence of a multitude of factors including soft tissue movements, individual difference, marker size, clothing and so on. As the effects of these factors have yet to be elucidated, a technique that allows individual- and condition-specific determination of the joint center location is desirable. This paper presents such a calibration technique for identifying the elbow and shoulder joint centers through the determination of instantaneous helical axes.

REVIEW AND THEORY

Kinematically, an instantaneous joint center (IJC) can only be identified as an axis which passes through it—the instantaneous helical axis (IHA) along which the instantaneous motion of one segment member of the joint relative to the other occurs (Woltring et al., 1994). The problem of determining IHA is simplified in the special case when one member of joint is kept motionless; since the axis now coincides with the absolute axis of rotation of the moving segment, various methods of deriving the axis of rotation of rigid body (Panjabi, 1979; Spiegelman et al., 1987; Crisco et al., 1994; Woltring et al., 1994) can be used to locate the axis on which the joint center ideally should reside. If we assume that the relationship between this axis and the corresponding joint surface marker varies only with the relative configuration between two segments involved (whereas the aforementioned multiple factors remain invariant), the mapping between this varying relationship and a set of positions obtained under the 'simplified' conditions may then be extended to the situations when both members are in motion.

The purpose of this study is to establish an experimental and kinematic analysis scheme that allows instantaneous helical axes (IHAs) to be calibrated based on the above concepts and assumption. The scheme is illustrated by an experiment conducted to determine the IHAs for identifying shoulder and elbow joint centers. The effect of the relative rotation between the adjacent segments on the IHA location and orientation is also examined.

PROCEDURES

Subjects and Tasks

Four subjects, two males and two females, participated in the experiment. Five reflective markers (radius=1.5 cm) were attached to the right upper extremity: three placed at the acromion process (AP), the lateral epicondyle (LE), and the mid-breadth dorsal groove of the wrist (MW); two attached to the ends of a rigid post grasped by the hand (P1 & P2). Three voluntary full-range motion tasks were performed by the subjects while seated: 1) an elbow flexion/extension with the upper arm fixed in a vertical configuration; 2) a shoulder flexion/extension with the torso fixed in an upright posture; and 3) a shoulder abduction/adduction with the torso fixed in an upright posture. In task 1, the subjects were instruct to stiffen the wrist joint; in tasks 2 and 3, a fixture was attached to the arm to rigidify the elbow joint in an angle of approximately 90 degrees. Thus, with respect to each joint concerned, the proximal member was immobilized, and the kinematics of the distal (moving) member can be determined from 3 markers affixed to it: markers P1, P2, and LE for the elbow during task 1; markers MW, LE, and AP for the shoulder joint during tasks 2 and 3.

Data Collection and Analysis

A MacReflex^{TM} motion analysis system with four cameras was employed to collect the movement data at a frequency of 25 Hz. The recording period was 5 seconds (125 frames) during which the subjects were able to complete 1 to 2 cycles of the specified motion. The data of one full range of motion were processed.

On the processed data of each task considered, the following procedures of kinematic analysis were performed to determine the IHA with respect to two instantaneous positions:

1) coordinates of 3 markers on the moving segments were used to establish a local coordinate system for each instant;
2) the rotation matrix **R** was determined from the two local coordinate systems;
3) the rotation angle ϕ between the two positions and the orientation of IHA represented by a unit vector **h** were derived from the **R** using the standard 3D kinematics algorithms (Spoor et al., 1980);
4) a plane was formed by two instantaneous locations of a marker (relatively more distant to the estimated IHA) and the **h** as the normal direction; and
5) in that plane, a point on the IHA was then determined using a method of locating 2D center of rotation similar to Spiegelman et al. (1987) and Crisco et al. (1994).

A 10 frame separation between the two instants was adopted to ensure that, for most time frames in consideration, ϕ was in a range associated with the smallest numerical error (Spiegelman et al., 1987).

For each determined IHA, two parameters were derived:

1) $|\mathbf{d}|$—the distance from the respective surface marker to the IHA represented as the magnitude of **d**, a vector from the marker to a point on IHA that is closest to the marker;
2) θ—the angle between **d** and the moving segment.

The relative motion between two adjacent segments were quantified as follows: elbow flexion/extension—the included angle between the forearm and the upper arm; the shoulder flexion/extension—the angle of the upper arm measured in sagittal plane with respect to the vertical torso (flexion+/extension-); the shoulder abduction/adduction—the angle of the upper arm measured in frontal plane with respect to the vertical torso (abduction+/adduction-). Therefore, a mapping between each IHA parameter and the corresponding relative motion angle, both in a time series, can be obtained to further examine the characteristics of the IHA in relation to the changing configuration of the joint.

RESULTS AND DISCUSSION

Table 1 summarizes the means and standard deviations of $|\mathbf{d}|$ and θ for the four subjects. For elbow flexion/extension, the mean values of $|\mathbf{d}|$ varied in a range of 0.7 cm while the θ seemed to be widely dispersed across the subjects. Our analyses also revealed that the IHA of the elbow remained perpendicular to both the upper arm and forearm during the motion. This, and the constancy of the $|\mathbf{d}|$ value, verified that elbow flexion/extension is a distinctive 2-dimensional motion, and the $|\mathbf{d}|$ can thus be considered as the distance from the surface marker to the IJC.

Figures 1 and 2 present the $|\mathbf{d}|$ and θ as functions of the relative motion between two adjacent segments during shoulder flexion/extension and abduction/ adduction, respectively. Note that near the two ends of each motion, the computed $|\mathbf{d}|$ values seem to be erratic due to the pathological case resulted from a small ϕ (<10 deg). Otherwise, $|\mathbf{d}|$ varied within a range that appears to be in agreement with previously reported 2 inch distance from the acromion to the shoulder joint center (Dempster, 1955). As portrayed in the right panel of Figure 1, there existed a correlation between the flexion/extension angle and the θ: the two angles were of about the same magnitude throughout the motion. This suggests that, regardless of forearm

position, **d** always points vertically down as viewed from a perspective perpendicular to the sagittal plane. A similar correlation was also exhibited by the shoulder abduction/adduction. However, instead of pointing vertically down, **d** had a component along the lateral-to-medial direction, the magnitude of which increased as the upper arm became less abducted.

The results from this study provide insightful but not sufficient information for locating the IJC. An average center of rotation (ACR) can be further determined using methods such as described in Angeles (1986) and Holzreiter (1991). However the determination of a single average joint center does not reflect the moving nature of the IJC. Additionally, such methods normally do not work well when the motion is distinctively 2-dimensional. The inter-subject variability in the characteristics of IHA, as demonstrated in this study, appears to justify the need of individualized calibration. It is a viable technique before some heuristics or models developed from empirical investigations become available.

REFERENCES

Angeles, J. ASME J. Dyn Sys, Meas & Contr, 1986.
Crisco et al. J. Biomechanics, 1994.
Dempster, W.T. WADC Tech Report, 1955.
Holzreiter, S. J. Biomechanics, 1991.
Panjabi, M. J. Biomechanics, 1979.
Spiegelman et al. J. Biomechanics, 1987.
Spoor et al. J. Biomechanics, 1980.
Woltring et al. J. Biomechanics, 1994.

ACKNOWLEDGMENT

This work was supported by research grants from Chrysler Corporation and Ford Motor Company.

Table 1. The means and standard deviations of the derived parameters used to characterize the IHA.

	Elbow Extension/Flexion		Shoulder Extension/Flexion		Shoulder Abduction/adduction	
	|**d**| (cm)	θ (deg)	|**d**| (cm)	θ (deg)	|**d**| (cm)	θ (deg)
Subject 1	2.8±1.0	43±44	6.7±2.8	46±22	8.5±0.8	110±8
Subject 2	3.1±0.7	93±42	6.4±0.8	40±16	7.7±0.8	108±18
Subject 3	2.4±0.6	33±20	4.9±2.6	62±26	9.0±0.7	104±18
Subject 4	2.6±0.9	98±47	8.1±1.4	48±26	8.3±0.7	82±11

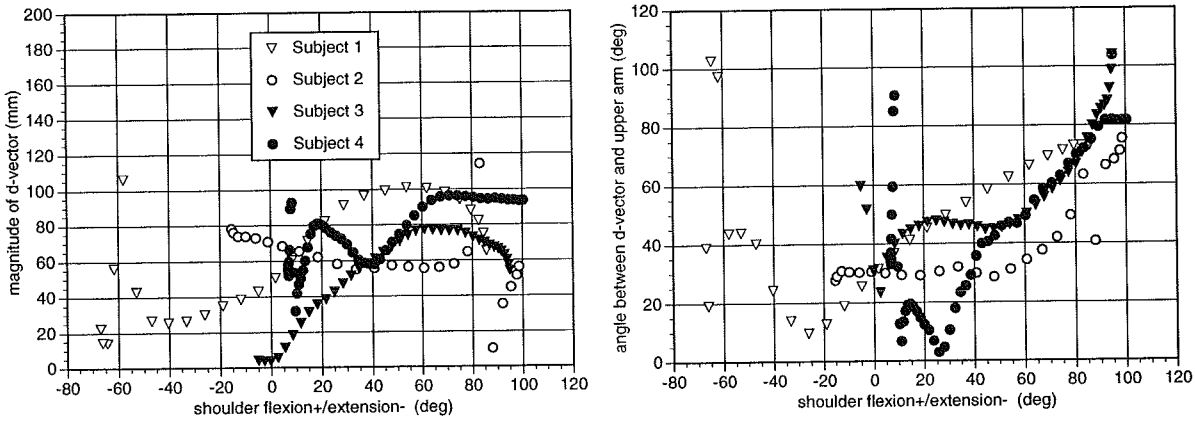

Figure 1. The IHA parameters as functions of relative shoulder flexion/extension angle.

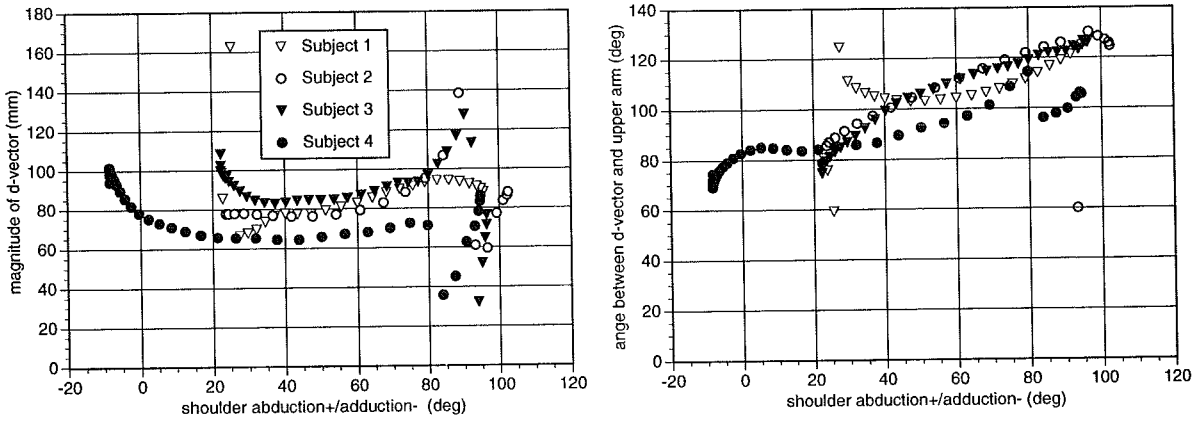

Figure 2. The IHA parameters as functions of relative shoulder abduction/adduction angle.

A REDUCED SURFACE MARKER SET FOR UPPER LIMB KINEMATICS: HEURISTICS AND OPTIMIZATION

M.A. Nussbaum, X. Zhang, D.B. Chaffin, B.S. Stump, U. Raschke
Center for Ergonomics, The University of Michigan, Ann Arbor, MI, 48109-2117 USA

INTRODUCTION

A method is presented whereby the 3-d location of the upper limb joints [shoulder (S), elbow (E), and wrist (W)] may be determined given a set of surface marker coordinate data. As part of a study of upper limb kinematics during both reaching tasks and while operating automated material handling devices, surface marker coordinates are obtained from an optoelectronic system. While the system yields highly accurate marker location data, analysis is significantly slowed by the need to associate tracked points with physical joints ('tracking'). In our experience, tracking time may increase nearly as the square of the number of markers. In the interest of efficiency, transformation algorithms (marker location -> joint center) were created that would allow for estimation of joint centers using a minimal number of surface markers. A description and application of these techniques, and the results from an experiment to validate the methods are presented here for the right upper limb.

REVIEW AND THEORY

With multiple (≥3) markers placed on each body segment, one can define and follow a local coordinate system imbedded in that segment thus determine displacements and rotations. Unfortunately, this necessitates a large number of markers, some of which are too close to accurately track, and requires inordinately large tracking times. Alternatively, motions of surface markers placed over joints can be used as direct estimates of segment kinematics. This approach, however, does not allow for indentification of axial rotations and is sensitive to skin movement artifact. As an alternative, we have developed a heuristic method that can be used alone or in combination with an optimization method to estimate joint locations.

Heuristic Method: The central assumption is that a constant magnitude vector exists between a surface marker and the underlying joint center. These vectors (surface-> joint: s2j) were derived from a review of the literature:

- S- 5cm caudal to acromial process along torso long axis.
- E- half the thickness of the elbow joint inter-epicondyle) and normal to plane formed by S, E, and W markers.
- W- half the thickness of the wrist, normal to long axis of forearm and vector formed by lateral axis of hand (see marker placements below).

The elbow s2j vector is modified when the included elbow angle exceeds ~160 degrees, and the plane formed by the S,E, and W markers becomes a non-robust reference plane for the direction of the elbow. In this case, using prior empirical results, the rotation of the s2j vector for the elbow was approximated as 1/3 of the hand rotation about the forearm long axis. Initial results with these heuristics showed that they were severely degraded by inaccurate initial marker placement. To 'fine-tune' the method, it was combined with an optimization procedure.

Optimization Method: An objective was formed as a function of the estimated S, E, and W joint locations, and its minimization (using simulated annealing [SA]) was assumed to provide a valid estimate of joint location. The following unconstrained objective, determined *ad hoc* to be relatively efficient, was used:

$$\sum_j w_1(s2j_j - \overline{s2j_j})^2 + \sum_j w_2(X_j - \overline{X_j})^2 + \sum_i w_3(l_i - \overline{l_i})^2$$

where the bar indicates estimates (surface->joint center vector, joint locations using the heuristic method, and the link length respectively). Thus, a weighted sum of squared error is minimized between estimated distances for the j joints and i segments. The results presented below were determined with weights: w_1=1 and w_2=w_3=10.

The SA procedure was terminated with a consistent converge criterion ('temperature'<0.0001). A complete motion (~125 samples) could be processed in <20 seconds on a PC. Several methods are being used to validate these procedures. For the present case, the estimated upper and lower arm segment lengths were determined in each trial and the rms error (w.r.t. the nominal or measured length) within a trial used to quantify the accuracy of estimations. Hence, it was assumed that over a subset of the range-of-motion, calculated link lengths should be constant.

PROCEDURES

A minimal set of five surface markers was determined necessary to estimate the location of the shoulder, elbow, and wrist of one upper limb. All markers were 2.5 cm spheres covered with reflective tape and placed as follows:

1. over cranio-lateral aspect of acromial process.
2. 8mm cranial to lateral epicondyle.
3. mid-breath of dorsum of wrist, at the level of lunate-capitate junction.

4,5 a 20 cm post with markers at either end is held at palmar fold (forearm rotation) with fingers flexed.

Six subjects participated in the experiments (3M, 3F). A 4-camera MacReflex™ system was used to obtain 3-d marker coordinates for 5s trials at 25Hz. After

anthropometric data were obtained, subjects performed 11 trials consisting of different upper arm motions. Subjects were seated and efforts were made to insure minimal torso flexion and lateral bending. The trials were designed to incorporate many (if not all) of the degrees of motion freedom in the upper limb. Wrist motion was specifically minimized. Each trial included one or more of the following: 1) elbow flexion/extension; 2) forearm pronation/supination; 3) shoulder flexion/extension; 4) shoulder internal/external rotation; 5) shoulder abduction/adduction. Some trials involved free movements of multiple joints, whereas others involved limitations in the freedom of one or more joints.

The transformation algorithms were used to obtain two sets of estimated joint locations with approximately 125 points per trial. Validation consisted of 1) qualitative evaluation of predicted joint trajectories; and 2) quantitative analysis of consistency in predicted segment lengths. The effect of the two algorithms (independent variable) on the rms error in the two predicted segment lengths within a trial (dependent variables) was determined using one-way ANOVA and treating subjects as a random blocking factor (significance = $\alpha \leq 0.05$). Further error analysis allowed for an estimate of the precision in single joint locations.

RESULTS

Estimated joint center trajectories using the heuristic method were smooth and anatomically 'feasible' without exception. Joint trajectories estimated using the optimization method showed occasional high frequency 'noise' that was easily removed using a low-pass filter.

The means of the rms error (across subjects and motion trials) in estimated segment lengths were 0.46 and 0.53 cm (not sig. diff., p=0.07) for the upper and lower arms respectively (Figure 1). For each segment, the rms error was significantly lower using the optimization method (p<0.001).

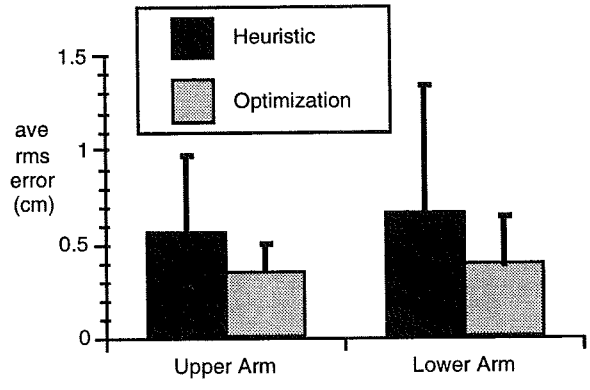

Figure 1. Means (sd) of the rms error in predicted segment lengths using the two surface marker -> joint center transformation methods.

The expected rms error of a single joint location prediction can be estimated using:

$$\text{var(length)} = \text{var(a-b)} = 2\text{var(a)}$$
$$\text{sd(a)} = \text{sd(length)} / \sqrt{2}$$

where a and b are the proximal and distal joint positions and their respective variances assumed equal and independent. Since the sd of segment length is roughly the average rms error, and this average was 0.61 and 0.37 cm for the heuristic and optimization methods respectively, the sd for single joint position estimates is 0.43 and 0.26 cm for the two transformation methods.

DISCUSSION

With the goal of reducing the number of surface markers needed to determine upper limb kinematics, thus increasing the efficiency in marker tracking for large-scale experiments, methods using heuristics and optimization were developed. The methods were able to transform 3-d surface marker coordinates to joint centers using only 5 markers for the upper extremity. This compares favorably with traditional marker configurations using 3/segment (e.g. Apkarian et al, 1989) to track local coordinate frames. In addition to the reduction in processing demands, the heuristics in combination were able to partially compensate for marker tracking errors and skin motion artifact. The methods are currently being extended to full-body kinematic analyses.

The transformation methods are based on the assumptions that segment link lengths are fixed and that joint centers-of-rotation (COR) are the physical centers of the joint surfaces. There is evidence for movement of the COR: movement of the shoulder COR within 6mm of center of the humeral ball (Poppen et al., 1976) and of gleno-humeral contact up to 2cm (Soslowski et al., 1992). Particularly for the S and E joints, if the COR is still assumed to be approximately the center of contact area, bone-bone translation will change the length of the idealized segment. These are potential sources of error in both the validation criteria and objective function used.

To overcome these limitations, present efforts are directed towards deriving more efficient objective functions and improved methods for estimating initial parameters (s2j vectors, link lengths). Experiments to determine instant helical axes using additional markers are being undertaken to further validate the transformation methods.

REFERENCES

Apkarian, J. et al. *J Biomech*, **22**, 143-155, 1989.
Poppen, N.K. et al. *J Bone Jt Surg*, **58-A**, 195-201, 1976.
Soslowsky, L.J. et al. *J Orth Res*, **10**, 524-535, 1992.

ACKNOWLEDGMENTS

This work was supported through grants by Ford Motor Company (#953187) and the Chrysler Corp. Challenge Fund

EFFICIENT CALCULATION OF MASS MOMENTS OF INERTIA FOR SEGMENTED HOMOGENOUS 3D OBJECTS

J.J. Crisco[1,2] and R.D. McGovern[1]
[1]Department of Orthopaedics, Rhode Island Hospital, Providence, RI
[2]Division of Engineering, Brown University, Providence, RI

INTRODUCTION

The equations for mass moments of inertia are rewritten using Green's theorem. This permits efficient calculation of the inertia for homogeneous 3D objects that are described by a stack of contours.

REVIEW

Determining the mass moments of inertia (I_{ij}, where $i,j \in [x, y, z]$) for 3D objects in the field of Biomechanics offers unique challenges. Classically this has been achieved by either physical measurements or by parametric approximation (e.g. approximating a limb segment as an ellipsoid). With the advent of medical imaging modalities, objects can readily be described by a 3D composition of voxels. The intensity of each voxel can be appropriately scaled producing a mass element (dm) which can be weighted and summed in 3D to determine the mass moments of inertia. While this method is both simple and accurate, it requires definition of every voxel in the object. This corresponds to increased memory usage and computation time for data manipulation. Large objects can require large amounts of data storage capacity and significant computation time. When the interior volume of an object is undefined, most of the data needed for this method is unavailable. These limitations reduce the utility of this method for large complex objects and cases where only the surface contours are available. Nagurka and Hayes (1980) previously addressed similar issues in 2D by defining cross sections as a collection of trapezoids and rectangles.

Motivated by our interest in 3D analysis, the purpose of this study was to develop an efficient approach to the determination of the mass moments of inertia (I_{ij}) of 3D objects.

THEORY

We begin by restating Green's theorem in 2D (Taylor and Mann, 1972). Let R be a cross section in the xy plane consisting of a finite number of simple closed curves that do not intersect each other. Let $F(x,y)$ and $G(x,y)$ be functions which are continuous and have continuous first partial derivatives in region R. Let C denote the contours of R, each oriented in such a way that the region is on the left as one advances along the curve in a counter-clockwise direction. Then Green's theorem states

$$\iint_R \left(\frac{\partial G}{\partial x} - \frac{\partial F}{\partial y} \right) dx\, dy = \oint_C F\, dx + G\, dy. \quad [1]$$

The mass moment of inertia about the x-axis is defined by

$$\mathbf{I}_{xx} = \iiint_R \left(z^2 + y^2 \right) dm, \quad [2]$$

where R is the region contained by the 3D object. Given the object is defined by contours C stacked in the z direction and employing Green's theorem, Eq. 2 can be rewritten as

$$\mathbf{I}_{xx} = \rho \int_R dz \oint_c z^2 x\, dy - \frac{1}{3} y^3\, dx, \quad [3]$$

where ρ is the density. Here we have arbitrarily chosen $F = -\frac{1}{3} y^3$ and $G = z^2 x$. Similar use of Green's theorem yields the mass moments about y and z:

$$\mathbf{I}_{yy} = \rho \int_R dz \oint_C \frac{1}{3} x^3 dy - z^2 y\, dx \quad [4]$$

and

$$\mathbf{I}_{zz} = \rho \int_R dz \oint_C \frac{1}{3} x^3\, dy - \frac{1}{3} y^3\, dx. \quad [5]$$

The products of mass moments of inertia can also be rewritten as

$$\mathbf{I}_{xy} = \rho \int_R dz \oint_C \frac{1}{2} x^2 y \, dy, \qquad [6]$$

$$\mathbf{I}_{xz} = \rho \int_R dz \oint_C \frac{1}{2} x^2 z \, dy, \qquad [7]$$

and,

$$\mathbf{I}_{yz} = \rho \int_R dz \oint_C -\frac{1}{2} y^2 z \, dx. \qquad [8]$$

In most applications the 3D object is described by a collection of points. For this case we assume the object is represented by *sn* contours with z-coordinates *z(s)*, where $s = 1$ to *sn*. Each contour *s* is a set of points whose *xy*-coordinates are given by *x(s,p)* and *y(s,p)*, where $p = 1$ to *pn(s)*. Let

$$dx(s,p) = x(s,p+1) - x(s,p),$$

$$dy(s,p) = y(s,p+1) - y(s,p),$$

$$u(s,p) = \frac{x(s,p+1) + x(s,p)}{2}, \text{ and}$$

$$v(s,p) = \frac{y(s,p+1) + y(s,p)}{2}.$$

Then, the mass moment of inertia about the *x*-axis can be written as

$$\mathbf{I}_{xx} = \rho \sum_{s=1}^{sn} z(s) \left(\sum_{p=1}^{pn(s)-1} \left(u(s,p) z(s)^2 \, dy(s,p) - \frac{1}{3} v(s,p)^3 \, dx(s,p) \right) \right)$$

The discrete versions of Eqs. 3 - 8 are similarly derived.

DISCUSSION

The method presented here permits the efficient calculation of the mass moments of inertia for 3D objects defined by a stack of 2D contours, which are assumed to be homogeneous in density. The contours may have complex shapes and any number of holes as long as the holes are digitized in a clockwise direction. The centroid and volume of the object are also readily calculated using this method. This method is advantageous over the voxel summation methods when the density is homogeneous, intensity to density scale is unknown, or computation time and memory requirements are concerns. For 2D cross-sectional properties, the speed and accuracy of this method are effectively the same as that previously described by Nagurka and Hayes (1980). The method presented here, however, does not require the cross sections to lie in the first quadrant and is directly applicable to complex 3D objects.

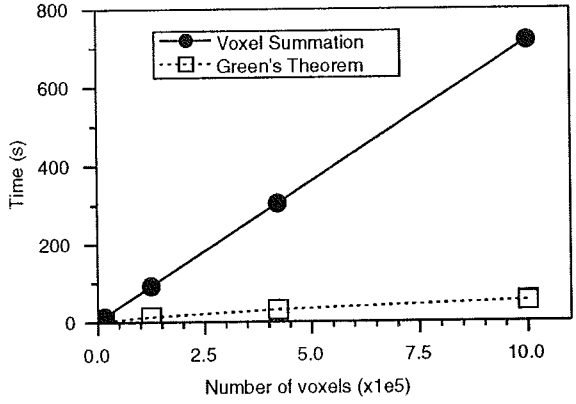

Figure 1. Typical computation times for the mass moments of inertia. The 3D object was a cube of various dimensions, normalized by the number of voxels. The computer code was written in MATLAB (Mathworks Inc., Natick, MA) and executed on a Power Macintosh 7100/80.

REFERENCES

Nagurka M.L. and Hayes W.C. An interactive graphics package for calculating cross-sectional properties of complex shapes, J Biomechanics, 13:59-64, 1980.

Taylor A.E. and Mann W.R. Advanced Calculus, pp. 482-490, Xerox College Publishing, 1972.

ACKNOWLEDGMENTS

We would like to acknowledge Erik Hult and Manohar Panjabi for their contributions.

A FOURTEEN SEGMENT GEOMETRIC-BASED MULTIPLE LINEAR REGRESSION MODEL FOR CALCULATING SEGMENT MASSES

K.J. Chesnin[1], M.P. Besser[2], L. Selby-Silverstein[2], W. Freedman[1], R. Seliktar[1]
[1]Biomedical Engineering and Science Institute, Drexel University, Philadelphia, PA 19104
[2]Human Performance Laboratory, Thomas Jefferson University, Philadelphia, PA 19107

INTRODUCTION

The accurate calculation of segment masses, *in vivo*, is important for the determination of whole-body center of mass (COM) and joint kinetics. A geometric-based multiple linear regression model for the calculation of the mass of fourteen body segments has been developed. This model is customized to the individual using thirty four anthropometric measurements and is gender specific. The accuracy of this model has been evaluated and compared with two previously published models[4,9], using data available from three published cadaver studies[1-3]. The output of our model was found to correlate well with the measured data and it compared favorably with the two other models that were evaluated.

REVIEW AND THEORY

There are many methods available for estimating segment masses, *in vivo*, including: MRI, CT, scaling cadaver data to body mass, regression equations, and stereophotometrics. Some of these methods are excessively time consuming and/or prohibitively expensive. Ratios of segment mass to body mass and regression equations are quick and inexpensive[1-4]. However, the methods in the literature[1-4,6,8] often are developed from small, homogeneous cadaver samples, comprised mostly of men. Thus, their application to various living populations, especially those that vary from the cadavers samples, e.g: children, women, and people with disabilities, may result in significant error. Other methods, such as geometric models and stepwise regression equations, have been developed to increase the sensitivity of the models to individual morphological variations. However, many of these methods are limited in their applicability, since they are derived from small, homogeneous cadaver samples. Further, due to the difficulty in testing the accuracy of segment mass models *in vivo*, their accuracy is often unknown. Our model is based on the model of Vaughan et al[8]. They developed geometric-based multiple linear regression equations for the determination of lower extremity segment masses, using data from six male cadavers[1].

The model developed here has an advantage in that its theoretical basis seeks to parallel the natural geometric form of the human body, rather than relying purely on statistical inference from a generally small and homogeneous sample of cadavers. The purpose of this work is to develop an accurate model for the calculation of body segment masses *in vivo*, that is quick, inexpensive, and can be applied to various populations. The model is intended for use in calculating whole-body COM and joint kinetics.

METHODS

Multiple linear regression equations were derived from published anthropometric and stereophotometric volume data, from 31 men[5] and 46 women[7], collected *in vivo*, and density data from cadavers[3]. The body segments were modeled as regular geometrical solids and were assumed to have a constant density. All the body segments were modeled as cylinders, except the feet and head, which were modeled as right pyramids and a sphere, respectively. The regression equations for estimating segment masses all have the general form of equation 1, where ρ is segment density, and length is a composite anthropometric parameter that depends on the geometric model of the segment.

$$M = \rho[C_1 (\text{Body mass}) + C_2 (\text{Length})^3 + C_3] \quad (1)$$

The accuracy of our model has been estimated using anthropometric and segment mass data from three published cadaver studies (Clauser et al., 1969; Chandler et al., 1975; Clarys et al., 1986). The accuracy of our model has also been compared with two commonly used methods; a ratio method[3,4,6] that scales segment mass as a ratio of total body mass and a multiple linear regression model[9] that uses total body mass and stature as predictors. The former was developed from the data of eight cadavers segmented by Dempster (1955), and adjusted by Clauser et al., and is a commonly used method[6]. The latter model (Zatsiorsky et al., 1990) was developed from *in vivo* gamma radiation experiments, with a large sample of young Russians: 100 men and 15 women[9].

Percent errors, sum of absolute error as percent total body mass (equation 2, where M_i is the measured mass of segment i, C_i is the calculated mass of segment i, and M_b is total body mass.), and intraclass correlation coefficients (ICC) for segment mass data were calculated comparing each of the segment mass estimation models to data from three published cadaver studies[1-3]. Several foot and hand anthropometric measurements were not directly measured in the cadaver studies, but were estimated from the data available. Further, the raw data from Clauser et al. were not available; the data used were right and left side averages for each subject.

$$\sum_i \frac{\left| M_i - C_i \right|}{M_b} \cdot 100 \quad (2)$$

RESULTS AND DISCUSSION

Due to varying segmentation procedures and experimental protocols, data from the three cadaver studies were analyzed separately. Our model segments the body in a manner most similar to Chandler et al. The other models and cadaver studies segment the body slightly differently.

Table 1 reveals the total percent of body mass that is allotted to the wrong segment by each model, and is indicative of the accuracy of the models when used for

calculating whole-body COM. The results indicate that our model worked best with the data of Chandler et al. The Dempster model worked best with the cadaver data of Clauser et al. However, the data from Clauser et al. were right and left side averages, thus the resultant error is an underestimate of the actual error, as there are normally right and left side asymmetries. The regression model of Zatsiorsky et al. showed higher errors than the other two models.

Table 2 indicates that the model developed here shows good correlation (> 0.70) for most segments. The model is least correlated with the smaller body segments: the hand, foot, and forearm. However, foot height, foot breadth, and hand length, which are used in our model, were not directly available and were estimated from the data. This would result in increased errors in the calculation of foot and hand masses for those cadavers. Also, when calculating the whole-body COM the smaller segments have less of an impact, as seen in figure 1, depending on the motion of interest. However, errors in segment mass may result in increased errors in calculated joint forces due to inertial forces, depending on the motion and joint of interest.

Figure 1 shows that our model compared favorably with the other two models that were evaluated. This figure also illustrates that errors in calculating the mass of larger segments has more influence on the calculation of whole-body COM. It should be recognized that varying segmentation procedures will affect these results.

Using cadaver data to examine the accuracy of models used for calculating body segment masses *in vivo*, is not ideal, due to pre- and post-mortem tissue changes, fluid losses, etc. Further, it is difficult to combine the data from different studies, due to varying experimental protocols. However, we are unable to safely, directly measure segment masses *in vivo*, and hence must rely on cadaver data. While the data analyzed do not provide a direct measure of the accuracy of the models when applied *in vivo*, it provides insight into their utility.

The model developed here is customized to the individual using anthropometric measurements. Therefore, it should be better suited for calculating segment masses of populations not well represented in cadaver studies (e.g: children, women, and people with disabilities), than are simple statistical models that assume some average morphology. Our model was developed using *in vivo* data[5,7] and thus should represent the shape of the living human better than data from cadavers. Further, these data were collected from a much larger and morphologically diverse sample than that used in most cadaver segmentation studies[1-4]. Our model has been shown to calculate segment masses with some accuracy and compared favorably to the two other models evaluated. Our model is inexpensive, quick, and accounts for individual fluctuations in segment shapes using anthropometric measurements, thus increasing its clinical and research utility.

REFERENCES

1) Chandler, RF et al., Investigation of the Inertial Properties of the Human Body, AMRL Technical Report 74-137, 1975.
2) Clarys, JP et al., Hum Bio 58, pp. 771-782, 1986.
3) Clauser, CE et al., Weight, Volume, and COM of segments of the Human Body, AMRL-TR-69-70, 1969.
4) Dempster, WT, Space Requirements of the Seated Operator, WADC Technical Report 55-159, 1955.
5) McConville, JT et al., Anthropometric Relationships of Body and Body Segment Moments of Inertia, AFAMRL Technical Report 80-1191, 1980.
6) Winter, DA, Biomechanics and Motor Control of Human Movement, John Wiley & Sons, 1990.
7) Young, JW et al., Anthropometric and Mass Distribution Characteristics of the Adult Female, FAA-AM-83-16, 1983.
8) Vaughan, CL et al., Dynamics of Human Gait, Human Kinetics Publishers, 1992.
9) Zatsiorsky, VM et al., Contemporary problems of Biomechanics, CRC Press, 1990 pp. 272-291.

Table 1 Mean and standard deviation of sum of absolute error as percent total body mass.

Cadaver study		Model		
		Chesnin	Dempster	Zatsiorsky
Chandler et al.	$\bar{x}$	7.1	8.2	20.7
	σ	2.9	1.8	4.5
Clarys et al.	$\bar{x}$	12.2	15.2	14.2
	σ	2.0	3.5	7.4
Clauser et al.	$\bar{x}$	9.5	6.1	17.3
	σ	2.4	1.9	4.0

Table 2 Range of ICC comparing segment mass for each model to three published cadaver studies[1-3].

	Chesnin	Dempster	Zatsiorsky
Head	0.65 - 0.94	0.34 - 0.73	0.22 - 0.70
Torso	0.88 - 0.97	0.92 - 0.97	0.63 - 0.86
R. U. arm	0.82 - 0.93	0.78 - 0.95	0.82 - 0.97
L. U. arm	0.88 - 0.93	0.78 - 0.94	0.86 - 0.97
R. forearm	0.22 - 0.63	0.72 - 0.94	0.72 - 0.93
L. forearm	0.22 - 0.48	0.71 - 0.91	0.70 - 0.94
R. hand	0.21 - 0.88	0.35 - 0.95	0.60 - 0.82
L. hand	0.21 - 0.81	0.58 - 0.93	0.60 - 0.83
R. thigh	0.78 - 0.93	0.53 - 0.92	0.27 - 0.91
L. thigh	0.78 - 0.98	0.54 - 0.96	0.27 - 0.88
R. calf	0.74 - 0.95	0.66 - 0.81	0.57 - 0.88
L. calf	0.76 - 0.96	0.66 - 0.86	0.55 - 0.93
R. foot	0.66 - 0.91	0.51 - 0.78	0.73 - 0.76
L. foot	0.58 - 0.90	0.25 - 0.70	0.64 - 0.77

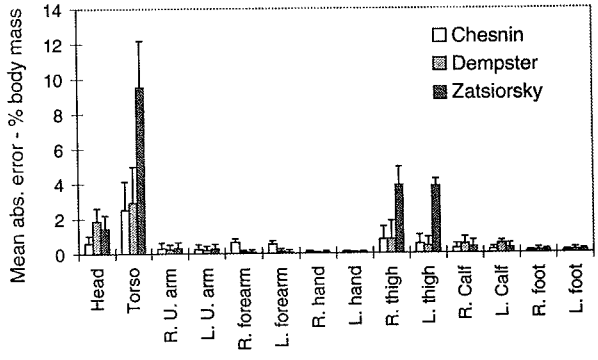

Figure 1 Example of mean absolute error, per segment, in percent body mass for each model. Raw data from Chandler et al (1975), (n=6).

TIME-FREQUENCY (WAVELET) ANALYSIS OF GROUND REACTION DATA IN WALKING AND RUNNING

WILLIAM M. SLOBODA, VLADIMIR M. ZATSIORSKY
Biomechanics Laboratory, Department of Kinesiology, The Pennsylvania State University

The use of the wavelet transformation for analyzing ground reaction force (GRF) data is proposed and demonstrated. The method permits: (a) time localization of the wavelet coefficients which represent the contributions of varying frequency, e.g. high frequency oscillations are mainly present immediately after foot contact with the ground; (b) reconstruction of the signal from the coefficients; (c) estimation of the contribution of the low and high frequency components of the signal, in particular the percentage of energy in the original system accounted for by an individual frequency bandwidth, (d) document the differences in various GRF signals through the energy at different frequency bands.

REVIEW AND THEORY

Analysis of human gait frequently makes use of Ground Reaction Forces (GRF's) recorded during walking and running. These forces have traditionally analyzed either in the time domain—as variations of magnitude of the signal, or in the frequency domain—via the spectral distribution for the entire time duration. The wavelet transform is a mathematical technique that allows for quantitative analysis in the time-frequency domain. The purpose of this research is to apply this technique to GRF's recorded during human locomotion and to compare the wavelet technique with the harmonic analysis.

PROCEDURES

Ten healthy female college students performed a series of walking and running trials at 1.0, 1.5, 2.0, 2.5, 3.0 m/s over an AMTI Force Plate. Data was collected for the right foot as it contacted the platform which was centered over a two meter distance. Velocities were obtained by recording the time it took to cover the two meters using a pair of electronic photocells set at neck level. A walk or run up distance was provided to ensure constant velocity through the two meters. Data from the force platform was transmitted to a computer using an ADT-Data Acquisition Board (National Instruments), digitized at 500 hz and saved using the AMTI Bedas Software. All forces were normalized with respect to the subjects body weight.

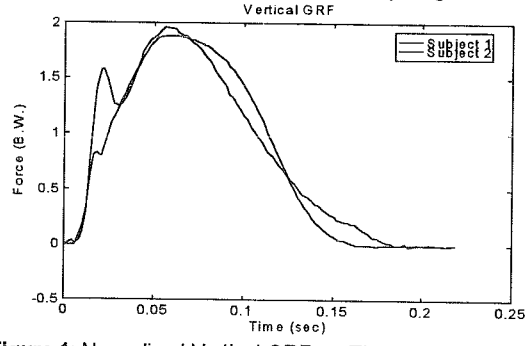

Figure 1: Normalized Vertical GRF vs. Time

RESULTS

Figure 1 shows data from two subjects both running at 2.0 m/s. A qualitative inspection of the two curves shows a large variation in the initial peak. The magnitude of this peak is directly correlated with the degree of heel strike for a given runner. Subject two clearly shows a much larger initial peak, hence lands with a much greater degree of heel strike when compared to subject one. This distinction is the classic separation of runners into a heel strike or forefoot strike category which is often useful when evaluating additional gait parameters. Because this initial peak occurs over a much shorter time than the full contact period its frequency should be much higher. For that reason the spectral distribution of the two curves should reflect the variation of this higher frequency contribution. Most analysis of this type are based on the Fast Fourier Transform (FFT) which converts signals from the time to the frequency domain using the following algorithm:

$$H_k = \sum_{j=0}^{N-1} h_j \, e^{-i 2\pi \; j \, k / N}$$

hj: GRF curve at point j
N = number of sample points
H_k: amplitude at frequency k

The spectral distribution (based on FFT) for both subjects is shown in Figure 2.

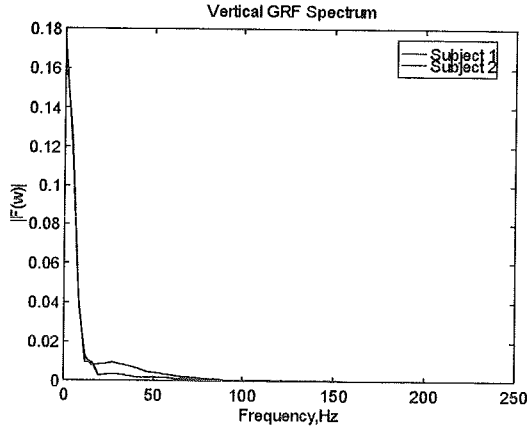

Figure 2: FFT of Vertical GRF's

Unfortunately, as can be seen from the spectral distribution, any differences between the two subjects, though obvious in the time domain, are difficult at best to discern in the frequency domain. And in neither case is there a quantitative measure of this fundamental difference in landing style for these two subjects. The wavelet transform provides such a measure. Shown in Figure 3 is the Discrete Wavelet Transform (DWT) for both subjects GRF's. This transform is computed using S-Plus software based on the algorithm:

$$W_h f(m,n) = \frac{1}{\sqrt{a}} \sum_{k=-\infty}^{\infty} f(k) h\left(\frac{k-b}{a}\right)$$

with $a = a_0^m$, where a ~ T (previous)

and $b = n b_0 a_0^m$, where b ~ j (previous)

Which simply states that for a given frequency range ~ 1/a at a given time = b, the magnitude of the original signal is represented by W_h—a wavelet coefficient— similar to the H_k from the FFT.

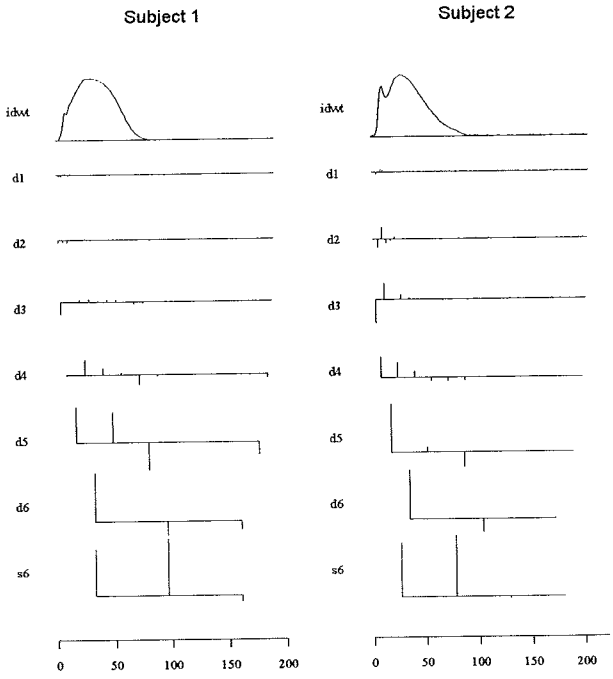

Figure 3: Wavelet Transform of Vertical GRF's.

Of even greater significance is that for the transform shown the energy of the original signal is preserved by the wavelet coefficients. These frequency scales or crystals are the horizontal levels labeled d1...6 and s6 at left and represent a decrease in frequency from top to bottom. In fact each crystal decreases by a factor of 2. Location from left to right within a given crystal corresponds to real time as seen in comparison with the original signal at the top of the figure. In this case the difference in higher frequency content due to the heel strike component for subject two is clearly visible when compared to subject one.

DISCUSSION

The wavelet transform clearly shows certain advantages for quantitatively analyzing differences in GRF's. Due to the simultaneous time-frequency nature of the transform as well as it's ability to preserve energy these differences may be summarized through a comparison of the energy contained in different crystals. Such a summary is shown in Figure 4.

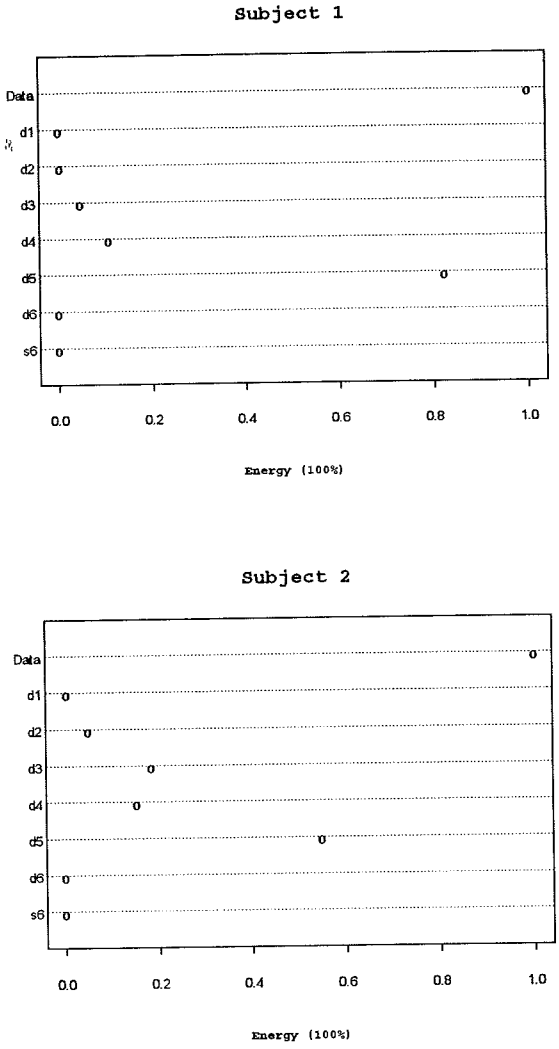

Figure 4: Energy Distribution by Scale Crystals.

Here the equal s6 and d6 levels have been set to zero which further amplifies the differences in the remaining crystals. In this manner only 4-5 numbers (% energy at a given crystal) quantitatively capture the differences between these two curves. For this reason the wavelet transform is a potentially powerful tool in the field of biomechanics.

REFERENCES

Walker, James S. (1991) Fast Fourier Transforms, CRC Press.

Young, Randy K. (1992) Wavelet Theory and Applications, Applied Research Lab, The Pennsylvania State University.

ACKNOWLEDGMENTS

A special thanks to Paul K. Canavan, PT and The Penn State Center for Sports Medicine for it's support and cooperation in this endeavor.

MODELLING OF THE FOOT TO IMPROVE SEGMENT POWER ESTIMATES IN THE VERTICAL JUMP

Wendy L. Carmichael and James J. Dowling

Department of Kinesiology, McMaster University, Ontario, Canada

INTRODUCTION

Vertical jump height is best predicted by the development of peak instantaneous power (Dowling, et al. 1993). This power was calculated for the whole body as the product of the ground reaction force and the vertical velocity of the center of gravity. In order to examine the development of that peak power, it would be useful to determine the flow of power which occurs within and between the segments contributing to the movement.

Segment power flow analysis is a method used to yield information about the generation, absorption and transfer of mechanical energy in human movements. Robertson, et al. (1980) compared the total segment power (TSP) of the thigh, leg and foot during walking to the rate of change of mechanical energy (RCE). Power measures were validated for all segments except the foot during the weight acceptance and the late push-off phase of the gait cycle. Theoretically, for any rigid segment, the RCE should be equal to the TSP and errors have been attributed to the "necessary assumptions concerning rigidity of the links and the position of the (moving) axes of rotation" (Ingen Schenau, et al. 1990).

The purpose of this study was to develop a foot model to improve segment power estimates in the vertical jump. In order to accomplish this goal, it was necessary to examine the effect of adding a forefoot segment to the traditional foot model and to determine a method to decrease the foot segment length variability.

METHODS

Sixteen university or club volleyball players (8 male, 8 female) volunteered to participate in this study. Infrared emitting diodes were placed on the toenail of the great toe, fifth m-p joint, distal tip of the lateral malleolus and the femoral condyle. Kinematics were recorded by an OptoTrak/3020 at 100 hz and synchronized with an AMTI force platform. The subjects performed maximum counter-movement and squat jumps. The inertial data of the foot segments were determined from water immersion, geometric models and literature values.

Figure 1 shows the power calculations for the traditional foot model (1-segment) and the two segment model (2-segment).

A) 1-segment model

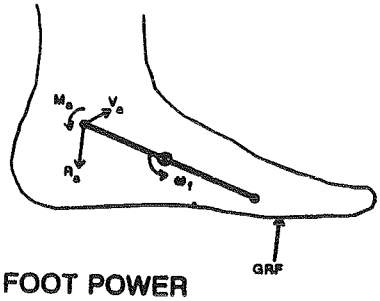

FOOT POWER

$$TSP = [JP + MP]_{prox}$$

$$JP_{prox} = \vec{R}_a \circ \vec{V}_a$$

$$MP_{prox} = M_a \circ \omega_f$$

B) 2-segment model

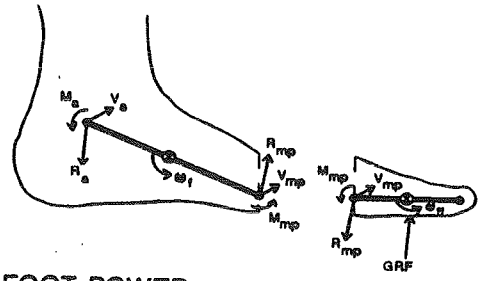

FOOT POWER

$$TSP = [JP + MP]_{prox} + [JP + MP]_{dist}$$

$$JP_{prox} = \vec{R}_a \circ \vec{V}_a \qquad JP_{dist} = \vec{R}_{mp} \circ \vec{V}_{mp}$$

$$MP_{prox} = M_a \circ \omega_f \qquad MP_{dist} = M_{mp} \circ \omega_f$$

FOREFOOT POWER

$$TSP = [JP + MP]_{prox}$$

$$JP_{prox} = \vec{R}_{mp} \circ \vec{V}_{mp}$$

$$MP_{prox} = M_{mp} \circ \omega_{ff}$$

Figure 1. Total segment power calculations A) one segment and B) two segment foot models.

In order to decrease the foot segment length variability, the position of the ankle marker was relocated by extending the leg segment in 1mm increments to a maximum of 50mm by minimizing the standard deviation of the foot segment length throughout the movement. These two manipulations yielded four foot models: one segment foot (1-segment), two segment foot (2-segment), one segment-modified ankle (1-segment-ankle), and the two segment-modified ankle (2-segment-ankle). Correlation coefficients and percent root mean square differences (%RMS) were used to assess the discrepancies between TSP and RCE for each of the four models.

RESULTS AND DISCUSSION

The combination of both modifications to the traditional foot model (i.e. 1-segment vs. 2-segment-ankle) resulted in dramatic improvements for the match between the TSP and the RCE (see fig. 2). The average correlation coefficient improved from -0.46 to 0.92 for the male group and from -0.50 to 0.77 for the female group in the countermovement jump. The %RMS differences decreased from 380.5% to 35.4% for the male group and from 466.9% to 71.6% for the female group. The squat jump results were similar.

Ankle joint re-definition succeeded in compensating for foot segment length changes in most cases, and indicates that a single point can be located to act as a hinge joint between the foot and leg segments throughout the vertical jump motion. Improvements associated with the addition of a forefoot segment to the traditional one segment model indicate that substantial power flow occurs through the metatarsal-phalangeal joint during vertical jump motions.

It should also be emphasized that the necessary addition of the forefoot segment and the location of the axis of rotation changed the calculated joint reaction forces and moments at the ankle joint when compared to the traditional foot model. These different forces and moments would also change the forces and moments calculated for the knee and hip joints in a linked segment analysis. Therefore, the good match between TSP and RCE found by Robertson, et al. (1980) for the leg and thigh segments for the entire gait stride should not be interpreted as an indication that the joint reaction forces and moments were accurate for the knee and hip for the entire stride. The errors at the ankle during weight acceptance and toe-off cause errors at the other joints at these times. The equations of dynamic equilibrium ensure a balance between RCE and TSP as long as the assumptions of rigidity are true and the axis of rotation is known. The equating of RCE and TSP will not detect an error in the input information such as errors in reaction forces or moments at the distal joint.

REFERENCES

Dowling, J.J., et al. *J. Appl. Biomech.* 9:95-110, 1993.

Ingen Schenau, G.J. van, et al. *J. Biomech.* 23:865-881, 1990.

Robertson, D.G.E., et al. *J. Biomech.* 13:845-854, 1980.

ACKNOWLEDGEMENT

The Authors wish to thank the Natural Science and Engineering Research Council of Canada for funding and the subjects for their participation.

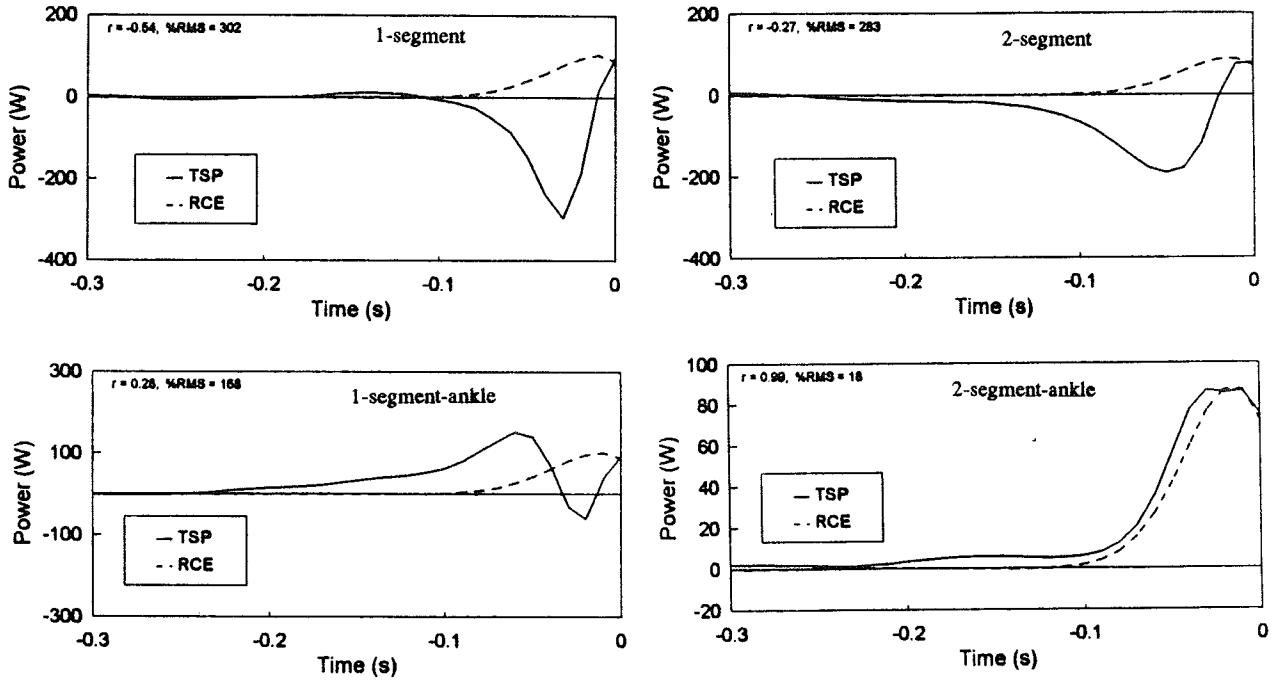

Figure 2. TSP (solid line) and RCE (dashed line) comparisons for the four foot models during the counter-movement jump of a single subject.

THE EFFECT OF SEGMENT PARAMETER ERROR ON GAIT ANALYSIS

D J Pearsall[1], P A Costigan[2]

[1] Department of Physical Education, McGill University, Montréal, Québec, Canada, H2W 1S4
[2] School of Physical Health & Education, Queen's University, Kingston, Ontario, Canada, K7L 3N6

INTRODUCTION

The extent to which errors in predicting body segment parameters(SP) affect the outcome of a biomechanical analysis of motion is not evident. The intent of this study was to address this question by quantitatively evaluating (1) the differences in SP estimates for a young, adult, male population based on predictive functions from various literature sources; and (2) the extent to which SP errors effect inverse dynamic analysis of walking motion.

REVIEW AND THEORY

Reducing systematic errors in motion analysis has focussed upon marker location, skin movement, and equipment accuracy; however, the significance of using generalized body SP has not been reviewed extensively. SP include measures of mass (MS), center of mass (CM) and moment of inertia (I) of body segments. Of the few quantitative reports, it has been noted that SP errors may be only as damaging as errors in acceleration data when estimating joint forces and moments[1] while others have suggested that SP errors may be more serious[2].

PROCEDURES

From a sample of 15 young, healthy males varying in body mass indices (18.8 to 27.3 cm/ kg^2) SP estimates of the leg and thigh were calculated according to predictive functions found in the literature and include equations that use ratios, regressions and geometric descriptions[3-5].

SP were varied to examine the effect of changing segment parameters on the kinetic output. The SP predict by Dempster's equations[3] were taken as the baseline level. Each SP was varied in steps over nine levels by a defined percentage (-40% to +40%) of the original SP baseline value.

Walking kinematic and kinetic data were collected for each subject. The three-dimensional motion of the right lower limb was recorded at 50 Hz using the WATSMART motion tracking system (Northern Digital, Waterloo). The body model used (Figure 1) consisted of leg and thigh segments.

Figure 1. Lower limb model used for kinetic estimates of hip.

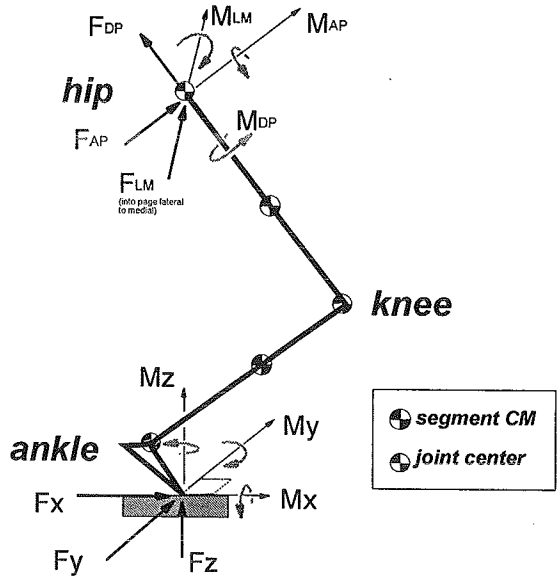

Inverse dynamic analysis was performed iteratively to compute hip forces and moments while simultaneously varying SP values over nine intervals within ± 40% of a baseline value. The output data were the forces and moments about the hip joint expressed in the thigh fixed-body coordinate system.

RESULTS

Substantial variation in SP were produced when various predictive formulae from the literature were used. In some cases, the differences were greater than 40% for MS and I values. A Duncan's multiple range test ($p<0.05$) was used to contrast the means of SP predicted. Significant differences were found for the MS, CM, and I segment parameters for both the leg and thigh.

Using repeated measures ANOVA, SP variations were found to significantly affect ($p<0.05$) most of the kinetic estimates, particularly during the swing phase. However, the absolute value of these differences were small, generally less than 1% of body weight. The one exception was the force in the distal-proximal direction where SP variations altered the force measures by up to 57% during stance and 62% during swing. (Figure 2)

DISCUSSION

Though nearly half of the kinetic measures were statistically affected by SP variation most effects were small. The SP influence may have been diminished by several factors including (1) unchanged kinematic and ground reaction force patterns, (2) the lack of interaction of SP used in the body model, and (3) the net mass of the thigh or the leg segments as compared to the whole body.

The small changes in the kinetic measures does not suggest that SP are unimportant in all human motion studies. In closed-chain situations, such as during gait stance, the limb accelerations are low when compared to the maximum achievable; thus the effect of SP are minimal. However, the effect of the SP would increase with skills that involve larger limb accelerations, such as running, and with open-chain skills that do not have large external loads, such as throwing. In addition, forward simulation of activities such as those just described would be more dependent on SP of the body model. The extent of this dependence is an issue for further investigation.

Figure 2. Hip forces during gait cycle as affected by changes in thigh mass.

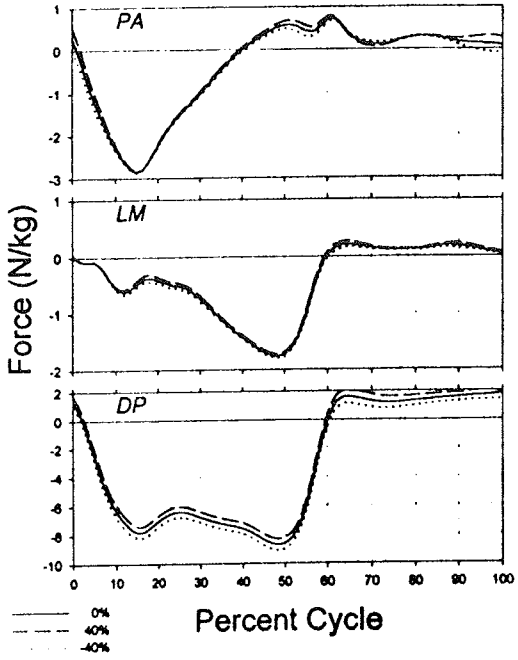

REFERENCES

1. Davis B L. Uncertainty in calculating joint moments during gait. *Proc 8th Euro Soc Biomech Conf*, Rome, Italy, 276, 1992.
2. Wu G, Ladin Z. *Proc 2nd Int Sympos on 3D Analysis of Human Movement.* , 106-108, 1993.
3. Dempster W T. Space requirements for the seated operator. WADC (TR-55-159), 1955.
4. Clauser C E, McConville J T, Young J W. Weight, volume and center of mass of segments of the human body. AMRL (TR-69-70) 1969.
5. Zatsiorsky V, Seluyanov V. The mass and inerital characteristics of main segments of the human body. *Biomechanics VIII-B.* Matsui H, Kobayashi K. editors, 1152-1159, 1983.

ACKNOWLEDGEMENTS

The authors would like to thank Dr. Urs Wyss for the use of the data from the Clinical Mechanics Group gait analysis laboratory (Queen's University) and the use of the QGAIT motion analysis software.

ROLES OF FLUID LOSS AND INTRINSIC PROPERTIES IN THE VISCOELASTIC BEHAVIOR OF THE HUMAN INTERVERTEBRAL DISC

Y. Michael Lu[1], William C. Hutton[2], and Vasanti M. Gharpuray[1]
[1]Department of Bioengineering, Clemson University, Clemson, SC 29634
[2]The Emory Spine Center, Emory University School of Medicine, Atlanta, GA

INTRODUCTION

Loss in disc height due to constant loading over long periods of time has long been known to be directly attributable to two major factors: intrinsic viscoelastic behavior of disc tissues and changes of fluid content in the nucleus[1,4]. These factors are also responsible for the rate dependent behavior of the disc. A thorough knowledge of the roles that these two factors play in a loaded disc is directly relevant to the study of the mechanical behavior of the disc under sustained loading and under cyclic loads. This knowledge is also of considerable clinical interest when interventions such as chemonucleolysis cause changes in nuclear fluid content over time. In this study the effect of the interplay between these two factors on the overall viscoelastic behavior of the disc was studied using the finite element method.

REVIEW AND THEORY

The fluid content of the disc varies with the applied load, and represents an equilibrium between the applied load, which causes fluid to be expelled from the disc, and the swelling pressure of the hydrophilic proteoglycans, which act to retain the fluid. At equilibrium, there is no net fluid loss or gain. Adams and Hutton[1] reported an overall fluid loss of 11% from cadaveric discs subjected to creep loading, equivalent to body weight, for four hours. In an in vivo study using MRI scans, Botsford et al.[4] found that the average diurnal disc volume decrease in lower lumbar discs was 16.2%; this volume decrease was presumed to be due to fluid loss. The fluid content has also been found to decrease with degeneration. In addition, Best et al.[2,3] showed that degenerated discs have greater hydraulic permeability than normal discs, which suggests that degenerated discs may lose fluid faster than normal discs under a compressive load.

Therefore, our primary objective was to develop a viscoelastic finite element model of a lumbar motion segment and to use the model to 1) determine the effect of different rates of fluid loss on the creep behavior of the disc and 2) to propose a fluid loss rate that best describes the physiological profile.

PROCEDURES

A three-dimensional finite element model of an intact L2-L3 motion segment was developed based on a fresh cadaveric lumbar spine using the software code ABAQUS. The model consisted of two vertebrae, the disc, endplates, ligaments and posterior bony structures. All solid elements were represented by brick elements, anular fibers and ligaments by cable elements and facet joints by interface gap elements. Anisotropy and geometric nonlinearity were accounted for in the model. The intrinsic viscoelastic behavior of the anular fibers and ligaments was described by the quasi-linear viscoelastic theory[9]: $\sigma(\varepsilon,t)= G(t)*\sigma^{e}(\varepsilon)$, where G(t) is the reduced relaxation function $0.95-0.044\ln(t)$; $\sigma^{e}(\varepsilon)$ is the instantaneous elastic stress.

The disc was subjected to a constant compressive load of 1000 N for one hour to simulate sustained light manual labor. ABAQUS provides the capability to reduce (or increase) the amount of fluid in the nucleus cavity by specifying a mass flow rate and therefore, changes in fluid content of the nucleus could be manipulated to simulate various fluid loss rates. Six different fluid loss profiles were examined in this study: 3 constant rates of 0%/hr (C0), 5%/hr (C5), and 10%/hr (C10) and 3 linearly decreasing rates L10, L15, and L20 (described in Table 1).

Table 1. The fluid loss rates for the six simulations.

Simulation	Fluid Loss Rate (% Nucleus Volume / per hour)	Total Fluid Loss From the Nucleus after One Hour
C0	0	0%
C5	5	5%
C10	10	10%
L10	15 at t=0 reduced to 5 at t=3600 s linearly	10%
L15	30 at t=0 reduced to 0 at t=3600 s linearly	15%
L20	30 at t=0 reduced to 10 at t=3600s linearly	20%

RESULTS

Figure 1 shows the time dependent behavior of the disc in terms of axial strain (disc height loss divided by original disc height) under a constant load of 1000N for a one-hour period. In the disc with 0% fluid loss (C0), changes in axial strain occurred mainly in the first ten minutes and then approached an equilibrium. This suggests that intrinsic viscoelastic properties of the anulus fibers contribute to the time-dependent behavior in about the first ten minutes only of sustained loading. Comparing the values at t=0 to those at t=3600 s, the intrinsic viscoelastic behavior contributes to a 4.1% increase in axial strain (cf. from 0.0884 to 0.092). Fluid loss, on the other hand, contributes more significantly . For example, after 3600 s of loading, fluid losses of 5% (C5), 10% (C10

or L10), 15% (L15), and 20% (L20) contributed to an increase in axial strain (or disc height loss), relative to the value of 0.0884 at t=0, of 23.7%, 48.0%, 70.6%, and 90.7%, respectively. As shown in Figure 1, when the fluid loss went to zero at t=3600 s (simulation L15), the changes in axial strain ceased.

DISCUSSION

Our results indicate that the viscoelastic behavior of the intervertebral disc depends to a large extent on the magnitude and rate of fluid loss from the disc, while the intrinsic properties of the disc tissue play a role only at the early stage of loading. This is in agreement with Adams and Hutton[1] who estimated that fluid content loss consists of two-thirds of the average height loss while the remaining one-third is due to creep deformation of the anulus fibrosus.

Before an external load is applied to a disc, the swelling pressure and physical pressure are in equilibrium. When load is applied, fluid is lost rapidly at first because the hydrostatic pressure in the disc suddenly outbalances the swelling pressure. As the disc loses more fluid, the swelling pressure increases. The fluid loss then slows as the driving force approaches zero[8]. This suggests that fluid loss decreases with time. The results of our simulations indicate that the three linearly decreasing rates of fluid loss (simulations L10, L15, and L20) provide the best physiological profile of fluid loss from a disc. The predicted axial strain curves and the experimental curves showed similar slopes (Figure 1). However, they differed in intercepts or instantaneous strains. Extreme variations in intercepts also exist in the experimental curves from different studies and from different testing samples in the same study. The contributing factors may include variations in cadaveric specimens (e.g., geometric variations, degeneration, pathology, etc.) and differences in the experimental protocols (strain measurements, gauge length, etc.) in different studies.

Fluid loss rate is also affected by pathology, since disease or degeneration alters the biochemical composition and molecular ultrastructure of the disc tissue. It is also already known that degenerated discs have a lower fluid content[7,8]. Best et al.[2] reported that the permeability coefficient (k) of the anulus of degenerated discs (1.11×10^{-15} m^4/Ns) was higher than that of normal discs (0.28×10^{-15} m^4/Ns) (i.e. degenerated discs lose fluid more quickly than normal discs). To compare our results to these experimental values, the average permeability coefficient (k) corresponding to the simulations in this study was calculated using Darcy's law. The calculated permeability coefficients (k) for L10, L15, and L20 were 0.37×10^{-15} m^4/Ns, 0.55×10^{-15} m^4/Ns, and 0.74×10^{-15} m^4/Ns, respectively; these values fall within the range of those given for normal and degenerated discs by Best et al.[2] These values also show that a higher fluid loss gives a permeability coefficient that is closer to that of a degenerated disc. This suggests that the model simulation L15 and L20 approximated degenerated discs while simulation L10 approximated normal discs.

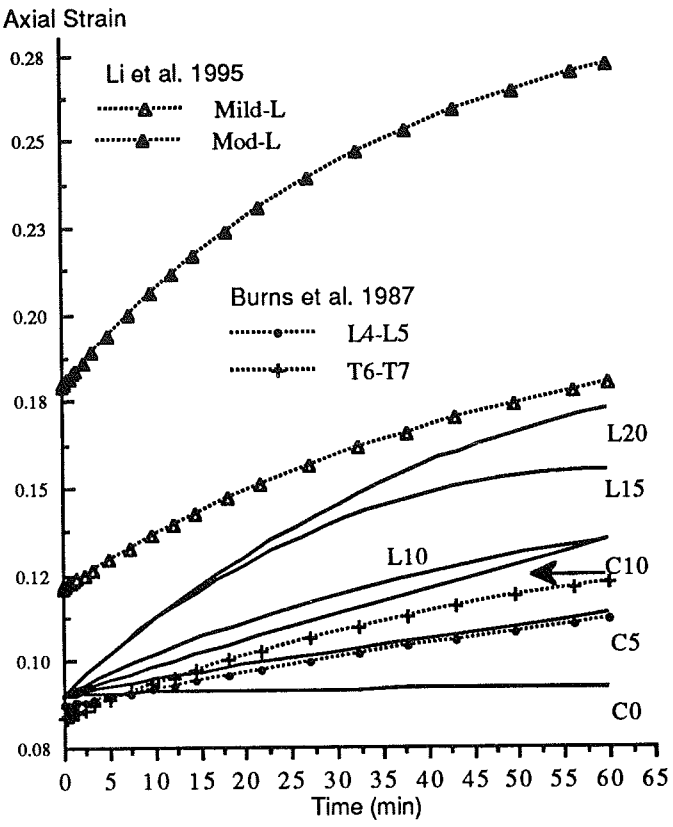

Figure 1 Axial strain versus time for a constant compressive load of 1000 N. The results from the model simulations are compared with other experimental results: Burns et al.[5] a lumbar disc (L4-L5); Li et al.[6], from lumbar discs of mild (Mild-L) and moderate degeneration (Mod-L).

REFERENCES

1. Adams MA, Hutton WC. Spine 1983; 8:665-671.
2. Best BA, et al., Tran Orthop Res Soc 1989; 14:354.
3. Best BA, et al., Spine 1994; 19(2):212-221.
4. Botsford DJ et al. Spine 1994; 19:935-940.
5. Burns ML et al. J Biomechanics 1984; 17:113-130.
6. Li S et al. J Biomechanics 1995; 28(7):779-790.
7. Pearce RH et al. J. Rheumatology (Suppl) 1983; 11:108-110.
8. Urban JPG et al. Spine 1988; 13, 179-187.
9. Yahia LH et al. J Biomed Eng 1991; 13:399-406.

ACKNOWLEDGMENTS

National Center for Supercomputing Applications (NCSA) (Grant No. BCS950002N), GHS/CU Cooperative Research and Education Program.

NONLINEAR FINITE ELEMENT ANALYSIS OF THE CERVICAL SPINE

L. Voo, J. Denman, F. Pintar, N. Yoganandan
Department of Neurosurgery, Medical College of Wisconsin, Milwaukee, WI 53226
and Neuroscience Research, Veterans Affairs Medical Center, Milwaukee, WI 53295

INTRODUCTION

Quantification of the internal biomechanical responses such as stress and strain, in various tissues of the cervical spine has many applications in injury prevention, surgery, and rehabilitation. Our current knowledge about biomechanics of the cervical spine mostly stems from cadaveric experiments. Finite element (FE) application in the cervical spine is relatively new. The reported models are either representing a single vertebra or whole cervical column with assumed geometry (Saito et al., 1991; Kleinberger, 1993; Bozic et al., 1994; Teo et al., 1994). Recent development in this area has produced a detailed C4-C6 linear model based on three-dimensional CT reconstruction (Voo et al., 1995; Yoganandan et al., 1996). Preliminary study of this model and complex structural properties of the cervical spine indicates a need for a nonlinear model.

This study has developed a nonlinear FE model of the lower cervical spinal segment (C4-C6). The model was validated under axial compression, and pure-moment flexion and extension modes. Stress distribution within various tissues under different loading conditions was also examined.

PROCEDURES

The model geometry for the bony tissues was obtained from computer-reconstruction of sagittal and coronal CT images of a 33 year old female cadaver. The soft tissue geometry was based on the anatomical details from cryomicrotome images. Mapped-mesh technique was used to obtain the FE mesh of eight-noded hexahedron elements for the vertebrae and intervertebral discs. The detailed model construction procedure was reported in another publication (Voo et al., 1995). The two-noded uniaxial elements for various ligaments were added with their insertion points identified from sequential cryosection slides. The final elements added were MSC/NASTRAN three-dimensional slideline contact elements to simulate the articular sliding contact in the facet joints. The contact elements were defined such that any node on either the superior or inferior surface of each joint would be considered in contact if it passed between any of the nodes on the opposite adjoining facet surface. The completed model consists of three lower cervical vertebrae (C4, C5, and C6), two intervertebral joints (C4-C5 and C5-C6), and five major cervical ligaments: anterior longitudinal, posterior longitudinal, ligamentum flavum, capsular, and interspinous (Figure 1). The model has a total of 9,722 elements and 34,842 total degrees-of-freedom. The ligaments were modeled by a total of 595 uniaxial nonlinear elements. The facet interfaces were simulated with 43 slideline contact elements.

Material properties of tissues for model input were obtained from literature and our own laboratory experiments. The material properties for the bony tissues and disc nucleus were assumed to be linearly elastic. The nonlinear stress-strain curves for the disc annulus were adapted from Yamada (Yamada, 1970). The nonlinear curves for the ligaments (anterior and posterior longitudinal, ligamentum flavum, joint capsule, and interspinous) were derived from our own experimental data. Elements representing the ligaments had near zero stiffness under compression.

Three different loading cases were considered in this study: axial compression, pure flexion, and pure extension. The model boundary conditions were defined to mimic the experimental conditions for validation. For all three load cases, nodes in the inferior surface of C6 were assigned zero displacements in all directions. For compression loading case, an uniformly distributed axial displacement was incrementally applied to the superior surfaces of the C4 vertebra while displacements in other direction were set to zero. This simulated the boundary condition in the experiments (Shea et al., 1991; Pesigan, 1989). For flexion and extension loading cases, a rigid structure was created on the surfaces of C4, and a pure moment in the near-sagittal plane was applied incrementally. The C4 top was not constrained; similar to the experiments of Shea et al. The material properties were the same for all three loading cases reported in this study. The model simulations were performed in MSC/NASTRAN program.

Model load-displacement responses and experimental curves were plotted together for the validation purpose. Stress distribution in various tissues, such as middle (C5) vertebra, intervertebral discs, and ligaments, was also obtained and analyzed.

RESULTS & DISCUSSION

The model load-displacement responses agreed well with the comparable experimental curves (Figures 2 and 3). The flexion-extension responses closely matched the experimental curve from Shea et al until the load reached approximately 1.5 Nm (Figure 2).

The stress distribution within spinal components was consistent with their structural behavior. For example, under extension moment loading, tensile stress was found in the anterior longitudinal ligaments while all the other ligaments were not stressed. Discs had tensile stress in the anterior portion and compressive stress in the posterior portion. A similar stress pattern was found in the vertebral body of C5, i.e., anterior portion was under tension and posterior portion under compression.

Under compressive loading, maximum principal stress in the superior endplate of C5 was along the lateral direction while in the inferior endplate, it was along the anteroposterior direction. The stress magnitude in the inferior surface was higher than that in the superior surface. This is likely due to the unique saddle shape of the cervical vertebral body (see Figure 1) which is not present in the thoracic or lumbar spines. The superior and inferior surfaces of the cervical vertebral body curve upward at the left and right sides while they curve downward at the anterior and posterior sides. The higher stress in the inferior region of the body may indicate a higher propensity for trauma to initiate from this region. This finding may explain the mechanism of burst fractures with vertebral fragments retropulsed into the spinal canal at its inferior end..

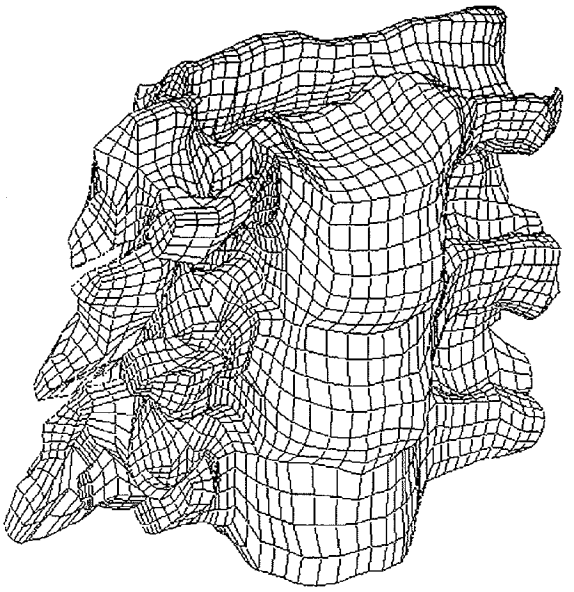

Figure 1: Superior-anterior view of the C4-C6 model (ligaments are not shown)

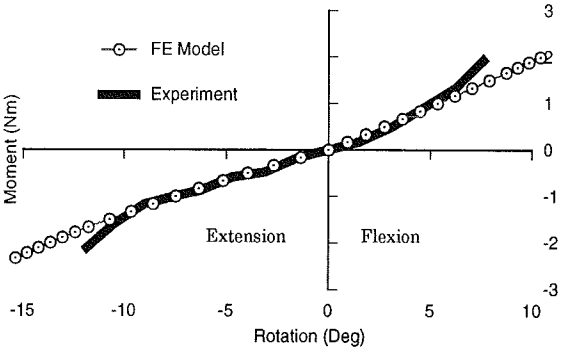

Figure 2: Nonlinear FE model response with validation in flexion-extension

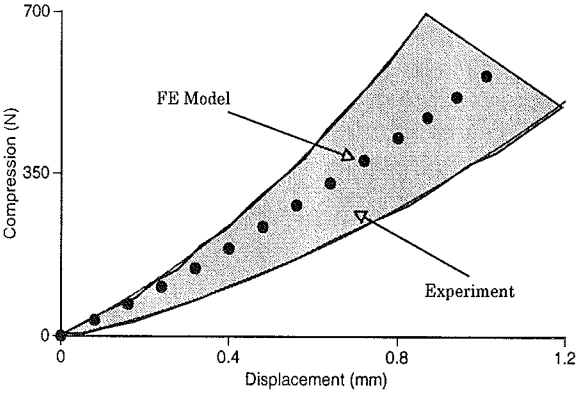

Figure 3: Nonlinear FE model response with validation in compression.
Shaded area represents experimental data.

REFERENCES

Bozic, K.J. et al. J Spinal Disord, 7, 102-110, 1994.
Kleiberger, M. Proc 37th Stapp Car Crash Conf, 261-272, 1993.
Pesigan, M.F. M.S. Thesis, Marquette Univ, 1989.
Saito, T. et al. Spine, 16, 494-502, 1991.
Shea, M. et al. J Biomech, 24, 95-107, 1991.
Teo, E. et al. Med & Biol Eng & Comput, 32, 236-238, 1994.
Voo, L.M. et al. Adv Bioeng, 31, 13-14, 1995.
Yamada, H. Strength of Biological Materials, (pp. 84-92), Williams & Wilkins, 1970.
Yoganandan, N. et al. J Biomech, (in press), 1996.

ACKNOWLEDGMENTS

This research was supported in part by the Research Project Development Grant (1995) of the Cervical Spine Research Society, PHS CDC Grant R49CCR 507370, and the Department of Veterans Affairs Medical Research Service.

MECHANICAL PROPERTIES AND INJURIES RESULTING FROM ANTERIOR AND POSTERIOR SHEAR LOADING OF THE SPINE AT DIFFERENT LOAD RATES

V.R. Yingling, S.M. McGill
Department of Kinesiology, University of Waterloo, Waterloo, Ontario, Canada

INTRODUCTION

The purpose of this study was to quantify the effect of the rate of shear loading on several functional parameters on a homogenous sample of porcine spinal motion segments. Specifically, load deformation curves yielded the ultimate load to failure, the stiffness and the deformation to failure of the spinal motion segments. The resulting injury from the applied shear loads were quantified via dissection and high resolution planar x-rays.

REVIEW AND THEORY

Understanding the etiology of spinal injury is powerful knowledge in the design of appropriate rehabilitation and prevention strategies. Compressive injuries continue to be a main focus of spinal injury research. However, shear loading is a significant mode of loading in-vivo and is suspected to play a role in injury. The lordotic curve of the lumbar spine places a continual shear load on the motion segments. Furthermore, normal load handling movements which involve flexion of the upper body can generate an applied shear load equal to approximately half of body weight (Potvin et. al., 1991). During activity these applied shear loads increase due to the acceleration and inertia of the load.

Injury is commonly defined as occurring when the load on a tissue exceeds its tolerance value. Previous research has focused on understanding the factors which affect the tolerance of a tissue. These factors include both material properties and loading conditions of the spinal motion segment. The composite material of the vertebral motion segment affects the tolerance of the tissue since each tissue exhibits differing material properties and are affected by age, gender, level of activity and diet. The posture during loading, the direction of loading (anterior/posterior), and the rate of loading also affect the tolerance of spinal motion segments. Lumbar motion segments are made of viscoelastic tissue thus indicating the possible effect of loading rate on the injury mechanisms of the tissue.

PROCEDURES

Cervical porcine spines of domestic pigs (mean live weight of 80kg) were collected immediately after death and frozen (20° C). Thawed spines were stripped of their musculature and sectioned into two specimens, C3-C4 and C5-C6. The specimens were examined for degeneration and only grade I specimens were used in testing (Galante, 1967).

The specimens were mounted into stainless steel cups using dental plaster (Denstone Miles Inc) and wires, looped around the pedicles and anterior processes, to secure the specimen to the cup. The cups were placed into a custom designed jig to ensure a pure shear load was applied to the specimens. The jig was placed into an Instron Dynamic Testing Machine (Model 8511). One end of the motion segment remained stationary while the other end moved in a casing mounted on linear bearings for frictionless movement. A 5000 N load cell, which recorded the load resisted by the specimen, was in series with the actuator and the casing containing the specimen. The specimens were loaded at either 100 N/s and > 7,000 N/s under both anterior and posterior shear loading.

Load deformation curves were collected at 100 hz to obtain the mechanical parameters of the specimen. Deformation to failure, ultimate shear load at failure and the stiffness of the specimen were recorded from the curves. Failure was defined as a 6% drop in the load signal.

The Students t-test ($p < 0.05$) was used to test for significant differences between load rates under anterior and posterior loading for the dependent variables, ultimate load to failure, deformation to failure and stiffness.

RESULTS & DISCUSSION

Table 1: Mechanical properties of the spinal motion segment under Anterior and Posterior loading for 100 N/s and > 7,000 N/s [mean (sd)].

Stiffness (N/mm)	Deformation to Failure (mm)	Ultimate Load to Failure (N)
Anterior Shear Loading (100 N/s) N=10		
202 (42.4)	11.9 (2.3)	2111 (160.6)
(> 7,000 N/S) N=4		
353.6 (79.7)	8.23 (1.3)	2773.1 (537.5)
Posterior Shear Loading (100 N/s) N=10		
147.9 (24.3)	14.1 (2.9)	1706 (210.2)
(> 7,000 N/s) N=5		
190.6 (36.1)	10.55 (.5)	1727.8 (288.2)

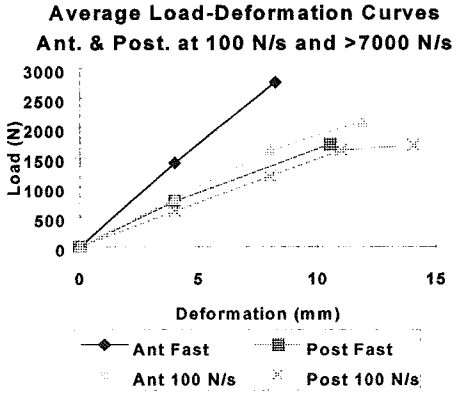

Figure 1: Load-Deformation Curves for Anterior and Posterior Shear Loading (Average Curves).

The current results compare favourably with trends and magnitudes found in the literature. Cripton et. al. (1995) found anterior shear stiffness to be greater than posterior shear stiffness (155 N/mm > > 104 N/mm) in human lumbar vertebral motion segments. Under destructive constrained testing Cripton et. al. (1995) found ultimate load to failure values of approximately 2500 N under anterior loading compared to (2111 N - 2773.1 N) found in the current study.

No significant differences were found between the stiffness, deformation to failure and ultimate load at failure between quasi-static loading (100 N/s) and loading rates greater than 7,000 N/s for both anterior and posterior loading (Table 1). However the injury patterns differed from slow to higher loading rates as well as between anterior and posterior loading. At low load rates anterior loading does not appear to result in bony injury at least there was no visual confirmation on the x-ray, consequently the injury may be primarily to the soft tissue. Posterior loading may have soft tissue injury as well as bone avulsions of the inferior posterior portion of the vertebral body. At higher load rates and in anterior shear the injuries found included fractures of both the facet face and pars interarticularis and bone avulsion at the annulus vertebra junction. Posterior shear loading resulted in wedge fractures and facet damage.

A limitation of the study may be the application of pure shear loading which may be rare in-vivo. Also, the use of a porcine model may be a limitation, however, an animal model affords control over the specimen homogeneity, specifically age, weight, diet, activity level and genetic background. The porcine animal model remains a reasonable analog of the human spine given the similar architectural and biomechanical properties to humans.

In conclusion, the site of injury and severity of injury differed for a porcine spinal motion segment dependent on the rate of loading yet the mechanical properties did not differ significantly. The soft tissue resisting posterior loading may result in lower stiffness values and larger deformations under posterior loading. The main message for humans appears to be shear loading, either anterior or posterior, influence the type and extent of injury and that injurious levels are reached at approximately 1700-2700 N under a range of loading rates.

REFERENCES

1. Cripton, P. et. al. Symposium: Injury prevention through biomechanics. 111-126, 1995.

2. Galante, J.O. Acta Orthop. Scand. #100. 5-91, 1967.

3. Potvin, J.R. Clin. Biomech. 6:88-96, 1991.

COMPONENT MECHANISMS IN SPINAL CORD INJURY
- AN ANIMAL MODEL FOR DRUG TREATMENT PROTOCOLS -

G.M. McNeice[1], W.A. Lee[1], K.C. Lennon[1], C.D. Riddle[1], R.L. Ferguson[1], M. LaBerge[2],
[1]Greenville Hospital System Medical Education & Research, [2]GHS/Clemson University
Biomedical Cooperative, Greenville, S.C. 29605, USA

INTRODUCTION

Spinal cord injury models continue to be used to study the pathophysiology of injury and the potential of various therapeutic treatments. Recent NIH (Young et. al., 1995) supported studies have aimed at standardizing the impact trauma to the cord in the rat model. The present authors have discussed some potential errors inherent in the NYU proposed model (McNeice et. al., 1994, 1995) and introduced a refined rat model using a miniature accelerometer that allows the biomechanics of the impact to be established. The NYU model excludes the effect of cord compression on the neurologic deficit, a factor often seen in human injuries. The present study demonstrates the successful application of this refined model to drug therapy of the impacted cord as well as introduces an extension of the model to include the effects of cord compression. Compression levels of 65% and 85% are demonstrated.

REVIEW AND THEORY

Clinical and animal studies have indicated that early treatment using glucocorticoids may lessen the degree of neurologic deficit. This has led to a current national emergency treatment protocol that requires the administration of methlyprednisolone (MP) within eight hours of the trauma. Although MP has been shown to reduce neurologic deficit in laboratory animals, it has only been marginally effective in clinical studies. There are many contributing factors including dosage, time of administration and the degree of injury to the cord. In attempts to study these factors, many researchers continue to use animal models to establish drug type and dosage. These models use various methods to traumatize the cord such as direct impact, clip compression or static compression. In all cases, the cord is free to return to its original anatomical shape following the trauma. In the case of human injuries, this seldom happens. In addition to the impact force, permanent cord compression caused by bony fragments (burst), canal compromise (bilateral facet dislocation) or other residual deformation effects contribute to the degree of injury. With regard to the selection of drug type and treatment protocols, how do these factors affect the ultimate performance and efficacy of the drug selected? The animal model should be capable of addressing each factor separate as well as in combination.

MODEL AND PROCEDURE

In this ongoing study the authors have established an animal model that will address the following component mechanisms of spinal cord injury:

A. Instantaneous Impact without Compression
B. Compression followed by Decompression
C. Permanent Compression
D. Combined Impact and Compression

The model makes use of the rat with cannulation of the jugular for placebo and drug delivery, and a refined drop mass impact trauma device with a miniature accelerometer that allows full biomechanical impact analysis at the cord interface. To provide cord compression, cylindrical metal rod implants of different diameters (1.6 & 2 mm dia., referenced as R1.6 & R2.0) were designed and placed extradurally to span the partial laminectomy at the T9 vertebra. Neurological deficit was assessed using an extended Tarlov hind limb motor response scale. Sequential video records were kept of each animal and its ability to ambulate, up to six weeks post injury. These tapes allowed multiple trained personnel, blinded to the study, to evaluate the output from the model.

APPLICATION

Application has been made to mechanism A using methylprednisolone (MP) with trauma levels between 40 and 60 gm. cms. of absorbed energy (McNeice et al.,1994). Twenty seven (27) Long Evan hooded rats were studied. Thirteen (13) received placebo (sterile saline) and fourteen (14) MP. Total drug/placebo dosage of 150 mg/kg was administered to each of the 27 animals. This dosage is similar to the approved ER protocol used in most states. A bolus of 60 ml/kg was delivered over a one minute time interval and within two minutes of the trauma. Additional injections of 30 mg/kg were derived at 2, 4, and 6 hours post-trauma. Application was made to Category B without

drug treatment. Both immediate (10 R1.6 & 3 R2.0) and subsequent decompression (4 R1.6 & 0 R2.0) were studied on seventeen (17) animals. Application was made to mechanism C without drug treatment. Permanent compression was studied on 24 animals (14 R1.6 & 10 R2.0). Studies of mechanism D are ongoing.

RESULTS AND DISCUSSION

Results from mechanism A indicate that early (5 min. post injury) administration of MP does have a positive effect (recovery to 70% normal compared to 50% normal without MP using the Wilcoxon rank sum test, p=.04). Preliminary results from mechanisms B and C, in the form of mean and standard deviation, are presented in Figure 1. Results from mechanism B (see Figures 1 & 2) indicate that for 65% cord compression, immediate or subsequent total decompression does result in hind limb functional recovery up to as much as 80% of normal. However, immediate decompression of an 85% compressed cord as seen in Figure 1 showed no recovery above 30% of normal. Preliminary results from mechanism C indicate that permanent 65% cord compression caused 50% deficit levels (Figures 1 & 2) while 85% cord compression (Figure 1) causes severe deficit (30% normal). Additional studies involving MP in mechanisms A through D are ongoing.

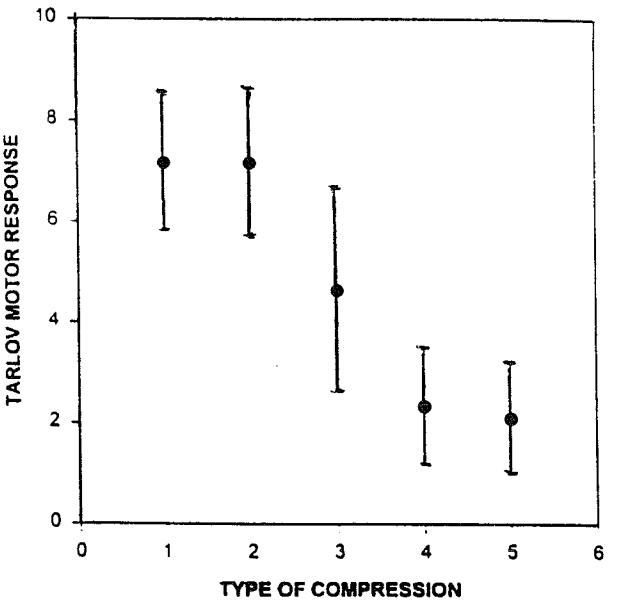

Figure 1: Effect of Cord Compression on Motor Response

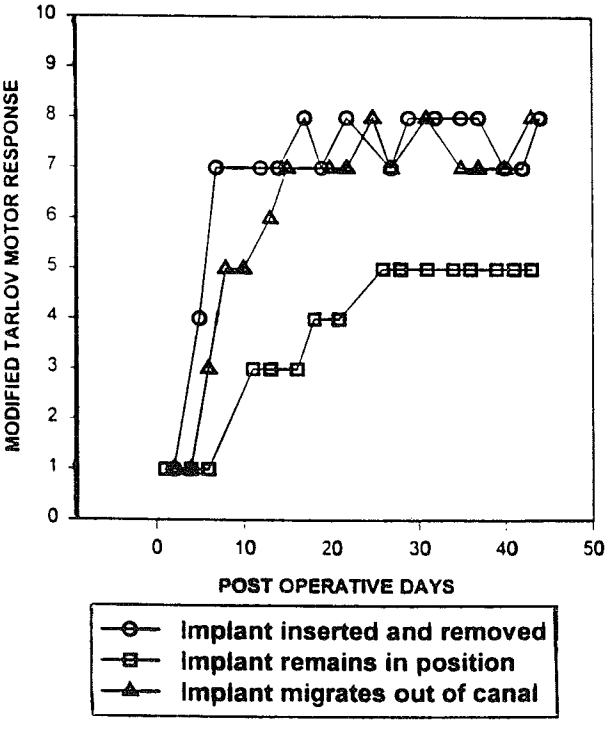

Figure 2: 65% Spinal Cord Compression (Typical)

REFERENCES

McNeice G.M. et al. A refined spinal cord contusion device with measurement at the impact interface. Twelfth Annual Neurotrauma Symposium, Miami Beach, Florida, November 12-13, 1994

McNeice G.M. et al. Example of the "Trauma Window" for SCI Research with Application to a Refined Impact Interface Spinal Cord Contusion Device, 3rd International Neurotrauma Symposium, Toronto, Ontario, July 1995.

Young W et al. Phamacological Treatment of spinal Cord Injury - Experimental and Clinical Studies, 3rd International Neurotrauma Symposium, Toronto, Ontario, July 1995.

ACKNOWLEDGMENTS

Appreciation is expressed to Clemson University faculty and staff at the Godley Snell Research Center and the GHS/CU Biomedical Cooperative for their continuing assistance and support of this study.

BIOMECHANICAL EVALUATION OF TRANSVERSE PROCESS FIXATION OF THE THORACIC SPINE

J. E. Hale, S. Thanapipatsiri, D. Fenton, D. P. K. Chan
Department of Orthopaedics, University of Virginia, Charlottesville, VA 22908

INTRODUCTION

Posterior segmental instrumentation of the thoracic spine can be accomplished by means of pedicle screw fixation, laminar fixation, spinous process fixation, or transverse process fixation. Given the potential for direct spinal cord injury, pedicle screw fixation has been employed sparingly in the thoracic region. Likewise, the use of sublaminar wire or supralaminar hooks carries the risk of neurological complication. In addition, laminar and spinous process fixation cannot be accomplished in the absence or deficiency of the laminae (e.g., spina bifida, post-laminectomized spine, fractures of the posterior bony elements).

REVIEW AND THEORY

Transverse process fixation provides three major advantages over other techniques: (a) implants do not invade the spinal canal thereby decreasing the risk of spinal cord injury, (b) implant attachment is possible even in the absence of the laminae or spinous process, and (c) a greater moment arm is provided for correction of rotational deformity in scoliosis. However, the strength of the transverse process has not been thoroughly investigated. The objectives of this study were to assess the strength of thoracic transverse process fixation constructs using stainless steel wire and Mersilene tape, and to compare the strength of transverse process fixation constructs with that of spinous process button-wire fixation construct.

PROCEDURES

Eight human thoracic spinal columns (C7-T11) with costo-transverse joints and proximal portion of the ribs intact were obtained from 5 male and 3 female fresh unembalmed cadavers (average age: 68 yrs, range: 61 to 72 yrs). Radiographic studies were performed on all specimens to exclude metastatic spinal disease and other destructive lesions of the spine. Prior to mechanical testing, specimens were disarticulated and embedded in self-curing dental acrylic to the level of the vertebral body-pedicle junction, with the posterior bony elements exposed.

For each vertebra, three fixation constructs were evaluated:
1) Transverse process wire fixation (TW). Double strands of 18 gauge stainless steel wire were placed around the left transverse process and fastened with all wires twisted together.
2) Transverse process tape fixation (TT). Mersilene tape (Ethicon, Inc.), 5 mm wide, was placed around the right transverse process and fastened with a surgical knot as advocated by Gaines and Leatherman [1981]. The tape was used to investigate the effect of implant-bone interface area on the strength of the transverse process fixation construct.
3) Spinous process wire fixation (SW). An 18 gauge button-wire (Wisconsin wire) was passed through a drill hole at the base of the spinous process and fastened with a symmetrical twist as recommended by Drummond [1988].
The order of testing was the same for all specimens (TW, TT, SW) and was chosen to minimize the effect of a particular test on the results of any subsequent tests.

Tensile loads were applied to each construct using a materials testing machine (MTS Model 858 Bionix, Minneapolis, MN) operating at a constant load rate of 10 N/sec. Loading was applied until either the bony structure or the means of fixation failed. Specimens were positioned such that the direction of the applied load was perpendicular to the surface of the bony structure being tested. Ultimate tensile force (UTF) was determined from the load-displacement data (maximum load) for each test and a multi-variate analysis of variance performed to determine statistical significance between groups.

RESULTS

A total of 73 thoracic vertebrae were studied (Figure 1). Eleven transverse process-tape constructs (16%) failed by rupture of the Mersilene tape. All other constructs failed by bony fracture. Specimens exhibited varying degrees of osteoporosis as indicated by bone mineral density values at L3 (mean = 0.72, range 0.53 to 0.86, n = 6). Weak positive correlations between bone mineral density and ultimate tensile force were noted for each fixation construct.

The mean ultimate tensile force for each fixation construct was calculated for the upper (T1-2), middle (T3-7), and lower (T8-10) thoracic spine (Table 1) and differences between groups assessed at $p<0.01$, unless otherwise noted. For the upper thoracic spine, UTF values for TW and TT constructs, while not different from each other, were both statistically different from UTF values for the SW construct. For the middle and lower thoracic spine, statistical differences were noted between SW and TW ($p<0.05$, T8-10) and between TW and TT, but not between SW and TT.

DISCUSSION

Mean UTF values were reasonably consistent with corresponding data from previous studies. Wenger et al. [1982] determined the strength of segmental fixation constructs using 16 gauge stainless steel wire attached to the transverse process and spinous process of human vertebrae. The strength of transverse process constructs of the upper and mid-thoracic region were 331.5 N and 237.4 N, respectively. Strengths of 286.7 N and 421.1 N were reported for attachment to the spinous processes of the mid- and lower thoracic region, respectively.

Based on experimental measurements of ultimate tensile force, transverse process wire fixation was inferior to spinous process wire fixation at all levels in the thoracic spine. In the upper levels of the thoracic spine, transverse process tape fixation does not provide any advantage over transverse process wire fixation. Interestingly, the highest mean ultimate tensile forces occurred in this region. However, in the lower thoracic spine, transverse process tape fixation proved superior to wire fixation and provided a suitable alternative to spinous process wire fixation.

REFERENCES

Gaines and Leatherman, Spine 6:483-8, 1981.
Drummond, Orthop Clin North Am 19:281-90, 1988.
Wenger et al., Orthop Trans 6:23-4, 1982.

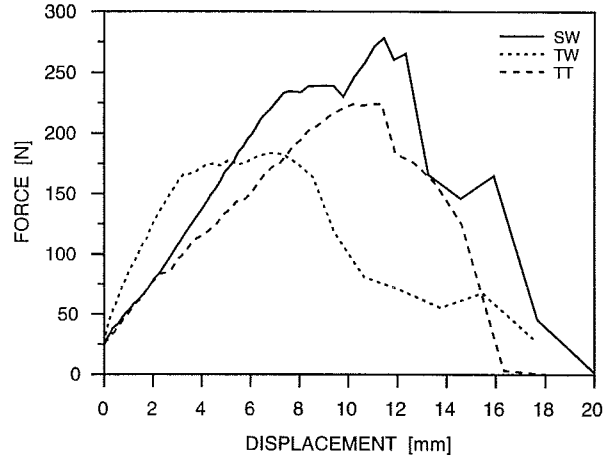

Figure 1. Representative force-displacement response for spinous process wire (SW), transverse process wire (TW), and transverse process tape (TT) fixation constructs attached at the mid-thoracic spine level.

Table 1. Mean ultimate tensile force (std.dev.) of fixation constructs for upper, middle, and lower thoracic spine in Newtons.

	TW	TT	SW
UPPER THORACIC	265.9 (108.4)	270.4 (82.1)	423.7 (178.3)
MIDDLE THORACIC	185.2 (69.1)	259.6 (82.1)	326.7 (137.1)
LOWER THORACIC	197.1 (64.1)	260.6 (72.2)	343.9 (155.6)

NAMES INDEX